Session 5

Wednesday August 24, 2022

10:45am – 12:15pm

O5.1 – ACL

O5.2 – Balance and Falls

O5.3 – Musculoskeletal Modelling & Simulation 1

KNEE CARTILAGE STRESSES IN MEDIAL FEMORAL CARTILAGE 6 MONTHS AFTER ACL RECONSTRUCTION: A FINITE ELEMENT ANALYSIS

Kelsey Neal[1], Jack R. Williams[1], Ashutosh Khandha[1], Lynn Snyder-Mackler[1], Thomas S. Buchanan[1]
[1]University of Delaware, Newark DE
email: kaeneal@udel.edu

Introduction

Medial tibiofemoral osteoarthritis (OA) is common after ACL reconstruction (ACLR)[1]. Alterations in gait biomechanics, such as reductions in peak knee flexion angle (pKFA) and medial compartment force (MCF), may contribute to disease development[2]. Altered gait, in turn, may impact cartilage stress distribution; however, little is known about alterations in cartilage stress distribution after ACLR. The purpose of this study was to compare peak medial femoral stresses between the involved and uninvolved limbs 6 months after ACLR. We hypothesized that the involved limb would see lower stresses when compared to the uninvolved limb.

Methods

15 subjects (12 female, age: 23 ± 7 years, BMI: 22.9 ± 2.3 kg/m²) completed gait analysis during overground walking 6-months after ACLR during which kinematic (120 Hz), kinetic (1080 Hz), and surface electromyography (1080 Hz) data were collected bilaterally. These data were used as inputs into a validated EMG-informed neuromusculoskeletal model to calculate subject-specific joint contact forces[3]. Each subject's pKFA, MCF at pKFA and lateral compartment force (LCF) at pKFA were then used as the inputs to a finite element (FE) model.

Geometry for the FE model was obtained from one subject (female, age:19) through segmentation of a MRI scan taken 6-months after ACLR. Cartilage and meniscal structures were meshed using hexahedral elements via an open-source software developed by Rodrigues-Vila et. al 2017[4]. Bone geometries were meshed using triangular shell elements in Hypermesh (HyperWorks, Altair Engineering, Inc, Troy, MI). The meshed geometries were assembled by using tie constraints to connect the cartilage and meniscal horns to the bones. Knee ligaments were added using 1D truss elements in Abaqus CAE (Dassault Systems Simulia Corp., Providence, USA). (**Figure 1A**)

A reference point (RP-C) was placed at the center of the transepicondylar axis and coupled with the femur elements. Two additional reference points were placed at the center of the medial (RP-M) and lateral (RP-L) joint compartments on the transepicondylar axis and coupled to RP-C. Simulations were run for each subject's involved and uninvolved limb's data. All FE model inputs were applied quasi-statically to the femur while the tibia was fixed in all directions. Peak KFA was applied to RP-C and the model was allowed to settle into position. Once settled, MCF and LCF were applied to RP-M and RP-L, respectively. The output of interest was Von Mises stress for each element.

For each simulation, the medial femoral cartilage was divided into anterior, central, and posterior regions of interest (**Figure 1B**) and peak von Mises stress was found within each region. The region average was then calculated for each limb. A two tailed paired students t-test ($\alpha = 0.05$) was performed to assess differences between limbs.

Results and Discussion

Our hypothesis was supported, the involved limb experienced lower stresses (vs. uninvolved limb) in all three regions of cartilage (**Figure 2**). These differences were significant in the anterior region ($p = 0.037$) and approached significance in the central ($p = 0.063$) and posterior ($p = 0.079$) regions.

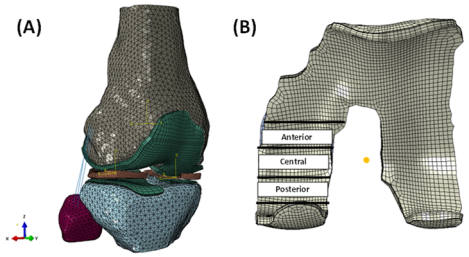

Figure 1: (A) Full FE model and global coordinate system. (B) Regions of interest for medial femoral cartilage

Interestingly, among the subjects assessed, only pKFA was significantly lower in the involved limb (vs. uninvolved). There were no differences between limbs in MCF (**Table 1**). These data suggest that, after ACLR, individuals may modify their gait to avoid applying stresses to their cartilage rather than specifically to reduce load. Thus, isolated examination of loading after ACLR may tell an incomplete story of the true state of cartilage. Future work should assess the association between altered cartilage stresses and long-term cartilage health.

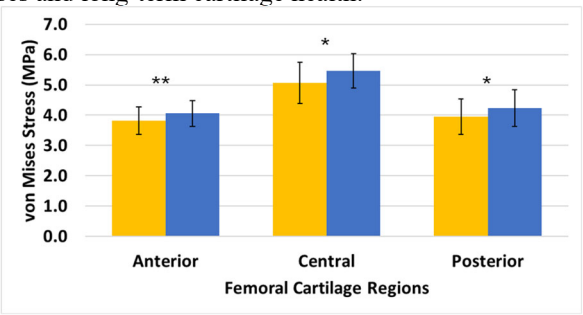

Figure 2: Peak von Mises stress in the medial femoral cartilage of the involved (yellow) and uninvolved (blue) limbs 6 months after surgery. ** =statistical significance * = Approaching significance

Table 1: Averaged biomechanical model inputs for all subjects

Limb	MCF (BW)	LCF (BW)	pKFA (°)
Involved	2.90 ± 0.61	1.71 ± 0.51	19.46 ± 3.23
Uninvolved	2.91 ± 0.43	1.66 ± 0.45	21.5 ± 3.15
P-Value	0.961	0.554	< 0.001**

Significance

Stresses within the cartilage differ between limbs after ACLR and could be a mechanism for eventual OA development.

Acknowledgments

NIH: R01-HD087459

References

1. Wellsandt E, et al. 2016. *Am. J. Sport. Med.* 2. Slater L V., et al 2017. *J. Athl. Train.* 3. Manal K, Buchanan TS. 2013. *J. Biomech. Eng.* 4. Rodriguez-Vila B, et al. 2017. *Comput. Methods Biomech.*

CORRELATIONS BETWEEN PRE-LANDING KNEE KINEMATICS AND LANDING FORCES

Ling Li, Yu Song, Maddy Jenkins, Boyi Dai*
Division of Kinesiology and Health, University of Wyoming, Laramie, WY, USA
Email: bdai@uwyo.edu

Introduction

Anterior cruciate ligament (ACL) injuries often occur when athletes perform jump-landing and cutting tasks [1]. Landing with great peak vertical and posterior forces at a small knee flexion angle may increase ACL loading. Compared to double-landings, single-leg landings result in more risky knee movement patterns due to the greater external loading and limited leg strength [2]. Females also have higher ACL injury rates compared to males in most sports events [3]. Most ACL injuries occurred within 50 ms after initial ground contact [1], while peak ACL strain could occur approximately 55 milliseconds (ms) before initial ground contact during non-injury landing tasks [4]. As the timing of ACL injuries after landing is shorter than simple reaction time (>100 ms), ACL injuries are not likely the result of inappropriate responses after landing but perturbed pre-landing preparation. Therefore, the purpose of the current study was to examine the relationships between pre-landing knee kinematic variables and peak ground reaction forces during landing. The findings might provide information to understand the role of pre-landing kinematics on landing mechanics associated with increased ACL loading.

Methods

Twenty-six male and 26 female recreational athletes were recruited in this study (Females: 20.70 ± 2.09 years, 1.70 ± 0.06 m, 64.05 ± 9.43 kg; Males: 23.22 ± 2.63 years, 1.78 ± 0.05 m, 76.58 ± 8.07 kg). Sixteen retro-reflective markers were attached to participants' body segments [2]. Participants were instructed to jump forward from a 30 cm box placed half of the participant's body height from the force platform and land with either both legs or the dominant leg [2]. Kinematic variables included the minimal knee flexion angle in pre-landing (MKF), timing of minimal knee flexion angles in pre-landing (Timing of MKF), range of motion (ROM), and average knee flexion angular velocities (KFV) between the minimal knee flexion angle and initial ground contact. Knee flexion angles (KF) at initial contact, ROM and KFV within 50 ms after initial contact were extracted. Peak vertical (PVF) and posterior (PPF) ground reaction forces within 50 ms after landing were calculated. Pearson correlation analyses were performed.

Results and Discussion

The ROM and KFV before landing had significant correlations with PPF during the double-leg landing task (Table 1). The MKF, ROM, and KFV before landing also had significant correlations with PPF during the single-leg landing task (Table 2). These results indicated that a greater knee flexion range of motion and a faster knee flexion velocity might represent a more active soft-landing preparation and resulted in decreased peak posterior ground reaction forces that are associated with decreased ACL loading.

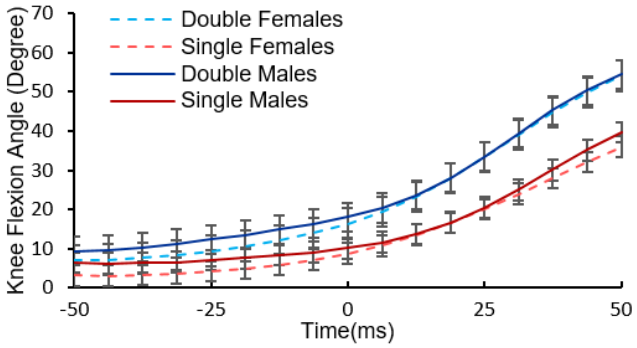

Figure 1. Knee Flexion Angles 50ms before and after Landing

Significance

ACL injuries occurred shortly after landing, highlighting the importance of pre-landing knee motion in affecting peak ACL loading during landing. The current findings support that actively flexing the knee prior to landing could better prepare individuals for a soft landing to decrease impact forces during landing, particularly in the posterior direction.

Acknowledgments

Ling Li's graduate assistantship was provided by the Wyoming INBRE (P20GM103432).

References

[1] Dai et al., 2014. *J Sport Health Sci*, 3(4), 299-306.
[2] Li et al., 2020. *J Biomech*, 109, 109906
[3] Montalvo et al., 2019. *Br J Sports Med*, 53:1003–12
[4] Englander et al., 2019. *Am. J. Sports Med*, 47(13), 3166-3172

Table1. Coefficient of correlation (p values) between kinematic data and ground reaction force during the double-leg landing task

	Prior to Initial Landing				Initial Landing	50 ms after Landing		
	Timing of MKF	MKF	ROM	KFV	KF	ROM	KFV	Timing of PF
PVF	0.22(0.13)	-0.11(0.44)	-0.11(0.42)	**-0.32(0.02)**	-0.17(0.22)	-0.10(0.49)	-0.10(0.49)	-0.31(**0.03**)
PPF	-0.12(0.40)	-0.19(0.17)	**-0.35(0.01)**	**-0.38(0.00)**	**-0.42(0.00)**	-0.25(0.07)	-0.25(0.07)	-0.27(0.05)

Table2. Coefficient of correlation (p values) between kinematic data and ground reaction force during the single-leg landing task

	Prior to Initial Landing				Initial Landing	50 ms after Landing		
	Timing of MKF	MKF	ROM	KFV	KF	ROM	KFV	Timing of PF
PVF	0.20(0.17)	-0.09(0.53)	0.11(0.44)	0.01(0.93)	-0.01(0.95)	-0.00(0.99)	-0.00(0.99)	0.10(0.50)
PPF	-0.24(0.09)	**0.31 (0.02)**	**-0.36(0.02)**	**-0.46(0.000)**	0.04(0.76)	0.12(0.38)	0.12(0.38)	-0.16(0.26)

ENERGY ABSORPTION STRATEGIES IN ADOLESCENT MALES AND FEMALES WITH AND WITHOUT AN ACL INJURY

Christine C. Smith[1*], Nicholas J. Romanchuk[2], Michael J. Del Bel[3], Sasha Carsen[4], Daniel L. Benoit[1-3]
[1]School of Human Kinetics, University of Ottawa, Ottawa, ON, Canada
[2]Ottawa-Carleton Institute for Biomedical Engineering, University of Ottawa, Ottawa, ON, Canada
[3]School of Rehabilitation Sciences, University of Ottawa, Ottawa, ON, Canada
[4]Department of Surgery, Division of Orthopaedic Surgery, University of Ottawa, Ottawa, ON, Canada
email: *christine.smith@uottawa.ca

Introduction

Over the last two decades, there has been an increase in anterior cruciate ligament (ACL) injuries [1]. Specifically, the adolescent population (ages 6-18) has seen a 2.3% increase in injury rate (Beck et al., 2017); furthermore, adolescent females are three to nine times more likely to tear their ACL compared to male counterparts [1]. Considering that approximately ¼ individuals will experience a re-injury [2], new methodologies ought to be developed to improve the current ACL rehabilitation measures. Since energy absorption strategies can provide important insight into functional capacity and movement quality, they should be considered in ACL rehabilitation programs [3]. Therefore, the purpose of this study was to evaluate kinematics and kinetics in the lower extremity joints during a drop-vertical jump (DVJ) task in female and male ACL-injured and control individuals.

Methods

Fifty-four (37 females) ACLi patients, aged 11-18, with confirmed ruptures and 68 (39 females) control participants, aged 10-18, were recruited to participate in this study. All participants performed a DVJ task which consisted of stepping of a raised platform set at the height of their tibial plateau, landing onto the force plates, performing a maximal vertical jump, and again, landing onto the force plates. 3D kinematics were collected using a 10-camera infrared motion analysis system at 200Hz (Vicon, Nexus, Oxford, UK) and ground reaction force data (GRF) was collected simultaneously using two force plates (Bertec Corp., Columbus, USA) sampled at 2000Hz. The DVJ task was normalized from initial contact (GRF > 10N) until maximum knee flexion, only the first landing was evaluated. Statistical Parametric Mapping (SPM) independent t-tests were used to determine differences in the hip, knee, and ankle angles and moments. The Benjamini-Hochberg procedure was completed to determine the effect of any statistically significant values.

Results and Discussion

ACLi females displayed lower knee flexion moments, ankle flexion angles, and ankle flexion moments compared to ACLi males, while female controls show lower ankle flexion moments and higher knee flexion angles compared to male control and ACLi females, respectively (Table 1). Finally, ACLi males displayed lower knee flexion moments compared to male controls. There were no statistically significant differences at the hip joint.

Higher flexion angle values in the knee and ankle during landing from a drop jump may be allowing the lower extremity to absorb the energy in a manner that protects the ACL during the eccentric phase [4], which was not seen in our results. Having the knee and ankle in a more extended position at landing has been suggested as a potential risk for ACL injury, while higher knee flexion, as seen in our female controls, is suggested in ACL prevention programs as a safer landing strategy [5]. The lower knee and ankle flexion moments observed in our injured group may be harmful if it is due to lower muscular activation, which would not allow the lower extremity joints to absorb the energy in a safe and effective manner [5].

Significance

While there are some studies that evaluate energy absorption strategies in relation to ACL injuries in the adult population, this is one of the first to do so in the ACL injured adolescent population. Energetic analysis is comprised of kinematic and kinetic components and provides important insight into functional capacity and movement quality. Furthermore, if we can understand how energy absorption is altered following an ACL injury, we can begin to modify these variables through targeted training to decrease the risk of injury and/or re-injury.

References

[1] Agel et al., 2005. *Am J Sports Med.* 524-530, 33(4)
[2] Wiggins et al., 2016. *Am J Sports Med*. 1861-1876, 44(7)
[3] Norcross et al., 2010. *Clin Biomech*. 1031-1036, 25(10)
[4] Devita et al., 1992. *Med Sci Sports Exerc*. 108-115, 24(1)
[5] Decker et al., 2003. *Clin Biomech*. 662-669, 18(7)

Table 1: Statistically significant results from the statistical non-parametric mapping independent *t*-tests run on the kinematic and kinetic variables; including the Benjamini-Hochberg procedure, correcting for a false discovery rate of 0.05

Task	Comparisons	Variable	Statistical Significance	Benjamini-Hochberg	Corrected Significance
DVJ	FACL / MACL	KFM	0.004	0.0111	FACL < MACL
		AFA	$1*10^{-4}$	0.0055	
		AFM	0.0085	0.0222	
	FCON / MCON	AFM	0.0202	0.0333	FCON < MCON
	FACL / FCON	KFA	0.0064	0.0167	FCON < FACL
	MACL / MCON	KFM	0.0177	0.0278	MCON < MACL

Note: SPM assessments of normality yield multiple time-varying *p*-values, only the smallest *p*-value shown.
Note: FACL: female ACL injured, MACL: male ACL injured, FCON: female control, MCON: male control, KFM: knee flexion moment, AFA: ankle flexion angle, AFM: ankle flexion moment, KFA: knee flexion angle

KNEE JOINT MOMENT CONTRIBUTIONS INCREASE FROM RUNNING TO WALKING AFTER ACLR DURING INCLINE BUT NOT DECLINE LOCOMOTION

Eric B. Finley[1], Hillary H. Holmes[1], Jaimie A. Roper[1]
Auburn University, Auburn, AL
Email: ezf0016@auburn.edu

Introduction

Anterior cruciate ligament reconstruction (ACLR) results in altered knee joint loading during locomotion.[1,2] The knee joint moment is defined as the individual joint torque contributing to the overall summation of the support moment.[2] The sum of the knee joint moment and moment contributions from the hip and ankle define the support moment and are necessary for lower limb support and may provide insight into the development of joint degeneration. Incline and decline locomotion are a part of the real-world environment; therefore, recognizing the impact of incline and decline walking and running on knee joint moment changes is crucial for understanding mechanisms of gait rehabilitation following ACLR. We sought to compare the knee joint moment contributions (JMC) changes during incline and decline walking and running between individuals with ACLR and healthy controls. We expected that individuals with ACLR would have reduced knee JMC between incline and decline walking to running compared to healthy controls.

Methods

Thirty-four individuals volunteered in this study: 17 with an ACLR and 17 age, height, and sex-matched controls [(12 males and 22 females), height (1.7 ± 0.1m), mass (73.0 ± 11.7Kg), age (21 ± 2 years)]. All individuals within the ACLR group had a unilateral tear. Participants walked (1.0m/s) and ran (1.8m/s) at an incline of 4°, incline of 10°, decline of 4°, and decline of 10°. Peak moments during the stance phase were normalized to body mass and averaged for the last ten strides in the involved limb. The knee JMC was expressed as a percentage, calculated as the ratio of the averaged peak moment in the last ten strides at one point to the support moment of that limb (M_k = Peak knee moment/ $\Sigma M_a + M_k + M_h$).[3,4] Change scores were calculated as the difference between knee JMC in walking and running under each condition (Knee $_{\text{change score}} = M_k$ running– M_k walking). A 2x4 analysis of variance was used to investigate the change in knee joint contribution from walking to running in incline and decline running.

Results and Discussion

Change scores for knee JMC from running to walking were significantly different between groups during both incline conditions (incline 4° and incline 10°, ($F(1,32)= 63.9$, $p<.001$, and $F(1,32)= 40.4$, $p<.001$), respectively), but not decline (decline 4° and decline 10°,0 ($F(1,32)= 0.55$, $p = 0.46$, $F(1,32)= 0.04$, $p=0.84$), respectively). The knee JMC change score decreased by 17% (incline 4°) and 39% (incline 10°) for the control group, while the knee JMC score for ACLR group increased by 6% (incline 4°) and 9%(incline 10°) (**Figure 1.**) There was not a significant difference in knee JMC between the ACLR group and controls during decline 4° and decline 10°,0 ($F(1,32)= 0.55$, $p = 0.46$, $F(1,32)= 0.04$, $p=0.84$), respectively.

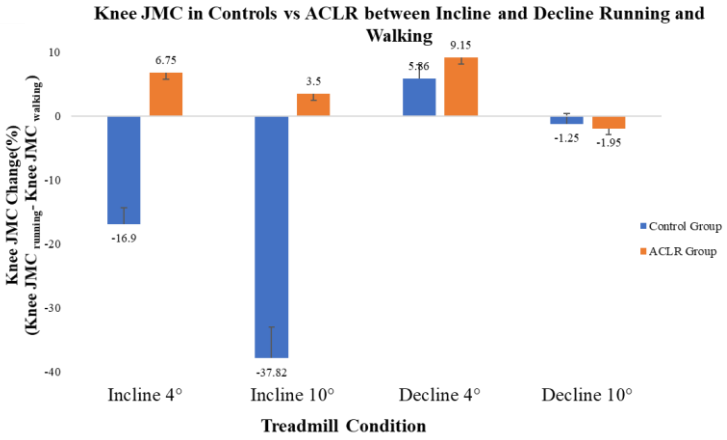

Figure 1. Knee JMC between running and walking for groups expressed as a change score percentage. Knee JMC are lower in the control group and higher in the ACLR group during incline locomotion. *JMC denotes joint moment contribution.

Significance

Our findings provide insight into potential protocols for ACLR rehabilitation that target incline and decline treadmill running and walking for individuals with ACLR. Increased knee JMC during incline locomotion for individuals with ACLR could pre-dispose individuals for re-tear and joint degeneration. To better protect the knee joint after ACLR, rehabilitation measures should consider simulating the decrease in knee JMC observed in healthy controls during incline locomotion. Future research should better understand how incline running and walking along with JMCs from the hip and ankle affect human locomotion post ACLR to enhance rehabilitation protocols and address pre-disposing mechanisms for knee joint pathologies.

Acknowledgments

This study was funded by an Auburn University seed grant. E.B.F. is funded by an Auburn University Presidential Graduate Fellowship.

References

1. Gardinier, Emily S., et al. "Altered loading in the injured knee after A.C.L. rupture." *Journal of Orthopaedic Research* 31.3 (2013): 458-464.
2. Devita, Paul, et al."Gait biomechanics are not normal after anterior cruciate ligament reconstruction and accelerated rehabilitation." *Medicine and science in sports and exercise* 30 (1998): 1481-1488.
3. Winter, D. A. (1980). Overall principle of lower limb support during stance phase of gait. *Journal of biomechanics*, *13*(11), 923-927.
4. Winter, D. A. (1984). Kinematic and kinetic patterns in human gait: variability and compensating effects. *Human movement science*, *3*(1-2), 51-76.

LIMB UNDERLOADING TRANSMITS LESS DYNAMIC TIBIOFEMORAL CONTACT FORCES AFTER ACLR

Amanda E. Munsch[1*], Alyssa Evans-Pickett[2], Hope Davis-Wilson[2,3], Brian Pietrosimone[2], Joshua D. Roth[4], and Jason R. Franz[1]
[1]Joint Dept. of BME, UNC-Chapel Hill and NC State, NC, USA, [2]Exercise and Sport Science, UNC Chapel Hill, NC, USA, [3]Physical Medicine and Rehabilitation, CU Anschutz Medical Campus, CO, USA, [4]Dept. of Orthopedics, UW-Madison, Madison, WI, USA
email: *aemunsch@live.unc.edu

Introduction

Changes in limb and joint loading after anterior cruciate ligament reconstruction (ACLR) may contribute to the development of post-traumatic osteoarthritis by altering the magnitude of force applied to the cartilage during each step. Individuals with ACLR often walk with a less dynamic vertical ground reaction force (vGRF), exemplified by a reduced first peak vGRF, elevated midstance vGRF, and reduced peak knee extensor moment (pKEM) compared to uninjured controls [1]. In contrast, higher first peak vGRF has been shown to associate with better biochemical cartilage health measures and greater pKEMs associate with thicker cartilage [2,3]. This alludes to vGRF as a modifiable target with potential to mitigate the prevalence of osteoarthritis in individuals with ACLR. In fact, our group recently demonstrated that increasing peak vGRF resulted in decreased biomarkers of cartilage breakdown immediately following a 20m walking protocol [4]. The mechanism by which altering limb loading affects the biological cartilage response to walking remains unclear. We posit that less dynamic limb loading (i.e., vGRF) may yield less dynamic cartilage loading (i.e., contact forces), which may in turn limit nutrient and waste exchange necessary for preserving cartilage health. Our purpose was to evaluate the effects of first peak vGRF biofeedback on tibiofemoral contact forces relevant to the development of post-traumatic osteoarthritis in individuals with ACLR. We hypothesized that reduced first peak vGRF would produce less dynamic limb-, joint- and tissue-level loading, evidenced by smaller vGRF, pKEM, and contact force values in early stance and larger vGRF and contact force values at midstance.

Methods

23 ACLR participants (12F, mean±SD: age: 20.6±3.8, BMI: 24.7±3.3, mos. since surgery: 8.6±2.6) walked at their preferred speed (1.26±0.1 m/s) on an instrumented treadmill while we recorded bilateral GRFs and pelvis and lower extremity marker trajectories. From a 5-minute walk in Session 1, first peak vGRF values were averaged to obtain target values of ±5% usual walking values. Modified vGRF loading conditions (underloading: -5%, control loading, overloading: +5%) lasting 3,000 steps at preferred speed were then presented in random order (Sessions 2-4). In overloading and underloading sessions, visual biofeedback presented participants' real-time bilateral first peak vGRF as the height of two vertical bars and their target value (Fig. 1A). Participants did not receive biofeedback during the control trial. We identified the ACLR leg stride with the first peak vGRF that best matched the target value (biofeedback conditions) or average first peak vGRF values from Session 1 (control condition). Those data drove musculoskeletal simulations via the Concurrent Optimization of Muscle Activations and Kinematics (COMAK) framework in OpenSim [5]. Knee joint angles, moments, and tibiofemoral joint contact forces were estimated using the scaled Lenhart 2015 model with generic ligament properties and assessed using one-way rmANOVAs (α=0.05).

Results and Discussion

Compared to normal walking, first peak vGRF increased and decreased during the overloading and underloading conditions, respectively (all $p<0.001$). This elicited less dynamic limb loading; midstance vGRF *decreased* by 8% for overloading and *increased* by 7% for underloading (all $p<0.001$, Fig 1B). pKEM subsequently increased by 85% (overloading) and decreased by 60% (underloading) (all $p<0.001$). Control and overloading conditions produced two distinct contact force peaks during stance on both tibial plateaus (Fig. 1C). However, the underloading condition did not produce a distinct medial contact force peak during early stance – a hallmark of less dynamic loading at the tissue level. Indeed, compared to control loading, underloading elicited 16% smaller medial contact force during early stance ($p<0.001$) and 14% higher medial contact force during midstance ($p=0.022$) (Fig. 1C). However, we found no loading condition effects on contact force impulse and thus cumulative load for either tibial plateau ($p\geq0.136$).

Significance

Limb-level underloading observed in individuals with ACLR may contribute to heightened risk of osteoarthritis development by transmitting less dynamic loads to tibiofemoral articular cartilage. Less dynamic stance phase loading may inhibit nutrient and waste exchange necessary for cartilage remodelling.

Acknowledgments

Supported by NIH grants: R21AR074094 and F31AR078013.

References

[1] Davis-Wilson et al., 2020. *MSSE*. 52(4).
[2] Pietrosimone et al., 2016. *Am J Sports Med*. 44:425-432.
[3] Schmitz et al., 2015. *J Athl Train*. 52(6).
[4] Luc-Harkey et al., 2020. *J Athl Train*. 55(10).
[5] Smith et al., 2016. *J Knee Surg*. (29)2.

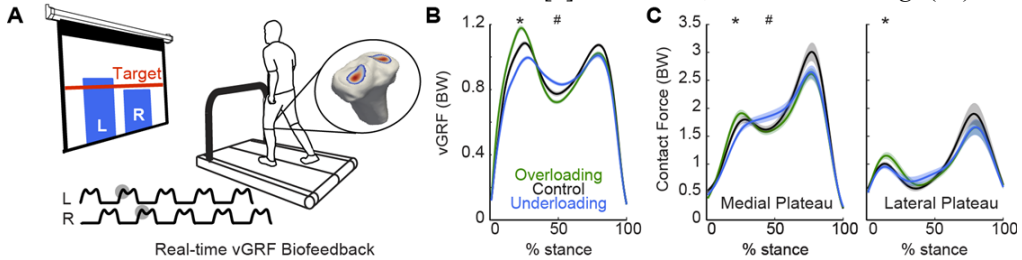

Figure 1. (A) Biofeedback cued participants to walk with ±5% change in vGRF **(B)** vGRF. **(C)** Medial and lateral vertical tibiofemoral contact forces. Main effects of condition during early stance (*) and midstance (#).

DECREASES IN BONE MINERAL DENSITY ARE RELATED TO GAIT ASYMMETRIES FOLLOWING ACL RECONSTRUCTION

Meredith K. Owen[*1], Kelsey A. Reeves[1], Cale Jacobs[2], Darren L. Johnson[2], Chris S. Fry[3], and Brian Noehren[1,2]
[1]Department of Physical Therapy, University of Kentucky, Lexington, KY
[2] Department of Orthopaedics and Sports Medicine, University of Kentucky, Lexington, KY
[3]Department of Athletic Training and Clinical Nutrition, University of Kentucky, Lexington, KY
email: [*]mow229@uky.edu

Introduction

Anterior cruciate ligament (ACL) tears and subsequent reconstructions are common among athletic populations and result in a cascade of negative changes in gait mechanics, including decreased knee extensor moments and decreased ground reactions forces on the affected limb [1]. Additionally, several reports indicate that the bone mineral density (BMD) of the involved lower extremity is reduced following ACL reconstruction [2,3]. While gait and BMD changes have been reported independently, the relationships between these key metrics have yet to be well defined. Potentially, reduced loading on the involved limb as compared to the uninvolved limb may contribute to reductions in BMD. Therefore, we hypothesized that there would be associations between changes in BMD and the limb symmetry index (LSI) of the knee joint moment, knee flexion angle, and vertical ground reaction force (vGRF) following an ACL-reconstruction.

Methods

10 individuals (9 female, age = 18.9 ± 4.2, height = 1.6 ± 0.1 m, weight = 66.3 ± 8.7 kg) who underwent ACL reconstruction had BMD scans before surgery. Participants were rescanned six months following surgery at which time gait biomechanics were recorded during walking.

BMD was measured using dual-energy X-ray absorptiometry. A region of interest (ROI) at the distal femur was defined following protocols established by Bakkum et al. and consists of 0-10% of the distal femur [4].

Sagittal plan knee joint kinematics, kinetics, and vGRF were measured 6 months after surgery using instrumented motion analysis. Fifty-two reflective markers were placed at specific anatomical and tracking locations. A standing static calibration was recorded first and then participants walked at a self-selected speed. Kinematic and kinetic data were collected at 200 and 2000 Hz, respectively. Kinematic data were filtered using a 4th order Butterworth filter at 8 Hz. Joint moments and angles were determined. Limb symmetry indices, as determined by dividing the value for the affected limb by the unaffected limb, were calculated for each variable. Pearson's product moment correlations were calculated for all variables. Significance was set a 0.05.

Results and Discussion

Average values for all variables at the 6-month post-reconstruction timepoint are reported in Table 1. Change in BMD (BMD loss) is calculated as the difference between the pre-surgery measure and 6-month measure ($BMD_{pre\text{-}surg}$ - BMD_{6mo}).

BMD loss and GRF LSI were found to be strongly correlated (r = -0.62, p = 0.03), as were BMD loss and knee moment LSI (r = - 0.57, p = 0.04). Change in BMD and knee flexion angle were moderately but not significantly correlated (r = -0.51, p = 0.07).

Table 1: Average values for all variables of interest

Variable	Average
BMD loss (g/cm^2)	0.30 (0.11)
GRF LSI	0.97 (0.05)
Knee Extensor Moment LSI	0.70 (0.49)
Knee Flexion Angle LSI	1.06 (0.44)

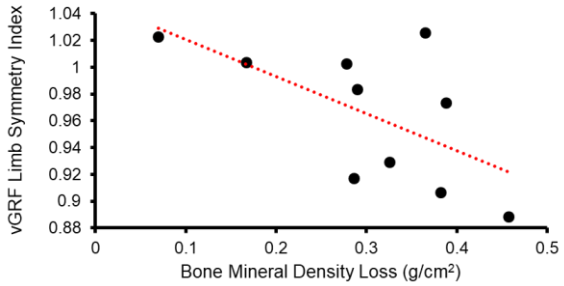

Figure 1: Relationship between bone mineral density loss and the limb symmetry index for the vertical ground reaction force during walking.

BMD loss in the affected limb 6 months after ACL-reconstruction is strongly correlated to measures of limb asymmetries during walking gait. Limb asymmetries appear to be highly sensitive to changes in BMD, where even a modest 10% reduction in GRF symmetry was associated with large losses of BMD.

Significance

Up to 50% of individuals will develop post-traumatic osteoarthritis secondary to an ACL reconstruction. Understanding and addressing areas associated with this increased risk are crucial for informing treatment methods. Changes in BMD have been linked to the progression of osteoarthritis [5] and are often the result of decreased loading and/or inactivity [6]. The results of the present study indicate that as gait mechanics normalize between limbs, there is less of a reduction in BMD. Potentially, targeting improved limb gait symmetry may help reduce losses in BMD. Future work will seek to expand these preliminary findings to a larger data set and evaluate additional factors that could be associated with the loss of BMD after surgery.

Acknowledgments

The project described was supported by the National Institutes of Arthritis and Musculoskeletal and Skin Disease (NIAMS) through grant R01 AR072061.

References

[1] Slater et al., 2017. *J Athl Train.* 52:847-860.
[2] van Meer et al., 2013. *Osteoarthr.* 22:154-161.
[3] Reiman et al., 2006. *JOSPT.* 36:837-844.
[4] Bakkum et al., 2014. *Med Eng & Phys.* 36:387-390.
[5] Goldring, S., 2008. *Rheum Dis Clin.* 34:561-571
[6] Järvinen et al., 1997. *J Bone Joint Surg Am.* 79:263-2

EVALUATING DIFFERENCES IN THE CONTRIBUTION OF EACH LOWER LIMB DURING THE DROP VERTICAL JUMP IS CRUCIAL IN FEMALE ACL INJURED PEDIATRIC POPULATION

Joana F. Hornestam[1,2], Blake S. Miller[3], Sasha Carsen[1], Daniel L. Benoit[2,3*]
[1]Children's Hospital of Eastern Ontario, 401 Smyth Road, Ottawa, ON K1H 8L1, Canada
[2]School of Rehabilitation Sciences, University of Ottawa, 451 Smyth Road, Ottawa, ON K1H 8M5, Canada
[3] School of Human Kinetics, University of Ottawa, 125 University, Ottawa, ON K1N 6N5, Canada
email: *dbenoit@uottawa.ca

Introduction

Anterior cruciate ligament (ACL) injury and re-injury rates are high in adolescents and even more frequent in females[1]. Decisions on clearance for return-to-play and rehabilitation progression typically requires performance assessment during functional tests. Vertical jump performance and muscle strength tests are common tools used by clinicians to make these decisions[2]. However, it is still not clear how vertical jump measurements should be analyzed and interpreted in an ACL injured adolescent age group.

The aim of this study was to evaluate differences in drop vertical jump heights in female adolescents with an ACL injury, as well as healthy controls, and to investigate differences in the contribution of each lower limb to this performance.

Methods

Thirty-two female adolescents with ACL injury (ACLi, 15.2 ± 1.5 yrs, 164.0 ± 6.5 cm, 63.7 kg) and thirty-eight uninjured (CON, 13.2 ± 1.7 yrs, 161.7 ± 8.1 cm, 50.6 kg) participated in this study. Pelvis, thigh, and shank motions were recorded using a 10-camera motion analysis system (Vicon, Nexus, Oxford, UK), while the participants performed double-legged drop vertical jumps (DVJ) on two force plates (Bertec Corp., Columbus, USA) for 3 trials.

The raw jump height (i.e., non-normalised distance between the maximum pelvic vertical position to its average vertical position in the static trial) and the jump height normalized to dominant leg length were compared between groups, using an independent samples t-test. The maximum knee extension velocity and vertical ground reaction force (GRFz) before take-off were compared between limbs (i.e., injured vs. contralateral limb in the ACLi and dominant vs. non-dominant limb in the CON), using a paired samples t-test. The mean differences (MD) and 95% confidence interval ($CI_{95\%}$) were also reported.

Results and Discussion

There was no difference in the raw jump height between ACLi and CON groups (MD = 3.22cm, $CI_{95\%}$ = -0.17, 6.62). However, the normalized jump height was lower in the ACLi, than CON (MD = 0.05cm, $CI_{95\%}$ = 0.01, 0.08) (Table 1).

Table 1. Participant jump heights

	ACLi	CON	*p*
Raw Jump Height (cm)	28.36 ± 8.60	31.58 ± 5.54	0.063
Normalized Jump Height	0.32 ± 0.09	0.37 ± 0.06	0.020*

Results are reported as mean and standard deviation. ACLi: ACL injured group. CON: uninjured group. *p*: *p*-values. *$p < 0.050$.

In the ACLi, the GRFz (MD = 42.89N, $CI_{95\%}$ = 23.22, 62.57) the maximum knee extension velocity (MD = 92.13°/s, $CI_{95\%}$ = 64.44, 119.83) was greater in the contralateral limb, compared to the injured limb. No differences were observed in the CON for these two variables (MD = 11.74, $CI_{95\%}$ = -3.27, 26.74 and MD = 7.65, $CI_{95\%}$ = -10.567, 25.86, respectively) (Table 2).

Table 2. Participant jump mechanics (cm)

		Limb 1	Limb 2	*p*
GRFz (N)	ACLi	632.41 ± 103.80	675.30 ± 96.14	<0.001*
	CON	533.47 ± 115.54	545.20 ± 116.30	0.122
Max. Knee Extension Velocity (°/s)	ACLi	718.47 ± 137.61	810.61 ± 130.47	<0.001*
	CON	789.30 ± 164.46	796.94 ± 161.81	0.400

Results are reported as mean and standard deviation. Limb 1: ACLi injured limb and CON non-dominant limb. Limb 2: ACLi contralateral (healthy) limb and CON dominant limb. *p*: *p*-values. *$p < 0.001$.

The findings of this study show that the raw jump height measurement does not differentiate ACL injured female adolescents from uninjured. However, when normalized to leg length, the jump height was approximately 12% lower in the ACLi than in the CON, indicating the importance of this normalization[3] in these populations. Nevertheless, limiting vertical jump assessments only to jump heights does not highlight the differences in the contribution between limbs. In the ACLi, the contralateral limb had greater knee extension velocity and GRFz, by 13% and 7% respectively, compared to the injured limb. This higher contribution, or shielding, of the contralateral limb to drop vertical jump height may lead to joint overloads and increase risk of injury to the contralateral limb[4].

Significance

Clinicians assessing ACL injured female adolescents using the DVJ should (i) normalize jump height to the dominant leg length and (ii) evaluate differences in mechanical contributions between lower limbs since ACL injured females use more of their non-injured limb to jump, than their injured limb. This approach would help identify limb asymmetries, improve rehabilitation procedures, and potentially help prevent re-injuries in female ACL paediatric population.

Acknowledgments

We would like to acknowledge Michael Del Bel, Joanna Geck, and Chrissy Smith for their assistance in data processing.

References

1. Werner et al., 2016. *J Pediatr. Orthop. 36*: 447–452.
2. Laudner et al., 2015. *IJSPT*. 10(3): 272-280.
3. Rojas-Reyes et al., 2020. 38th ISBS Conference. 328-332.
4. Webster & Hewett, 2019. *Sports Medicine.* 49: 917–929.

PREDICTING PERSISTENT CHEMOTHERAPY-INDUCED NEUROMOTOR DYSFUNCTION

Lise Worthen-Chaudhari^[1], Patrick Schnell^[2], Ajit MW Chaudhari[3], Scott M Monfort[4], Maryam B Lustberg[5]
[1]Department of Physical Medicine & Rehabilitation, [2]Center for Biostatistics, [3]School of Health and Rehabilitation Sciences, The Ohio State University, Columbus, OH, [4]Department of Mechanical and Industrial Engineering, Montana State University, Bozeman, MT, [5]School of Medicine, Yale University, New Haven, CT
^Co-first authors email: lise.worthen-chaudhari@osumc.edu

Introduction

Neurotoxic chemotherapy drugs extend life for many cancer survivors, however, these agents also induce sensorimotor neuropathy for up to 80% of breast cancer survivors for whom they are prescribed (Jung et al. 2005). Effects of chemotherapy-induced neuropathy include pain, impaired gait and balance, increased fall risk, and reduced quality of life. While oncologists may consider reducing the dose of chemotherapy agent administered once symptoms are self-reported by the client, treatment planning would likely benefit from prognostic and objective criteria.

We sought to assess postural control as such a prognostic indicator. Specifically, we evaluated whether postural control responses obtained just prior to chemotherapy infusion could identify those individuals who would present with persistent neuromotor dysfunction 1-3 months post-chemotherapy. We hypothesized that persistent balance dysfunction would be predictable based on center-of-pressure (COP) data collected immediately prior to each dose infusion.

Methods

This secondary analysis of postural control data drew from two previously published studies among (a) individuals with breast cancer (stages I–III) who were initiating taxane-based treatment (Monfort et al. 2016) and (b) individuals who were middle-aged and healthy (Worthen-Chaudhari et al., 2018).

Survivor data: Twenty-five individuals received 4 cycles of chemotherapy at an equivalent dosage and returned 1-3 months post-treatment for follow-up (FU) testing (Monfort et al., 2016). Postural control was measured immediately prior to each chemotherapy cycle (timepoint 1-4) and at FU (timepoint 5) using a 30 second task of quiet standing with eyes closed (QEC).

Normative control data: Worthen-Chaudhari et al., 2018 estimated the typical distributions of balance function and measurements for relevant postural control These values represent the manifold of balance behavior that we can expect to see demonstrated by an unimpaired neurosensorimotor system. We then assessed COP data collected from survivors, comparing their values to the control manifold of behavior in terms of a) absolute value and b) change from pre-chemotherapy values.

Outcome measures: COP 95% ellipse area (COPa), COP variability in the frontal plane (RMSml); COP velocity in the frontal plane (COPvml).

Analysis: We defined *dysfunction* as either (a) *deficits* at any single timepoint as center-of-pressure (COP) values below the 5th percentile of the normal population or (b) *decrements* relative to pre-chemotherapy function. Using receiver operator characteristic (ROC) analysis, we evaluated performance of balance deficits and/or decrements in predicting balance dysfunction at FU.

Results and Discussion

Balance dysfunction (> 95% prediction interval (PI) of normative data) persisted at FU for 15 out of 25 (60%) of survivors evaluated (95% CI 39–79%). Using a threshold of 1.480 within-subject standard deviations (SD) above normative mean, in biomechanical measures (COPa, RMSml, COPvml) collected before each chemotherapy infusion, we were able to predict treatment-induced balance dysfunction at FU, some after a single chemotherapy dose, with 87% sensitivity and 70% specificity (Figure 1).

Significance

We demonstrate a novel, prognostic, quantitative approach to identify clients who are at risk of developing persistent neurologic deficits due to cancer treatment. Approaches like this, that combine biomechanical quantification with predictive analytics, stand to improve treatment planning and survivorship outcomes by identifying those who might benefit from dose reduction and early intervention for neurologic sequela of cancer treatment.

Acknowledgments

This research was supported by grants from the NIH and NSF including 1R21AG068831; R03CA182165-01; DGE-1343012.

References

B.F. Jung, D. Herrmann, J. Griggs, A.L. Oaklander, R.H. Dworkin, Neuropathic pain associated with non-surgical treatment of breast cancer, PAIN. 118 (2005) 10.

Monfort, S. M., Pan, X., Patrick, R., Singaravelu, J., Loprinzi, C. L., Lustberg, M. B., & Chaudhari, A. M. (2016). Natural history of postural instability in breast cancer patients treated with taxane-based chemotherapy: a pilot study. *Gait & posture*, *48*, 237-242.

Worthen-Chaudhari, L. C., Monfort, S. M., Bland, C., Pan, X., & Chaudhari, A. M. (2018). Characterizing within-subject variability in quantified measures of balance control: A cohort study. *Gait & posture*, *64*, 141-146.

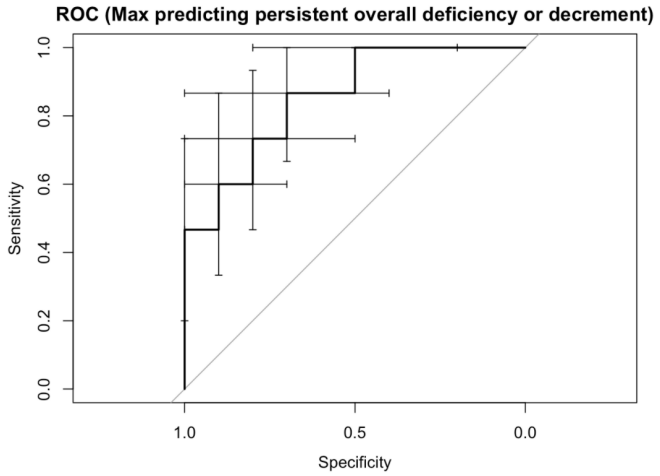

Figure 1: ROC analysis results predicting persistent, treatment-induced balance dysfunction among survivors receiving neurotoxic chemotherapy.

Identifying predictive variables for levels of Brain Trauma in Youth Ice Hockey

Thomas Hoshizaki*, Andrew M. Post[2,3], Clara Karton[2], Michael Robidoux[2], Blaine Hoshizaki[2] and Michael Gilchrist[3]
[1]Injury Biomechanics and Aging Laboratory, University of Waterloo, ON, Canada
[2]Neurotrauma Impact Science Laboratory, University of Ottawa, ON, Canada
[3]School of Mechanical and Materials Engineering, University College Dublin, Republic of Ireland
email: tbhoshiz@uwaterloo.ca

Introduction

Brain trauma is a concern in youth ice hockey due to its potential short and long term negative effects on brain health. Improved helmets are one method of reducing the magnitude of brain strains from impacts to the head in youth ice hockey. However current standards use adult impact parameters with linear acceleration as the performance metric; a metric with low correlations to strains in the brain tissue linked to concussion and repetitive brain trauma. As a result, current youth helmets are not tested to youth parameters of mass, velocity, and compliance, and use test metrics that are not associated with brain trauma. To improve helmets for youth ice hockey players and to reduce risk of brain trauma, methods must be developed to impact the helmet in ways that commonly occur when they play ice hockey. Also, youth specific test metrics must be developed; metrics that have a high association with strain in the brain tissues for youth players. Peak, duration, time to peak, slope to peak and integral of head impact acceleration curves as well as Gadd Severity Index (GSI) and Head Injury Criterion (HIC) represent unique dynamic response characteristics associated with brain tissue strain[1]. Understanding the relationship between impact events and these associated dynamic response characteristics for competition level and age provides a guide to improve head trauma management in youth ice hockey. The purpose of this research was to examine the relationship between these curve characteristics for youth ice hockey reconstructions to identify the kinematic variable with the highest association with maximum principal strain (MPS) in the brain tissues for three levels of play: Initiation (U6); Competitive, non-contact (U8, U10, U12); and Competitive contact (U15, U18).

Methods

Video analysis: Ice hockey game videos were analyzed for head contact events such as head-to-head, head-to-shoulder, head-to-elbow, head-to-hand/punch, head-to-ice, head-to-glass, head-to-boards, and other. The head contacts were also categorized by impact location, and velocity was determined through Kinovea analysis (Kinovea 0.8.20, 2016). Thirty games of each level were analyzed and separated into 3 groups: initiation (U6) competitive non-contact (U8, U10, U12), and competitive contact (U15, U18).

Laboratory reconstruction: All head impact events (except for "other") were reconstructed in the laboratory. Head impacts were reconstructed using an appropriately sized helmeted Hybrid III headform (6yo, 5th, or 50th) depending on age group. The headforms were equipped with accelerometers in a 3-2-2-2 array for the three-dimensional measurement of kinematics for each impact event at 20 kHz using a DTS collection module and filtered using a CFC 180 filter. The helmet used was of similar model to those used by the youth ice hockey players, which had a VN impact liner and cage. The collision events (elbow, shoulder, punch, and head-to-head) used a pendulum or linear impactor system with an appropriate surrogate striker to reflect the compliance of the event. The events where the youth player impacted an immobile object (head-to-ice, boards, glass) used a monorail drop rig with an ice, boards, or glass anvil. The impacts produced the linear and rotational acceleration time histories that were used as input for finite element (FE) modelling of the human brain to determine the MPS. A 6 year old FE model was used for the Initiation group [2], with a scaled down version of the University College Dublin Brain Trauma Model[3] used for the other groups. The MPS results were classified into the following levels of brain trauma: Very low (<0.08), Low (0.08-0.169), Medium (0.17-0.259), High (0.26-0.349), and Very High (>0.35). These categories were based upon research in injury biomechanics that identified relationships between physiological brain responses to axonal stretch and reported concussion, sub-concussion, and clinical outcomes[1].

A linear regression analysis was used to establish the relationship between the dynamic response characteristics of the head impacts with brain tissue strain within each brain trauma category.

Results and Discussion

Competitive, non-contact

Strain category	Event type (sample size)	Variable with highest R^2	R^2
Very low (0-8%)	Ice (3)	GSI	1.00
	Boards (21)	Peak resultant rotational acceleration	0.708
	Glass (8)	Peak y-axis rotation	0.501
	Elbow (41)	Velocity	0.776
	Head (18)	Peak resultant rotational acceleration	0.856
Low (8-16%)	Ice (7)	Peak resultant rotational acceleration	0.745
	Boards (11)	Peak resultant rotational acceleration	0.617
	Shoulder (18)	Peak z-axis linear acceleration	0.556
	Head (6)	Duration x-axis linear	0.988
Medium (16-26%)	Boards (4)	HIC	0.971

Competitive, contact

Strain category	Event type (sample size)	Variable with highest R^2	R^2
Low (8-16%)	Ice (6)	Peak resultant rotational acceleration	0.874
	Boards (8)	Velocity	0.564
	Glass (12)	Peak resultant rotational acceleration	0.383
	Shoulder (13)	Peak y-axis rotational acceleration	0.415
	Elbow (9)	y-axis linear acceleration duration	0.633
	Head (9)	Resulant rotational acceleration duration	0.602
Medium (16-26%)	Boards (4)	Velocity	0.986
	Elbow (4)	Peak x-axis linear acceleration	0.921

Figure 1: Linear regression results for the competitive, non-contact and competitive, contact categories.

Rotational acceleration metrics had the highest association with MPS for each category examined in this research (Figure 1). The relationship between kinematic variables varied by strain magnitude level as well as event type, suggesting that efforts to develop a test metric for the evaluation of youth ice hockey helmets need to be specific to brain trauma mechanisms. This data demonstrates that the impact data within each age category is unique, and as a result suggests that helmet technologies specific to competitive level needs to be developed.

Significance

This research indicates that metrics to evaluate the protective capacity of youth ice hockey helmets must be focused on rotational characteristics as well as age and competitive level.

Acknowledgments

This research was supported by NSERC and CCM Hockey.

References

[1] Post et al., 2012. *J Sport Eng Tech*. 226(P3-4).
[2] Koncan et al., 2019. J Sport Eng Tech. 233(2), 277-291.
[3] Horgan et al., 2004. IJCrashworthiness. 9(4), 401-418.

THE EFFECTS OF AGING AND ROBOTIC FEEDBACK ON DYNAMIC BALANCE TRAINING BIOMECHANICS

Ava D. Segal[1*], Peter G. Adamczyk[2], Andrew J. Petruska[1], and Anne K. Silverman[1]
[1] Dept. Mech. Engr., Colorado School of Mines, Golden, CO, USA; [2]Dept. Mech. Engr., University of WI, Madison, WI, USA
email: *asegal@mines.edu

Introduction

Targeted balance training can mitigate the pervasive balance decline with aging [1]. However, effective therapy programs rely on long-term adherence, which remains challenging [2]. Gamifying balance therapy with goal-directed feedback can increase training adherence, leading to functional balance improvements [3]. Further, larger improvements in balance control may be realized through customized training programs tailored to balance skill. However, personalized training currently relies on a therapist's intuition to adjust the challenge level due to a lack of direct performance measures during training [4]. Therefore, the purpose of this study was to quantify the underlying biomechanics of older and younger adults during dynamic balance training with and without robotic feedback, which can provide insights to guide targeted balance therapy.

Methods

Eight healthy younger adults (25.6±7.8 yrs, 5M/3F) and six healthy older adults (68.2±4.6 yrs, 3M/3F) provided informed consent to participate in this IRB-approved study. Participants performed balance trials barefoot on a wobble board with medial borders of the feet touching, both with and without robotic feedback. A full-body marker set consisting of seventy 14-mm reflective markers were tracked with a seven-camera motion capture system (200 Hz, Qualisys, **Fig 1A**). Four markers were also placed on the wobble board. Bilateral muscle activations of the tibialis anterior (TA) and vastus lateralis (VAS) were collected using wireless surface electromyography (EMG) sensors (2000 Hz, Delsys). An IMU-based motion controller (**Fig 1B)** was secured to the wobble board. Euler angles from the IMU (pitch/roll) were calculated, transmitted wirelessly (~45 Hz) and mapped to velocity (linear/angular) for robot control (**Fig 1C**).

In the no feedback condition, participants tilted the wobble board forward/backward and side-to-side in a controlled manner avoiding touching the board's edge to the floor. Two repeated 40-s trials were collected in each direction. Participants then performed two minutes of structured practice driving the car with board tilting motion. Next, they navigated the robot through a figure-eight maze for three repeated one-minute trials. Trajectories were lowpass filtered (cutoff=6 Hz, bidirectional 4th-order Butterworth) and used to compute kinematic metrics (Visual3D, **Fig 1D**). For each trial, path length was calculated as the summed Euclidean x-y distance between successive samples across 30-s for the wobble board, ankle and knee angles and body center of mass (COM) position. EMG signals were bandpass filtered (20-500 Hz), full-wave rectified, and lowpass filtered (cutoff=6 Hz).

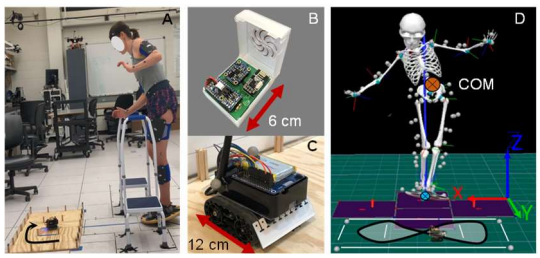

Figure 1: (A) Experimental setup (B) IMU-based motion controller (C) Robotic car platform D) Full-body modeling and figure-eight maze.

These linear envelopes were normalized at each time-step by the linear envelope mean peaks (3 reps) of functional tasks that isolate each muscle: (1) VAS: 90-deg squat, (2) TA: single leg lateral posterior reach (stance leg). Total normalized muscle activity (iEMG) was calculated by integrating the normalized linear envelope across a 30-s time window. Linear mixed-effects models tested for metric differences (p<0.05), with age and feedback as fixed effects and participant slopes and intercepts as random effects. (R, 4.1.2).

Results and Discussion

Older and younger participants performed more whole-body COM motion training without feedback compared to robotic feedback (p<0.05, **Fig 2**), possibly due to faster, less controlled movements. This pattern persisted for the older participant wobble board angles (p<0.05) and approached significance for the knee angles (0.05<p<0.09*)*. The older participants' TA muscles were also more active compared to the younger participants ($p\leq$0.01) with a similar trend for the VAS muscles, perhaps due to antagonist co-activations to compensate for age-related neuromuscular deficits [5]. Higher muscle activity persisted during robotic feedback training for the older participants yet did not produce greater motion compared to the younger participants. These findings suggest robotic feedback requires more precise movements, which is likely more challenging for older adults.

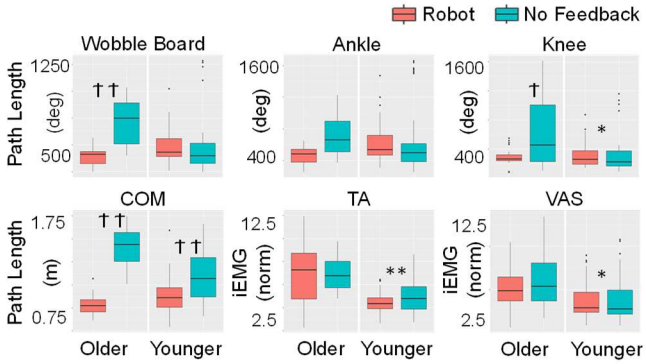

Figure 2: Age (*) and feedback (†*)* effects for total path length and muscle activity (iEMG) across 30-s balance trials. Double symbols: (p<0.05), Single symbol (0.05<$p\leq$0.1).

Significance

Feedback can affect training performance and has potential to provide more effective, engaging, and individualized therapy programs. Biomechanical evaluation during training can identify mobile balance performance metrics (e.g., wobble board dynamics) for monitoring at-home training progress.

Acknowledgments

NSF GRFP (Grant No. DGE-1646713) funded this research.

References

[1] Sherrington, C., et al, 2008. *J Am Geriatr Soc*. 56(12): 2234-43.
[2] Schneider, J.K. et al., 2003. *J Gerontol Nurs*. 29(9): 21-31.
[3] Kosse, N.M. et al., 2011. *J Cyber Ther Rehabil*. 4(3): 399-407.
[4] Van Diest, M. et al., 2013. *J Neuroeng Rehabil*. 10(1): 101.
[5] Mixco et al., 2012. J Motor Behavior. 44(1): 1-11.

FRONTAL PLANE ANKLE STIFFNESS INCREASES WITH LOAD INDEPENDENT OF MUSCLE ACTIVATION

Zoe Villamar[1,2*], Eric J. Perreault[1,2,3], Daniel Ludvig[1,2]
[1]Department of Biomedical Engineering, Northwestern University, Evanston, IL
[2]Shirley Ryan AbilityLab, Chicago IL, [3]Department of Physical Medicine and Rehabilitation, Northwestern University, Chicago, IL
email: *zoevillamar2018@u.northwestern.edu

Introduction

Ankle sprains are the most common musculoskeletal injury, typically resulting from excess inversion of the ankle. One way to reduce the probability of sprains would be to increase the stiffness of the ankle in the frontal plane [1]. Recent studies from our group have shown that frontal plane stiffness increases with the bodyweight loading that occurs during standing [2]. However, this study did not control for the separate effects of axially loading the joint and activation of the muscles that surround the ankle, a phenomenon that is known to increase ankle stiffness [3]. The objective of this study was to determine whether axial loading in the absence of muscle activation would increase the frontal plane stiffness of the ankle. We hypothesized that ankle stiffness would increase with an increase in axial load, while muscle activity would remain constant. If axial loading does increase stiffness independent of muscle activity, this would demonstrate that load-dependent passive structures play a role in stabilizing the ankle, and that alterations or damage to these structures may lead individuals to be more susceptible to ankle sprains.

Methods

Fifteen individuals (8 males) participated in this study. All had no known neurological or connective tissue disorder, and no ankle impairments. Subjects were seated with their ankle fixed to a rotary motor via a fiberglass cast (**Fig. 1A**). Knee and ankle angle were at 90 degrees of flexion. The desired load was set by applying pressure to the knee. Electromyographic (EMG) data were collected from the tibialis anterior (TA), lateral gastrocnemius (LG), medial gastrocnemius (MG), soleus (SOL), peroneus longus (PL), and peroneus brevis (PB) to assess any load-dependent changes in muscle activity. Small rotational perturbations were applied to the ankle in the frontal plane to estimate stiffness. We characterized the ankle's impedance, the dynamic relationship between an imposed movement and the resultant resistive torque, by computing a non-parametric impulse response function (IRF) between the measured ankle angle and the measured torque in the frontal plane. We then parameterized the impedance IRF to a 2nd order model containing stiffness, viscosity, and inertia.

We used a linear mixed-effects model to test our hypothesis that frontal plane stiffness increased with load. Ankle stiffness was the dependent variable, axial load was an independent continuous factor, sex a fixed factor, and subject a random factor. To check whether muscle activity contributed to changes in stiffness, we computed a separate linear mixed-effects model for each muscle, where EMG was the dependent variable, axial load was a continuous factor, and subject was a random factor.

Results and Discussion

Ankle stiffness increased linearly with the applied load (**Fig. 1B**; $R^2 = 0.96$). This increase occurred with a slope of 0.084 +/- 0.005 [Nm/rad]/[N], ($p < 0.001$). These results imply that the ankle is approximately 3 times stiffer when loaded by 50% of the subject's body weight than when unloaded.

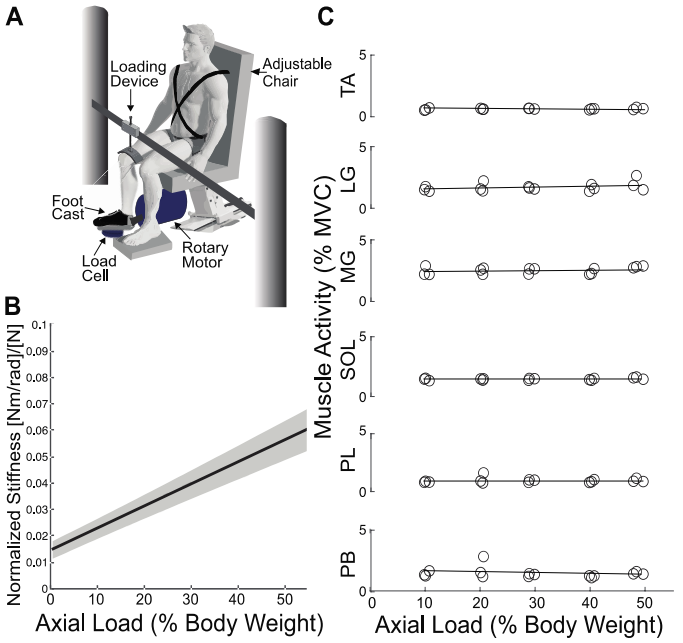

Figure 1: (**A**) Experimental Set-Up (**B**) Ankle stiffness increases with axial load across all subjects. The solid line shows the group average from the linear mixed-effects model, with the shaded area showing the 95% confidence intervals of the fit. (**C**) Mean EMG for each muscle for a representative subject. Lines represent least squares fit to the data.

The increase in ankle stiffness was not due to muscle activity (**Fig. 1C**). Across all subjects, there was little effect of load on muscle activity, with the dependence of EMG on load ranging from -0.018 to 0.034 %MVC/% body weight, with none reaching significance (all $p > 0.10$).

Under axial-loading conditions in cadavers, nearly all the torque resisting imposed frontal plane rotations is due to the articular surfaces [4]. This resistive torque, a similar measure to the stiffness we measured, increases with axial loading [5]. While our results cannot directly point to a mechanism behind the effect of axial load, our results agree with cadaver studies pointing to a greater contribution of the articular surfaces.

Significance

These results demonstrate that axial loading is a significant contributor to maintaining frontal plane ankle stiffness. Any disruption to this mechanism of increasing stiffness could result in an increased probability of ankle sprains.

Acknowledgments

NIH T32 HD07418

References

[1] Hubbard, 2008. *Foot Ankle Int*. 29(3): p. 305-11. [2] Matos et al., 2021. *J Biomech.* 124: 110565. [3] Mirbagheri et al., 2000. *Exp Brain Res.* 135(4): p. 423-36. [4] Stormont et al., 1985. *Am J Sports Med,* 13(5): p. 295-300. [5] Stiehl et al., 1993. *J Orthop Trauma.* 7(1): p. 72-7.

BIOMECHANICAL EFFICACY OF HIP PROTECTORS VARY ACROSS DESIGN, FALL ORIENTATION, BIOLOGICAL SEX AND TROCHANTERIC SOFT TISSUE THICKNESS

Steven P. Pretty*, Rebecca A. Knarr, and Andrew C. Laing
Department of Kinesiology and Health Sciences, University of Waterloo, Waterloo, ON
email: *spretty@uwaterloo.ca

Introduction

Hip fractures are a prevalent and severe health concern in older adults, with sideways falls onto the hip being implicated in most cases [1]. Soft-shell hip protectors represent a promising strategy to reduce the forces applied to the proximal femur and subsequent fracture risk during a fall through a combination of energy absorption and shunting [2]. Continuous protectors directly overly the proximal femur and act to smooth out local stiffness, whereas horseshoe-shaped protectors wrap around the proximal femur and act to form a bridge over the bone. Previous research in young females has found these protectors are more effective among low-BMI individuals, likely due to lower trochanteric soft tissue thickness (TSTT) overlying the proximal femur [2,3]. Improved understanding of factors influencing hip protector efficacy could inform the development of next-generation hip protectors and subject-specific recommendations. The purpose of this study was to compare hip protector efficacy (force magnitude and localization reduction) across design, fall orientation, biological sex, and TSTT. It was hypothesized that: 1) Both continuous and horseshoe-shaped hip protectors will reduce force magnitude and localization. 2) Hip protectors will be more effective among males and low-TSTT participants, as well as during lateral fall orientations, compared to females, high-TSTT participants and upright fall orientations respectively.

Methods

Thirty young adults (14 female) underwent transverse plane ultrasound imaging and were stratified into low-, mid- and high-TSTT groups based on values observed in older adults [4]. Each participant completed a series of six unpadded pelvis-release fall simulations and then repeated these simulations wearing both a continuous and a horseshoe shaped hip protector (18 trials total). Within each pad condition, participants completed three lateral (upper body flat) and three upright (upper body braced) pelvis-releases. In both fall orientations, the pelvis was isolated in a nylon sling and raised 5 cm above the ground before being released by an electromagnet. Participants' lateral left hips impacted a rigid pressure plate (Footscan, RSscan International), sampled at 500 Hz. Peak force was determined through spatial integration of all 4096 sensors (64x64 grid). All subsequent analysis was performed at the time of peak force. Peak pressure magnitude was taken as the highest value recorded in a single sensor and contact area was calculated (number of non-zero sensors * sensor area). Separate mixed model ANOVAs were utilized to assess the effect of fall orientation, sex, TSTT and padding on peak force, peak pressure, and contact area.

Results and Discussion

With respect to hypothesis 1, both the continuous and horseshoe-shaped protectors significantly reduced peak force ($p < 0.01$) and localization (inferred through reductions in peak pressure ($p < 0.01$) and increases in contact area ($p < 0.01$)). These findings support previous work, suggesting soft-shell hip protectors are biomechanically effective, while having higher user compliance than their hard-shell counterparts [2].

These protective effects, however, varied across pad design, fall orientation, biological sex, and TSTT (pad-interaction effect $p < 0.05$). The continuous protector reduced peak force 10.6% and increased contact area 13.2% compared to 3.8% and 28.5% with the horseshoe-shaped protector ($p < 0.01$). The continuous protector was more effective than the horseshoe-shaped protector at reducing peak pressure among low- (70.1% vs 57.0%) and mid-TSTT participants (60.4% vs 44.8%) ($p < 0.01$) but no differences were observed across pad designs in high-TSTT participants (40.0% vs 32.6%) ($p = 0.13$). The current analysis suggests the continuous protector is likely more effective than the horseshoe-shaped protector particularly among lower-TSTT individuals, who represent an elevated fracture risk. Based on our findings related to contact area, future continuous pad designs may benefit from a larger surface area. In addition to our results, protector design should balance end-user comfort/preference with biomechanical efficacy in order to maximize compliance.

In partial support of hypothesis 2, across both pad designs, the force and pressure reductions were greater in males (9.6% and 59.1%) and low-TSTT (11.2% and 59.5%) participants than females (4.7% and 33.3%) and high-TSTT (2.7% and 36.1%) participants, respectively (all $p < 0.05$). Hip protector use also increased contact area among males (36.9%) more than females (8.7%) ($p < 0.01$). Our results suggest that males and low-TSTT individuals would benefit most from hip protector use; however, coupling of the current data with tissue level models is necessary to draw conclusions about absolute fracture risk reduction. High-TSTT females (who had the least protective effects from hip protectors) may differentially benefit from interventions targeting underlying bone strength rather than impact attenuation.

In contrast to hypothesis 2, fall orientation did not influence the peak force or pressure attenuation provided by the hip protectors ($p > 0.10$). Contact area increases during lateral releases (26.9%) were greater than during upright releases (14.9%). These results contrast previous literature suggesting differences in hip protector efficacy across studies could be explained by methodological differences in fall orientation [2,3].

Significance

Our findings have implications to both hip protector design and clinical implementation. Ongoing work will couple the current data with tissue models to gain insights at the fracture risk level.

Acknowledgments

This research was funded by grants from the Natural Sciences and Engineering Research Council of Canada (RGPIN-2015-03636 and 416587), the Canadian Foundation for Innovation (Grant #25351), and the Ontario Ministry of Research and Innovation (Grant #25351 and ER14-10-236).

References

[1] Hayes et al., 1993. *C Tissue Int.* 52:192-8
[2] Laing & Robinovitch, 2008. *Osteo Int.* 19:1067-75
[3] Choi et al., 2010. *Clin Biomech.* 25:63-9
[4] Lafleur et al., 2021. *JAB.* 37:556-64

GENERATION OF TRANSVERSE PLANE LINEAR AND ANGULAR MOMENTA DURING 90 DEGREE TURNS

Mitchell Tillman[1*], Antonia Zaferiou[1]
[1]Stevens Institute of Technology, Hoboken, NJ USA
email: mtillman@stevens.edu

Introduction

Turning while walking comprises up to half of all steps during walking [1], and 90˚ turns are especially common. To accomplish a turn, multiple mechanical objectives must be simultaneously managed at the whole-body level: balance maintenance, and the transverse-plane goals of body center of mass (COM) trajectory redirection and body facing direction reorientation. These are accomplished via linear and angular momenta regulation. If we better understand the role of each leg towards the required changes in momenta during different types of turns, we can better assist people who struggle to balance during turns.

Turn strategy classifications at the whole-turn level or per step typically require a specific number of footfalls. However, the transverse-plane mechanical objectives to rotate and translate the body exist regardless of the stepping strategies used during a turn. The purpose of this study was to examine strategies used during each foot's gait phases to accomplish the transverse-plane mechanical objectives of pre-planned and late-cued 90° turns, regardless of the number or sequence of steps used.

We hypothesized that in pre-planned and late-cued turns, (1) during inside (left) steps the body generates a larger change in transverse-plane angular momentum (Ht) to redirect the body facing direction towards the turn vs. outside (right) steps, and (2) during outside footfalls, a larger change in COM velocity is generated in the new direction of travel vs. the inside foot's steps.

Methods

Ten healthy young adults participated in this study (3 f, 7 m; 25±4.2 yrs; 73.9±14.8 kg; 1.79±0.1 m) after providing informed consent in accordance with the IRB. A 15-segment whole-body kinematic model [2] was constructed using optical motion capture data (200 fps; Optitrack, USA). Participants were instructed to imagine that they were walking in a grocery store in three contexts. Participants performed a set of 10 pre-planned 90˚ and 10 late-cued 90˚ turns to the left. Upon reaching the intersection a visual late cue was provided on an 84" monitor at the end of the perpendicular aisle, indicating whether to turn or not. Transverse-plane angular momentum (Ht) was computed and normalized to dimensionless form [3], as well as horizontal COM velocity in the direction of the turn (equivalent to mass-normalized linear momentum). Positive Ht rotated the body towards the turn while negative velocity translated the COM towards the new direction of travel (**Fig. 1**). Turns began at the heel strike prior to transverse-plane pelvis heading angle increasing three standard deviations above person-specific straight-line gait values (**Fig. 1**, green circle). Turns ended at the first heel strike after pelvis heading angle decreased below that same threshold with respect to the new direction of travel (**Fig. 1**, red circle). A left step is the interval from left to right heel strike, and vice versa. Left double support is the double support phase within a left step, and vice versa. We computed changes in Ht and COM velocity during each foot's double and single stance phases. Within each foot, we averaged these metrics across multiple steps, if multiple steps of that foot occurred. Sign tests compared all stance phases across participants with Bonferroni adjustments for multiple (6) comparisons, bringing α to 0.008.

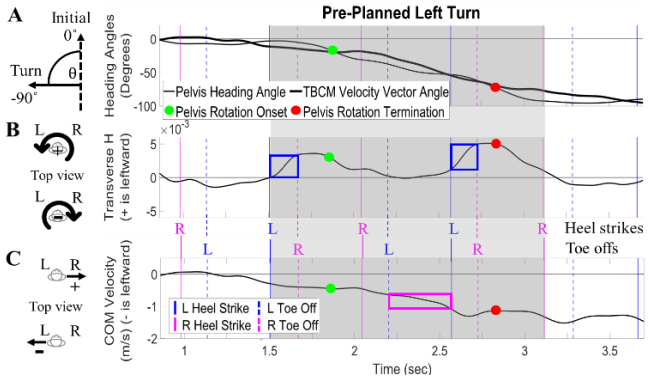

Figure 1. Exemplar pre-planned left turn: (**A**) pelvis heading and COM velocity angle relative to original direction of travel, (**B**) angular momentum (Ht), (**C**) COM velocity in the new direction of travel. The left step's double support phases with large Ht changes are indicated with blue boxes. The right step's single support phase with a large change in COM leftward velocity is indicated with a pink box.

Results and Discussion

The change in Ht was largest during the left step's double support phase (ΔHt_{avg} 0.003 during pre-planned, 0.003 during late-cued) vs. the three other gait phases (p=0.002 for each comparison). The change in COM velocity in the direction of the turn was largest during the right step's single support (Δv_{avg} -0.37 m/s during pre-planned, -0.65 m/s during late-cued) vs. the three other gait phases (p=0.002 for each comparison). These findings were observed despite a diversity of stepping behaviors. During pre-planned turns, participants used three to five steps and during late-cued turns participants used two to four steps. Future research will investigate if people tended to initiate turns with the left or right foot, and if generating the requisite momenta tended to occur in a sequence (e.g., rotation prior to translation).

Significance

Despite a diversity of stepping behaviors observed, we found distinct roles of each gait phase towards generating momenta during pre-planned and late-cued turns. These results suggest that during turns, changes in body facing direction is accomplished most during the inside (left) step's double support phase and changes in COM trajectory occur more during outside (right) single stance phase. Our findings align with the understanding that during straight-line gait, the net change in COM velocity is leftward during right foot single support phases and that Ht changes leftward after left heel strikes [4]. Therefore, our current findings suggest that healthy young adults leverage the dynamics observed during straight-line gait to generate the transverse-plane momenta required by turns.

Acknowledgments

This work is funded by NSF CAREER Award #1944207.

References

[1] Glaister et al., 2007. *Gait & Posture.* 25:289-294.
[2] Dumas et al., 2007. *J Biomech*. 40: 543-553.
[3] Vistamehr et al., 2016. *J Biomech*. 49(3): 396-400.
[4] Neptune et al., 2019. *J BME*. 141:1-9.

BALANCE AND POSTURAL CONTROL IN EXPERIENCED AND NOVICE YOGA PRACTITIONERS

Angeliki Vazaka[1], Sean Maudsley-Barton[1], Richard Mills*[1]
[1]Department of Sport and Exercise Sciences, Musculoskeletal Science and Sports Medicine Research Centre, Manchester Metropolitan University, UK
email: *richard.mills@mmu.ac.uk

Introduction

It is widely accepted that yoga interventions can improve balance [1] and reduce fall risk factors, improve health-related quality of life [2], and are an attractive form of exercise [3,4] among older people. However, there is currently a paucity of research on the potential for balance improvement through yoga (and therefore the risk of falling) in young-to-middle age adults, who also regularly experience falls [5].

Therefore, the aim of this study was to identify whether long-term yoga practice has an effect on yoga practitioners' balance performance by comparing experienced and novice practitioners in three poses. We hypothesized that experienced yoga practitioners would exhibit greater control of centre-of-pressure (CoP) measures, evidenced by lower sway area, path length, mean and root mean square velocities, and higher sway frequencies.

Methods

Sixteen female adults participated in this study (mean ± SD: age 31.8 ± 12.2 years, height 150.4 ± 42.5 cm, body mass 61.2 ± 7.4 kg). Based on experience level, participants were allocated to either the experienced (5+ years; n=8) or novice yoga practitioner (<1 year; n=8) groups. Balance performance was evaluated in three different conditions: two-legged quiet stance, and the one-legged 'tree' and 'warrior III' yoga poses. Participants performed each pose on their self-reported dominant and non-dominant legs while standing on a force plate (100 Hz). CoP data were filtered using a 2nd order Butterworth filter with cut-off frequency of 12 Hz [6]. The CoP 95% confidence ellipse area, path length, root mean square velocity, mean velocity, sway frequencies, were obtained.

.

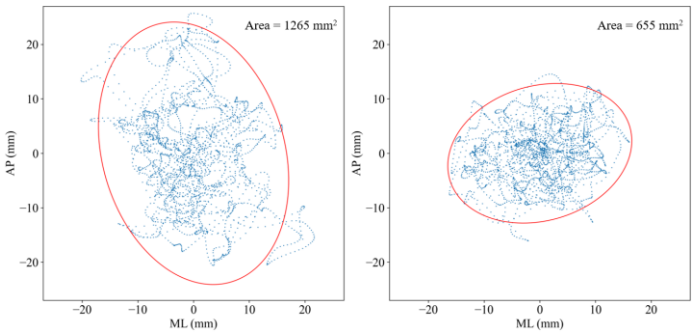

Figure 1: Example stabilograms for novice (left) and experienced (right) yoga practitioners in the warrior III pose. The 95% confidence ellipse is shown in red, with sway total area presented at the top. AP = anteroposterior; ML = mediolateral

Results and Discussion

Balance performance in experienced and novice yoga practitioners was found to be significantly different in the one-legged poses, with the experienced group exhibiting greater control as reflected in CoP measures. These results are likely attributable to a training effect favouring the experienced group. Both groups demonstrated worse performance with more difficult poses while two-legged quiet stance performance revealed no differences between groups, a possible consequence of the relatively non-challenging nature of the pose. Whilst the experienced group swayed over a smaller area (p<0.001), they swayed faster than the novice group (p<0.001), reflective of more frequent corrections for their centre-of-mass (COM) displacement. No significant difference was identified between dominant and non-dominant leg for either group. In conclusion, experienced yoga practitioners appear to have better postural control in yoga-specific poses than novices while they choose to correct for their COM displacement by swaying faster.

Significance

Risk of falls has been studied extensively (c.f. [7]), especially in older populations, however younger to middle-aged adults are often overlooked with regards to falls and/or risk of falling. For example, it has been reported that while falls were experienced less frequently than elderly individuals (35% of those aged >65 years), they were not insignificant in young (20-45) and middle-age (46-65) adults (18 and 21%, respectively), with women reporting a higher percentage of injurious falls in each age category [8]. Similarly, when adjusting for environmental factors (i.e., weather), 30% of young adult participants regularly experienced falls [5]. It is suggested that something other than activity levels -- such as general balance and gait characteristics -- is likely responsible. The results of our study suggest that practicing one-legged yoga poses may be beneficial in reducing the risk of falling. Therefore, future work should investigate, longitudinally, the effects of yoga interventions on balance, and particularly, its association with falls in both younger and older adults. Future work should also aim to generalise results to other, non yoga-specific balance tasks.

References

[1] Jeter et al., 2014. *J Altern Complement Med.* 20:4.
[2] Sivaramakrishnan et al., 2019. *Int. J. Behav. Nutr. Phys. Act.* 16:33
[3] Tiedermann et al., 2018. *Public Health Res. Pract.* 28(2):e28011801
[4] Keay et al., 2018. *Pilot Feasibility Stud.* 4:74
[5] Heijnen & Rietdyk 2016. *Hum. Mov. Sci.* 46
[6] Rochefort et al., 2017. *Orthop. J. Sports Med.* 5:3
[7] Blodgett et al., 2022. *Ageing Res. Rev.* 73:101501
[8] Talbot et al., 2005. *BMC Public Health* 5:86

PERSONALIZING A STATIC OPTIMIZATION OBJECTIVE FUNCTION FOR POST-STROKE GAIT

Mohammad S. Shourijeh*, Di Ao, Marleny Vega, Benjamin J. Fregly
Rice Computational Neuromechanics Lab, Department of Mechanical Engineering, Rice University, USA
email: *shourijeh@rice.edu

Introduction

Reliable estimation of muscle forces during human movement could facilitate the development of improved interventions for disorders such as stroke [1]. Muscle forces cannot be measured noninvasively using standard experimental methods, nor can they be computed via rigid body dynamics alone due to the muscle redundancy problem (i.e., more muscles than degrees-of-freedom (DOF) in the human musculoskeletal system). Because of its simplicity, static optimization (SO) is frequently used to resolve the muscle redundancy problem. However, generic musculoskeletal modeling frameworks have been incapable of estimating muscle activations and, therefore, muscle forces accurately [2].

Model personalization has been a significant step forward in individualizing neuromusculoskeletal parameters, especially in pathologic cases such as stroke [3]. However, accurate estimation of muscle activations/forces may also require personalization of the muscle redundancy problem. This study explored personalization of a static optimization cost function for an individual post-stroke and how personalization affects estimated muscle activations and forces.

Methods

Previously published walking data (motion, ground reaction, and EMG for 50 trials—5 speeds, 10 trials each) collected from a subject post-stroke were used for this study [3]. A modified OpenSim (v4.0; [4]) model with 31 degrees of freedom (DoFs; 5 per leg) and 35 leg muscles was used for the initial musculoskeletal analysis, including scaling and inverse kinematics and dynamics. An EMG-driven method calibrated musculotendon parameters in the model [3].

The inverse problem was formulated as a two-level optimization. The outer loop optimization minimized the error between the estimated muscle activations and the experimental EMG activations:

$$\min_{w,\, a^{Bg}} \sum_{k=1}^{N} \sum_{i=1}^{35} (a_{ik} - a_{ik}^{EMG})^2$$

where N is the number of trials. The optimization design variables of the outer loop were muscle-specific activation weights (w) and background activation levels (a^{Bg}).

The inner loop optimization was a custom SO defined as

$$\min_{a_{ik}} \sum_{i=1}^{35} w_i {a_{ik}}^2$$

subject to $M_j = \sum_{i=1}^{35} r_{ij} F_i^T (j = 1, \ldots, 5)$ and $a_i^{Bg} \leq a_i \leq 1$ where w_i and a_i^{Bg} are the muscle-specific weights and background activations optimized in the outer loop optimization problem, r is muscle-tendon moment arm, and F^T is muscle-tendon force.

Results and Discussion

We used several sets of trials for the inverse optimization problem to assess the sensitivity of the optimized parameters to the training set. Personalized muscle weights and background activation levels from the variations of training sets were nearly identical (>0.95 cosine similarities). The mean of the Pearson correlation coefficient between the estimated activations and EMG activations increased from 0.68 for SO to 0.93 for the inverse optimization (Figure 1).

Significance

This study showed that personalizing an objective function for the muscle redundancy problem in populations with neurological disorders is necessary. Although traditional static optimization is not accurate for estimating muscle activations, we showed that personalized custom static optimization could have the potential to be used for such estimations, which can have a great impact on how the interventions are designed for pathologic populations.

Acknowledgments

This work was funded by the Cancer Prevention and Research Institute of Texas (grant RR170026).

References

[1] Erdemir A et al. (2007). Clin. Biomech. 22: 131–154.
[2] DeMers S et al. (2014) J. Ortho. Research 32.6: 769-776.
[3] Meyer AJ et al. (2017). PLoS One. 12.
[4] Delp SL et al. (2007). Biom. Eng. IEEE T. 54: 1940–195

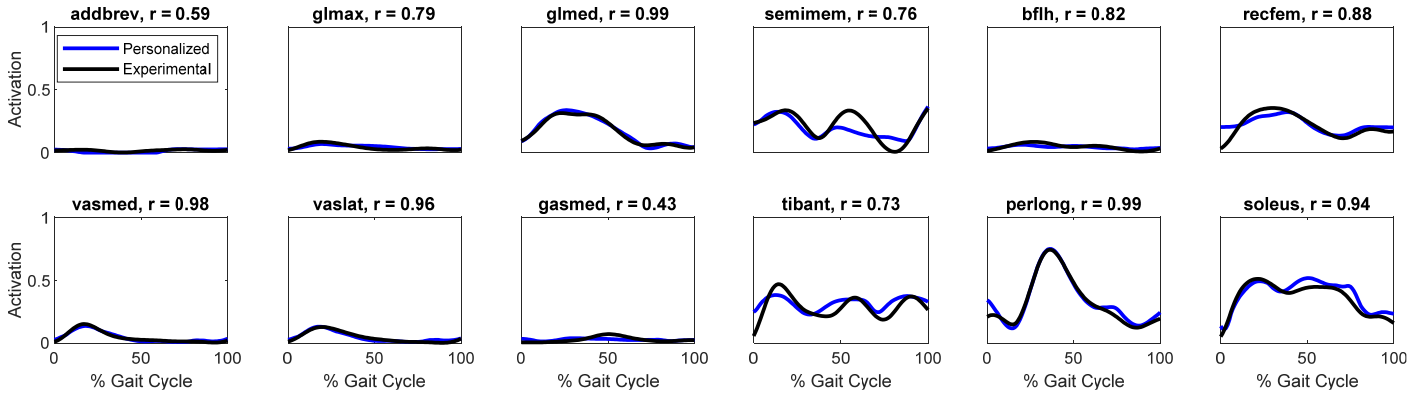

Figure 1: Representative muscle activation estimates of a trial at the self-selected walking speed from the personalized SO versus processed EMG for adductor brevis (addbrev), gluteus maximus (glmax), gluteus medius (glmed), semitendinosus, rectus femoris (recfem), vastus medialis (vasmed) and lateralis (vaslat), gastrocnemius lateralis (gaslat) and medialis (gasmed), tibialis anterior (tibant), peroneus longus (perlong), and soleus.

SENSITIVITY OF INTERNAL TIBIAL FORCES AND MOMENTS TO STATIC OPTIMIZATION JOINT MOMENT CONSTRAINTS AT THE FOOT AND ANKLE

Michael Baggaley[1]*, W. Brent Edwards[1], Timothy R. Derrick[2]
Human Performance Laboratory, University of Calgary, Calgary, Alberta
Department of Kinesiology, Iowa State University, Ames, Iowa
email: *michael.baggaley1@ucalgary.ca

Introduction

Static-optimization-based musculoskeletal modelling is often used to estimate the internal forces and moments acting on the human body. The static optimization routine is constrained such that the computed muscle forces must be able to produce the joint moments from inverse dynamics analysis. The flexion-extension and abduction-adduction moments at the hip and the flexion-extension moments at the knee and ankle are typically used as constraints; however, at the foot/ankle some studies have included the inversion-eversion moment at the ankle while others have used the inversion-eversion moment at the subtalar joint [1,2].

To date, no systematic evaluation has been performed to determine the sensitivity of internal forces and moments to joint moment constraints at the foot and ankle. The present study examined internal forces and moments at the tibia due to the high prevalence of stress fractures at this location.

Methods

17 (9M/8F, 25.7±6.9 yrs, 22.3±2.1 kg/m^2) participants ran on an instrumented treadmill while motion-capture and force platform data were collected. Participants ran at 0° and a speed of 3.33 m/s. Ankle joint contact force was estimated using inverse dynamics-based static optimization [1], with muscle moment arms, orientations, and force bounds obtained from a scaled musculoskeletal model [3]. Three sets of joint moment constraints were used in the static optimization routine. All sets included the flexion-extension and abduction-adduction moments at the hip and the flexion-extension moment at the knee, but the three sets differed in the constraints used at the foot/ankle. 1) flexion-extension at the ankle (Sag), 2) flexion-extension and inversion-eversion at ankle (Sag+Front), and 3) flexion-extension at the ankle and inversion-eversion at the subtalar (Sag+SubT). Internal tibial forces and moments were quantified at a cross section located at the distal 1/3rd of the tibia, by ensuring static equilibrium with all applied forces and moments. Linear mixed effects models were fit for each of the dependent variables. Statistical significance of the effect of constraint was established using likelihood ratio tests. Post-hoc testing was performed using Bonferroni adjusted pair-wise comparisons (adjusted α=0.008).

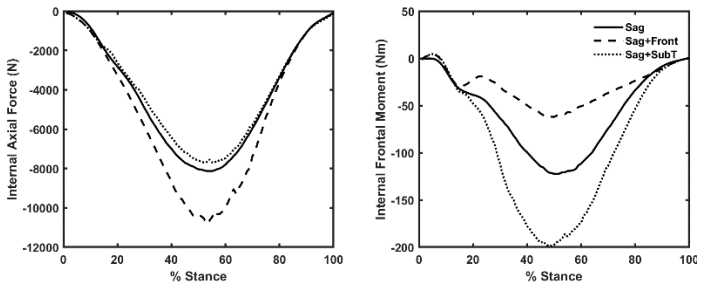

Figure 1: Time-normalized data of the internal tibial axial force (left) and the frontal plane bending moment (right) in each constraint condition.

Results and Discussion

A main effect of constraint was observed for internal axial and mediolateral force ($\chi^2(2)\geq86.60$,$p<0.001$), and frontal and transverse plane moments ($\chi^2(2)\geq48.58$,$p<0.001$). Sag+SubT resulted in larger internal mediolateral force ($p<0.001$), frontal ($p<0.001$) and transverse ($p<0.001$) plane moments, compared to Sag and Sag+Front. Internal axial force was greatest in SAG+FRONT, compared to Sag and Sag+SubT ($p<0.001$) with a mean difference of approximately 3000 N.

Alterations to the ankle joint contact force magnitude ($\chi^2(2)=65.81$,$p<0.001$) and orientation ($\chi^2(2)\geq74.31$,$p<0.001$) were responsible for changes to internal tibial forces and moments. Peak resultant ankle joint contact force was greatest in Sag+Front (~17 BW), compared to Sag (~13 BW) and Sag+SubT (~12 BW). The ankle joint contact force angle was oriented more in the axial direction in the Sag+Front condition compared to Sag and Sag+SubT ($p<0.001$). By comparison, the ankle joint contact force angle was oriented more in the medial direction in Sag+SubT, compared to Sag and Sag+Front ($p<0.001$).

Internal tibial forces and moments were sensitive to static optimization joint moment constraints, with larger forces and moments predominately observed in the Sag+SubT condition. Constraining models to replicate the inversion-eversion ankle moment produced very high axial forces, due to the relatively small muscle moment arms about the inversion-eversion axis of the ankle [4]. It also resulted in a reduction in the internal frontal plane moment, which may underestimate frontal plane bending of the tibia.

In contrast, previous work in a finite element simulation, which used the Sag+SubT constraints to derive muscle forces, demonstrated realistic tibia bending angles compared to *in vivo* data [2], suggesting that these may be more appropriate constraints to use for human locomotion out of the combinations examined herein.

Significance

Estimates of internal tibial loading derived from static-optimization-based musculoskeletal modelling were sensitive to the joint moment constraints at the foot and ankle in the static optimization routine. Constraining the static optimization routine to replicate the ankle flexion-extension and subtalar inversion-eversion moments accounts for movement about the anterior-posterior axis of the foot and ankle without resorting to high muscle forces to meet joint moment constraints.

References

[1] Derrick T et al. 2016. *J Biomech*. 49: 429-35.
[2] Haider et al., 2020. *J Biomech Eng.* 142: 021010.
[3] Edwards WB et al. 2008. *Clin. Biomech*. 23: 1269-78.
[4] McCullough et al. 2011. *Foot Ankle Int.* 32: 300-306.

PREDICTIVE MODEL FOR FUNCTIONAL LIMB LENGTH ASSESMENT DURING PROSTHETIC GAIT

Therese E. Parr[1], Brandon Lawhorn[2], John D. DesJardins[1]
[1]Clemson University, Department of Bioengineering, Clemson, SC
[2]Prisma Health, Center for Prosthetics and Orthotics, Greenville, SC
email: jdesjar@clemson.edu

Introduction

Leg length discrepancy (LLD) causes lateral asymmetry which is related to chronic pain in the back, hip, and knee [1]. LLD is especially pronounced in transfemoral amputees and must be regularly managed during their lifetime with each new prosthesis or component. Common clinical methods for measuring LLD do not account for gait deviations caused by static or dynamic axial malalignment, or muscle weakness or shortening. A new scientific measurement, termed *dynamic leg length* (DLL), has recently been established and is based on the functional metrics of the lower extremity according to bony limb segment length, structural deformity, and kinematic joint angles [2]. A previous model was developed to determine effective leg length and the sensitivity of toe clearance and hip-toe distance to the joint angles of the lower limb during swing phase of gait [3]. We hypothesize that a predictive analytical model of dynamic leg length could be developed that uses patient-specific anthropometric length inputs to better predict the functional inequalities of persons with LLD during critical periods of gait such as swing toe clearance and late stance forward propulsion.

Methods

A model was produced using literature-based inputs (anthropometric data [4] and dynamic joint angles) and trigonometric principles to determine lengths for hip joint center to heel (HJC-HEEL), hip joint center to ankle joint center (HJC-AJC), and hip joint center to forefoot/toe (HJC-FF) for the gait cycle (Figure 1). The sensitivity of the model was assessed by varying input lengths for the thigh, shank, toe, and heel by +/-5%.

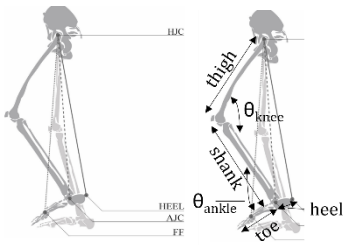

Figure 1. Dynamic leg length model outputs (left) established by the segment lengths and dynamic joint angles (right) (*figure adapted from Khamis, S., et al. 2018*)

Validation of the model was performed against experimental kinematic motion capture DLL data of forty healthy subjects [5] with a percent difference over a ten-step gait cycle. Similarly, a sensitivity analysis was calculated for the differences in maximum, minimum, and overall range between the standard and altered models. Retrospective anatomical segment length data for eight amputees was collected by the collaborating Certified Prosthetist-Orthotist and assessed for limb symmetry (% difference, std deviation) of the normalized values of all subjects.

Results and Discussion

The mathematical model yielded an accuracy of 98.65% for HJC-HEEL, 99.4% for HJC-AJC, and 98.60% for HJC-FF when compared to the experimental gait data (Figure 2). This model matched the experimental results on LLD detection within less than 1.2 cm, which is within the clinical value of acceptability [6]. A superior knee joint center (KJC) resulted in the most change in DLL range (max-min), while the posterior and anterior AJC resulted in the most change in overall DLL. The inconsistencies (standard deviation) of the prosthetic side were 10-20% larger than the sound side (Figure 2).

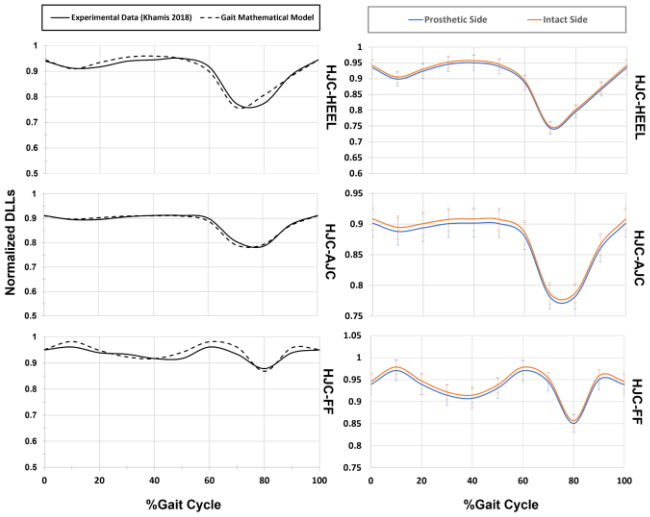

Figure 2. Validation of dynamic leg length model against experimental motion capture data (left) and sensitivity of retrospective amputee prosthetic vs sound side data (right)

Overall, the variations to the toe and the heel resulted in a higher average percent change than the changes to thigh or shank. Model suggestions include an inferior KJC or anterior AJC for a shorter leg length during swing (and hypothetically eased toe clearance, or less risk for tripping) and an inferior KJC or posterior AJC for a longer leg length during pre-swing (and hypothetically more forward propulsion). Limitations of this model for amputees include styles of prosthetic knee and ankle joints, as well as residual limb anatomy changes and pistoning.

This model shows how small static inequalities measured for typical LLD may result in larger biomechanical effects during critical gait periods, such as swing toe clearance and late stance forward propulsion. The DLL model established in this study is an accurate representation of DLL for amputees or (otherwise able-bodied) persons with LLD, which can give a more functional approach to measuring LLD without requiring the use of motion capture or other costly materials/methods.

Significance

The mathematical model of DLL provides a novel approach for encouraging functional symmetry for persons with LLD or amputees and aids clinicians in making more accurate prescriptions and adjustments of the thigh, shank, toe, or heel. Optimizing functional symmetry can help ease foot clearance issues, as well as reduce chronic pain in the back, hip, and knee.

References

[1] Friberg O. *Prosthet Orthot Int* 1984; 8: 124–129.
[2] Khamis S, Carmeli E. *J Orthop* 2017; 14: 276–280.
[3] Moosabhoy MA, Gard SA. *Gait Posture* 2006; 24: 493–501.
[4] Winter DA. *Biomech and Motor Control of Human Mvmnt.* 4th ed. John Wiley & Sons, Inc, 2009.
[5] Khamis S, et al. *Sensors (Switzerland)* 2018; 18: 1–9.
[6] Knutson GA. *Chiropr Osteopat* 2005; 13: 1–10.

SIMULATING CONTROL AND DYNAMICS OF HUMAN LAND AND STOP TASKS

Rodolfo Amezcua[1*], Henryk Flashner, PhD[1], Jill L. McNitt-Gray, PhD[2,3]
[1]Departments of Aerospace and Mechanical Engineering, [2]Biological Sciences, [3]Biomedical Engineering
University of Southern California, CA, USA. *Email: rodolfo.amezcua@usc.edu

Introduction

To study the control and dynamics of land-stop tasks, we propose the use of a four-link model. During the task, a braking action is implemented after initial foot contact, followed by control of the system center of mass (CM) via a telescoping inverted pendulum (TIP) equipped with springs and dampers along its radial and angular coordinates. Our aim is to validate this model and control strategy with experimental data during a series of landings where the participant intentionally regulated the magnitude of the ground reaction forces (GRFs) upon contact. The coefficients of the springs and dampers are estimated for each landing condition, assuming the same rigid ground model at initial toe and heel impact events. These coefficients of the control under each condition can represent impedance control during task execution.

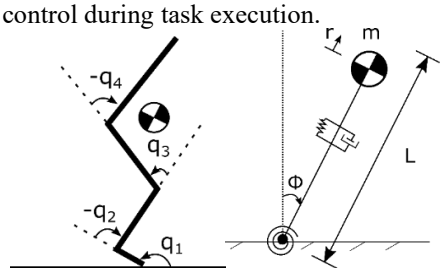

Figure 1: Left: Four-link model. Generalized coordinates starting with q_1 correspond to the foot, shank, thigh, and upperbody respectively. Right: Impedance control strategy. TIP equipped with springs and dampers used to control the CM position of the four-link model.

Methods

A female participant with a background in gymnastics provided informed consent and performed a series of self-regulated landings from a 0.445 meter platform. The three types of landings were characterized as normal, soft, and hard according to the magnitude of the GRF. Kinematic data in the sagittal plane was captured at 11000 frames per second with a 1.5mm/pixel resolution. Ankle, knee, hip, and shoulder points were tracked with available Matlab software [1]. A cubic smoothing spline was applied to the data to attenuate high frequency noise.

Modeling

The dynamics of the human body are derived under rigid body assumptions using coordinates described in Figure 1. The land-stop task is divided into an impact phase, defined as twice the time to peak vertical GRF observed in data, and post-impact phase. The impact phase begins when the toes contact the ground. At this point a rigid impact ground model [2], that assumes an instantaneous change of angular velocities but no change in angular positions, is used. A braking action, achieved with derivative control, is applied during this phase. When the heel contacts the ground, the rigid impact ground model is applied once more. During the post-impact phase, first feedback linearization is applied followed by an impedance and null space control design to regulate the CM. At the task-space level, the model's CM is rendered a TIP, with linear and cubic stiffness and damping terms in both the radial and angular directions. The model constraint forces are the GRFs acting on the human during landing. The coefficients of the braking action are chosen to minimize the sum of square error (SSE) of the data and simulated GRF. The coefficients of the desired impedance are chosen to minimize the SSE of the data and simulated CM position.

Results and Discussion

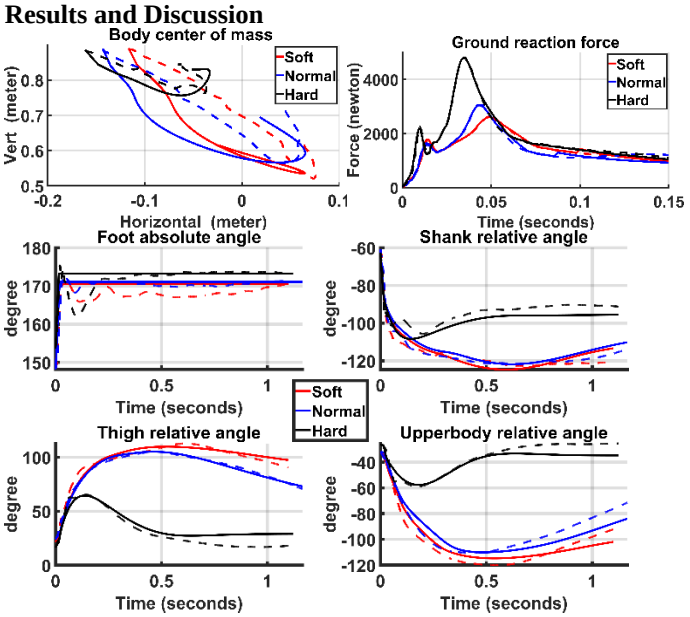

Figure 2: Top left: CM position comparisons for various landing conditions. Top right: Vertical GRF comparisons. Bottom four: Angular position comparisons of the four-link model for various landing conditions. For all plots, solid lines are simulation and dashed are experimental data.

The four-link model, under the proposed control and using a rigid impact ground model, reproduces well the joint angle position data and vertical GRF across various landing conditions. The switching in control logic from braking during impact to impedance during post-impact is what allows both the force and position simulation to match the data.

Significance

The optimized impedance coefficients suggest that the body can regulate landing behavior, such as CM and joint angle positions, and modulate GRF by adjustment of coefficients corresponding to a braking action during impact and a TIP equipped with springs and dampers during post-impact. These coefficients show an increase in magnitude going from soft to hard landing conditions suggesting that the body becomes more rigid when producing GRFs of larger magnitude. Furthermore, by using a rigid rather than compliant ground model, the complexities of identifying a nonlinear function describing the ground and fitting its parameters is not needed. This allows for an alternative study of the control implemented during land-stop tasks.

References

[1] Hedrick, T. L. (2008). *Bioinspiration & biomimetics*, 3(3).
[2] Westervelt, E.R. (2018). *Feedback Control*, CRC Press.

OPTIMAL CONTROL GAIT SIMULATIONS OF OLDER ADULTS PREDICT FOOT PLACEMENT TRENDS NOT CAPTURED BY REFLEX-BASED MODELS

Varun Joshi[1*], Katherine A. Boyer[2] and Brian R Umberger[1]
[1]School of Kinesiology, University of Michigan, Ann Arbor, MI
[2]Department of Kinesiology, University of Massachusetts, Amherst, MA
email: *varunjos@umich.edu

Introduction

Predictive simulations using reflex-based models of walking have provided important insights on the effects of age-related physiological changes on gait performance, such as the link between reduced muscle strength and poorer walking economy [1]. However, these models are limited in the range of behaviours they can produce, which could limit their utility. Optimal control techniques [2] are a common alternative to reflex-based control [1], yet the similarities and differences in results obtained with these two contrasting approaches are not well characterized. In this study, we sought to investigate these differences and determine the relative benefits of these two modeling approaches as the basis for a systematic study of the effects of muscle fatigue on gait in older adults.

Methods

An 11 degree of freedom musculoskeletal model, actuated by 18 Hill-type muscles [2] was modified to match the body mass distribution, joint range of motion, muscle strength, muscle mass, and muscle properties of both young and old healthy adults [1]. Symmetric and periodic predictive simulations of walking for this model were generated using IPOPT in OpenSim Moco [3]. The optimal control problem was set up to minimize either a) metabolic cost of transport (MCOT) based on the Bhargava model [4] or b) fatigue of transport (FOT) determined from the sum of squared muscle activation [1].

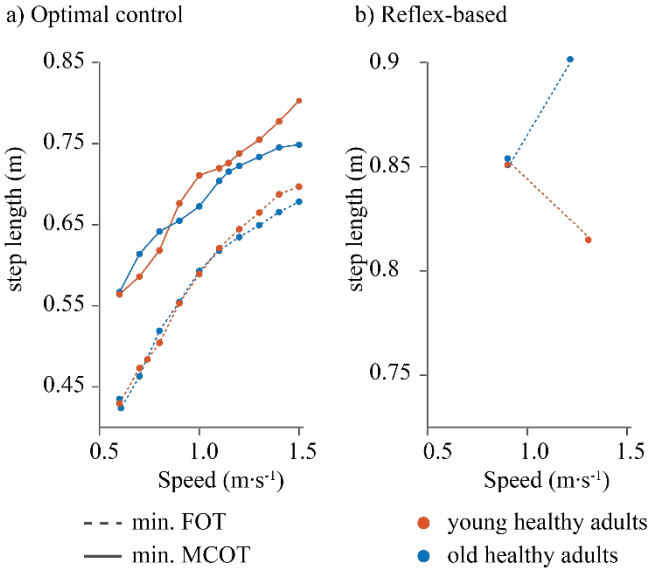

Figure 1: Optimal values of Step length (m) as a function of speed ($m \cdot s^{-1}$) for musculoskeletal models scaled to represent young healthy (red) and old healthy (blue) adults from a) optimal control based models and b) reflex-based models. Results for minimized MCOT (solid lines) and minimized FOT (dashed lines) show different values but similar trends – simulated older adults take shorter steps at medium to high speeds than their young counterparts.

Control parameters for the 2-D reflex-based models of older adults developed by Song and Geyer [1] were optimized by solving for the minimum FOT using a covariance matrix adaptation evolution strategy. For both models, solutions were generated for walking speeds set to 0.6 - 1.5 m s^{-1} in steps of 0.1 m s^{-1}.

Results and Discussion

Step lengths for the solutions to the optimal control problem matched expected qualitative trends – older adults take shorter steps than their younger counterparts at medium to high speeds (Fig 1a). However, the transition point in these trends depends on the cost function used in the optimal control problem. MCOT predicted a difference in step length by age above 0.8 $m \cdot s^{-1}$, while FOT predicted the difference above 1.0 $m \cdot s^{-1}$. MCOT also predicted longer steps in general for both young and old models at all speeds when compared to FOT. The step lengths predicted with MCOT were the expected magnitude for young adults, but the differences between young and old were less than reported experimentally [5].

Solutions generated by minimizing FOT for reflex-based models show the opposite trend; i.e., step lengths predicted for older adults were longer than their younger counterparts for the same walking speed. This suggests that while reflex-based models capture some age-related trends, such as increased fatigue and reduced walking speeds in older adults [1], they achieve these results with kinematics that do not match realistic walking behavior. Whether this is a result of modeling limitations or choices of cost functions for generating steady-state gait requires further evaluation.

Significance

In order to use musculoskeletal models effectively, it is important to understand the relative strengths and limitations of different modeling approaches. The results of this study show that models based on optimal control might better represent the steady-state kinematics of human walking due to the large space of possible gaits they can generate, while reflex-based models offer the ability to capture transient behavior.

Acknowledgments

This work was funded by NIH grant 5R01AG068102-02

References

[1] Song and Geyer, 2018. *J. Physiol 596*(7), pp.1199-1210.
[2] Nguyen et al., 2019. *IEEE TNSRE 27*(7), pp.1426-1435.
[3] Dembia et al., 2020. *PLOS Comput. Biol.* 16(12), e1008493.
[4] Bhargava et al., 2004. *J Biomech 37*(1), pp.81-88.
[5] Boyer et al. 2017. *Exp Gerontol* 95, 63-70.

OPTIMAL MUSCLE FIBER LENGTHS FOR HUMAN WALKING

Alex N. Denton[1*] and Brian R. Umberger[1]
[1]Locomotion Research Laboratory, School of Kinesiology, University of Michigan, Ann Arbor, MI.
email: [*]alxdent@umich.edu

Introduction

Muscle fiber length is a key architectural feature of the muscle-tendon unit, and the force-length relationship is a major determinant of the contractile behavior of muscle. When muscles operate at the optimal fiber length, force can be generated with minimum activation and low energy cost due to ideal cross-bridge formation [1]. The impacts of individual muscle architecture on function of the whole musculoskeletal system are poorly understood, but of considerable interest.

Relative muscle fiber lengths vary considerably across species and are likely subject to selective pressures. Fiber lengths also vary among humans, while exercise and aging can lead to within-subject changes in muscle fiber length [2,3]. Experimental approaches to studying the effects of muscle architecture in humans are limited to cross-sectional studies and time-consuming longitudinal interventions. Musculoskeletal modeling and simulation is a complementary approach that allows muscle parameters to be varied systematically, or optimized for various performance criteria [4,5]. In this study, we used a modeling approach to determine how optimal muscle fiber length (i.e., length at which muscle fibers generate peak active force) in lower limb muscles affects the neuromuscular effort of walking. Neuromuscular effort was defined as muscle excitation integrated over the stride and summed across muscles. Minimizing neuromuscular effort is indicative of preferred gait characteristics [6], which also coincide with minimum metabolic cost. We hypothesized optimizing muscle fiber lengths in all muscles would permit walking with systematically lower neuromuscular effort across muscles.

Methods

Predictive simulations of human walking at 1.3 m/s were generated using OpenSim Moco with a sagittal plane model consisting of 9 segments, 11 degrees of freedom, and 18 lower limb muscle-tendon actuators (nine per limb) [7]. The fiber length corresponding to peak isometric force was optimized for each muscle. The parameter search spaces were ±35% of the default optimal fiber lengths, which ensured that no optimal parameter values were restricted by the search bounds. The optimal control problem was set to minimize the sum of cubed muscle excitations, which has been shown to lead to realistic gait simulations [8]. The solution of this optimization problem was used to estimate neuromuscular effort and metabolic energy consumption overall, and for each muscle in the model. Predicted metabolic cost was calculated using a model of muscle energy consumption [9].

Results and Discussion

Optimal muscle fiber lengths were 7.6% shorter on average in the optimized solution. As a result, neuromuscular effort decreased 8% overall, with a similar 6.7% decrease predicted for metabolic cost. While overall neuromuscular effort decreased, individual muscles exhibited a range of responses, with the gluteus maximus experiencing the greatest increase (+33%) and the iliopsoas experiencing the greatest decrease (-37%) (Fig 1). Neuromuscular effort predominantly increased

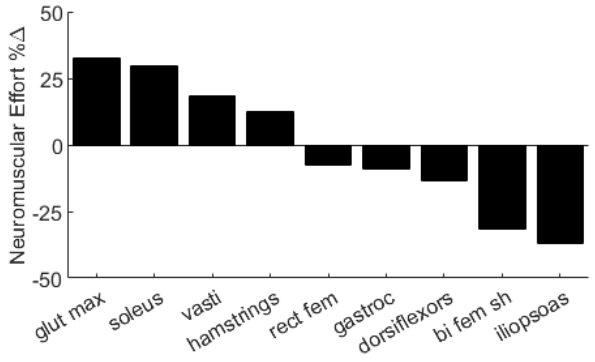

Figure 1: Change in overall neuromuscular effort when optimizing all lower limb muscle fiber lengths during walking compared to the default model parameters.

across the hip, knee, and ankle extensor muscles. These increases were more than offset by decreases in most of the flexor muscles, particularly the uniarticular hip and knee flexors (Fig 1). Thus, contrary to our hypothesis, achieving the greatest overall decrease in effort required increased effort in several muscles.

While optimal muscle fiber lengths decreased on average, there were similar mixed results across muscles, with increases for some muscles (e.g., gluteus maximus: +27%) and decreases for others (e.g., biceps femoris short head: -33%).

We followed the main results by targeting the optimal fiber length in the soleus muscles only, which had experienced a large increase in effort when all muscles were simultaneously optimized (Fig 1). In the isolated case, soleus neuromuscular effort decreased by 3%, overall effort decreased by 2%, and metabolic cost decreased by 4%. These substantially different results for the soleus emphasize the complex interactions among muscles in whole body movements, and the unpredictable effects on effort and metabolic cost.

Significance

Numerous external and internal factors affect the demands of walking, yet neuromuscular effort and metabolic cost were both quite sensitive to optimizing a single parameter: optimal muscle fiber length. The potential reduction in effort and metabolic cost implies that muscle fiber lengths are not tuned to minimize the demands of walking, which likely reflects evolutionary trade-offs associated with the need to perform other tasks beside level walking at preferred speed.

References

[1] Gordon et al., 1966. *J Physiol*. 184: 170-192.
[2] Salzano et al., 2018. *J Biomech*. 80: 1-7
[3] Morse, et al., 2005. *Acta Psychiatr. Scand*. 183: 291-298.
[4] Bobbert, 2001. *J Exp Biol*. 204: 533-542.
[5] Wong et al., 2016. *PloS one*. 11: e0150019.
[6] Stenum et al., 2016. *J Exp Biol*. 219: 2809–2813.
[7] Nguyen et al., 2019. *IEEE TNSRE*, 27: 1426-1435.
[8] Ackermann et al., 2010. *J Biomech*. 43: 1055-106.
[9] Bhargava et al., 2004. *J Biomech*. 37: 81-88.

INVESTIGATION OF THE PRE- AND POST-THR LOAD SHARING IN THE PROXIMAL FEMUR DURING WALKING

Mohamed Z. Bendjaballah[1] and Wissal M. Mesfar[1]
[1]Biomedical Technology Department, College od Applied Medical Science, King Saud University, Riyadh, Saudi Arabia
email: bendja@ksu.edu.sa

Introduction

Total hip replacements (THRs) present nowadays a high clinical success rate but bring about a number of complications as well[1]. The knowledge of internal loads acting on bones during daily activities is crucial for the proper understanding of their biomechanics. An implant that is several times stiffer than bone induces a loss in bone density as a consequence to the drop in the bone's physiologic loading. Numerical and experimental studies were carried out to minimize the drop in bone's load yielded to the implant[2]. This load sharing mechanism has been investigated in numerous analytical, experimental and numerical studies. The composite beam theory expresses, for instance, how a tensile force transfers through a composite structure made of two bonded straight bars having different Young's moduli and cross-sectional areas[3]. Similar formulations exist for beams under bending and shafts under torsion[4-7]. When applied to intramedullary straight stems, this theory is found to reasonably estimate the load shared between the stem and bone in the middle region of a long stem but fails near the implant's ends since the loading is carried proximally by the implant alone and distally by the bone alone. Furthermore, the use of curved implants within orthotropic bone material models further invalidates the results even at mid-stem sections[2]. To address these limitations, the current numerical study aimed to investigate the zonal load transfer occurring between a hip implant and a femur through the computation of internal forces and moments in various levels of the intact and implanted femoral shaft. These results along with data on the stress distribution in the bone may help in the prediction of stress shielding sites and intensities.

Methods

Intact and prosthetic computer-aided design (CAD) models of a proximal femur were developed. CT-scan images have served for the development of the intact model (Figures 1a). For the prosthetic model, a cementless implant, inspired from a Depuy SUMMIT commercial design was developed and the femoral head sectioned prior to the accurate placement of the prosthesis (Figure 1b). As long as walking activity is concerned, the hip joint force and the glutei, tensor fascia latae and vastus lateralis muscle forces were set up based on Heller's work[8]. The FE models (figures 1c and 1d) consider a bonded contact between all models' constituents in addition to an 'encastre' condition applied to the distal femur. To investigate the load sharing mechanism, static nonlinear analyses were performed and the elemental stress-based internal forces and moments computed over 35 sections demarcated along the femoral shaft (Figure 1e).

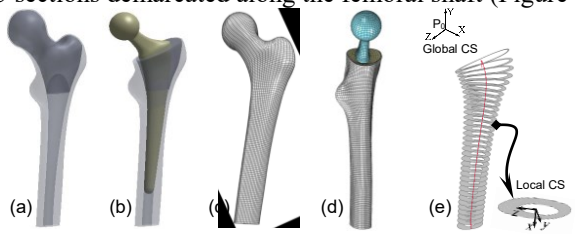

Figure 1: Intact and prosthetic CAD and FE models (a-d), also shown is the set of equidistant slices demarcated along a curved path of the femoral shaft and the global and local coordinate systems (e).

Results and Discussion

The internal forces and moments for the intact and prosthetic models were computed for a set of 35 sections, among which, results pertaining to 5 characteristic sections were presented in figure 2. These sections are located at the proximal most region, distal to the glutei insertion, distal to the tensor fascia latae and vastus lateralis, proximal and distal to the implant's tip.

In general, the shear forces and torsional moment were found to be negligible compared to their counterpart compressive force and bending moments, respectively. Cancellous bone had an insignificant contribution to the overall load sharing. The cortical rim that carried most of the internal loads in the intact model has been found to concede most of its share to the implant particularly in the proximal most regions.

The glutei were found to partially neutralise the internal compressive force in the intact cortical bone. This trend reverses to tension in the absence of compressive load, borne almost entirely by the implant.

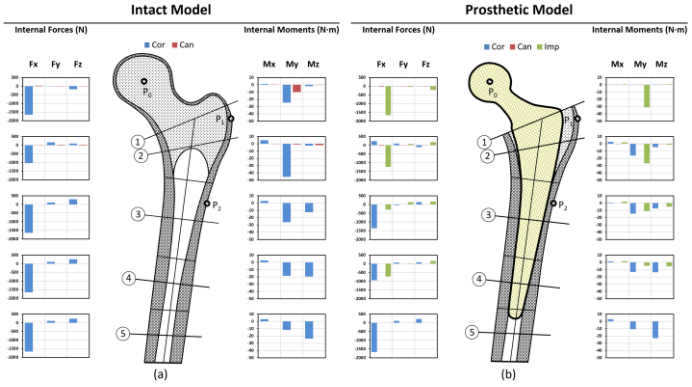

Figure 2: Load sharing mechanism at various locations of the femoral shaft. Sagittal views of: (a) intact model and (b) prosthetic model. Also shown, are the point of application of the joint force P_0 and muscles' attachment sites P_1 and P_2.

Significance

Despite being computed for an entire cross-section, the internal forces and moments used for the investigation of the load sharing mechanism remain a good indication of the amount of load the bone loses in favour of the surrounding implant at any specific site. When combined with data on the stress distribution developed in bone at the vicinity of the implant, such findings may be valuable in the prediction of stress shielding sites that may arise in bone particularly at the calcar region also known as gruen zone7.

References

[1] Berry et al., 2002. *J. Bone Joint Surg. Am.*, 84A, 171–177.
[2] Mandell, 1998. PhD-Dissertation.
[3] Timoshenko and Gere., 1972. Mechanics of materials.
[4] Duda et al., 1997. *J Biomech.*, 30(9):933-41.
[5] Van Mow and Huiskes, 2005. Basic Orthop. Biomech. and Mech. Biology, Lippincott Williams & Wilkins.
[6] Huiskes, 1980. *Acta Orthop Scand* [Suppl], 185.
[7] Huiskes, 1984. Functional behavior of orthopaedic materials.
[8] Heller et al., 2005. *J Biomech.*, 38(5):1155-6.

Session 6

Wednesday August 24, 2022

1:30pm – 3:00pm

O6.1 – Muscle Mechanics

O6.2 – Rehabilitation

O6.3 – Tissue Mechanics 2

O6.4 – Upper Limb 1 – Shoulder

O6.5 – Wearable Sensors 1

COLLAGEN DISTRIBUTION BEST EXPLAINS VARIATION IN DIAPHRAGM MUSCLE TISSUE STIFFNESS ACROSS AGE AND DISEASE STATES

Ridhi Sahani[1*], C. Hunter Wallace[2], Kaitlyn Hixson[1], and Silvia S. Blemker[1]
[1]University of Virginia, Department of Biomedical Engineering
email: rs8te@virginia.edu

Introduction

The development of fibrosis has devastating impacts across several neuromuscular disorders such as Duchenne muscular dystrophy (DMD). As healthy muscle is replaced with noncontractile fibrotic tissue, changes in passive muscle properties such as increased stiffness contribute to muscle dysfunction. Fibrosis is often quantified by collagen levels, neglecting collagen's complex organizational structure in the extracellular matrix (ECM) surrounding (epimysium) and within muscle tissue (intramuscular), and the role of collagen amount on tissue stiffness is debated. Thus, we seek to examine to extent to which collagen amount, distribution, and structure account for variation in tissue stiffness across age and disease states.

Here we focused on the diaphragm muscle, as respiratory insufficiency is a leading cause of death in DMD, but increased collagen amount does not explain increased diaphragm muscle stiffness in *mdx* (dystrophin null) mice [1]. Previous studies do not account for collagen organization or biaxial properties of diaphragm muscle, which sustains both along- and cross-muscle fiber loads *in vivo*. Therefore, we characterized collagen organization and biaxial passive properties to examine relationships between collagen structure and diaphragm stiffness.

Methods

Diaphragm muscle was isolated from 6-month-old *mdx* (n=4), 12-month-old *mdx* (n=4), 6-month-old WT (n=2), and 12-month-old WT (n=2) mice. Collagen organization: Total collagen area fraction (number of collagen pixels/total pixels in sample) and intramuscular collagen fraction (number of intramuscular collagen pixels/total number of collagen pixels) were measured from picrosirius red stained diaphragm muscle cross-sections imaged with circularly polarized light microscopy. Collagen fiber direction and collagen fiber strength of alignment were measured from scanning electron microscopy (SEM) images of the epimysium (**Fig. 1A**) [2]. Mechanical properties: Equibiaxial passive testing was performed to measure along- and cross-muscle fiber stiffness at low (3%) and high (8%) strain (**Fig. 1B**) [3]. Statistical analyses: Simple linear regression was performed to determine whether each organization parameter could predict stiffnesses. Multiple linear regression was then performed for each stiffness as a linear function of the organization parameters, excluding age and disease state. F-tests were used to compare regressions. All tests were performed in R (α=0.05).

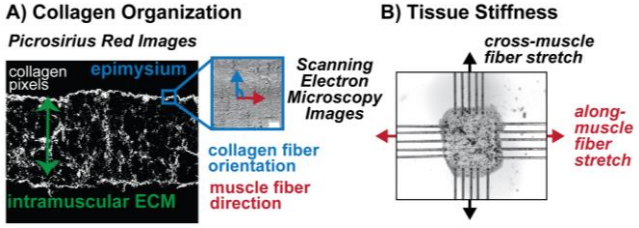

Figure 1: Collagen organization (A) and tissue stiffness (B).

Results and Discussion

Cross-muscle fiber low strain (3%) stiffness was best predicted by collagen alignment and intramuscular collagen amount, while high strain (8%) stiffness was best predicted by collagen area fraction and intramuscular collagen fraction. Both low and high strain along-muscle fiber stiffnesses were best predicted by collagen alignment and intramuscular collagen fraction. Intramuscular collagen fraction was the only significant predictor of tissue stiffnesses from simple regression, with positive relationships between intramuscular collagen fraction and stiffnesses. However, no significant differences were found between the multiple and simple regression models ($p>0.05$), suggesting that an increased proportion of collagen within the intramuscular ECM is the best predictor of increased tissue stiffness. Although collagen alignment and area fraction were not significant independent predictors of tissue stiffness, they helped account for variation in the data and their role on tissue mechanics must be explored further. Intramuscular collagen fraction was a stronger predictor of cross- relative to along-muscle fiber stiffnesses, and tissue samples were stiffer in the cross- relative to along muscle fiber direction. As epimysial collagen fibers were oriented in the cross-muscle fiber direction (70-90°) and produce force when stretched in tension, we posit that collagen regulates cross-muscle fiber diaphragm properties and future studies will incorporate *in vivo* measurements to determine the role of collagen organization on both passive and active diaphragm muscle properties.

Table 1. Regression analyses with intramuscular collagen fraction (simple regression) and **additional predictors* (multiple regression)

Stiffness Prediction		Simple Regression	Multiple Regression	
Cross-muscle fiber	3%	R^2=0.61, p=0.0018	R^2=0.65, p=0.0035	**collagen alignment*
	8%	R^2=0.71, p=0.00035	R^2=0.73, p=0.0011	**collagen area fraction*
Along-muscle fiber	3%	R^2=0.35, p=0.0025	R^2=0.37, p=0.05	**collagen alignment*
	8%	R^2=0.34, p=0.026	R^2=0.45, p=0.028	**collagen alignment*

Significance

The methods presented here allowed us to predict structure-function relationships that cannot be directly measured. Our results suggest that the distribution of collagen has a significant impact on passive tissue stiffness, highlighting the need to characterize collagen organization across muscles and diseases. Further, we must account for the role of collagen structure on passive muscle properties to better understand diaphragm muscle dysfunction in DMD, as well as the multitude of other fibrotic diseases.

Acknowledgments

Thank you to the National Institutes of Health for funding (Grant # U01AR06393) and the UVA Biotechnology Training Program (Grant # T32GM136615).

References

[1] Smith et al., 2014. *Am J. Phys.* [2] Sahani et al, (*in press*) *J. Appl. Phys*. [3] Wallace, 2021[PhD Thesis] *Univ. of Virginia*.

THREE DIMENSIONAL AND MICROSTRUCTURAL EFFECTS IN CEREBRAL PALSY AFFECTED MUSCLE

Ryan N. Konno[1*], Nilima Nigam[1], James M. Wakeling[1,2], and Stephanie A. Ross[2,3]
[1]Department of Mathematics, Simon Fraser University, Burnaby, Canada
[2]Department of Biomedical Physiology and Kinesiology, Simon Fraser University, Burnaby, Canada
[3]Department of Physical Therapy, University of British Columbia, Vancouver, Canada
email: *rkonno@sfu.ca

Introduction

Skeletal muscle has a complex three dimensional structure making it difficult to fully understand and model. One of the main reasons for this difficulty is that its structure crosses many physical length scales. On the microscopic scale there are the sarcomeres inside the muscle fibres, which are responsible for the active force production in muscle. The muscle fibres themselves are embedded in a matrix of collagen fibres called the extracellular matrix (ECM). Altogether the muscle transfers force to the skeletal system on the macroscopic scale. During muscular diseases, changes can occur to these microstructural components; however, it is difficult to determine, using experimental techniques, the causation between the changes in the microstructure and the overall muscle mechanics.

Cerebral palsy results from an upper motor neuron lesion in the brain and leads to changes in the skeletal muscle structure; in particular, contracture occurs resulting in reduced overall mobility. The structural changes can include variations in the volume fraction and stiffness of the ECM, as well as changes to the lengths of the sarcomeres within the muscle fibres [1]. Due to the complex nature of the microstructural changes, we utilised a modelling approach to examine the individual contributions of different microstructural changes to whole muscle mechanics in CP affected muscle.

Methods

To investigate the three dimensional mechanics of muscle in cerebral palsy, we utilise a continuum mechanical model of muscle developed in previous studies [2,3]. The mathematical model consists of a fibre-reinforced nonlinearly elastic material. In particular, we have one dimensional fibres, which include effects from the contractile units, embedded in a three dimensional base material, which includes contributions from the ECM and other cellular components. We varied the volume fraction (α) of the ECM in the muscle, as well as the length of the sarcomeres (c_{sarco}). Changes in the sarcomere length were modelled by changes in the intrinsic passive force-length properties of the fibres.

Results and Discussion

To evaluate the mechanical behaviour of muscle, we performed stress-strain experiments. From these tests we measured the corresponding stiffness modulus as the rate of change of the stress-strain curve at a given length. We found that the ECM had the largest effect on the overall stiffness of the muscle (Figure 1). This agrees with previous studies (eg. [4]) that the ECM has the largest contribution to the passive stiffness of muscle in CP. While the change in sarcomere length did result in an increase in the stiffness of muscle, it was not as large as the ECM component.

Furthermore, we find that the increase in sarcomere length does not linearly increase the stiffness in the whole muscle. For a large enough increase in the sarcomere length (> 150% increase in length), there was a decrease in the whole muscle stiffness (Figure 1). The reason for this is the three dimensional and nonlinear effects of the muscle model. If we were to only consider a one or two dimensional model, these results would not be seen. To fully understand the mechanics of skeletal muscle, three dimensions are required.

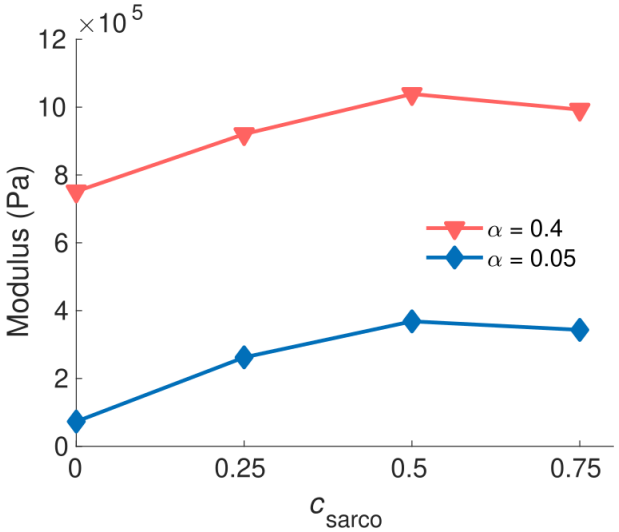

Figure 1: Whole muscle stiffness at optimal length of the muscle versus the shift in the sarcomere length (c_{sarco}). α is the volume fraction of the extracellular matrix.

Using this model, we are better able to understand the influence of the microstructure on the overall mechanics of CP affected muscle. We found that the extracellular matrix, while not consisting of a large fraction of the muscle volume, has a substantial effect on muscle stiffness. Additionally, to fully understand the mechanics of both diseased and healthy muscle three dimensions need to be considered, as an increase in stiffness on the microstructural level may not correspond to an increase in stiffness on the macroscopic level.

Significance

Causation between changes in the microstructure and overall muscle mechanics are difficult to determine using experimental techniques. Using our modelling approach, we are able to isolate the effects from individual microstructural contributions, which can provide insights into the mechanics of both diseased and healthy muscle. Additionally, this work demonstrates the importance of considering three dimensional behaviour when investigating the mechanics of skeletal muscle.

Acknowledgments

We would like to acknowledge funding from NSERC Discovery Grants to NN and JMW.

References

[1] Lieber RL et al. (2019). *J. Appl. Physiol.*, **126**: 1492-1501.
[2] Wakeling et al. (2020). *Front. Physiol.,* 11:813.
[3] Konno et al. (2021). *PLoS ONE.*, 16(4): e0249601.
[4] Smith et al. (2011). *J. Physiol.* 589(10): 2625-2639.

VALIDATING A MUSCULOSKELETAL MODEL FOR SIMULATING MUSCLE MECHANICS AND ENERGETICS DURING HUMAN HOPPING

Luke N. Jessup[1*], Glen A. Lichtwark[1], Luke A. Kelly[1], Andrew G. Cresswell[1]
[1]Centre for Sensorimotor Performance, School of Human Movement and Nutrition Sciences, The University of Queensland, Australia
email: *luke.jessup@uq.edu.au

Introduction

The efficacy of computational modelling of musculoskeletal (MSK) systems for simulating metabolic cost depends heavily on how well the modelling can account for changes in muscle mechanics. While this has become an area of emphasis, MSK modelling has rarely been explored outside of walking and/or a narrow range of movement conditions and/or small perturbations in movement or movement choice.

This study aimed to determine whether a current MSK model could be validated to simulate muscle mechanics and energetics across a wide range of human two footed hopping tasks known to drastically alter metabolic rate in a way that is hard to predict with simple mechanical metrics.

Methods

Data here is presented from n = 3 (3 males; age 25.7 ± 2.0 (mean ± SD); height 177.0 ± 5.6 cm; mass 76.9 ± 11.3 kg. We have collected and plan to present data from n = 10.

Experimental data came from each participant performing 19 x 4 min trials: 7 partly constrained (hop frequency (*f*) or height (*h*) specified), 8 fully constrained (both *f* and *h* specified), and 4 unconstrained (neither f nor h specified). Steady-state metabolic energy expenditure was measured from the final 2 min of each trial. Kinematics and kinetics were measured simultaneously at 3 min (11-camera motion analysis system and 2 x force plates). Electromyography data was collected from lateral gastrocnemius (LG), medial gastrocnemius, soleus (SOL), tibialis anterior, vastus lateralis (VL), rectus femoris, and biceps femoris. Ultrasound imaging was used to measure fascicle length changes from LG, SOL, and VL.

We used a scaled, whole body OpenSim model (Lai et al., 2017) along with inverse kinematics and inverse dynamics (based on the kinematic and kinetic data) to simulate muscle excitations and fascicle dynamics using OpenSim Moco. Muscle dynamics were then input to OpenSim's Umberger Muscle Metabolics Probe (Uchida et al., 2016) to simulate metabolic cost. Where possible, the base model's muscle and tendon properties were tuned to improve the agreement between experimental and simulated mechanics.

Seven conditions per participant are used here for comparison – low hop height (LH; 2.8 ± 0.2 Hz, 9.3 ± 0.7 cm), medium hop height (MH; 2.1 ± 0.2 Hz, 14.1 ± 0.6 cm), high hop height (HH; 1.8 ± 0.03 Hz, 19.9 ± 0.9 cm), low hop frequency (LF; 1.9 ± 0.2 Hz, 10.5 ± 3.0 cm), low-medium hop frequency (LMF; 2.2 ± 0.1 Hz, 8.0 ± 0.9 cm), medium-high hop frequency (MHF; 2.6 ± 0.1 Hz, 8.0 ± 2.5 cm) and high hop frequency (HF; 3.0 ± 0.02 Hz, 6.9 ± 2.1 cm).

Results and Discussion

Qualitative analysis of the experimental and simulated muscle activity showed a good relationship between their general shape and pattern, although a substantial time lag was always evident between the two due to how activation dynamics are implemented in OpenSim Moco. An r^2 value of 0.93 was calculated between the experimental and simulated metabolic power. Values (r^2) of 0.92, 0.97 and 0.93 were calculated for LG, SOL and VL fascicle shortening, respectively. Values (r^2) of 0.79, 0.91 and 0.83 were calculated for LG, SOL and VL fascicle shortening velocity, respectively.

These results show promise for using MSK models to simulate relative changes in muscle mechanics and whole-body energetics, although simulated and real values often differ in absolute terms. We concur with the sentiment of other validation studies – that there are a host of areas for simulation to improve in. For instance, handling dynamic inconsistencies in high force conditions, determining the cost of negative work, formulating more accurate muscle models and cost functions, and dealing with nuances such as electromechanical delays.

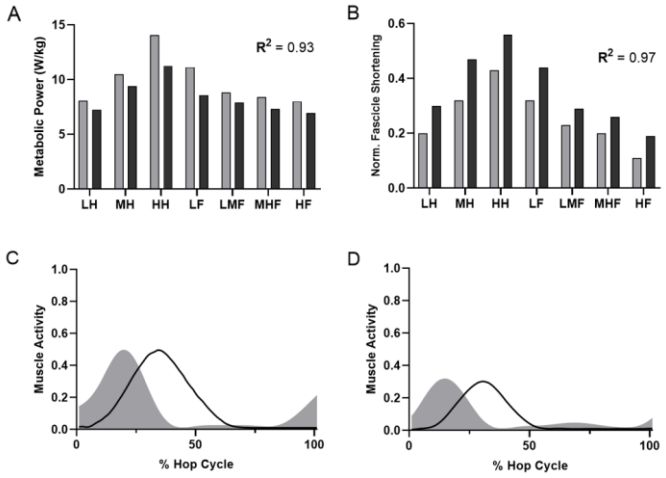

Figure 1: Experimental (grey) and simulated (black) metabolic power (W/kg; Fig. 1A) and normalised SOL fascicle shortening (Fig. 1B) averaged between participants for each condition, and muscle activity of SOL (Fig. 1C) and VL (Fig. 1D) across the hop cycle for the LH condition of one participant.

Significance

This research demonstrates that changes in metabolic cost can be estimated across a range of movement conditions, which makes such models suitable for predicting generalised lower limb movements. Appropriate tuning of the parameters in such models using biological data such as that collected here will aid in applying such models to improve human performance, health and rehabilitation.

Acknowledgments

This research is funded by an Australian Research Council Future Fellowship Award (DP200101476). We also thank Nick Bianco for his advice and guidance.

References

Dembia, C. L. PLoS Comput. Biol. 16, 2020
De Groote, F. Proc. R. Soc. B. 288, 2021
Gutmann, A. K. J. Exp. Biol. 220, 1654-1662, 2017
Lai, A. Ann. Biomed. Eng. 45, 2762-2774, 2017
Uchida, T. K. PLoS One. 11, 2016

THE CAPACITY OF THE IN-SERIES MUSCLES TO GENERATE STRAIN IN THE ILIOTIBIAL BAND

Laura A. Hutchinson[1*], Glen A. Lichtwark[1], Luke A. Kelly[1]
[1]The University of Queensland, St. Lucia, QLD, Australia
email: *laura.hutchinson@uq.edu.au

Introduction

The iliotibial band (ITB) is a unique anatomical structure in humans, believed to be important for bipedal locomotion. One curious feature of the band is that it transmits force across the lateral knee from two seemingly antagonist muscles: gluteus maximus (GM) and tensor fascia latae (TFL). While we have previously hypothesised that there may be different force transmission pathways from each muscle through the ITB, there is currently a lack of empirical evidence [1]. We have developed a technique using a Kanade-Lucas-Tomasi (KLT) [2,3] algorithm to track ITB length changes during isolated contractions of GM and TFL via ultrasound imaging.

Here we explore the regional variation of ITB strain as well as the influence of knee posture on ITB strain during isolated contractions of TFL and GM. We hypothesized that isolated contraction of the TFL will result in an increase in ITB strain in the anterior region of the ITB with limited strain in the posterior region and that the opposite would occur with GM contraction. We further hypothesized that there would be more strain in the ITB during contraction of either muscle when the knee is flexed compared to a straight leg.

Methods

Fifteen healthy participants (9m/6f, a:29±7years, h:175±7cm, w:78±11kg) gave written, informed consent. Two sets of fine-wire electrodes were inserted across the motor points of TFL and the superior portion of GM. Two flat ultrasound transducers (Telemed, 110Hz) imaged the ITB on the distal, lateral side of the femur (Figure 1). Both were aligned with the fibers of the ITB with the posterior probe angled slightly off the long axis of the thigh to achieve this. Joint movement was assessed by a string potentiometer attached between the transducers and Gerdy's tubercle. A constant current electrical stimulator (Digitimer) was programmed to deliver "trains" of electrical stimulation (60 rectangular pulses, 110Hz) through the fine wires. Participants were instructed to relax in two separate supine postures: knee bent (90°) and knee straight and received three stimulations trains in each posture to each muscle separately.

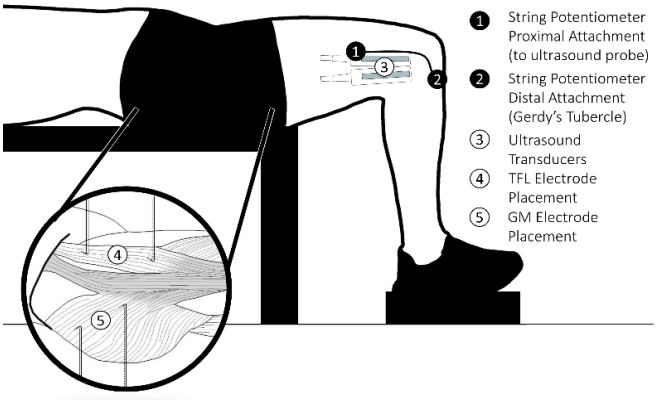

Figure 1: Participant experimental set-up including TFL and GM fine wires, two ultrasound probes, and string potentiometer.

In MATLAB, the ITB region was manually selected by an operator and the points were tracked using the built-in KLT point-tracking algorithm (vision.PointTracker). Combining the string potentiometer and the ultrasound tracking displacements, the ITB strain during each trial was calculated.

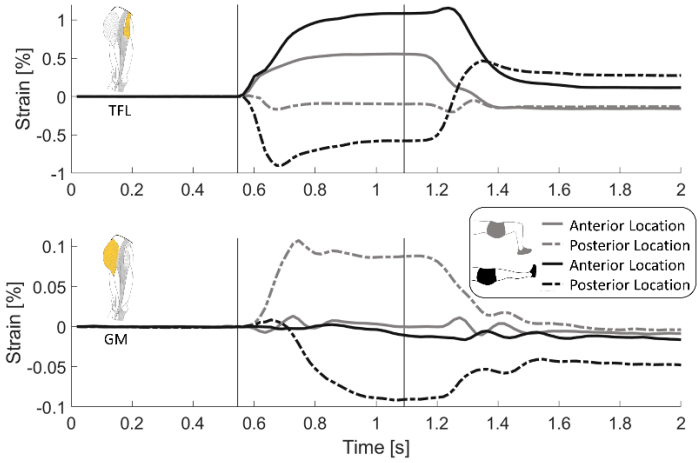

Figure *2*: Strain measured using anterior probe (solid lines) and posterior probe (dashed lines) in a bent knee posture (grey) and a straight knee posture (black) during TFL stimulations (top) and GMax superior stimulations (bottom). The vertical lines indicate the timing of the applied stimulation.

Results and Discussion

During isolated contractions (stimulations) of the TFL we found that the anterior probe measured more positive strain (stretching) than the posterior probe for both the bent knee (P=0.003) and the straight knee condition (P=0.0001) (Figure 2, top).

During isolated contractions of the superior portion of GM, we found that the posteriorly positioned probe measured more positive strain than the anteriorly positioned probe for only the bent knee condition (P=0.007) (Figure 2, bottom).

We suspect that skin artifact due to subtle knee postural changes may cause underestimates of the changes of length of the string potentiometer, causing the negative strain values and are likely more representative of zero strain conditions.

Significance

Our results demonstrate the capacity of the different in-series muscles to generate strain in the ITB and that this capacity varies with posture and ITB region. We have begun to highlight the complex relationship between the ITB and its in-series musculature in the hopes of elucidating its potential functions and why some athletes develop ITB syndrome, while others do not.

References

[1] Hutchinson et al., *Sports Med.*, 2022
[2] Lucas & Kanade, *7th Int. Jt. Conf. Artif. Intell.*, 1981.
[3] Tomasi & Kanade, *Carnegie Mellon Univ. Tech. Rep.*,1991.

IS SARCOMEROGENESIS REQUIRED FOR MUSCLE FASCICLE LENGTH INCREASES?

Loren Z.F. Chiu[1], Torstein E. Dæhlin[1], and Zachary A. Fielding[1]
[1]Faculty of Kinesiology, Sport, and Recreation, University of Alberta
email: Loren.Chiu@ualberta.ca

Introduction

Physical activity, such as stretching exercise, may elicit increases in muscle fascicle length [1]. In animal studies, increased fascicle length is the result of sarcomerogenesis, leading to an increased number of sarcomeres in series [2]. However, this research is difficult to replicate in humans. Moreover, it has been argued that other mechanisms are responsible for increased fascicle lengths.

Computational modelling may be used to examine the consequences of increased fascicle length with and without sarcomerogenesis. Specifically, the presence or absence of sarcomerogenesis will differently affect sarcomere length excursion for the muscle lengths corresponding to full joint range of motion (ROM).

The purpose of this research was to model an increase in muscle fascicle lengths with either a fixed serial sarcomere number or an increased serial sarcomere number. It was hypothesized that 10-20% increases in fascicle length with a fixed serial sarcomere number would cause a shift in sarcomere length excursion to long sarcomere lengths that would not be physiologically realistic.

Methods

A computational model was developed based on muscle and skeletal parameters measured on three cadaver specimens. The baseline model describing the anatomy and forces of the quadriceps is previously published [3]. Briefly, the quadriceps muscles were modelled as distributed force systems, allowing multiple fascicles to be incorporated into each muscle. Based on the fascicle lengths and orientations, which change as a function of muscle length excursion with knee flexion, maximum 3D forces exerted by each muscle could be estimated.

Using the vastus lateralis from the baseline model, fascicle length was modelled to increase by 10% and 20% [1]. As pennation angle does not increase following muscle stretching interventions [1], fascicle orientations were not altered. Maximal muscle force was assumed to occur at -60º knee flexion in the baseline model, thus, the number of sarcomeres in series was calculated by dividing 2.7 µm (optimal sarcomere length) into fascicle length at this joint angle.

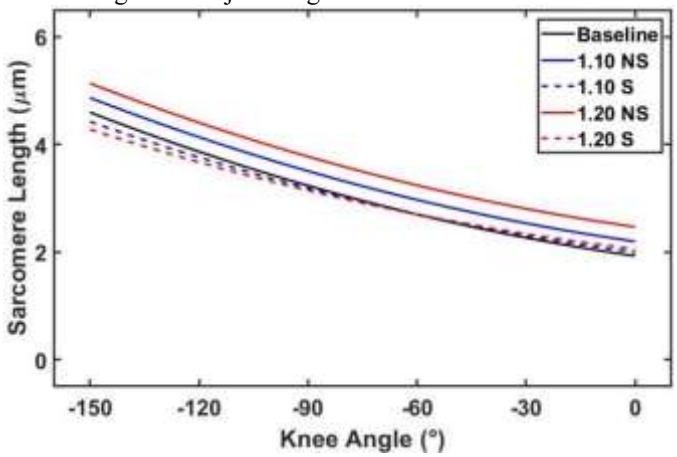

Figure 1: Vastus lateralis sarcomere length in specimen 1 for 10% (1.10) and 20% (1.20) fascicle length increases with (S) and without (NS) sarcomerogenesis.

The number of sarcomeres in series for each fascicle were calculated. For the sarcomerogenesis model, serial sarcomere number was increased so that optimum length remained at -60º knee flexion. For the no sarcomerogenesis model, serial sarcomere number was held constant. Sarcomere length as a function of knee flexion angle was determined for all conditions. Additionally, the knee flexion angle where sarcomeres were at optimal length was determined.

Results and Discussion

Optimal sarcomere length (2.7 µm) remained at -60º for both the 10% and 20% increased fascicle length models with sarcomerogenesis. The sarcomere length excursion across the knee flexion ROM decreased (Figure 1). With greater knee flexion (longer muscle length) increasing fascicle length with sarcomerogenesis led to shorter sarcomere lengths compared to the baseline model. With less knee flexion (shorter muscle length), increasing fascicle length with sarcomerogenesis resulted in longer sarcomere lengths compared to the baseline model. Taken together, increased fascicle lengths resulting from sarcomerogenesis allows sarcomeres to operate nearer to optimal sarcomere length and away from extreme long and short lengths where force generating capacity is decreased.

Without sarcomerogenesis, the knee flexion angle where sarcomeres were at optimal length changed to -42º to -45º for 10%, and -21º to -32º for 20% fascicle length increases. At all knee flexion angles, sarcomere lengths were longer when fascicle length increased without sarcomerogenesis. This shift to longer sarcomere lengths indicates that lack of sarcomerogenesis would place sarcomeres at optimal length nearer to extension, where the muscle is shorter, and that sarcomeres would operate primarily on the descending limb of the force-length relation.

As exercise programs involving muscle stretching generally observe a shift in maximum force to occur at longer, not shorter muscle lengths [4], an increase in fascicle length without sarcomerogenesis does not seem plausible. This is highlighted by the extreme sarcomere lengths that would be required, as sarcomeres have 0% force beyond 4.5 µm.

Altogether, realistic increases in fascicle length likely require sarcomerogenesis. Increasing serial sarcomere number is beneficial as sarcomeres operate along a narrower length range, nearer to the optimal length for force generation.

Significance

This data provides theoretical support for sarcomerogenesis as the mechanism for increased fascicle length following stretching exercise. Further, as relative muscle force can be predicted from sarcomere length, the muscle force and joint angle relation may be used to assess the presence of sarcomerogenesis in humans following exercise interventions.

References

[1] Simpson et al., 2017. *Scand J Med Sci Sports*. 27:1597-1604.
[2] Williams & Goldspink, 1971. *J Cell Sci*. 9:751-767.
[3] Chiu & Dæhlin, 2021. *J Biomech.* 120: 110347.
[4] Brughelli & Cronin, 2007. *Sports Med*. 37: 807-826

REPEATED GLYCEROL INJECTIONS LEADS TO PASSIVE STIFFENING IN SKELETAL MUSCLE

K. Josh Briar[1]*, Alex M. Noonan[1], Stephen H. M. Brown[1]
[1]Human Health and Nutritional Sciences, University of Guelph, Guelph Ontario
email: Kbriar@uoguelph.ca

Introduction

Skeletal muscle has an exceptional capacity to remodel following injury or in response to various diseases. Currently, several experimental rodent models utilize glycerol injections to chemically induce muscle damage and elicit controlled and reproduceable muscle regeneration [1]. Glycerol damages the plasma membrane resulting in myofibre necrosis and regeneration and leads to the accumulation of fat and collagen deposition between fibres [2]. However, this model has not been fully characterized, particularly in relation to effects on biomechanical characteristics, and the effects of multiple glycerol injections are unknown.

Therefore, the purpose of the current work was to explore the influence of multiple glycerol injections on skeletal muscle passive stiffness. It was hypothesized that multiple glycerol injections would lead to greater muscle stiffness when compared to control saline injections.

Methods

Male (n=12) and female (n=12) C57BL/6 mice received 15µm injections of either glycerol (50% v/v) (experimental) or sterile saline (control), to the erector spinae muscles (L1-L5 bilaterally) at day 0 and every 14 days for 42 days (4 injections total). Mice were euthanized 14 days after the final injection; erector spinae muscles were immediately dissected and prepared for either histology or mechanical testing.

Muscle histology

Muscle samples were dissected and flash frozen. After sectioning, muscle slides were stained with picrosirius red (collagen) and fast green (muscle fibres) to detect fibrosis.

Passive mechanical testing

Muscles were chemically permeabilized and bundles of fibres (n=72) were extracted and tested using a cumulative stretch-relaxation protocol to quantify passive mechanical characteristics [3].

Results and Discussion

Multiple glycerol injections were found to have a statistically significant impact on skeletal muscle passive stiffness. Specifically, the passive elastic modulus was significantly higher in the glycerol group when compared to the saline group ($p=0.009$; Figure 1). No sex effects were present. In addition, 8 fibre bundles (27%) from the glycerol group (compared to zero in the saline group) failed in their mid-substance during the mechanical testing, suggesting a weakness or brittleness present in these muscles.

The current findings demonstrate that repeated intramuscular glycerol injections resulted in a significant increase in the passive stiffness of the muscle, likely due to a proliferation and possibly reorganization of the collagen fibres within the muscle.

Preliminary histological data (Figure 2) shows a greater amount of intramuscular collagen, which supports this idea.

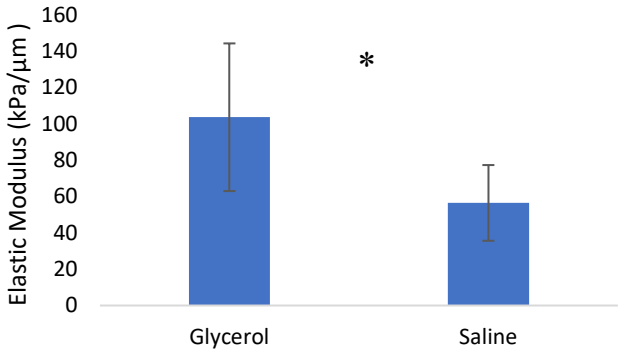

Figure 1*:* The passive elastic modulus for the mouse erector spinae muscles in the glycerol and saline injection groups. (*) indicates a significant between glycerol and saline injection conditions. Error bars indicate the standard error for each experimental group.

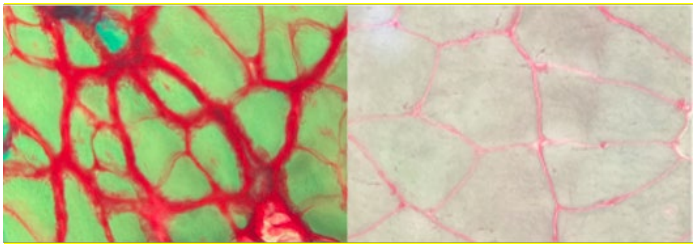

Figure 2: Representative muscle histology. Muscle sections stained with picrosirius red (collagen) with fast green (fibres). Glycerol injected mice (left) demonstrate increased collagen deposition when compared to saline mice (right).

Significance

Our results demonstrate that multiple intramuscular glycerol injections can induce *de novo* skeletal muscle fibrosis and increase the passive stiffness of the muscle in young wild type mice. This method of intramuscular glycerol injection may be of interest to researchers investigating skeletal muscle pathology and will allow for insight into the mechanisms underlying skeletal muscle fibrosis, tissue stiffening, and its possible treatments.

Acknowledgments

Funding for this study was provided by the Natural Sciences and Engineering Research Council of Canada.

References

[1] Mahdy et al., 2015, *Annals of Anatomy – Anatomischer Anzeiger* 202:18-27.
[2] Biltz et al., 2020. *J Physiol* 598 : 2669-2683.
[3] Noonan et al., 2020, *Experimental Gerontology,* 137, 110968.

IN VIVO VASTUS LATERALIS FASCICLE LENGTH SHORTENING DURING MAXIMAL ISOMETRIC CONTRACTIONS

Bryan Yu[1] and Walter Herzog[1]
[1]Human Performance Laboratory, University of Calgary, Calgary, Canada
Email: bryan.yu1@ucalgary.ca

Introduction

The force-length relationship describes the force generating potential of skeletal muscle during maximal, steady-state, isometric contractions, and it can be observed on all structural levels of the muscle [1]. In human testing, the force-length relationship is affected by the dissociation of fascicle (contractile element), and whole muscle-tendon unit length [2]. Fascicle lengths during isometric knee extension testing (probably the most common human muscle testing) are shortening for two reasons (i) shortening caused by the extension of the knee during contraction due to compliance of the dynamometer and human soft tissues and (ii) shortening caused by the elongation of muscle elastic tissues with increasing force [3].

The amount of fascicle shortening associated with each factor is not known but is important for accurate and reliable estimates of the *in vivo* force-length properties of human skeletal muscles. The purpose of this study was to quantify the amount of vastus lateralis (VL) fascicle shortening caused by each of these factors.

Methods

Sixteen sub-elite speed skaters participated in the study. Participants performed nine maximal voluntary isometric knee extensions with the left leg ranging from 20° to 120° knee flexion (0°=full extension) in a randomized order. They were positioned on a dynamometer (THE HUMAC NORM, Computer Sports Medicine Inc., Stoughton, MA, USA) with the back supported and the hip joint angle set at 80°.

2-D leg kinematics were recorded with two markers (medial malleolus and medial femoral epicondyle) using a high-definition camera. Knee angles were determined using Dartfish (Version 10, Dartfish, Switzerland).

Ultrasound images of VL were obtained using B-mode ultrasonography (60mm, LV8, Telemed, Lithuania). The ultrasound probe was attached to the skin above the VL (~50% of femur length). Fascicle lengths were measured using ImageJ (NIH, USA).

Knee joint angles and VL fascicle lengths were obtained for the passive and fully activated conditions. Second order polynomial approximations were used to calculate fascicle shortening from force production alone. The fascicle shortening caused by knee angle changes was then calculated as the difference between the total fascicle shortening and the shortening just caused by the increasing VL force.

Results

The greatest change in total fascicle shortening occurred between 30° to 22° knee flexion, and the lowest change occurred between 120° to 112° (Figure 1).

Fascicle shortening caused by VL force gradually decreased as the knee angle increased (85% to 40%) while, correspondingly, fascicle shortening caused by changes in knee angle increased with increasing knee angles (Figure 1).

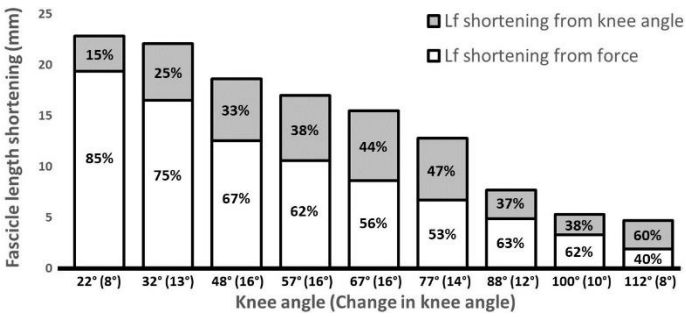

Figure 1: Total vastus lateralis fascicle length (Lf) shortening as a function of final knee angles. Angles in parenthesis indicate the knee angle change due to dynamometer and soft tissue compliance.

Discussion

In many human studies, fascicle length changes of muscles are given as the difference of fascicle lengths measured in the passive muscle and the fully activated muscle [4-6]. The implicit assumption underlying such results is that fascicle shortening occurred at the expense of elongations of elastic structures in the muscle [4-6]. Here, we demonstrate that this assumption is likely not correct for the human knee extensor muscles, as even careful strapping of subjects into the dynamometer allows for extension of the knee with force production due to the compliance of the dynamometer-human leg system. Furthermore, the contribution of muscle elastic elements and dynamometer compliance to fascicle shortening depends crucially on the knee joint angle at which the testing is performed. Fascicle shortening during "isometric" muscle testing will not only affect the force-length properties of muscles due to the changed length of fascicles but also due to the residual force depression associated with the mechanical work produced by fascicle shortening [7].

Significance

Knowing the change in fascicle length during "isometric" human muscle testing is crucial in understanding the true force-length properties of the tested muscles.

Acknowledgments

Funding: NSERC Canada

References

[1] Gordon et al., 1966. *J. Physiol.* 184, 170-192.
[2] Kulig et al., 1984. *E. S. S. Reviews.* 12, 417-466
[3] Arampatzis et al., 2004. *C Biomech.* 19, 277-283
[4] Ito et al., 1998. *J. A. Physiol*. 85, 1230-1235
[5] Reeves and Narici, 2003. *J. A. Physiol*. 95, 1090-1096
[6] Ichinose et al., 1997. *A. Anatomica*. 159, 78-83
[7] Chen et al., 2019. *J. A. Physiol.* 126, 1066-1073

EFFECT OF CUSTOMIZED ADAPTIVE TREADMILL CONTROL ON STEP LENGTH AND TRAILING LIMB ANGLE

Kayla M. Pariser[1*], Margo C. Donlin[2], Kaitlyn E. Downer[1], Jill S. Higginson[1,2]
[1]Department of Mechanical Engineering, University of Delaware, Newark, DE, USA
[2]Department of Biomedical Engineering, University of Delaware, Newark, DE, USA
email: pariserk@udel.edu

Introduction

Walking speed is one of the most used measures of gait performance as it directly correlates with functional mobility and can predict future health status in a wide range of populations [1]. Because of its importance to overall wellbeing, increasing walking speed is a common target outcome of gait rehabilitation [2]. However, because speed is a complex function of gait mechanics like step length (SL), propulsion, and trailing limb angle (TLA) [3], many rehabilitation protocols designed to increase gait speed exhibit mixed effectiveness perhaps due to failure to target individual-specific impairments that contribute to decreased walking speed.

To enable targeted treadmill rehabilitation programs, we developed a customizable adaptive treadmill (ATM) controller that changes belt speed in real time due to changes in user step length, propulsive impulse, or anterior-posterior position on the treadmill [4]. With this controller, the relative importance of each input on the overall belt speed can be adjusted via gain functions. The **objective** of this study is to determine the effect of increased SL gain in the ATM controller on user SL, TLA, and walking speed. We **hypothesized** that as the gain on step length was increased relative to the gain on the propulsive impulse that average SL, average TLA at the event of peak propulsive force, and average self-selected walking speed would all increase.

Methods

The ATM controller determines the new belt speed (v_{i+1}) based on the weighted sum of the current speed (v_i) and intermediate speeds due to user step length ($v_{Avg,SL}$), propulsive impulse ($v_{Avg,propulsion}$), and position on the treadmill ($position^2$, Eq. 1). The unitless gain functions α, γ, and β define the importance of changes in step length, propulsion, and position on the overall belt speed. In this study β was left unchanged and the ratio of α/γ was modified to test user response to preferential weighting on step length over propulsion.

$$v_{i+1} = v_i + \alpha(v_{Avg,SL}) + \gamma(v_{Avg,propulsion}) - \frac{v_i(\alpha+\gamma)}{2} \pm \beta(position^2) \quad (1)$$

Twenty-two young, healthy adults with no history of musculoskeletal injury impacting gait (11 male, 24 ± 3 years, 1.72 ± 0.11 m, 76.52 ±11.29 kg) participated in the study. Each subject was outfitted with 42 retroreflective markers for motion capture and completed four one-minute walking trials at their self-selected walking speed on an instrumented split-belt treadmill (Bertec Corp., OH, USA). The four ATM conditions were randomized: Baseline (α = γ = 1.5), Low SL ratio (α = 1.25γ), Mid SL ratio (α = 1.5γ), High SL ratio (α = 1.75γ). Motion capture (Motion Analysis Corp., CA, USA, 100 Hz) and ground reaction force data (2000 Hz) was recorded during each trial. Average walking speed, SL, and TLA were calculated. TLA was defined as the angle between the lab vertical axis and a straight line from the hip joint center to the 5th metatarsal of the trailing limb [4]. Data from five subjects is presented here. One-way ANOVAs will be run when the full data set is ready for analysis.

Results and Discussion

Preliminary results indicate that increasing the ratio of the gain on SL relative to the gain on propulsion, α/γ, increases SL, TLA, and walking speed. Similar to the literature, as TLA and SL increase so does walking speed [5]. Four out of five subjects achieved their greatest SL, TLA, and fastest self-selected walking speed with the Mid ratio condition (Figure 1). While data analysis is still in preliminary stages, this may suggest that there is a threshold where emphasizing SL in the control function makes it more difficult to maintain self-selected walking speed and as a result the user chooses to take smaller steps beyond this threshold.

This study demonstrates that an ATM controller can be customized to promote increased user SL, TLA, and walking speed. Since increased walking speed and modifying the mechanisms by which walking speed is achieved are common goals of gait rehabilitation, these results show promise for the use of this customized ATM as a tool in gait training programs.

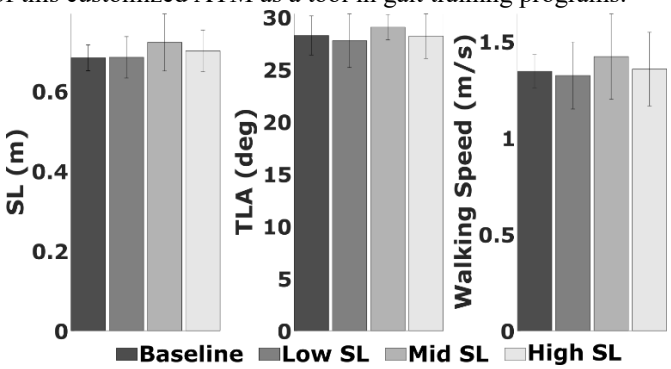

Figure 1: Group average ± 1 standard deviation, SL (left), TLA (middle), and self-selected walking speed (right). On average, all outcome measures were greatest for the Mid ratio condition.

Significance

A customizable ATM may be an effective therapeutic intervention to target individual-specific impairments in SL and TLA, and ultimately walking speed. Future work will seek to understand the impact of this ATM controller on the gait mechanics of individuals post-stroke.

Acknowledgments

Funding: NSFGRFP, University of Delaware Helwig Mechanical Engineering Fellowship, Delaware Space Grant College and Fellowship Program, NIH P30 GM 103333.

References

[1] Fritz S, Lusardi M, 2009. *J Geriatr Phys Ther.* 32: 2-5.
[2] Bowden M et al., 2008. *Neurorehabil Neural Repair.* 6: 672-675.
[3] Hsiao H et al., 2016. *J Biomech.* 49: 388-395.
[4] Ray N et al., 2018. *J Biomech.* 78: 143-149.
[5] Hedrick E et al., 2021. *J Biomech.* 115: 11013.

INDIVIDUALS POST-STROKE CHANGE ENERGETICS OF MULTIPLE LOWER LIMB CONSTITUENTS DURING GAIT WHILE WEARING A PASSIVE-DYNAMIC ANKLE FOOT ORTHOSIS

Jacob T. Skigen[1*], Corey Koller[2], Keira Morgan[1], Luke Nigro[3] and Elisa S. Arch[2,4]
[1]Department of Biomedical Engineering, University of Delaware, Newark, DE
[2]Biomechanics & Movement Science Program, [3]Department of Mechanical Engineering, [4]Department of Kinesiology & Applied Physiology, University of Delaware, Newark, DE
email: *jtskigen@udel.edu

Introduction

Passive-dynamic ankle-foot orthoses (PD-AFOs) are commonly prescribed to individuals post-stroke to supplement weakened plantar-flexor muscles in their paretic limb. Our previous research demonstrated stiffness-customized PD-AFOs capacity to reduce lower extremity mechanical cost of transport (COT) for individuals post-stroke when walking compared to walking with No AFO or with their standard-of-care (SOC) AFO. [1] The purpose of this study was to investigate how individuals achieve this COT reduction.

We hypothesized COT reductions would be driven primarily by decreases in the subjects' paretic ankle work.

Methods

Eight individuals (mean (SD) age 65.1 (6.9) years; height 1.72 (0.13) m; mass 82.4 (14.8) kg; 3 male, 4 female) with single chronic stroke took part in this study. Instrumented gait analysis was conducted using an instrumented treadmill and motion capture cameras as participants walked without any AFO and then with their SOC AFO at their self-selected waking speed determined via a 10 Meter Walk Test without an AFO. A PD-AFO was stiffness customized and manufactured for each participant based on the peak paretic plantar-flexor moment during stance from the No AFO data. Participants were given the PD-AFO to wear for four weeks, then returned to the lab for an instrumented gait analysis with the PD-AFO at the same self-selected walking speed from the initial visit.

Data were processed and analyzed in Visual 3D. COT was calculated per limb for each condition as positive limb work (summed hip, knee, ankle, and distal foot, all normalized by body mass) summed with the absolute value of negative limb work over the gait cycle, scaled by stride length. [1] Finally, The Constituent Lower Extremity Work (CLEW) approach was used to quantify and visualize how energetics of the 14 lower extremity constituents (bilateral positive and negative ankle, knee, hip during stance and swing, and positive and negative distal foot during stance only) changed with PD-AFO use. [2]

Results and Discussion

All subjects with full data sets saw decreases in total COT (paretic + nonparetic limbs) with the PD-AFO compared to No AFO and all but one decreased total COT compared to the SOC AFO. While wearing the PD-AFO, six subjects decreased the net COT in their paretic limb and seven decreased the net COT in their nonparetic limb compared to No AFO. Conversely, seven decreased the net COT in their paretic limb and six decreased the net COT in their nonparetic limb compared to their SOC AFO (Table 1). Interestingly, on average, subjects showed reductions in over half of the constituents' work with the PD-AFO use compared to both the No AFO and SOC AFO conditions (Table 1), and these changes were all relatively small (<0.19 J/kg).

The results of this study support our previous findings that showed stiffness-customized PD-AFOs enable COT reductions. However, the results do not support our hypothesis as to how these reductions were achieved. Instead of total COT reductions being driven by the ankle or even a few primary constituents, results indicated that the decrease in total COT was due to a summation of small changes across the entirety of both limbs. This suggests that, for individuals post-stroke, PD-AFOs do not simply cause direct enhancement of plantar flexor function; instead an adaptation or reorganization of much of the lower limb system appears to occur.

Table 1. Number of lower limb constituents that decreased work magnitude and magnitude of change in COT (J/kg/m) with the PD-AFO compared to both the No AFO and SOC AFO. ±COT could not be calculated due to technical error.

	No AFO vs PD-AFO				SOC AFO vs PD-AFO			
	Paretic		*Nonparetic*		*Paretic*		*Nonparetic*	
Subject	*#*	*ΔCOT*	*#*	*ΔCOT*	*#*	*ΔCOT*	*#*	*ΔCOT*
P1	5	-0.01	11	-0.13	3	-0.01	6	-0.1
P2	4	-0.05	11	-0.29	5	0.12	8	-0.31
P3	12±	-±	-±	-±	11	-0.55	12	-0.16
P4	10	0	13	-0.2	9	-0.06	7	0.02
P5	14	-0.04	12	-0.54	14	-0.05	10	-0.17
P6	8	-0.55	7	-0.4	9	-0.32	6	-0.58
P7	7	-0.54	5	-0.17	4	-0.03	5	0.19
P8	8	-0.27	12	-0.04	9	-0.59	9	-0.01
Mean	*8.5*	*-0.21*	*8*	*-0.25*	*10*	*-0.19*	*8*	*-0.14*
SD	*3.38*	*0.25*	*3.74*	*0.17*	*2.97*	*0.27*	*2.36*	*0.23*

Significance

This study provided valuable insight into how the post-stroke musculoskeletal system interacts with stiffness-customized PD-AFOs. Further, this study highlighted the importance of looking at the entirety of the lower limbs rather than just the constituent being targeted by a given assistive device. Future work can investigate whether the change in COT observed while wearing a stiffness-customized PD-AFO corresponds to a change in muscle activation patterns. Additionally, future studies can investigate whether subjects' self-organized changes are optimal for reducing COT or if training can improve their performance. This study combined with future work will help to optimize the design and prescription of PD-AFOs as well as rehabilitation and training strategies to meet patients' needs and improve their quality of life.

Acknowledgments

This work was supported by USAMRAA through the Orthotics & Prosthetics Outcomes Research Program under Award No. W81XWH-18-1-0502. Opinion, interpretations, conclusions, and recommendations are those of the author and not necessarily endorsed by USAMRAA.

References

[1] Koller, C. et al. Proc. ASB Annual Meeting, 2021
[2] Ebrahimi, A. et al. Gait Posture, 56, 49-53, 201

STANCE-PHASE MEDIAL COMPARTMENT TIBIOFEMORAL COMPRESSIVE FORCES DURING DOWNHILL WALKING IN PATIENTS FOLLOWING TOTAL KNEE ARTHOPLASTY

Tanner A Thorsen[1], Chen Wen[2], Songning Zhang[2]
[1]The University of Southern Mississippi
[2]The University of Tennessee, Knoxville
email: tanner.thorsen@usm.edu

Introduction

Following unilateral total knee arthroplasty (TKA), downhill walking is still a necessary part of daily life. Previous studies that reported knee joint biomechanics of patients walking downhill following TKA have used inverse-dynamics based knee abduction moment to detail the joint loading in the medial compartment of the knee [1]. Although these variables have often been used as surrogate for compressive force, they do not directly indicate the magnitude nor behavior of stance-phase compressive forces at the medial compartment of the knee (MCF).

While understanding the behavior of compressive forces in both limbs post-TKA is important for the improvement of prosthetic design and development of rehabilitation protocols, obtaining in-vivo compressive forces is costly and invasive. Musculoskeletal modelling and simulation provide a toolset that allow for the estimation of knee joint compressive forces in both the replaced and non-replaced limbs of patients with TKA *in-silico*. Furthermore, data analysis techniques such as Statistical Parametric Mapping provide the opportunity to examine a biomechanical variable throughout the entirety of a task as opposed to a single discrete value (i.e., maximum, or minimum) [2]. It was hypothesized that MCF would be smaller in the replaced limb and that MCF would be greater throughout the duration of stance during downhill walking compared to level walking.

Methods

Kinematics (240 Hz) and ground reaction forces (1200 Hz) were recorded simultaneously while twenty-five TKA patients (11 male, 68.6 ± 4.9 years, 22.1 ± 11.7 months post-op) walked over level ground and downhill at a slope of 10° on a customized adjustable instrumented ramp system. A modified gait2392 model with a knee that includes hinge joints for medial and lateral knee compartments [3] was used to estimate muscle forces with static optimization and MCF with joint reaction analysis (3.3, OpenSim, Stanford University). Stance phase MCF was evaluated with a 2×2 (Limb × Slope) Statistical Parametric Mapping repeated measures ANOVA (SPM{F}). Limb and Slope main effects and their interaction were deemed significant when the SPM{F} trajectory crossed the critical threshold [2]. Effect size for all significant regions were computed from the mean difference (md) between the two waveforms throughout the significant duration and were reported using Cohen's d.

Results and Discussion

Our hypothesis regarding increased MCF in the non-replaced limb and increased MCF throughout stance were not supported as results of SPM{F} test revealed only a significant main effect of slope on MCF (Figure 1A). MCF between slopes was greater in level walking during 10-30% of stance ($p<0.001$, md=0.31 BW, d=0.60), yet larger during downhill walking between 46-77% stance ($p<0.001$, md=0.33 BW, d=0.85). Stance-phase MCF between slopes are presented in Figure 1B. Two additional significant regions were identified at the start, 1-4% ($p=0.04$, md=0.11 BW, d=0.67) and end of stance phase 88-100% ($p=0.005$, md=0.21 BW, d=0.56).

Significance

Contrary to our hypotheses, stance phase MCF was not different between replaced and non-replaced limbs, nor was it different through the entirety of the stance phase of gait during downhill walking. In fact, MCF was different between slopes cumulatively only 63% of stance. Interestingly, during the duration often associated with the loading-response (10-30%, figure 1B), MCF was greater during level walking, yet during the duration of stance associated with push-off (46-77%), MCF was greater in downhill walking. These data may suggest that downhill walking at a 10° slope may be a safe form of exercise and rehabilitation following TKA in that balanced joint loading was observed between limbs and that downhill walking only increases MCF near push-off for about 30% of total stance.

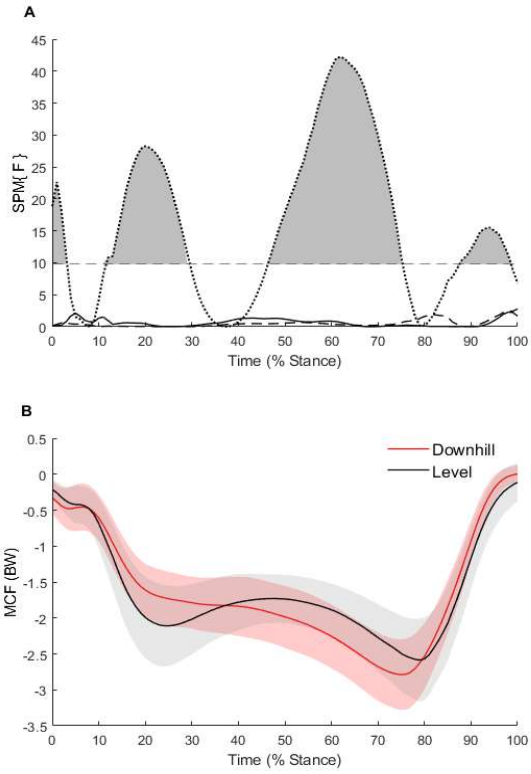

Figure 1: **A)** Results of the SPM 2-way ANOVA with the results of main effect A, Limb, indicated by the dashed line, main effect B, Slope, indicated by the dotted line, and the interaction indicated by the solid line. The critical threshold is indicated with the dashed gray line, and regions of significance are shown as shaded gray areas. **B)** MCF time-series plots normalized to 101 data points and normalized to body weight. Shaded regions represent standard deviations.

References

1. Wen, C., et al. (2021). J Sport Health Sci. In press.
2. Pataky, Todd C. (2013). J Biomech. 48(7). 1277-85
3. Lerner, Z., et al. (2015). J Biomech, 48(4), 2780-278

CAN A UNILATERAL PASSIVE HIP BRACE DIMINISH WALKING ASYMMETRY?

Kayla M. Kowalczyk[1*], Philippe Malcolm[1]
[1]Department of Biomechanics, University of Nebraska at Omaha, Omaha, NE, USA
email: kkowalczyk@unomaha.edu

Introduction

Approximately 200 million Americans suffer from at least one neurological disorder (i.e., stroke or Multiple Sclerosis (MS)) that may lead to asymmetric biomechanics during walking gait [1,2]. Walking asymmetries may consist of temporal (i.e., stance or swing time) and spatial (i.e., step or stride length) alterations between the left and right limbs [3], increasing the metabolic cost of daily activities and fall risk for the affected populations [4]. Previous studies examined the efficacy of interventions (i.e., unilateral weighting or split-belt walking) as forms of rehabilitation for asymmetric walking. Although these interventions produced symmetrical walking patterns [5], split-belt treadmills are large and expensive. Developing accessible, inexpensive rehabilitative methods that lead to symmetrical walking patterns is necessary to improve neurologically afflicted populations' lives.

Passive exoskeletons have shown effectiveness at influencing walking patterns. MS patients using a passive device successfully altered hip joint range of motion and power [2]. Developing similar devices at low costs and for long-term use outside of therapeutic or laboratory settings may potentially create long-term retention in neurological populations. The purpose of this proof-of-concept investigation was to apply passive posterior resistance unilaterally while walking on a split-belt treadmill in healthy participants. We hypothesized the passive hip exoskeleton would help reduce step length asymmetries induced by the split-belt perturbation.

Methods

We assigned fifteen healthy participants (9 male, 24.13 ± 2.47 years, 172.6 ± 9.8 cm, 72.2 ± 11.9 kg) into three experimental groups: Split-Belt only (SO), Exoskeleton only (EO), and Split-Belt and Exoskeleton together (EXSB). All participants completed a baseline walking trial at 1.0 ms^{-1} for three minutes. Participants walked for 20 minutes in an experimental trial following the baseline trial with their assigned perturbation. A 20-minute post-experiment trial immediately followed experimental conditions. Split-belt velocities were at 0.75 ms^{-1} for the slow-belt and 1.25 ms^{-1} for the fast belt, with the slow belt placed under the dominant limb of participants in both split-belt groups. We put the passive hip exoskeleton on the dominant limb of the participants in both exoskeleton groups, acting in parallel with the hamstring muscles.

A Vicon 16-camera system recorded kinematic data at 100 Hz. Force data were collected on a Bertec Split-Belt Treadmill at 1000 Hz. We used Visual 3D and MATLAB to process raw data and perform statistical analyses. We used the last 60 seconds of the baseline condition and the first and last 60 seconds of the experimental and post-intervention trials. An alpha level of 0.05 was set for one-way repeated measure ANOVA tests.

Results and Discussion

Figure 1 displays step length symmetry index values across the entire collection period for the participants in the SO group seen in Figure 1 (we created similar graphs for the other two experimental groups). RANOVAs indicated no significant differences across time points for the EO ($p = 0.45$). Significant differences were found in the EXSB ($p = 0.021$) and the SO ($p = 0.0007$) groups across time points. Post-hoc paired t-tests indicated a significant increase in SI values from the baseline to the first 60 seconds of the experimental trial for EXSB ($p = 0.029$) and SO ($p = 0.013$) groups. SI values from the first 60 seconds of the post-intervention trial were not significantly different from the baseline for EXSB ($p = 0.16$) group. In contrast, the SO had significantly higher SI values ($p = 0.028$).

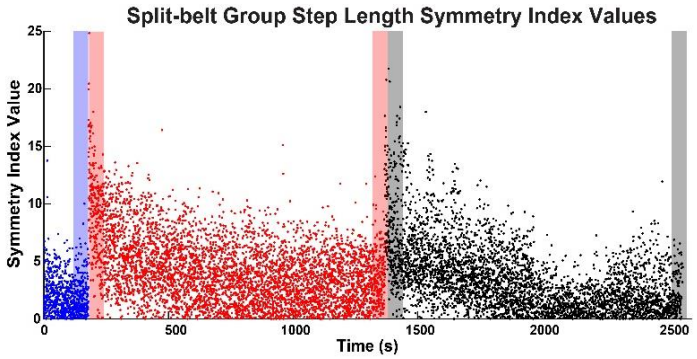

Figure 1: Step length symmetry index (SI) values for the split-belt only group across the entire collection period. Blue dots represent baseline SI values, red dots represent SI values during the experimental intervention, and black dots represent SI values after the intervention was removed. Shaded regions show the 60s areas used for statistical analyses.

These results indicate that wearing the exoskeleton while walking on a split-belt increased step-length SI values compared to baseline in healthy participants. However, typical increases in step length SI after removing the split-belt perturbation did not occur in the EXSB group. The addition of the exoskeleton helped subjects maintain step length symmetry between legs during the post-intervention trial.

Significance

These preliminary results show the potential of a low-cost passive device to influence walking gait asymmetries. Future research may investigate the device's effectiveness as a rehabilitative to reduce asymmetry in patient populations.

Acknowledgments

I want to thank the Office of Research and Creative Activity and the NIH COBRE grant (no. P20GM109090) for helping to fund this project.

References

[1] Feigin VL, et al., *JAMA Neurol* **78**, 165-176, 2021.
[2] Neuman RM, et al., *J Neuroeng Rehabil* **18**, 1-13, 2021.
[3] Lewek MD and Randall EP, *J Neurol Phys Ther* **35**, 116-121, 2011.
[4] Patterson KK, et al., *Arch Phys Med Rehabil* **89**, 304-310, 2008.
[5] Reisman DS, et al., *Neurorehabil Neural Repair* **27**, 460-468, 2013.

MARKERLESS MOTION CAPTURE AND CLINICAL ASSESSMENT YIELD COMPARABLE MEASURES OF SINGLE-LEG HOP PERFORMANCE

Kayla D. Seymore[1,2*], Naoaki Ito[1,2], Elanna K. Arhos[1,2], Haraldur B. Sigurðsson[2,3], Kenneth V. Cruz Rodríguez[2,4], Lynn Snyder-Mackler[1,2], Karin Grävare Silbernagel[1,2]
[1]Biomechanics and Movement Science Program, University of Delaware, Newark, DE, USA
[2]Department of Physical Therapy, University of Delaware, Newark, DE, USA
[3]School of Health Sciences, University of Iceland, Reykjavík, Iceland
[4]Department of Mechanical Engineering, Recinto Universitario de Mayagüez, Mayagüez, Puerto Rico
*email: seymorek@udel.edu

Introduction

The single-leg hop test battery [1] is used to identify readiness to return to sport following injuries, such as anterior cruciate ligament injury and subsequent reconstruction (ACLR) [2,3]. Measures of hop distance and limb symmetry index (LSI) collected in a clinical setting may be insufficient to identify relevant lower limb movement impairments [4]. Markerless motion capture (mocap) is a modern technology with the ability to quantify kinematics without the use of retroreflective markers or extensive setup, making it more feasible in a clinical setting than traditional mocap. Advancements in markerless mocap technology may allow clinicians to readily obtain relevant biomechanics during a hop test, such as knee kinematics. Since the technology is new and has been seldom studied, it is unknown whether using markerless mocap provides comparable measures of hop performance to clinical measures. The purpose of this study was to compare measures of hop distance and limb symmetry collected by a physical therapist to those obtained using markerless mocap.

Methods

Thirty-nine participants with and without a history of knee surgery (22 female, 17 male, 27 healthy, 7 ACLR, 5 other knee surgery, 28±8 years, 171±9 cm, 72±12 kg, 7±4 years since surgery) performed a forward hop for distance as part of the single-leg hop test battery. Eight high speed cameras (Sony RX0-II, Sony Corp., Minato, Japan, 120Hz) were used to collect motion data. The hop test was administered by a licensed physical therapist. Participants were asked to hop as far as possible, starting with their toes behind a marked point, and "stick the landing". Landing position of the heel was used to measure the farthest distance hopped. The hop was performed first on the uninvolved limb then involved limb. The involved limb was defined as the injured or non-dominant limb. Two practice trials preceded two successful hop trials. The average hop distance of two trials was reported for each limb and LSIs were calculated (LSI = [involved limb / uninvolved limb] * 100).

Theia 3D (Theia Markerless Inc., Kingston, Canada) was used to generate 3D model files for each trial. The model files were processed in Visual 3D (v6, C-Motion Inc., Germantown, USA). Take-off and landing events were defined from the velocity of foot segment heel and toe positions. Hop distance was calculated as the linear distance between the toe at take-off and heel at landing.

Limits of agreement (LOA) and percentage error between the markerless mocap and clinical measures of hop distance were calculated and visually inspected with Bland-Altman plots [5,6]. Pearson correlation was used to determine the relationship between LSI for each measurement method. All statistical analyses were performed in SPSS (Version 28, IBM Corp., Armonk, USA). Alpha was set at 0.05.

Results and Discussion

Hop distance measured by a physical therapist and markerless mocap had acceptable agreement [6], with a 4% margin of error between methods. Markerless mocap measured approximately 5 cm greater hop distance than the physical therapist on average (LOA: 1.213-9.456 cm; **Fig. 1**). LSI between methods was strongly (near perfectly), positively correlated (markerless mocap: 99±15% vs clinician: 100±18%, r=0.992, p<0.001). Our data suggests that using markerless mocap can provide clinicians with accurate hop distances and limb symmetry indexes. Markerless mocap's added benefit of joint kinematic data may provide clinicians further insight into patient hop biomechanics. Markerless mocap still requires access to equipment and a spacious facility, as well as setup and data processing time.

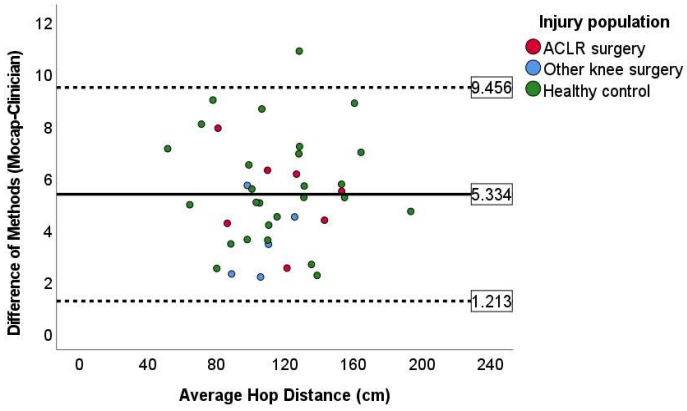

Figure 1: Bland-Altman plot of average difference in hop distance between markerless mocap and clinical measurement methods for each participant. Limits of agreement (dotted line --) shown above and below mean difference (solid line –) pooled for injury population and limb.

Significance

Markerless mocap is an exciting new technology in the field of biomechanics. With the ability to quantify both spatiotemporal and kinematic measures during functional activity, markerless mocap could continue to provide accurate clinical data in addition to informing clinicians of useful patient biomechanics.

Acknowledgments

Theia Markerless Inc. provided the cameras and software used in this research study.

References

[1] Noyes et al., 1991. *Am J Sports Med.* 19:513-18.
[2] Adams et al., 2012. *J Orthop Sport Phys Ther.* 42:601-14.
[3] Grindem et al., 2016. *Br J Sports Med.* 50:804-8.
[4] Wellsandt et al., 2017. *J Orthop Sports Phys Ther.* 47:334-8.
[5] Bland & Altman, 1986. *Lancet.* 1:307-10.
[6] Critchley & Critchley, 1999. *J Clin Monit Comput.* 15:85-91.

BOTULINUM NEUROTOXIN IMPROVES VASTI MUSCLE BALANCE, PATELLAR TRACKING, AND PAIN IN PATIENTS WITH CHRONIC PATELLOFEMORAL PAIN SYNDROME

Saikat Pal[1*], Jang-Hwan Choi[2], Scott Delp[3] and Michael Fredericson[3]
[1]New Jersey Institute of Technology, Newark, NJ, USA
[2]Ewha Womans University, Seoul, South Korea
[3]Stanford University, Stanford, CA, USA
Email: pal@njit.edu

Introduction

Patellofemoral (PF) pain syndrome is common, accounting for 1 in 4 knee injuries diagnosed in sports medicine clinics [1]. A possible mechanism of PF pain is elevated stress at the cartilage-bone interface due to excessive lateral tracking of the patella arising from an imbalance in the vasti muscles [2]. A promising treatment to alleviate PF pain is injection of botulinum neurotoxin type A (BoNT-A) into the distal third of the vastus lateralis (VL) muscle [3]. BoNT-A is theorized to weaken the VL muscle, resulting in improvement in VL:VM (vastus medialis) muscle balance, patellar tracking, and pain. Prior studies have reported improvements in PF pain following BoNT-A treatment [3, 4]; however, evidence of improvements in VL:VM muscle balance and patellar tracking is sparse. The **purpose** of this study was to quantify the effects of BoNT-A on VL:VM muscle balance, patellar tracking, and pain score in patients with chronic PF pain. We tested three hypotheses: BoNT-A in combination with a 6-week home exercise program 1) reduces VL:VM cross-sectional area (CSA) ratio; 2) reduces lateral patellar maltracking (patellar tilt and bisect offset); and 3) improves pain score.

Methods

We recruited 13 (9F, 4M) participants with chronic PF pain (>6 months) who failed conservative treatment. All participants were between 18-50 years of age and reported pain scores >3/10 on a visual analog scale during specific physical activities.

All participants underwent ultrasound-guided BoNT-A injections to the distal third of the VL muscle followed by a 6-week home exercise program to strengthen their VM muscle. We obtained the following outcome measures pre and post BoNT-A + home exercise: **1)** VL:VM CSA ratio from C-arm cone-beam computed tomography (CT) scans during non-weight-bearing condition with the knee at full extension. An axial slice at the level of the distal appearance of the rectus femoris muscle was created, and VL and VM CSAs were manually outlined. **2)** Patellar tilt and bisect offset values from C-arm CT scans during upright, weight-bearing condition with the knee at full extension. An oblique-axial plane intersecting the center of the patella and the most posterior points of the femoral condyles was created. Patellar tilt is the measure of the angle formed by lines joining the posterior femoral condyles and the maximum width of the patella. Bisect offset describes the percentage of the patella lateral to the midline of the femur. **3)** Functional pain score during daily activities using the Anterior Knee Pain Scale [5]. In addition, we obtained pain scores 2 to 4 years post intervention.

All participants were classified into normal tracking and maltracking groups based on their patellar tilt and bisect offset values [2]. Differences in outcome measures pre and post BoNT-A + home exercise were assessed using one-tailed, paired sample *t* tests (if data passed normality) or Wilcoxon signed rank tests (if data failed normality). A one-way repeated measures ANOVA was used to test the effect of the intervention at two time points post intervention, followed by post hoc comparisons.

Results and Discussion

BoNT-A + home exercise resulted in 18% ($p < 0.001$) reduction in VL:VM CSA ratio (Fig. 1A). The reduction was driven by participants classified as maltrackers (21%, $p < 0.001$, Fig. 1B).

BoNT-A + home exercise resulted in 19% ($p = 0.020$) and 5% ($p = 0.025$) reductions in patellar tilt & bisect offset, respectively (Figs. 1C, 1E). The reductions were only in maltrackers (patellar tilt: 26%, $p = 0.001$, Fig. 1D; bisect offset: 8%, $p = 0.014$, Fig. 1F). Next, change in bisect offset was associated with change in patellar tilt ($R^2 = 0.650$, $p < 0.001$, Fig. 1G). Four participants classified as maltrackers transitioned to normal tracking after the intervention (Fig. 1G).

The repeated measures ANOVA produced a significant effect at the two time points post intervention ($F(2, 22) = 9.86$, $p = 0.004$, Fig. 1H). Post hoc comparisons showed pain scores improved immediately after intervention (13%, $p < 0.001$) and remained improved at 2+ years follow up (12%, $p = 0.011$).

Significance This study provides new evidence in support of BoNT-A for treatment of chronic PF pain. The results showed improvements in vasti muscle balance, patellar tracking, and pain only in maltrackers classified under weight-bearing; we observed no such differences when participants were classified under non-weight-bearing condition. This suggests that classification of PF pain patients under weight-bearing condition may identify the individuals who will most benefit from BoNT-A treatment.

References [1] Devereaux et al., 1984. *Br J Sports Med*. 18; [2] Pal et al., 2011, *Am J Sports Med*. 39; [3] Singer et al., 2011. *Br J Sports Med*. 45; [4] Silbert et al., 2012. *Disabil Rehabil*. 34; [5] Kujala et al., 1993. *Arthroscopy*. 9.

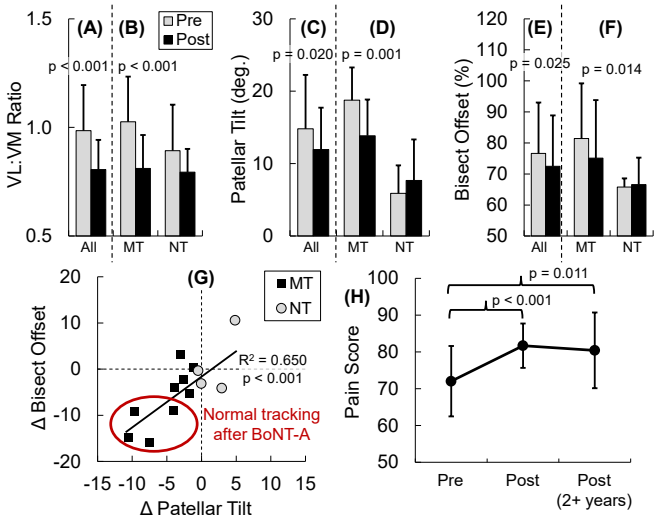

Average (+1 SD) VL:VM CSA ratio (A, B), patellar tilt (C, D), and bisect offset (E, F) from pre and post BoNT-A + home exercise intervention from (A, C, E) all participants and (B, D, F) participants classified into maltracking (MT) and normal tracking (NT) groups. (G) Relationship between change in patellar tilt and change in bisect offset. (H) Average (±1 SD) pain scores from pre, post, and 2+ years follow up.

Tibiofemoral joint contact characteristics from MRI during weightbearing with lateral wedge insoles for knee osteoarthritis

Calvin T.F. Tse [1,2], Michael B. Ryan[2], Michael A. Hunt[1*]
[1]Motion Analysis and Biofeedback Laboratory, University of British Columbia, Vancouver, BC
[2]Kintec Footlabs Inc., Surrey, BC
email:* michael.hunt@ubc.ca

Introduction

Poorly distributed joint loading is a recognized risk factor for progression of joint degradation associated with tibiofemoral osteoarthritis (TFOA) [1]. Lateral wedge insoles (LWI) are shoe inserts that alter the interaction between the foot and the ground and have been well documented to reduce the external knee adduction moment [2] – an indirect measure of knee joint load distribution. Currently, little is known about how LWI affects the internal tibiofemoral loading environment. A previous study used upright open magnetic resonance imaging (openMRI) to evaluate tibiofemoral joint contact of patients with TFOA during upright standing with and without a lateral heel wedge [3]. However, investigations involving sulcus length LWI and weightbearing postures emulating the midstance period of gait would better represent the effect of LWI interventions during activities of daily living.

Methods

Eligible participants had knee pain and radiographically confirmed TFOA, primarily in the medial compartment. A 0.5T openMRI scanner took coronal slice images of the knee with participants weightbearing with orthotic insoles, in a posture that mimicked the foot flat period of the stance phase of gait (Fig. 1). Participants maintained 90% bodyweight throughout all scans, aided by real-time visual feedback of the vertical force beneath the stance limb. The imaging order of four insoles was randomized: flat control insole (FLAT), 5° LWI (WEGD), custom arch support (V-ARCH), arch supported LWI (WEDG+V-ARCH).

Figure 1*. Participant posture during imaging in openMRI*

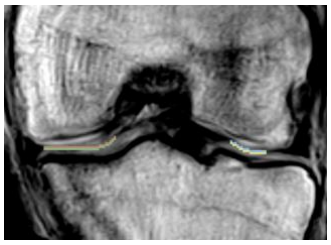

Figure 2. *MRI slice with tibia and femur contact segments highlighted in coloured pixels.*

Areas of tibiofemoral joint contact were identified in Slicer (Fig. 2) and joint contact outcomes were calculated for each compartment. Contact area was the product of the number of contact voxels with the voxel dimensions. Contact centroid was calculated as the mathematical mean location of contact voxels, and registered and normalized to tibial plateau dimensions. A centroid value of zero in the medial-lateral (M-L) and antero-posterior (A-P) directions corresponded to the medial and posterior boundaries, respectively. Differences between insole conditions for each outcome were compared with repeated measures ANOVA and pairwise comparisons.

Results and Discussion

Fourteen patients with TFOA (3M/11F; mean age = 61.8 [5.6] years; KL1-2-3-4 = 0-9-4-1) completed openMRI scans in all insoles. Table 1 summarizes the joint contact outcomes between insole conditions. Contact area in the medial compartment was significantly increased with WEDG only, and unchanged in the lateral compartment with any insole when compared to FLAT. A greater surface area of contact may distribute an identical load over a greater area and help unload the medial compartment by minimizing focalized pressure peaks.

Contact centroids in the medial and lateral compartments were not significantly different between any insoles. Previous research has shown that LWI have minimal effect on modifying the frontal plane knee angle during gait [2]. Added to our finding of unchanged M-L contact centroid locations with insoles may be another indication of the small effect that LWI have on modifying knee position.

Significance

This research that explored openMRI-based outcomes of the weightbearing knee in a posture that mimics gait provided a functionally relevant in vivo assessment of the internal tibiofemoral loading environment while using LWI. The observed increase in medial compartment contact area adds to previous reports of the dynamic load modifying effects of LWI to better understand their mechanisms of treatment for TFOA.

Acknowledgments

Authors were supported by the Canadian Institutes of Health Research, Natural Sciences and Engineering Research Council of Canada, and the Pedorthic Research Foundation of Canada.

References

[1] Andriacchi et al 2015. *Ann Biomed Eng*. 43(2): 376-387.
[2] Shaw et al., 2018. *Br J Sports Med*. 52(4): 238-253.
[3] Barrance et al., 2014. *Clin Biomech*. 29(9): 997-1002.

Table 1. Medial and lateral compartment tibiofemoral joint contact characteristics for each insole condition.

Joint Contact Outcome	FLAT	WEDG	V-ARCH	WEDG+V-ARCH
Medial Contact Area (mm^2)	499.7 [196.0]	**561.6 [210.2]**	547.1 [212.4]	575.5 [206.8]
Lateral Contact Area (mm^2)	327.0 [166.6]	323.1 [143.7]	307.6 [145.0]	321.2 [144.4]
Medial Contact Centroid M-L (% Tibia Width)	20.4 [2.8]	20.5 [2.4]	20.4 [2.3]	20.6 [2.5]
Lateral Contact Centroid M-L (% Tibia Width)	70.6 [4.4]	70.1 [4.9]	70.7 [5.2]	70.5 [4.5]
Medial Contact Centroid A-P (% Tibia Depth)	52.3 [6.4]	49.9 [6.4]	50.8 [8.0]	52.0 [5.6]
Lateral Contact Centroid A-P (% Tibia Depth)	55.4 [7.0]	54.3 [6.0]	53.2 [8.2]	54.9 [5.7]

Values reported as mean [standard deviation]. **Bolded values** indicate a significant difference compared to FLAT ($p < 0.05$).

AMBULATORY STATUS IN ACUTE SPINAL CORD INJURY IMPACTS THE EFFICACY OF ZOLEDRONIC ACID TO ATTENUATE CHANGES IN HIP BONE DENSITY AND STRENGTH

Laura E. Crack[1*], Ifaz T. Haider[1], Joana Barroso[2], Narina Simonian[2], Thomas J. Schnitzer[2], and W. Brent Edwards[1]
[1]University of Calgary, Faculty of Kinesiology, Human Performance Lab
[2]Northwestern University Feinberg School of Medicine, Department of Physical Medicine and Rehabilitation
email: laura.crack@ucalgary.ca

Introduction

Bone loss leading to skeletal fracture is a well-known complication of spinal cord injury (SCI)[1]. The bone loss occurs below the level of neurological lesion from a combination of neurogenic changes and mechanical disuse. We recently demonstrated the efficacy and safety of a once-yearly infusion of zoledronic acid (Zol) to attenuate bone loss after SCI[2]; however, the influence of ambulatory status was not examined. The objective of this study was to investigate the effect of Zol and ambulatory status on bone and strength changes in acute SCI. We hypothesized that Zol would mitigate bone and strength loss, and that participants with greater ambulation would demonstrate less bone and strength loss than their non-ambulatory counterparts.

Methods

Sixty participants with acute SCI (<120 days after injury) were recruited for a double-blind, placebo-controlled trial, registered at clinicaltrials.gov (NCT02325414). The study was open to both males and females, but approximately 80% of participants were male. Upon entrance into the study, participants underwent baseline testing, which included a CT scan of the hip and the Walking Index for SCI II (WISCI) to assess ambulatory status. Participants were then randomized into two groups. Thirty participants were given an intravenous zoledronic acid (5 mg), and thirty participants were given matching placebo (saline). The sixty participants were subsequently followed for one year with re-assessment of the hip and WISCI score at 6- and 12-months. CT scans taken at each time point were segmented to quantify trabecular bone mineral density (BMD) and cortical bone mineral content (BMC) at the femoral neck and trochanteric regions. Bone strength was calculated for each region using a Compressive Strength Index (CSI) that integrated BMD and geometry information. A repeated measures generalized linear model was used to determine statistical differences as a function of treatment group over the year following treatment and WISCI score (as a proxy measure of ambulation status).

Results and Discussion

A significant interaction ($p<0.01$) between treatment group and time from baseline, while controlling for WISCI score as a covariate, was observed for trabecular BMD and cortical BMC at the trochanteric region and trabecular BMD at the femoral neck, but not cortical BMC. Participants receiving placebo experienced a decrease in BMD over the year. According to the estimated marginal means, non-ambulatory participants (WISCI=0) in this group experienced the greatest loss in BMD (approximately 8%), while ambulatory participants (WISCI=20) experienced BMD loss to a lesser extent (approximately 2-3%). Conversely, the group receiving Zol experienced some BMD loss in non-ambulatory participants (approximately 3%) and no loss in BMD among ambulatory participants. Non-ambulatory participants receiving placebo experienced the greatest loss of trochanteric cortical BMC (approximately 4%), while Zol users saw no loss in BMC, regardless of ambulatory status.

In the placebo group, loss of compressive bone strength was demonstrated with a significant treatment group and time from baseline interaction (Figure 1;$p<0.001$). Based on estimated marginal means, the greatest loss of compressive strength was seen the placebo group, especially among non-ambulatory participants (approximately 10%). Within the Zol group, non-ambulatory participants demonstrated a decline in compressive strength (3-5%), while ambulatory participants experienced a minimal gain in compressive strength (less than 1%).

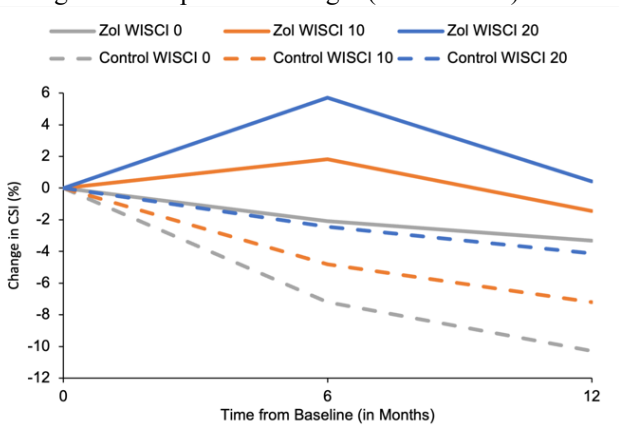

Figure 1: Comparison of the change in compressive strength index at the femoral neck from baseline by ambulatory status in the Zol and placebo groups.

These findings suggest that both administration of Zol and greater ambulation status after SCI have mitigating effects on bone and strength loss. Thus, people with SCI who receive an infusion of Zol at the time of their injury and regain ambulation over the first year experience the strongest protective effect against bone and strength loss. Those who receive a Zol infusion and do not regain ambulation still experience attenuating effects, but to a lesser extent and may remain at risk for significant bone density and strength loss and associated complications.

Significance

Bone loss after SCI is a source of considerable morbidity, and in some cases mortality, for which there is no current standard of care. This work suggests that Zol has the potential to mitigate bone loss after SCI, but the degree of personal ambulation has an impact on drug treatment efficacy. Other treatments may be required in tandem with Zol for those individuals who do not regain ambulation, and therefore, experience greater bone loss after SCI.

Acknowledgments

This research was supported by Department of Defense U.S. Army Medical Research and Materiel Command (grant # SC130125).

References

1. Biering-Sorensen, F. et al. Eur J Clin Invest. 1990;20(3). 2. Edwards, W.B. et al. J. Bone Miner. Res. 2021; 00.

QUANTIFYING THE CONTRIBUTION OF DIETARY MINERAL INTAKE TO CORTICAL BONE MECHANICAL PROPERTIES UNDER COMPRESSIVE LOADING USING FINITE ELEMENT ANALYSIS

Mahsa Zojaji[1], Tyler Rowsell[2], Mandy E. Turner[2], Austin P Lansing[2], Rachel M Holden[2], Michael A Adams[2], Heidi-Lynn Ploeg[1]
[1,2] Queen's University, Kingston, ON, Canada;
email: 18mz62@queensu.ca

Introduction

Chemical composition alters the mechanical behaviour of cortical bone in rat models [1]. Hydroxyapatite (HA) is the main bone mineral component consisting of calcium (Ca) and phosphate (P) where the ratio of Ca to PO_4 ranges from 1.37 - 1.87 in healthy bones [2]. The normal regulation of bone mineral metabolism becomes altered in common bone disorders such as osteoporosis and chronic kidney disease (CKD) [1]. Dietary PO_4 intake has increased substantially in North America over the past 20 years due to widespread use of inorganic PO_4 food additives. Foods containing phosphate additives have low Ca:PO_4. Considering the load-bearing property of cortical bone, the mechanical behaviour of the cortical bone needs to be assessed in situations when the relative proportions of minerals in the diet vary. The purpose of this study was to determine whether, in a rat model of CKD, changes in the dietary Ca:PO_4 altered the compressive stiffness of cortical bone. This was accomplished using finite element analysis (FEA) on micro computed tomography (µ-CT)-based finite element (FE) models of rat tibias.

Methods

The left tibias of 30 male Sprague-Dawley rats (14 weeks old; 400-450g, N=10 per dietary group: Ca:$P0_4$ 0.3%:0.5%, 1.2%:1.0%, and 0.6%:0.5% for the normal group) (Hilltop Lab Animals Inc. PA, USA) were excised and stored in acetone at 4°C. The proximal region of the tibia was scanned *ex vivo* using a micro-CT (VECTor4CT, MILabs, Utrecht, NL). Images were reconstructed with a voxel size of 10 µm (MILabs Rec software, MILabs, Utrecht, NL) and binarized (Fig. 1 Left) to separate bone from background using the BoneJ plug-in available in ImageJ showing representative images of the dietary interventions [3,4]. Using the thickness map (Fig. 1 Right b), cortical bone borders were identified and segmented using a MATLAB algorithm [3].

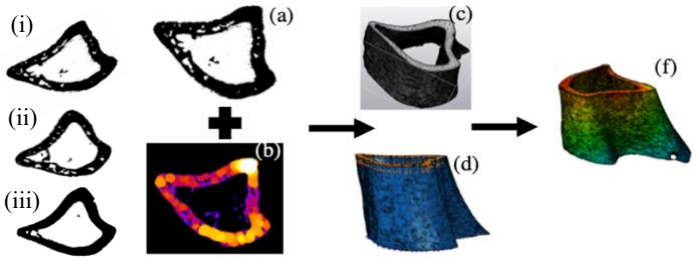

Fig. 1: Left: Binary images of cross-sections of rat tibias modified with Ca:$P0_4$: (i) 0.3%:0.5%, (ii) 1.2%:1.0%, (iii) 0.6%:0.5% (normal). Right: Workflow of generating µ-CT-based FE models: (a) Binary image (b)Thickness map (c) 3D STL model (d) FE-model with boundary conditions (f) FEA displacement results from compression test.

Apparent density (ρ_{app}, g/cm^3) of each model was calculated using HA phantom calibration. Apparent elastic modulus (E, MPa) of 5,253 MPa, 7,087 MPa, and 12,237 MPa were assigned to the tibias with Ca:$P0_4$ of 0.3%:0.5%, 1.2%:1.0%, and 0.6%:0.5% for the control group, $E = 3711.4(\rho_{app})^{1.87}$ [5]. A mesh with 10-node quadratic tetrahedral elements was generated (Abaqus CAE/2017) for one representative bone in each group. The proximal end of the FE model was fixed, and an axial displacement of 0.08 mm was applied to the distal end (Fig. 2.d) [5,6]. Stiffness was calculated as a ratio of maximum reaction force to the maximum deflection.

Results and Discussion

In comparison to the FEA stiffness of the bone from the normal group, the FEA stiffness of the representative bones from the groups with 1.2%Ca:1.0%PO_4 and 0.3%Ca:0.5%PO_4 were 46% and 60% lower (Fig 2.). This difference is due to the change of material properties and bone structure. The current study showed compressive cortical bone stiffness was related to dietary Ca:PO_4 intake. In comparison to the normal diet group's cortical porosity (0.29±0.048%), the cortical porosity in the 1.2%Ca:1.0%P and 0.3%Ca:0.5%P experimental groups were 0.40±0.052% and 0.47 ±0.058%, respectively.

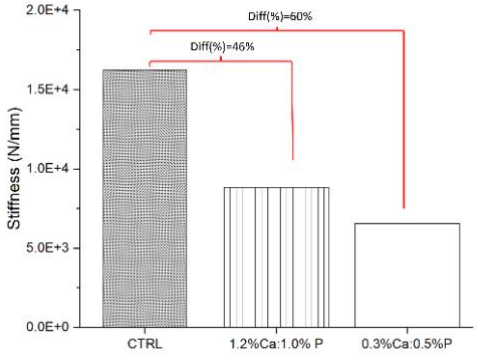

Fig. 2: Stiffness predicted with FEA for dietary groups (Ca: PO_4 0.6% 0.5%, 1.2%:1.0% and 0.3%:0.5%.

Further investigation is needed to verify and validate these results. Future work includes *in silico* assessments of flexural rigidity and bending strength in each model will be assessed.

Significance

Bone mechanical properties, bone mineral density, and cortical bone chemical composition are commonly assessed in clinical and preclinical trials to diagnose bone disorders and predict fracture risk. A better understanding of relationship between bone mechanical behaviour and dietary mineral intake may inform the treatment of common bone diseases. Further investigation is needed to study the impact of increasing dietary intake of inorganic PO_4 and its ratio to Ca on the mechanical behaviour of bones [7].

Acknowledgments

We acknowledge the support of Queen's Bone and Joint Biomechanics Lab, Centre for Health Innovation, Kingston Health Sciences Centre, Natural Sciences and Engineering Research Council of Canada (NSERC), and Dr. Kimberly A. Woodhouse Fellowship, funding from the Translational Institute of Medicine at Queen's University, Kingston, ON and the Queen's Cardio Pulmonary Unit.

References

[1] Iwasaki et al., 2011, *J Bone*, 48 (6):1260-1267.
[2] Shaker et al., 2018, *Endotext.*, MDText.com, Inc; 2000.
[3] Ang et al., 2018, *engrXiv*, engrxiv.org/w86ke.
[4] Doube et al., 2010, *J Bone* 47(6):1076-9.
[5] Zhao et al., 2018, *J Bone Joint Res*. 7(8):524-538.
[6] Cory et al., 2010, *J Biomech*. 43:953–960
[7] Hench et al., 2002' *J* Science, 5557(295)104.

A CRITICAL EVALUATION OF CORTICAL BONE FRACTURE TOUGHNESS TESTING METHODS

Daniel Y. Dapaah and Thomas L. Willett*
Systems Design Engineering, University of Waterloo, Waterloo, Ontario, Canada
Corresponding authors' email: *thomas.willett@uwaterloo.ca

Introduction

Fracture mechanics approaches have been used for more than three decades to quantify the fracture resistance of cortical bone. The J-integral Resistance (J-R) curve as defined in ASTM E1820 [1] is currently the most widely used method for cortical bone fracture toughness quantification. Because a single sample is used, an important component of this method is the accurate tracking of the crack extension. An inexpensive approach known as the unloading compliance method has been widely used to tackle this including with cortical bone. This approach uses the unloading compliance (UC) from a series of unload-reload cycles during the fracture test to estimate the crack extension through a standard calibration equation. However, because cortical bone is a viscoelastic micro-damaging material [2,3], it violates two of the assumptions for this method being: no energy loss during the unload-reload cycles and changes in unloading compliance should only be due to crack extension.

Here, we show that the use of the unloading compliance method inaccurately estimates the crack extension, leading to roughly 26-49% overestimation of various fracture toughness measurements of bovine cortical bone compared to the standard optical approach.

Methods

Ten paired single edged notched bend (SENB) samples of dimension ~50mm×4mm×4mm were prepared from five young steer tibiae. All samples underwent a 3-point fracture test during which a microscope mounted on a digital camera took images of the crack tip region. This allowed optical measurement of crack extension. However, from each pair, one underwent a fracture test involving a series of unload-reload cycles at regular intervals while the other was continuously loaded until fracture/instability.

For each pair, three different J-R curves were developed by combining one of the testing regimes and determining crack extension either by the UC method or optically as detailed below:

Approach name	Testing regime	Crack extension
UC	Unload-reload	UC
OMC	Unload-reload	Optically
Optical	Continuous loading	Optically

From each J-R curve, three parameters: the crack initiation toughness (J_{IC}), propagation toughness (T_R) and fracture toughness at instability (J-int) were computed (Figure 1). Further, the crack extension between the UC and OM-C approaches were compared and reported as mean absolute percentage error (MAPE).

Two tailed paired t-tests were used to test for statistical differences between any two of the three approaches for all three fracture toughness parameters.

Results and Discussion

A MAPE of 72.8±39.2 % (mean ± SD) was obtained between the crack extension measures for OM-C and UC approaches which is greater than the15% error allowance stated in ASTM E1820 [1] indicating the inaccuracy of the UC method.

There was a statistical difference between the UC and Optical approaches for all three fracture toughness parameters (see Table 1). The lack of statistical difference between OM-C and UC approaches seems to suggest this difference is the combined errors of crack extension estimated by the UC method and the energy loss due to unload/reload cycles. OM-C is statistically different from Optical only for J-int most likely because, at this point, the energy lost due to unload/reload cycles is sufficient to detect a difference.

There is ongoing work to extend this to human cortical bone samples.

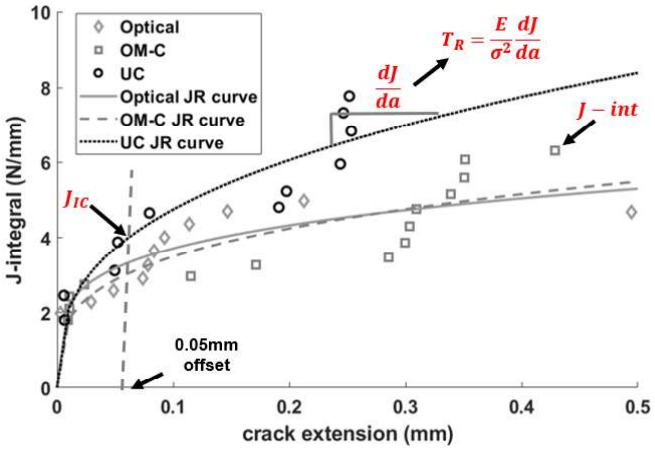

Figure 1: Representative J-R curves for the three approaches as well as illustration of the fracture toughness parameters.

Table 1: Fracture toughness measurements for bovine samples.

	J_{IC} (N/mm)	T_R	J-int (N/mm)
UC	2.92±1.63*	4.61±3.46*	5.36±1.61*
OMC	2.83±0.73	2.66±1.16	4.90±1.27*
Optical	2.31±0.71**	2.36±1.30**	4.10±1.15**

* Statistical difference from Optical
** Statistical difference from UC

Significance

This study highlights the need to critically consider how fracture toughness methods for engineering materials are translated for use in cortical bone studies. Using appropriate as well as accurate approaches for fracture toughness determination in cortical bone is important to understanding how changes in the bone tissue affects its fracture resistance. Such understanding is imperative towards finding key determinants for bone fragility and fracture.

Acknowledgments

The authors thank the CIHR, CFI, ORF and the NSERC Training in Global Biomedical Technology Research and Innovation for research grant and student funding.

References

[1] ASTM. Standard Test Method for Determining J-R Curves of Plastic Materials. ASTM Stand Test Method 2013
[2] Anderson TL. Fracture mechanics: Fundamentals and Applications. Boca Raton: CRC Press LLC; 2005.
[3] Currey JD. The structure and mechanics of bone

PASSIVE FORCE ENHANCEMENT IS NOT ABOLISHED BY MUSCLE SHORTENING

Shuyue Liu[1*], Heron Baptista de Oliveira Medeiros[2], Heiliane de Brito Fontana[2] and Walter Herzog[1]
[1]Human Performance Laboratory, Faculty of Kinesiology, University of Calgary, Calgary, Canada
[2] Department of Morphological Sciences, Federal University of Santa Catarina, Florianópolis, Brazil
email: *shuyliu@cucalgary.ca

Introduction

Passive force enhancement is a mechanical property of skeletal muscle that was discovered about two decades ago [1]. It is defined as the increase in steady-state passive force observed following stretching of an active muscle compared to the corresponding passive force following stretching of the same muscle to the same length passively. Passive force enhancement is considered an important contributor to the residual force enhancement property [4]. However, the molecular mechanisms producing the passive force enhancement remain unknown. It has been proposed that titin, a large, spring-like protein in sarcomeres might be responsible for passive force enhancement by increasing its stiffness when a muscle is actively stretched [2]. The stiffness of titin can be increased in two conceptual ways: (i) by calcium binding to titin, thus increasing molecular bond strengths [3]; and (ii) by binding of proximal segments of titin to a rigid filament (actin), thus shortening titin's free spring length [4].

In 2003, Herzog et al. [5] showed that passive force enhancement is long lasting (minutes). However, casual observation revealed that the passive force enhancement was abolished instantaneously when the (cat soleus) muscle was shortened to its original length and stretched back to the final length where the passive force enhancement had occurred. This serendipitous observation provided important clues about the molecular mechanisms causing passive force enhancement, but it was never repeated and tested systematically.

The purpose of this study was to test whether the passive force enhancement could indeed be abolished instantaneously using a mechanical trigger, i.e., shortening a muscle fibre to its original length. We hypothesized, in analogy with the incidental observation made on the cat soleus muscle, that passive force enhancement is an inherently long-lasting property but is abolished instantaneously by shortening a muscle to its pre-stretched length.

Methods

Skinned single fibres (n = 19) from New Zealand white rabbit psoas muscles were used for all testing. Each fibre was stretched passively first and an actively second from an average sarcomere length of 2.4 µm to 3.6 µm. In the passive tests, after force reached a steady-state at 3.6 µm, fibres were exposed to three passive shortening-stretch cycles from 3.6 to 2.4 and back to 3.6 µm (Figure 1). The first shortening-stretch cycle occurred in 200 ms, the second in 6 s and the third in 14s. Force at steady-state after each shortening-stretch cycle was recorded and compared to the forces in the active stretch protocols and between the different shortening-stretch cycles. In the active stretch experiment, fibres underwent the same protocol as for the passive experiments, except that fibres were stretched while activated and deactivated 30 s after the end of the active stretch. Forces were normalized to the fibre cross-sectional area and expressed as Stress (mN/mm^2).

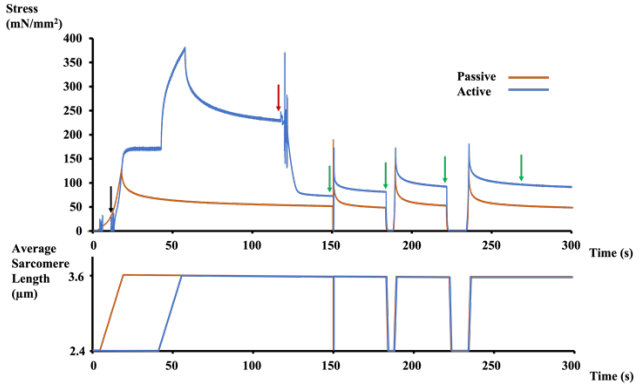

Figure 1: Stress-time curves and sarcomere length-time for an exemplar fibre undergoing passive (orange) and active (blue) stretching. The black arrow indicates the instant of activation and the red arrow the instant of deactivation. Force measurements were made as indicated by the green and red arrows.

Results and Discussion

The average stress of fibres after active stretch at a sarcomere length of 3.6 µm was 198 ± 16 mN/mm^2, and the stress after deactivation was 85 ± 6 mN/mm^2. The corresponding average stress at the steady state after passive stretching was 52 ± 4 mN/mm^2. There was a significant increase in passive force after the active compared to the passive stretch protocols indicating a substantial amount of passive force enhancement. Stress following the passive stretches remained the same after all shortening-stretch cycles, while passive stress increased with increasing duration of the shortening-stretch cycles in the actively stretched fibres (91 ± 7, 99 ± 7, and 102 ± 7 mN/mm^2 respectively), resulting in an increase in the passive force enhancement over time.

In complete contrast to our hypothesis, passive force enhancement was not abolished by fibre shortening to its original length. Rather, force enhancement increased with the duration of the shortening-stretch cycle indicating a recovery of passive force that only occurred in the actively stretched fibres.

Significance

The results of this study point to a fundamental recovery property of passive force enhancement not previously observed that is favoured by short sarcomere lengths and time. It resembles the refolding characteristics of titin's PEVK and immunoglobulin domains, a hypothesis to be tested in future experiments.

Acknowledgments

NSERC, CIHR, The Killam Foundation, Canada Research Chair Programme, NIH, ISB and ELAP.

References

[1] Herzog and Leonard, 2002. *J. Exp. Biol.*, 205:9, 1275–1283.
[2] Leonard and Herzog, 2010. *Am. J. Physiol.* 299:1, C14–C20.
[3] Labeit *et al.*, 2003. *PNAS*, 100:23, 13716–13721.
[4] Edman et al. 1982. *J. Gen. Physiol.*, 80:5, 769–784.
[5] Herzog et al. 2003. *J. Exp. Biol.*, 206:20, 3635–3643.

FRACTURE OF BLOOD CLOT: EFFECTS OF LOADING RATE, RED BLOOD CELL AND PLATELET

Shiyu Liu[1], Farshid Ghezelbash[1], Aram Bahmani[1], Zhen Yang[1], Zhenwei Ma[1], Guangyu Bao[1] and Jianyu Li[1*]
[1]Department of Mechanical Engineering, McGill University, Montréal, Québec, Canada
email: *jianyu.li@mcgill.ca

Introduction

Blood clots form at injury sites (i.e., hemostasis) or inside blood vessels (i.e., thrombus). They can fail mechanically via crack propagation within the bulk of the clot (cohesive failure; Fig. 1) or at the interface between the clot and neighbouring tissues (adhesive failure; Fig. 1). The clot fracture might lead to fatal conditions such as haemorrhage, embolism and stroke [1]. Comprehending the fracture behaviour (cohesive/adhesive) of blood clots is critical to uncover root causes of related disorders, as well as to develop therapeutic interventions. Recent studies shed a light on the cohesive fracture of blood clots [1-3] however few works to date on its adhesive fracture. In this study, we employed a holistic framework to characterize cohesive and adhesive fracture behaviours of blood clots, and investigated the effects of loading rate, red blood cell (RBC) and platelet (PLT) on the fracture of bovine blood clots.

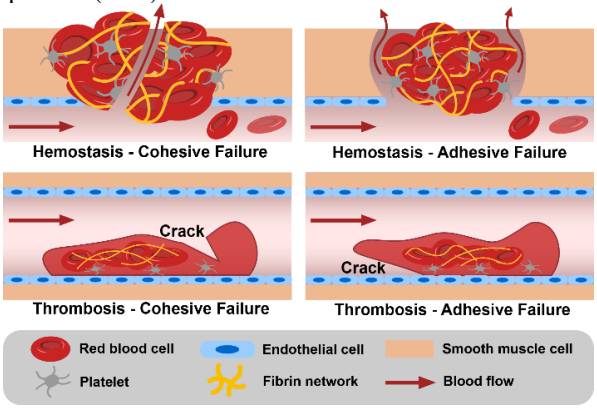

Figure 1: Schematic illustrations of the cohesive and adhesive failure of the blood clot in hemostasis (top) and thrombosis (bottom)

Methods

To characterize cohesive fracture of bovine blood clots as function of loading rate, we carried out pure shear tests to determine fracture energy, commonly used for soft materials such as hydrogels [2]. Adhesion energy of blood clots on various substrates (e.g., skin, muscle) was measured with varying loading rates in 90o peeling tests [2]. While the fibrin content was fixed, blood clots with varying RBC and PLT contents were prepared and tested to evaluate their mechanical properties (i.e., fracture energy, adhesion energy, stiffness, and hysteresis). Scanning electron microscopy (SEM) was used to determine likely structural differences due to variations in RBC and PLT. Finally, we developed and validated a rate-independent finite element model, capturing cohesive and adhesive failure in the blood clots.

Results and Discussion

The measured fracture energy of the bovine blood clot (18.3 ± 1.4 J/m^2; Fig. 2A) was substantially higher than its adhesion energy on all tissues tested (maximum for muscle: 5.6 ± 2.1 J/m^2; Fig. 2B). The results demonstrate that blood clot is more predisposed to adhesion failure under physiological conditions. As a poroviscoelastic material [4], the blood clot showed marked rate-dependence for cohesive fracture (18.3 ± 1.4 J/m^2 vs 38.1 ± 8.7 J/m^2 for 1% and 100% loading rate; Fig. 2B). Interestingly, the effect of loading rate was much less pronounced for the adhesion energy (1.6 ± 0.1 J/m^2 vs 2.6 ± 1.4 J/m^2 for 1% and 100% loading rate on skin). Increasing the RBC content in the whole blood from 30% to 70% augmented cohesive (82%) and adhesive (81%) fracture energy, Fig. 2C. PLT induced more contraction and residual stresses in the clot; therefore, higher PLT content was inversely proportional to cohesive fracture toughness. However, since PLT has strong adhesion to collagen, increasing PLT content significantly increased the adhesion energy (Fig. 2D); SEM images showed mixed failure conditions of cohesive and adhesive for higher PLT content under peeling tests. Our finite element model accurately predicted loading/unloading responses of the blood clot under tension and compression as well as cohesive and adhesive crack propagation in pure shear and 90° peeling tests.

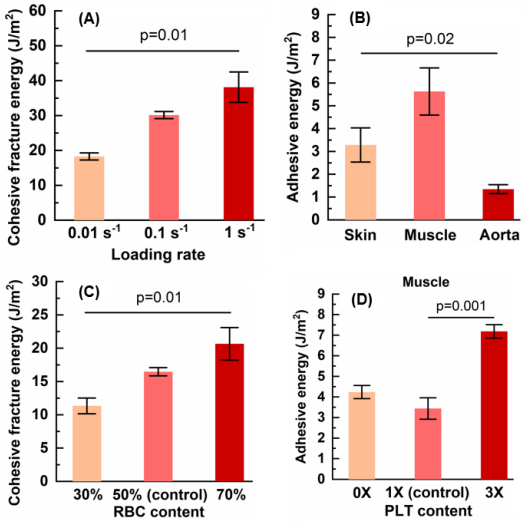

Figure 2: Cohesive fracture energy at various (A) rates and (C) RBC content. Adhesion energy of blood clots for different (B) substrates and (D) PLT contents. At each group, n=4; ANOVA was used to estimate p-values.

Significance

The mechanical integrity of the blood clot facilitates hemostasis and prevents life-threatening conditions as a result of cohesive/adhesive crack propagation in thrombus. Here, we quantified comprehensively cohesive and adhesive fracture properties of the clot under different physiologically relevant conditions (e.g., loading rate, RBC/PLT content). This study highlights the importance of improving adhesion properties of the blood clot as therapeutic strategies for hemostasis.

Acknowledgments

Supported by NFRF-Exploration and FRQNT-Team grants.

References

[1] Tutwiler et al., 2020, *Sci. Adv.*, 6(35), eabc0496.
[2] Liu et al., 2021, *Extreme Mech. Lett.*, 48:101444.
[3] Fereidoonnezhad et al, 2021, *Acta Biomater.*, 127: 213-228.
[4] Ghezelbash et al, 2021, *JMBBM*, Under Review.

EFFECTS OF CEMENT LINE GEOMETRY & PROPERTIES ON XFEM CRACK PROPOGATION IN TRABECULAE

Pavel Rahovich[1], Krishna S. Challagulla[1], W. Brent Lievers[1*],
[1]Bharti School of Engineering and Computer Science, Laurentian University, Sudbury, Ontario, Canada
email: *blievers@laurentian.ca

Introduction

The ageing population faces a higher risk of bone fracture. The majority of these fractures occur in skeletal regions that have large proportions of trabecular bone such as the vertebrae, hip, and forearm [1]. Therefore, it of interest to understand how changes to the architecture and microstructure of trabeculae with age may affect fracture risk.

Trabeculae are composed of small regions called bone structure units (BSUs), separated from each other by a thin layer of cement line, that develop due to remodelling activity. The cement line is considered to be a highly mineralized material that is stiffer and more brittle than the surrounding tissue. Recent work [2] has shown that the size of BSUs decrease with age, leading to an increased proportion of cement line in the trabeculae. However, the consequences of these changes on crack propagation remain unknown.

Therefore, this study investigates the role of the cement line geometry and material properties on the strain-to-failure of an idealized 2D trabecula.

Methods

A 300x150µm 2D region of trabecular tissue was represented as a set of 120x50µm hexagonal BSUs (Fig. 1). The sidewall angle (θ) was varied to test how this parameter affected the crack propagation path. The BSUs were separated by a 5µm cement line to resemble the biological "brick and mortar" structure.

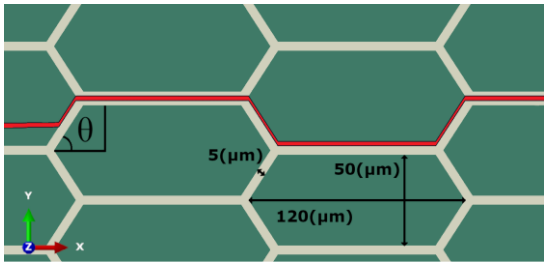

Figure 1: A unit cell model representing a matrix of hexagonal trabecular BSU (green), separated by cement lines (white). The crack path for this geometry is highlighted in red.

Extended finite element method (XFEM) modelling was used to model crack propagation via a cohesive segments approach using ABAQUS software. The maximum principal strain criterion (MAXPE) was chosen to model crack propagation in the BSUs. The fracture criterion f is defined as:

$$f_{MAXPE} = \{\langle \varepsilon_{max} \rangle / \varepsilon^0_{max}\}$$

where ε_{max} is the maximum principal strain and ε^0_{max} is the critical damage initiation strain. Damage is initiated when ($f_{MAXPE} > 1$) with the maximum principal orientation being used as a normal vector for the crack propagation.

A dual interface damage model [3] was adopted for the cement line, were the MAXPE criterion was used to model propagation through the cement line, and the quadratic nominal strain criteria (QUADE) was introduced for propagations along the cement line. The damage was initiated when ($f_{MAXPE}, f_{QUADE} > 1$). The QUADE criterion was defined as:

$$f_{QUADE} = \left\{\frac{\langle \varepsilon_n \rangle}{\varepsilon^0_n}\right\}^2 + \left\{\frac{\langle \varepsilon_s \rangle}{\varepsilon^0_s}\right\}^2$$

where ε_n is the normal strain, ε_s is the shear strain and ε^0_n and ε^0_s are critical interface strains. For this study it was assumed that $\varepsilon^0_n = \varepsilon^0_s$. Vectors oriented perpendicular to the cement line's interface were used as crack normals for the QUADE criterion.

Each model was subjected to tensile displacement in the vertical direction. MAXPE values were kept constant at 0.004, and QUADE and θ were varied to assess the effects of cement line material properties and geometry on the crack path and the macroscopic strain to failure.

Results and Discussion

The strain at which the crack propagated through the entire model was recorded for each simulation. The crack path was also noted as either through or around the BSUs (Fig. 1). The failure strains are plotted versus θ and QUADE (Fig. 2). Lower failure strains (blue) were noted when a crack propagated through the BSUs, whereas in higher strains (yellow) the crack followed the cement line. The sharp drop in strain when transitioning from one mode to another demonstrates an interaction between the θ and QUADE values.

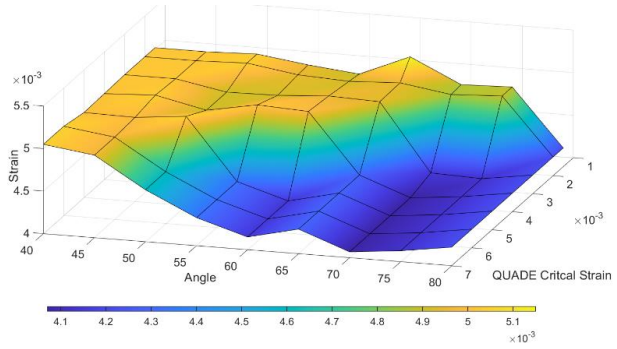

Figure 2: A 3D graph of macroscopic failure strain required to propagate a crack through a unit cell of trabecular bone as a function of BSU angle (θ) and cement line failure strains (QUADE).

Significance

This study demonstrates that the geometry and material properties of the cement line alter the crack path and macroscopic strain to failure in trabecular bone under tensile loading. Future studies should investigate how age-related changes in BSU size and other material properties also alter the overall crack resistance of the trabecular bone. These studies will expand our knowledge of the microstructural and compositional changes that lead to higher fracture risk with age.

Acknowledgments

The authors gratefully acknowledge the financial support of the Natural Sciences and Engineering Research Council of Canada (NSERC RGPIN-2015-05019).

References

[1] Chen et al., *Int J Endocrinol*. 213234, 2013. [2] Lamarche, 2020, MASc thesis, Laurentian University. [3] Gustafsson et al. *J Mech Behav Biomed Mater*, 90:556-565, 2020

EFFECT OF MITRACLIP ON MITRAL VALVE LEAFLET STRESSES AND CHORDAL FORCES IN FUNCTIONAL MITRAL REGURGITATION REPAIR

Gediminas Gaidulis[1,2*] and Muralidhar Padala[1,2]
[1] Structural Heart Research and Innovation Laboratory, Carlyle Fraser Heart Center at Emory University Hospital Midtown, Atlanta, GA, USA
[2] Division of Cardiothoracic Surgery, Emory University School of Medicine, Atlanta, GA, USA
email: *gediminas.gaidulis@emory.edu

Introduction

Functional mitral regurgitation (FMR) is a disease that alters the geometry of the mitral valve (MV), the left-sided atrioventricular valve of the heart, leading to inadequate closure and backward leakage of the valve. MitraClip is a medical device that repairs FMR by clipping MV leaflets together at the leakage (or regurgitant) site. It is the only medical device approved for FMR repair despite the data showing a high rate of long-term FMR recurrence after such repair **[1]**,**[2]**. The deployment of MitraClip causes the occurrence of unphysiological biomechanical effects, that might be a potential cause for FMR recurrence. We report a patient-specific computational model of the MV, that shows a significant increase in MV leaflet stresses and tension forces in the chordae tendineae after MitraClip implantation.

Methods

3D echo dataset was obtained in a post-myocardial infarction pig with FMR. Echo images were segmented, and geometry of mitral annulus, leaflets, and papillary muscles was reconstructed. Chordae tendineae were created according to ex-vivo findings, as chordae are not visible on echo. FMR state was induced after displacing the papillary muscles and thus pre-straining the chordae. The physiologic transvalvular pressure gradient was applied on the leaflets to simulate valve closure. As a result, systolic configuration of the MV affected by FMR was created with two noticeable regurgitant gaps. The arms of MitraClip were modeled as two 9x5 mm rigid rectangular plates. The device was positioned in systole at a conservative clipping height of 4.5 mm (half of the device height) to prevent overstretching the leaflets while still preserving a sufficient contact area. Angular displacement θ_i was prescribed to the plates to draw them together and grasp the leaflets (**Figure 1A**). Two devices were deployed to assure the elimination of both regurgitant gaps **(Figure 1B)**. After the deployment, valve opening was simulated by removing pressure gradient, and post-repair diastolic configuration of the MV was obtained **(Figure 2A)**.

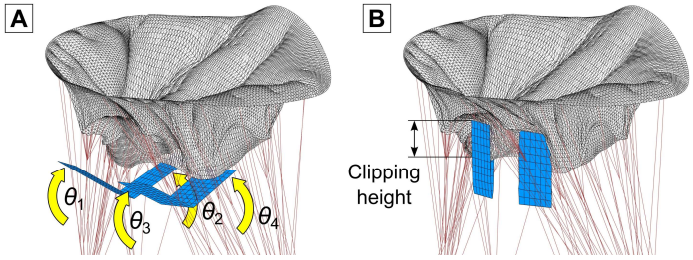

Figure 1: MitraClip deployment in systole: (A) a pair of devices positioned for arm closure and leaflet grasping; (B) MV leaflets clipped together at the regurgitant sites.

Results and Discussion

Systolic and diastolic configurations of pre- and post-repair MV models with stress distribution on the leaflets are shown in **Figure 2B**. After MitraClip deployment, both regurgitant gaps were largely eliminated and coaptation of the leaflets increased. However, tethering of the valve was not relieved. In systole, maximum tension force in marginal chordae increased from 0.41 N to 0.58 N, and significant increase in leaflet stresses was observed, with a peak value going up from 2.04 MPa to 8.81 MPa. In diastole, high stresses remained, with a peak value of 3.50 MPa after MitraClip deployment, compared to 1.91 MPa in pre-repair model. Maximum diastolic tension force in marginal chordae before the repair was 0.02 N, while after MitraClip implantation such force increased to 0.50 N.

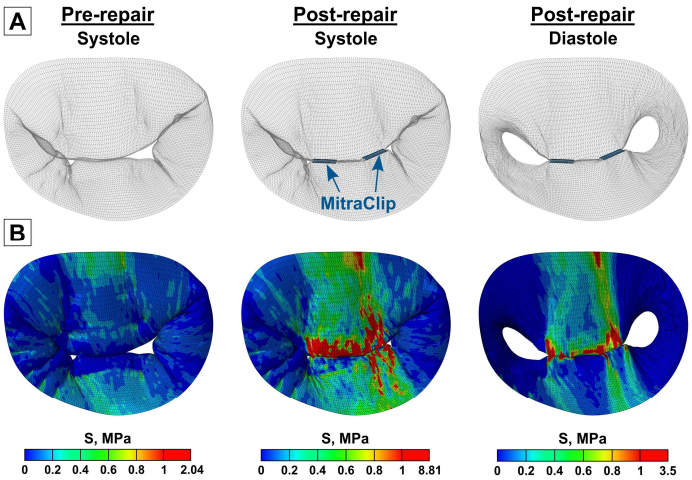

Figure 2: Simulation of FMR repair using MitraClip: (A) two devices were deployed in systole and valve opening was simulated to obtain diastolic configuration of post-repair model; (B) stress distribution in pre- and post-repair models in systole and diastole.

Our computational model demonstrates that MitraClip deployment reduces FMR and restores leaflet coaptation. On the other hand, the computational results show that both leaflet stresses and chordal tension forces after MitraClip implantation exceed pre-repair systolic peak values not only in systole but in diastole as well. This indicates that post-repair MV is experiencing high-level leaflet and chordal tethering throughout the whole cardiac cycle. Such unphysiological elevated stresses and forces occurring after MitraClip implantation can increase the risk of fibrosis and thus lead to FMR repair failure.

Significance

The presented patient-specific computational model allows to evaluate the biomechanical effects of FMR repair using MitraClip. In particular, the obtained results suggest that a potential cause for a high rate of recurrent FMR after MitraClip implantation might be the occurrence of unphysiological elevated stresses and forces caused by the device deployment.

References

[1] De Bonis et al., 2016. *Eur J Cardiothorac Surg*. 50: 488-494.
[2] Ooms et al., 2022. *J Am Soc Echocardiogr*. 35: 105-115.e8.

SIMILAR STRENGTH DEFICITS EXIST IN PATIENTS WITH ECCENTRIC AND CONCENTRIC GLENOHUMERAL OSTEOARTHRITIS

Margaret S. Coats-Thomas[1-3]; Emma M. Baillargeon, DPT, PhD[4]; Daniel Ludvig, PhD[1,2]; Constantine P. Nicolozakes, PhD[1-3]; Guido Marra, MD[5]; Eric J. Perreault, PhD[1,2,6]; Amee L. Seitz, DPT, PhD[3,7]

[1]Biomedical Engineering, Northwestern University, Evanston IL 60208, USA; [2]Shirley Ryan AbilityLab, Chicago IL 60611, USA; [3]Feinberg School of Medicine, Northwestern University, Chicago IL 60611, USA

email: margaret.coats-thomas@northwestern.edu

Introduction

Total shoulder arthroplasty (TSA) for glenohumeral osteoarthritis (OA) fails more often in patients with asymmetric glenoid erosion (eccentric deformity) compared to overall TSAs.[1] Failures are thought to result from strength imbalances between agonist/antagonist rotator cuff muscles. Patients with eccentric compared to concentric (symmetric erosion) deformities demonstrate increased intramuscular fat in antagonist muscles, which should impair external rotation strength.[2-3] Existing unidimensional strength assessments[4] do not describe the 3-dimensional (3D) strength-generating capacity needed for daily tasks or consider pain. Thus, it is currently unknown if 3D strength imbalances exist in patients with eccentric deformities.

Our objective was to determine if strength imbalances in external compared to internal rotation exist in patients with eccentric compared to concentric deformities. We also considered the influence of pain. If strength imbalances exist in patients with eccentric deformities, directed rehabilitation may be necessary to correct imbalances and help reduce TSA failures.

Methods

We enrolled 47 participants (57 shoulders) in the eccentric (n=18; mean age±SD yrs, 68±12), concentric (n=20, 68±9), and control groups (n=19, 65±13). Participants were seated with their casted arm attached to a 6 degree-of-freedom load cell in 45° of scapular plane abduction. Participants performed maximal isometric contractions in 26 equally spaced directions guided by visual feedback. Weight-normalized strength magnitude (Nm/kg) was computed as the Euclidian norm of the three principal axis magnitudes derived from principal components analysis of the 26 measures.[5] To test for strength imbalances, we quantified relative strength in opposing directions (strength balance) by computing the 3D center of the torque space as the vector mean of the 26 measures normalized by strength magnitude. Patients with OA rated their day-of shoulder pain before testing and with each maximal contraction (torque-dependent pain). Pain ratings across all torque directions were summed to determine pain balance. A linear model was used to test for differences in strength magnitude (univariate) and strength balance (multivariate). Pain metrics were found to be non-normally distributed, so Kruskal-Wallis tests were used to test for differences in day-of pain, torque-dependent pain, and pain balance. For all, $\alpha = 0.05$ with Bonferroni corrections for multiple comparisons.

Results and Discussion

Strength balance did not differ between eccentric and concentric groups (**Fig. 1**; p=0.23; mean diff along X Y Z: [0.90, -3.5, 0.62]; Hotelling's T^2: 4.5), suggesting no external to internal rotation imbalances. Strength balance in the eccentric (p=0.001) and concentric (p<0.001) groups differed from control participants ([-1.9, -6.9, -0.18], 20.9; [-2.8, -3.4, -0.80], 24.1, respectively), favoring abduction, external rotation, and extension. Weight-normalized strength magnitude was 16.5% lower in patients with eccentric compared to concentric deformities but did not reach statistical significance (p=0.22; mean diff: -0.04 Nm/kg, 95% CI: [-0.10, 0.02]). Strength magnitude was reduced by 38.5% in the eccentric (p<0.001) and 26.4% in the concentric (p=0.009) group compared to control participants (-0.13 Nm/kg, [-0.19, -0.07]; -0.09 Nm/kg, [-0.15, -0.03], respectively). Day-of (p=0.49) and torque-dependent (p=0.59) pain did not differ between deformity groups (diff in mean rank: -5.7; 95% CI:[-17.4, 6.0]; 2.0, [-5.1, 9.0], respectively). The X (p=0.56), Y (p=0.71), and Z (p=0.70) components of pain balance also did not differ between deformity groups (X: -2.1, [-9.1, 4.9]; Y: 1.3, [-5.7, 8.3]; Z: -1.4, [-8.4, 5.6]), suggesting no direction-specific pain differences.

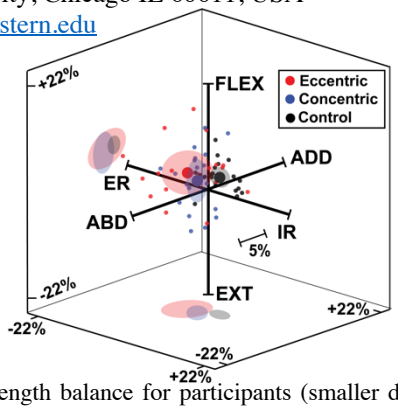

Figure 1: Strength balance for participants (smaller dots) and groups (larger dots). Shaded ellipses = 95% CIs. FLEX/EXT: flex/extension; IR/ER: internal/external rotation; ADD/ABD: abd/adduction.

Patients with eccentric compared to concentric deformities demonstrated no external to internal rotation strength imbalances, though strength balance did differ between patients with OA and control participants. There was more variability in strength balance in the eccentric group (95% CI volume, $\%^3$: 856.5) compared to the concentric group (356.3) and control participants (90.3). As three distinct glenoid wear patterns have been described in patients with eccentric deformities[6], the observed variability suggests patients with different wear patterns may adopt unique forms of kinematic or muscular compensation.

Significance

Our findings do not support a clinical theory proposed to explain TSA failures in patients with eccentric deformities. However, we saw high variability in the eccentric group. Our findings direct future work to explore if unique compensation methods contribute to variability and play a role in TSA failure.

Acknowledgments

ASB, NIH (F31AR077426), Northwestern Depts. of Physical Therapy & Human Movement Sciences and Orthopaedic Surgery

References

[1]Walch et al. 2012. *JSES*. [2]Donohue et al. 2018. *JBJS*. [3]Yoon et al. 2018. *Orthopedics*. [4]Sperling et al. 2008. *Int J Shoulder Surg*. [5]Baillargeon et al. 2019. *J EMG Kines*. [6]Otto et al. 2021. *JSES*.

MUSCLE TORQUE GENERATOR MODEL FOR A TWO DEGREE-OF-FREEDOM SHOULDER JOINT

Sydney M. Bell[1*] and John McPhee[1]
[1]Systems Design Engineering, University of Waterloo, Canada
email: *sm3bell@uwaterloo.ca

Introduction

Muscle Torque Generators (MTGs) reduce the complexity of muscle models to a single torque at the joint, while maintaining position and speed-dependant qualities of muscle forces [1]. While useful, these models can only be applied to one plane of motion and are often implemented with one MTG per degree-of-freedom (DOF) [2]. With joints such as the hip or shoulder having multiple DOF, there is a need for a model that can provide muscle torques for 3D motion. To the best of our knowledge, no research has been published on multiple DOF MTGs to date.

Two of the main components of MTG models are the torque-angle and the torque-speed scaling functions [1]. These functions are typically defined in terms of one DOF, i.e. a single joint angle. In this research, surfaces that define these functions as a coupling effect of flexion and horizontal abduction motions are evaluated for a two DOF shoulder joint.

Methods

One female subject (25yr, 175cm, 80kg) participated in the study. Isometric and isokinetic data was gathered using a dynamometer (Biodex System 4 Pro, Biodex, USA) and the coordinates were defined according to ISB standards, with θ_1 representing the elevation of the humerus and θ_2 the plane of elevation [3]. Isometric torques were gathered from 25 positions, with $60 < \theta_1 < 160$ degrees and $0 < \theta_2 < 120$ degrees. A total of 50 isokinetic concentric and eccentric torques were gathered with $-45 < \dot{\theta}_1 < 45$ deg/s and $-45 < \dot{\theta}_2 < 45$ deg/s. Maximum torque values were regressed against average torques to produce a maximal dataset as described in [4].

A curve-fitting solver (MATLAB 2020b) was utilized to fit different polynomial surfaces with varying degrees to the data, and the surfaces were evaluated using the Root Mean Square Percentage Error (RMSPE).

Results and Discussion

The isometric data that described the torque-angle scaling function was best fit using a polynomial surface with two degrees for θ_1 and three for θ_2 (RMSPE of 6.2%). Figure 1 shows the comparison of the surface function against values in the literature. In the case of flexion, the function underestimates the torque output. However, the model follows the literature results and decreases in torque with an increase in flexion.

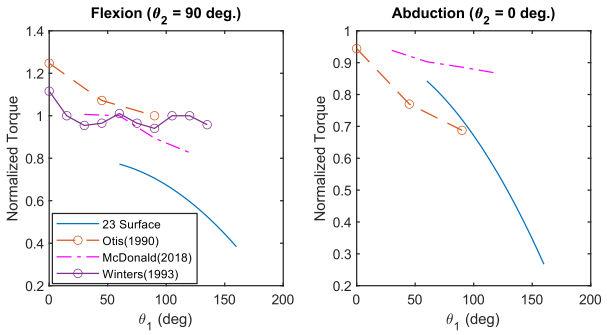

Figure 1: Comparison of the torque-angle polynomial surface function against values in the literature for flexion and abduction [5, 6, 7].

The isokinetic data that described the torque-speed scaling function was fit using two curves, one for concentric motions and another for eccentric as done in [4]. A surface with two degrees for $\dot{\theta}_1$ and one for $\dot{\theta}_2$ (RMSPE of 13%) was selected for the concentric motion, and a surface with three degrees for $\dot{\theta}_1$ and one for $\dot{\theta}_2$ (RMSPE of 10%) was selected for the eccentric. Figure 2 shows the comparison of the surfaces against values in the literature. The expected trend of a decrease in torque with higher speeds is present; however, surfaces for both motions underestimate the torque [4]. The eccentric torque was also expected to be greater than the concentric torque, which was not present in flexion. The unexpected results could be attributed to the limited sample size.

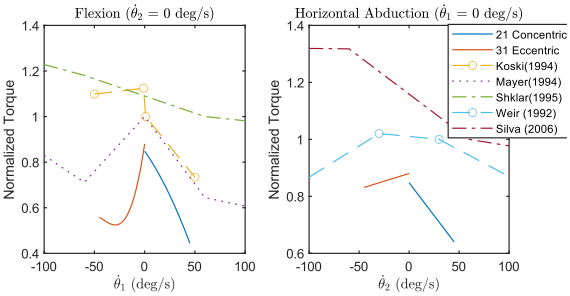

Figure 2: Comparison of the torque-speed polynomial surface against values in the literature for flexion and horizontal abduction [8-12].

Overall, a reasonable torque-angle scaling surface model has been presented for a two DOF MTG of the shoulder. Progress has been made towards a torque-speed scaling function, but a larger sample size is required.

Significance

Steps towards an easy-to-use two DOF MTG model for the shoulder have been made, with a viable torque-angle polymetric surface being observed. Faster simulations of complex motions will be enabled, with applications including optimization of athlete performance [13] and the design of assistive devices [14].

Acknowledgments

This research was funded by the Natural Sciences and Engineering Research Council of Canada.

References

[1] Inkol et al., 2020. *Multibody Syst Dyn*.10.1007/s11044-020-09747-9
[2] MacKenzie et al., 2009. *Sports Eng*. 10.1007/s12283-009-0020-9
[3] Wu et al., 2005. *J Biomech.* 10.1016/j.jbiomech.2004.05.042
[4] Yeadon et al., 2006. *J Biomech.* 10.1016/j.jbiomech.2004.12.012
[5] Otis et al., 1990. *Am J Sports Med.* 10.1177/036354659001800201
[6] McDonald et al., 2018. *Appl Ergon.* 10.1016/j.apergo.2017.10.004
[7] Winters et al., 1993. *J. Biomech.* 10.1016/0021-9290(93)90045-g
[8] Koski et al., 1994. *Clin Biomech*. 10.1016/0268-0033(94)90031-0
[9] Mayer et al., 1994, Int J Sports Med. 10.1055/s-2007-1021105
[10] Shklar et al., 1995. *Clin Biomech.* 10.1016/0268-0033(95)00007-8
[11] Weir et al., 1992. *J Orthop Sports Phys Ther.* 10.2519/jospt.1992.15.4.183
[12] Silva et al., 2006. *Br J Sports Med.* 10.1136/bjsm.2005.023408
[13] Jansen et al., 2020. *Multibody Syst Dyn.* 10.1007/s11044-020-09723-3
[14] van den Bogert et al., 2012. *J Biomech Eng.* 10.1115/1.400668

Deltoid muscle drives movement compensation after a severe rotator cuff tear

Joshua Pataky[1*], Lyndsay Engle[1], Vijitha Seelam[1], Sujata Khandare[1], Zoe Moore[1], April D. Armstrong[2], Meghan E. Vidt[1,3]
[1]Biomedical Engineering, Pennsylvania State University, University Park, PA, USA
[2]Orthopaedics and Rehabilitation, Penn State College of Medicine, Hershey, PA, USA
[3]Physical Medicine & Rehabilitation, Penn State College of Medicine, Hershey, PA USA
email: *jjp6192@psu.edu

Introduction

Rotator cuff tears (RT) are common in older adults, negatively affecting mobility and function[1]. RT severity ranges from a partial thickness supraspinatus tear to a massive 3-tendon tear, including the supraspinatus (S), infraspinatus (IS), and subscapularis (SS) tendons. A prior model-based study of static postures showed increased muscle compensation with increased RT severity[2], suggesting specific muscles could be identified to avoid further injury[3]. It has also been shown that glenohumeral joint loading decreases with increased tear severity during task performance[4]. It is unclear how muscle activations change with increased RT severity driving observed decreases to joint loading magnitude. Thus, our objective is to determine how muscle force and activation change with increased RT severity during functional task performance to identify compensatory muscles, which will help guide treatment and avoid further injury.

Methods

A computational model of the upper limb[5] was developed in OpenSim (v.3.3)[6], representing mean muscle force-generating properties of healthy older adult males. Eight models were developed to represent increasing RT severity by systematically reducing peak isometric force of S, IS, and SS muscle actuators[4]. Kinematics for forward reach, functional pull, axilla wash, and upward reach to 90° and 105° humeral flexion were measured from 9 older adults with RT and 9 age-, sex-matched controls in a prior study[7]. Simulations were performed with each combination of RT severity model and task kinematics (n=144 simulations/task) using the Computed Muscle Control[8] tool in OpenSim. Muscles of interest include anterior, middle, and posterior deltoid (AD, MD, PD), IS, SS, teres minor (TMi), teres major (TMa), clavicular, sternal, and ribs portions of pectoralis major (CPM, SPM, RPM), and thoracic, lumbar, and iliac compartments of latissimus dorsi (TL, LL, IL) muscles. Average predicted muscle force was quantified as both magnitude and percentage of total force for each muscle for each task with a two-way (RT model, muscle) ANOVA with Tukey post-hoc test. Average predicted muscle activation for each task was assessed with two-way (RT model, task) ANOVA with Tukey post-hoc test. Analyses were performed using SAS (v.9.4, SAS Institute, Inc., Cary, NC, USA), with significance at $p<0.05$.

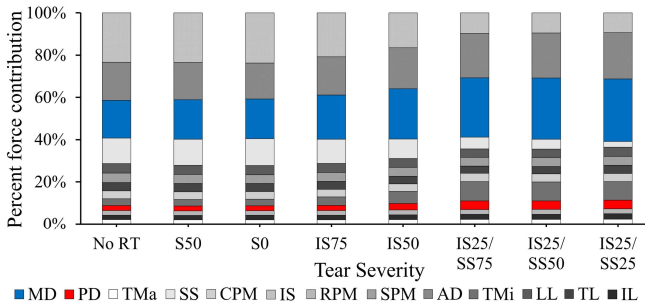

Figure 1: Muscle force normalized to total muscle contributions from all shoulder muscles for axilla wash task.

Results and Discussion

No difference in predicted muscle force or activation was seen between control and cuff tear groups. Tear severity and muscle were important interactions and main effects for predicted muscle force for all tasks for muscle forces (all $p<0.05$). For the axilla wash task, force contributions of MD and PD increased by 12.7% ($p<0.0001$) and 1.9% ($p<0.0001$), respectively, in the greatest tear severity model when compared to the no tear model (Fig. 1).

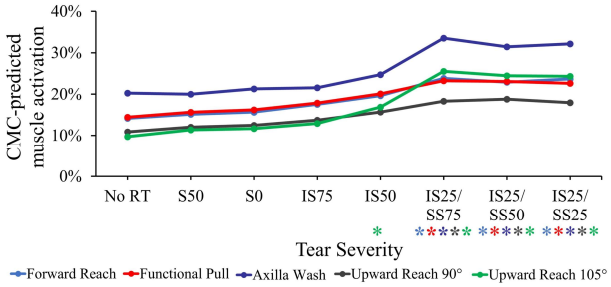

Figure 2: Predicted posterior deltoid muscle activation for all functional tasks, with significant comparisons between the greatest tear severity and no tear models shown (*$p<0.05$).

For predicted activation, there were no interactions between task and tear severity for all muscles. Task was important for all muscles (all $p<0.05$), while tear severity caused increased (MD, PD, ID, TMi, CPM, SPM) or decreased (SS, TL, LL) activations (all $p<0.05$). Predicted activation of PD in the greatest tear model increased during the forward reach (9.5%, $p=0.01$), functional pull (8.2%, $p=0.04$), axilla wash (11.9%, $p=0.02$), upward reach to 90° (7.1%, $p=0.02$), and upward reach to 105° (14.6%, $p<0.0001$) tasks when compared to the no tear model (Fig. 2).

Significance

After severe RT, functional tasks elicit compensatory responses from uninjured muscles, most prominently the MD and PD. As previous work has shown[4], increased tear severity leads to a posterior-superior shift in glenohumeral loading. The identified muscles provide ideal targets for strengthening to avoid injury due to sustained increased muscle activation[3]. Ongoing work explores functional tasks that use broader ranges of the upper limb work envelope to further understand identified compensatory responses.

Acknowledgments

Penn State start-up funds (Vidt).

References

1. Lin JC. et al. J. Am. Med. Dir. Assoc. 2008;9(9):626-632.
2. Khandare S. et al. J. Electromyogr. Kinesiol. 2019;(18):30516-9.
3. Bencke J. et al. Front. Physiol. 2018; 9:445.
4. Pataky J. et al. Clin. Biomech. 2021; 90:105494.
5. Saul KR. et al. Comput. Methods Biomech. Biomed. Eng. 2015;18(13):1445-58.
6. Delp SL. et al. IEEE Trans Biomed Eng. 2007;54(11):1940-50.
7. Vidt ME. et al. J. Biomech. 2016;49:611-617.
8. Thelen DG. et al. J. Biomech. 2003;36(3):321-328.

COMPUTATIONAL MODELING OF GLENOHUMERAL CONTACT AND TRANSLATION

Morgan J. Dalman[1*] and Katherine Saul[1]
[1]Department of Mechanical and Aerospace Engineering, North Carolina State University, Raleigh, NC, USA
email: *mdalman2@ncsu.edu

Introduction

Altered humeral head translation (HHT) and glenohumeral contact forces (GHCFs) are key features underlying shoulder injury and disability such as rotator cuff tears and osteoarthritis [1]. Accurate predictions of HHT and GHCF are essential for improving tendon repair, joint replacement, and physical therapy. Direct measurement of HHT and GHCF has been achieved using techniques such as in vivo fluoroscopy [2,3], instrumented joint prostheses [4,5], and cadaveric models [6], but predictive musculoskeletal models of the glenohumeral (GH) joint have typically used a simplified ball and socket shoulder representation which cannot capture HHT. Therefore, our goal was to augment an existing upper limb musculoskeletal model to include GH contact and evaluate predicted HHT and GHCFs.

Methods

An existing upper limb computational musculoskeletal model representing an adult male [7] was augmented to include GH joint contact between the glenoid fossa and the humeral head with surfaces defined from MR images (Figure 1). Blankevoort ligaments [8] representing the corocohumeral ligament and the superior, medial, and inferior GH ligaments were included [9-11]. Three degrees of freedom were added to allow for HHT. Humeral and glenoid cartilage contact pressure was computed as a function of the depth of penetration between the contacting cartilage surfaces via an elastic foundation model implemented using Forsim [12].

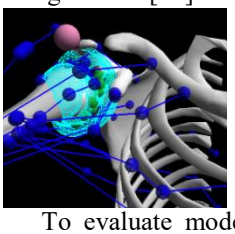

Figure 1: Upper limb musculoskeletal model. Muscle lines of actions (blue), contact surfaces (cyan) and Blankevoort ligaments (green).

To evaluate model performance, a passive scapular plane elevation task was simulated to mimic experimental conditions in a cadaver study [6] and two fluoroscopy studies [2,3]. The elbow, forearm, and wrist were locked in a neutral extended posture. Initial equilibrium was determined over 0.5s to allow surfaces to come into initial contact and settle. The arm was then passively elevated from 0-180° over 2.5s. Three conditions were simulated: constant 2%, 5%, and 7% muscle activation. Predicted HHT were calculated in an anatomical reference frame aligned with the glenoid fossa and compared to the literature values [2-3,6]. Predicted peak GHCF at 90° was compared to literature values for in vivo active straight arm abduction in instrumented prosthesis studies [4,5].

Results and Discussion

Predicted SI HHT with 2% activation fell within the overall range of reported values (Figure 3a), but was most similar to the truly passive cadaveric experiments as compared to in vivo passive elevation during which moderate levels of muscle activation is likely [13]. As we increased the applied constant muscle activation to explore this effect, the humeral head translational path more closely replicated HHT reported in fluoroscopy studies (Figure 3b). Peak predicted GHCF during the simulated passive task was 298.9 - 557.1N at 90° scapular plane elevation. This is consistent with previously reported GHCF during elevation of 400 – 700N [4,5].

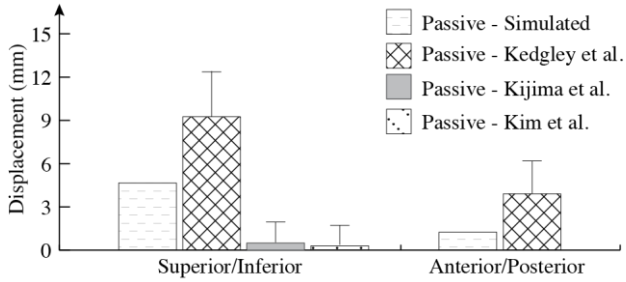

Figure *2*: Magnitude of HHT in the superior-inferior direction (mm) during passive scapular elevation between 30-90°.

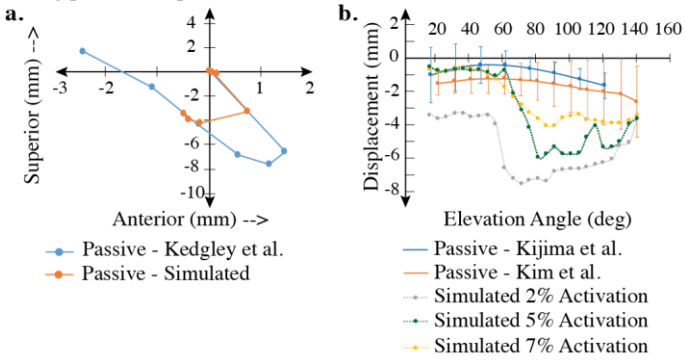

Figure *3*: (a) HHT path (mm) during passive scapular elevation between 30-90° (b) SI HHT paths (mm) during passive scapular elevation between 15-140° compared with fluoroscopy studies.

Ongoing work will continue to refine the application of muscle coordination to address the unequal muscle activation during passive tasks and simulate active shoulder tasks. In addition, the influence of altered muscle or ligament function as following injury on HHT and GHCF will be explored.

Significance

This work provides an initial framework by which GHCF and HHT can be simulated and predicted in the shoulder. The outcomes of this work represent a critical step in understanding the interactions among musculoskeletal properties, muscle and joint loading, and shoulder function.

References

[1] Yamamoto et al. (2010). *J Shoulder Elbow Surg.* **19**:116-120.
[2] Kijima et al. (2015). *J Shoulder Elbow Surg.* **24**:1817-1826.
[3] Kim et al. (2020). *Clinical Biomechanics*. **75**:104990.
[4] Bergmann et al. (2006). *J Biomech*. **40**:2139-2149.
[5] Bergmann et al. (2007). *J Biomech*. **44**:1543-1552.
[6] Kedgley et al. (2007). *J Shoulder Elbow Surg.* **17**:132-138.
[7] Holzbaur et al. (2005). *Ann Biomed Eng.* ***33***:829-840.
[8] Blankevoort et al. (1991). *J Biomech Eng*. **113**(3):263-269.
[9] Massimini et al. (2012). *J Orthop Surg Res*. **7**:29
[10] Boardman et al. (1996). *J Shoulder Elbow Surg.* **5**:249-254.
[11] Lee et al. (1999). *Clinical Biomechanics*. **14**:471-476
[12] Lenhart et al. (2015). *Ann Biomed Eng.* **43**(11):2675-2685.
[13] Cross et al. (2020). *JSAE*. **4**:1-8.

EFFORT AND STIFFNESS CONSIDERATIONS FOR EMERGENT SHOULDER MUSCLE ACTIVITY PATTERNS

Daanish M. Mulla* & Peter J. Keir
Department of Kinesiology, McMaster University, Hamilton, ON, Canada
email: mulladm@mcmaster.ca

Introduction

The human neuromusculoskeletal system has the tremendous capability to perform motor tasks using several movement strategies, with each kinematic "solution" feasibly accomplished through potentially an infinite combination of muscle load-sharing patterns [1]. Biomechanical models commonly assume that motor behaviour is governed by effort considerations (e.g., minimizing muscle activations). Although optimal effort principles can describe and predict several aspects of motor behaviour, minimizing effort alone can result in unsatisfactory predictions of muscle load-sharing. Effort-based objective functions penalize increased co-activation of muscles that do not alter the net joint moments although these patterns are often observed in experimental measurements of muscle activity. Muscle co-activation is presumably important for increasing joint stiffness, particularly at the shoulder as muscles are the primary stabilizers of the glenohumeral joint. Recently, trade-offs between effort and stability were explored with a biomechanical model of the cat hindlimb, with relatively small increases in effort from a minimal effort solution predicting large increases in stiffness [2]. Our work aims to evaluate the extent to which effort and stiffness considerations may explain emergent muscle activity patterns at the shoulder. Focusing on the modelling framework, the purposes of this exploratory study are to: (1) identify the set of optimal muscle activity patterns accounting for both effort and stiffness, and (2) evaluate effort and stiffness costs for non-optimal feasible muscle activity patterns.

Methods

The Delft Shoulder and Elbow Model (DSEM) was used in the current study [3]. Muscle elements were combined from 138 to 41 lines of muscle actions to allow exploring the range of feasible muscle activity patterns computationally tractable. Isometric contractions were investigated by setting the model in a static posture with an external load applied at the hand. To predict muscle activations, a multi-objective optimization was formulated based on two objective functions: minimizing effort ($\sum$ activations^2) and maximizing stiffness [4] at the glenohumeral joint. As effort and stiffness are competing objectives, a single globally optimal solution cannot be found. Rather, each objective was weighted iteratively to identify the set of optimal muscle activity patterns at varying levels of minimizing effort and maximizing stiffness. The effort and stiffness costs were normalized to the number of muscles and globally maximum stiffness solution, respectively. A hit-and-run search [1] was used to investigate the landscape of all feasible muscle activity patterns (or "solutions") for each isometric contraction.

Results and Discussion

Representative simulations from an isometric contraction with a 0.5 kg mass held at the hand in a 45° thoracohumeral elevated posture are presented in Figure 1. Examining the set of optimal solutions with varying weights for each objective (effort and stiffness), rapid increases in glenohumeral joint rotational stiffness were observed with small increases in effort from the minimal effort solution. Further increases in effort contributed to diminishing increases in stiffness. The trade-off in effort towards increased joint stiffness may explain emergent muscle co-activation patterns that effort objectives alone cannot predict [2]. It should be noted that some muscles were predicted to remain inactivated even with incremental weight added to the stiffness objective function, which may be due to the consideration of joint rotational stiffness in one axis alone. To survey effort and stiffness costs across all non-optimal feasible muscle activity patterns, a hit-and-run search method was used to sample 10^7 solutions. The sampled feasible solutions produced effort (range: 0.14-0.27) and stiffness (range: 0.28-0.71 Nm/rad) costs far away from the optimal set of activity pattern, with ongoing work attempting to evaluate whether this is due to the likelihood of those costs in the landscape of solutions and/or computational challenges when sampling uniformly from high-dimensional spaces. In the future, we aim to collect electromyography of shoulder muscles to identify where individuals lie on the effort-stiffness landscape and evaluate the predictive ability of a multi-objective optimization combining both effort and stiffness to predict motor behaviour.

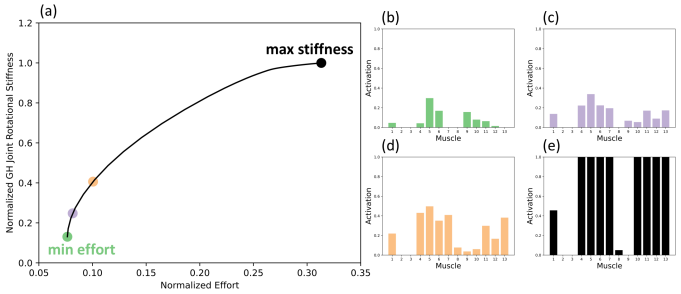

Figure 1: (a) Effort and glenohumeral (GH) joint rotational stiffness costs for optimal solutions based on varying weights for each objective (black line), with the globally minimum effort and maximum stiffness solutions labelled. (b-e) Predicted activity patterns of the glenohumeral muscles for 4 selected optimal combinations of effort and stiffness.

Significance

Static optimization based biomechanical models systematically underpredict muscle co-activation based on effort objectives alone. Motivated by recent work [2], we aimed at incorporating stiffness objectives in an optimization modelling framework to not only aid in improving predictions of muscle load sharing at the shoulder, but also enhance our current understanding of how neuromechanical factors may shape motor behaviour.

Acknowledgments

Thank you to the National Sciences and Engineering Research Council of Canada (NSERC CGS-D and DG) for their funding.

References

[1] Cohn et al. (2018). *Front Comput Neurosci*. 12:62.
[2] Sohn & Ting (2018). *bioRxiv*. https://doi.org/10.1101/477083
[3] Blana et al. (2008). *J Biomech*. 41:1714-1721.
[4] Hu et al. (2011). *J Neurophysiol*. 105:1633-1641.

NORMALIZATION OF SHOULDER COMPLEX KINEMATICS AFTER ROTATOR CUFF REPAIR

Alyssa J. Schnorenberg[1,2*], Dara Mischkel[3], Steven I. Grindel[3], and Brooke A. Slavens[1]
[1]Rehabilitation Sciences and Technology, University of Wisconsin-Milwaukee, Milwaukee, WI, USA
[2]Biomedical Engineering, Marquette University, Milwaukee, [3]Orthopedic Surgery, Medical College of Wisconsin, Milwaukee
email: *paulaj@uwm.edu *corresponding author

Introduction

In the U.S.A., an estimated 300,000 rotator cuff repair surgeries are performed each year [1]. Rehabilitation after surgery is necessary to reestablish function while allowing the repaired cuff to heal [2]; however, it is often a long process [3]. Although the optimal rehabilitation protocol is still being deliberated, most aim to restore active range of motion (ROM) by 3-4 months [3-4]. A primary goal is for the injured shoulder motion to become symmetrical, or normalize, with the contralateral arm motion [5]. Studies have demonstrated normalization of shoulder kinematics 1-2 years after surgery [5]; however, how this occurs within the first year is unknown. Thus, the aim of this study was to perform a longitudinal biomechanical evaluation of shoulder complex joint normalization in patients during the first 6-months of rehabilitation following a rotator cuff repair.

Methods

Ten adults (mean ± SD age: 62.3 ± 6.6 years; 5 males) with a supraspinatus tear participated in three evaluations: before surgery and 3- and 6-months after surgery. A Vicon motion capture system tracked 27 reflective markers on the upper body while five trials of maximal abduction were performed with each arm. The thoracohumeral (TH), sternoclavicular (SC), acromioclavicular (AC), and glenohumeral (GH) joint angles were calculated over the task duration using an inverse kinematics model [6]. Average peak elevation angles for the group were computed and compared between the injured and asymptomatic contralateral arms for each joint at each visit using the Wilcoxon signed rank test ($p<0.05$). The p-value was corrected via the Benjamini-Yekutieli method ($p<0.0029$).

Results and Discussion

The angular profiles for each joint of the injured arm at each visit are compared to the contralateral arm in Figure 1. The plots clearly show the reduction in elevation angles for the injured arm throughout the task during the pre-op and 3-month post-op visits compared to the injured arm at 6-months post-op and the contralateral arm. Injured arm peak elevation angles of the TH, AC and GH joints were significantly lower at pre-op when compared to 6-months and to the contralateral arm (Table 1). The only significant difference at 3-months, was lower TH peak elevation than at 6-months. This is likely due to the high standard deviations across all joints at 3-months. Profiles indicate normalization occurred at 3-months for the TH, SC an GH joints, but moderate normalization occurred for the AC joint. The average 6-months profiles indicate normalization for all joints.

Examining each participant's data provides further insight. At 3-months post-op, when compared to the contralateral arm, 6 of the 10 participants exhibited lower AC elevation (avg deficit: 34°), and 7 of 10 participants exhibited lower TH (avg deficit: 63°) and GH elevation (avg deficit: 57°). These deficits are clinically relevant as they would impede the execution of many upper extremity activities of daily living. Some data also suggests the AC and GH joints compensated for one another, presumably to attain higher TH elevation angles. At 6-months, however, only 2 participants exhibited a deficit at the AC joint (avg deficit: 18°), 4 at the GH joint (avg deficit:15°), and 0 at the TH joint. This indicates that compensation strategies may still exist at 6-months. Proper rehabilitation within 3 months post-op is key to good functional outcomes [3-4]. However, this study indicates that active ROM was not restored by 3-months, and instead most joint normalization occurred between 3- and 6-months post-op.

Table 1: Average (±1 SD) peak elevation angles for the injured arm at each visit and contralateral arm, * indicates significant differences with the contralateral arm; ǂ with the injured arm at 6-months (*$p<0.0029$*).

	TH Elevation	SC Elevation	AC Upward Rot.	GH Elevation
Contralateral	-128 (14)	-37 (8)	-54 (17)	-84 (14)
Pre-Op	-70 (20) * ǂ	-30 (9)	-6 (18) * ǂ	-43 (18) * ǂ
3-Months	-81 (36) ǂ	-30 (10)	-35 (32)	-43 (28)
6-Months	-130 (12)	-40 (6)	-63 (13)	-81 (20)

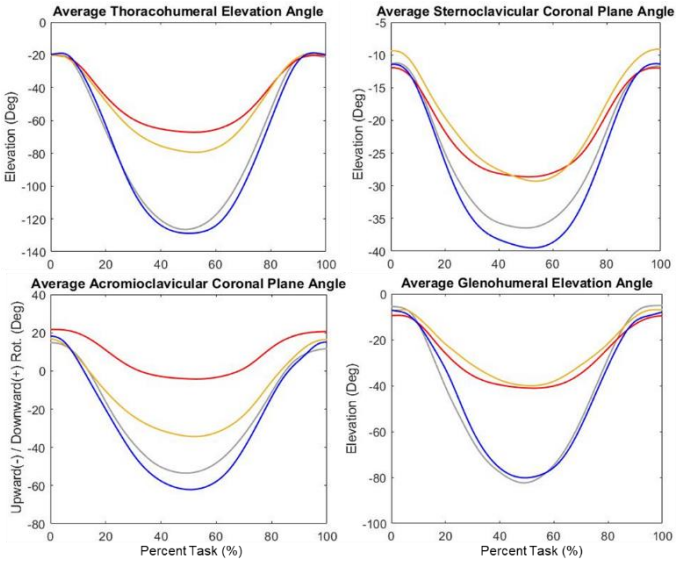

Figure 1: Average elevation angles of the injured arm at pre-op (red), 3- (yellow) and 6-months (blue) post-op and the contralateral arm (grey).

Significance

Knowledge of the normalization of shoulder complex kinematics after rotator cuff repair is essential to improve and shorten post-operative recovery. This work suggests targeted rehabilitation interventions need to be developed to achieve current 3-month post-op goals or the protocol timeline may need to be adjusted to set realistic patient expectations.

Acknowledgments

This work was supported by the Medical College of Wisconsin, Department of Orthopaedic Surgery Intramural Grant Program.

References

[1] M. Crawford, 2014. *AAOS* Now, 34. [2] A. Arshi, et al., 2015. *Arthrosc*, 31:2392-2399. [3] S. Vollans & A. Ali, 2016 *Surgery*, 34:129-133. [4] C. Jung, et al., 2018. *Obere Extrem*, 13:45-61. [5] A. Kolk, et al., 2016. *J Shoulder Elbow Surg*, 25:881-889. [6] A. J. Schnorenberg, et al., 2014. *J Biomech*, 47:269-276.

PREDICTIVE MODEL FROM FACTORIAL ANALYSIS OF FACTORS AFFECTING GLENOID BASEPLATE MICROMOTION IN REVERSE SHOULDER ARTHROPLASTY

Kenna Bartlett[1,3*], Kevin Nguyen[1,3], Lawrence F. Torkan[1,3], J. Timothy Bryant[1,3], Ryan T. Bicknell[1,2,3], and Heidi-Lynn Ploeg[1,3]
[1] Centre for Health Innovation, Queen's University, Kingston, ON, Canada
[2] Department of Surgery, Queen's University, Kingston, ON, Canada
[3] Department of Mechanical Engineering, Queen's University, Kingston, ON, Canada
email: * 16kkb3@queensu.ca

Introduction

Reverse shoulder arthroplasty (RSA) is commonly used to treat patients with a variety of disorders [1, 2]. Loosening of the glenoid component, one of the principal modes of failure, is the main complication leading to revision [3, 4]. Excess micromotion contributes to glenoid loosening. For optimal RSA implant osseointegration, the micromotion between the baseplate and the bone must not exceed 150 µm. The purpose of this study was to test the effects of four factors on glenoid baseplate maximum micromotion and create a predictive model to determine the micromotion of factor combinations.

Methods

A half-fractional factorial experimental design (2^{k-1}) was used to assess four factors at two levels: central element type (peg or screw), central element cortical engagement according to length (13.5 or 23.5 mm), anterior-posterior (A-P) peripheral screw type (non-locking or locking), and cancellous bone surrogate density (10 or 25 pcf) [5]. This created eight unique conditions, where each was repeated five times for a sample size of 40 (N = 40).

Glenoid baseplates were implanted into high- or low-density Sawbones™ rigid polyurethane foam blocks and cyclically loaded at 60° for 1000 cycles at 1 Hz (500 N compressive force range). Micromotion at the four peripheral screw positions was recorded using linear variable displacement transducers (LVDTs). Micromotion was quantified as the displacement range at the implant PU interface, averaged over the last 10 cycles of loading. From the factorial analysis, a predictive model was determined for the glenoid baseplate maximum micromotion ($\hat{y}$).

$$\hat{y} = \beta_0 + \beta_1 X_1 + \beta_2 X_2 + \beta_3 X_3 + \beta_4 X_4 + \beta_{1,2} X_1 X_2$$

Where, X_i (Central element length, central element type, bone density, peripheral screw type) are coded variables and β_i and β_{ij} are regression coefficients. A regression analysis of the measured and predicted micromotion determined the strength of the model.

Results and Discussion

The predictive model for the baseplate maximum micromotion of all repeated trials ranged from β_0 = [79.4, 118.0] µm, β_1 = [-91.3, -133.5] µm, β_2 = [-86.7, -144.3] µm, β_3 = [-21.7, -59.3] µm, β_4 = [-13.0, -71.5] µm, $\beta_{1,2}$ = [72.1, 113.5] µm, and R^2 = 0.95. This predictive model is shown in **Figure *1*** with a 95% confidence interval. This model can be used to predict the glenoid baseplate micromotion of the eight factor combinations not tested.

No significant effects were observed when varying A-P peripheral screw type or bone surrogate density. There were significant interactions between central element type and length ($p < 0.001$). Baseplates with short central elements lacking cortical bone engagement generated 373% greater micromotion at all peripheral screw positions compared to those with long central elements ($p < 0.001$). Central peg fixation generated 360% greater micromotion than central screw fixation ($p < 0.001$).

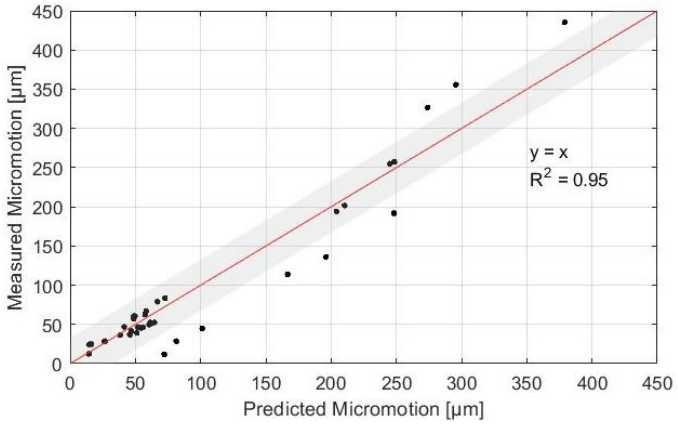

Figure 1: Regression analysis of the micromotion predicted by the model versus measured by the LVDTs for the eight combinations tested. An R^2 of 0.95 was found.

Both the physical testing and predictive model showed that a long central screw and long central element that engaged in cortical bone reduced RSA baseplate micromotion, as hypothesized. An interaction exists between central element type and the length required to achieve purchase with the cortex. This suggests that a central screw that cortically engages with the scapula may reduce post-operative micromotion.

Significance

A limitation of this study is that not all factor combinations were tested which limits the statistical evaluation of the interactions. Another limitation was that all tests were performed with a bone surrogate under lab conditions; however, these data may inform the design of future cadaveric testing. The proposed predictive model allows for all factor combinations to be considered, thus more accurately analyzing the four different factors. These findings can inform future preclinical analyses and ultimately surgical decision-making regarding baseplate fixation elements to minimize the risk of glenoid loosening and thus, the need for revision surgery.

Acknowledgments

Financial support was provided by Queen's University Faculty of Engineering and Applied Science. We acknowledge the support of the Kingston Health Sciences Centre, Centre for Health Innovation, National Sciences and Engineering Research Council of Canada (NSERC) and NSERC MediCREATE program.

References

[1] Hast et al., 2019, *J. Biomech.* 101: 109628
[2] Zumstein et al., 2011, *J Shoulder Elbow Surg.* 20(1): 146-57
[3] Farshad et al. 2010, *Int Orthop.* 34(8): 1075-82
[4] Kwon et al. 2010, *Bull NYU Hosp Jt Dis.* 68(4): 273-80
[5] Torkan et al. 2021, *JSES.* In Press

CHARACTERIZATION OF TERRAIN SLOPE USING JOINT ANGLE PRINCIPAL COMPONENTS AND HIERARCHICAL CLUSTERING

Sara E. Harper[1*], Jack A. Martin[2], Peter G. Adamczyk[2], and Darryl G. Thelen[2]
University of Wisconsin-Madison Departments of [1]Biomedical Engineering and [2]Mechanical Engineering
email: *seharper@wisc.edu

Introduction

Evaluations of natural movement dynamics are of interest in quantifying workload measures in healthy individuals on unconstrained terrain. While field-based evaluation of kinematics has made tremendous advances, the field-based assessment of kinetics remains elusive. Kinetic measures are particularly relevant in evaluating cumulative loading or workload during prolonged locomotion. We recently showed that walking speed and slope can predict a significant portion of the variation in Achilles tendon loading when walking on variable terrain [1]. Walking speed can be easily tracked via wearable sensors; however, it is more challenging to assess the slope of individual steps. The purpose of this study was to assess the potential for using ankle and knee kinematics to estimate terrain slope of individual steps as a step toward using normative data to estimate cumulative triceps surae work over a sloped walking course.

Methods

Eleven healthy young adults (5F/6M, mean ± SD: 23.3 ± 2.5 years, height 1.8 ± 0.13 m, mass 76.5 ± 13.6 kg) navigated an outdoor course (800 m) while a wearable shear wave tensiometer (SWT) and inertial measurement unit (IMU) system recorded continuous measures of Achilles tendon wave speed, ankle angle, knee angle, and geographical position. A total of 4734 strides were collected. Terrain slope was mapped by securing an IMU to a bicycle and traversing the course. For each stride, we evaluated walking speed based on horizontal displacement of an IMU secured to a belt worn about the waist. Position along the course was tracked by the waist mounted IMU, and then used to discern ground incline from the slope look-up table [1]. Net soleus work per step was calculated from muscle force and length, derived from calibrated wave speed and joint angles, respectively [2].

Principal component analysis (PCA) was performed on ankle angle waveforms. The minimal set of principal components (PCs) accounting for at least 90% of the variance was retained for analysis. Hierarchical clustering was performed using retained PCs to divide strides into distinct groups based on ankle angle. To match the 11 bins describing observed slopes, a cut-off was chosen such that 11 clusters would be formed. The mean slope of strides within each cluster was determined and compared to the observed slope of the strides in that cluster (Figure 1). To relate these kinematic-derived clusters to muscle-tendon loading, the mean soleus work per step within each cluster was determined. These steps were repeated using concatenated ankle and knee angle waveforms for PCA and clustering.

Results and Discussion

Ankle angle-derived clusters were associated with differences in slope, as expected (Figure 1). However, data from each cluster was spread over a broad range of observed slopes, likely due to remaining variability in the data and potential bias due to unequal numbers of strides in each slope bin. Each participant's data were distributed across clusters, indicating no strong subject-specificity. The addition of knee angle data to PCA and clustering yielded better agreement between cluster slopes and observed slopes, particularly at steep inclines, as indicated by the larger range of mean cluster slopes as well as larger percentages of appropriately sorted strides.

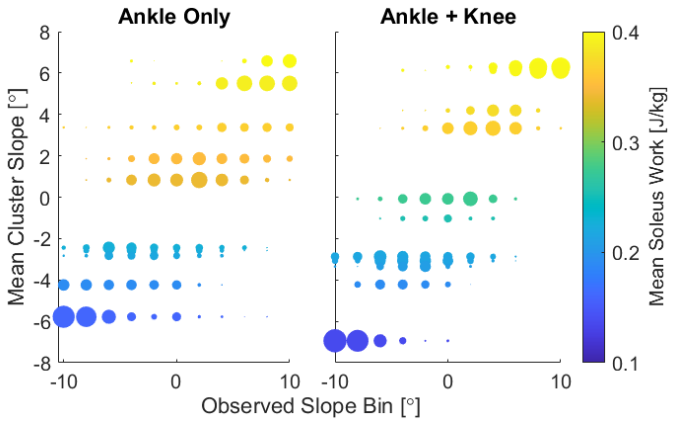

Figure 1: Mean slope of clustered strides based on combined ankle + knee angle PCs compared to clusters based solely on ankle angle PCs. Each row of data points belongs to one cluster, and point size reflects the percentage of strides from each bin corresponding with each cluster.

Similarly, estimated mean soleus work varied across clusters. This is expected given previous findings of slope-dependent increases in ankle work [3-5]. The addition of knee angle enriched the spread of work estimates by better distinguishing intermediate levels of soleus work.

These results suggest that walking joint kinematics could be used to estimate terrain slope. Coupled with walking speed, such data could be used to predict cumulative work done by the triceps surae muscles during walking on variable terrain. While generalized estimates of muscle-tendon loading could be provided through this approach, subject-specific measures would likely still require direct measurement, particularly in cases of injury.

Significance

Wearable sensors could provide unique opportunities to characterize cumulative biomechanical loading, which is relevant for understanding the cause and treatment of overuse injuries. This study shows that joint angle trajectories have sufficient information to ascertain slope, which is a key determinant of loading during outdoor locomotion.

Acknowledgments

Funded by the WARF Accelerator Program, NIH grants R42AR074897 and TL1TR002375, DOD CRMRP RESTORE W81XWH-21-2-0006, and NSF GRFP DGE-1747503.

References

[1] Harper+, 2020. *Sensors.* [2] Ebrahimi+, 2020. *Front Sports Act Living.* [3] McIntosh+, 2006. *J Biomech.* [4] Montgomery+, 2018. *R Soc Open Sci*. [5] Yang+, 2019. *J Biomech*.

FUSION OF VIDEO AND IMU DATA VIA DYNAMIC OPTIMIZATION OF A BIOMECHANICAL MODEL

Owen Pearl*, Ashwin Godura, Sarah Bergbreiter, Eni Halilaj
Department of Mechanical Engineering, Carnegie Mellon University, Pittsburgh PA, USA
Email: *opearl@andrew.cmu.edu

Introduction

Inertial sensing and video-based motion tracking [1] offer flexibility and accessibility for gait analysis, but their accuracy remains insufficient for many biomechanics applications. Inertial measurement units (IMUs) and video data both suffer from noise, but they have complementary strengths that can be leveraged to overcome their individual limitations. Data fusion with a biomechanical model could improve estimation of kinematics compared to prior unconstrained (i.e., model-free) fusion approaches [2]. Given the computational cost associated with biomechanical modeling, its use should be recommended judiciously. The goal of this work was to determine the sensor noise conditions under which fusion of video and IMU data with a biomechanical model outperforms (1) unconstrained fusion of IMU and video data [2] and (2) dynamic optimization of a biomechanical model using IMU data only [3].

Methods

Three markerless tracking approaches were compared: (1) fusion via dynamically constrained optimization, (2) fusion via unconstrained optimization, and (3) dynamically constrained optimization using only IMU data. We derived the equations of motion for a nine degree-of-freedom model (Figure 1) in their explicit form and simultaneously tracked joint center (keypoint) and IMU (acceleration and angular velocity) trajectories constrained to the model's equations of motion.

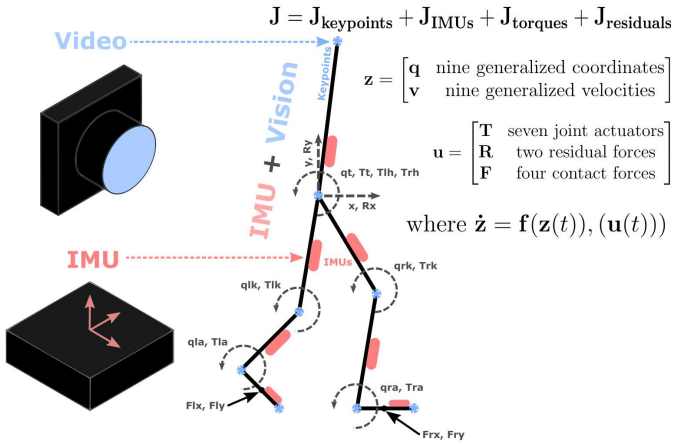

Figure 1: Video and IMU data are fused into a single optimal control trajectory tracking problem, where the state of a planar musculoskeletal model is optimized to produce joint center trajectories and inertial profiles that match the experimental data.

Each modeling approach was tested on data with different levels of noise to determine scenarios under which one modeling approach performs better than others. IMU and keypoint trajectories were generated synthetically from a public marker-based motion capture dataset of a single subject walking [4]. Noise representative of *low*, *medium,* and *high* sensor accuracy conditions was added to both keypoint and IMU data. Signal-to-noise ratios (SNRs) of 10, 20, and 30 dB and root-mean-square errors (RMSE) of 8, 4, and 1 cm, were used to model these conditions in the IMU and keypoint data, respectively. We compared kinematics across conditions and modeling approaches using a repeated measures ANOVA.

Results and Discussion

IMU and video fusion via dynamic optimization performed better than alternative methods when the accuracy of IMU data was low and keypoint accuracy was high. At the intersection of these conditions, fusion via dynamic optimization improved estimation of joint angles by a mean (± std) 1.0° (± 0.6°) compared to unconstrained fusion ($p = 0.0436$) and by 1.3° (± 0.9°) compared to IMU-only dynamic optimization ($p = 0.0380$). When the IMU data accuracy was low, fusion via dynamic optimization improved prediction of joint center positions by 1.1 (± 0.5) cm over unconstrained optimization ($p = 0.0002$), independently of keypoint accuracy, and by 4.3 (± 2.8) cm over IMU-only dynamic optimization ($p = 0.0017$). When keypoint accuracy was high, these improvements were 1.3 (± 0.5) cm over IMU-only dynamic optimization ($p < 0.0001$) and 0.7 (± 0.5) cm over unconstrained fusion ($p = 0.0051$), across all IMU accuracies.

Fusion via unconstrained optimization outperformed the alternatives when IMU data was of high accuracy and keypoint data was of low to medium accuracy. Unconstrained optimization improved prediction of joint center positions by 0.3 (± 0.3) cm over constrained fusion ($p = 0.0033$) and by 2.8 (± 2.0) cm over IMU-only dynamic optimization ($p < 0.0006$). It improved prediction of joint angles by 1.9° (± 0.7°) ($p < 0.0001$) and 0.8° (± 0.4°) ($p < 0.0001$) over the other two methods, respectively. However, unconstrained optimization was characterized by a one-sided dependence on IMU SNR ($r = -0.93$) and little sensitivity to changes in keypoint RMSE ($r = 0.03$).

Fusion of IMUs and video with a model can reduce sensitivity to noise and improve kinematic predictions in real-world applications, especially when IMU data are of low accuracy (~10 dB SNR). Low accuracy IMU data are common when IMU sensors are slightly misplaced (± 5 cm) or misaligned (± 10°) [5] or when subjects exhibit soft-tissue motion with a magnitude at the high end of the range for low-BMI individuals (± 5 cm) [6].

Significance

IMU and video fusion with a dynamically constrained model is an advantageous approach for processing noisy data, which augments the growing toolbox of next generation motion capture techniques that will enable better rehabilitative treatments.

Acknowledgments

This work supported by NSF DGE1745016 and DGE2140739.

References

[1] Cao, et al., 2019. *ArXiv:1812.08008.*
[2] Halilaj, E., et al. 2021. *J. Biomech.*
[3] Dorschky, E., et al., 2019. *J. Biomech.*
[4] John, C., et al. 2012. *J. Biomech.*
[5] Fan, B., et al. 2021. *IEEE Sensors Journal.*
[6] Fiorentino, N., et al. 2017. *Gait & Posture.*

USING OPENSIM TO VALIDATE AND COMPARE IMU-BASED KINEMATIC ESTIMATION METHODS

Michael V. Potter[1], Stephen M. Cain, Lauro V. Ojeda, Reed D. Gurchiek, Ryan S. McGinnis, and Noel C. Perkins
[1]Department of Physics and Engineering, Francis Marion University
email: michael.potter@fmarion.edu

Introduction

Wearable inertial measurement units (IMUs) provide means to measure human kinematics without traditional laboratory constraints (e.g., high-cost equipment, limited capture volume). However, accurately estimating anatomical joint angles and many other traditional kinematic measures from body-worn IMU data requires advanced signal-processing methods to overcome many challenges (e.g., correcting for integration drift errors).

While many methods have been developed for estimating human kinematics from IMU data, they often have significant limitations for general applicability to biomechanical studies including reliance on unknown assumptions (i.e., black-box methods), outside equipment for initialization, anatomical calibration, and/or specific movement assumptions (e.g., normal or level-ground walking). Thus, validation and comparison of such methods require accurate validation data sets from a broad range of movements, which may be difficult to obtain. We present a method to simulate realistic IMU data from existing motion capture data sets using the open-source biomechanics platform OpenSim [1]. Importantly, the biomechanics community could utilize the proposed method to aid in establishing high-quality data sets that act as standards for comparison between various IMU-based methods.

Methods

Generation of Realistic IMU Data using OpenSim

Existing data sets from marker-based motion capture are utilized to generate simulated IMU data for real human motions. A subject-specific biomechanical model is created in OpenSim with associated markers (Fig. 1). The standard inverse kinematics methods are used to solve for the generalized coordinates of the biomechanical model. A second biomechanical model is then created in OpenSim that is identical to the first except the markers are deleted and virtual IMUs are added. These virtual IMUs are created as small rigid bodies that are weld-jointed to associated bones (e.g., a right thigh IMU welded to the right femur) at locations where the real IMU would likely be attached (see Fig. 1). The generalized coordinate motion solution from the first model (the results of inverse kinematics) is applied to the model with virtual IMUs. The BodyKinematics tool within OpenSim is then used to calculate the positions and orientations of the virtual IMUs throughout the trial. These IMU positions and orientations are finite-differentiated at a desired IMU sampling frequency and gravitational acceleration is added to yield simulated IMU acceleration and angular rate data. Finally, realistic sensor noise characteristics can be simulated and added, for example, by adding a fixed bias or random Gaussian noise to the signals.

Comparison of Simulated and Experimental IMU Data

For the proposed method to be effective, the simulated IMU data must be similar to real IMU data. Data from a subject equipped with both reflective markers and IMUs on the lower limbs during a one-minute treadmill walk are used to evaluate the method. Simulated IMU data are generated as described above at locations near the experimental IMU mounting locations and compared to experimental IMU data. No bias or noise are added to the simulated data in this study as they could skew comparisons.

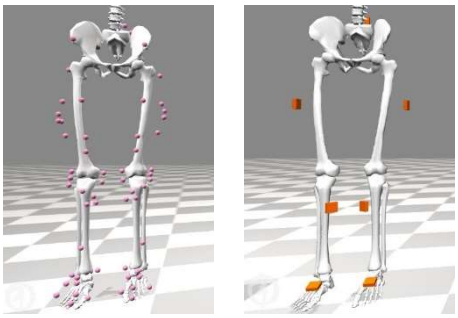

Figure 1: Equivalent OpenSim biomechanical models with markers (left) and virtual IMUs (right).

Results and Discussion

Figure 2 shows a sample comparison of the simulated and experimental IMU signals. Notice the good qualitative agreement between the signals. Pearson correlation coefficients between simulated and experimental IMU signals are determined for each IMU signal (acceleration and angular rate, 7 IMUs, 3 axes each). The correlation coefficient is greater than 0.5 in 37 of the 42 signals (88%). As seen in Figure 2, differences may be attributed to differences in the frequency content of signals and sensor errors (e.g., noise and bias) that can be modeled. Differences may also arise from small differences in the positions of the real and virtual IMUs. These results demonstrate that the proposed method does generate realistic simulated IMU data.

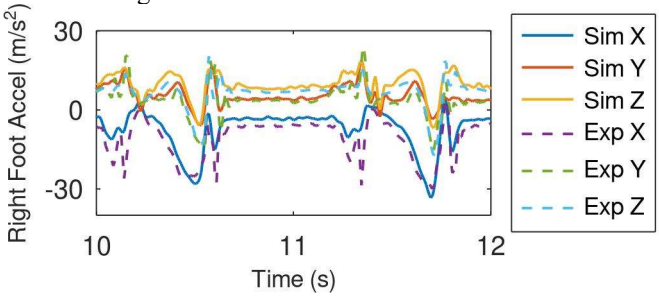

Figure 2: Sample right foot IMU acceleration for simulated (Sim) and experimental (Exp) IMUs in the sensor X, Y, and Z axes.

Significance

Accurate IMU-based methods for estimating human kinematics provide opportunities for many new and exciting biomechanical study designs. While many such methods are being developed, it is difficult to evaluate each method due to the difficulties in obtaining reliable validation data sets. The proposed method here offers significant benefits to the development and validation of various IMU-based methods by leveraging existing motion capture data sets to generate realistic IMU data. Further, comparisons between IMU-based methods are complicated because each method is evaluated using different validation data sets. The biomechanics community could utilize the proposed method to aid in establishing high-quality data sets that act as standards for comparison between various IMU-based methods.

References

[1] Delp et al., 2007. *IEEE Trans. Biomed. Eng.* 54(11).
[2] Potter et al. 2021. *PLOS ONE.* 16(4): e0249577.

USING CONSUMER-GRADE WEARABLE SENSORS TO PREDICT ACHILLES TENDON FORCE DURING RUNNING

John J. Davis IV[1*], Stacey A. Meardon[2], and Allison H. Gruber[1]
[1]Indiana University-Bloomington School of Public Health
[2]East Carolina University College of Allied Health Sciences
email: *jjd1@iu.edu

Introduction

Overuse injuries in runners are caused by gradual accumulation of damage from large, repetitive internal biomechanical forces that occur with each step of running. While these internal forces can be estimated in a motion capture lab using musculoskeletal modeling techniques, the inability to track these forces during day-to-day training outside of the lab is a major limitation in sports biomechanics. Wearable sensors offer a possible solution to this problem if sensor data could be used to predict internal forces without relying on in-lab motion capture.

Predicting internal biomechanical forces using gait metrics from consumer-grade wearable sensors is attractive given their popularity worldwide. Our purpose was to test whether gait metrics measured by consumer-grade devices can improve predictions of peak Achilles tendon force, compared with predictions made using only the runner's speed and body weight.

Methods

Six habitual runners (≥3x/wk) completed a 38-minute (instrumented) treadmill run in a motion capture lab at speeds ranging from 70%-125% of preferred (3.09-4.02 m/s) while equipped with a chest-worn accelerometer (HRM-Run, Garmin Ltd, Olathe KS, USA) and foot pod (Stryd Inc, Denver CO, USA) to measure speed. Peak Achilles tendon (AT) force of each step was estimated using a scaled musculoskeletal model [1] constrained to match experimental kinematic and kinetic data, while minimizing muscle activation squared. Sensor-measured gait metrics (speed, cadence, vertical oscillation, ground contact time, step length, vertical ratio, and ground contact time balance) for each step were aligned with motion capture data yielding several thousand pairs of model-derived peak AT force and sensor-measured gait metrics for developing predictive models.

We developed three progressively more sophisticated statistical learning models to predict peak AT force for each step from sensor-measured gait metrics: (1) **Intercept-only model**; (2) **Speed+weight**; (3) **Speed+weight+gait metrics**. AT force was predicted using generalized additive models (R package '*mgcv*'), a regression approach which allows for smooth, nonlinear effects of predictor variables. Because of the small number of subjects, body weight was fit as a linear effect. Model 1 was a baseline 'guess-the-average' model which predicted AT force for an unseen subject from the average AT force the model was trained on. It is equivalent to developing a linear regression model with only an intercept, and no predictor variables. Model 1 would be used if a researcher assumed differences in AT force both within and across subjects were negligible, and that loading cycles (i.e. total steps) were the dominant factor driving injury development. Model 2 predicted AT force using body weight as a linear effect and speed as a smooth nonlinear effect. Model 3 included the same variables as Model 2 plus smooth nonlinear effects of all sensor-measured gait metrics.

Predictive performance of the three models was assessed using mean absolute percentage error (MAPE) in subject-wise cross-validation: each model was trained on data from five subjects, then tested on the sixth. This process was repeated for each subject. Prediction errors were compared to the inherent variability of personalized lab-based AT force derived by averaging musculoskeletal model-calculated peak AT force at each speed (**Lab-based data**).

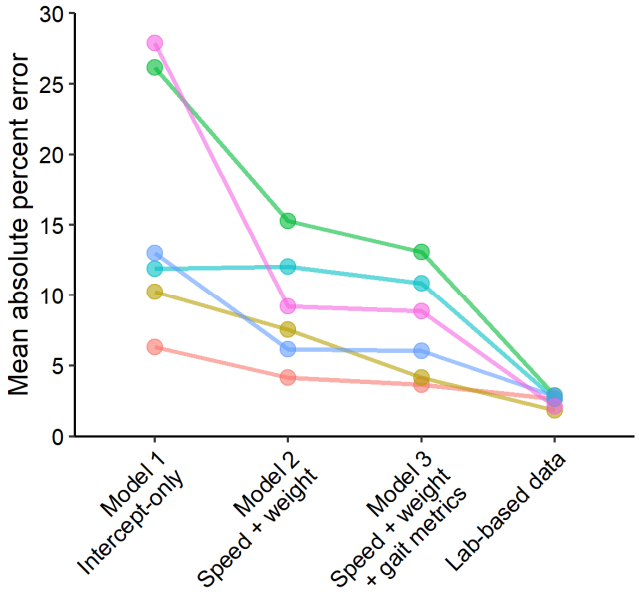

Figure 1. Cross-validated predictive performance for each model. Each subject's results are represented by separate lines. Adding sensor-based data improved model performance for all subjects compared to a model fit only to running speed and weight.

Results and Discussion

Cross-validated MAPE for Model 3 outperformed Models 1 & 2 (Wilcoxon p=0.03). Prediction error decreased for all six subjects in Model 3 versus Model 2. Gait metrics like cadence and vertical oscillation are associated with internal biomechanical forces [2], likely explaining why Model 3, which incorporated sensor-measured gait metrics, outperforms Model 2, which only considers speed and weight. As data collection continues, we aim to build more powerful predictive models developed on larger subject pools to improve model performance.

Significance

Sensor-based models of internal forces could allow researchers to study biomechanical loads and injury risk on an unprecedented scale, and clinicians could monitor biomechanical loading during return-to-running programs following injury.

Acknowledgments

Funding: American Society of Biomechanics; World Athletics, American College of Sports Medicine; De Luca Foundation; Stryd, Inc.

References

1. Catelli et al., 2018. *Comput Methods Biomech Biomed Engin*. 22(1):21-4.
2. Lenhart et al. 2014. *Med Sci Sports Exerc*. 46(3)557-64.

UNDERSTANDING COMPLIANCE FOR CONSUMER-GRADE WEARABLES: A CASE STUDY USING FITBIT DATA

Loubna Baroudi[1*], Ronald F. Zernicke[1], Muneesh Tewari[1], Sung Won Choi[1], Stephen M. Cain[2]
[1]University of Michigan, Ann Arbor, MI, USA and [2]West Virginia University, Morgantown, WV, USA
email: *lbaroudi@umich.edu

Introduction

With advancements in wearable technologies, measures of human movement can be captured outside the lab. Real-world data—although lower in resolution compared to lab measurements—offer large amounts of information on an individual's natural behavior. However, there is one fundamental requirement to be able to collect these data: subjects must be wearing the sensor. Subjects' compliance impacts whether or not sufficient data are collected to accurately capture the metrics of interest. There is no consensus on how to define a compliant subject (e.g., the required amount of wear time) to answer different research questions or to answer the same research question. In the studies using the Fitbit, the most common methods to define compliance (if any) use a threshold on daily wear time or step count to pre-process the data [1, 2]. However, it is unclear how threshold choices might influence results, or how results from different studies can be compared. In the current study, we aimed to demonstrate: (Aim 1) how different definitions of compliance can influence scientific results, and (Aim 2) how the definition of compliance is dependent on the research question. We used two examples to illustrate this work: (1) the evaluation of the average daily step count and (2) the evaluation of the average number of steps taken in a minute.

Methods

Fitbit data were collected between 2020 and 2021 on a population of 2,107 students from the University of Michigan over 90 days. This study was approved by the U-M Medical School Institutional Review Board.

For Aim 1, the average daily step count was calculated using three definitions of daily compliance: (*None*) all data were used, (*StepCount1000*) a day was kept if the step count was greater than 1,000, and (*WearTime80*) a day was kept if the wear time was greater than 80% (evaluated using minute-by-minute heart rate data). The change in average daily step count was assessed at the level of the population and the individual.

Aim 2 focused on how a subject's data can be insufficient for the evaluation of daily step count but not necessarily for the evaluation of the average number of steps taken in a minute. *WearTime80* were used for calculation of the average daily step count since it was the most stringent definition. For steps taken in a minute, the measurements of steps in a minute given by Fitbit were used. The number of values needed to converge to an average was calculated using the coefficient of variation of the standard deviation for a growing number of values. Subsequently, the number of days necessary to obtain that number of values was computed.

Results and Discussion

	None	*StepCount1000*	*WearTime80*
Mean	5,798	6,320	6,696
SD	3,162	3,032	3,362
N	2,038	2,023	1,855

Table 1: Daily step count. Mean daily step count, standard deviation (SD), and sample size (N) across the three definitions of compliance.

Aim 1: As expected, an increase in average daily step count and a decrease in sample size were observed from *None* to *WearTime80* (Table 1). Only a small change was observed in the average daily step count between the different definitions (max 15%). Those small changes can be explained by the high level of compliance observed in this population (14.5 hours/day). However, individuals with low levels of compliance presented large changes in the estimate of average daily step count (Figure 1). Having no threshold on compliance consistently led to a large underestimation of the average daily step count. *StepCount1000* and *WearTime80* can lead to similar estimates (e.g., for Subject 3), but generally give different estimates. Those changes showed how different definitions of compliance can lead to critical differences in the assessment of someone's level of physical activity.

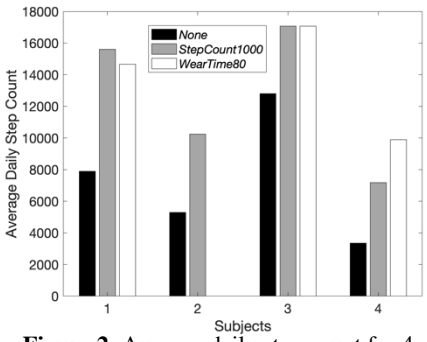

Figure 2: Average daily step count for 4 subjects using the 3 definitions of compliance. (Note: Subject 2 did not have any day with a wear time greater than 80%)

Aim 2: An average of 5.3 days was required to converge to an average value of steps taken in a minute. One hundred and forty four participants did not have any day with a wear time greater than 80% but had more than 5.3 days where they wore the Fitbit. Thus, the average daily step count for 144 participants could not be established, but the average number of steps they take in a minute could still be evaluated. The definition of compliance must be adapted to the research question to ensure data are valid and used appropriately.

Significance

Datasets collected using consumer-grade wearables over long periods of time enable new research that includes measures of daily movements. Standardized methods for the analysis of these datasets, however, need to be developed. The current study presents evidence on the sensitivity of scientific results to the processing of data with regard to compliance. Consequently, similar research questions should adopt standard definitions of compliance, with the understanding that compliance can be defined differently depending on the research question.

Acknowledgments

This work was supported by the Taubman Medical Research Institute, Edith S Briskin/Shirley K Schlafer Foundation and NIH grants (K24HL156896, R01HL146354). This work was also supported (in part) by a Scientific Research Initiative grant from the Biosciences Initiative of the University of Michigan.

References

[1] Faust L, et al. *16th ACM/IEEE Intl Conf,* Pages 55-60, 2016
[2] Hardcastle S J., et al. *PLOS One,* Pages 1-16, 2020

EVALUATING HOW WELL MARKERLESS MOTION CAPTURE APPROACHES MEASURE TRUNK KINEMATICS

Jacob J. Banks[1,2*], Joanna N. James[1], Andrew C. Lynch[1], Andrew P. White[1,2], Dennis E. Anderson[1,2]
[1]Center for Advanced Orthopaedic Studies, Beth Israel Deaconess Medical Center, Boston, MA, United States
[2]Department of Orthopaedic Surgery, Harvard Medical School, Boston, MA, United States
email: *jbanks3@bidmc.harvard.edu

Introduction

Obtaining accurate biomechanical data using marker-based motion analyses can be difficult, expensive, and time-consuming. Recent advances in markerless tracking approaches have demonstrated promising results for accurately quantifying lower limb gait parameters[1]. However, markerless approaches have not been thoroughly examined for their efficacy in tracking trunk kinematics during lifting.

Therefore, the purpose of this study is to assess the ability of markerless approaches to quantify trunk kinematics. We compared spine and pelvis kinematics from video and IMU-based markerless approaches against a "gold standard" marker-based system to ascertain the utility of markerless motion capture for a sagittal and non-sagittal lifting task.

Methods

Four healthy, young, and fit participants (♂=2; 29±7 years; 23.5±2.9 BMI) consented to an institute review board approved protocol. A full-body set of 97 motion capture markers (Vicon Motion Systems), four IMUs (Xsens Tech.) at the T1, T8, L3, and S1 vertebral levels, and two video-cameras (Vicon Motion Systems) capturing frontal and left lateral images were recorded in unison. Participants performed two crate lifts (to waist height and return) of 10% body mass: 1) lateral left-handed lift from a 30 cm step, and 2) 2-handed sagittal plane lift from the floor.

Video-images were analysed with OpenPose software[2] to identify 25 anatomical landmarks, 3D positions from coincident video-based landmarks were calculated using direct linear transformations. Total spine and pelvis kinematics from all three approaches were estimated by inverse kinematic analysis with a scaled full-body thoracolumbar spine musculoskeletal OpenSim model[3,4]. Coupling constraints were applied in the model to reduce the spinal (and also, in the case of the video-based models, the pelvis tilt) degrees of freedom from fifty-one to a determinate three[5].

Kinematics were time normalized and averaged across three lift repetitions. Within-participant lift comparisons of RMSE and zero-lag cross correlation values (*r*-values) were made between the markerless and marker-based approaches.

Results and Discussion

In general, both the IMU and video-based approaches matched the marker-based spine flexion/extension and pelvic tilt well, and pelvic list during the lateral lift (Table & Fig. 1). However, both markerless approaches struggled to track the more subtle transverse plane movements, spine lateral bending, and pelvic list during the sagittal lift.

IMU-based systems rely on fused coordinates between units and the assumption they are securely attached to the body segment of interest. The video-based approach greatly simplifies the trunk from estimated shoulder and hip joint centers. The accuracy of their estimated location may depend on the placement and number of cameras used, which was not examined here. It should also be noted that marker-based measures, while considered a "gold standard", can have poor reliability for some outcomes such as rotation during a lateral bend[6].

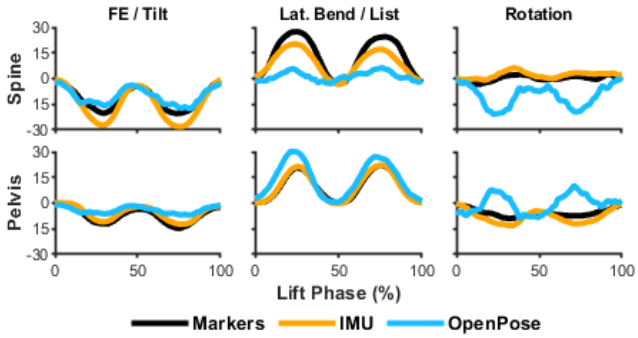

Figure 1: Average spine and pelvis kinematics (in degrees) from markers, IMUs, and OpenPose[2] video analyses during the lateral lift.

Significance

This study demonstrates the potential of alternative approaches to capture trunk movement. Some movements were tracked quite well, with respect to a marker-based approach, but others were not. Thus while certain outcomes may be viable, future studies should seek to optimize and further characterize markerless approaches for evaluating trunk kinematics and their impact on other biomechanical outcome measures.

Acknowledgements

This work was funded by a BIDMC Carl J Shapiro Department of Orthopaedic Surgery 2021-2022 Faculty Research Grant.

References

1. Stenum et al. (2021) *Plos Comp. Bio.* 17 (4)
2. Cao et al. (2018) *arXiv:1812.08008*
3. Delp et al. (2007) *IEEE Trans. BME* 37
4. Burkhart et al. (2020) *J. Bmch.* 112
5. Alemi et al. (2021) *Frontiers Bio. Biotech.* 9
6. Mousavi et al. (2018) *J. Bmch.* 79

Table 1: RMSE and cross-correlation (*r*) average (±SD) values between trunk coordinates from marker-based and markerless (IMU and video-based) approaches and the total range of motion during the lift (RoM; in degrees).

		Lateral Lift						Sagittal Lift					
		Spine Flex/Ext	Spine Lat. Bend.	Spine Axial Rot.	Pelvic Tilt	Pelvic List	Pelvic Rotation	Spine Flex/Ext	Spine Lat. Bend.	Spine Axial Rot.	Pelvic Tilt	Pelvic List	Pelvic Rotation
Markers vs. IMU	r	.95 ± .06	.96 ± .02	.66 ± .33	.78 ± .38	.97 ± .03	.47 ± .93	.96 ± .04	.47 ± .51	-.11 ± .69	.97 ± .02	-.05 ± .76	.21 ± .83
	RMSE	7.0 ± 2.9	7.1 ± 2.2	5.1 ± 2.5	3.1 ± 1.5	3.0 ± 1.0	7.2 ± 4.7	11.1 ± 2.5	2.1 ± .90	5.3 ± 2.8	9.6 ± 3.9	4.1 ± 2.3	4.4 ± 2.6
Markers vs. Video	r	.80 ± .26	.38 ± .38	.12 ± .83	.79 ± .24	.94 ± .07	.44 ± .58	.95 ± .03	.31 ± .41	.00 ± .43	.97 ± .02	-.22 ± .61	-.03 ± .49
	RMSE	5.0 ± 2.9	15.9 ± 4.6	14.0 ± 10.0	5.6 ± 5.0	7.7 ± 3.6	10.1 ± 6.1	20. ± 5.8	5.4 ± 2.0	8.6 ± 3.1	13.8 ± 3.4	7.4 ± 4.0	11.1 ± 3.3
RoM from Markers		22.1 ± 8.5	34.8 ± 15.6	12.7 ± 4.3	17.3 ± 7.1	23.8 ± 3.6	12.4 ± 5.3	49.0 ± 6.5	4.6 ± 1.4	5.4 ± 2.0	48.8 ± 14.2	5.2 ± 2.1	7.1 ± 2.2

ESTIMATION OF ARM ELEVATION THROUGH WEARABLE TECHNOLOGY ACROSS SIMULATED WORK TASKS

Jacklyn Kurt[1], Caitlyn Mei[2], Vignesh Sivan[2], Clark Dickerson[1] and Stewart McLachlin[2*]
[1]Kinesiology & Health Sciences, University of Waterloo, ON, CANADA
[2]Mechanical & Mechatronics Engineering, University of Waterloo, ON, CANADA
Email: stewart.mclachlin@uwaterloo.ca

Introduction

Occupational shoulder musculoskeletal disorders continue to contribute to workplace burden. A leading cause of these disorders is frequent overhead exertions. Overhead work is generally defined as working with the hands above the acromion, or over 60° shoulder flexion or abduction [1].

Current field assessments of overhead work often rely on ergonomists performing in person visual job analysis in addition to video analysis to provide posture counts, percentages of time spent working in arm postures, and to document tools or weights in the hands. Recent advances in wearable device technologies like smartwatches presents a potentially ideal non-invasive and remote platform to overcome on-site data collection and assessment challenges, but require validation for this application.

The goal of this study was to investigate the accuracy of using inertial measurement unit (IMU) sensors in a smartwatch to identify arm elevation during work tasks. It was hypothesized that use of machine learning techniques would yield accurate overhead prediction with a single wrist-worn inertial sensor.

Methods

13 right-handed, university-aged participants each completed 36 trials of simulated overhead work tasks (drilling, pushing, and materials handling) for 60s at three different arm elevation angles: 30°, 75°, and 120° (Figure 1). Percentage of time in an elevated position ranged from 20-80% within repeated 10s intervals. Motion was captured using a 10 camera VICON setup at 50Hz, a smartwatch (Tic E Android Wear) recording 6-axis IMU sensor data at 100Hz, and a video camera. Arm angles were extracted using a modified version of the SLAM geometric model throughout the task [2]. Motion capture and IMU data were synced using timestamps. IMU data points were labelled as overhead work if the arm elevation angle exceeded 50°.

A Random Forest classifier model was implemented for the IMU data to predict if the arm was in an overhead position for a period of time (split into 0.25-1s segments). The total overhead time for the task was then summed for the predicted elevated time segments. The dataset was (stratified) split in three different ways by organization: subject, temporal, and task. The model was trained and evaluated using K-fold cross-validation for each of the splitting techniques.

Figure 1: Simulated drilling task pictured with shoulder elevation angles of 30°, 75°, and 120° from left to right.

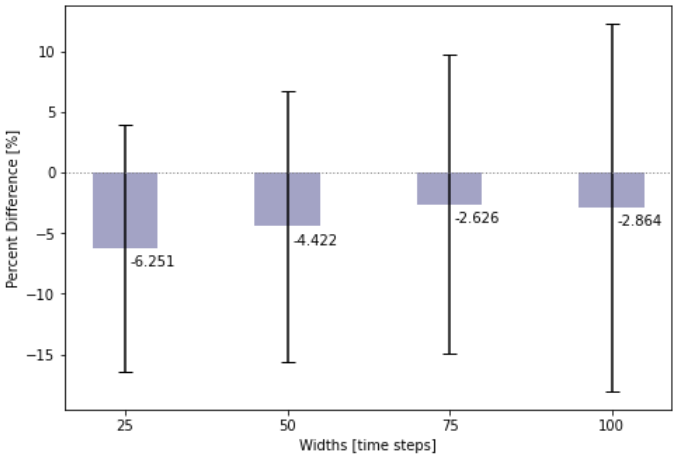

Figure 2: Stratified subject splitting: percent difference between predicted and actual overhead time on unseen test subject data based on different time step widths (corresponding to the 0.25-1s segments).

Results and Discussion

Stratified subject splitting model performance scoring on unseen test subject data yielded good results with an average of 87% accuracy for the predicted overhead arm position using 1s time segment widths. In general, the longer time steps demonstrated improved model performance for overhead prediction. When evaluating the overhead time prediction across all trials, the model was able to achieve less than 3% difference between the predicted and actual time (Figure 2).

Stratifying the dataset temporally yield improved results in model performance, up to 92% accuracy for overhead prediction. Stratifying by task (training on 2 overhead tasks and testing on the third) had the poorest performance overall (up to 75% accuracy), with large differences seen in the summated time of predicted vs. actual overhead work (up to 100% different). In this case, the current algorithm may not perform well with unseen tasks, and likely some task-specific training would be needed in practice.

Significance

Direct data-driven knowledge of exposures such as time spent in high arm elevation is essential, yet in-the-field identification of shoulder hazards has been historically difficult. This project fused new methods and inexpensive technology to present a novel method to estimate risk of overexposure in the workplace. This study could help to revolutionize job assessment for shoulder exposures, as arm elevation is one of the few risk factors routinely linked to shoulder pathologies.

Acknowledgments

Funding support was provided by a CRE-MSD seed grant. Caitlyn Mei was supported by an NSERC USRA for this project.

References

[1] Grieve and Dickerson, 2008, Occupational Ergonomics
[2] Dickerson, Chaffin DB, Hughes RE. 2007. CMBBE.

Session 7

Wednesday August 24, 2022

3:30pm – 5:00pm

O7.1 – Animal Models and Comparative Biology

O7.2 – Artificial Intelligence

O7.3 – Footwear/Feet

O7.4 – Musculoskeletal Modelling & Simulation 2

Thematic Poster Session 3 – Explaining Locomotion Costs

Stride-by-Stride Variability Impacts on Running Economy

Iain Hunter[1*], Jared Steele[1], Kaleigh Renninger[2], & Cameron Weeks[1]
[1]Brigham Young University
email: *iain_hunter@byu.edu

Introduction

As runner's performance improves, the variables that segregate them become harder to discern. Running economy (RE), at the higher levels, is a driving force behind that separation. While many factors influence RE such as metabolic adaptations within the muscle like increased mitochondria and oxidative enzymes, the ability of the muscles to store and release elastic energy by increasing muscle stiffness, and biomechanical factors. How consistent runners are in their movements may also play a role in running economy. Consistency of movements can be tested simply with calculating a standard deviation of a running mechanics measurement. Coordination variability (CV) also provides a valuable method for testing movement consistency [4].

CV describes a movement patterns' organization based on the allotted degrees of freedom [4]. The complexity of the integration between the musculoskeletal and neuromuscular systems allow for variations in movement to complete a similar task [6,1]. From an injury perspective, it has been shown that greater experience with a task leads to increases in variability to distribute load across working tissues which can be a protective mechanism[4]. From a performance perspective, decreases in the timing of leg muscle activation leads to improvements in RE [2]. This can help explain why an individual with a higher RE will have a lower variability of movement. This idea led to our hypothesis that runners with lower variability would have a lower oxygen uptake while running at 3.83 m/s.

Methods

Participants for the current study included 39 males (26.59 ± 8.69 years) with a variety of running experience (11.49 ± 7.91 years) and weekly mileage (48.59 ± 21.26). All individuals were injury free in the 6 months before their data collection and reported being comfortable running on a treadmill. All subjects ran in the Saucony TypeA running shoe (Boston, MA).

Kinetic data were collected while each participant ran on a 1 × 3 m dual-belt treadmill instrumented with two force plates (Bertec Corp; Columbus, Ohio) at 3.83 m/s. Kinematic data were captured at 240 Hz using a thirteen-camera motion capture system (Vicon Motion Systems, Oxford, UK. Peak force, ground time, stride rate, and joint angles were calculated using Visual 3d (Washington DC, USA). Oxygen uptake (K5, Cosmed, USA) was collected throughout the duration of the run with running economy being identified the median value of the final 10 minutes of the 15 minute run at 3.83 m/s.

Kinetic data were used to calculate stride rate, peak force, and ground time along with the standard deviation of each. Kinematic data were used to calculate CV using hip/knee sagittal plane angles.

Two linear regressions were performed. One for RE with the average standard deviation of peak force, stride rate, and ground contact time. A second regression for RE to CV. Alpha was set at 0.05.

Results and Discussion

Variability of movement as described through the average of the standard deviations of stride rate, peak vertical force, and ground contact time is slightly correlated with running economy as measured through oxygen uptake when running at 3.83 m/s (R^2 = 0.102, p=0.030, Figure 1). Surprisingly, the CV was not correlated with running economy (p=0.513).

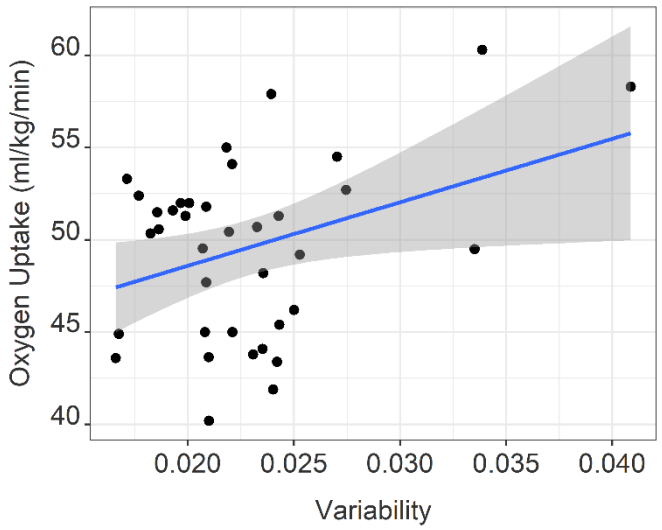

Figure 1: Oxygen uptake at 3.83m/s versus Variability of movement determined as the average standard deviation of peak force, stride rate, and ground time.

Step-by-step movement variability is only weakly correlated with running economy. Other physiological, biomechanical, and perhaps psychological factors account for the majority of variation in running economy between runners.

One final consideration is that of injury risk. In an attempt to minimize movement variability to decrease RE, injury risk may increase.

Significance

This study shows the impact that movement variability has RE. If movement variability can be minimized through various modalities of training, there may be a small impact on performance.

Acknowledgments

We would like to thank Saucony (Boston, MA) for providing the footwear for this study.

References

[1] Boyer et al, 2014. *J App Biomech*, *30:* 649–654.
[2] Li, 2014. *Gait & Posture* 39: 634–637.
[3] Hafer et al, 2015. J Sports Sci, 34: 1388-95.
[4] Hafer et al, 2019. *Med Sci Sports Exer*, *51:* 1438.
[5] Hamill et al, 1999. *Clin Biomech*, 14: 297–308.
[6] Saunders et al, 2004. *Sports Med, 34:* 465–485.

Metabolic Cost and Vigor in Human Gait

Matthew Mulligan[1] and Brian R. Umberger[1]
[1]School of Kinesiology, University of Michigan, Ann Arbor, MI
email: *mbmulli@umich.edu

Introduction

Even though human gait tends to be stereotypical, there are inter-individual and between-group differences in several gait parameters. Examining how the performance criteria underlying these gait behaviors are modulated will advance our understanding of the differences between individuals or between groups (e.g., young vs. old). Much of the existing literature has focused on factors such as metabolic cost and muscle activation in the selection of gait parameters, such as preferred gait speed [1]. However, most of the experimental evidence for this form of optimization is indirect, making it unclear if energetic minimization is a driver or consequence of task performance.

In addition to criteria such as energy or effort, recent work has shown that in the valuation of motor behavior, time may play a critical role in task performance. This may be a result of the body ascribing an implicit cost to the duration of the task. There is an emerging body of literature suggesting that the time required for task performance, termed *vigor,* is selected for in motor behavior [2,3]. However, this work has predominantly explored non-locomotor tasks, leaving the relationship between vigor and energetic cost in locomotion relatively uncharacterized. In addition to creative experiments that manipulate underlying performance criteria, musculoskeletal simulation is a powerful approach to quantify the effects of performance criteria on motor behavior [4]. Through this approach, it is possible to examine optimization for energetics alone, vigor alone, and the interplay between the two. Thus, the purpose of this study was to quantify the independent and combined roles of energy cost and vigor in gait performance.

Methods

We employed a 2-D musculoskeletal model [4] implemented in OpenSim Moco. The model included 9 segments, 11 degrees of freedom, and 18 lower limb musculotendon actuators (nine per limb). We first generated predictive simulations minimizing metabolic cost alone, and metabolic cost scaled to distance traveled alone. Here, no further constraints were placed on the model in order to identify the gait behaviors corresponding to these energy criteria alone. To test the effect of prioritizing vigor alone, we performed a predictive simulation where we minimized the time taken to generate a periodic stride with the stride length fixed at the value corresponding to normal walking at 1.3 m/s [5].

To test the combined effects of energy cost and vigor, we generated 8 sets of simulations for walking speeds ranging from 0.5 m/s to 1.9 m/s in increments of 0.2 m/s to determine how various weights on vigor (i.e., minimum time) impact the predicted walking speed. In each set of simulations, the stride length was fixed to the value corresponding to the typical speed-frequency relationship [5]. For each stride length, we generated simulations where the weight on metabolic cost was fixed and the weight on vigor was progressively increased over 8 conditions (weights from 0-10). As a result, for each of the 8 fixed distances, we generated 8 predictive simulations (64 total simulations) to assess the combined effects of metabolic cost and vigor on gait speed.

Results and Discussion

Minimizing metabolic cost alone resulted in the model standing in place to incur the lowest possible cost, as expected. Minimizing metabolic cost over distance predicted walking at 1.15 m/s, which is slower than typical preferred walking speeds (~1.3 m/s). Prioritizing vigor alone (i.e., minimizing time) resulted in a running gait with a speed of 4.05 m/s, which was the fastest speed that could be achieved with the fixed stride length. Thus, neither metabolic cost or vigor alone predicted the normal human walking speed.

For all eight of the fixed stride lengths, there were logarithmic relationships between the weight on vigor and the walking speed produced. Specifically, with a fixed weight on metabolic cost, increasing the weight on vigor led to an increase in gait speed. but with diminishing effects at greater vigor weights (e.g., Fig 1A). Across the fixed stride lengths, the weight on vigor required to achieve the corresponding target speed was greater for faster target speeds (Fig 1B). Thus, prioritization of movement vigor may play a role in the common behavior of walking at speeds greater than that which minimizes the metabolic cost of transport.

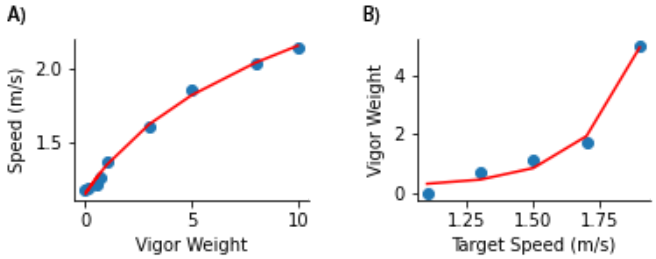

Figure 1. A) Simulated gait speed as a function of vigor weight for the stride length corresponding to 1.3 m/s. The relationship was logarithmic across all target speeds. B) Vigor weight yielding the target speed across stride lengths. In general, increasing vigor weight was required to generate a faster prescribed speed.

Significance

Our preliminary simulation results suggest a possible role for movement vigor as a factor weighted against metabolic cost of transport in the selection of gait speed. More work is needed to test the generality of these findings, as well as possible interactions with other performance criteria such as gait stability.

References

[1] Ralston, H. 1958. Int Z Angew Physiol, 17(4), 277-283.
[2] Berret, B, et al. 2016. J Neurosci, 36(4), 1056-1070.
[3] Shadmehr, R. et al. 2016 Curr Biol 26(14), 1929-1934.
[4] Nguyen, V, et al 2019. IEEE TNSR 27(7) 1426-1435.
[5] Bertram, J. et al 2005. J Exp Biol 208(6), 979-991.

ON THE ACHILLES TENDON MOMENT ARM LENGTH AND THE FORCE-LENGTH-VELOCITY RELATIONSHIP DURING RUNNING

Eric C. Bennett[1*] and Jared R. Fletcher[1]
[1]Department of Health and Physical Education, Mount Royal University. Calgary AB Canada
email: ebenn841@mtroyal.ca

Introduction

The impact of the length of the Achilles tendon moment arm (AT_{MA}) on the energy cost of muscle during running has been contentious. A short AT_{MA} has been associated with a lower running oxygen cost[1,2]. In theory, a short AT_{MA} allows for a lower muscle fascicle shortening velocity for a given ankle joint rotation[3], reducing active muscle volume and muscle energy cost. Short AT_{MA} also increases muscle forces for a given joint moment, elevating muscle energy cost. In contrast, a long AT_{MA} decreases muscle energy cost by reducing fascicle force for a given joint moment, but requires a higher shortening velocity for a given joint rotation. Using a theoretical within-subject approach, we estimated that increasing AT_{MA} from 30 to 40 mm increased muscle energy cost by 33% in runners which was partially attributed to changes in muscle fascicle shortening velocity and the operating range on the force-velocity relationship[4]. However, fascicle shortening velocity was not directly measured nor was the operating range on the muscle force-length relationship considered. Here, we aimed to determine the operating ranges of the force-length-velocity relationships during running where AT_{MA} differed in order to examine the impact of AT_{MA} on the energy cost of muscle contraction.

Methods

We measured AT_{MA} in 19 male and female participants (24±3 years, 75±11 kg, 177±7 cm) using the tendon travel method. We classified individuals having 'SHORT' (n=10, 29.5±1.9 mm) or 'LONG' (n=9, 36.6±2.5 mm) AT_{MA} based on a bimodal distribution of AT_{MA} (difference in AT_{MA} $p<0.001$). They ran at a speed of 2.5 $m \cdot s^{-1}$ on a motorized treadmill for 10 minutes while ultrasound images of their right medial gastrocnemius (MG) were collected. Fascicle forces were calculated from an instrumented insole algorithm[5] and fascicle velocities were calculated from fascicle length change measured during stance. Sarcomere lengths during stance were estimated from fascicle length and the average number of sarcomeres in series in the MG[6]. Fascicle velocity was expressed relative to MG maximal shortening velocity. MG energy cost was calculated from estimates of muscle forces and shortening[4]. All data were averaged over 10 consecutive stance phases.

Results and Discussion

Long AT_{MA} were significantly correlated with a reduced muscle energy cost (r^2=0.13, p=0.02). There were no significant differences in the force-length operating ranges during stance between groups (Figure 1). Both groups operated on the ascending limb of the theoretical force-length relationship. There was no significant main effect of group on measured muscle forces during stance (p=0.07). Shortening velocity was significantly higher in LONG compared to SHORT at both 5% (p=0.029) and 60% (p=0.05) of stance (Figure 2). Contrary to our hypothesis, short AT_{MA} did not result in significantly higher muscle forces but did show lower shortening velocities during periods of stance. Plantarflexion moment must have been lower in individuals with short AT_{MA}, perhaps as a result of a reduced forefoot length in runners with short AT_{MA}.

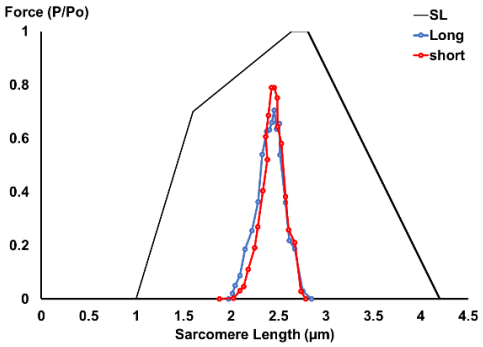

Figure 1: Sarcomere length operating range for short (red) vs. long (blue) AT_{MA}. The sarcomere force-length relationship for maximally-activated human sarcomeres are shown in black.

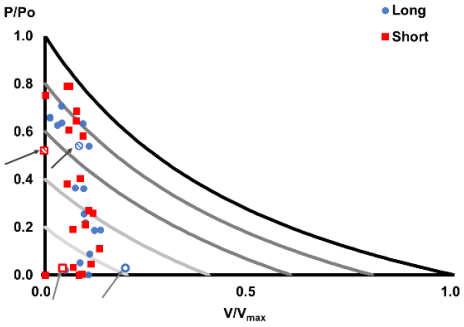

Figure 2: The force-velocity relationship with varied level of activation (grey lines, 20, 40, 60 and 80% maximal activation). The black line shows 100% activation. Red squares represent forces and velocities during stance for short AT_{MA} while blue circles represent long AT_{MA}. Light grey arrows show force and velocity 5% of stance, and dark grey arrows show force and velocity at 60% of stance.

Significance

The results of this study show the direct impact of AT_{MA} on the *in vivo* force-length-velocity operating range during submaximal running. Regardless of AT_{MA}, MG fascicles operate on the ascending limb of the force-length relationship, and shorten relatively slowly, regardless of AT_{MA}. which has fundamental impacts on muscle energy cost *in vivo*. We also show a weak, but significant correlation between AT_{MA} and muscle energy cost. These data suggest that biomechanical factors other than the force-length-velocity relationship help determine *in vivo* muscle and whole-body energy cost during running.

Acknowledgments

Supported by NSERC's Undergraduate Student Research Award.

References

[1] Mooses et al., 2014. *J Sport Sciences 33*: 136-144
[2] Scholz et al., 2008. *J Experimental Biology 211:* 3266-3271
[3] Nagano and Komura 2003. J Biomech. *36*: 1675-1681
[4] Fletcher and Macintosh 2018. *J Biomech. 79*: 100-102
[5] Hullfish and Baxter 2020. *Gait & Posture, 79*: 92-95.
[6] Bobbert MF et al., *J Biomech 1986;19*:887–98

EFFECTS OF INDUCED MOTOR FATIGUE ON WALKING MECHANICS AND ENERGETICS

Pei-Chun Kao[1,2*], Colin Lomasney[1,2], Amie Russell[2,3]
[1]Dept of Physical Therapy and Kinesiology, University of Massachusetts Lowell
[2]New England Robotics Validation and Experimentation (NERVE) Center, University of Massachusetts Lowell
[3]Dept of Biomedical Engineering, University of Massachusetts Lowell
email: PeiChun_Kao@uml.edu

Introduction

Lower-body robotic exoskeletons can be used to reduce the energy demand of locomotion and increase the endurance of wearers. Motor fatigue has been shown to reduce neuromuscular performance of an individual, leading to adaptive changes in gait spatiotemporal parameters to maintain walking stability [1]. To optimize exoskeleton wearer's performance, understanding how motor fatigue also affects walking mechanics and energy expenditure can help better design exoskeletons for providing versatile assistance [2] to the changing physical capacity of an individual due to motor fatigue.

Methods

We used treadmill walking at 1.25 m/s with progressively increased inclination (2.5° for every five minutes) to induce motor fatigue. The criteria to be considered as having reached motor fatigue include: (1) Borg rating of perceived exertion > 17/20, (2) reaching 85-90% of maximum predicted heart rate, and (3) vertical jump height reduced by ≥20%. If the vertical jump height was not reduced by ≥20%, another round(s) of treadmill walking protocol would be resumed from the last inclination setting. The last inclination angle was 7.5° for five subjects and 10° for seven subjects. The accumulated treadmill walking time to induce motor fatigue was 36.8 ± 7.9 minutes.

Twelve healthy young subjects (9M, 3F) walked on an instrumented treadmill at 0° before and after the fatiguing protocol. We recorded kinematics, ground reaction force, and the rate of oxygen consumption and carbon dioxide production. We computed net metabolic power (P_{met}, W/ kg) and average (positive and negative) mechanical power (P^{+}_{mech} and P^{-}_{mech}, W/kg) for each joint and the sum of the ankle, knee, and hip [3], which were used to derive the efficiency of positive mechanical work (η^{+}_{work}) and the contribution of an individual joint to the total average mechanical power.

Results and Discussion

Subjects had significantly greater net VO2 and P_{met} after the fatiguing protocol (POST) compared to the baseline (PRE) by ~16% on average (**Table 1**). For mechanical power, subjects had increased Total P^{+}_{mech} by ~4% but had similar P^{-}_{mech} during POST. Thus, the efficiency of positive mechanical work was reduced, from 0.27 at PRE to 0.24 at POST, by ~10%.

For the contribution of each joint to the total average mechanical power (**Table 2**), ankle joint had significantly reduced its contribution to the total positive power but increased its contribution to the total negative power during POST compared to PRE. On the contrary, knee joint increased its contribution to the total positive power but reduced its contribution to the total negative power during POST. The contribution of hip to total positive or negative power was not changed at POST.

These results showed that ankle joint's capability in generating positive mechanical power was affected by the inclined treadmill walking protocol the most. While greater positive mechanical power was generated at the knee joint after fatiguing to compensate for the reduction in ankle positive power, the disproportionate increase in net metabolic power resulted in a reduced efficiency of positive mechanical work.

Ankle joint was found to be a less metabolic costly source for positive mechanical power during walking compared to other joints and it was suggested that powering ankle joint is less "metabolic" beneficial [4]. Our results suggest that providing exoskeleton assistance at the ankle joint to make up the reduction in positive mechanical power generation due to motor fatigue may help reduce the energy expenditure of walking.

Significance

Understanding how motor fatigue affects walking mechanics and energy expenditure may lead to better designs of the exoskeletons such as the development of adaptive exoskeleton controllers or multi-joint exoskeletons that can adjust the strategies of providing assistance to the changing physical capacity of the wearers.

Acknowledgments

Supported by NSF IIS-1955979.

References

[1] Kao and Pierro, 2018. PloS One. 13(7):e0201433.
[2] Nuckols et al, 2020. PLoS One. 15(8):e0231996.
[3] Farris and Sawicki, 2012. J. R. Soc. Interface. 9:110-18.
[4] Sawicki and Ferris, 2008. J Exp Biol. 211:1402-13.

Table 1. Energetics and mechanics data (group mean ± STD) before (PRE) and after (POST) the motor fatiguing protocol.

parameters	PRE	POST	p-value
net VO2 (ml/min/kg)	10.84 ± 2.13	12.59 ± 2.34	< 0.001
P_{met} (W/ kg)	3.62 ± 0.72	4.15 ± 0.79	< 0.001
η^{+}_{work}	0.27 ± 0.06	0.24 ± 0.06	< 0.001
Total P^{+}_{mech} (W/kg)	0.95 ± 0.18	0.98 ± 0.20	0.03
Total P^{-}_{mech} (W/kg)	-1.03 ± 0.16	-1.01 ± 0.10	0.33

Table 2. The percentage of total average positive and negative power contributed at the ankle, knee, and hip joints before (PRE) and after (POST) the motor fatiguing protocol (* p<0.05; ** p< 0.01)

	PRE (contribution of individual joint, %)			POST (contribution of individual joint, %)		
	Ankle	Knee	Hip	Ankle	Knee	Hip
Total joint positive power (Total P^{+}_{mech})	35.1 ± 7.2	19.0 ± 2.9	45.9 ± 8.1	32.8 ± 7.1*	21.4 ± 4.3*	45.8 ± 10.2
Total joint negative power (Total P^{-}_{mech})	41.6 ± 4.7	49.8 ± 5.1	8.6 ± 3.0	46.2 ± 2.5**	45.3 ± 2.6*	8.5 ± 3.5

HOW HUMANS ADAPT STEPPING TO PERFORM LATERAL MANEUVERS

David M. Desmet[1*], Joseph P. Cusumano[2], and Jonathan B. Dingwell[1]
[1] Department of Kinesiology, Pennsylvania State University, University Park, PA, USA
[2] Department of Engineering Science & Mechanics, Pennsylvania State University, University Park, PA, USA
email: *dmd78@psu.edu

Introduction

Humans often perform maneuvers when traversing their environments to avoid obstacles or navigate complex terrain (e.g., Fig. 1A). Humans readily accomplish these tasks primarily by modulating their foot placement [1]. During continuous, straight-ahead walking, humans multi-objectively enact regulation of primarily step width (w) and secondarily lateral body position (z_B) via their left (z_L) and right (z_R) foot placements [2].

Humans regulate w to maintain lateral balance [3] and z_B to remain on their desired path [1]. Although prior work has postulated a "stability-maneuverability trade-off" during lateral maneuvers [4], the nature of this trade-off has not been well defined.

Here, we quantified how humans regulate lateral stepping during non-steady-state lateral lane-changing maneuvers. We hypothesized that humans would adapt regulation of w and z_B during such maneuvers in a manner consistent with the proposed stability-maneuverability trade-off.

Methods

20 young healthy adults each performed 4 lateral lane-change maneuvers between two parallel paths centered 0.6m apart in a virtual environment. Step-to-step time series of z_L, z_R, z_B, and w were obtained from motion capture data (Fig. 1B).

At each step of the lateral maneuver, foot placements were plotted in the $[z_L,z_R]$ plane. In this plane, diagonal, orthogonal Goal Equivalent Manifolds (GEMs) exist for both w and z_B that define all combinations of foot placements resulting in constant w or z_B, respectively (Fig. 1C). To determine the w and z_B stepping goals and the relative regulation of each variable, we quantified the locations and variance structure, respectively, of fitted variability ellipses at each step (Fig. 1C-D).

Results and Discussion

During continuous walking, the center of the variability ellipse aligns with the intersection of the w or z_B GEMs. Participants most commonly took 3 non-steady-state steps to complete the lateral maneuver, indicated by the centers of the fitted ellipses falling between the initial and final stepping goals: a small preparatory step, a large transition step, and a small recovery step.

The variability ellipses were more isotropic at the preparatory and transition step, indicating a trade-off in w for z_B regulation from step to step. The transition step had the most isotropic variability ellipse, indicating that the maneuverability requirements of a given step dictate the relative trade-off in w for z_B regulation. Areas (i.e., sizes) of the stepping ellipses also increased at the preparatory, transition, and recovery steps (Fig. 1D).

The lateral maneuver assessed here was relatively abrupt and thus challenging to complete. The results of this analysis indicate that humans are able to adapt lateral stepping regulation from step to step in response to such walking tasks.

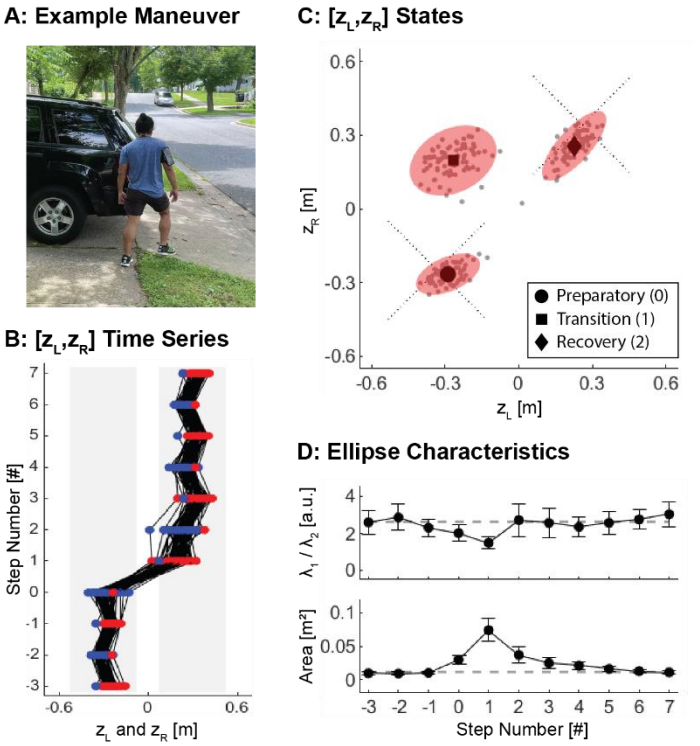

Figure 1: (A) Humans often encounter environmental contexts which require locomotor adaptability. (B) Time series of left (z_L; blue) and right (z_R; red) foot placements during the experimentally imposed lateral maneuver. (C) Stepping data during the preparatory, transition, and recovery steps projected onto the $[z_L,z_R]$ plane. (D) Fitted 95% prediction ellipse characteristics at each step: aspect ratio (top), calculated as the ratio of the eigenvalues of the covariance matrix of the ellipse, and area (bottom).

Significance

Prior work postulated a "stability-maneuverability trade-off" during lateral maneuvers. Indeed, humans select foot placements during adaptive walking tasks between those that would be optimal with respect to stability or maneuverability [4]. However, the nature of such a trade-off has not been well defined. Here, we demonstrate a novel method of interpreting stepping data to quantify how humans trade-off stability for maneuverability during lateral maneuvers

Acknowledgments

NIH / NIA Grant #: R01-AG049735 & R21-AG053470

References

[1] Bruijn & van Dieën, 2018. *J R Soc Interface*. 15, 1-11
[2] Dingwell & Cusumano, 2019. *PLoS Comp Bio.* 15, e1006850
[3] Kuo, 1999. *Int J Rob Res*. 18, 917-930
[4] Acasio et al., 2017. *Gait Posture*. 52, 171-177

HEADS OR TAILS: WHERE SHOULD A FISH STORE EXTRA MASS TO MAXIMIZE ITS JUMP DISTANCE?

Kazem Alambeigi[1], Emily M. Standen[2] and Thomas K. Uchida[1*]
[1]Department of Mechanical Engineering, University of Ottawa, Ottawa, Canada
[2]Department of Biology, University of Ottawa, Ottawa, Canada
*email: tuchida@uottawa.ca

Introduction

The mangrove rivulus (*Kryptolebias marmoratus*) is a small freshwater amphibious fish that relies on "tail-flip jumping" for terrestrial locomotion [1], in which it lifts its head off the ground, folds its body, and launches itself over its tail. This activity appears to be powered by red muscle tissue [2]. Recent work has revealed that rivulus of similar size and red muscle mass show variation in jump performance that appears to be related to differences in gonad and organ mass [3]. Because muscle mass and total body mass were similar among these individuals, we hypothesize that mass distribution contributes to the observed differences in jump performance.

Computational models and simulations can provide insight into the mechanical principles underlying human and animal movement [4]. When coupled with optimization, we can explore biological systems and scenarios that would be difficult or impossible to study using experiments alone. For example, Geyer and Herr [5] used optimization to elucidate the control strategy humans use to walk, Ong et al. [6] isolated the effects of muscular and neurological deficits that often co-occur, and Bishop et al. [7] studied the role of a dinosaur's tail during locomotion.

We use a single-shooting optimization strategy in OpenSim version 4.1 [4] with a planar, three-segment model to predict the jumping motion of the rivulus and to explore how the location of an added mass affects jump distance.

Methods

The model comprised three rigid segments representing the head, body, and tail. Revolute (pin) joints connected the head to the body and the body to the tail. The centre of mass of the tail was connected to ground with a planar joint, which constrained the model to a vertical plane. A compliant contact model was used to generate forces between the fish and the ground. Two contact spheres were added to each body segment. Motors were used to approximate the muscle-generated moments about the vertebral column; the torques they applied were parameterized as functions of time. The covariance matrix adaptation evolution strategy (CMA-ES) was used to find the motor torque parameters that resulted in maximum jump distance.

Each simulation consisted of three phases. In phase 1, the head segment was free to rotate while the body and tail segments remained fixed to the ground by constraining the corresponding joints. In phase 2, the body was released from the ground but the tail remained fixed. Finally, in phase 3, the tail was released from the ground, allowing the model to take flight. This modelling strategy was used to capture the rivulus's ability to adhere itself to flat surfaces and reflects the strategy it uses to jump.

The motor torque parameters for a "nominal" jump were sought first; this solution was then used as the initial guess for optimizations in which an additional mass was attached to the model. The additional mass (12.5% of the model's original mass) was attached at one of nine equally spaced locations along the length of the fish. The jump distance relative to the distance jumped by the "nominal" model was calculated for each of these nine weighting conditions.

Results and Discussion

Despite the model's simplicity, the optimal jump resembled that of a rivulus (Figure 1). When mass was added to the end of the head segment, jump distance increased by about 18% relative to the "nominal" case (Figure 2). Jump distance decreased as the added mass was moved posteriorly. This result is in contrast to observations of the biological system, where fish with mass concentrated in the middle of the body appear to have increased jump distance and endurance, suggesting that mass distribution alone does not explain differences in jump performance.

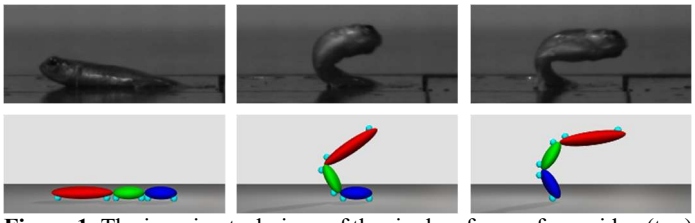

Figure 1: The jumping technique of the rivulus: frames from video (top) and OpenSim simulation of three-segment model (bottom) comprising head (red), body (green), and tail (blue) body segments, each with two contact spheres (cyan).

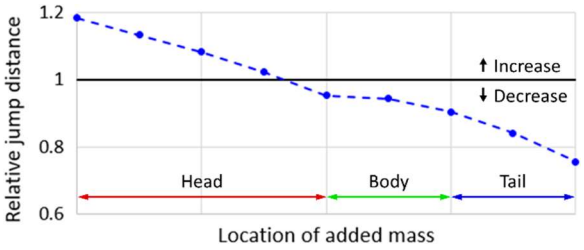

Figure 2: Jump distance of the models with added mass (relative to that of the model with no added mass) vs. the location of the added mass.

Significance

We have used modelling and simulation to explore the effect of mass distribution on jump distance in the rivulus. This framework enables one to investigate the effects of model and simulation parameters on jump distance in isolation of other factors. Future work includes calibrating the model from *in vivo* measurements, investigating other factors that may explain jump performance, and experimental validation.

Acknowledgments

We acknowledge the support of the Natural Sciences and Engineering Research Council of Canada (NSERC).

References

[1] Styga et al., 2017. *J Exp Zool A*. 327: 620–634.
[2] McFarlane et al., 2019. *J Exp Biol*. 222: jeb213348.
[3] Turko et al., 2022. *J Exp Biol*. (Submitted)
[4] Seth et al., 2018. *PLoS Comput Biol*. 14: e1006223.
[5] Geyer and Herr, 2010. *IEEE Trans Neural Syst Rehabil Eng*. 18: 263–273.
[6] Ong et al., 2019. *PLoS Comput Biol*. 15: e1006993.
[7] Bishop et al., 2021. *Sci Adv*. 7: eabi7348.

DEVELOPMENTAL PLASTICITY OF WALKING ENERGETICS AND SWING-PHASE MECHANICS IN CHRONICALLY LIMB-LOADED FOWL

Kavya Katugam[1*], Talayah Johnson[1], Ian Dechene[1], Suzanne Cox[1], Stephen Piazza[1], and Jonas Rubenson[1]
[1]Department of Kinesiology, Pennsylvania State University
email: *kavya@psu.edu

Introduction

Humans and other animals adapt to expend the least amount of energy to complete a movement task, both over acute [1-3] and evolutionary timeframes [1,4]. Whether adaptations in locomotor economy occur in response to altered life history (e.g. environmental fluctuations, or training in humans) remains less clear. Further, the mechanical underpinning to developmental adaptations in locomotor economy have not been well explored.

Here we test the hypothesis that a reduction in mechanical limb work contributes to the lower metabolic cost of carrying externally applied limb mass after chronic loading. Specifically, we hypothesize that (1) limb-loaded animals (LL) locomote with added limb mass using less mechanical power (Watts/kg) than control (CON) animals, and (2) the increase in mechanical power between unweighted and weighted conditions will be smaller for LL animals than CON animals. We also explore whether the associated changes in metabolic cost that result from limb loading can be explained by adaptations in mechanical power.

Methods

To study the effect of load stimulus during development on locomotor mechanics, we applied a mass equal to 3.5% body mass unilaterally to the lower right limb of a group of guinea fowl continuously from 1-16 weeks of age (limb-loaded group, LL; n = 5). We raised a second group of birds in the same conditions but with no external limb loading (CON; n = 5). At 16 weeks of age, birds' limb joints and body segments were marked and video recorded (100 Hz) walking on a treadmill at 0.5 m/s in both unilaterally loaded and non-loaded conditions. An inverse dynamic formulation was used to analyse swing-phase kinematics of the right limb. Five strides per load condition were used to generate averages per animal and used to compute group averages. Further, we compared mechanical data to previously collected metabolic data on the same animals in the same conditions [5]. Locomotor mechanical power was computed by dividing mechanical work (for each joint individually as well as the total limb work) by stride time.

Results and Discussion

LL animals preserved joint angles when unilaterally loaded versus unloaded ($p = 0.27$), while CON animals increased peak angle flexion by 7% when unilaterally loaded ($p < 0.05$, Figure 1). When unilaterally loaded, both CON and LL animals increased ankle, knee, and hip joint moments and instantaneous power during limb swing.

Both CON and LL animals performed more positive ankle, knee, hip, and total locomotor power (Watts/kg) when loaded compared to when unloaded. Contrary to our first hypothesis, when unilaterally loaded, LL animals performed 43% more total positive power than CON animals ($p < 0.05$, Figure 2). Contrary to our second hypothesis, the average increase in positive mechanical power between unweighted and weighted conditions for CON animals was 199% (0.23 Watts/kg, $p < 0.001$), which was significantly lower than the 243% increase in LL animals was (0.36 Watts/kg, $p < 0.05$, Figure 2).

Despite the greater increase in mechancial power of unilateral limb loading in LL animals, the mass-specific metabolic power of walking with this limb loading was 26% lower in LL animals compared to CON animals ($p < 0.05$) [5]. It remains possible that there are adaptations in mechanics occurring in the unloaded limb (analyses ongoing) that will help elucidate the relationship between limb mechanics and energetics.

Animals subjected to chronic limb loading (LL) maintain gait kinematics of their loaded limb at the expense of greater mechanical power. Despite the higher mechanical cost, these animals nevertheless have a remarkably low metabolic cost of carrying additional mass. Thus, it is likely that growth-period adaptations for economy arise via adaptations at the muscular level as opposed to gross mechanics.

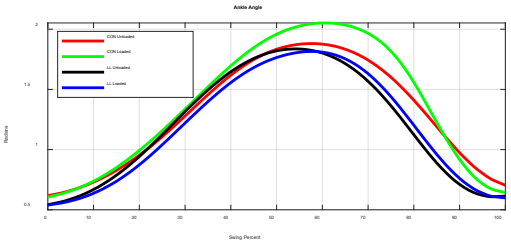

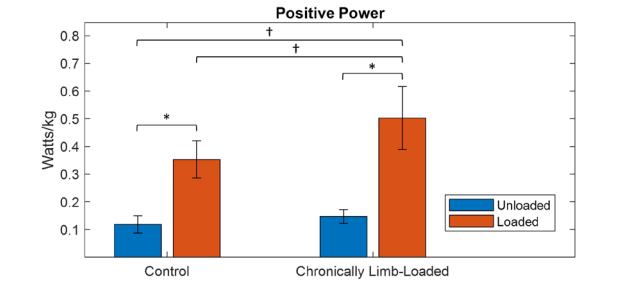

*indicates significant differences between load conditions ($p < 0.05$)
†indicates significant differences between CON and LL ($p < 0.05$)

Significance

This study is among the first to establish mechanisms for growth-period adaptations in locomotor economy. Further focus on muscular adaptations will help determine the physiological basis for load-induced metabolic plasticity.

Acknowledgments

Supported by NIH Grant R21AR071588.

References

[1] Alexander, 2003. *Prin Animal Loc*.
[2] Barnes & Kilding, 2015. *Sports Med,* 45: 37-56.
[3] McCann & Higginson, 2008. *Sports Med,* 7: 158-162.
[4] Dawson & Taylor, 1973. *Nature*, 246: 313-314
[5] Johnson, 2021. *PSU KINES Master's Thesis*

COMPARING ACTIVE CONTRACTILE PROPERTIES WITHIN AN INTRGRATED GROUP OF MUSCLES: THE ABDOMINAL WALL

Aliza R. Siebenaller*, Alex M. Noonan and Stephen H. M. Brown
Human Health and Nutritional Sciences, University of Guelph, Guelph, Ontario, Canada
email: *asiebena@uoguelph.ca

Introduction

The abdominal wall muscles (external oblique (EO), internal oblique (IO), rectus abdominis (RA), and transverse abdominis (TrA)) are an anatomically and functionally integrated group that play a critical role in moving and stabilizing the spine. While the passive mechanical properties of the individual abdominal wall muscles have been studied previously [1], the active contractile properties have yet to be described. The aim of this study was to measure the active contractile properties of single muscle fibres from EO, IO, RA, and TrA in the rat. It was hypothesized that there would be no difference in specific force, active modulus, unloaded shortening velocity, or rate of force redevelopment between muscles.

Methods

Muscle samples were taken from the EO, IO, RA, and TrA of 6 skeletally mature male Sprague-Dawley rats. Single muscle fibres were isolated from each sample and were processed as per Roche et al. [2]. Each muscle fibre was tested to determine its specific force (maximal force/cross-sectional area), active modulus (i.e. normalized stiffness), unloaded shortening velocity (V_o), and rate of force redevelopment (k_{tr}).

Fibre type was then determined for each fibre via gel electrophoresis (SDS-PAGE). Fibre type distributions were additionally determined for each muscle from a subset of 3 rats. To do this, larger bundles of fibres of each muscle were fibre typed and analyzed using ImageJ software.

A one-way ANOVA and Tukey's HSD multiple comparison test were performed with muscle as the independent variable and rat coded as a random effect. The dependent variables were specific force, active modulus, V_o , and k_{tr}.

Results and Discussion

Of the 86 fibres tested only two were found to be type IIa and none were type I. Type IIx, IIb and IIx/b hybrid fibres were thus combined for statistical analysis, providing a total of 84 fibres for comparison: 20 EO, 20 IO, 22 RA, and 22 TrA. There were no significant differences found between muscles for specific force, active modulus, and unloaded shortening velocity. Rate of force redevelopment was found to be significantly different only between TrA and EO, with TrA being greater than EO ($p < 0.05$) (Figure 1). Fibre type distributions followed the same order of abundance for all muscles; type IIb being the most abundant, followed by type IIa/x, and type I being the least abundant.

It was hypothesized that there would be no difference amongst muscles for measures of specific force, active modulus, unloaded shortening velocity, and rate of force redevelopment. This was confirmed for the first three variables, but rejected for rate of force redevelopment as TrA was found to have a 62% higher k_{tr} than EO.

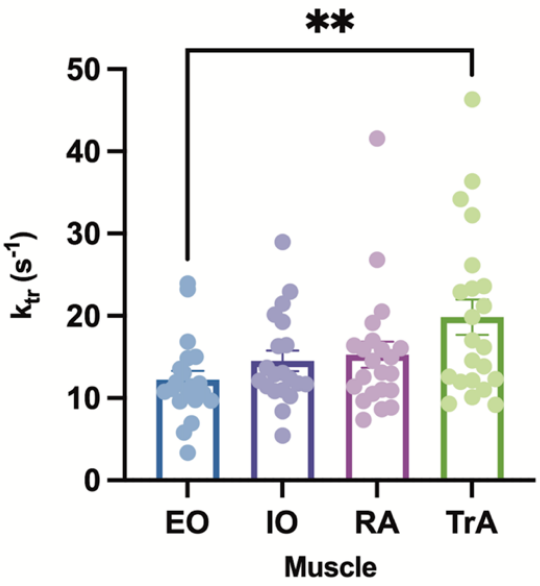

Figure 1: Mean (±SEM) rate of force redevelopment (k_{tr}) of EO, IO, RA, and TrA. One-way ANOVA, ** indicates statistical significance ($p = 0.0285$). Tukey's HSD test significant only for TrA vs. EO with a mean difference of 7.627 ($p < 0.05$, 95% C.I. = 1.669, 13.585).

Significance

TrA having a greater rate of force redevelopment than EO suggests that TrA cross-bridges may be able to transition faster between low and high force-generating states. It is interesting to note that of the abdominal wall muscles, EO and TrA are the two with the most similar fibre orientation but most different in terms of depth (EO being most superficial and TrA deepest with IO in between), thus contributing to the composite laminate-like structure of the abdominal wall. Perhaps diversity in cross-bridge kinetics reduces redundancy and further contributes to the functional aspects of this composite design. However, it must be noted that the rate of force redevelopment variable measured here is specific to single fibres, and how quickly the whole muscle is able to develop and transfer force will also depend upon the compliance of intramuscular and extramuscular (tendon and aponeurosis) connective tissues. The functional significance of the difference in k_{tr} between EO and TrA is unknown and will need to be studied further.

Acknowledgments

Funding was provided by the Natural Sciences and Engineering Research Council (NSERC) of Canada.

References

[1] Brown et al., 2012. *J Orthop Res.* 30: 1321-1326,
[2] Roche et al., 2015. *J Vis Exp.* 100: e52695.

INVESTIGATING THE EFFECTS OF A GRADUAL VCD-INDUCED OVARIAN FAILURE MODEL OF PERIMENOPAUSE ON MUSCLE CONTRACTILITY IN SINGLE FIBRES OF FEMALE MICE

Parastoo Mashouri[1], Jinan Saboune[2], Glen W. Pyle[2], Geoffrey A. Power[1]
[1]Neuromechanical Performance Research Lab, Human Health and Nutritional Sciences, University of Guelph, Guelph, ON N1G2W1, Canada.
[2]Laboratory of Molecular Cardiology, Biomedical Sciences, University of Guelph, Guelph, N1G2W1, Canada, [3]IMPART Investigator Team, Dalhousie Medicine, Saint John, New Brunswick, E2K 5E2, Canada.
email: gapower@uoguelph.ca

Introduction

Throughout menopause, estrogen deficiency is associated with a loss of muscle mass and strength [1-4]. In ovariectomized (OVX) rodent models, estrogen deficiency impairs muscle contractile performance owing to altered contractile protein function, but not changes to Ca^{2+} sensitivity [4]. While OVX models quickly reduce circulating sex-hormones, a model with greater ecological validity and gradual decrease in physiological levels of circulating estrogens is warranted. The purpose of this study is to characterize the effects of menopause on single muscle contractility from a slow-type muscle (soleus; SOL) and fast-type muscle (extensor digitorum longus; EDL) using a VCD-induced perimenopause mouse model. Muscle contractility will be assessed using rate of force redevelopment (ktr), instantaneous stiffness (k), and calcium sensitivity. Thus, the hypotheses for this investigation are: (i) Ca^{2+} sensitivity is expected to remain unaltered in fibres from the menopause group compared to the control group; (ii) specific force and instantaneous fibre stiffness are expected to be lower in tissue from menopausal mice compared to control tissue, with a greater effect on slow-type fibres; (iii) ktr values are expected to be slower in tissue from menopausal mice, with a greater effect on slow-type fibres.

Methods

Perimenopause was induced in sexually mature CD1 female mice by injecting 4-vinylcyclohexene diepoxide (VCD) for 15 consecutive days to cause gradual ovarian failure over 120 days. Mice showed acyclicity in estrus cycles by day 120 indicating the end of perimenopause and the start of the menopause phase. Single muscle fibres were dissected from the extensor digitorum longus (EDL) and soleus (SOL) muscles, and chemically permeabilized. A single muscle fibre was mounted between a force transducer and length controller and activated across varying Ca^{2+} concentrations (pCa 4.5-7.0).

Results and Discussion

Ktr: There was a main effect of muscle ($F(1,98) = 18.561$, $p<0.001$), whereby the EDL muscle was 69% faster than the SOL muscle. Additionally, there was an interaction of group x muscle ($F(1,98) = 8.717$, $p=0.004$), whereby the control EDL was 18% faster than the VCD EDL, and the control SOL was 44% slower than the VCD SOL. Stiffness: There was a main effect of muscle ($F(1,98) = 9.523$, $p=0.003$), whereby the EDL muscle had 25% less stiffness than the SOL muscle. pCa50: There was a main effect of muscle ($F(1,98) = 5.000$, $p=0.028$), whereby the EDL muscle was 1% more sensitive to calcium than the SOL muscle. Thus, there were no differences in Ca^{2+} sensitivity across groups for both fast and slow type muscles. Across all measures, the VCD group did not perform differently than the control group.

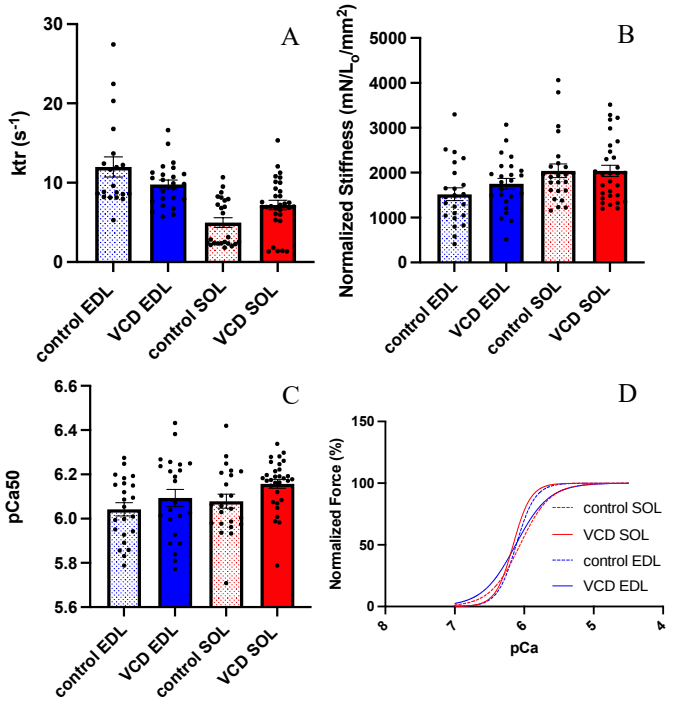

Figure 1A: Single fibres from the EDL, regardless of group produced the fastest ktr. **B:** Active instantaneous stiffness was lowest in fibres from the EDL muscle. **C:** There does not appear to be any differences in Ca^{2+} sensitivity as indicated by similar pCa50 values across groups and fibres. **D:** Force-pCa curve demonstrating similar pCa50 values across all muscles and groups.

Significance

My project will offer new insight into the effects of menopause on Ca^{2+} sensitivity and skeletal muscle contractility with the possibility to delay the negative effects of menopause on skeletal muscle contractility through exercise. More notably, my data will strengthen the present menopause literature by offering better understanding on how different fibre-types are affected throughout the perimenopause phase, which may inform opportunities to delay the negative effects of menopause on muscle function.

Acknowledgments

Supported by NSERC and HSFC.

References

[1] Power et al., 2013. J. *Sport Health Sci.* 2, 215-226.
[2] Sipila et al., 2003. *J. Med. Sci. Sports.* 13, 19-25.
[3] Lowe et al., 2010. *Exerc. Sport. Sci. Rev.* 38, 61.
[4] Cabelka et al., 2019. *Exp. Gerontol.* 115, 155-164.

HOW MUSCLE FORCES IMPACT TENDON STRAIN DURING LOCOMOTION: A DIRECT COMPARISON OF *IN-VIVO* AND *IN-VITRO* TENDON PROPERTIES IN SHEEP

Fransiska M. Bossuyt[1*], Tim Leonard[1], Andrew Sawatsky[1], W. Michael Scott[2], and Walter Herzog[1]
[1]Human performance Lab, Faculty of Kinesiology, University of Calgary, CA
[2]Faculty of Veterinary Medicine, University of Calgary, CA
email: *fransiska.bossuyt@ucalgary.ca

Introduction

Hysteresis and stiffness are tendon properties defined from force-strain curves that play a role in the efficiency of movements [1]. However, *in-vitro* obtained tendon hysteresis values are typically much lower and within a smaller range as compared to the *in-vivo* obtained values defined from estimated strains and forces while tendon stiffness values are more consistent [2]. Importantly, tendon strain has never been obtained with the corresponding directly measured *in-vivo* muscle forces thereby limiting our understanding of how muscles and tendon interact. The aim of this study was to determine the hysteresis and stiffness of a sheep hindlimb tendon *in-vivo* and to compare the *in-vivo* results with those obtained from *in-vitro* experiments that replicated the *in-vivo* conditions. Based on the literature, it was hypothesized that *in-vivo* obtained hysteresis would be greater as compared to the *in-vitro* hysteresis with no major differences in tendon stiffness.

Methods

Following training of six sheep to walk on a motor-driven treadmill, the medial gastrocnemius tendon was isolated and surgically instrumented (Figure 1). A custom-made "E"-shaped buckle-type force transducer [3] was used to measure muscle forces at 1040Hz. Sonomicrometry was used to measure tendon lengths at 520Hz [4]. All signals were transmitted by telemetry to a custom-built amplifier and synchronized with the use of an electronic synchronization pulse. Following 3 days of post-surgical recovery, *in-vivo* data were collected while the sheep walked on the treadmill (Figure 1). Due to technical difficulties and ongoing data-collection, this abstract will present results of one sheep only. Three consecutive steps for walking at 1.96m/s were chosen and used for further analysis. Force and sonomicrometry data were filtered with a low-pass (10 and 50Hz, respectively) 4th order recursive Butterworth filter. The muscle tendon unit, including part of the calcaneus, was dissected for the *in-vitro* experiments which took place 24h post-mortem and included calibration of the tendon force transducer. The tendon was clamped in a mechanical testing machine with a 10kN load cell and preloaded with 14.9N (Instron). A 20-min rest period was followed by 101 conditioning cycles to 1% strain at 0.5 Hz, and 51 test cycles using strain rates and peak forces that had been measured during the *in-vivo* walking conditions. The tendon was kept hydrated using a 0.9% saline solution every 2-min. Tendon strain was calculated as (length-length$_{ref}$)/length$_{ref}$)*100. *In-vivo* tendon strains were measured for a segment of the tendon length (length$_{ref}$ = shortest segment length observed *in-vivo*), while *in-vitro* tendon strains were measured for the entire tendon length (length$_{ref}$ = tendon length at zero strain). Hysteresis was defined as the difference in area between the force vs strain loading and unloading curves relative to the area under the force vs strain loading curve. Stiffness was defined as the slope between the 30-40th frame prior to the end of each loading cycle of the force vs displacement curves. This work was approved by the University of Calgary Veterinary Sciences Animal Care committee.

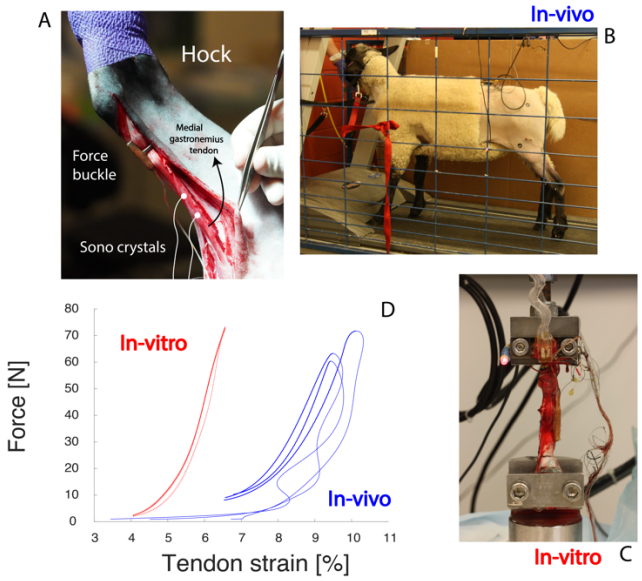

Figure 1: (A) surgically instrumented medial gastrocnemius tendon, (C) tendon clamped in Instron, (D) Force vs strain curve for 3 step cycles of a sheep walking on treadmill at 1.96 m/s (B)(blue line) and replication of the *in-vivo* strain rate and peak force *in-vitro* (red dashed line)(thick lines represent the loading and thin lines the unloading phases).

Results and Discussion

In line with the hypothesis, the hysteresis obtained for the *in-vivo* conditions (58, 64, and 49%) were greater than those obtained *in-vitro* for comparable loading conditions (14%, 13%, and 14%). While our *in-vitro* results are in line with previous *in-vitro* studies, our large *in-vivo* hysteresis values obtained from direct measurements exceeded previous estimations from *in-vivo* human studies [2]. Interestingly, the *in-vivo* stiffness (397 N/mm, 318 N/mm, 364 N/mm, for steps 1, 2, and 3) was different from the *in-vitro* stiffness (55 N/mm, 55 N/mm, 54 N/mm). These results suggest that muscular contractions and the *in-vivo* environment may impact the force-strain relationship.

Significance

The presented differences in *in-vivo* and *in-vitro* obtained tendon properties when directly comparing the same tendon and loading conditions warrant caution when making use of *in-vitro* studies to predict *in-vivo* musculoskeletal loading as commonly done in musculoskeletal modelling and simulation studies.

Acknowledgments

Early postdoc mobility funding from the Swiss National Science Foundation to FMB (187793). The Killam Foundation, the Canada Research Chair programme (CIHR), and NSERC (RGPIN-2020-03920).

References

[1] Voigt M et al. (1995) J Biomech. 28(3): 281-291. [2] Finni T et. al. (2012). J Appl Physiol. 114: 515-517. [3] Kaya et al, 2006. J Biomech. 39(15): 2752-66. [4] Caputi A et al. (1991). J Biomech. 25: 1067-1074.

CHANGES IN RODENT GAIT KINEMATICS AT DIFFERENT WALKING VELOCITIES

W. Brody Hicks[1*], Jack Dienes[2], George J. Christ[2, 3], and Shawn D. Russell[1, 3]
[1]University of Virginia, Depts. of [1]Mechanical Eng., [2]Biomedical Eng., and [3]Orthopaedic Surgery, Charlottesville, VA, USA
Email: *wbh2nz@virginia.edu

Introduction

The rodent hindlimb model system is frequently utilized to analyze hindlimb pathologies and their treatments. Joint kinematics are commonly used to evaluate both normal and pathologic gait, but there is still little understanding of the effect of locomotion speed on normal rodent hindlimb kinematics. Gillis and Biewener[1] presented changes in sagittal plane kinematics at the hip and knee as rodents employed different gait phases (walk, trot, transverse gallop) and identified a distinct speed bin where the rats utilized a walking locomotion pattern (17-48 cm/s). This lab has recently worked to establish a normative database for 3D kinematics and kinetics in the walking velocity bin[2]. However, our work has led us to notice subtle changes in joint kinematics as a function of walking speed, even within the walking locomotion pattern. In order to comprehensively understand the contributions of pathology to rodent gait in future studies, we need to better understand how velocity can alter joint kinematics within the walking phase.

Methods

15 twelve-week old female Lewis rats were labeled with motion capture markers and recorded using Vicon Nexus software as they voluntarily walked down an instrumented walkway at a self-selected speed. Simulations were performed on subject specific versions of a modified OpenSim 3D rat hindlimb model[2] to calculate hindlimb joint kinematics. Each rat's simulation data was then separated into two bins based on walking velocity: slow (17-29.5 cm/s) and fast (35.5-48 cm/s). Analysis of the joint kinematic curves and was performed using Statistical Parametric Mapping (SPM1) MATLAB code and paired t-tests (α=0.05). Spatiotemporal parameters were calculated using marker positions acquired from Vicon Nexus and were evaluated using paired t-tests (α=0.05).

Results and Discussion

The slow group exhibited significantly slower velocity, shorter strides, slower strides, and more time in stance than the fast group (see Table 1, $p<0.001$ in all parameters). Sagittal plane kinematics at the hip, knee, and ankle all display significant differences consistent with a phase shift between the fast and slow groups. Peak hip extension occurs earlier in the gait cycle for the fast velocity group, leading to earlier hip flexion in swing phase ($p=0.005$). This phase shift is also evident in hip rotation kinematics, as the hip externally rotates earlier through swing for the fast group ($p=0.001$). The knee is characterized by more knee extension in late stance for the fast group ($p<0.001$), and less knee flexion in swing ($p<0.05$). In the ankle, peak dorsiflexion occurs earlier in the gait cycle, and the animals are reaching higher peak plantarflexion values in the fast group ($p<0.001$). In swing, the fast group is more plantar-flexed than the slow group ($p<0.05$). These kinematics indicate the phase shift associated with the fast group spending a lower percentage of the total gait cycle in stance, and are likely associated with an increase in propulsive force for the fast group.

Table 1: Spatiotemporal Parameters for fast and slow groups.

	Slow	Fast
Stride Length (cm)	11.18±0.01	13.87±0.01
Stride Time (s)	0.46±0.07	0.34±0.02
Velocity (cm/s)	24.82±2.93	40.65±3.24
Percent Stance (%)	67.05±5.22	60.00±3.70

The lower stance percentage at faster walking velocities explains the transition to earlier peak extension angles in the hip and knee, as well as earlier peak plantarflexion in the ankle. As the animals increase their walking velocity, the knee extension and ankle plantarflexion excursions toward foot off decrease in magnitude, indicating that they are pushing off more in a shorter time as they maintain their higher velocity.

Significance

This work shows that changes in walking velocity contribute to kinematic differences in normal rodent gait. Walking velocity must be considered when evaluating kinematic differences in rodent gait as a response to hindlimb pathology. Previous work from this lab shows that animals walk slower after injury. As a result, it is necessary to understand the relationship between walking speed and joint kinematics to characterize kinematic changes due to injury vs. kinematic changes due to change in walking velocity. Furthermore, this work reveals the need to further explore joint kinetics in both normal and injured rats at different walking speeds to better understand why animals walk slower after injury.

Acknowledgments
We would like the members of the MAMP and Christ Laboratories for their contributions to this work.

References

[1] Gillis et al, 2001. *J. Experimental Biomechanics.*, 204: 2717-2731 [2] Dienes et al, 2021 *Scientific Reports* (in review) [3] Johnson et al, 2008. *J Biomech* 41(3) 610-619.

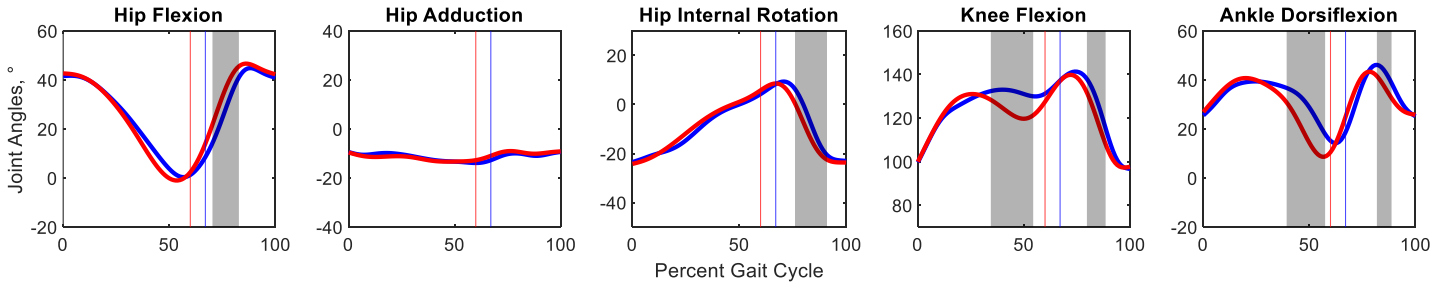

Figure 1: Kinematics Comparisons between slow (blue) and fast (red) velocity groups for the hip, knee, and ankle. Areas of significant difference between groups are shown as grey shaded regions with their respective p-values. (SPM1, paired t-test, $p < 0.05$). Foot off for each group plotted as vertical line.

NEUROMUSCULAR CONTROL STRATEGIES IN WALKING VERSUS RUNNING ON UNEVEN TERRAIN

M. Janneke Schwaner[1*], Joanne C. Gordon[2], Andrew A. Biewener[3], and Monica A. Daley[1]
[1]University of California, Irvine, CA, USA, [2] Royal Veterinary College, UK, [3]Harvard University, Cambridge, MA, USA
email: *mjschwan@uci.edu

Introduction

Agile and stable movement requires integration of complex sensorimotor networks to meet rapidly varying mechanical demands and substrate interactions. Motor commands arise from a synthesis of feedforward control and reflex-mediated feedback responses and are constrained by whether adjustments are required in short or longer timescales. Guinea fowl negotiating obstacles at slow speeds exhibit both anticipatory and reflex-mediated stride-to-stride muscle activity changes [1]. In contrast, at fast speeds, stride-to-stride variability is reduced, suggesting a shift toward feedforward control and a higher intrinsic stability. Stride cycle timing varies during obstacle negotiation at slow speeds, but not at fast speeds, consistent with feedforward limb cycling at high speeds and greater reflex modulation at slower speeds. Guinea fowl with induced proprioceptive deficit in the gastrocnemius show an increase in feedforward activation, but otherwise maintain a similar movement strategy for running over obstacles [2]. Here we investigate the effect of gastrocnemius proprioceptive deficit on the sensorimotor control of walking in guinea fowl. We hypothesize that, compared to intact birds, birds with proprioceptive deficit will reduce reliance on reflex-mediated modulation of muscle activity while walking on obstacle terrain.

Methods

Self-reinnervation procedures were performed on birds, during which the nerve that innervates the lateral gastrocnemius muscle was surgically cut and immediately repaired [2], [3]. After a 13–16-week recovery period, during which birds were familiarized with the treadmill, *in vivo* muscle transducers were implanted into the lateral gastrocnemius. Transducers included 2 sonomicrometry crystals, 2 EMG electrodes and an E-shape force transducer (tendon buckle) placed around the common gastrocnemius tendon. After 24-hours of recovery, each bird was recorded while walking and running on a treadmill fitted with 5cm high obstacles spaced to allow ~5–7 steps between obstacle encounters [1], [2].

Sonomicrometry, EMG, and tendon buckle data were analysed using in-house MATLAB scripts, to obtain muscle activity, work, and force data.

Results and Discussion

We found that reinnervated birds showed delayed obstacle recovery in walking, with the largest increase in EMG activity occurring in the stride after obstacle contact (Fig. 1). Additionally, we found that the gastrocnemius muscle increased force, but not work during obstacle encounters when walking, suggesting a shift towards isometric contraction.

When comparing the effects of proprioceptive deficit in walking versus running, we found reinnervated birds maintained similar strategies as intact birds during running but shifted towards a work-minimizing control strategy for obstacle negotiation during walking. Further analysis of limb and joint mechanics is needed to test whether reinnervated birds increase reliance on more proximal muscle groups, such hip and knee extensors, while walking over uneven terrain.

Future research using unexpected perturbations could parse out the role of visual input versus proprioception for navigating complex terrains.

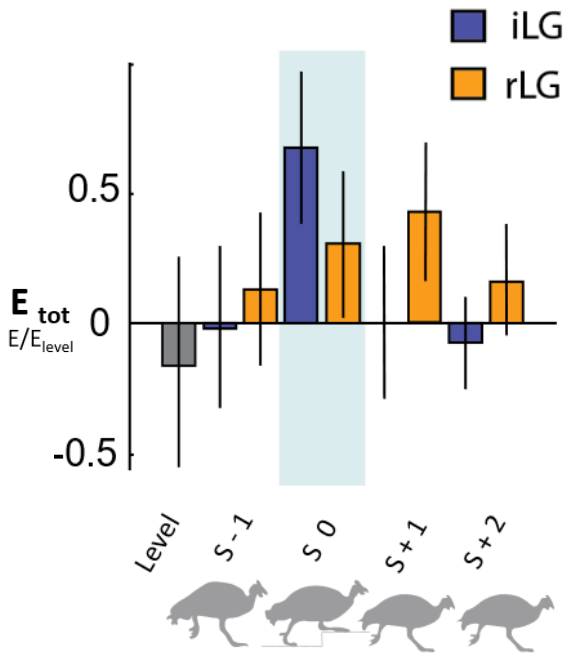

Figure 1: Muscle activity (E_{tot}) during walking in level and obstacle trials. Intact birds (blue) exhibit a reflex-mediated increase in muscle activity on the obstacle stride (S 0), whereas reinnervated birds (orange) show reduced reflex-mediated response and a greater increase in activity in the first (S+1) and second (S+2) recovery strides after the obstacle.

Significance

Navigating complex terrains requires dynamic interactions between the environment, the sensory system, and the musculoskeletal system. However, the mechanisms of sensorimotor adaptation and plasticity remain poorly understood. By understanding these mechanisms and their interactions in guinea fowl as a model system, we hope to provide insight into recovery from nerve damage in humans and improve strategies for rehabilitation and physical therapy.

Acknowledgments

NIH, NIAMS 5R01AR055648 (A.A.B); Biotechnology and Biological Sciences Research Council BB/H005838/1 (M.A.D) and Doctoral Training Studentship (J.C.G, M.A.D); NSF-IOS, 2016049 (M.A.D).

References

[1] Gordon et al., 2015. *J of Exp Biol*. 218: 104646.
[2] Gordon et al., 2020. *eLife*. 9: e53908
[3] Carr et al., 2010. *Proc of ASB*.

PREDICTING KNEE ADDUCTION MOMENT RESPONSE TO GAIT RETRAINING

Nataliya Rokhmanova[1,2*], Katherine J. Kuchenbecker, Peter B. Shull, Reed Ferber, and Eni Halilaj
[1]Department of Mechanical Engineering, Carnegie Mellon University, Pittsburgh PA, USA
[2]Max Planck Institute for Intelligent Systems, Stuttgart, DE
email: *nrokhman@andrew.cmu.edu

Introduction

Personalized gait retraining has shown promise as a conservative intervention for slowing knee osteoarthritis (OA) progression [1,2]. Changing the foot progression angle is an easy-to-learn gait modification that often reduces the knee adduction moment (KAM), a correlate of medial joint loading. Deployment to clinics is challenging, however, because customizing gait retraining still requires gait lab instrumentation. Innovation in wearable sensing and vision-based motion tracking could bring lab-level accuracy to the clinic, but current markerless motion-tracking algorithms cannot accurately assess if gait retraining will reduce someone's KAM by a clinically meaningful margin. To assist clinicians in determining if a patient will benefit from toe-in gait, we built a predictive model to estimate KAM reduction using only measurements that can be easily obtained in the clinic.

Methods

For data-driven predictive models to generalize, the training data must be large and variable. Since a large dataset of both baseline and toe-in gait does not exist yet, we generated the data synthetically. Our approach consisted of four steps:

(1) Optical motion capture and ground reaction force data from 12 knee OA patients walking on an instrumented treadmill at baseline and toe-in [2] were used to learn patterns of how the foot center of pressure, knee joint center, and ground reaction force—used to compute KAM—change with increasing toe-in angle. A leave-one-out approach was used to assess the generalizability of the learned patterns to new subjects.

(2) The learned toe-in gait patterns were then used to synthesize toe-in gait from an optical motion capture dataset of 138 subjects [3] and compute KAM changes. We calculated KAM with the lever-arm method and used the reduction in the first peak of KAM from baseline to synthetic toe-in as the outcome to be predicted by the final model.

(3) We trained a linear regression model with LASSO to predict first peak KAM reduction from six input features that can be easily collected in the clinic: height (HT), bodyweight (BW), baseline walking speed, static knee alignment, baseline foot progression angle, and target toe-in angle. The data were split into training (N=110), validation (N=14), and test (N=14) sets.

(4) For independent validation with a dataset collected in a different environment, we collected optical motion capture data from 15 healthy subjects walking at baseline and toe-in gaits.

Results and Discussion

The synthetic toe-in data generation approach correctly captured the first peak KAM reduction in both the cross-validation and the independently collected datasets (Fig 1A). The first KAM peaks were estimated with a mean absolute error of 0.174 (±0.135) %BW*HT in the cross-validation and 0.170 (±0.101) %BW*HT in the independent set. The true reduction in the first peak of KAM for the independent set was 0.620%BW*HT, more than three times this error. Knee joint center and center of pressure patterns were estimated with an RMSE of 14 mm, or within the range of motion capture accuracy [4].

The predictive model using six easily-obtained features estimated the first peak KAM reduction with an error that was lower than baseline within-subject variability across steps (Fig. 1B). In the synthetic test set, the trained model predicted KAM reduction to a mean absolute error of 0.095%BW*HT (±0.072). In the independent set, the mean absolute error was 0.134%BW*HT (±0.0932), which was smaller than the average standard deviation of the first peak at baseline (0.306%BW*HT). As the model performed comparably on both sets, the feasibility of training predictive models on synthetic data further extends the value of existing motion capture datasets. The model corresponding to the minimum mean squared error used all six features even after regularization was applied. The toe-in angle was the strongest predictor of KAM reduction, and higher weight and valgus angle during static alignment were related to a smaller KAM reduction. While toe-in angle and alignment have been previously related to KAM reduction, more investigation is needed to determine the effect of weight on retraining outcomes. Prior research has shown that some patients reduce KAM more with a toe-out gait [1]. Adding toe-out gait data from other laboratories could extend this proof-of-concept model to identify a patient-specific gait with the greatest therapeutic benefit.

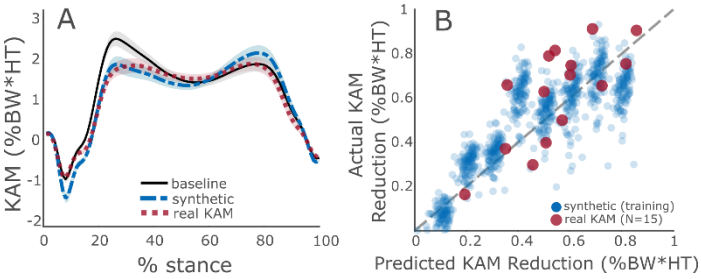

Figure 1: Independent validation (N=15) showed that (A) synthetic KAM accurately captured true KAM during toe-in gait and (B) the predictive model generalized well to new subjects.

Significance

Predicting whether a patient will respond to therapeutic gait retraining without comprehensive gait analysis could cut down the time and experimental resources that currently prevent gait retraining from being deployed to clinics. Coupled with wearable haptic systems that patients can take home to practice newly prescribed gaits, predictive models like the one presented here could accelerate the clinical translation of a highly promising intervention shown to slow OA progression.

Acknowledgments

This work was supported by NSF grants DGE1745016 and DGE2140739. We thank Owen Pearl for his assistance in data collection.

References

[1] Uhlrich, SD, et al. ISB 2021; [2] Shull, PB, et al. J. Biomech 2013; [3] Ferber, R, et al. J. Biomech 2016; [4] Peters, A, et al. Gait & Posture 2010.

Opening the black box: Using explainable AI to understand what a neural network learns from lateral pinch simulations

Kalyn M. Kearney[1], Joel B. Harley[2], Jennifer A. Nichols[1]
[1]J. Crayton Pruitt Family Department of Biomedical Engineering, University of Florida, Gainesville, United States
[2]Department of Electrical and Computer Engineering, University of Florida, Gainesville, United States
email: *kalynkearney@ufl.edu

Introduction

Machine learning approaches can infer complex biomechanical relations. Yet, many models are regarded as a "black box," lacking interpretability and limiting user confidence. While various works have recently advanced the field of explainable artificial intelligence (XAI)[1,2], very few have applied these methods to explain time-series biomechanical data. A notable example, Horst et. al[3] employed layer-wise relevance propagation to classify gait patterns from measured kinetic and kinematic data. This work presented a robust, interpretable model to provide data-driven gait analysis. XAI may provide clinical and scientific insights for a variety of other tasks beyond gait.

Here, we expand the use of XAI to the upper extremity, which is a complex, high degree-of-freedom system. Our objective was to reveal what a deep long short-term memory model (LSTM) learns from forward dynamic lateral pinch simulations. We used Shapley Additive Explanations (SHAP) to explain our LSTM's predictions. Known for consistent interpretations, SHAP considers all possible predictions for an observation using all possible combinations of features[4]. Importantly, we interpret SHAP values for our LSTM in the context of prior literature, providing both confidence in and insight from our model.

Methods

We developed an LSTM, which is a type of neural network, to predict lateral pinch thumb-tip forces from muscle activations. The LSTM included 14 inputs representing simulated muscle activations for 5 wrist and 9 thumb muscles. There were 3 hidden layers with 16 nodes each and 3 output nodes corresponding to 3-component thumb-tip forces. The LSTM used an RMSE loss criteria and an Adam optimizer. The LSTM underwent parameter tuning via random search, and 5-fold cross validation was used.

To provide observations to train our LSTM, we simulated lateral pinch data with varied anthropometric scaling and target forces. Using OpenSim v. 4.1, we scaled a thumb model[5] to random masses and bone lengths representing 5th-95th percentile young adults[6]. Each scaled thumb model was used in computed muscle control (CMC) simulations[7]. Target thumb-tip forces ranging from 40 N to 80 N in 5 N increments were CMC inputs. We applied these forces palmarly at the thumb-tip, as well as with 25% distal, 25% ulnar, and 25% radial deviations. Altogether, each scaled thumb model (525 total) was run through CMC 36 times (9 forces x 4 directions). Forward dynamics was then used to estimate thumb-tip forces resulting from the muscle activations from CMC. Muscle activations from CMC acted as LSTM inputs and thumb-tip forces from forward dynamics acted as outputs.

Data preprocessing included (1) removing simulations that failed to complete, (2) linearly interpolating all simulations to the same number of time points, (3) truncating the simulations to remove noise end effects, and (4) removing unphysical and unstable simulations. We then shuffled and split the resulting 6,590 simulations into training and testing datasets (80/20 split).

We analyzed the performance and predictions of the LSTM. Here, we report the RMSE of our LSTM evaluated on test data to elucidate the LSTM's ability to predict forces from muscle activations. To explain the predictions of the LSTM, we calculated SHAP values for 1000 random test observations. Briefly, SHAP values are calculated by first permuting all model features and training a distinct model (i.e. the LSTM) for each combination. The SHAP value for a feature is the average of the marginal contributions across all permutations of model features.

Results and Discussion

The LSTM predicted forces from muscle activations with low error. RMSEs for the LSTM were 1.64 N, 0.932 N, and 0.692 N for the distal, dorsal, and ulnar force directions, respectively. For each observation, the absolute error in the LSTM's prediction generally followed a normal distribution centered about 0 N.

The SHAP values of the five features most important for the LSTM's predictions are displayed in Fig. 1. Consistent with observations from cadaver specimens[8], the LSTM predicted a large negative dorsal force when activation of the *flexor pollicis longus* (FPL) was high and the *extensor pollicis brevis* (EPB) was low (Fig. 1, when FPL & EPB are red, SHAP value for F_y is large). Fascinatingly, the LSTM's prediction of thumb-tip force was substantially impacted by the activation of wrist muscles (Fig 1, *extensor carpi ulnaris*, ECU, and *flexor carpi ulnaris*, FCU). This result is consistent with prior literature, as wrist posture is known to affect lateral pinch strength[9].

In summary, we present two key findings: (1) the LSTM was able to learn the mapping between simulated muscle activations and simulated thumb-tip forces with low error and (2) interpreting the LSTM via SHAP revealed impacts of muscle activations on thumb-tip forces consistent with prior literature.

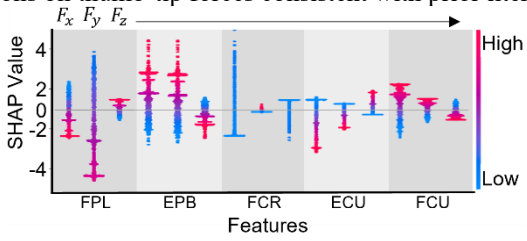

Fig. 1: SHAP values from 1000 test observations for the most important features predicting thumb-tip force in distal, dorsal, and ulnar directions (F_x, F_y, and F_z, respectively). Colors represent muscle activations.

Significance

The present work exemplifies not only the robustness of deep models for predicting upper extremity biomechanics, but that these models no longer need be considered a totally "black box."

Acknowledgments

Funding from National Science Foundation Graduate Research Fellowship and NIH NIBIB Trailblazer Award (R21EB030068).

References

[1] Roscher et al., 2020. *IEEE Access*. 8: 42200-42216. [2] Samek et al. 2017. *arXiv preprint*. [3] Horst et al. 2019. *Sci. Rep*. 9(1): 1-13. [4] Lundberg et al. 2017. *Proc. 31st NeurIPS*. [5] Nichols et al. 2017. *J Biomech*. 58: 97-104. [6] Fryar et al. 2016. *Vital Health Stat 3*. 39: 1-46. [7] Thelen et al. 2003. *J Biomech*. 36: 321-328. [8] Pearlman et al. 2004. *J Orthop Res*. 22(2): 306-312. [9] Dempsey et al. 1996. *Int. J. Ind. Ergon.* 17(3):273

EXAMINING MACHINE LEARNING CLASSIFICATIONS WITH EXPLAINABLE AI AIDS INTERPRETATION OF WRIST BIOMECHANICS

Isaly Tappan[1], Erica M. Lindbeck[1], Jennifer A. Nichols[2], and Joel B. Harley[1]
[1]Department of Electrical and Computer Engineering, University of Florida
[2]J. Crayton Pruitt Family Department of Biomedical Engineering, University of Florida
email: i.tappan@ufl.edu

Introduction

The last decade has seen advances in the speed, reliability, and accuracy of biomechanical data collection. As datasets increase in size and complexity, biomechanists have turned to artificial intelligence (AI) to aid their analyses. However, a significant drawback of using AI is its black-box character, which obfuscates the reason for any given prediction. To alleviate this, explainable AI (XAI) has evolved to elucidate complex relationships between input data and the decisions of an AI system. Here, we explore whether local explanations (i.e., explaining what features best explain individual classifications) can enhance the interpretability of biomechanics data derived from musculoskeletal simulations. We use XAI to explain how a machine learning algorithm classifies simulated lateral pinch data as belonging to either healthy or types of surgically altered wrists. This simulation-based classification task is analogous to using biomechanical movement and force data to clinically diagnose a pathological state.

Methods

A simulation dataset was generated using published models and methods [1] in OpenSim. Briefly, three models were created to represent the healthy wrist and two surgeries for wrist osteoarthritis (PRC: proximal row carpectomy and SE4CF: scaphoid-excision four-corner fusion). Simulations of lateral pinch (n = 315) were generated by varying the anthropometric scaling (90-110% of baseline) and target thumb-tip endpoint force (10-50N in increments of 10N). Each simulation can be thought of as data from a synthetic patient. Simulation outputs included a 3D thumb-tip endpoint force and six joint angles across the wrist and thumb for a total of nine time-varying features. A random forest classifier [2] composed of 100 trees was trained to predict wrist impairment using 15-fold cross-validation (93% training simulations and 7% testing simulations).

Within every unique validation fold, an XAI framework known as Local Interpretable Model-Agnostic Explanations (LIME) [3] was applied to each time point in the testing set, thereby producing nine feature importance scores per time point per subject. The feature importance score indicates how much the prediction probability of the top class would change if the given feature were perturbed, with negative values indicating the feature contributed toward a class other than the top prediction. Following cross-validation, the importance scores were averaged across time to produce nine final feature importance values (i.e., scores defined for each synthetic subject). The final values were subsequently averaged across each classification to produce explanations specific to each impairment (nonimpaired, PRC, SE4CF). Final values were also averaged across musculoskeletal model sizes (produces explanations for combinations of target force and impairment classification), and across target forces (produces explanations for combinations of model size and impairment classifications). From these averages, we can evaluate whether explanations for identifying impairment change based on the characteristics (size and strength) of the synthetic patients.

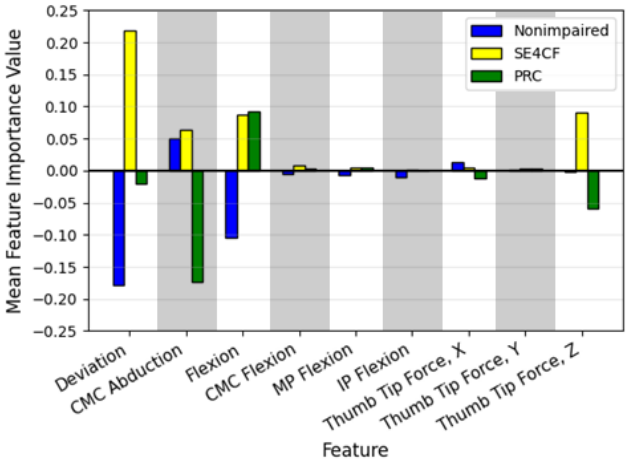

Figure 1: Final feature importance values averaged across impairment classification.

Results and Discussion

Our results demonstrate that LIME can be used to identify and explain the biomechanical features helpful for distinguishing nonimpaired and impaired synthetic patients. For example, the magnitude of the feature importance value for wrist flexion is large for all three conditions, but it is only negative in the nonimpaired condition (Fig. 1). This suggests that wrist flexion aids the classifier in distinguishing between nonimpaired and impaired states. Following this classification, the results show that a combination of radial-ulnar deviation and carpometacarpal (CMC) abduction can be used to further distinguish SE4CF versus PRC. This is illustrated by the difference in sign between the SE4CF and PRC importance values for radial-ulnar deviation and CMC abduction. Mean importance values across model sizes and target forces (not shown) illustrate the same trends, indicating these factors do not substantially influence which features are important. In addition, the explanations highlighted by LIME align with experimental data demonstrating that wrist flexion and radial-ulnar deviation are important for distinguishing these conditions [4].

Significance

This work demonstrates that XAI can identify the most important features for classifying impairments and how these features change with synthetic patient size and strength. Thus, XAI can effectively remove the black-box character of AI when used in biomechanical analyses. This capability could aid in elucidating the biomechanical mechanisms underlying impairment.

Acknowledgments

Funding from NIH NIBIB Trailblazer Award (R21EB030068).

References

[1] Nichols et al., 2017. *J Biomech*. 58.
[2] Pedregosa et al., 2011. JMLR 12: 2825-2830.
[3] Ribeiro et al., 2016. ACM SIGKDD: 1135-1144.
[4] Nichols et al., 2015. *J. Biomech*. 30.

GROUND REACTION FORCE ESTIMATION FROM WEARABLE SENSORS DURING FREE RUNNING

Seth R. Donahue[1*], Michael E. Hahn[1]
[1]Bowerman Sports Science Center, Department of Human Physiology, University of Oregon, Eugene OR
email: sethd@uoregon.edu

Introduction

Machine learning and wearable sensors have shown potential for the estimation of biomechanical variables in the laboratory [1]. Previous work has demonstrated portions of ground reaction force (GRF) waveforms can be estimated with machine learning, and kinetic variables can be calculated from these waveforms with minimal error [2]. However, these systems are yet to be validated in a real-world environment across a range of running velocities and slopes.

The purpose of this study was to implement a bidirectional long short term memory network (BD-LSTM) for the estimation of GRF waveforms from participants free running on a 5 mile course. It was expected that impulse from estimated GRF waveforms would have an RMSE of 0.030 BW*s, which was similar to the average estimation error reported recently [2].

Methods

This study was approved by the UO Institutional Review Board. Data were collected from 16 recreationally trained runners (8 female, age: 23.15 years, height: 167.77 cm, mass: 65.00 kg). Each participant was equipped with Loadsol force sensing insoles, (sf = 100 Hz) (Novel Electronics, St. Paul, MN). Three inertial measurement units (IMUs) were mounted on each participant, two bilaterally on the dorsal aspect of each foot, and one attached near the sacrum on the participant's waistband (sf = 200 Hz) (Casio, Tokyo, JPN). Participants also wore a Garmin GPS (sf = 1 Hz) (Kansas City, KS). Participants were instructed to run a 5-mile course at their own pace. Three participants were excluded from analysis, due to GPS malfunction.

All analyses were performed offline in custom Matlab programs (Mathworks, Natick, MA). Acceleration data from the IMUs were corrected with a Kalman filter, aligning the vertical axis with gravity. Measured GRFs were normalized to body weight. All data were synchronized and resampled to 100 Hz. Input into the BD-LSTM were linear acceleration and angular velocities were divided into 1 second windows. Outputs were 1 second estimated GRF waveforms. A BD-LSTM consisting of four layers was used to estimate GRF waveforms from IMU data. The estimated GRF waveforms were filtered with a 2nd order low pass zero lag Butterworth filter (f_c = 15 Hz). Model behavior was assessed using leave one out cross validation (LOOCV) analysis.

Errant estimated kinetic data were removed by setting estimated force <5% BW to 0 BW, and foot contacts <100 ms and > 500 ms were removed from the analysis. Initial contact was identified by the first instance of force > 5% BW and toe off was determined by the last instance of force > 5% BW.

Foot contacts were grouped by slope > 5° (incline), between 5° and -5° (level ground) and < -5° (decline), and by running velocity at 0.25 m s^{-1} intervals from 2.25 m s^{-1} to 5.25 m s^{-1}. For a velocity and slope combination to be included in the analysis, a minimum of 10 consecutive steps were required for each slope and velocity combination. For each foot contact stance average GRF and impulse values were calculated from the estimated waveforms and compared to the measured GRFs. Bias in the estimate was calculated with mean difference and 95% limits of agreement (LoA).

Results and Discussion

There were 85,406 analyzed foot strikes. Each presented data point represents the average value of each velocity and slope combination for each participant. Average impulse calculated from measured GRFs during level ground running in the current study was 0.360 BW*s compared to 0.340 BW*s reported recently for level treadmill running [2].

Average root mean squared error (RMSE) for estimated impulse was larger than the anticipated RMSE of 0.030 BW*s: 0.0397 ± 0.0150 BW*s for level ground running, 0.0446 ± 0.021 BW*s for decline, and 0.039 ± 0.023 BW*s for incline running. The mean difference between measured and estimated impulse was -0.020 BW*s (Figure 1). This resulted from an underestimation of stance average GRFs, which had a mean difference (-0.113 BW). Compared to recently reported estimation error of 0.030 BW*s for impulse [2], estimation error from the current work was slightly higher, likely due to the collection of data in a free running environment, compared to the controlled environment of the laboratory.

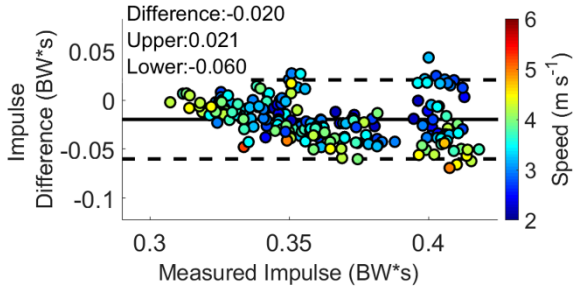

Figure 1: Bland-Altman plot of the differences between measured and estimated impulse for all measured foot contacts.

Limitations of this work include errors in the GPS data synchronization process, with slight errors in the estimation of velocity and altitude. Further, corrections were made to the force sensing insole data (approximately 500 footfalls had an issue with floating baseline that had to be set to 0). Lastly, an iterative corrections algorithm was used to address discrepancies between IMU and the force sensing insole internal clocks.

Significance

This is the first work to collect inertial and kinetic data during a free run and use a BD-LSTM to estimate GRF waveforms. It is now possible to estimate basic spatial temporal and kinetic variables from a machine learning model focused on running outside the laboratory.

Acknowledgments

This work was part of an industry sponsored project, supported by Casio, and was also supported by the Wu Tsai Human Performance Alliance and the Joe and Clara Tsai Foundation.

References

[1] Halilaj, E. et al., *JBiomech*, 81, 1-11, 2018.
[2] Alcantara, R. et al., *PeerJ,* 10, e12752, 2022.

MULTI-DIMENSIONAL DYNAMIC TIME WARPING DISTANCE BASED APPROACH FOR THE RECOGNITION OF HIGH KNEE FLEXION POSTURES IN INERTIAL SENSOR DATA

Annemarie F. Laudanski[1*], Arne Küderle[2], Felix Kluge[2], Bjoern M. Eskofier[2], and Stacey M. Acker[1]
[1]Department of Kinesiology and Health Sciences, University of Waterloo, Waterloo, ON, Canada
[2]Department of Computer Science, Friedrich-Alexander Universität, Erlangen, Germany
email: *annemarie.laudanski@uwaterloo.ca

Introduction

Cyclic and prolonged adoption of high knee flexion postures, where the flexion angle exceeds 120°, have been associated with increased risk for joint tissue degeneration and knee osteoarthritis development [1]. Despite this risk, the frequent adoption of such postures is standard within many occupations, including floor laying, tile setting, mining, and childcare [1, 2]. In order to inform injury prevention initiatives, quantitative, occupation-specific physical demands data must be obtained.

Inertial measurement units (IMUs) offer a reliable and non-intrusive approach to continuously measure postural adoption in workplace settings, however the interpretation of such data presents challenges not typically experienced in laboratory based collections. Without a researcher present during collections, an alternative method of identifying adopted postures from the inertial data is required. While the physical demands of childcare, as they relate to high flexion postural adoption, have previously been analyzed using sensor-based approaches in 2 studies; both defined knee straining postures to include only kneeling, squatting and seated postures [3, 4]. Therefore, the objective of this study was to develop a means by which childcare-specific high knee flexion postures could be identified from IMU data, ultimately allowing for the continuous measurement of such exposures in childcare settings.

Methods

Forty-eight participants were recruited to complete 3 repetitions of 9 postures (7 high flexion and 2 upright, Table 1) frequently adopted by childcare workers under unloaded and loaded (12 kg) conditions (except for the supported kneeling and stooping motions). Participants were instrumented with 7 IMUs, attached bilaterally to the superior aspect of the mid-foot, the lateral aspect of the lower and upper leg, and at the base of the sacrum.

To identify the adopted childcare postures based on these IMU data, a multi-dimensional Dynamic Time Warping (MD-DTW) distance based classification model was developed. IMU signals were first calibrated based on isolated motion trials about the hip and knee as well as a 10 m walk trial; and ankle, knee, and hip flexion angles were subsequently estimated [5, 6]. These data were then time and scale normalized to 101 points and between -1 and 1 respectively and divided such that data from 33 participants were split into training and testing datasets (80% and 20% respectively) while the remaining 15 participants were withheld for classification performance validation on novel data. DTW distances (D) for each joint angle were calculated, with warping paths constrained within 5-samples, and combined using iteratively determined unique weightings as in Equation 1 below.

$$1.\quad D_{MD-DTW} = 0.25 \cdot D_{ankleL} + 0.25 \cdot D_{ankleR} + 0.75 \cdot D_{kneeL} + D_{kneeR} + 0.7 \cdot D_{hipL} + 0.7 \cdot D_{hipR}$$

Each high flexion movement was identified based on the MD-DTW distances during the training and testing of a 5-fold cross validated nearest neighbour classifier (k = 1). The model was tested on novel data from the subjects on which it was trained (testing data) as well as on novel subject data (validation data).

Results and Discussion

Overall accuracies of 84.9% and 72.0% were reached when classifying postures on testing and validation data respectively. Movement precision, recall, and specificity can be found in Table 1. This model proved highly accurate in distinguishing upright from high flexion postures, and high precision values were observed in distinguishing all kneeling postures.

Table 1: Precision (P), recall (R), and specificity (S) (%) for novel testing data and novel subject validation data from 9 childcare postures classified using MD-DTW nearest neighbour classification

	Testing Data			Validation Data		
Movement	P	R	S	P	R	S
Dorsiflexed Kneeling	92	92	99	78	76	96
Plantarflexed Kneeling	91	81	97	89	91	98
Flatfoot Squatting	68	76	96	53	44	91
Heels-Up Squatting	71	69	96	45	58	93
Child-Chair Sitting	72	80	97	66	52	92
Adult-Chair Sitting	83	83	98	54	68	95
Supported Kneeling	97	92	99	91	87	98
Stooping	100	100	100	94	79	98
Standing	100	97	100	99	95	99

The highest rates of misclassification were observed between flatfoot and heels-up squatting and between child-chair and adult-chair sitting. While grouping these postures would yield higher overall classification rates, the interpretation of unique postures adopted by childcare workers remains the ultimate goal of this research and the current model allows for the analysis of such data within the limits of the precisions here presented.

Significance

In this work – the first application of MD-DTW to the identification of childcare specific high knee flexion postures – the generally high classification rates on novel data indicate strong potential for the proposed model's application to the quantitative measurement of postural requirements in numerous childcare settings. While the movements analysed in this study replicated those observed in childcare settings, the proposed model could be applied in numerous occupations to inform musculoskeletal injury prevention initiatives.

Acknowledgments

Funding provided by the Canadian Foundation for Innovation, NSERC Canada, and the ISB International Travel Grant.

References

[1] Coggon et al., 2000 *Arthritis Rheum* **43**(7); 1443-1449
[2] Laudanski et al., 2021 *Ergonomics*; 1-12
[3] Holtermann et al., 2020 *Ann. Work Expo.* **64**(6); 586-595
[4] Burford et al., 2017 *Ergonomics* **60**(12); 1718-1729
[5] Seel et al., 2014 *Sensors* **14**; 6891-6909
[6] Küderle et al., 2018 *Curr. Dir. Biomed. Eng* **4**(1); 439-442

ESTIMATION OF KNEE ADDUCTION MOMENT DURING WALKING USING WEARABLE SENSOR DATA WITH AN OPTIMIZED SEQUENCE-BASED ARTIFICIAL RECURRENT NEURAL NETWORK

Yu-Pin Liang and Li-Shan Chou
Department of Kinesiology, Iowa State University, Ames, IA, USA
email: yupinl@iastate.edu

Introduction

Peak knee adduction moment (KAM) during walking has been reported as a sensitive biomechanical marker for predicting the risk of knee osteoarthritis [1, 2]. However, its requirement for equipment and technical processing significantly restricts clinicians' access to such important data. Recent advances in wearable sensor technologies offer an opportunity to bridge this gap. Moreover, an emerging recurrent neural network (RNN) model, the Long Short-Term Memory (LSTM), is capable of making predictions based on time series data. Studies [3] have employed wearable sensors to estimate knee joint moment, which did not account for sequential information from the input data and required a significant amount of computational time. The purpose of this study was to estimate KAM during walking using data measured from accelerometers with the RNN-LSTM modeling.

Methods

Twelve male and 12 female adults were recruited for the study. Motion data from a total of 9 walking trials with three different walking speeds (self-selective, slow and fast) were collected using a 12-camera motion analysis system. Concurrently, two tri-axial accelerometers were placed at the medial (Med) and lateral (Lat) sides of the femur epicondyles. KAM was calculated with the Visual3D. The data were randomly assigned to be the training (80%) and testing (20%) dataset (24 subjects x 9 =216 data).

The time-series linear accelerations data along superior-inferior (SI), medial-lateral (ML), and anterior-posterior (AP) directions of the femur are sampled from two wearable sensors. Thus, a total of six variables were available for input features (2 sensors x 3 axes). A 6-folds cross-validation was used to estimate the model performance by selecting different feature combinations. The initial model included all 6 features, then followed by models with 5 features. The combination that yielded the lowest root mean square error (RMSE) was kept for the next feature elimination iteration. The model with the combination of the lowest number of features that delivers the lowest RMSE was selected as the optimal neural network model with the implementation of principal component analysis afterwards.

The output vector was KAM during the stance phase. The model consisted of three LSTM blocks followed by a fully connected layer and a dropout layer with a dropout probability of 0.2. The mini-batch size was 5, and the learning rate was 0.01 with a maximum number of epochs 1000. RMSE was used to estimate how well the model fit the testing dataset.

Results and Discussion

The model that includes Lat_AP, Lat_ML, Lat_SI, and Med_ML accelerations yielded the lowest RMSE (0.196 ± 0.004; Fig. 1). Furthermore, the combination of Lat_ML, Lat_SI, and Med_ML accelerations also performed similarly (RMSE=0.204 ± 0.020). With the optimal combination of input vectors, the model had an overall RMSE of 0.0993 in the testing dataset (Fig. 2).

Since walking speed has a strong association with the peak KAM, it is reasonable that the Lat_AP acceleration is included in the optimal model. Similarly, the vertical ground reaction force is a primary contributor to the knee joint moment, which could be reflected by the Lat_SI acceleration. Although there are discrepancies between the KAMs estimated from wearable sensor data and those calculated with instrumented gait analysis over the stance phase, these differences are relatively small for the peak KAMs, which are the most important indicator for knee osteoarthritis.

Significance

The combination of wearable sensor data and the RNN-LSTM modeling demonstrates a strong potential to eliminate barriers from clinician's access to the informative knee kinetic data.

References

[1]Sharma L, et al. (1998). Arthritis & Rheumatism, 41:1233-40
[2]Zhang Y, Jordan JM (2010). Clin Geriatr Med, 26(3):355-369.
[3]Stetter BJ (2020). Front Bioeng Biotechnol, 24:8-9.

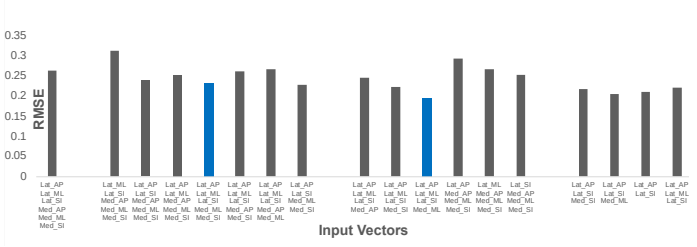

Figure1. Mean RMSEs for models with different combinations of input features while performing the cross-validation.

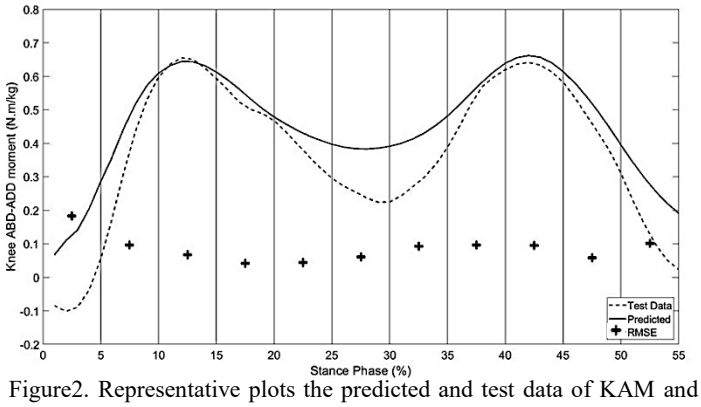

Figure2. Representative plots the predicted and test data of KAM and overall RMSE in every 5% of stance phase.

A RANDOM FOREST REGRESSION TO PREDICT JOINT ANGLES ACROSS VARIOUS GAIT PHASES

David Hollinger[1*] and Michael Zabala[1]
[1]Department of Mechanical Engineering, Auburn University, Auburn, AL, USA
email: *dzh0063@auburn.edu

Introduction

Volitional and seamless control of exoskeletons is essential to the often-stated goal of metabolic cost reduction. Optimal control requires accurate timing of peak ankle joint power which occurs during toe-off phase [1]. Peak hip flexion power subsequently follows and generates limb motion into the swing phase. Therefore, joint angle estimation errors occurring during the toe-off phase may result in worsened exoskeleton performance outcomes due to delayed ankle and hip. Several studies using machine learning models have performed well to predict lower limb joint angles [1]. However, such studies do not assess the performance during critical phases of the gait cycle. Therefore, the purpose of this study is to combine EMG and IMU from sensors worn on the torso and lower limbs to systematically compare lower limb joint angle prediction accuracy during various phases of walking gait. We hypothesize that regions before and after the toe-off phase will have the best overall prediction performance because high muscular information typically occurs during toe off phase of walking [2].

Methods

25 healthy volunteers (age 21.97 ± 2.75 years) performed three overground walking trials on two separate test days in the Auburn University Biomechanical Engineering Lab. Subjects wore 79 markers utilizing point cluster method [3]. Sixteen IMUs and 14 EMG sensors (Trigno by *Delsys Inc.)* were attached bilaterally to the lower limb (gluteus maximus, biceps femoris, rectus femoris, gastrocnemius, tibialis anterior, rectus abdominis, erector spinae, and foot mounted IMU). The first walking trial of each session was used to train the machine learning algorithm (Random Forest Regressor) while the second walking trial was set aside for testing. The Random Forest Regressor included EMG, IMU and joint angles as training and testing features to predict joint angles. Prediction results were partitioned into distinct gait phases corresponding to regions of high muscular information [2]. Walking trials were normalized to 0-100% of the gait cycle beginning and ending with left heel strike. The time windows for the gait phases of interest were split into intervals of 15% of the gait cycle. Pre and post heel strike (PreHS and PostHS) regions were bounded within ±15% of heel strike while pre and post toe-off (PreTO and PostTO) regions were bounded within ±15% of toe-off. The 15% window duration was chosen because this is approximately equal to delays between 100 ms and 125 ms, which are considered optimal for myoelectric prosthesis controllers [4]. A single factor ANOVA was used to compare joint angle predictions of PostHS, PreTO, PostTO, and PreHS phases and were repeated for the ankle, knee, and hip. Bonferroni corrected post-hoc paired t-tests were performed following significant repeated measures ANOVA testing ($p<0.05$).

Results and Discussion

Prediction performance for each phase of gait is reported in Figure 1. Prediction accuracy for the ankle angle was significantly greater than the knee and hip during PreHS and PostHS. Conversely, predictions for hip angles outperformed ankle and knee predictions during PreTO and PostTO. More broadly, prediction accuracy was best during PreHS and PostHS regardless of joint.

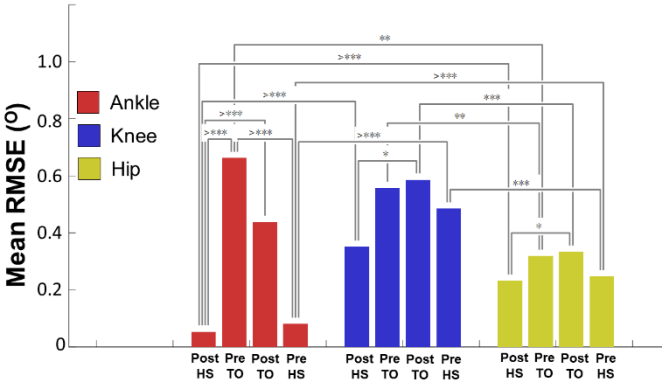

Figure 1: Comparison of prediction performance across gait phase regions for post hoc t-tests after performing Bonferroni correction. *, **, and *** indicates statistically significant result ($p \leq 0.05$, ≤ 0.01, ≤ 0.001).

Table 1: RMSE for various phases of the gait cycle between the predicted and ground truth angles of the test trial.

RMSE (deg)	PostHS	PreTO	PostTO	PreHS
Ankle	0.0533	0.662	0.438	0.081
Knee	0.351	0.557	0.586	0.485
Hip	0.231	0.319	0.333	0.247

Significance

This study demonstrates how a random forest regressor is capable of predicting the temporal relationship of the gait cycle and performs reasonably well at predicting lower limb joint angles regardless of gait phase. However, it is worth noting that prediction performance may change depending on gait phase. Changes occurring during toe off were more difficult to predict compared to heel strike. Therefore, biomechanists should consider the user's gait phase for optimal control of a wearable exoskeleton. The results of this study may be helpful for designing low-level torque control of an exoskeleton during various phases of the gait cycle.

Acknowledgments

We would like to thank the U.S. Army Combat Capabilities Development Command (CCDC) for funding this study. PAO number PR2022_57932

References

[1] Malcolm P, Quesada RE, Caputo JM, Collins SH
J Neuroeng Rehabil. 2015 Feb 22; 12():21.
[3] Farrell and Herr, *33rd Annual Int. Conf. Of the IEEE EMBS*
[2] Andriacchi, et al.*Journal of Biomechanical Eng 1*20(6):743-9
[4] Ferrel and Weir, IEE Trans. Neural Sys. & Rehab. Eng.

THE EFFECTS OF SHOE-SOLE STIFFNESS ON SPRINT-CYCLING PERFORMANCE

Ross D. Wilkinson*, Nell Crosby, and Rodger Kram
Locomotion Laboratory, Department of Integrative Physiology, University of Colorado, Boulder, CO, USA
email: ross.wilkinson@colorado.edu

Introduction

The cycling industry is rife with unsubstantiated claims about the performance benefits of stiff-soled cycling shoes. Carbon fiber is championed as the premier outsole material because it is lightweight, and its stiffness supposedly maximizes the transmission of force from the foot to the pedal. Indeed, our lab has found that full-carbon cycling shoes with clipless pedals improve sprint performance compared to running shoes with classic toe clips[1]. But we have found negligible effects between nylon, fibreglass, and carbon-fiber outsoles on sprint performance[2]. Thus, we sought to determine the outsole stiffness at which there is a "breakpoint" in sprint performance, which we hypothesized would occur at a sole stiffness between a flexible running shoe and nylon.

Methods

We compared maximal 1 s crank power between 3 cycling shoes with different outsole materials (in order of decreasing stiffness): 1) Nylon, 2) 85A thermoplastic polyurethane (TPU), and 3) 64D TPU. 26 recreational and competitive adult cyclists volunteered (M = 13, F = 13). Subjects self-reported ≥4 h of cycling per week and ≥1 year of road cycling experience. Subjects rode the same model of road bicycle (Specialized Venge) equipped with a crank-based mechanical power meter (SRAM Quarq DZero), which was modified to output high-frequency data at 65 Hz instead of the usual 1 Hz. The sprint course was 50 m long on a 9.1% uphill slope. Subjects performed a total of 9 sprints: 3 in each of the 3 outsole conditions. Subjects rested for 5 min between each sprint. The order of conditions was randomized within 3 blocks of 3 sprints. The cycling shoes appeared identical to the subjects as they were custom-made to have the same uppers. We devised a simple testing apparatus (see Figure 1) to quantify the longitudinal-bending stiffness of each shoe using Equation 1.

$$k = \frac{F_1 r_2}{tan(\frac{d}{r_1})} \quad (1)$$

Results and Discussion

There was a moderate decrease (ES = –0.59, p = 0.020) in maximal 1 s crank power from Nylon to 85A TPU, with an average difference of –3.1% (95% CI: –5.7% to –0.5%). There was a large decrease (ES = –0.83, p = 0.001) from Nylon to 64D TPU, with an average difference of –5.8% (–9.4% to –2.2%). There was a negligible decrease (ES = –0.50, p = 0.054) from 85A TPU to 64D TPU, with an average difference of – 2.6% (95% CI: –5.2% to 0.0%).

Significance

Overall, we find that sprint performance is nearly constant across a wide range of sole stiffness. Cycling shoes could be designed with more compliant soles without significantly sacrificing sprint performance. Relaxing the stiff-sole design constraint may allow for other benefits, such as comfort and walkability.

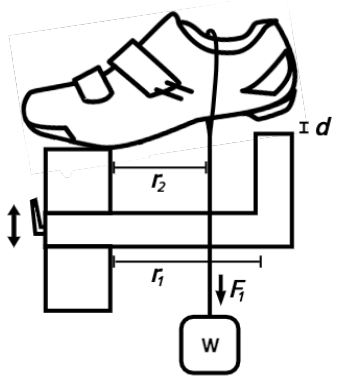

Figure 1: Longitudinal stiffness test setup. We affixed the shoe directly to a support beam via flathead screws through the two posterior cleat holes. d = displacement from shoe sole to contact point. d was set to 10 mm for each test using a sliding rail system shown on the left. F_1 = force applied to the shoe due to the hanging weight (w). r_2 = moment arm from the fulcrum to the cord, which was used to calculate the torque applied to the sole. r_1 = moment arm from the fulcrum to the contact point, which was used to calculate the angular displacement of the sole.

Figure 2: Mean percentage difference (±95% CI) in maximal 1 s crank power across a spectrum of shoe-sole stiffnesses. An exponential curve (blue line) was fit to the cycling-shoe data (blue circles) only. Note: We were able to collate our results with our previous findings[1, 2] due to the inclusion of the nylon-soled shoe within all 3 studies. We also quantified the stiffness of the current and previously tested shoes, which allowed us to compare maximal 1 s crank power along a stiffness spectrum.

Acknowledgments

Equipment and funding supplied by Specialized Bicycle Components, Inc.

References

[1] Burns & Kram, 2020. *Footwear Sci*. 12(3): 185-192.
[2] Hurt & Kram, 2021. *Footwear Sci*. 13(1): 69-77.

BOA-ENABLED PERFORMANCE FIT WRAP UPPERS IMPROVE POWER TRANSFER DURING SUBMAXIMAL AND SPRINTING IN ROAD CYCLING

Bethany Kilpatrick[1*], Kathryn Harrison[1], Eric Honert[1], Daniel Feeney[1]
[1]BOA Technology, Denver, CO
email: *Bethany.Kilpatrick@boatechnology.com

Introduction

Power output is a critical component of competitive road cycling. In long-distance races that can span from 50 to over 300km, it is essential to have efficient energy expenditure while maintaining a steady power output. Among the many components that impact cycling performance, cycling shoes are integral in transferring force into the pedals. Stiffer cycling shoes can increase maximal power output[1] and positively affect joint mechanics during steady state riding[2] with no additional metabolic cost[2,3]. While shoe uppers can influence ankle work and range of motion during agility movements,[4,5] no studies have investigated the impact of shoe uppers on cycling performance.

The purpose of this study was to investigate if there was a difference in power output and metabolic economy between a BOA Performance Fit Wrap (PFW) configuration and a three-strap Velcro (V) configuration (Fig. 1). We hypothesized that PFW upper configurations would increase power output during 15-second sprints following steady, submaximal riding.

Methods

We recruited 13 male recreational cyclists who rode greater than five days per week. The cyclists tested two identical road cycling shoe soles, one shoe with a PFW that consists of a dual-dial wrapping configuration and the second shoe with three straps of Velcro (Fig. 1). The cyclists rode for seven minutes in each shoe twice in a counterbalanced order (i.e., A-B-B-A). Subjects were instructed to maintain a constant power output, which was determined as approximately 70% predicted maximum heart rate and a rating of perceived exertion of 5/10 during the warm-up. The next two minutes comprised two 15-second sprints followed by 45 seconds of self-selected easy riding between. Oxygen uptake and carbon dioxide output were measured during minutes 3-5 of steady-state riding in order to estimate energetic expenditure (EE). Steady state and sprinting power outputs were measured via a cycle ergometer. Data were converted into Z-Scores for each subject and entered into a random intercept, random slope probabilistic model with priors centered on 0 as shown below. The percent of the posterior greater than 0 and the 95% credible intervals are presented for each power metric.

$$DV \sim Normal(\mu_i, \sigma)$$
$$\mu_i \sim \alpha + \beta x_i$$
$$\alpha \sim Normal(0,1)$$
$$\beta \sim Normal(0,1)$$

Figure 1: The BOA Performance Fit Wrap configuration (left) and the three-strap Velcro configuration (right).

Config.	Power output Steady (W)	Power output Sprint (W)	EE (W/kg)
PFW	193.63 (33.3)	638.19(226.05)	13.33(3.49)
Velcro	179.77(32.47)	575.03(178.63)	13.37(3.55)

Table 1: Averages and standard deviations for steady state power output, sprint power output, and steady state energy expenditure (EE) for Velcro and Performance Fit Wrap (PFW) configurations.

Results and Discussion

PFW shoe uppers increased cycling power during sprinting and- surprisingly- were associated with greater power output during steady state riding with no change in EE. Despite asking subjects to maintain an equal power output and providing 3-second smoothed average power feedback during riding, PFW increased power during the submaximal riding (estimate 6 watts, 94% posterior > 0, 95% CI: -0.2% to 4.79%) with no change in RPE or energetic expenditure. Similarly, there was an increase in sprint power output in PFW than in V (estimate 64 watts, 97% posterior > 0, 95% CI: 0.14 to 15.5%).

Although previous studies have investigated how shoe uppers influence performance in agility movements[3], this is the first study to test the impact of upper construction on cycling performance. Notably 11/13 subjects had the greatest peak power in the PWF condition. Moreover, since there was no change in EE or RPE between the two conditions despite an increase power output, we conclude subjects experienced greater power transfer in PFW. Increased power output with the PFW uppers could be due to improved fit causing a greater connection between foot and midsole. This in turn would create less movement variability between the shoe and the foot on the downstroke. Because there is limited movement within the shoe, there is a more direct transfer of power from the shoe to the pedal.

Significance

This research is significant because it is the first of its kind in the field of cycling. This research validates previous research that shoe uppers have a positive influence on performance[4,5]. This information is useful to cyclists who participate in competitive long-distance races.

References

1. Burns & Kram (2020). *Footwear Science*, *12*(3), 185-192.
2. Fletcher, et al., (2019). *Journal of sports sciences*, *37*(13), 1457-1463.
3. Straw & Kram (2016). *Footwear Science*, *8*(1), 19-22.
4. Subramanium et al., (2021) *J Sports Sciences*, 1-9.
5. Harrison et al., (2021). *Footwear Science*, *13*(2), 167-180.

AUTOMATED THREE-DIMENSIONAL DISTANCE AND COVERAGE MAPPING IN THE PRESENCE OF HALLUX VALGUS

Andrew Behrens, Kepler Alencar Mendes de Carvalho, Matthieu Lalevee, Nacime Barbachan Mansur, Cesar de Cesar Netto, and Kevin Dibbern
[1]Department of Orthopaedics and Rehabilitation, University of Iowa, Iowa City, IA
Email: andrew-behrens@uiowa.edu

Introduction

Hallux Valgus (HV) deformity is a common deformity of the medial column and second ray of the foot involving the proximal phalanx, first and second metatarsals, and the intermediate and medial cuneiforms that results in the often painful protuberance of the first metatarsal head medially. Recently, rapid advances in our understanding of complex rotation components in this deformity have occurred thanks to the detailed multiplanar views of these foot structures under load afforded by weightbearing CT (WBCT) imaging (1,2,3). This work sought to develop an automated methodology for assessing the complex changes in distances and coverage between bones of medial column to better understand their 3D relations.

The use of distance mapping (DM) in analyzing 3D relative positions between the joint surfaces (joint interaction) in the foot and ankle has recently come into prominence for the detailed insights it can provide into the effects of weight bearing on both healthy and pathologic conditions (4,5). Dibbern et al., in an important study expanded upon 3D DM of WBCT to assess Subluxation through the introduction and use of Colored Coverage Maps (CM). These maps based on DM identify areas of adequate joint interaction, joint subluxation, and impact. This new visualization technique aimed to semantically divide DM into meaningful regions of coverage and joint impacts in 3D, with more interpretable and potentially clinically useful maps, facilitating the understanding of areas of interest where subluxations and impacts may occur (4). However, these methods relied upon manual identification of coverage regions.

This study sought to expand upon these methods and describe surface-surface interaction in the first and second metatarsophalangeal joint (MTPJ), the metatarsosesamoid joint, and the first and second tarsometatarsal joint (TMTJ), using an automated DM and CM approach that can be applied to large datasets in the future.

Methods

In this IRB approved study, 9 unilateral feet diagnosed with Hallux Valgus were compared to 5 controls.

Disior Bonelogic 2.0 was used to create STL models of all bones proximal to the 1st distal phalanx. Models were then analyzed in MATLAB to measure distances along the entire surface of the first and second metatarsophalangeal joint (MTPJ), the metatarsosesamoid joint, and the first and second tarsometatarsal joint (TMTJ) were measured. The surface of the first MTPJ was divided into a 2x2 grid using the principal axes of the joint surface in order to provide a more detailed analysis. The head, base, and interfacing regions with each sesamoid were selected using relationships between bones and geometric properties of each bone. Using the distance along the normal direction of vectors projected between all opposed surfaces, measurements were performed in all articulating regions.

Due to the highly curved surfaces of nonarticular regions, such as the space between the first and second metatarsal bones, aberrantly large typical distances can be produced. These distances are unrelated to loading and deviate significantly from neighbouring regions. To account for this, the averaged normal directions from each point to the opposed surface was used to compute distances in highly curved/uneven regions.

Results and Discussion

Changes in coverage percentages of Hallux Valgus cases relative to controls are indicated in the attached Figures 1 & 2.

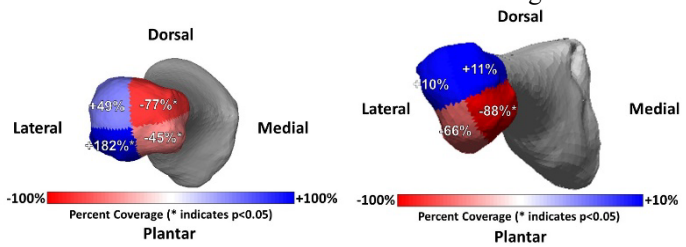

Figures 1 & 2: Summary of coverage changes on the 1st (left) and 2nd (right) metatarsals.

Significant subluxation was observed on the medial side of the 1st metatarsal in Hallux Valgus cases. A corresponding increase in coverage was also observed on the lateral side of the 1st metatarsal head. The 2nd metatarsal head also experienced both significant subluxation and increases in coverage.

In addition to the coverage on the 1st and 2nd metatarsal head, the mean joint space width (JSW) in each joint was also calculated. In the 1st MTPJ, an 8.5% decrease in JSW was observed but this value was not significant ($p = 0.335$). Decreases in JSW were als observed in the metatarsosesamoid joint.

Our results support the occurrence of significant coverage and JSW changes in the forefoot in patients with Hallux Valgus deformity.

Significance

To our knowledge, this study is the first to evaluate distance and coverage in Hallux Valgus patients. Additionally, it is the first to use fully automated methods to compute joint coverage in the forefoot. These results can be used to plan larger studies evaluating subtle changes in distance and coverage in Hallux Valgus and may eventually be used to create patient specific care protocols. The methods developed in this study will enable larger and prospective studies evaluating the effects of different components of Hallux Valgus deformity on patient outcomes and surgical correction.

References

1. De Cesar Netto, C. and M. Richter (2020). Foot Ankle Clin 25(1): 31-45.
2. Collan L, Kankare JA, Mattila K. Foot Ankle Surg 2013;19(3):155–61
3. Welck MJ, Singh D, Cullen N, et al. Foot Ankle Surg 2018;24(4): 314–9.
4. Dibbern KN, et Al. Foot Ankle Int. 2021 Jun;42(6):757-767.
5. Siegler S, et Al. J Biomech. 2018 Jul 25;76:204-21

THE EFFECTS OF WALKING SPEED ON MULTISEGMENT FOOT KINEMATICS

Nayeli Marcial[1*], Usha Kuruganti[1], Victoria Chester[1]
[1]Andrew and Marjorie McCain Human Performance Laboratory, University of New Brunswick, Fredericton, Canada
email: *nmarcial@unb.ca

Introduction

Research studying the effect of speed on foot kinematics have shown that speed significantly influences foot and ankle kinematics. The appreciation of speed-mediated effects is critical for increasing our understanding of foot mechanics in young and older adults. While previous studies have examined the effect of speed on multisegment foot (MSF) kinematics in young and older adults, few studies have tested a broad range of speeds [1-2] and/or included the midfoot segment [2]. Therefore, the purpose of this study was to examine differences in MSF kinematics between young and older adults during walking at five different speeds (very slow, slow, typical, fast, and very fast). The 5-segment foot model [3] and the range of speeds tested provides a comprehensive examination of foot mechanics and facilitates the development of age and speed-matched databases for further studies.

Methods

Sixteen young participants (8 males, 8 females, mean age 23.62±3.73 years) and fifteen older participants (8 males, 7 females, mean age 71.64±5.94 years), with no known lower-extremity disease/disorder/injuries, were recruited. A 12-camera Vicon T160 motion capture system (Oxford Metrics Group Ltd., UK) was used to track thirty-six retro-reflective markers placed on the tibia and foot following a modified version of a 5-segment foot model [3]. Significant group differences ($p<0.05$) in mean max and min relative angles in stance between foot segments, were analyzed using a one-way ANOVA or if indicated, Kruskal-Wallis test. Statistical analyses were completed using R Studio (RStudio 2018, USA).

Results and Discussion

Results showed significant differences in MSF kinematics between young and older adults in stance across speeds, suggesting that speed significantly influences foot mechanics. In the sagittal plane, older adults exhibited a significantly decreased mean max ankle (shank-foot) dorsiflexion (DF) angle during stance as walking speed (WS) increased from very slow to typical WS compared to younger adults. Similarly, older adults showed a decreased mean max ankle plantarflexion (PF) angle during stance as WS increased from very slow to typical WS compared to young adults (Table 1). A significantly increased mean min PF angle for the midfoot-metatarsus (mid-met) during stance was also evident for older adults across speeds. In addition, older adults exhibited an increased mean max mid-met PF angle during stance as speed increased from slow to very fast compared to young adults. In the frontal plane, older adults showed a significantly reduced mean min midfoot-calcaneus (mid-cal) eversion (EVE) angle during stance as WS increased from very slow to fast WS compared to young adults. Also, older adults exhibited a decreased mean max EVE angle during stance across speeds compared to young adults (Table 1). Moreover, older adults showed a significantly increased mean min cal-met EVE angle during stance from slow to fast WS. An increased mean max cal-met EVE angle during stance was also evident for slow and typical WS compared to young adults (Table 1). In the transverse plane, older adults showed significantly increased mean min and max mid-met adduction (ADD) angles during stance at the very slow speed compared to young adults.

It is plausible that the ankle max PF and DF angles in older adults are purposefully decreased to maintain greater foot-floor contact to extend the support base [4], and thus increase their stability and balance. Reduced mid-cal eversion (EVE), as well as increased mid-met PF and ADD angles, may suggest a trend towards a less pronated dynamic foot position for older adults during walking across speeds. Reduced cal-met EVE motion in older adults may suggest a lesser activation of the midtarsal locking mechanism. Thus, the foot may become less flexible, affecting its adjustment to the surface. This suggests a functional decline for older adults in their ability to adapt to the terrain. Overall, older adults showed a less propulsive gait pattern and less foot mobility, especially at the midfoot, at different speeds.

Significance

This research provided critical information of the foot and ankle across a range of speeds, increasing our understanding of foot mechanics and function in older adults. The data provided can be used as a reference database to identify atypical gait patterns, e.g., patients with planus and cavus feet. Hence, the findings may provide guidance to improve gait performance.

References

[1] Van Hoeve et al., (2017). *Medicine,* 96(35).
[2] Arnold et al., (2014). *Gait & Posture*, pp. 689-694.
[3] Leardini et al., 2007. *Gait & Posture,* pp. 453-462.
[5] Kerrigan, et al., (1998). APM&R, pp. 317-322.

Table 1. Descriptive statistics of the mean max and min peak relative MSF angles during stance for young and older adults, across five different walking speeds. * indicates significant difference ($p<0.05$).

MSF Kinematics	Very Slow		Slow		Typical		Fast		Very Fast	
	Mean±Std.Dev. (°)		Mean±Std.Dev. (°)		Mean±Std.Dev. (°)		Mean±Std.Dev. (°)		Mean±Std.Dev.(°)	
	O	Y	O	Y	O	Y	O	Y	O	Y
Max DF sha-foot angle	10.9±3.8 *	6.2±2.2 *	9.4±4.4 *	5.7±2.8*	8.0±4.1 *	5.6±2.9 *	7.5±4.2	5.8±3.2	6.7±3.8	6.1±5.3
Max PF sha-foot angle	-13.1±7.9 *	-18.1±7.3 *	-14.1±6.6 *	-19.2±5.2 *	-19.6±6.6 *	-23.8 ±5.7 *	-21.7±8.1	-25.1±6.1	-21.3±8.5	-25.5±6.1
Min EVE mid-cal angle	5.6±4.1 *	9.8±3.7 *	6.4±4.3 *	11.0±3.8 *	6.6±4.9 *	10.9±3.6 *	6.1±4.7 *	10.5±3.9 *	7.1±4.1	9.7±3.2
Max EVE mid-cal angle	11.2±3.7 *	17.2±4.4 *	11.7±4.7 *	18.5±4.9 *	12.4 5.1*	18.1±4.0 *	11.6±4.9 *	17.3±5.1 *	12.0±4.2 *	16.1±3.4 *
Min PF mid-met angle	-79.5±6.8 *	-73.9±7.2 *	-81.1±7.4 *	-74.6±5.6 *	-81.3±8.1 *	-75.8±5.9 *	-80.3±7.1 *	-75.2±4.9 *	-82.9±7.1 *	-76.3±5.6 *
Max PF mid-met angle	-74.9±7.1	-69.6±6.9	-76.4±7.1 *	-70.2±5.5 *	-75.6±6.1 *	-70.5±6.1 *	-74.3±6.4 *	-70.1±4.7 *	-76.9±6.5 *	-70.1°±6.1 *
Min ADD mid-met angle	8.6±8.7 *	8.0±4.8 *	11.5±4.6	8.7±4.9	9.2±7.2	8.8±4.1	9.3±7.6	8.8±4.1	8.8±8.4	9.2±4.5
Max ADD mid-met angle	12.3±8.1 *	12.1±5.0 *	15.6±4.7	12.9±4.9	14.2±7.1	13.5±4.6	14.3±7.4	13.2±4.5	13.7±8.2	14.2±4.5
Min EVE cal-met angle	9.2±8.1	6.8±7.1	9.4±4.8 *	5.6±6.6 *	7.7±6.3 *	3.5±6.5 *	7.2±6.5 *	4.5±4.3 *	8.5±7.0	4.2±6.7
Max EVE cal-met angle	15.5±6.6	14.0±6.3	16.3±4.5 *	13.5±6.0 *	16.5±5.0 *	13.1±6.9 *	16.2±5.5	13.0±4.6	16.8±6.3	14.0±7.1

A Soft 3-Dimensional Force Sensor for In-Shoe Ground Reaction Force Measurement

Jonathan D. Miller[12]*, Andrew J. Miller[2], Lance L. Frazer[3], Tylan N. Templin[3], Travis D. Eliason[3], and Cory J. Berkland[124]
[1]University of Kansas, Department of Chemical and Petroleum Engineering, Lawrence, KS
[2]Axioforce LLC., Lawrence, KS
[3]Southwest Research Institute, San Antonio, TX
[4]University of Kansas, Department of Pharmaceutical Chemistry, Lawrence, KS
email: jdmiller@ku.edu

Introduction

Measuring ground reaction forces from human movements is a heavily utilized tool in the field of biomechanics and sport performance[1]. However, these measurements are currently limited to movements that can be performed on stationary, bulky, and expensive 3D force plates. In-shoe 3D ground reaction force measurement would enable the analysis of many new types of movements which cannot be performed on force plates, advancing our understanding of human locomotion. Design methods for magnetic soft 3D force sensors have recently been described[2], and may provide a platform for an in-shoe 3D force measurement system.

Methods

Magnetic soft 3D force sensors were constructed according to methods presented by Miller et al.[2] and shoe insoles were fabricated with silicone rubber resin and 3D printed insole molds. Five magnetic soft 3D force sensors were integrated into each shoe insole and data were transmitted wirelessly to a nearby computer at 100 Hz.

The insoles were inserted into an unmodified pair of training shoes and worn by a participant. The participant performed 3 countermovement jumps and 3 bodyweight squats on a dual force plate set up to directly compare traditional 3D force plates to the shoe insoles. Data from the first movement of each type was used in an optimization procedure to determine the calibration parameters for each sensor that convert raw magnetic output to units of force for each axis (x, y, and z). These parameters were used to establish movement specific calibrations.

Data from the force plates and the shoe insoles were compared for each movement not used for calibration by calculating two-way random effect single measures intraclass correlation coefficients and mean biases on the peaks from each axis (x, y, and z). Data from left and right shoe insoles for each movement resulted in 8 peak force measurements for analysis for each axis.

Results and Discussion

The shoe insoles demonstrated good to excellent agreement with the force plates which are considered the gold standard for force measurement in biomechanics research. The agreement between the force plates and shoe insoles for peak forces in the Z-axis (vertical) from the countermovement jumps and bodyweight squats was good (ICC = 0.861). However, the agreement between devices was excellent for peak forces in both the, X-axis, (ICC = 0.982) and the Y-axis (ICC = 0.965) from these movements. The means were biased by 15.9 N and by 31.5 N in the X- and Z-axes respectively, indicating the insoles tended to overestimate the peak force in these directions. However, there was minimal bias in peak forces in the Y-axis (-0.013 N).

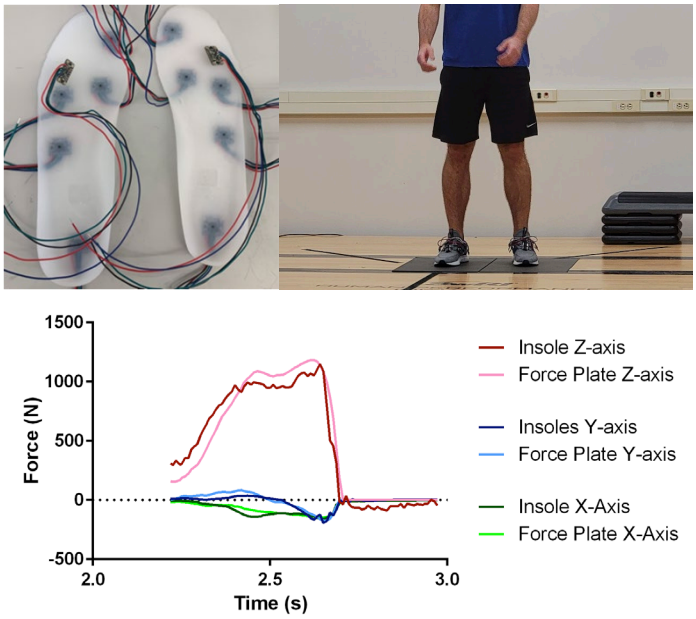

Figure 1: Images of the 3D force sensing shoe insoles (top left) and of the insole/force plate set up during testing (top right). Force data from the insoles and force plates plotted against time for the braking and propulsive phases of a countermovement jump (bottom).

Significance

This work describes the fabrication of shoe insoles capable of measuring and wirelessly transmitting 3D ground reaction force data when inserted into a normal pair of training shoes. The peak forces measured from the insoles during countermovement jumps and bodyweight squats have good to excellent agreement with gold standard 3D force plates in terms of reliability, but tended to overestimate forces in the X- and Z-axes. It is likely the performance of the insoles could be improved by the inclusion of more force sensors, and increasing the sampling rate. Further research is needed to validate the insoles as a 3D force measurement system without the need for a force plate.

Acknowledgments

We gratefully acknowledge support from Honeywell Federal Manufacturing & Technologies as a part of Department of Energy Contract DE-NA-0002893.

References

[1] D. T. McMaster, N. Gill, J. Cronin, M. McGuigan, *Sports Med.* 2014.
[2] J. D. Miller, D. Cabarkapa, M. J. Hermes, A. C. Fry, C. J. Berkland, *Advanced Materials Technologies*. 2021.

COMPARISON OF INCLINE VS BLOCK HEEL-RAISE EXERCISE TRAINING ON VERTICAL JUMP

Torstein E. Dæhlin[1], Loren Z.F. Chiu[1]
[1]Faculty of Kinesiology, Sport, and Recreation, University of Alberta
email: eriksend@ualberta.ca

Introduction

Foot muscle strength is purported to affect performance in propulsive tasks, such as running and jumping. Previous research has attempted to use isometric and concentric exercise modes to increase foot muscle strength [1, 2]. However, the effect of these exercise modes on vertical jump performance are inconsistent [1, 2]. An alternative action of the intrinsic and extrinsic foot muscles is to act eccentrically to control the centre of pressure and oppose foot arch deformation [3, 4]. Heel raise exercise has a midfoot moment supporting the foot arch; this moment is larger when heel raise is performed on an inclined surface compared to an elevated block [4]. The purpose of this research was to investigate the hypothesis that 11 weeks of incline heel-raise exercise would be more effective at improving vertical jump performance and toe flexor strength compared to conventional (block) heel-raise.

Methods

Thirty-three competitive female volleyball players volunteered for the study and were randomly allocated to an incline (n = 17) or block (n = 16) heel-raise exercise group. The groups completed a block-periodised incline or conventional heel-raise exercise program three times per week for 11 weeks. Before, in week 7, and after the training intervention, vertical countermovement and 3-step approach jumping mechanics was assessed using stereophotogrammetry and force platforms. Additionally, toe flexor strength of the hallux and 2nd through 5th digits was assessed using a seated toe grip test with the toes neutral and dorsiflexed. Time-by-group mixed ANOVAs were used to compare changes in jump height and toe flexor strength. Additionally, net joint moment work performed at the ankle, knee, and hip during jumps was explored as explanatory variables.

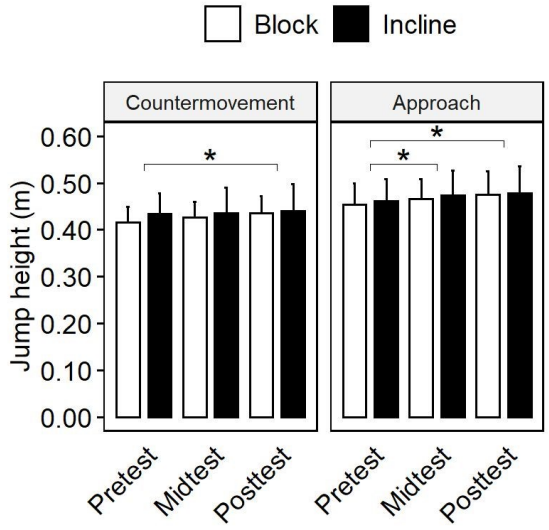

Figure 1: Jump heights in the block and incline groups at pre- mid- and posttest during vertical countermovement and 3-step approach jumps. *Main effect for time: Significant with respect to pretest ($p < 0.05$).

Results and Discussion

Three participants in the incline, and five participants in the block exercise groups withdrew from the study. Thus, 14 participants completed the incline (age: 16 ± 1 yrs., height: 1.77 ± 0.08 m, mass: 67.1 ± 11.1 kg) and 11 participants completed the block (age: 17 ± 2 yrs., height: 1.80 ± 0.07 m, mass: 70.3 ± 7.2 kg) heel-raise exercise program.

In contrast to our hypotheses, no significant time-by-group interactions were observed for any variable. Main effects for time indicated that the sample as a whole experienced changes from pre- to mid- and/or posttest. Specifically, participants improved their and approach jump height from pre- to mid-test (Δ1.19 ± 2.47 cm; $p = 0.047$; Figure 1). Additionally, participants improved vertical countermovement (Δ1.24 ± 2.25 cm; $p = 0.022$) and approach jump (Δ1.89 ± 2.51 cm; $p < 0.002$) height from pre- to posttest (Figure 1). This indicates that heel-raise exercise may be effective for improving vertical jump height. However, as there were no differences in the work performed at the ankle, knee, or hip joint during vertical countermovement or approach jumps ($p > 0.050$), it remains unclear through what mechanism these heel-raise variations may affect vertical jump performance.

In addition to improvements in vertical jump performance, participants improved hallux flexor strength from pre- to mid-test with both the toes neutral (Δ0.23 ± 0.45 N/kg; $p = 0.002$) and dorsiflexed (Δ0.20 ± 0.42 N/kg; $p = 0.005$). Similarly, hallux strength was greater with the toes neutral (Δ0.29 ± 0.49 N/kg; $p < 0.001$) and dorsiflexed (Δ0.25 ± 0.51 N/kg; $p = 0.003$) at post- compared to pre-test. This finding supports previous research reporting that midfoot net joint moments are of a considerable magnitude in heel raise exercises [4]. The results of this study support the hypothesis that exercises where the intrinsic and extrinsic foot muscles act eccentrically to oppose foot deformation or control the centre of pressure may be utilized to improve foot function.

Significance

The present research provides support of the use of heel-raise exercises to improve foot muscle strength. Exercise and clinical professionals seeking to improve foot muscle strength may therefore consider heel-raise exercises for this purpose.

Acknowledgments

The first author was supported with a Vanier Canada Graduate Scholarship.

References

[1] Chiu & Dæhlin, 2021. *J Strength Cond Res, 35*(12), 3308-3314.
[2] Goldmann et al., 2013. *J Sports Sci, 31*(4), 424-433.
[3] Hashimoto & Sakuraba, 2014. *J Phys Ther Sci, 26*(3), 373-376.
[4] Kelly et al., 2012. *Clin Biomech, 27*(1), 46-51.

SINGLE-SEGMENT, MULTI-SEGMENT, AND PLANAR ANGLE FOOT KINEMATIC DATA FOR CLASSIFYING AUTISTIC GAIT PATTERNS IN CHILDREN

Ashirbad Pradhan[1*], Karansinh A. Padhiar[1], Victoria Chester[1]
[1]Andrew and Marjorie McCain Human Performance Laboratory, Faculty of Kinesiology, University of New Brunswick, Fredericton, Canada
Email: vchester@unb.ca

Introduction

Previous research has demonstrated that children with autism walk with atypical ankle kinematics and kinetics [1-3]. Although these studies have utilized single segment foot (SSF) data, to date, no studies have examined multisegment foot (MSF) kinematics and the corresponding planar angles in children with autism. Further, due to the lack of tools and data, machine learning analysis has not been performed on SSF, MSF, and planar angle foot kinematics for identifying atypical gait. The purpose of this study was to investigate the classification of gait patterns in children with autism using foot kinematic (SSF, MSF and planar angles) data.

Methods

A total of 40 children: 19 autism (age=10.4±2.9 yrs; height: 1.42±0.1 m; weight: 41.2±17.0 kg) and 21 controls (age=11.3±2.90 yrs; height: 1.48±0.1 m; weight: 44.3±16.3 kg) participated in the study. A12-camera Vicon T160 motion capture system (Oxford Metrics Group Ltd., UK), sampling at 100 Hz, was used to track thirty-six retro-reflective markers (9 mm diam.) that were placed on the medial and lateral tibia and anatomical landmarks of the foot using a modified version of a 5-segment MSF model used [4].The MSF features were extracted from the angles between the shank (Sha), calcaneus (Cal), midfoot (Mid), and forefoot (Met) rigid segments, whereas, the SSF features were extracted from the angles between the rigid shank and foot segments. These features included the angular value at heel-strike (HS) and toe-off (TO), range-of-motion (ROM), maximum (MAX) and minimum (MIN) angle during stance (ST) and swing (SW), and their corresponding time occurrences. MAX and MIN planar angles during stance were computed [4]. The MSF, SSF, and planar features, individually and combined, served as input to a support vector machine (SVM) classifier with a radial basis function (RBF) kernel. A wrapper-based sequential forward feature selection algorithm was used for selecting the feature subset that contributed to the most accurate classification of Autism and Control gait patterns. The model performance was validated using leave-one-out cross-validation and the mean performance evaluation metrics (Table 1) were reported after hyper-parameter tuning. Additionally, the entire feature set (MSF+SSF+Planar) was ranked using ANOVA F-value to determine the individual feature importance for classifying autism and control gait patterns. Visual3D and Python was used for data analysis.

Results and Discussion

The individual (Cal-Met, Cal-Mid, Mid-Met, Sha-Cal, and Sha-Foot) segments gave an average classification accuracy of 84%. However, combining all the five segments showed a significant increase in accuracy (96.3%) using only 37 features (out of 233). The features from the planar angles had an average accuracy of 73.4%, among which those from the V2G angle were the highest (78.8%). Combining all the eight planar segments improved the accuracy score to 91%. It was also observed that combining MSF and planar angles resulted in the same performance as MSF, but utilized a relatively lower number of features (#Features=29) out of 273. This signifies that adding planar segments to MSF contributed by reducing the number of features considered. The feature ranking (Fig. 1) suggested that among all the extracted features (#Features = 273), the top ten features were comprised of six MSF angle features and four planar angle features. This suggests that although MSF angles resulted in higher classification performance, both MSF and planar angles contributed to the high accuracy of classifying autism and control gait patterns.

Table 1: Classification performance evaluation using RBF SVM.

Segment	Angle	#Features	Accuracy (%)	Specificity (%)	Sensitivity (%)
SSF	Sha-Foot	8	83.8	84.2	83.3
MSF	Cal-Met	14	81.2	63.2	97.6
	Cal-Mid	14	83.8	76.3	90.5
	Mid-Met	5	77.5	81.6	73.8
	Sha-Cal	12	83.8	86.8	81
SSF + MSF		37	96.3	94.7	97.6
Planar	F2G	3	76.3	55.3	95.2
	F2Ps	4	71.3	65.8	76.2
	F2Pt	4	66.3	63.2	69.1
	MLA	5	77.5	65.8	88.1
	S2G	3	77.5	60.6	92.9
	S2F	2	68.8	57.9	78.6
	S2V	3	71.3	65.8	76.2
	V2G	3	78.8	63.2	92.9
Planar_All		23	91.2	86.8	95.2
SSF + MSF + Planar		29	96.3	94.7	97.6

Figure 1 Feature ranking of MSF and Planar angle features using ANOVA-F scores.

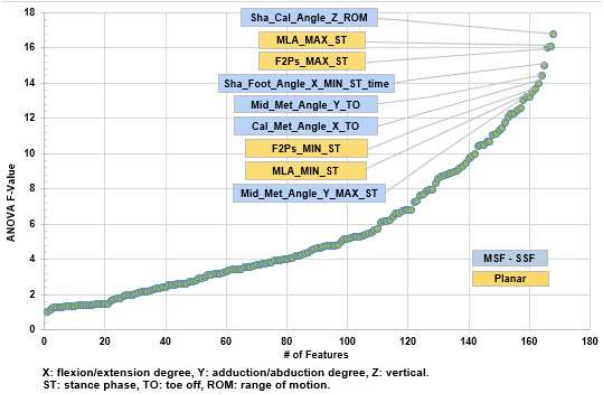

X: flexion/extension degree, Y: adduction/abduction degree, Z: vertical.
ST: stance phase, TO: toe off, ROM: range of motion.

Summary

Our results suggest that gait patterns in children with autism can be classified with high accuracy of 96.3% using the SSF, MSF, and planar angle-based kinematic data. Further, this can lead to a better understanding of atypical ankle/foot motion in children with autism and assist in more effective treatments.

References

[1] Calhoun, M et al. (2011). Cli. Biomech., 26(2), 200-206.
[2] Ilias, S et al (2016). IEEE IEACon (pp. 275-279).
[3] Galea, V. (2012). Year Bk Sports Med. Elsevie. 376–377.
[4] Leardini et al. (2017). Gait & posture, 25(3), 453-462.

RECONSTRUCTION OF PATIENT-SPECIFIC TIBIOFEMORAL JOINT ARTICULATIONS FROM MARKER TRAJECTORIES AND ANTHROPOMETRICS

Claire E. Warren[1], Michele Conconi[2], Nicola Sancisi[2], Allison L. Clouthier[1] Sasha Carsen[3] and Daniel L. Benoit[4]
[1]School of Human Kinetics, University of Ottawa, Canada
[2]Department of Industrial Engineering – DIN, University of Bologna, Italy
[3]Division of Orthopaedic Surgery, CHEO (the Children's Hospital of Eastern Ontario), Ottawa, Canada
[4]School of Rehabilitation Sciences, University of Ottawa, 451 Smyth Rd, Ottawa, Canada
email: *claire.warren@uottawa.ca

Introduction

Patient-specific modelling through incorporating magnetic resonance imaging (MRI) improves biofidelity with respect to articulations, particularly at the knee [1]. However, these models can be both labour and time intensive, and access to MRI is not possible for all researchers. Principal component analysis (PCA) has been used to facilitate the reconstruction of articular surface features from existing morphology in adults [2]. The purpose of this research was to determine if patient-specific articulations of the tibiofemoral joint (TFJ) could be reconstructed from marker positions and anthropometrics in paediatric knees.

Methods

Magnetic resonance images (MRI) of 12 ACL-injured (ACL-I) adolescents (6 male, 6 female, Tanner Stage: 3.91 ± 1.2) were used to segment the femur and the tibia of each subject. Articular surfaces of the femur and tibia were simplified as best-fitting spheres to preserve contact. Six OpenSim marker positions of the anterior superior iliac spine, hip joint centre, medial/lateral epicondyles and medial/lateral malleoli were scaled to patient anthropometrics and extracted. Markers positions were aligned to the MRI segmented bones in Rhinoceros and their new positions extracted [3].

Principal component analysis (PCA) was performed to enable reconstruction of the positions and radii of the best-fitting spheres from marker trajectories and anthropometric measurements of the leg. Four sets of observations were tested: 1. MRI-Aligned markers of the femur and tibia; 2. MRI-aligned markers of the femur and tibia and anthropometric measurements; 3. MRI-Aligned femur markers only (reconstruct femur only); and 4. MRI-aligned femur markers and anthropometric measurements related to the femur. A leave-one-out cross validation was performed to ensure each knee was equally considered part of the PCA training sample or used to validate the reconstruction accuracy. Average root mean squared error (RMSE) was calculated for all tests.

Results and Discussion

Of the four sets of features used to run PCA, the combination of markers and anthropometrics related to the femur only (test 4) performed the best. For this test, RMSE were under 1mm for reconstructed lateral femoral radii and 5 mm for all reconstructed medial femoral radii. Reconstructed sphere centroids had a RMSE of 9.86 ± 8.8 mm or lower.

Difficulty in reconstructing tibial articulation spheres could be due to the asymmetry of the tibial plateau morphology [4]. The shape of the femoral condyles can be simplified to circular representations [5], and the evolution of distal femur shape has remained relatively static over the last 400 million years compared to the tibial plateau [6]. In contrast, we observed, and others [7], observant important differences in lateral tibial morphology between knees. To summarize, this research shows that simplifications of articular contacts can be reconstructed requiring use of medical images, however tibial reconstruction remains a challenge.

RMSE of Articular Contact Sphere Reconstruction								
	All Markers		All Markers, All Anthropometrics		Femur Markers Only		Femur Markers & Anthropometrics Only	
Feature [mm]	RMSE [mm]	SD [mm]	RMSE [mm]	SD [mm]	RMSE [mm]	SD [mm]	RMSE [mm]	SD [mm]
TLx	40.18	34.23	18.03	13.23	----	----	----	----
TLy	63.61	42.65	20.31	17.31	----	----	----	----
TLz	173.92	135.30	51.87	31.35	----	----	----	----
TMx	20.13	13.12	8.67	8.20	----	----	----	----
TMy	21.76	14.75	11.68	10.49	----	----	----	----
TMz	6.65	7.49	5.57	4.03	----	----	----	----
FLx	10.33	15.65	12.16	10.78	25.15	37.82	9.68	8.83
FLy	4.54	4.77	12.98	12.80	4.54	6.76	5.07	4.66
FLz	7.66	8.31	6.82	5.28	9.15	14.29	5.52	4.14
FMx	17.77	15.66	10.68	8.01	25.83	38.56	7.20	8.98
FMy	12.72	11.95	13.45	14.49	25.72	38.19	6.64	8.88
FMz	15.11	13.38	12.13	10.43	31.80	47.24	4.37	4.25
Radius TL+FL	39.07	35.11	22.76	20.20	----	----	----	----
Radius TM-FM	20.38	26.98	21.20	17.84	----	----	----	----
Radius FL	----	----	----	----	1.77	2.66	0.44	0.31
Radius FM	----	----	----	----	17.28	26.11	4.89	4.94

Table 1: Root mean squared error (RMSE) of the PCA generated articular contact spheres.

Significance

Eliminating the need for medical images to generate simplifications of articular contacts can make patient-specific modelling accessible to all researchers, regardless of equipment. Furthermore, relying on external markers and anthropometrics to build these knee models means that they can be easily scaled to accommodate growth, for example during adolescence or through a knee rehabilitation protocol.

Acknowledgments

The authors would like to thank the Natural Sciences and Engineering Research Council (NSERC) for the financial support during the completion of this research.

References

[1] Conconi et al., 2021. *IEEE Trans Biomed Eng,* 68(3). 1084-92
[2] Clouthier et al., 2019. *Med. Eng. Phys.* 66 :47-55
[3] Smale et al., 2019. *J. Biomech.* 83:9-15.
[4] Hashemi et al., 2008. *J Bone Joint Surg Am.* 90(12) :2724-34
[5] Monk et al. 2014. *Bone Joint J.* 96 :1623-30
[6] S.F. Dye. 2003. *Clin Orthop Relat Res.* (410): 19-24
[7] Wahl et al. 2012. *J Bone Joint Surg,* 94(3),217-26

CREATING PERSONALIZED THUMB MODELS FROM SPARSE SIMULATION DATASETS USING DEEP LEARNING

Erica M. Lindbeck[1*], Maximillian T. Diaz[2], Jennifer A. Nichols[2] and Joel B. Harley[1]
[1] Department of Electrical and Computer Engineering, University of Florida
[2] J. Crayton Pruitt Family Department of Biomedical Engineering, University of Florida
*email: elindbeck@ufl.edu

Introduction

Despite recent advances in musculoskeletal modelling, current models remain inadequate for personalized medicine. For example, models at the wrist commonly exhibit errors in estimated muscle forces in the range of 20-50%, but these errors can be as high as 180% [1]. While subject-specific models are likely to yield superior performance and thus be better suited for patient care, measuring subject-specific parameters remains time intensive and impractical in a clinical setting. Here, we investigate whether subject-specific parameters can be estimated from easily obtainable clinical measurements (height, weight, pinch force) through the use of deep learning. We specifically examine how increasing force data complexity from 1D to 3D, and from peak forces to time series, improves such estimates.

Methods

We generate unique models by uniformly scaling the height, weight, bone density (BD), tendon slack length (TSL), optimal fiber length (OFL), physiological cross-sectional area (PCSA), and pennation angle (PA) of the bodies of a generic OpenSim lateral pinch model [2]. Scaling factors are selected based on known distributions of each parameter in adults [3,4]. Using 50 random models, we generate activation patterns using computed muscle control (CMC). One of these 50 activation patterns is then randomly chosen for each new model to use in forward dynamics, emulating variability in how people perform a lateral pinch task.

To train neural networks, 50,000 randomly scaled models are generated, and forward dynamics is performed to estimate lateral pinch force. These pinch force estimates, along with height and weight scaling factors, are used as inputs for the neural networks. Eight independent networks are trained, each with a different input representation based on 3 binary choices: (i) forces are either 1D or 3D, (ii) forces are either singular peak force or time series, and (iii) height and weight are either included or excluded.

For each representation of network inputs, an 80/20 train-test split is performed, then 5-fold cross-validation is used on the training data to determine the optimal network hyperparameters: number of hidden layers, learning rate, layer size, and nonlinear activation function. The final neural networks are then trained on the training set using the optimal hyperparameters for each input representation. The root mean square error (RMSE) of the predictions produced on the test set are compared to determine the usefulness of the different input representations for predicting 5 musculoskeletal parameters: BD, TSL, OFL, PCSA, and PA.

Results and Discussion

Our results suggest that height and weight, though most easily obtained, are the least useful for predicting modeling parameters. On average their inclusion as network inputs decreases the RMSE by at most 0.47% for each parameter. Using 3D and time series data (Fig. 1) provides larger improvements, and the combination of all three changes that increase input measurement complexity reduces error more than any one change. Further, changing from 1D peak forces to 3D time series with height and weight reduces error more than changing from distribution-based guesses to estimates based on 1D peak forces.

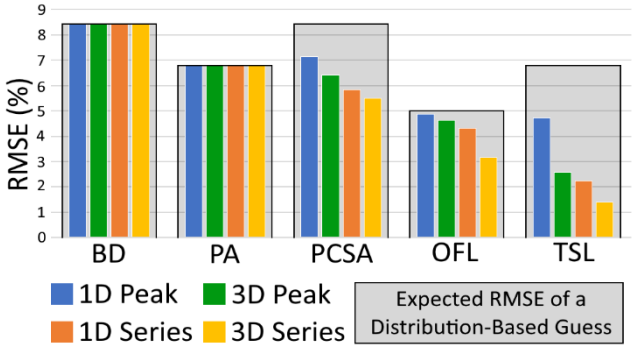

Figure 1: RMSE of parameter estimates generated by neural networks that included height and weight. From left to right, color bars represent increasing complexity of force data representations. Gray boxes are the standard deviation of the parameter distribution, which is equivalent to the expected error of a random guess from that distribution.

We observe that TSL is always the parameter best predicted by the networks. Even with 1D peak forces, TSL scaling can be predicted with less than 5% error, while 3D time series forces can lead to TSL predictions with RMSE less than 1.4%, much less than the 6.67% error expected from random guessing. In contrast, while OFL prediction errors are reduced to 3.1% with 3D time series, other input representations produce errors of 4.3-4.9%, much closer to the expected error random guessing (5%). We find that PA and BD cannot be predicted using lateral pinch forces. We suspect PA is unpredictable because small deviations in near zero angles will not affect force production due to the small angle approximation. Similarly, BD is unpredictable because very small masses and inertias in the hand do not meaningfully affect an isometric pinch task. Use of measurements from additional isokinetic tasks may enable better predictions for BD in future work.

Significance

The results of this study indicate that by using external force sensors and easily obtained biometrics, some musculoskeletal parameters of a human hand models may be quickly personalized to specific simulated subjects. Thus, this work provides the foundation for systems capable of generating personalized models suitable for analysis and guidance during treatment of musculoskeletal pathologies in the hand. Additional tasks, new measurements, and real-world validation with experimental data may enable personalization of more parameters and improve the accuracy of current parameter predictions.

Acknowledgments

This work was supported by the NSF GRFP under Grant No. AWD04512-1842473 and the NIH NIBIB (R21EB030068).

References

[1] De Monsabert et al., 2018. *Ann Biomed Eng.* 46(1): 71-85.
[2] Nichols et al., 2017. *J Biomech.* 58: 97-104.
[3] McPhee et al. 2018. *J Gerontol A Biol Sci Med Sci,* 73(10):1287-1294
[4] Blake et al. 2005. *Osteoporos Int.*, 16:2149–2156

THE EFFECT OF SUBTALAR JOINT AXIS DEFINITION ON MUSCLE MOMENT ARMS OF THE FOOT

Julia M. Noginova[1], Hunter J. Bennett[2], Stacie I. Ringleb[2]
[1]Naval Medical Center Portsmouth, Portsmouth, VA
[2]Old Dominion University, Norfolk, VA
email: sringleb@odu.edu

Introduction

Frequently, the subtalar joint (STJ) is overlooked or restricted in biomechanical models by "locking" the joint or using a generic 1 DOF STJ axis definition. Since the STJ is responsible for the foot's acceptance and transmission of load during dynamic tasks, inaccurate representation may negatively impact the results of simulations. [1]. Specifically, it was shown that the orientation of the STJ axis significantly affected ankle range of motion during walking and STJ moments during walking and running [2] and moving the STJ origin from the heel to the ankle resulted in a significant decrease in STJ moment when Inman's mean orientation were set [3].

In the OpenSim Lai model [4], the 1DOF STJ axis is defined with origin location based at the most distal part of the calcaneus and the axis of rotation oriented in such a way that it intersects with the center of the talus (**Delp**) [5]. While there are no STJ specific standards, the ISB standards for ankle joint recommend that the calcaneus coordinate system origin should be coincident with that of the ankle, i.e. midway between the two malleoli of the talus [6]. To better understand the source of these differences, it is necessary to evaluate how these changes to orientation affect key model definitions, such as moment arms that determine a muscle's function. Therefore, the purpose of this study was to determine how the STJ origin location and axis orientation definitions affect the muscle moment arms of the ankle/STJ throughout STJ range of motion.

Methods

Overground walking was obtained from the 3rd, 4th, and 6th Grand Knee Challenge Competition [7]. The standard Lai model was scaled for each subject and adjusted to include the pelvis and lower instrumented limb. The STJ axis was modified by changing the location of the origin from the default location at the distal point of the calcaneus **(Heel)** to a new location at the talocrural axis **(Ankle).** The STJ axis orientation was set to match Inman's mean inclination/deviation angles in both conditions [8]. This was chosen to highlight how changes to location can affect varying orientation models when compared to default (**Delp**). With the model set in anatomical position, OpenSim was used to evaluate muscle moment arms vs STJ angle (from -20° to +20° of passive STJ motion) for the major ankle muscles defined in the model.

Results and Discussion

The default STJ oblique axis in the Lai model runs directly from the heel axis location through the ankle axis location. Thus change to STJ origin location has no significant effect on relative location of the muscle insertion to STJ axis and resulting muscle moment arms of the ankle (Fig 1a). Therefore, it may be sufficient to use **Heel** location if there are no changes to STJ axis orientation. However, when defining the STJ orientation based on Inman's mean inclination/deviation angles, the origin location dramatically influenced how the 1DOF rotational axis crosses through the talus (Fig 1a). Since the muscle functions actuating the joint are heavily dependent on the distance and relative location to the joint axis of rotation, these changes become significant to the model.

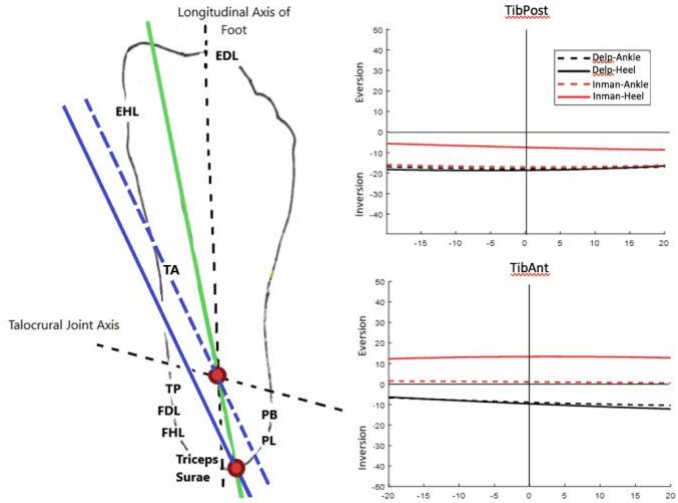

Figure 1*:* (a) Relationship between STJ axis and surrounding muscle insertions when using default Delp (green) or Inman (blue) axis orientations. (b) Muscle moment arm vs STJ angle for two representative major ankle muscles highlighting the functional differences when using **Heel** (solid) vs **Ankle** (dotted) origin locations.

For many of the muscles shown in Fig 1a, like TibPost, setting the origin location to the ankle resulted in muscle moment arm values that closely match the default **Delp** values and make the invertor/evertor action of the muscles less extreme (Fig 1b). However, for a few key muscles, like TibAnt, even with the new origin location, the muscle insertion still falls on or laterally to the STJ axis. This makes the TibAnt function as an evertor within the model, instead of an invertor.

Significance

Subject-specificity is becoming increasingly important in models; however, unlike the attention that the knee and ankle receive, the STJ is often under-appreciated. This work demonstrates that considerable attention needs to be placed on the location of the axes when modifying the STJ orientation as this can affect the function of the muscles within the model.

References

[1] Nichols, J. et al. *Ann Biomed Eng*. 2017
[2] Noginova, J. et al. ASB Conference, 2018
[3] Noginova, J. et al. ASB Conference, 2021
[4] Lai, A.K. et al. *Ann Biomed Eng*. 2017
[5] Delp, S. et al. *IEEE Trans Biomed*. 1990
[6] Wu et al. *J. Biomech.* 2002
[7] Fregly et al. *J Orthop Res*. 2012
[8] Inman. The Joints of the Ankle. Williams & Wilkins, 1976

MEASURING AND MODELING *IN VIVO* HUMAN GRACILIS PASSIVE FORCE

Lomas S. Persad[1], Benjamin I. Binder-Markey[2], Alexander Y. Shin[1], Richard L. Lieber[3,4] and Kenton R. Kaufman[1],
[1]Department of Orthopedic Surgery, Mayo Clinic, Rochester, MN, [2]Drexel University, Philadelphia, PA
[3]Shirley Ryan AbilityLab, Chicago, IL, [4]Hines VA Medical Center, Chicago, IL
Email: Kaufman.Kenton@mayo.edu

Introduction

Subject-specific human musculoskeletal models rely heavily on the use of animal data and a variety of assumptions to model the subject being studied. To accurately model an individual, models are scaled from a default configuration to one that represents a subject's segment length and musculotendon parameters. Therefore, it is important to validate the musculotendon parameters and test the limitations of subject-specific musculoskeletal models. The aim of this study was to measure *in vivo* gracilis muscle-tendon unit (MTU) length and passive tension during knee motion and compare these data against musculoskeletal model predictions.

Methods

Gracilis MTU length and passive tension were measured intraoperatively in nineteen subjects undergoing a free functioning muscle transfer surgery to restore upper limb function by transfer of the gracilis into the biceps brachii location. *In situ* gracilis MTU length and passive tension were measured at four joint configurations (JC1-JC4) designed to gradually lengthen the gracilis muscle. MTU length was measured by holding one end of a suture proximally at the muscle's origin then threading the suture parallel to the MTU and marking the MTU insertion location on the suture using surgical clips. *In vivo* passive tension was measured using a buckle force transducer placed on the distal gracilis external tendon. After the MTU was harvested, it was weighed then spread along a sterile surgical towel adjacent to a ruler and photographed. Muscle and tendon slack length were measured from this image when the muscle was at true slack length with zero passive tension. Muscle fiber length was calculated from the gracilis' fiber:muscle length ratio (1).

Intraoperative MTU length and passive force data were compared to predictions obtained from two previously published OpenSim models (2,3) that had different passive force-length (FL) curves (4,5). These models were linearly scaled to the subject's segment length and were used to predict passive tension in two configurations. First the default configuration, where the models were only scaled. Second a modified configuration, where the models were scaled, the gracilis maximum isometric force (Fmax) was adjusted to subject-specific values, and our previously published data (6) were used to define the gracilis passive FL curve.

Results and Discussion

Experimental average passive tension ranged from 1.3 ± 0.9 N at JC1 to 20.2 ± 11.4 N at JC4. The greatest error for both models and configurations occurred in JC4 (Fig. 1A&B) when the knee was fully extended. For the default configuration, on average, Model 1 overestimated passive tension by 720% whereas Model 2 underestimated passive tension by 69% at JC4. When the modifications were made, Model 1's error decreased to 207% and Model 2's error increased to 86% (Fig. 1B).

Previously we showed that both models significantly overestimated MTU and muscle fiber length where individual fiber length errors exceeded 45% in JC 4 (7). Greater fiber length errors were observed for Model 2. However, when predicting passive tension, Model 2 had smaller errors compared to Model 1 (Fig 1A). Since both models predicted MTU length similarly, the differences in passive tension error reported here were due the model's tendon slack length parameter and passive FL curve.

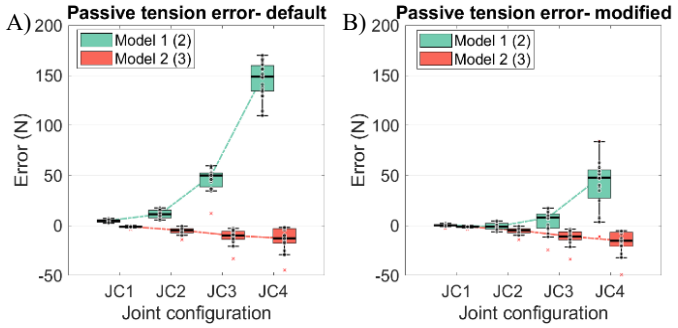

Figure 1: A) Passive tension error for the default models. B) Passive tension error for the modified models. Hip abduction (HA) and knee flexion (KF) angles for each JC were set to (HA, KF). JC1 (45°, 130°), JC2 (45°, 90°), JC3 (45°, 45°) and JC4 (60°, 0°). Hip flexion was constant at 60° for each of the four JCs. (n=19).

In addition to adjusting Fmax and the passive FL curve, optimal fiber length and tendon slack length were also adjusted to further investigate the influence of subject-specific musculotendon values on both models. The addition of these two parameters resulted in errors greater than 390% in JC4, due to an overestimation of MTU length, which led to longer normalized fiber length and greater predicted passive tension.

Model 1 highlights the improvement of using subject-specific data however both models have significant muscle fiber length errors due to errors in predicted MTU length. Despite substituting all experimental subject-specific muscle parameters, significant errors still occurred due to the underlying scaling and MTU length errors that were not first addressed.

Significance

This study quantifies the error resulting from current open-source musculoskeletal models to predict subject specific gracilis passive tension in a muscle where direct measurements were made. The novel MTU data were directly measured *in vivo* and thus serve as a "gold standard" against which to compare the models. Significant errors were observed at full knee extension. Subject-specific values can improve model prediction however significant errors remain due to the MTU length and scaling errors that exist.

Acknowledgments

Supported by VA grants I01 RX002462 and IK6 RX003351.

References

[1] Ward *et al.* (2009). *Clin Orthop Relat, Res.* **467**:1074-1082. [2] Lai *et al.* (2017). *Ann Biomed Eng*, **45**: 2762-2774. [3] Hamner *et al.* (2010). *J Biomech*, **43**: 2709-2716. [4] Millard *et al.* (2013). *J Biomech Eng*, **135**: 1-11. [5] Thelen (2003). *J Biomech Eng*, **125**:70-77. [6] Persad *et al.* (2021). *J Exp Biol*, **224(17)**. [7] Persad *et al.* (2021). *J Biomech*, **26**:125:110592.

ELASTICITY TENSOR APPROXIMATION APPLIED TO A FINITE ELEMENT MUSCLE MODEL

Manuel Lucas Sampaio de Oliveira[1*], Thomas K. Uchida[1]
[1]Department of Mechanical Engineering, University of Ottawa, Ottawa, Ontario, Canada
*email: mdeol080@uottawa.ca

Introduction

Computational models of muscle force generation are used to represent the mechanical function of muscles in simulations of movement. Muscle models have improved our understanding of muscle structure and function. For example, Blemker et al. [1] used a muscle model to understand the contribution of different features of biceps architecture (e.g., fiber length and fascicle curvature) to producing nonuniform strains within the muscle, and Weickenmeier et al. [2] created a model of the masseter to understand muscle forces during biting. These studies used finite element models, which are computational models where each component of a physical system is divided into small pieces (called "elements") that embody the behaviour of the material.

Muscle models can be implemented in Ansys, a popular finite element analysis software, via user material ("USERMAT") subroutines. These subroutines provide as outputs the Cauchy stress and the tangent modulus (also referred to as the elasticity tensor or material Jacobian). The Cauchy stress is relatively straightforward to calculate; however, the tangent modulus is more complicated due to the presence of a fourth-order tensor, making the calculations more cumbersome to program and more time-consuming to evaluate. To reduce the computational expense of computing the elasticity tensor, we implement and verify an approximation of the elasticity tensor proposed by Miehe [3] and apply it to a muscle material model.

Methods

We used the strain energy function reported by Blemker et al. [1] to calculate the Cauchy stress ($\boldsymbol{\sigma}$) and elasticity tensor ($\mathbb{C}^J$) in our USERMAT subroutine. The Cauchy stress was defined using the force–length relationship of a muscle fiber and by assuming that the muscle material is incompressible.

The elasticity tensor was calculated using the deformation method proposed by Miehe [3]. The method is based on the perturbation of the deformation gradient by a small perturbation parameter ε, following a four-step procedure: i) calculation of the perturbation ($\Delta\mathbf{F}$) on the gradient matrix ($\mathbf{F}$); ii) calculation of the perturbed gradient matrix ($\tilde{\mathbf{F}}$); iii) calculation of the perturbed Cauchy stress ($\tilde{\boldsymbol{\sigma}}$) and perturbed Kirchhoff stress ($\tilde{\boldsymbol{\tau}}$); and iv) use of the perturbed Kirchhoff stress to calculate the elasticity tensor ($\mathbb{C}^J$) as follows:

$$\mathbb{C}^J = \frac{1}{J\varepsilon}(\tilde{\boldsymbol{\tau}} - \boldsymbol{\tau}),$$

where J is the determinant of the deformation gradient ($\mathbf{F}$).

We proposed three tests to explore force, displacement and contact scenarios. All tests were performed using a single muscle filament with one fixed end and one free end (where the boundary conditions were applied). In the force test, force was applied at each node of the free end. In the displacement test, a displacement was applied on the face of the free end. In the contact test, two filaments with opposite fiber directions were bonded together at their free ends and both were activated. We used these tests to verify our implementation of the muscle model [1] and approximation of the elasticity tensor [3].

Results and Discussion

From the force test, we verified that as the muscle activation increases, the muscle stretches less to reach the same level of force generation (Figure 1). The displacement test allowed us to verify that the passive component of force depends only on the muscle stretch. In the contact test, we compared the simulated stress with the theoretical stress at the contact interface at various levels of activation. The error in stress was less than 1% for all conditions. Similar errors were reported by Nazari et al. [4], who verified their muscle model with similar tests.

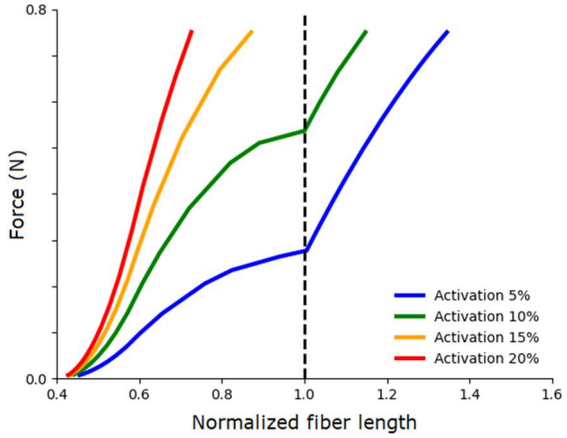

Figure 1: Verification using force test. Force (N) measured on the free end of the fiber vs. fiber length normalized by the optimal fiber length. The colours blue, green, yellow and red represent, respectively, activations of 5%, 10%, 15% and 20%. Passive force is zero when the fiber is shorter than its optimal length (i.e., normalized length of 1.0).

Significance

The approximation method for the elasticity tensor [3] has been used previously for several hyperelastic materials [5]. The implementation of this method facilitates the development of a hyperelastic material model into commercial finite element software. This work applies the approximation method to a muscle material model in Ansys to improve computational efficiency while simplifying the implementation. A similar method can be applied to other muscle models, making them faster, more accessible and easier to replicate [6]. Finite element models of muscle that are fast, easy to use, and freely available will facilitate detailed studies of muscle behaviour during human movement.

Acknowledgments

We acknowledge the support of the Natural Sciences and Engineering Research Council of Canada (NSERC).

References

[1] Blemker et al., 2005. *J Biomech*. 38: 657–665.
[2] Weickenmeier et al., 2017. *J Biomech Eng*. 139: 121007.
[3] Miehe, 1996. *Comput Methods Appl Mech Eng*. 134: 223–240.
[4] Nazari et al., 2013. *J Speech Lang Hear Res*. 56: 1909–1923.
[5] Sun et al., 2008. *J Biomech Eng*. 130: 061003.
[6] Dao and Tho, 2018. *Appl Bionics Biomech*. 2018: 7631818.

THE AGING ACHILLES TENDON: MODEL-PREDICTED CHANGES IN CALF MUSCLE NEUROMECHANICS

Maggie M. Wagner[1], William H. Clark[2], and Jason R. Franz[1]
[1]Joint Department of Biomedical Engineering, UNC Chapel Hill & NC State University, Chapel Hill, NC, USA
[2]Department of Ecology, Evolutionary and Organismal Biology, Brown University, Providence, RI, USA
email: magwag98@live.unc.edu

Introduction

The triceps surae muscle-tendon unit contributes significantly to forward propulsion in walking by transmitting forces from the lateral gastrocnemius, medial gastrocnemius (MG), and the soleus (SOL) through subtendons that intertwine to form the Achilles tendon (AT). In young adults, there is evidence that these subtendons can slide relative to one another, facilitating some level of independent actuation [1]. However, two hallmark age-related changes to the AT are likely to affect triceps surae muscle neuromechanics and potentially force production. First, animal literature reveals older tendons exhibit interfascicular adhesions [2], which we suspect deleteriously diminishes independent actuation. Indeed, our *in vivo* work suggests that a reduced capacity for subtendon sliding correlates with smaller peak ankle moments in older adults [3]. Second, the majority of human studies report that older tendons are more compliant than younger tendons, which we suspect elicits shorter triceps surae muscle operating lengths, thus reducing their force generating capacity [4]. However, the independent and interdependent neuromechanical effects of these hallmark age-related changes are poorly understood, largely because they are difficult to isolate and quantify *in vivo*. Our earlier modelling work attempted to fill this gap, but those walking simulations were confounded by complex patterns of inter-joint kinematics and activation and limited to one level of force generation [5]. Thus, the purpose of this study was to use a series of hill-type musculoskeletal models to simulate the effects of age-related decreases in AT stiffness and/or a reduced capacity for subtendon sliding on triceps surae neuromechanics during fixed-end contractions across a physiological range of muscle forces.

Methods

We developed hill-type models of triceps surae muscle-tendon unit dynamics in Simulink [5]. We manipulated the model in two ways. First, we simulated age-related changes in tendon stiffness by varying peak tendon strain at maximum isometric force (i.e., 3%, 6%, 9%). Second, we simulated a reduced capacity for subtendon sliding by including a 20 cm shared AT that connects the MG and SOL and reduced their respective independent tendon lengths accordingly. For both, we had 3 activation conditions: 1) SOL alone, 2) MG alone, and 3) combined SOL and MG. Thus, we interrogated a total of 18 models and determined the excitations necessary to match a fixed, net MG+SOL force requirement, prescribed as a percentage of those estimated from measured walking data (i.e., 25%, 50%, 75%, and 100% of peak walking force [%WF]) [3]. When stimulated together, we preserved the ratio of activations determined by relative physiological cross-sectional areas. Our primary outcomes included requisite muscle excitation and fiber length changes needed to generate the prescribed force.

Results and Discussion

When activated alone or together, increased tendon compliance elicited greater fiber shortening (Fig. 1A) and thereby increased SOL and MG excitation requirements (Fig. 1B) to meet each prescribed force level, regardless of the presence of a shared tendon. These effects were common to both muscles and increased with increasing force demand. For example, for SOL-only activation without a shared tendon, requisite excitation and fiber length change to generate 100 %WF increased by 17% and 212% across the range of peak tendon strains, respectively. The presence of a shared tendon mitigated those effects, but only when muscles were activated separately. Compared to independent muscle-tendon actuators, the presence of a shared tendon elicited a redistribution of relative force production from MG (-40 N) to SOL (+40 N) when the muscles were activated together to achieve 100 %WF. Those inter-muscular differences were consistent with those found previously in walking, mirrored requisite activations and fiber length changes, and increased with tendon compliance more than increasing force demand.

Significance

Our model predictions provide a road map for understanding the complex changes in muscle neuromechanics elicited by two hallmarks of the aging Achilles tendon across a physiological range of muscle forces in the absence of inter-joint kinematics.

Acknowledgments

Supported by NIH (R01AG051748), BME Lucas Scholars Program, and UNC Chancellor's Science Scholars Program.

References

[1] Clark and Franz, 2018. *PeerJ*. 6: e5182. [2] Thorpe et al., 2013. *Eur Cell Mater*. 25: 48. [3] Clark and Franz, 2021. *Sci Rep.* 21264. [4] Onambele et al., 2006. *J Appl Physiol*. 100(6): 2048. [5] Franz and Thelen, 2016. *J Biomech*. 49(9): 1403.

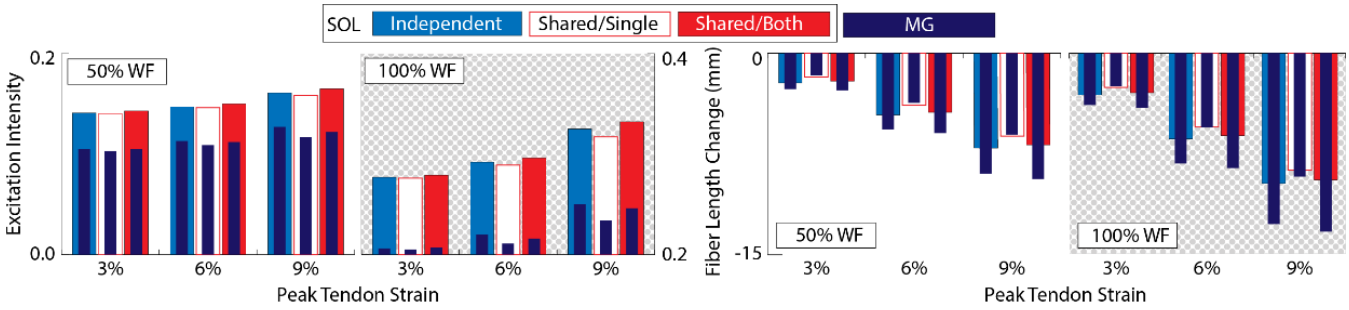

Figure 1. Simulated effects of tendon compliance and inter-fascicle adhesions on soleus and medial gastrocnemius neuromechanics during fixed end contractions across a range of physiological force levels. Soleus (SOL) shown with medial gastrocnemius (MG) inset.

A 3D modeling exploration into quantifying soleus muscle stiffness

Katherine R. Knaus[1*] and Silvia S. Blemker[2]
[1] University of California San Diego, Department of Bioengineering, La Jolla, CA, USA; *email: kknaus@ucsd.edu
[2] Department of Biomedical Engineering, University of Virginia, Charlottesville, VA, USA

Introduction

Muscle stiffness is a biomechanically important description of the structure-function relationship between tissue deformation and loading. This stiffness is neuromechanically determined by combining active and passive non-linear properties. Also, it contributes to performance as a component of joint quasi-stiffness, relating moment and angular motion [1]. Quantifying muscle stiffness *in vivo* relies on assumptions from limited measurements to estimate stress and strain. Methodological approaches to quantify stiffness therefore vary with the available measurements and may not be comparable between studies. Further, the stiffness of an intact muscle is governed by the arrangement and material properties of fibers and extracellular components [2], which often can't be fully characterized experimentally to compare with quantifications of stiffness of the muscle as a whole. Computational modeling makes it possible to quantify muscle stiffness in a context where tissue material properties as well as geometry and architecture are known, and multiple measurements can be made to examine these effects.

The soleus muscle plays an important role in ankle function, so its stiffness influences locomotive performance. Soleus architecture is complex with multi-pennate compartments of short fibers with large interdigitating aponeuroses. It is difficult to intuit soleus mechanical function and especially complicated to characterize its stiffness. We hypothesize that differences in muscle stiffness arising from mechanical and neural conditions vary between the tissue and organ scales and that methodological differences in characterizing whole muscle stiffness augment this variation. Our goal is to use a finite element model (FEM) of the soleus to test this hypothesis by quantifying muscle stiffness using different experimental approaches and directly comparing to prescribed material properties.

Methods

3D geometry for the soleus FEM was made based on MR images [3]. FEM muscle architecture, constructed with fibers originating and inserting onto aponeuroses surfaces, was used to assign a fiber direction to each tetrahedral element of transversely isotropic muscle material. Fascicle tracts were created for the FEM architecture and mapped to the FE mesh so that simulations predict both tissue deformation and associated fascicle behavior. Model predictions of passive architecture changes and eccentric tissue displacements were validated diffusion and dynamic imaging [3]. Muscle passive lengthening of 20cm was simulated to calculate stiffness.

To quantify stiffness, we calculated stress in two ways. For the first (σ_{ACSA}), reaction force at the distal end of the muscle was divided by the anatomical cross-sectional area (ACSA) at half the muscle length. Second (σ_{PCSA}), force was divided by the physiological cross-sectional area (PCSA) computed as *volume*cos(average pennation angle)*(average fascicle length)*. Strain was calculated in three ways: from the muscle belly length change (ε_m), the average fascicle strain (ε_f), or average element strain to represent sarcomeres (ε_s). Modulus, found as slopes of lines fit to each stress-strain curve, served as a metric of stiffness and compared to material properties of muscle and aponeurosis.

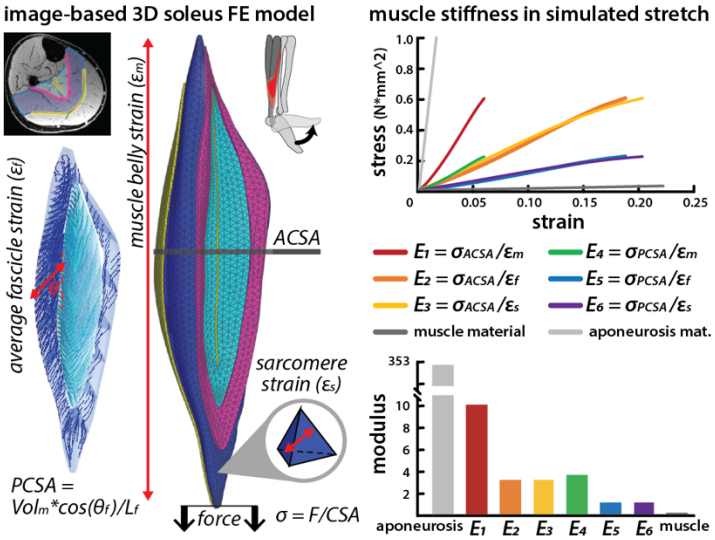

Figure 1: Muscle stress-strain curves were created with 6 different methods to quantify stiffness modulus of simulated soleus lengthening.

Results and Discussion

Methodological differences in calculated stiffness resulted in varied estimates of muscle stiffness for a muscle of a given morphology with a prescribed lengthening. All calculations of muscle stiffness were greater than the stiffness of the muscle material but much less than aponeurosis material. Modulus was greater with stress calculated using ACSA instead of PCSA. Strain in the muscle belly resulted in higher moduli than using fascicle or sarcomere strains. Calculations of stiffness that incorporate measurements of muscle architecture are therefore more accurate in elucidating the tissue properties.

These results demonstrate the role of morphological effects on muscle-level mechanical properties, especially in muscle with complex architecture and connective tissue structures like the soleus. Further, this work highlights how experimental approach can lead to differences in characterization of muscle stiffness that are not dependent on the muscle's neuromechanical properties.

Significance

Quantifying muscle stiffness provides insight to how mechanical properties are modulated by structural and neural factors. This is important for investigating cases where muscle phenotypic structural changes are associated with altered function such as aging, pathological conditions, and adaptations to training. This work reveals how different methodologic approaches result in variations in presumed stiffness. Separating characterization of stiffness by scale further elucidates how different constituents influence muscle biomechanics (aponeuroses, ECM, titin, etc.).

Acknowledgments

Thank you Tendonados and funding from grant #R01AG051748.

References

[1] Krupenevich et al. (2020). *J Appl Biomech*, **36(4)**:209-216
[2] Ward et al. (2020). *Frontiers in Physiology*, **11**:211
[3] Knaus et al. (2022). *J Biomech*, **130**:110877

Session 8

Thursday August 25, 2022

9:30am – 11:00am

O8.1 – Motion Analysis/Methods

O8.2 – Movement Disorders

O8.3 – Orthopaedic Biomechanics

O8.4 – Sports Injuries 2 – Head Trauma

O8.5 – Trunk & Spine 2

A COMPARISON OF FORCE PLATE-BASED CENTER OF MASS ESTIMATION ALGORITHMS

Alexandre Banks[1*], Rose He[1], Luke Dillman[1], Chris McGibbon[1] and Jon Sensinger[1]
[1]Institute of Biomedical Engineering, University of New Brunswick, Canada
email: *j.sensinger@unb.ca

Introduction

Estimating horizontal centre of mass (CoM) is an important biomechanics process that can be used for clinical and scientific analysis, as well as to regulate self-paced treadmill algorithms. Many laboratories use motion-capture to estimate CoM, while others prefer to use force-plate based estimates, either because they cannot access motion-capture or because the risk of losing a marker or the post-processing of motion-capture outweigh the benefits. Several groups have recently proposed force-plate based estimates of CoM, which all rely on converting forces to accelerations, and then twice integrating the acceleration to obtain the estimated position. In this work we compare two of those methods against an algebraic method that avoids the need to integrate acceleration. We hypothesize that compared with a benchmark of motion-capture based CoM estimates, the algebraic force-plate estimate will have a greater sample-by-sample accuracy than conventional integration-based techniques.

Methods

Informed consent was obtained from 23 able-bodied subjects in this study and received approval from the UNB Ethics Review board. Subjects walked at their preferred speed for five minutes on a CAREN instrumented treadmill featuring an OptiTrack motion-capture system. We estimated CoM offline using three different methods.

The first method (I1) integrated the anterior/posterior force-plate measurement to obtain an estimate of CoM position. This integration results in drift away from the true CoM. Estimates were recentred at each heel-strike through Kalman filter sensory fusion. The technique is described in greater detail here [1]. Our only deviation from this technique was to use a butterfly detection of heel-strike [2] rather than the 20% weight threshold used by [1].

The second integration method (I2) used the same approach as I1 but did a hard recentre whenever the anterior/posterior forces transitioned from positive to negative or vice versa. This method is described in greater detail by [3].

The algebraic method (A1) uses the model proposed by Kajita et al [4] to algebraically relate Centre of Pressure (CoP) to CoM using the Zero Moment Point framework [5]:

$$CoM = CoP + \frac{L}{g}a,$$

where L is the length from the floor to the CoM, defined in this study as 55.1% of the total height of the person [6], and a is the acceleration, defined as the force divided by the subject's mass.

Error between each of the three force-plate methods and a marker-based approach (using four iliac spine markers [7]) was found. The standard deviation of this error was recorded for each subject and assessed across subjects using an ANOVA in SPSS. The static offset was not considered as this does not affect standard deviation calculations.

Results and Discussion

The algebraic estimate of CoM was found to have significantly less standard deviation error across subjects (5.0 ± 2.3 cm) than commonly used integration techniques (I1: 15.1 ± 3.5 cm, p=0.046; I2: 23.3 ± 23.9 cm, p<0.001). The integration techniques are typically accurate when they are recentered at each foot-contact (Figure 1), but often wander – a known property of integrating noisy signals that results in Brownian diffusion. It accordingly makes sense that the algebraic method, which does not rely on integration, provides a more accurate CoM estimate.

The algebraic method also avoids the 180° phase-lag associated with integrating a second-order differential equation, which is a useful feature for real-time control applications such as self-paced treadmill applications.

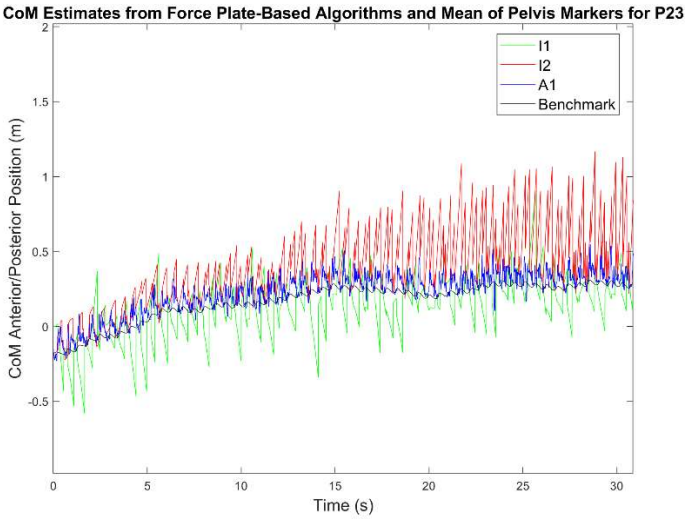

Figure 1: Example of the 3 force-plate based CoM estimates and the benchmark motion-capture estimate for 30 seconds of walking.

Significance

It has been demonstrated that a simple algebraic equation provides an accurate estimate of CoM. This equation is more precise than existing integration approaches, avoids phase-lag, and is clearer to implement. It should accordingly be used for force-plate applications when motion-capture is not available.

Acknowledgments

This work was funded by NSERC and NBHRF.

References

1. Song et al (2020). Using force data to self-pace an instrumented treadmill and measure self-selected walking speed. JNER.
2. Roerdink et al (2008). Online gait event detection using a large force platform embedded in a treadmill. J Biomech.
3. Zatsiorsky and King (1997). An algorithm for determining gravity line location from posturographic regordings. J Biomech.
4. Kajita et al. (2002). A realtime pattern generator for biped walking. IEEE ICRA.
5. J. Reher et al (2020). Dynamic Walking: Toward Agile and Efficient Bipedal Robots. Annual Reviews.
6. McConville et al (1980). Anthropometric relationships of body and body segments moments of inertial.
7. Pavei et al (2017). On the estimation accuracy of the 3D body center of mass trajectory during human locomotion. Front Physio.

TRANSFORMING GAIT: DEEP LEARNING POWERED SPATIOTEMPORAL VIDEO GAIT ANALYSIS

R. James Cotton[1,2,*], Emoonah McClerklin[1], Anthony Cimorelli[1], Ankit Patel[3], Tasos Karakostas[1,2]
[1]Shirley Ryan AbilityLab
[2]Department of Physical Medicine and Rehabilitation, Northwestern University
[2]Department of Neuroscience, Baylor College of Medicine
email: *rcotton@ric.org

Introduction

Human pose estimation (HPE) from uniplanar video is a rapidly advancing field that offers great promise to human movement science and rehabilitation. For example, recent algorithms reliably detect 2D joint keypoints in an image and even estimate 3D joint locations fairly accurately. This potential is tempered by the smaller body of work ensuring the outputs are clinically meaningful. In contrast, gait analysis produces precise clinically relevant measurements including kinematics and step timing. Using a dataset of more than 9000 uniplanar videos from an instrumented gait analysis lab, we trained a neural network to map 3D joint location sequences and the height of individuals onto interpretable biomechanical outputs including gait cycle timing characteristics and selected sagittal plane kinematics and spatiotemporal gait parameters.

Methods

Our video analysis pipeline includes several stages of pretrained algorithms followed by a neural network that we trained to the gait parameters (Figure 1 shows an overview of this process). Pretrained HPE steps include localizing the subject in a frame with a bounding box, detecting 2D keypoints and lifting these to 3D joint locations [1]. This 3D joint location sequence is then tokenized, concatenated, and passed through a neural network based on a transformer architecture with positional encoding [2]. After training the gait transformer outputs sagittal plane hip and knee kinematics, foot position and velocity, pelvic velocity, and the timing of bilateral foot contact and toe off.

To train the gait transformer, we used more than 9000 videos acquired in the frontal plane from hundreds of subjects evaluated in a clinical gait analysis laboratory with simultaneously acquired motion capture data. Videos were passed through the pretrained pipeline to obtain corresponding inferred 3D joint location trajectories. The sagittal plane measurements were retained from the motion captured data. The timing of gait events detected from force plates were represented with four quadrature encoded pairs.

Individual gait cycles were detected from the outputs and for each cycle the velocity, step length, cadence, double support, and single support times were computed.

Results and Discussion

We tested the accuracy of the trained gait transformer on a subset of the dataset withheld for validation. For the foot off and contact event timing, the median error was 25ms for foot contact events and 27ms for foot off events, with the 90% percentile error being 83ms. Subjects typically performed several gait analysis trials in each condition (e.g. with and without walkers or braces) and the average gait parameters from each annotated gold standard cycle were compared with the gait transformer outputs. The correlation for cadence was 0.99, for double support was 0.93, for walking velocity was 0.91, for step length was 0.78 and for single support was 0.76.

While the outputs of most HPE algorithms are of limited clinical value, data annotated with clinically relevant variables, like gait kinematics, can be used to train additional layers to produce similar outputs from video. Whether these outputs are sufficiently accurate will depend on the clinical question and it is likely the accuracy will continue to improve with advances in HPE. A key benefit of this approach is the ease of use, given that video can be obtained with only a smartphone, although the accuracy will need further validation from data obtained this way

Significance

Gait analysis based on uniplanar video may reduce barriers to using it and create novel opportunities. For example, it could enable longitudinal, quantitative monitoring of gait changes during a course of physical therapy visits. However, the accuracy of novel approaches will need validating for each of these opportunities, and it will need to be determined if this accuracy is sufficient for the clinical question and application.

Acknowledgments

This work was generously supported by the Research Accelerator Program of the Shirley Ryan AbilityLab

References

[1] Chen et al., 2020. CVIU 192:102897. “Uniplanar human pose estimation: A survey of deep learning-based methods”
[2] Vaswani et al., 2017. NeurIPS. “Attention is All You Need.”

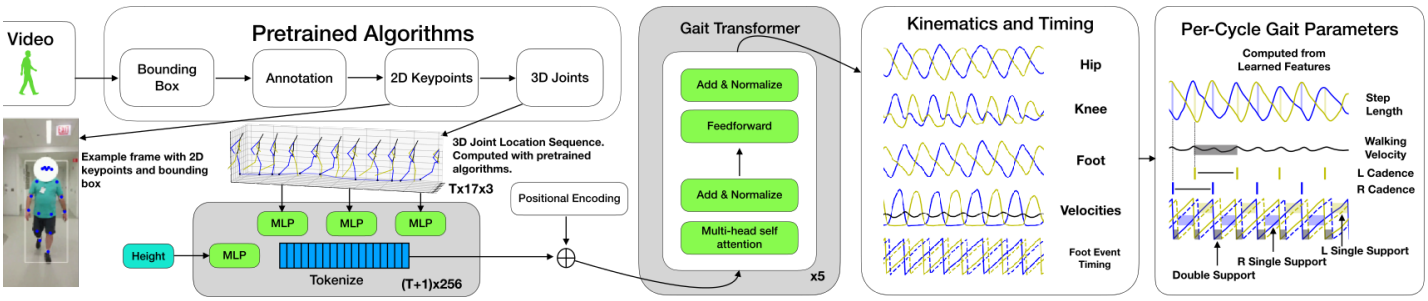

Figure 1: Overview or gait transformer pipeline. Videos are passed through several pretrained algorithms to produce a sequence of 3D joint locations. These are tokenized and passed through the gait transformer which produces sagittal plane kinematic trajectories and timing information. From this several spatiotemporal parameters can be extracted.

A GENERALISED SMOOTHING APPROACH FOR CONTINUOUS, PLANAR, INVERSE KINEMATICS PROBLEMS

Andrew J. Pohl[1*], Matthew R. Schofield[2] and Reed Ferber[1]
[1]Human Performance Laboratory, Faculty of Kinesiology, University of Calgary
[2]Department of Mathematics and Statistics, University of Otago
email: *andrew.pohl@ucalgary.ca

Introduction

Bayesian approaches to solve inverse kinematics problems (BIK) [1, 2] have a major advantage over traditional optimisation-based solutions [3] in that they are able to propagate uncertainties inherent to the observation of motion capture markers to the estimated kinematic quantities of interest (i.e. joint angles). To date, BIK have solved the inverse kinematics problems on a frame-by-frame basis, which if repeatedly applied, gives estimates that are discontinuous likely lead to large errors. We propose representing latent kinematic parameters as smooth continuous functions parametrised by finite basis expansions in an approach we refer to as 'generalised smoothing'[4]. We hypothesised that this approach would reduce root mean square error (RMSE) of joint angle estimation for simulated, planar BIK problems.

Methods

To construct a continuous, planar IK problem with a known solution, the kinematics of the right leg were estimated via an optimisation approach [3] for a single stride of treadmill running. The resulting segment angles and translations were smoothed via a LOWESS smoother and used as the 'ground truth' on which to simulate 1000 sets of noisy marker trajectories.

For each set of simulated marker trajectories estimates of knee joint angle (KJA) were computed from previously published 'time independent' BIK approach [1,2] and compared to those from the 'generalised smoothing' approach. For generalised smoothing, kinematic parameters within the rigid body measurement model of the time-independent approach were modelled as evolving in time via a dimension 12 Fourier basis function (segment angles and measurement noise) or cubic B-spline (hip joint centre).

Results

Both time independent and generalised smoothing provide unbiased estimates of knee joint angle (Fig. 1a-b). In support of our hypothesis, the time independent model produced knee joint estimates that were discontinuous and had greater variance than those from the generalised smoothing approach. In addition, estimates from the generalised smoothing approach had less uncertainty with credible intervals 0.026 rad narrower on average. Also in support of our hypothesis, the generalised smoothing approach halved average RMSE of the time independent model: 0.006 rad vs. 0.013 respectfully (Fig. 1c-d). The cost of this improved performance is computation time with the generalised smoothing approach taking 943s on average compared to 487s for the time independent approach.

Discussion

BIK quantifies the uncertainty in kinematic estimates absent in current optimization approaches [1,2] but to date such approaches have resulted in discontinuous estimates of kinematic parameters. Given the underlying dynamics which govern human motion, we would expect kinematic parameters to be continuous and evolve smoothly over time. A Bayesian generalised smoothing approach enforces this constraint resulting in significantly reduced error with less uncertainty while maintaining unbiased and well calibrated estimates. This result is particularly important when considering estimates of kinematic derivatives with the error in derivative estimation from time-independent approaches increasing considerably given a need to rely on finite-difference approximations. In contrast, derivatives for the generalised smoothing approach can be obtained analytically and are smooth with the degree of smoothness dependent on the a-priori selection of basis dimension.

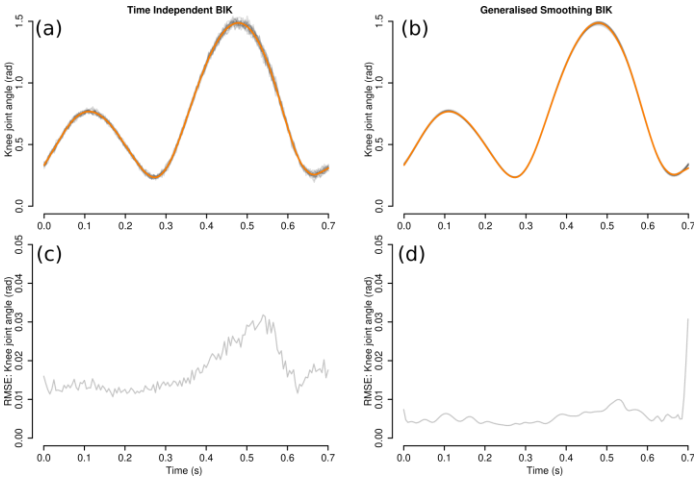

Figure 1: Posterior mean when estimating KJA for 20 independent simulations (grey lines) with true values in orange (top). RMSE for KJA estimates (bottom). Time independent BIK (left), generalised smoothing (right)

Significance

A generalised smoothing approach significantly reduces RMSE of current state-of-the-art Bayesian approaches to estimate gait kinematics from noisy motion capture data. As a result, generalised smoothing should form the basis for future estimation of gait kinematics. This approach has the potential to be incorporated in more complex models to better estimate the kinematic effects of potential interventions or treatments within repeated measures or case control studies.

Acknowledgments

NSERC CREATE Wearable Technology Research and Collaboration Training Program; Alberta Graduate Excellence Scholarship; Alberta Innovates Graduate Student Scholarship.

References

[1] Pataky, Vanrenterghem & Robinson., 2019. *J Biomech.* 91:324-329.
[2] Pohl, Schofield & Ferber., 2021. *J Biomech.* 126:110597.
[3] Lu & O'Connor., 1999. *J Biomech.* 32(2):129-134
[4] Ramsey et al., 2007. *J R Stat.* 69(5):741.

CAN BODY SEGMENT ANGLES DURING COMMON MANUAL WHEELCHAIR USER MOVEMENTS BE CALCULATED FROM LINEAR ACCELERATION DATA?

Stephen M Cain*[1], Meegan G Van Straaten[2], Sydney M Lundell[2], Kathylee Pinnock Branford[1], Omid Jahanian[2], Melissa MB Morrow[2]
[1]West Virginia University, Morgantown, WV and [2]Mayo Clinic, Rochester, MN
email: *stephen.cain@mail.wvu.edu

Introduction

Wearable inertial measurement units (IMUs), which measure linear acceleration and angular velocity, enable high-resolution measurements of human movement outside of the laboratory. A primary challenge in long-duration data collections (days-long) is the limited battery life of IMUs, which limits the run time of research-grade IMUs to <24 hours, requiring study participants to charge sensors at home. This burden placed on participants often results in incomplete datasets due to depleted sensor batteries. An alternative to IMUs are accelerometers, which measure only linear acceleration and have run times of ~2 weeks.

Accelerometers measure the sum of the linear acceleration of the sensor with respect to inertial space and the acceleration due to gravitational attraction [1]. If the linear acceleration of a sensor with respect to inertial space is close to zero (velocity not changing), measurements can be used to calculate the tilt of the sensor (and underlying body segment angle) with respect to vertical. If the sensor is accelerating (velocity is changing), it is impossible to separate sensor acceleration from gravitational acceleration and therefore impossible to accurately calculate sensor tilt [1]. A common approach in biomechanics is to filter accelerometer signals to attempt to separate sensor acceleration from gravitational acceleration before calculating sensor tilt [2, 3]. In this pilot study, we explored the differences between accelerometer- and IMU-based calculations of body segment angles with respect to vertical for common manual wheelchair user movements. We expected small differences between approaches for low-acceleration movements and larger differences for high-acceleration movements.

Methods

In this IRB-approved study, we collected data from a manual wheelchair user (30 years old, MWC user 9 years, T3 injury level, AIS Grade A) during a 1-hour long data collection that included transfers, propulsion (level and inclined on varying surfaces), and reaching tasks. Six wireless IMUs (Opal, APDM Inc.) placed on the participant's wrists, upper arms, chest, and back collected data at 128 Hz. Study team members recorded activity start and end times. We employed two different filtering approaches (low-pass at 1 Hz, 5 Hz) to calculate segment angles relative to vertical for the forearms, upper arms, and thorax [2,3]. IMU-based calculations of segment elevation angles [1] served as our ground truth to evaluate the accuracy of accelerometer-only calculations. Root-mean-square differences, concordance correlation coefficients ($-1<\rho_c<1$, which capture bias and scaling differences [4]), and differences in calculated ranges of motion quantified differences between IMU- and accelerometer-based calculations.

Results and Discussion

Accelerometer-based approaches yielded body segment angles for the MWC user that were quite different from the IMU-based approach (Figure 1). The largest differences were found for the body segment and task with the largest accelerations (forearm during **propulsion**; RMS Diff.>15.0°, $|\rho_c|<0.26$); the smallest differences were found for the body segment and task with the smallest accelerations (thorax during **reach**; RMS Diff.<1.6°, $|\rho_c|>0.90$). Large task-specific differences are hidden when evaluating the entire trial (**all**; RMS Diff.<8.6°, $|\rho_c|>0.92$), suggesting that movements of interest should be evaluated separately. Low-pass filtering acceleration data at 1 Hz versus 5 Hz yielded segment angles closer to IMU-based angles; angles calculated from 5 Hz low-pass filtered data tended to overshoot IMU-based angles during dynamic movements, as evidenced by larger range of motion differences (Figure 1). Caution should be used when interpreting angles during movements with significant body segment accelerations. Alternative strategies are needed for quantifying arm use in MWC users with accelerometers.

Significance

Accelerometers have significantly longer battery life than IMUs (2 weeks versus <24hrs), making them an attractive option for long-duration real-world data collections. We found large differences between IMU-based and accelerometer-based calculations of body segment angles relative to vertical during common manual wheelchair user movements, which often require significant body segment accelerations. Body segment and joint angles calculated from accelerometer data should be interpreted with caution, especially for dynamic movements.

Acknowledgments

This research was supported by the NIH (2R01 HD84423).

References

[1] Titterton D and Weston J, 2004. [2] Laidig D and Seel T, *Current Dir in Biomed Eng*, 2017. [3] Chapman RM et al., *J Biomech*, 2019. [4] Lin LI-K, *Biometrics*, 1989.

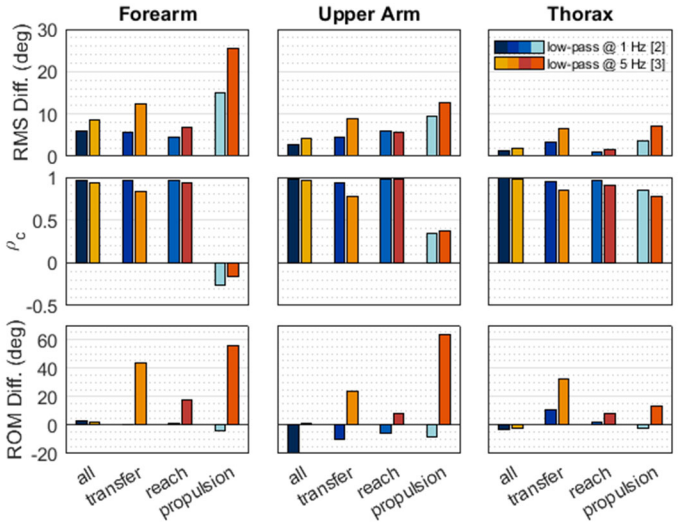

Figure 1: Differences in accelerometer- versus IMU-based calculations of body segment angles for the forearm, upper arm, and thorax during the entire trial (**all**), transfer from vehicle to wheelchair (**transfer**), a high reach task (**reach**), and propulsion up a ramp (**propulsion**). Differences are quantified by root-mean-square differences (**RMS Diff.**), concordance correlation coefficients ($\boldsymbol{\rho_c}$), and range of motion differences (**ROM Diff.**) for two different filtering approaches [2, 3].

FAST 3-D MOTION TRACKING WITH NOISY VIDEO AND IMU DATA

Soyong Shin[1*] and Eni Halilaj[1]
[1]Department of Mechanical Engineering, Carnegie Mellon University, Pittsburgh PA, USA
email: soyongs@andrew.cmu.edu

Introduction

Markerless motion tracking tools that use video and wearable sensing data are emerging as promising alternatives to traditional marker-based gait analysis, but several challenges limit their accuracy. Video-based approaches are data-driven and suffer from occlusion. Inertial-sensing-based approaches require precise calibration and suffer from drift. Fusion of these complementary modalities can reduce the negative effects of drift and occlusion, but it does not liberate us from the need for large training data and calibration practices. In clinical and home settings, careful sensor calibration by clinicians or patients is challenging and time consuming. The goal of this study was to build models that can accurately predict joint kinematics from a combination of video and inertial sensing data without requiring careful sensor-to-body calibration. Such models would enable fast data collection in clinics and patient homes.

Methods

To train the models, we used the AMASS marker-based motion capture dataset of 496 subjects performing a wide range of activities, including walking and range of motion, for a total of 3266 minutes of data [1]. A major advantage of the dataset is its size, while a limitation is the lack of video and inertial sensing data from which to build the predictive models. To address the later, we generated synthetic video and inertial data. Three-dimensional (3-D) locations of joint centers (keypoints) were extracted directly from the dataset. To model the noise present in keypoints extracted from two to four videos (e.g., via geometrically triangulated OpenPose results [2]), we added Gaussian noise ($\mu = 30$ mm, $\sigma = 22$ mm). We also attached virtual inertial measurement units (IMUs) on body segments based on marker-based orientations and computed linear accelerations and angular velocities (inertial data) via numerical differentiation. To model sensor-calibration errors, we applied random normally distributed rotations (μ=0 rad., σ=0.15 rad.) to the virtual IMUs.

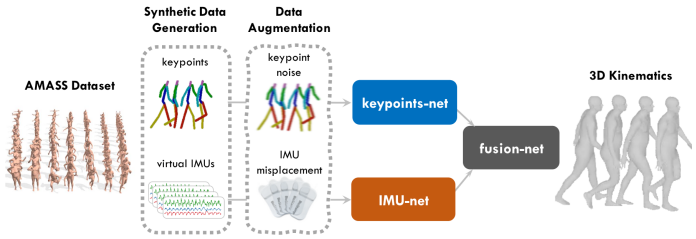

Figure 1. Overview. Synthetic keypoints and inertial data are extracted from marker-based data. Each data modality is input to Keypoints-net and IMU-net and fused by Fusion-net to estimate 3D kinematics.

The overarching architecture consisted of three sub-networks: keypoints-net, IMU-net, fusion-net (Fig. 1). Keypoints-net and IMU-net take sequences of synchronized keypoints or inertial data, respectively. Fusion-net fuses those intermediate features and estimates 3-D joint kinematics. We evaluated the performance of all three networks on real walking data from 2 subjects, which included 4 calibrated RGB cameras, 13 IMUs, and marker-based motion capture [3]. Model performance was compared using repeated measures ANOVAs. We also evaluated model sensitivity to sensor-calibration errors.

Results and Discussion

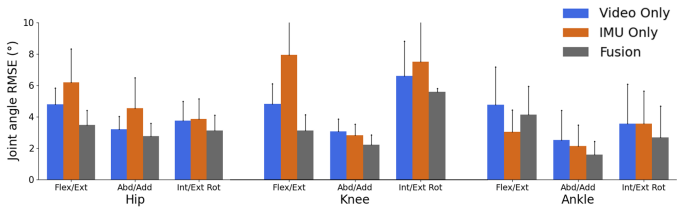

Figure 2. Model Performance. Fusion-net outperformed keypoints-net and IMU-net across most lower extremity degrees of freedom.

On independent data, the proposed fusion model predicted lower extremity joint angles with an RSME of 3.2° (± 1.3°), which is an improvement of 23% over the video-only model and 31% over IMU-only model ($p<0.0001$; Fig. 2). These networks performed better than commercial software for video-based analysis [3] and on par with IMU-based approaches reported in the literature that rely on sensor calibration. Since implementations of these algorithms are not publicly available, a direct comparison has not been carried out yet. We have exclusively tested our models on public datasets and are making the code publicly available to allow others to benchmark their accuracy.

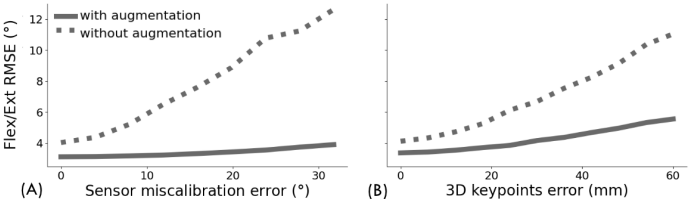

Figure 3. Effect of Data Augmentation. Knee flexion-extension angle error with and without data augmentation technique (A) across sensor miscalibration error and (B) across input keypoints quality.

Data augmentation improved the robustness of the fusion model, decreasing sensitivity to sensor misplacement (Fig. 3). In estimating the knee flexion-extension angle, fusion-net trained on data augmented for sensor-placement variability showed up to 70% higher accuracy than the baseline model. Furthermore, modeling noise in the keypoints improved model accuracy by 50%. Surprisingly, data augmentation improved model performance by over 20% even on precisely calibrated data.

Significance

Current markerless motion tracking approaches rely on accurate vision-based solutions that require multiple-camera systems and careful initial sensor-to-body calibration. The fusion model presented here is robust to noisy data, offering researchers and clinicians fast markerless motion tracking in clinics and homes.

References

[1] Mahmood et al., 2019. *ICCV*.
[2] Joo et al., 2019. *IEEE PAMI*.
[3] Trumble et al., 2017. *BMVC*.
[4] Kanko et al., 2021. *Journal of Biomechanics*.

ASSESSING TIME-VARYING LUMBAR FLEXION-EXTENSION KINEMATICS USING AUTOMATED POSE ESTIMATION

Paul N. Goncharow and Shawn M. Beaudette*
Department of Kinesiology, Faculty of Applied Health Sciences, Brock University, St. Catharines ON, CAN
email: *sbeaudette@brocku.ca

Introduction

In many cases, standardized movement tests can be done to assess individualized lumbar movement [1], including the potential association between lumbar spine motor control with the presentation and development of Low Back Pain [2]. Traditionally, lab-based methods to measure spinal movement are very expensive, time consuming, and invasive given the requirement of markers or sensors affixed to the skin.

The **purpose** of the current study was to compare concurrent planar time-varying angles of the lumbar spine (complex series of joints) and elbow (simple hinge joint) derived from DeepLabCut (DLC) [3], relative to those derived from gold-standard retroreflective kinematic systems (i.e., Vicon). It was **hypothesized** that DLC would be effective at tracking planar angles of both the lumbar spine and elbow relative to gold-standard alternatives (i.e., Vicon). Further we hypothesize that any error, potentially associated with out of plane movement, will be minimized for the elbow relative to the lumbar spine.

Methods

Fourteen participants (six males, eight females) volunteered to participate in the study. Participants were evenly partitioned into two groups (i.e., training and testing groups). To track spine and upper extremity kinematics a passive retroreflective 3D motion capture system, with time-synced 2D reference video was used (8 x Vicon Vero 2.2, 1 x Vicon Vue, Vicon Motion Systems Ltd.). Each participant completed a three maximum lumbar and elbow flexion range-of-motion (Max-fROM) tests.

Accuracy was quantified by observing the relative difference between planar elbow and spine flexion-extension data evaluated using DLC and Vicon, respectively. In contrast, precision was quantified in two ways. First, the (n = 3) standard deviation was quantified for each participant's Max-fROM trial to estimate cycle-to-cycle variability. This variability was compared between DLC and Vicon, and a larger variability was interpreted as a reduced cycle-to-cycle precision. Second, the variability in distribution of DLC-Vicon errors were inspected using Bland-Altman analysis, while accuracy was represented through any mean Bias, between-subject variability (i.e., precision) was inferred from the upper and lower levels of agreement. A statistical parametric mapping (SPM) approach was used to analyze ensemble mean and standard deviation time-varying data as a measure of DLC accuracy and precision relative to Vicon.

Results and Discussion

No notable statistically significant difference was identified between DLC and Vicon in terms of overall accuracy or cycle-to-cycle variability. Further, there were no statistically significant differences in the performance of DLC relative to Vicon when assessing the training vs. testing datasets. Bland-Altman analysis of time-varying elbow flexion-extension data the mean bias for the training dataset was observed to be -1.25°, with the upper and lower levels agreement at -0.11° and -2.40°. For the testing dataset this level of bias increased to -3.21°, with upper and lower levels of agreement at -1.23° and -5.19°. For the Bland-Altman analysis of the time-varying spine flexion-extension data the mean bias for the training dataset was observed to be -0.85°, with the upper and lower levels agreement at 0.66° and -2.35° . For the testing dataset this level of bias increased to 5.47°, with upper and lower levels of agreement at 8.10° and 2.84° (**Figure 1**).

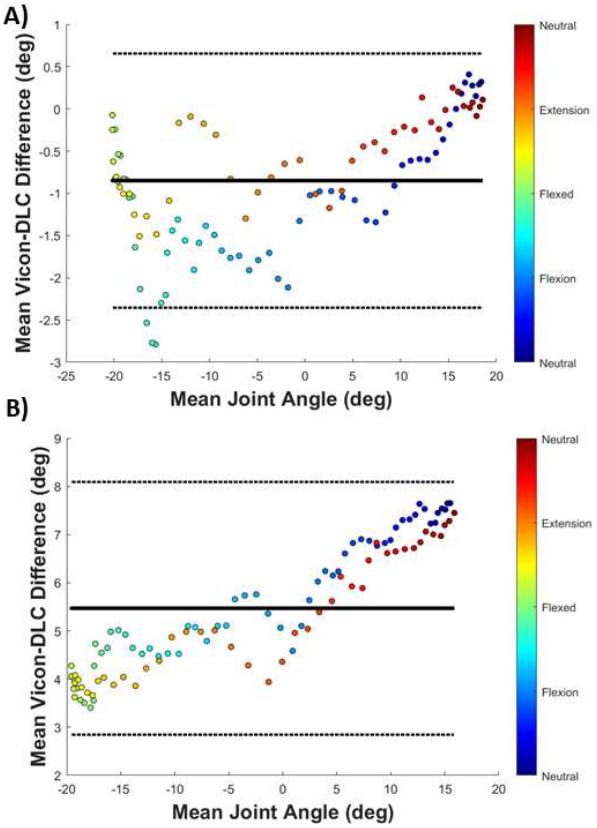

Figure 1: Bland-Altman plots depicting relative error in the estimation of lumbar flexion-extension in the training (A) and testing (B) groups.

Overall, planar angles derived using DLC are comparable to optoelectronic tracking. In general, errors are reduced for individuals included in the training dataset. Absolute elbow angle accuracy falls between 1.25 and 3.21°. Absolute lumbar angle accuracy falls between 0.85 and 5.47°.

Significance

This work suggests DLC is of acceptable accuracy when analyzing planar elbow and lumbar spine flexion in the sagittal plane. The workflow utilized here may have merit in the clinical assessment of lumbar movements when clinic visits are not permitted, extending the reach of a clinician in a telehealth environment.

Acknowledgments

SMB is supported by an NSERC Discovery Grant.

References

[1] Gatton & Pearcy, 1999. *Clin Biomech* 14(6): 623-31.
[2] O'Sullivan, 2005. *Man Ther* 10(4): 242-55.
[3] Mathis et al., 2018. *Nat Neurosci* 21(9): 1281-89.

JOINT KINETICS ASSESSMENT USING HIGH SPEED BIPLANAR VIDEORADIOGRAPHY AND MOTION CAPTURE

Gregor Kuntze[1*], Tomasz Bugajski[2], Harry Han[2], Emily Bishop[2], Ryan Baxter[2], and Janet L. Ronsky[1,2]
[1]Faculty of Kinesiology, University of Calgary, Calgary, AB, Canada
[2]Schulich School of Engineering, University of Calgary, Calgary, AB, Canada
email: gkuntze@ucalgary.ca

Introduction

Joint biomechanics form an important role in research of the mechanical contributions of osteoarthritis (OA) [1]. Motion Analysis (MA) and High Speed Biplanar Videoradiography (HSBV) technologies are utilized to quantify dynamic joint mechanics in OA. However, motion artifact of MA skin mounted markers contribute to uncertainty regarding differences between participants and the effects of interventions (e.g. bracing) [2].

The objective of this study was to implement a methodology to compare dynamic knee joint kinematics and kinetics between MA and HSBV systems. The focus of this study was on a lunge task. It was expected that differences in joint angles and moments between MA and HSBV would increase with greater knee flexion angles due to more substantial soft tissue motions.

Methods

MA (Motion Analysis, USA, 240Hz), ground reaction force (Bertec, USA, 2400Hz), and HSBV (60Hz) data for a lunge (MA+HSBV) and two static standing trials (trial 1 MA only; trial 2 MA+HSBV) were collected for one healthy male participant (age 25 years; weight 83.4kg; height 1.94m). Data were synchronized using a 5V square wave pulse. MA data were processed in Cortex (Motion Analysis). HSBV data were processed using custom software and femur and tibia bone poses were manually determined in Autoscoper (Brown University, USA) using subject-specific computed tomography (General Electric, USA) bone models (AMIRA, FEI, Germany).

Knee joint kinematics and kinetics were computed using custom code written in Matlab (MathWorks, USA). MA and HSBV global coordinate systems were first aligned to express all data with respect to the MA global coordinate system. Segment coordinate systems (foot, shank, thigh) were defined [3] using static trial 1 (MA only), where all 32 reflective markers were visible. Thigh and shank coordinate systems were then transformed to static trial 2 (MA+HSBV) where pelvis markers were not visible due to wearing a lead vest during HSBV imaging. MA joint kinematics and kinetics were computed using approaches summarized in Robertson et al. [4]. HSBV derived kinematics and kinetics were computed in the same manner as MA derived data. First, femur and tibia bone models were aligned to the X-ray images of static trial 2. Therefore, resultant HSBV static to dynamic transforms would mirror those for MA data. Further, to enable knee joint moment calculation a hybrid approach (HSBV+) was chosen, where foot segment data not available in HSBV data was supplemented using MA data.

Differences between MA and HSBV+ derived joint angles and moments were computed using HSBV+ data as a gold standard reference and expressed with respect to the median and interquartile range (Q1,Q3).

Results and Discussion

MA and HSBV derived knee joint angle time series (Figure 1) for flexion and abduction supported the presence of increased magnitudes of differences between MA and HSBV approaches with greater knee flexion angles. Interestingly, HSBV also indicated greater internal rotation at lower knee flexion angles. Across the lunge movement, MA based angles underestimated knee flexion angles [median (Q1,Q3) 2.9 (0.6,7.5)°] and knee abduction angles [7.4 (4.1,14.4)°], and overestimated external rotation angles [-10.9 (-12.8,-5.7)°].

MA based knee joint moments underestimated knee extension moments [-0.04 (-0.05,-0.02) Nmkg^{-1}], and overestimated knee abduction moments [-0.03 (-0.05,-0.00) Nmkg^{-1}]. Differences in internal rotation moments were only small [-0.00 (-0.01,0.00) Nmkg^{-1}], likely due to similar angular velocities and accelerations for low magnitude angles with similar excursion patterns (Figure 1).

MA and HSBV joint angle and moment differences of a lunge agreed with those for stair ascent and sit-to-stand [4,5]. Larger angular differences with greater knee flexion angles also agree with previous observations [4,5]. However, larger internal/ external rotation differences at low flexion angles are unique and require further investigation. Median knee joint moment differences of ~5.5% peak knee moments may be an important consideration when investigating knee joint moment reduction interventions and when evaluating compartmental knee joint force distributions using computer models.

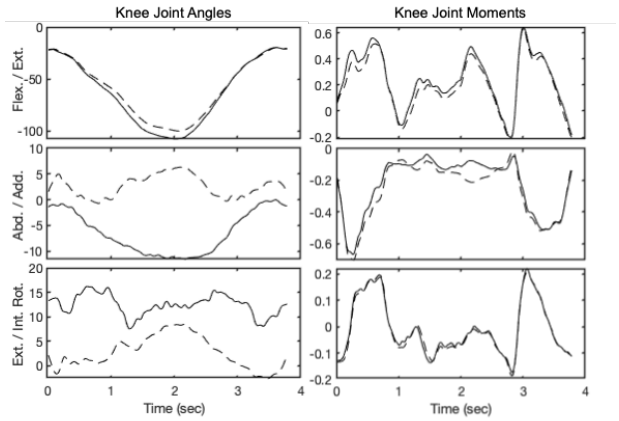

Figure 1: Knee joint angles (degrees) and moments (Nm/kg) for HSBV+ (solid) and MA (dotted) data.

Significance

These findings add to the knowledge base of methodological considerations and limitations when studying motions involving high flexion angles. Studies investigating dynamic joint function (e.g. bracing, modelling) may benefit from the use of HSBV to provide more accurate joint kinematics and kinetics estimates.

References

[1] Emery et al., 2019. *Nat. Rev. Rheumatol*. 15(7): 438-48.
[2] Smale et al.,2017. *J. Biomech*. 62: 132-9.
[3] Wu et al., 2002. *J. Biomech*. 35(4):543-8.
[4] Robertson et al., 2004. *Research Methods in Biomechanics*. 2nd edition.
[5] Tsai et al., 2011. *J. Biomech*. 44(6):1182-1188.
[6] Kuo et al., 2011. *Gait & Posture*. 33(3): 379:84

COMBINED AUDIOVISUAL AND HAPTIC BIOFEEDBACK SUPPORTS PLANTARFLEXOR RECRUITMENT IN INDIVIDUALS WITH CEREBRAL PALSY

Alyssa M Spomer*, Benjamin C Conner, Michael H Schwartz, Zachary F Lerner, and Katherine M Steele
*Department of Mechanical Engineering, University of Washington, Seattle, WA
Email: *aspomer@uw.edu

Introduction

Biofeedback is a promising non-invasive intervention to facilitate gait training in CP. Commonly, biofeedback systems are designed to provide extrinsic feedback on movement error using audio or visual cues; such systems have been broadly used in CP to improve muscle activity and joint kinematics[1]. However, more recently, haptic feedback (HF) systems, such as exoskeletons or vibrotactile arrays, have become popular as a means of providing intrinsic feedback which may be particularly important in CP where sensory processing is impaired[2]. To this end, Conner et al recently demonstrated that an ankle exoskeleton could be used to improve muscle activity and motor control in a small CP cohort[3].

While the success of these modalities highlights the potential of biofeedback for rehabilitation in CP, combining modalities may further amplify treatment effects. Prior research has demonstrated that robust error recognition drives adaptation, suggesting that biofeedback systems which present multimodal information may increase response magnitude[4]. However, the effect of combining audiovisual feedback (AVF) and HF in CP has not yet been investigated.

The aim of this study was to compare how individuals with CP modify plantarflexor activity while walking with AVF and HF, independently and in combination. The plantarflexors were targeted as they are critical for propulsion and often impaired in CP[5]. We hypothesized that combining AVF and HF would result in a larger increase in plantarflexor activity than either modality alone.

Methods

Eight individuals with diplegic CP (14.3±2.0 yrs; GMFCS I-III) walked at a self-selected speed (0.81 ± 0.10 m/s) using three feedback modalities, administered in randomized order: (1) AVF, (2) HF, and (3) AVF+HF. Each trial was separated into baseline (1 min.) and feedback (6 min.) phases.

Both feedback modalities were designed to target soleus activity on the more-affected limb. HF was administered using an untethered ankle exoskeleton that has been previously evaluated in CP[3]. This system imparts a *resistive* ankle moment during push-off proportional to the biological ankle moment. The AVF system was custom designed to display a real-time trajectory of soleus activity alongside a target score and play a tone each time the target score was reached. To balance motivation and challenge, the target score was programmatically adjusted to keep success rates between 50-75%. During AV-only feedback, participants wore the exoskeleton in zero-torque mode to reduce effects associated with device weight.

Bilateral electromyography (EMG) data were collected for the soleus for all trials (1000 Hz; Noraxon, Scottsdale, AZ). EMG data were high pass filtered (40 Hz), rectified, low pass filtered (10 Hz), and normalized to mean activity from the first baseline phase tested for each participant. Mean soleus activity for both limbs was then quantified for 30-second windows in early and late stages of the feedback phase to capture transient responses. Wilcoxon signed-rank tests with a Holm-Šídák correction for multiple comparisons were used to identify differences in soleus activity between feedback modalities ($\alpha = 0.05$).

Results and Discussion

When first exposed to each modality, participants significantly increased soleus activity in the targeted limb ($p < 0.03$). AVF + HF increased soleus activity by 40.8% [IQR: 12.4,62.6] compared with 8.9% [3.1,14.5] and 28.8% [17.6,53.7] for HF and AVF alone. Interestingly, by the end of the feedback phase, soleus activity during HF (2.1% [0.95,4.6]) had returned to baseline, while AVF (22.3% [13.7,35.3]) and AVF+HF (18.9% [8.7,37.3]) values remained elevated. Soleus activity in the non-targeted limb was minimally affected.

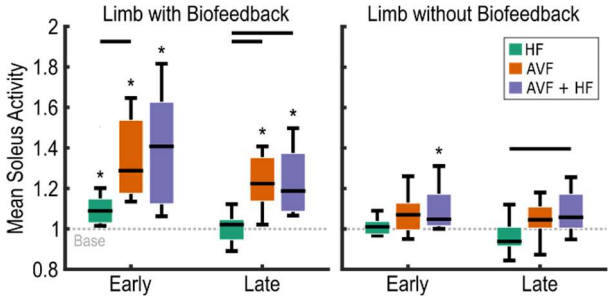

Figure 1: Mean soleus activity for both limbs during early and late stages of walking with AVF, HF, and AVF+HF compared to baseline. * denotes a significant difference from baseline walking. Horizontal bars indicate a significant different between modalities.

The significant increase in soleus activity with AVF and AVF+HF highlights the potential for these modalities to elicit desired training responses in CP. However, there was no additive advantage of combining AVF and HF after a single session and the effect of HF diminished over time. Since the purpose of the HF paradigm was to use resistance to create more challenging walking conditions these trends may indicate that further device acclimation may be necessary to promote consistent engagement across a training session. Future research will explore if response to each modality changes with additional training and what factors may underlie the inter-participant variability observed.

Significance

This study demonstrates the potential for combining AVF and HF modalities to support plantarflexor recruitment in CP. However, it also highlights the importance of characterizing the time-course response rather than simply reporting summary measures to assess intervention efficacy. Understanding how individuals adapt to different forms of biofeedback will inform future system design, ultimately improving non-invasive care options in CP.

Acknowledgments

Funding provided by NIH Award 1R15HD099664, NIH NINDS Award R01NS091056, and NSF GRFP Award DGE-1762114.

References

[1] MacIntosh A et al. *Disbil Rehabil.* **41**(20). 2019. [2] Shams L and Seitz AR. *Trends Cogn. Sci.* **12**(11). 2008. [3] Conner BC, et al. *J Biomech.* **126**(20). 2021. [4] Emken JL and Reinkensmeyer DJ. *IEEE T Neur Sys Reh.* **13**(1). 2005. [5] Brown JK, et al. *Dev Med Child Neurol.* **33**. 1991.

TREADMILL HANDRAIL USE INCREASES PARETIC SIDE MARGIN OF STABILITY IN INDIVIDUAL'S POST-STROKE

Oluwaseye P. Odanye[1], Emily A. Steffensen[1], Erica H. Hinton[1], Samuel Bierner[2], HaoYuan Hsiao[3], and Brian A. Knarr[1]
[1]University of Nebraska at Omaha, Omaha, NE, USA.
[2] University of Nebraska Medical Center, Omaha, NE, USA. [3] The University of Texas at Austin, Austin, TX, USA,
email: oodanye@unomaha.edu

Introduction

Mobility in post-stroke individuals is aided by their ability to attain mechanical gait stability while walking [1]. To ensure gait stability, healthy individuals actively control their mediolateral foot placement using the state of the stance limb, a neuromuscular strategy hard to attain post-stroke [2]. In stroke rehabilitation, assistive devices alter biomechanical outcomes that could ensure balance control [1]; for example, handrail use in treadmill walking impacts the walking mechanics by improving step symmetry and allowing increased walking speed [1][3]. Despite this evidence, there is limited information about how different handrail use conditions influence gait stability in post-stroke persons; therefore, in this study, we investigated how handrail use impacts mechanical gait stability for treadmill walking in post stroke patients. Previous studies adopted margin of stability (MOS) as a primary predictor of gait stability in healthy persons because it combines the center of mass (COM) position and velocity of an individual on a step-to-step basis[4]. Using the same MOS, we hypothesized that there will be increased margin of stability at the paretic lower limb at a self-selected handrail use condition over a no handrail use, and a light handrail use condition.

Methods

13 participants (Age: 59.31±13.16 yrs.; 8F, 5M; 1.31±0.86 yrs. since stroke) with a history of more than 6 months of stroke, and from an ongoing study, were included in this investigation. Participants were recruited if they were 19-80 years old, have had a single stroke, had no other surgical or medical conditions limiting their function, and could ambulate with or without a walking aid. A 16-camera motion capture system, with a 65-marker full body setup was used in collecting data, while the participants walked over a split-belt instrumented treadmill with handrails instrumented with force sensors. The participants were instructed to walk at their comfortable walking speed for 3 minutes under 3 conditions; no handrail use (NHR), light handrail use (LHR) and self-selected handrail use (SSHR), but 5 participants who could not walk without using the handrails were exempt from the NHR condition. Participants held the handrail with their non-paretic hand. For the LHR condition, we displayed real time feedback of the handrail support for the participants, and they were notified if the weight on the handrail was more than 5% of their body weight. MOS (calculated at initial contact as the minimum distance between the extrapolated center of mass in relation to the base of support which was quantified as the combined center of pressure while walking)[4], Step width (SW), and lateral foot placement (LFPL: calculated as the mediolateral distance between the center of mass and lateral malleolus at initial contact) were calculated from the collected data.

Results/Discussion

Overall, the participant's mean vertical SSHR force (36.38N) was more than the LHR force (19.72N). A mixed model analysis of the gait data showed significant main effect of handrail use on paretic mediolateral (ml) MOS ($F=4.685$, $P=0.02$) and non-paretic ml MOS ($F=3.713$ $p=0.042$). Pairwise comparisons of the handrail conditions showed a significant difference (Figure1) only between the LHR and SSHR conditions for the paretic ml MOS ($p=0.027$). There was no significant main effect for the handrail condition on the paretic anteroposterior MOS, and other pairwise comparisons were non-significant ($p > 0.05$). These findings indicated a possible increase in mechanical gait stability towards the SSHR use condition, seeing we also observed increased mean ml MOS for the paretic leg in the SSHR condition compared with the other two (Figure 1), and an observed main effect of handrail use on non-paretic LFPL ($F=14.510$, $p < 0.05$), such that its mean was lowest at the SSHR use condition. There was a main effect of handrail use on the SW of the paretic ($F=8.934$, $p=0.002$) and non-paretic ($F=9.108$, $p=0.001$) legs, specifically the mean paretic and non-paretic SW were least at the SSHR use condition. We speculated a sway to the non-paretic side as the participants leaned to the handrail support on the same side, moving the non-paretic leg closer to the body's center of mass, indicating an adaptive reliance on the handrail to add to their base of support, thereby allowing better gait stability. Future work will enable us to investigate how the activation of muscles in the paretic leg changes with handrail use, and if a shift in the center of mass toward the non-paretic limb decreases paretic limb loading as these could further impact rehabilitation of stroke patients.

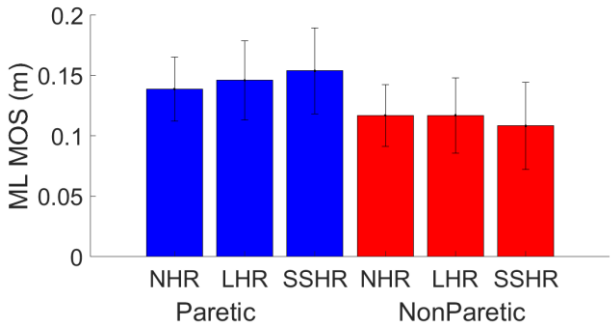

Figure1: Paretic and nonparetic mean mediolateral margin of stability.

Significance

The preliminary result in this research informs handrail use in treadmill rehabilitation of post stroke persons; it suggests that mechanical gait stability of the paretic limb is greater with increased handrail support, as a means to preventing falls and increasing walking speed in post-stroke individuals [1]. Future work is necessary to determine if this phenomenon is transferred from a treadmill setting to over ground walking.

Acknowledgment

This research is funded by the NIH (R15HD094194).

References

[1] T. Ijmker et al., *J. Neuroeng. Rehabil.*, vol. 12, no. 1, 2015,
[2] J. C. Dean et al., *J. Rehabil.* Res. Dev., vol. 52, 2015,
[3] H. Y. Hsiao et al., *J. Biomech.*, vol. 60, Jul. 2017,
[4] A. L. Hof et al., *J. Biomech.*, vol. 38, Jan. 2005,

FRONTAL-PLANE DEVIATIONS AND SPATIOTEMPORAL ASYMMETRY ARE ENERGY-OPTIMAL IN SIMULATED HEMIPARETIC GAIT

Russell T. Johnson and James M. Finley
Division of Biokinesiology and Physical Therapy, University of Southern California
email: rtjohnso@usc.edu

Introduction

As a result of neuromuscular impairments (e.g., hemiparesis), people post-stroke typically walk slower, display asymmetrical step lengths and step times, and have other kinematic deviations like hip hiking and hip circumduction [e.g., 1]. Our previous work using sagittal-plane musculoskeletal models with predictive simulation has suggested that spatiotemporal asymmetry may be an optimal gait pattern for individuals with hemiparesis [2], however sagittal-plane models are unable to make predictions on out-of-plane gait deviations, and it's unclear if the pattern of spatiotemporal asymmetries we found would hold for 3-D gait.

Therefore, our aim was to quantify the optimal step length and step time asymmetry, as well as the magnitude of hip hiking and hip circumduction, that emerge for 3-D musculoskeletal models with simulated hemiparesis via predictive simulation. Overall, this study will allow us to better understand the relationship between muscle weakness and gait performance, independent of other impairments that occur post-stroke.

Methods

We used a 3-D musculoskeletal model with 23 mechanical degrees-of-freedom and actuated by 84 muscle-tendon units and three coordinate actuators around the lumbar joint. We then created three hemiparetic models by uniformly reducing the peak isometric muscle force in all left-limb muscles by 20, 40, and 60 percent. We used OpenSim Moco to generate optimal control simulations of walking at 1.00 m/s with a weighted objective function to minimize the following two terms: 1) sum of the integrated muscle excitations cubed and 2) metabolic cost of transport (COT) [3]. The metabolic energy model was a smoothed version of the Bhargava 2004 metabolic energy model that is well suited for optimal control problems [4]. We held the muscle mass constant throughout the models, representing a loss of strength without a loss of muscle mass as would be present in the acute phase post-stroke.

Outcome measures included step length and step time asymmetry indices (Eq. 1).

$$Asym = \frac{X_{NP} - X_P}{X_{NP} + X_P} \times 100\% \quad (1)$$

Here, X_{NP} is the variable for the non-paretic limb, and X_P is the variable for the paretic side. Positive values of Asym indicate greater values on the non-paretic than the paretic limb. We also computed the hip hiking and hip circumduction magnitudes for each of the conditions based on the maximum value of pelvis list angle and hip abduction angle during paretic swing [5].

Results and Discussion

The symmetrical model walked with approximately equal step times and step lengths, while the hemiparetic conditions resulted in negative step time and step length asymmetries with greater values for each variable on the paretic versus nonparetic side (Table 1). The optimal gait in all conditions resulted in hip hiking, but the hemiparetic conditions resulted in an exaggerated the level of hip hiking (~5° greater) compared with the symmetrical condition. The hip adduction angle increased with hemiparesis compared with the symmetrical condition (9° greater), which is opposite what we expected to observe. However, this could be due to an interaction with the hip hiking pattern, where the hip hiking is sufficient to be able to clear the foot during swing phase. Finally, both measures of physiological effort within our objective function increased with hemiparesis. The integrated sum of the muscle excitations cubed increased by 146% and the metabolic COT increased by 7% in the 60% weak condition compared with the symmetrical condition.

Significance

Our results are consistent with previous work [2] by providing additional evidence that step length and step time asymmetries could be energy-optimal for people with hemiparesis. Further, results in the current study demonstrate that hip hiking may be an energy-optimal strategy for clearing the paretic limb during swing, but hip circumduction is not supported by our results as an optimal strategy. Therefore, clinical goals to restore symmetry and reduce hip hiking deviations may not be energetically optimal if the patient has lingering strength asymmetry.

Acknowledgments

Funding: NIH NCMRR R01HD091184

References

1. Finley JM & Bastian AJ, Neurorehab Neural Re. 31, 2. 2017.
2. Johnson RT et al., bioRxiv 2021.12.20.473515
3. Dembia CL et al., PLoS Comput. Biol. 16, 12. 2021.
4. Bhargava LJ et al., J Biomech. 37, 1. 2004
5. Kerrigan DC et al., Am J Phys Med Rehabil. 79, 3. 2000

Table 1: Outcome variables for each condition. Step time and step length asymmetries computed with Eq. 1. Kinematic deviations of hip hiking and hip circumduction during paretic side swing phase (positive values indicate hip adduction). The non-weighted sum of the integrated muscle excitations cubed and metabolic cost of transport (COT).

Model	Step Length	Step Time	Hip Hiking	Hip Circumduction	Muscle Excitations	Metabolic COT
Symmetrical	-0.3 %	2.0 %	8°	3°	0.016	3.35 W/kg/m
20% Weak	-12.7 %	-2.0 %	13°	10°	0.018	3.38 W/kg/m
40% Weak	-18.1 %	-6.0 %	12°	7°	0.026	3.44 W/kg/m
60% Weak	-14.8 %	-8.0 %	14°	12°	0.039	3.60 W/kg/m

LIMB-SPECIFIC POSTURAL INSTABILITY DURING QUIET STANCE AND ITS RELATION WITH WEIGHT DISTRIBUTION IN CHILDREN WITH CEREBRAL PALSY

Sydni V.W. Whitten[1], Katelyn S. Campbell[1], Karl M. Newell[1], Li Li[2], Gavin Colquitt[2], and Christopher M. Modlesky[1*]
[1]University of Georgia, Athens, GA [2]Georgia Southern University, Statesboro, GA
email: christopher.modlesky@uga.edu

Introduction

Cerebral palsy (CP) is a neurological disorder characterized by deficits in postural control.[1] Postural control is often assessed by measuring the center of pressure (COP) during quiet stance on a single force platform. A drawback of using a single platform is that the contribution of individual limbs to COP measures and weight distribution is not evaluated. For pathologies that exhibit asymmetrical deficits, like CP, assessing limbs separately may be beneficial to understanding the system as a whole and overall postural stability. However, studies examining postural control in children with CP using dual force platforms are scarce.

The primary purpose of this study was to determine if the postural control deficits in children with CP exhibited during quiet stance are present in the more (MAL) or less (LAL) affected limbs. The secondary purpose was to determine if the weight distribution during quiet stance is related to postural control deficits in children with CP. It was hypothesized that children with CP would have poorer postural control, exhibited by greater COP variability magnitude (sway distance↑ and velocity↑) and structure (entropy↓), than their typically developing peers (Con). A greater asymmetry in weight distribution during quiet stance would be associated with significant postural deficits.

Methods

Twenty-eight children with CP and 23 Con (5 – 11 y) were recruited for this study. Two force platforms (Bertec, Columbus, OH, 100 Hz) arranged in parallel were used to assess COP from the MAL and LAL during quiet stance. Each limb was placed comfortably and shoulder-width apart on individual platforms. COPnet was calculated by combining data from the 2 platforms.[2]

Participants completed 3 30s-trials of quiet stance. The COP data of the last 25s were filtered using a 5Hz 4th order Butterworth low pass filter. Sample entropy, sway distance, and sway velocity were calculated for both anteroposterior (AP) and mediolateral (ML) directions. Weight distribution on the MAL was presented as a percentage of the total vertical ground reaction force. Outcome variables were presented as the average of the 3 trials.

Group differences were evaluated using an independent-sample t-test if the data were normally distributed and a Mann-Whitney U test if the data were non-normally distributed. Spearman rho correlations were used to assess the relationship between percent weight distribution and COP measures.

Results and Discussion

The summary of the outcome variables is presented in Figure 1. Children with CP exhibited lower sample entropy and higher sway distance for COPnet and the LAL in the AP and ML directions (p<0.05). Children with CP also exhibited lower sample entropy and higher sway distance for the MAL, but only in the ML direction (p<0.05). Children with CP exhibited higher sway velocity for COPnet in the AP and ML directions (p<0.05). Children with CP also exhibited higher sway velocity for the LAL in the AP direction (p<0.05; Fig 1). However, there was no group difference in sway velocity in the MAL in either direction (p>0.05). Greater sway distance and velocity measures observed in children with CP indicate that they had a reduced ability to maintain balance and stability. The observation that, on the MAL, lower sample entropy and higher sway distance were only present in the ML direction, and sway velocity of the MAL was not significantly different between groups suggests that the postural deficit is more pronounced on the LAL.

Percent of weight distribution on the MAL was positively

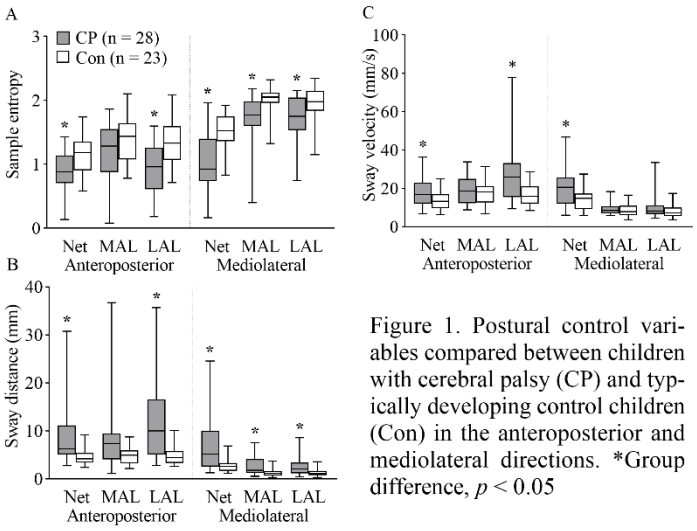

Figure 1. Postural control variables compared between children with cerebral palsy (CP) and typically developing control children (Con) in the anteroposterior and mediolateral directions. *Group difference, $p < 0.05$

related to sway distance (r_s=0.378-0.392; p<0.05) and velocity (r_s=0.370-0.555; p<0.053) in the AP and ML directions on the LAL, which suggests that greater weight distribution on the MAL is specifically associated with poorer postural control in the LAL. The greater number of group differences in COP variables on the LAL, especially with greater weight distribution on the MAL, may demonstrate a compensatory method of the LAL to alleviate muscle activity of the MAL.[3]

Significance

In addition to demonstrating a more structured and greater magnitude of the COP variability, using a dual-force platform enabled us to identify postural control deficits during quiet stance that were more pronounced on the LAL of children with CP, especially when there is greater weight on the MAL. The observed asymmetrical differences in limbs suggest a dual force platform paradigm is necessary to better understand the posture in populations that exhibit asymmetry. It is also needed to identify limb-specific intervention strategies that improve postural control in children with CP.

Acknowledgments

Funded by the National Institutes of Health (HD090126).

References

[1] Pavão et al., 2013. *Research Devel. Disabl.*
[2] Winter et al., 1993. *Neurosci Research Comm.*
[3] Fredjallah et al., 2002. *Clin Biomech*.

RELATIVE FOOT POSITION VISUAL FEEDBACK DURING WALKING IN PEDIATRIC CEREBRAL PALSY

Erik T. Hummer[1,2*], Melvin Mejia[1], Xuan Liu[1,2], and Peter J. Barrance[1,2]
[1]Center for Mobility and Rehabilitation Engineering Research, Kessler Foundation, West Orange, NJ, USA
[2]Children's Specialized Hospital Research Center, New Brunswick, NJ, USA
email: *Ehummer@KesslerFoundation.org

Introduction

Children with cerebral palsy (CP) often exhibit gait deviations, including limited knee extension at initial contact (IC), that are associated with reduced walking speed and asymmetric gait. Our previous research has reported promising potential for children to decrease knee flexion at IC in response to visual feedback on knee joint gait pattern deviations derived from inertial measurement units (IMUs) [1]. However, there is a continuing need to design feedback cues that are easy to interpret in young clinical populations. In this study we provided a different and potentially more easily interpreted cue that has the same clinical goal; i.e. to reduce knee flexion at initial contact and early stance. It was previously reported that higher maximal anterior foot position (AFP) relative to the pelvis is associated with longer steps and reduced knee flexion [2]; hence, our feedback rewards higher peak AFP during gait. The purpose of this study was to examine short term gait pattern adaptation in response to such feedback in a child with increased knee flexion at IC. We observed response to two variations of the feedback and gauged user experience through a questionnaire.

Methods

Results are presented from a single male participant (age = 11.9 yrs, right hemiplegic CP) and a habitual gait pattern with increased IC and early stance knee flexion. All activities were performed under informed consent per the institutional review board policies. In all testing the participant walked on a treadmill at a self-selected speed (0.6 m/s) with synchronized collection of lower extremity kinematics from four IMUs (60 Hz, Xsens, NL) and 3-dimensional motion capture (120 Hz, OptiTrack, Corvallis, OR, USA). The participant first walked for one minute without any visual feedback to measure baseline gait kinematics. Following this, the participant then walked for six minutes with visual feedback followed by 3 minutes of rest, repeated three times (4 bouts).

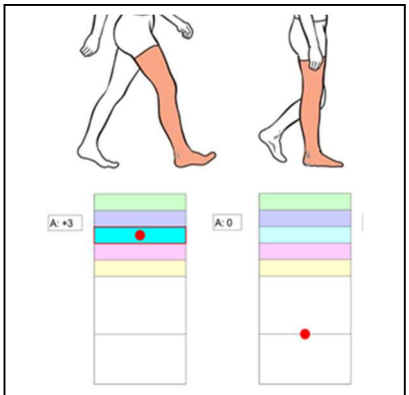

Figure 1: Representation of the feedback display, in which the red dot updates in real-time to the position of the paretic foot in relation to the pelvis.

During feedback bouts, a kinematic model utilizing 3D IMU orientations and segmental lengths for the paretic thigh and shank calculated relative foot position (X_{foot}). A red dot within the feedback display (Fig. 1), was updated in real-time to reflect X_{foot}. The feedback display incorporated five scoring zones and awarded points in ascending order from 1 point to 5 points. Points were awarded and displayed for the peak X_{foot} (AFP) for each step of the paretic limb. Bouts 2 and 3 also displayed a cumulative score during the trial. The intent of the feedback design was to reward and encourage steps with higher peak AFP, which we expected to be linked to lower knee flexion at IC.

Results and Discussion

Kinematic data from the 3D motion capture system is reported. Compared to baseline walking (37.0° ± 1.4°, mean and SD across steps), each of the four feedback bouts (33.9° ± 3.2°, 36.0° ± 4.4°, 32.8° ± 2.3°, and 33.8° ± 3.0°, respectively) displayed more knee extension at IC. In addition, the participant exhibited greater amounts of knee extension during the load-response phase (2-12% GC) within feedback bouts (Fig 2). The participant provided survey feedback that the interface was "easy" to understand and that it was "very fun" trying to change their walking. Hence, the data from this participant demonstrated adaptation of knee flexion kinematics as was intended in the design and formulation of this visual feedback display; i.e. improvements in knee kinematics were seen at IC and through stance phase. We did not observe clear differences in response dependent on whether cumulative score was displayed to the participant.

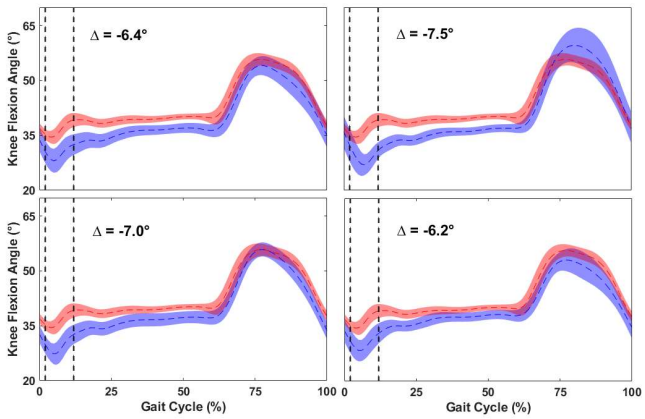

Figure 2. Ensemble curves across multiple steps for feedback bouts 1 (top left), 2 (top right), 3 (bottom left), and 4 (bottom right) comparing knee kinematics for baseline (red) and feedback (blue) with load-response designated by vertical dotted lines

Significance

Results from this study support the use of an easy to interpret cue relating to relative foot position. Designs such as this can be beneficial in gait training paradigms increasing user involvement and enthusiasm. Upon further testing with a larger sample, feedback systems such as this one may prove to be feasible in clinical settings in the treatment of paediatric CP by enhancing physical therapy mediated gait training.

Acknowledgments

Funding for this study was provided by Children's Specialized Hospital and Kessler Foundation.

References

[1] Liu et al., 2021. *J Rehabil Assit Technol Eng*. 8: 1-6.
[2] Balasubramanian et al., 2010. *Clin Biomech*. 25(5): 483-90.

THREE-DIMENSIONAL GAIT PATTERN IN CHILDREN: COMPARING TYPICALLY DEVELOPING AND HYPERMOBILE EHLERS-DANLOS SYNDROME

Anahita A. Qashqai[1*], Hyo Jung Jeong[1,2], Samantha R. Schwartz[1], Michael Muriello[3], Donald G. Basel[3], and Brooke A. Slavens[1]
[1] University of Wisconsin-Milwaukee, Milwaukee, WI, USA
[2] Orthopaedic and Rehabilitation Engineering Center, Marquette University, WI, USA
[3] Medical College of Wisconsin, Milwaukee, WI, USA
email: *anahita@uwm.edu

Introduction

Hypermobile Ehlers-Danlos syndrome (hEDS) is a rare genetic disorder affecting connective tissues that causes joint laxity, excessive joint range of motion, joint pain, fatigue, and joint instability during walking [1]. While there has been a lack of gait analysis in children with hEDS, three-dimensional (3D) gait has been investigated in adults with hypermobility [2]. However, the results of these studies have not been consistent and have not led to a collective understanding of walking patterns in hEDS [3]. The purpose of this study was to compare 3D lower-extremity joint kinematics, moments, and powers during walking in children with hEDS against typically developing children.

Methods

Ten children with hEDS (3 males, 7 females, age: 12.2 ± 2.8 years) and 10 age-matched typically developing children (3 males, 7 females, age: 13.2 ± 2.8 years) participated. We used a 15-camera Vicon T-Series motion capture system synchronized with four AMTI force plates to record marker trajectories and ground reaction forces. Five gait cycles performed at a self-selected speed were analyzed. The standard Vicon Plug-in Gait lower extremity inverse dynamics model was applied to compute joint dynamics [4]. To statistically analyze the entire gait cycle, statistical non-parametric mapping (SnPM) t-test [5] was used and compared 3-dimensional kinematics, moments, and powers during walking between two groups (p < 0.05). The spatiotemporal parameters were compared using Mann-Whitney U test.

Results and Discussion

Gait speed and cadence were not significantly different between the groups (p = 0.245, p = 0.160, respectively). Kinematics, moments, and powers were not statistically significant between hEDS and typically developing children, except for the ankle transverse plane. The average movement trajectory of ankle transverse plane in children with hEDS was shifted towards ankle adduction compared to typically developing children (Fig. 1a). The critical *t-statistics* = 2.300 was exceeded at time 59% (toe-off) with probability value of p=0.014, indicating hEDS had significantly greater ankle adduction in transverse plane during toe-off and early swing than the typically developing children (Fig. 1b). Our observations suggest potential differences in ankle biomechanics during walking that may be related to ankle joint instability reported in the hEDS population.

Significance

Despite significant differences in the ankle transverse plane, the gait dynamics in children with hEDS and typically developing children appeared to be similar. Understanding gait patterns in children with hEDS may identify contributors to joint instability during functional activities. Our findings could ultimately help prevent lower extremity injuries and lead to better treatment planning. This study could fill the gap in the literature for understanding the gait pattern of hEDS in pediatrics. Further research is underway with a larger population to determine a comprehensive gait analysis in children with hEDS.

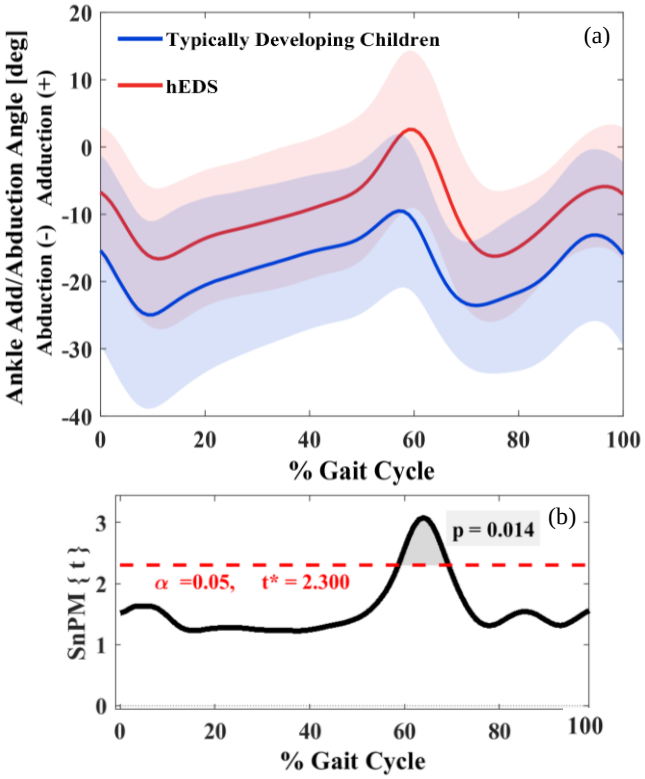

Figure 1: (a) Mean trajectories for ankle abduction/adduction angles during walking in hEDS (red) and typically developing children (blue). (b) one-dimensional statistical non-parametric mapping (SnPM) {t}: The black line depicts the test statistic continuum, and the red dashed line shows the critical threshold at α = 0.05. The critical threshold of critical *t-statistics* (t^*) = 2.300 was exceeded at time 59% (toe-off) with a probability value of p = 0.014.

Acknowledgments

We would like to acknowledge UWM college of Health Sciences for sponsoring this research through SPARC grant, Children's Hospital of Wisconsin Genetics Centre, and the Administration for Community Living, U.S. Department of Health and Human Services (90ARHF0006).

References

1. Castori, M. (2010). Am J Hum Genet, A, 152(3).
2. Galli, M. (2011). Dev Disabil Res Rev, 32(5), 1663-1668.
3. Bates, A. (2015). Gait & posture, 41(2), 361-369.
4. Kadaba, M. (1990). J Orthop Res, 8(3), 383-392.
5. Pataky, T. (2010). J. Biomech, 43(10), 1976-1982

IS CROUCH GAIT ADVANTAGEOUS IN THE PRESENCE OF PLANTARFLEXOR CONTRACTURE?

Elijah C. Kuska[1], Naser Mehrabi[1], Michael H. Schwarts[2], and Katherine M. Steele[1]
[1]Department of Mechanical Engineering, University of Washington, Seattle, WA, USA
[2]Center for Gait & Motion Analysis, Gillette Children's Specialty Healthcare, St. Paul, MN
email: kuskae1@uw.edu

Introduction

Cerebral Palsy (CP) is the result of a neurologic injury that alters motor control and often leads to secondary musculoskeletal impairments like weakness and contracture. These impairments restrict function and may alter gait. Typically, altered gait patterns in CP are considered disadvantageous and are the target of clinical interventions [1]. However, intervention outcomes remain variable and the cause of altered gait patterns in CP remains unclear. One theory is that specific gait patterns could be energetically advantageous given an individual's unique musculoskeletal morphology [2].

Computational models enable rapid investigation of causal mechanisms underlying altered gait. Previous modelling studies investigated altered gait that arose from musculoskeletal impairments [3,4] and how sensitive nondisabled (ND) gait is to these impairments [5]. Similar analyses could highlight potential advantages of altered gait patterns in the presence of impairments. In this research, we simulated ND gait and several common gait patterns in children with CP while iteratively increasing contracture. We hypothesized that crouch gait would be less sensitive to contracture. If supported, this would suggest that altered gait in CP could be an advantageous adaptation in the presence of impairments.

Methods

A dynamic sagittal plane musculoskeletal model comprised of seven rigid body segments (torso and bilateral thigh, shank, and foot) and 9 degrees-of-freedom was used for simulating gait. Each limb was actuated by eight Hill-type musculotendinous units. A direct collocation optimal control framework generated tracking simulations while minimizing kinematic tracking error and fatigue [6]. Simulations tracked either ND gait, or one of three crouch gait patterns seen in children with CP: mild, moderate, and severe crouch [7].

We simulated contracture in the soleus (SOL), gastrocnemius (GAS), and both plantarflexors (PFlex) by decreasing the tendon slack length of the affected muscle(s) [3,4]. Tendon slack length was iteratively decreased until the optimization no longer identified a feasible set of muscle activations to replicate each gait pattern.

Results and Discussion

Crouch gait tolerated different amounts of plantarflexor contracture compared to ND gait (**Figure 1)**. In particular, all crouch gait patterns were less sensitive to GAS contracture than ND gait (*i.e.,* the GAS tendon could be shortened more when tracking crouch as opposed to ND gait) and the contracture threshold increased with crouch severity. For the SOL, mild crouch had the greatest contracture threshold.

With contracture in both plantarflexors, ND gait had the highest contracture threshold. As crouch severity increased, PFlex contracture threshold decreased, indicating that more severe crouch deviations were more sensitive to PFlex contracture.

In CP, contracture of the GAS is more common and often more severe than contracture of the SOL. Most surgical procedures that address plantarflexor contracture in CP only target the GAS. Decreasing sensitivity to GAS contracture with increasing crouch severity may suggest this gait pattern is an advantageous adaptation. Considering our objective function, findings may indicate that crouch gait reduces fatigue caused by GAS contracture.

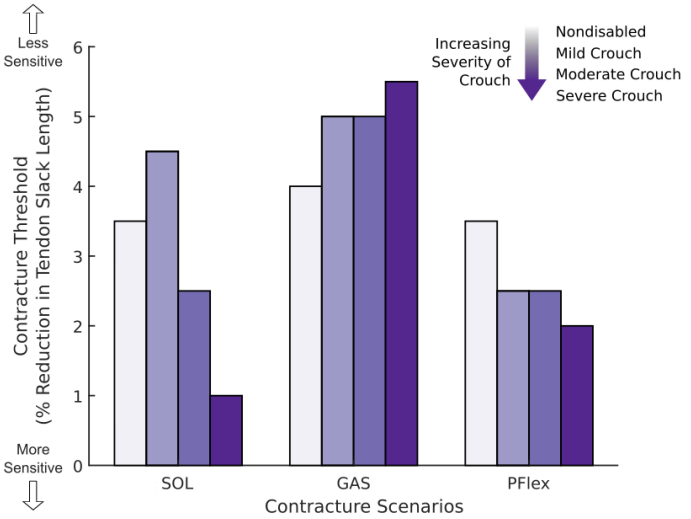

Figure 1: Contracture thresholds in soleus (SOL), gastrocnemius (GAS), and both (PFlex) for non-disabled (ND) gait and three crouch patterns of increasing severity.

Significance

This study demonstrates that altered gait patterns, like crouch, may decrease sensitivity to musculoskeletal impairments like contracture. Thus, altered gait patterns, commonly thought to be disadvantageous and targeted by clinical interventions, may be advantageous because they decrease sensitivity to impairments. Future investigations should consider additional gait abnormalities and neuromusculoskeletal impairments. Understanding advantageous adaptations in the presence of impairments can support the design of personalized treatments and improve treatment efficacy.

Acknowledgments

This work was supported by NIH Award R01NS091056.

References

[1] H. K. Graham, et al. *Nat Rev Dis Prim* 2. 2015.
[2] A. Falisse, et al. *Front Hum Neurosci* 14. 2020.
[3] C.F. Ong, et al. *PLoS Comput Biol.* 15(10) 2019.
[4] A.S. Fox, et al. *G & P.* 61. 2018.
[5] M.M. van der Krogt, et al. *G & P*. 36. 2012.
[6] N. Mehrabi, et al. *J Biomech* 90(84). 2019.
[7] A. Rozumalski and M.K. Schwartz, *G & P*. 30. 2009

Femoral and acetabular features explain acetabular contact pressure sensitivity to hip internal rotation in persons with cam morphology: A finite element analysis

Jordan Cannon[1], Jeffery W. Rankin, Kristi L. Lewton, Christopher M. Powers[1]
[1]Division of Biokinesiology and Physical Therapy, University of Southern California, Los Angeles, CA
email: cannonjo@usc.edu

Introduction

Femoroacetabular impingement syndrome (FAIS) is a clinical condition characterized by premature contact between the proximal femur and acetabulum [1]. The loss of femoral head-neck concavity associated with cam morphology leads to mechanical impingement during tasks involving hip flexion, internal rotation, and adduction [1]. Internal rotation with high degrees of hip flexion appears to be most problematic. This motion induces higher contact pressures on the anterior-superior acetabulum that increase the risk of chondrolabral damage associated with FAIS and future hip osteoarthritis [1-3]. While the magnitude of cam morphology has been reported to contribute to greater acetabular contact pressure [3], previous work suggests that elevated acetabular contract pressure when the hip is flexed and internally rotated may also be dependent on a number of morphological characteristics [1]. However, a comprehensive assessment of the primary contributors to mechanical impingement in persons with cam morphology has not been undertaken. The purpose of the current study was to determine which other bony characteristics contribute to acetabular contact pressure sensitivity to internal rotation in persons with a cam morphology.

Methods

Twenty participants (10 female, 10 male) with a documented cam morphology underwent CT scans of the pelvis and proximal femur to reconstruct 3D models. Morphological measurements of the acetabulum (anteversion angle, inclination angle, depth, and lateral center-edge angle (LCEA)) and femur (alpha angle and femoral neck-shaft angle (FNSA)) were obtained from the models. Finite element analysis (FEA) was used to estimate contact pressures. The femur and pelvis were modelled using homogeneous, isotropic, triangular shell elements with an elastic modulus of 17.0 GPa and a Poisson ratio of 0.30. FEA was performed in Abaqus using a hard contact algorithm and a surface coefficient of friction of 0.02. A resultant force of 1102 N derived from the OrthoLoad HIP98 database and scaled to the mean mass of our participants (72 kg) was applied at the center of the femoral head. Quasi-static loading simulations were performed at 3° increments of internal rotation (from 0-15°) with the hip flexed to 90°.

Participants' sensitivity to hip internal rotation was quantified as the slope of the linear least-squares regression fit between peak acetabular contact pressure and hip internal rotation. A stepwise regression was used to determine morphological predictors of sensitivity to internal rotation. The predictors were then included in a bootstrapped multiple linear regression analysis using 1000 iterations, resampling with replacement.

Results and Discussion

A range of sensitivity to internal rotation was observed across participants (Fig.1). Acetabular anteversion (r = -0.56, p=0.01), acetabular inclination (r = -0.50, p=0.02), and FNSA (r = -0.60, p = 0.005) were negatively correlated with sensitivity. LCEA was positively correlated with sensitivity (r = 0.56, p=0.01). Alpha angle (r = -0.25, p=0.28) and acetabular depth (r = -0.22, p=0.36) were not significantly associated with sensitivity. The stepwise regression model is shown in (Table 1). The bootstrap analysis revealed that a median value of 65% [37%, 89%] variance in sensitivity could be explained by the morphological variables selected by the stepwise regression.

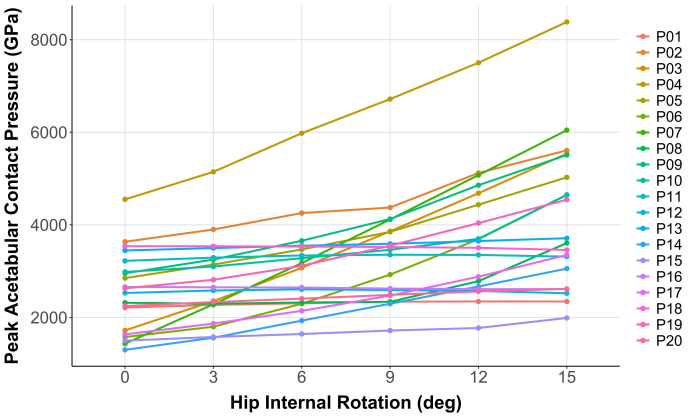

Figure 1: Peak acetabular contact pressure in each hip internal rotation posture with the hip flexed to 90^0 for each participant.

Table 1: Stepwise regression model. * Significant (p<0.05)

	Pressure sensitivity to internal rotation
Femoral Neck-Shaft Angle	-16.12* (-27.07, -5.16)
Acetabular Anteversion	-7.35* (-13.13, -1.58)
Acetabular Inclination	-4.82 (-9.80, 0.15)
Acetabular Depth	4.35 (-2.34, 11.04)
Constant	2,531.92* (1,145.71, 3,918.14)
Adjusted R^2	0.55
Residual Std. Error	65.03 (df = 15)
F Statistic	6.87* (df = 4; 15)

Lower FNSA, acetabular anteversion, acetabular inclination, and a deeper acetabulum were able to explain 65% of the variance in acetabular contact pressure sensitivity to hip internal rotation. This suggests that mechanical impingement and the concomitant acetabular contact pressure is modulated by multiple femoral and acetabular features in persons with a cam morphology.

Significance

Acetabular contact pressure sensitivity to hip internal rotation in persons with cam morphology is influenced by hip joint structure beyond that of the degree of cam morphology. Consideration of multiple measures of hip morphology may help identify persons with cam morphology most at risk of developing symptomatic FAI and future hip osteoarthritis.

Acknowledgments

International Society of Biomechanics Matching Dissertation Grant and USC Division of Biokinesiology & Physical Therapy.

References

[1] Ganz et al., 2003. *Clin. Orth. Rel. Res.*, 417.
[2] Jorge et al., 2014. *Comput. Methods Biomech. Biomed. Eng.,* 17(11).
[3] Bagwell & Powers, 2017. *Arthroscopy*, 33(10).

EFFECT OF HIP PRESERVATION SURGERY ON LEVEL AND SLOPED WALKING BIOMECHANICS

Brandon Nunley[1], Avneesh Chhabra[2], Ajay Kohli[2], Edward P. Mulligan[2], Emily F. Middleton[2], Joel E. Wells[2], & Nicholas P. Fey[3]
[1]University of Texas at Dallas, Department of Bioengineering
[2]University of Texas Southwestern, [3]University of Texas at Austin
email: Brandon.Nunley@UTDallas.edu

Introduction

Developmental dysplasia of the hip (DDH) and femoroacetabular impingement syndrome (FAI) are major causes of pain and dysfunction in young adults. Although DDH and FAI have different underlying morphology, walking difficulties are common to both. In DDH patients, hip joint instability leads to reduced hip flexion and extension moments during walking [1]. FAI patients may walk with reduced hip range of motion (ROM), especially during sloped walking. Limitations in hip ROM may be due to painful impingement or soft tissue restriction [2].

To improve symptoms, these patients increasingly opt for hip preservation surgery. A comprehensive gait analysis using varied walking conditions and advanced methods of analysis is needed to determine the extent of gait alterations brought on by these surgeries. The purpose of this study was to evaluate the effect of hip preservation surgery on lower limb joint biomechanics during level and sloped walking. We hypothesized that hip joint moments would increase post-operatively in DDH patient, and that hip flexion and extension angles would increase post-operatively in FAI patients for non-level walking conditions.

Methods

Ten patients (5 DDH, 5 FAI) who underwent preservative surgical treatment at UT Southwestern for their respective hip disease completed this study. The study was approved by the Institutional Review Board, and informed consent was provided.

Gait data were collected pre- and post-operatively with a minimum 1-year follow up. Patients performed a 1-minute walking trial at a self-selected speed for three conditions, which were incline (+10º), level (0º), and decline (-10º) walking. During the post-operative session, pre-operative speeds were matched. Forty-six passive reflective markers were used to estimate joint centers and track segmental motion. Kinetic and kinematic data were collected synchronously using a force-instrumented Bertec treadmill (1000 Hz) and 10-camera Vicon motion capture system (100 Hz). An 8-segment model was built in Visual3D. Variables of interest were hip, knee, and ankle sagittal plane joint angles, BW-normalized joint moments, and GRFs. Pre- and post-operative variables were compared using statistical parametric mapping with paired-samples t-tests (α=0.05) [3].

Results and Discussion

In post-operative DDH patients, few changes in joint angles were observed for the three walking conditions. However, alterations in joint moments were extensive during decline walking. Hip, knee, and ankle flexion and plantarflexion moments increased, supporting our first hypothesis. Due to high joint loading during the weight acceptance phase, decline walking was most impaired in the pre-operative DDH group and showed the largest improvement following preservation surgery.

Our second hypothesis, that hip flexion and extension angles would increase post-operatively in FAI patients, was only partially supported. Hip flexion angle was reduced during decline walking, and ankle dorsiflexion angle was increased across the gait cycle in all walking conditions. Hip extension moment was increased during incline walking, while hip and knee flexion moments increased during decline walking.

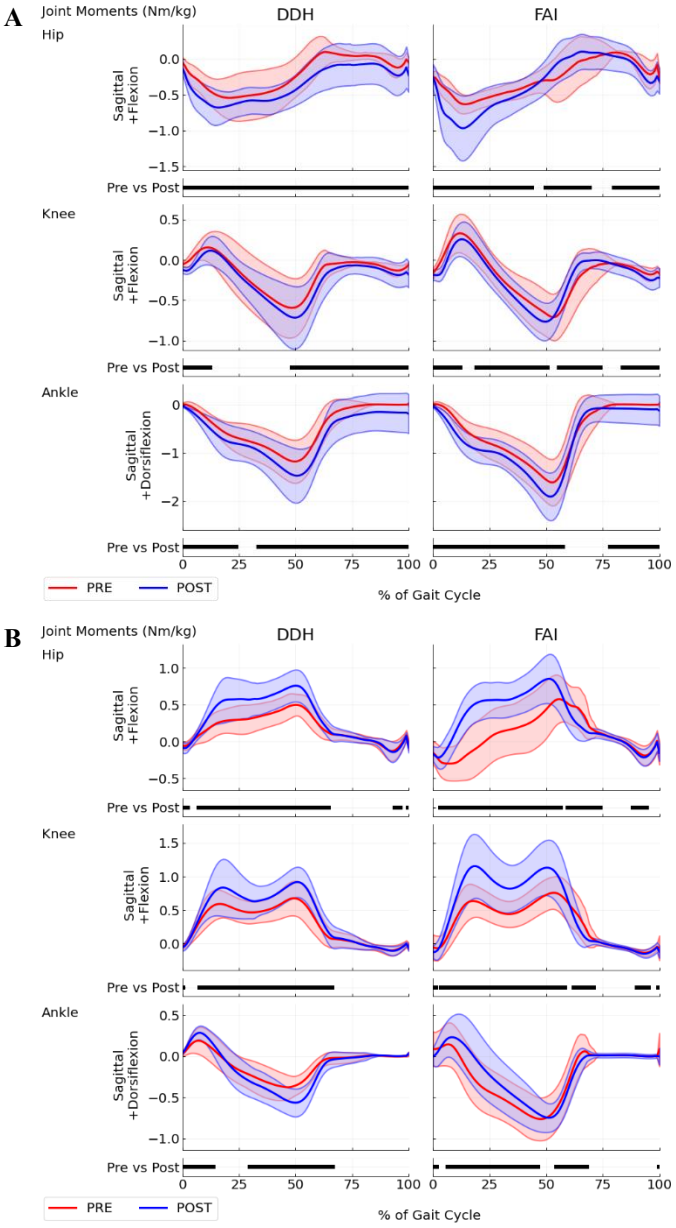

Figure 1. Joint moments during **(A)** incline and **(B)** decline walking.

Significance

Our results indicate that hip preservation surgeries affect gait biomechanics at not only the hip joint, but also the knee and ankle joints. As incline and decline walking are commonly impaired in hip patients, these walking conditions should be included in further studies and used as a measure of post-operative recovery.

References

[1] H. Endo et al, 2003; [2] M. J. Kennedy, M. Lamontagne, and P. E. Beaulé, 2009; [3] T. C. Pataky, 2012

ANKLE BIOMEHCNAICS OF PAITENTS WITH TKA DURING UPHILL WALKING

Songning Zhang[1*], Sean Brown[1], Kaileigh Estler[1], Walter Menke[1], Chen Wen[1], Harold Cates[2]
[1] Biomechanics/Sports Medicine Lab, The University of Tennessee, Knoxville, TN, USA
[2] Tennessee Orthopedic Clinic, Knoxville, TN, USA
email: *szhang@utk.edu

Introduction

Patients with unilateral total knee arthroplasty (TKA) showed reduced peak knee extension moment (KEM) of the replaced limb compared to healthy participants during uphill walking [1]. However, ankle biomechanics has not been explored during uphill walking in this patient group. Therefore, the purpose of this study was to compare ankle biomechanics of the replaced limb to the non-replaced limb of TKA patients and dominant limbs of healthy controls during walking on level (0°) and inclined surfaces of 5°, 10° and 15°.

Methods

Twenty-five TKA patients participated in this study from a local orthopedic clinic (68.8 ± 4.9 years, 1.70 ± 0.11m, 83.2 ±15.6 kg, 22.1 ± 11.72 months from surgery). Ten healthy participants served as healthy controls (69.1 ± 4.5 years, 1.74 ± 0.12 m, 75.0 ± 23 kg). 3D kinematic data were collected using a 12-camera system (Vicon). An adjustable instrumented ramp system with two separate walking surfaces bolted onto two force platforms (AMTI) was used to collect ground reaction force. Participants performed five trials each in level (0°) and uphill walking on 5°, 10° and 15° inclined surfaces. All joint moments were computed as internal moments. Peak joint moments were determined during loading-response (LR, first 50%) and push-off (PO, last 50%) of stance while peak angle and ROM were determined during the stance phase. A 3 x 4 (limb x group x slope) mixed model ANOVA was used to examine the interactions and main effects of selected dependent variables. A Greenhouse-Geisser correction was performed if the assumption of sphericity was violated. Post-hoc comparisons with Bonferroni adjustments were used to detect limb and slope differences.

Results and Discussion

The ANOVA results showed no significant limb x slope interaction for any of the examined sagittal- and frontal-plane kinematic and kinetic variables (Table 1). Only peak dorsiflexion angle was different between limbs with replaced limbs being greater than healthy control limb (p=0.041). All variables showed a significant slope main effect (all p<0.001). Post hoc comparison results showed that peak dorsiflexion angle and peak plantarflexion moment increased while peak dorsiflexion moment decreased, with the increased slopes during uphill walking (all p≤0.022). Fewer and less changes were observed for the frontal-plane variables. Peak eversion angle was reduced in all three slopes compared to level walking while peak LR inversion moment was also reduced at 10° and 15° conditions compared to level walking and at 10° compared to 5° slope condition (Table 1). These significant results were found while gait speeds were reduced in the increased slopes but not different between TKA and healthy participants.

These results show there is a compensation of the replaced limbs with greater dorsiflexion during uphill walking compared to the healthy counterparts. However, knee flexion and extension ROMs were smaller in replaced and non-replaced limbs [1] while similar kinematic compensations were not found in the hip [2]. Additionally, such compensation was not found in ankle plantarflexion moment during uphill walking. In addition, increased peak plantarflexion moments at greater slopes suggest uphill walking placed greater demand on ankle plantarflexors.

Significance

The lack of compensation from the ankle plantarflexors in the non-replaced limb is similar to the lack of difference of the peak hip LR extension moments between the replaced and non-replaced limbs in the same participant group during uphill walking [2]. These results suggest that the deficits shown by TKA patients in uphill walking is primarily in the knee joint, which are not compensated by the ankle or hip extensors of the non-replaced limbs.

Table 1. Average ankle joint angle (°), ROM (°) and peak joint moment (N/kg) data across different uphill slopes: mean ± STD.

Variable	Limb	0° (Level)	5°	10°	15°	Inter p (η^2_p)	Limb p (η^2_p)	Slope p (η^2_p)
Peak dorsiflexion angle	Replaced	11.95±3.66	13.52±3.44	17.63±3.46	22.87±3.56	0.204 (.051)	**0.046** (.103)	**0.001** (.111)
	Non-replaced	11.67±4.10	11.91±3.86	16.32±3.58	22.06±3.58			
	Healthy	8.58±2.15	9.85±1.82	14.66±2.07	21.09±2.86			
Peak eversion angle	Replaced	-10.15±3.22	-9.46±2.82	-8.80±2.80	-8.721±3.49	0.829 (.016)	0.491 (.025)	**<0.001** (.136)
	Non-replaced	-11.13±3.61	-10.04±3.23	-9.64±2.97	-9.791±3.07			
	Healthy	-9.81±2.66	-8.87±2.34	-8.95±3.03	-9.063±2.90			
Peak dorsiflexion moment	Replaced	0.27±0.10	0.20±0.09	0.10±0.06	0.03±0.03	0.073 (.076)	0.707 (.012)	**<0.001** (.851)
	Non-replaced	0.24±0.08	0.18±0.06	0.09±0.05	0.03±0.03			
	Healthy	0.31±0.13	0.18±0.09	0.08±0.05	0.03±0.03			
Peak plantarflexion moment	Replaced	-1.20±0.14	-1.27±0.15	-1.34±0.17	-1.37±0.21	0.750 (.016)	0.143 (0.067)	**<0.001** (.568)
	Non-replaced	-1.25±0.15	-1.29±0.15	-1.38±0.18	-1.42±0.19			
	Healthy	-1.32±0.13	-1.36±0.12	-1.46±0.12	-1.49±0.15			
Peak LR inversion moment	Replaced	0.11±0.07	0.09±0.05	0.07±0.05	0.08±0.06	0.225 (.049)	0.111 (.075)	**0.001** (0.111)
	Non-replaced	0.100±0.063	0.08±0.06	0.07±0.04	0.06±0.05			
	Healthy	0.05±0.05	0.05±0.03	0.04±0.04	0.06±0.05			

Note: η^2_p - partial eta squared, STD - standard deviation, LR - loading response

References

Wen, C. Cates, H.E., and Zhang, S. (2019) *Journal of Biomechanics*. 89: 40-47.

Zhang, S. et al. (2022) *9th World congress of biomechanics*.

QUATIFYING THE PRESSURE AND FORCE DISTRIBUTION ON THE PERINEAL REGION DURING HIP ARTHROSCOPY WHEN USING A PERINEAL POST: A POTENTAL MECHANSMS OF PUDENDAL NERVE PALSY

Nadeem Mamajiwala, Graeme Hoit, Jaskarndip Chahal, Tim Dwyer, Shgufta Docter, Jordan Farag
Daniel B. Whelan, Timothy A Burkhart[1]
[1]Faculty of Kinesiology and Physical Education, University of Toronto
email: timothy.burkhart@utoronto.ca

Introduction

Hip arthroscopy (HA) is a minimally invasive procedure used to treat a variety of hip pathologies including femoral acetabular impingement (FAI), acetabular labrum tears, or removal of loose bone or cartilage fragments. Between 2011 and 2018 there was an 85% increase in the use of HA. However, despite improvements in equipment and technique, there are still complications associated with HA. Approximately 1.8% of HA patients are diagnosed with a pudendal nerve injury, most commonly in the form of pudendal nerve palsy (PNP). PNP can result in external genital numbness and sexual dysfunction in both men and women.

During HA, the patient is supine with a perineal post positioned within the patient's perineal region. To improve visualization of the hip joint, the femoral head is distracted from the acetabulum by applying a distraction force to the femur while compressing the perineal region against the post. It has been suggested that prolonged compression of the pudendal nerve against the perineal post is a likely risk factor for the development of PNP. However, there is no biomechanical data quantifying the pressure and force distribution of the perineal post onto this region. Therefore, the purpose of this study was to quantify the biomechanical properties of perineal region compression during HA.

Methods

Twelve patients undergoing hip arthroscopy were recruited for this study from a single academic centre (mean [SD] age = 37[14] years; BMI = 24 [3 kg/m^2]). After proper calibration, a Tekscan pressure sensor (FlexiForce; Tekscan Inc. South Boston, MA) was securely fastened to the perineal post where it remained for the duration of the surgery. Data collection began just prior to the application of the traction force and continued until the traction was released.

Post-surgery, the Tekscan data were loaded into proprietary software where a region of interest was manually generated to isolate the perineal region from other contact areas (e.g., the thigh). The gluteal fold was distinguishable in the pressure data and was used as a border for the perineal ROI (Figure 1).

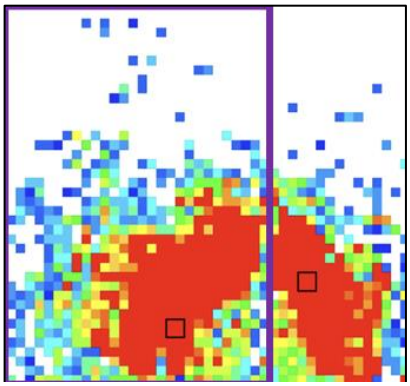

Figure 1: Representative pressure map showing the ROI (purple box) isolating the perineal region of a right hip.

The peak pressure, peak force, and contact area were extracted from each of the respective data sets; the total time of traction was also calculated (Figure 2).

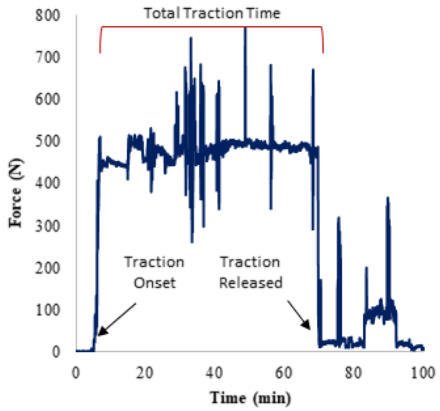

Figure 2: Representative contact force-time curve showing the onset and release of the traction force. The force at each time point is the peak force in the perineal region of interest. The peak force within the total traction time was extracted for analysis; this is similar for the peak pressure and contact area.

Results and Discussion

The mean (SD) peak force and pressure were 903 (464) N and 23.8 (7.2) kPa, respectively. The mean (SD) contact area was 0.36 (0.16) m^2. Traction was applied for an average of 72.6 (13.7) mins.

The forces measured on the perineal region reported here are almost three times higher than the 372 N (52% body weight) reported at the bicycle seat and perineal interface [1]. Wilson et al., suggest that these forces are large enough to generate injuries to the perineal region, including sexual dysfunction in both males and females. To our knowledge, this is the first study to quantify the biomechanical properties of the perineal region during HA, using a perineal post, for the duration of the surgery. Preliminary findings from the patient reported outcomes related to this study, suggest that patients who reported PNP tended to have greater forces and pressures over the duration of the study. Data continues to be collected and analysed to allow for a more robust analysis of this data.

Significance

injuries to the perineal region, specifically PNP, can have devastating long-term consequences for patients undergoing HA. The data reported in this study quantify, for the first time, the forces, pressures, and contact areas on the perineal region imparted by the perineal post. With this understanding, improved surgical approaches can be designed to reduce the magnitude of these injury inducing factors and decrease the risk of PNP.

References

[1] Wilson et al., 2007. C*lin Biomech.* 22, 1017-1023.

BIOMECHANICAL TESTING OF VERTEBRAL BODY TETHERING USING BIO-ROBOTIC SYSTEM

Daniel Jacobson[1], Alexander W Hooke, MA[1], A'nna Kelly[2], James Fizsimmons[1,2], Chunfeng Zhao, MD[1,2], A. Noelle Larson, MD[2], Todd A. Milbrandt MD, MS[2]
[1]Biomechanics Core, Mayo Clinic, Rochester, MN, USA
[2]Department of Orthopedic Surgery, Mayo Clinic, Rochester, MN, USA
email: jacobson.daniel@mayo.edu

Introduction

Adolescent idiopathic scoliosis (AIS) is the most common spinal abnormality in children and is prevalent in 2-3% of youth in the United States. Treatment options for AIS are determined based on curvature angle and risk of curve progression. Generally, observation and bracing treatments are used if the curvature angle is less than 40-50º, although larger angles require surgical intervention. Traditionally, posterior spinal fusion has been used to correct the scoliosis, however, this limits the spine mobility. Vertebral body tethering (VBT) is a new approach to surgically correct AIS with theoretical improved spine movement compared to fusion. Little information is available for the kinematics of the VBT instrumented spine. Therefore, the purpose of this study was to biomechanically evaluate VBT kinematics in human cadaveric spine using a novel robot system.

Methods

A spine from T8 to L5 was dissected from a fresh-frozen cadaver (female, age 41yrs) such that all soft tissue was removed with preservation of entire spinal columns and associated invertebral ligaments. The T8 and L5 vertebrae were potted in custom fixtures using a urethane resin. The spine was mounted to a 6 degree-of-freedom robotic arm (KUKA, Augsburg, Germany) equipped with a 6-axis load cell and controlled by simVitro software (Cleveland Clinic, Cleveland, OH, USA) (Fig 1). The spine was tested under 3 separate conditions (1-native, 2-VBT, 3-rigid fixation, steel rod 4mm in diameter) through 3 axes of motion, including axial rotation, lateral bending, and flexion/extension up to a 7.5Nm torque limit. The VBT spanned T10-L3 using six vertebral screws on the right-anterior of each vertebral body with the PET cord through each screw with approximately 400N of initial tension. The steel rod was installed in the same six vertebral screws.

Figure 1: Spine mounted to robot with anterior VBT

Results and Discussion

Both the VBT tether and rigid fixation significantly reduced the lateral bending range of motion, but the VBT tether less so. In axial rotation and flexion-extension motions, the VBT did not appear to have any impact on the range of motion, while rigid fixation had minor reduction in the overall range (Fig 2).

The purpose of this study was to understand the VBT influence on directional movement of the spine. Spine motion is mostly retained in both axial rotation and flexion-extension, while being slightly reduced in lateral bending. All axes had motion closer to native than that of rigid fixation.

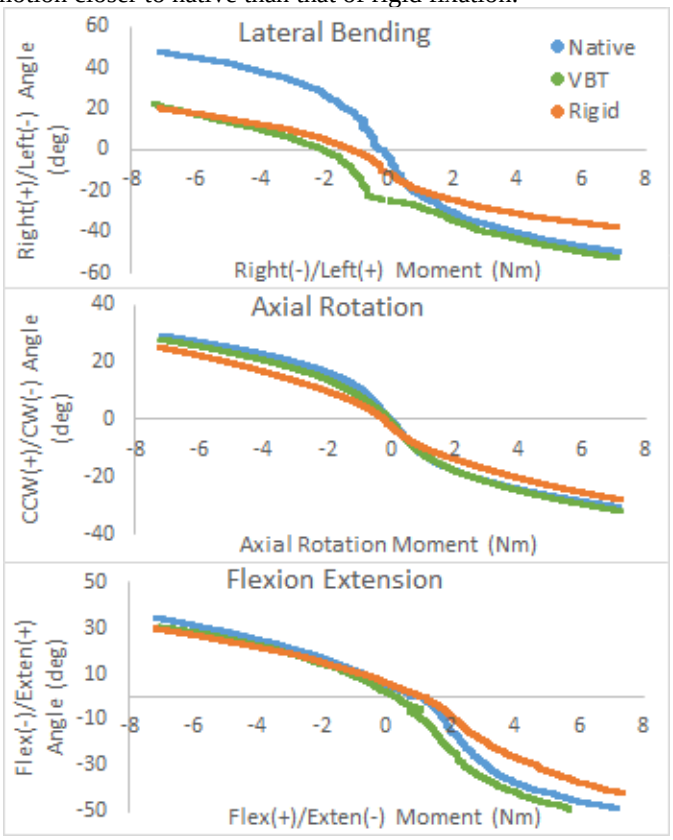

Figure 2: Range of Motion for Each Axis of Motion

Significance

VBT is a motion and growth preserving procedure to treat pediatric scoliosis that is growing in popularity. However, direct research on the exact mobility that is seen after this procedure is lacking. This study demonstrates some of its effects on biomechanical function. With a greater understanding of VBT implanted spine biomechanics, the optimal correction of deformity without spinal fusion can greatly improve adolescent patient health and reduce the complications related to instrumentation failure and spine fusion. Although only one case, this study demonstrates a novel methodology for spine mechanical evaluations and the influence of VBT on spine dynamics, thus providing valuable information for future studies.

Acknowledgments

This project was supported by the Mayo Clinic Wendel Clinician-Scientist Collaboration Grant and Mayo Clinic Biomechanics Core.

SEX-BASED DIFFERENCES IN HIP JOINT MUSCLE AND CONTACT FORCES DURING WALKING IN PEOPLE WITH HIP CARTILAGE DEGENERATION

Michael A. Samaan[1*], Thomas M. Link[2], Sharmila Majumdar[2], Richard B. Souza[2]
[1]University of Kentucky
[2]University of California-San Francisco
email: michael.samaan@uky.edu

Introduction

People with hip osteoarthritis (OA) walk with lower hip joint muscle and hip joint contact forces (JCF) compared to people without hip OA [1]. Females with hip OA ambulate with a higher peak hip adduction angle and adduction moment compared to males with hip OA [2]. To our knowledge, the sex-based differences in hip joint muscle forces, hip JCF and hip-related pain in people with hip joint cartilage degeneration have yet to be evaluated. Assessment of these biomechanical and clinical outcomes would provide insight into potential sex-based muscle- and gait-related interventions to prevent hip disease progression.

The purpose of this study was to investigate the sex-based differences in hip joint muscle and hip JCF during walking as well as self-reported hip pain in females and males with hip joint cartilage degeneration. We hypothesized that females with hip cartilage degeneration would ambulate with lower hip joint muscle forces and lower hip JCF and would self-report worse hip joint pain compared to males with hip cartilage degeneration.

Methods

This is a retrospective study of a longitudinal cohort data set [3]. All study participants underwent pelvic radiographs, 3D gait analysis at a fixed walking speed of 1.35m/s and hip joint magnetic resonance imaging (MRI). A total of 29 females (40 hips) and 25 males (33 hips) were tested in this study (Table 1). The presence of acetabular and femoral cartilage lesions was assessed with the Scoring Hip OA with MRI (SHOMRI), a previously validated technique [4]. Female and male participants that exhibited acetabular or femoral cartilage lesions were included in this study. Self-reported hip pain for each study hip was obtained using the Hip Disability & Osteoarthritis Outcome Score (HOOS) [5].

Previously published methods [6] were used to estimate hip joint muscle and hip JCF (femoral forces acting on the acetabulum) during the stance phase of walking (initial contact to toe-off) in OpenSim v4.2 [7]. All hip muscle forces and hip JCF were normalized to bodyweight. Chi-squared and independent t-tests were used to compare demographics, HOOS pain scores and severity of cartilage damage. Generalized estimating equations were used to assess differences in peak hip muscle forces and hip JCF during gait. Statistical significance was set at the 0.05 level.

Table 1: Demographics, Clinical and Structural Outcomes

	Females	Males	p-value
# Subjects/# Hips	29/40	25/33	X
Age (years)	53.8±13.5	53.9±13.1	0.89
BMI (kg·m^{-2})	23.1±3.48	24.4±2.91	0.54
HOOS Pain	89.5±12.7	93.1±12.6	0.58
Acetabular Lesions	1.82±1.71	1.27±1.44	0.67
Femoral Lesions	1.80±2.14	2.15±1.99	**0.02**
Kellgren-Lawrence (KL) Grades	KL 0, 1: 21 KL 2, 3: 19	KL 0, 1: 17 KL 2, 3: 16	X

Table 2: Hip Joint Muscle and Contact Forces (JCF), normalized by bodyweight

	Females	Males	p-value
Gluteus Medius	2.26±0.29	2.05±0.35	**< 0.01**
Gluteus Maximus	0.71±0.19	0.65±0.18	0.15
Adductors	0.51±0.14	0.61±0.14	**< 0.01**
Iliopsoas	2.52±0.53	2.57±0.46	0.66
Rectus Femoris	0.81±0.21	0.91±0.31	0.11
Anterior Hip JCF	1.55±0.21	1.43±0.21	**0.01**
Superior Hip JCF	5.29±0.65	5.45±0.79	0.35
Medial Hip JCF	1.62±0.25	1.59±0.32	0.66
Magnitude Hip JCF	5.66±0.68	5.78±0.84	0.52

Results and Discussion

There were no significant between group differences in age, BMI or HOOS pain scores ($p>0.05$). Males exhibited higher severity of femoral cartilage damage ($p=0.02$) yet similar ($p>0.05$) severity of acetabular cartilage damage as females (Table 1).

Females with cartilage degeneration walked with significantly higher (8.4%; $p=0.01$) peak anterior hip JCF compared to males with cartilage degeneration (Table 2). The peak superior, medial and magnitude of the hip JCF were similar between both groups ($p>0.05$). Females exhibited 10.2% higher gluteus medius peak muscle force ($p<0.01$) and 16.4% lower adductor muscle force ($p<0.01$) yet similar ($p>0.05$) gluteus maximus, iliopsoas and rectus femoris muscle forces.

The higher gluteus medius and lower adductor muscle forces exhibited by females with hip cartilage degeneration may lead to a higher abductor to adductor co-contraction. This higher abductor to adductor co-contraction may result in hip joint instability, leading to excessive anterior glide of the femoral head and the higher anterior hip JCF observed during walking in females with hip cartilage degeneration compared to males with hip cartilage degeneration.

Significance

Our results provide clinically relevant information on sex-based differences in neuromuscular strategies during gait in people with hip cartilage degeneration. This information can be used to develop sex-specific muscle- and gait-related interventions to optimize hip muscle forces and hip JCF to prevent hip disease progression in people with hip cartilage degeneration.

Acknowledgments

NIH P50-AR060752, R01-AR069006 and K24-AR072133.

References

[1] Diamond et al., 2020. *Osteo Cart*. 28(7): 924-931;
[2] Allison et al., 2018. *Gait Posture.* 65: 234-239;
[3] Liao et al., 2019. JOSPT. 49(12): 917-924;
[4] Neumann et al., 2019. Eur Radiol. 29(2): 578-587;
[5] Nilsdotter et al., 2003. BMC Musc Disord. 4;
[6] Samaan et al., 2019. J Biomech. 84: 138-146;
[7] Delp et al., 2007. IEEE Trans on BME. 54(11): 1940-1950.

PREDICTING POST-OPERATIVE WALKING SPEED BASED ON PRE-OPERATIVE GAIT MECHANICS

[1]Kristen Renner*, [2]Caitlyn Delaney, [3]Cherice Hill, [4]Laura Sands, [5]Robin Queen
[1]Department of Orthopaedic Surgery, University of Arizona College of Medicine [2]Department of Physical Therapy, Radford University [3]Department of Bioengineering, Clemson University [4]Center for Gerontology, Virginia Tech [5]Biomedical Engineering and Mechanics, Virginia Tech
email: *kristenrenner@arizona.edu

Introduction

Ankle arthritis (AA) is a degenerative disease associated with pain, reduced range of motion, and limitations in gait mechanics and walking speed [1]. Total ankle arthroplasty (TAA) is a surgical treatment for end-stage AA with the goal of pain relief and restoration of mobility and function [2]. Despite the benefits of TAA, walking speed 1yr post-TAA remains slower (1.20 m/s) than their peers (1.33 m/s) [3,4].

Decreased speed has been determined to be a predictor of impaired physical performance and overall function in older adults [5]. Benchmark speeds have been established for older adults as safety thresholds during various tasks. To be a safe community ambulator 0.8m/s is needed [6], 0.9 m/s is needed to safely complete housework independently [7], 1.1 m/s is associated with successfully and safely carrying groceries and completion of light yard work [8], and 1.3 m/s or faster is an indication of patients who can cross the street safely [6].

It is currently unknown if pre-operative kinetic and kinematic gait parameters may serve as useful predictive metrics during recovery. Therefore, the purpose of this study was to determine the ability of pre-operative gait parameters to predict walking speed 1yr post-TAA.

Methods

191 patients were assessed prior to and one year following TAA. Each patient completed a 3D gait assessment [7], and Visual 3D (C-Motion, Germantown, MD, USA) was used to identify the following variables of interest: ankle range of motion (A-ROM), peak plantarflexion (PF) moment (Nm/kg), peak PF angle, peak PF power (W/kg), and peak weight acceptance (WA-vGRF) and peak propulsive (P-vGRF) vertical ground reaction forces for the surgical (Sx) and nonsurgical (NSx) limbs.

Receiver operator curves (ROC) were generated for each variable to determine threshold values needed to achieve the walking speed benchmarks of 0.8 m/s, 0.9 m/s, 1.1 m/s, and 1.3 m/s at 1yr post-TAA. Each ROC curve represents the balance between sensitivity and specificity when the variable of interest is used to classify patients into groups [9]. The area under the curve (AUC) was used to determine a variable's potential to predict the ability to achieve each walking speed benchmark. All statistical tests were completed in R.

Results and Discussion

The AUC and threshold value to predict a given benchmark is shown in Table 1 along with the associated sensitivity and specificity. Only variables that had an AUC of at least 0.60 were included in the results, an AUC of 0.50 indicates a 50/50 chance of predicting if the patient reached the benchmark.

There were no variables classified with excellent or good predictive ability. The variable with the highest AUC was pre-op walking speed with an AUC between 0.73 and 0.78 (fair) for all the walking speed benchmarks tested. The NSx peak PF moment had fair predictive ability for 0.8 and 0.9 m/s and poor predictive ability at 1.1 and 1.3 m/s. Sx peak PF moment, NSx power and GRF peaks had poor or no meaningful (AUC<0.6) predictive abilities. The best predictor for all post-TAA walking speed benchmarks was pre-operative walking speed. This study investigated each variable of interest independently, the results of this study may be improved if we consider combining factors.

Significance

The most challenging level of functional independence was only achieved by 24.1% of the patients in this study, and over 80% were unable to walk at the speed of age matched healthy adults. Several gait metrics were associated with walking speed one year post-TAA which could be considered for future studies Pre-operative walking speed was the strongest predictor across all benchmark walking speeds. The associated cut-off values for these variables can be used in the development of pre-op intervention strategies which may improve post-TAA walking speed and therefore overall functional outcomes.

References

[1] Valderrabano et al., Clin Biomech. 2007. 22(8): p. 894-904. [2] Queen et al., JOR. 2017. 35(11): p. 2345-2355. [3] Queen et al., Foot & Ankle. 2012. 33(7): p. 535-542. [4] Bohannon et al., 2011. Physiotherapy. 97(3): p. 182-189. [5] Middleton et al., 2015. JAPA. 23(2): p. 314-322. [6] Perry et al., 1995. Stroke. 26(6): p. 982-989. [7] Ainsworth et al., 2011 Yearbook Of Sports Medicine. 43(8): p. 1575-1581. [8] Studenski, 2009. J Nutr Health Aging. 13(10):878. [9] Hodt-Billington et al., 2012. Physiother Pract Res. 28(2): p. 134-141.

Benchmark	0.8 m/s				0.9 m/s				1.1 m/s				1.3 m/s			
	AUC	Th	Sn	Sp	AUC	Th	Sn	Sp	AUC	Th	Sn	Sp	AUC	Th	Sn	Sp
Sx Moment	0.52	-1.33	0.82	0.82	0.62	-1.34	0.90	0.90	0.59	-1.35	0.79	0.79	0.64	-1.55	0.93	0.93
NSx Moment	0.70	-1.14	0.65	0.71	0.72	-1.19	0.70	0.68	0.64	-1.33	0.71	0.52	0.63	-1.54	0.89	0.36
NSx Power	0.58	-0.39	0.53	0.73	0.62	-0.41	0.57	0.68	0.60	-0.64	0.80	0.40	0.60	-0.49	0.54	0.69
Sx WA-GRF	0.56	1.02	0.65	0.58	0.50	0.97	0.90	0.23	0.60	1.02	0.73	0.46	0.69	1.06	0.86	0.44
NSx WA-GRF	0.56	1.04	0.88	0.37	0.59	1.04	0.90	0.39	0.56	1.03	0.74	0.44	0.69	1.02	0.63	0.71
Sx P-GRF	0.54	0.97	0.94	0.29	0.48	1.05	0.90	0.29	0.54	1.05	0.87	0.33	0.61	1.05	0.81	0.51
NSx P-GRF	0.54	1.04	0.88	0.35	0.57	1.03	0.87	0.40	0.59	1.06	0.84	0.36	0.62	1.08	0.87	0.44
Pre Speed	0.76	0.71	0.65	0.80	0.79	0.77	0.77	0.70	0.73	0.94	0.90	0.57	0.78	1.09	0.93	0.57

Table 1: Area under the curve (AUC), threshold (Th) values to predict a given benchmark along with the sensitivity (Sn) and specificity (Sp). An AUC ≥0.9 is excellent (green), 0.8-0.89 good (blue), 0.7-0.79 fair (yellow), and 0.6-0.69 poor (orange).

BRAIN TRAUMA EXPOSURE FOR AMERICAN TACKLE FOOTBALL PLAYERS 5 TO 9 AND 9 TO 14 YEARS OF AGE

A. Azadi[1], J. Cournoyer[1], C. Karton[1], D. Koncan[1], M.D. Gilchrist[2], R.C. Cantu, T.B. Hoshizaki[1]
[1]University of Ottawa, School of Human Kinetics, Ottawa, Canada
[2]University College Dublin, School of Mechanical and Materials Engineering, Dublin, Ireland

email: Amirhossein.azadi@uottawa.ca

Introduction

Repetitive head impacts (RHI) in American tackle football are associated with a variety of neurological impairments [1]. In youth American football players, associations between RHI and changes in white matter have been reported in athletes as young as seven years old [2]. The growing concern for brain health in youth American football players has led to the need for increased safety measures including an age-appropriate helmet. However, to develop a youth specific helmet, it is first necessary to understand the impact characteristics that create brain trauma in youth American tackle football. While youth football may appear to be similar to adult football, there may be differences in the frequency, magnitude, and type of head impact events. The purpose of this research was to understand differences in brain trauma sustained in youth American football players by comparing head impacts for two age groups of 5–9 and 9-14 years of age.

Methods

Video analysis: Video from 60 youth American football games was analyzed from two age categories: 30 games of 5-9 and 30 games for 9-14. The video was analyzed to identify the frequency and characteristics of head impacts. This was conducted by documenting the head impacts for 7 player positions from one of the two teams on the field (1 quarterback, 1 running back 1 wide receiver, 1 offensive lineman, 1 defensive lineman, 1 linebacker, and 1 defensive back) recording: event type, impact location and velocity. Event types consisted of head-to-head, head-to-shoulder, head-to-ground, head-to-hip/thigh, head-to-back/torso, head-to-knee/shin, or head-to-arm/hand. Impact locations were classified as front, front boss, side, rear boss, rear, and crown. The velocity of each impact was visually assessed and categorized as very low (0–2 m/s), low (2–4 m/s), moderate (4–6 m/s), or high (6 m/s +) and was confirmed when possible, using Kinovea (version 0.8.20, Bordeaux, France).

Laboratory reconstructions: Head-to head, head-to-ground, and head-to-shoulder events were selected for laboratory reconstructions as they made up 91% (682) and 85% (535) of all impacts in the 5–9 and the 9–14 age groups respectively. The impact conditions for which a frequency (>0) was observed were reconstructed in laboratory using a small NOCSAE head form fitted with a youth American football helmet. Head-to-ground impacts were conducted as free drops using a monorail drop rig without a neck onto a turf surrogate. Head-to-head impacts were reconstructed using a small NOCSAE head form fitted with an appropriately sized helmet as a pendulum (impacting mass = 5.2 kg) that was released into a stationary helmeted NOCSAE small headform. Head-to-shoulder impacts were conducted using a pendulum fitted with 7 cm of VN 602 foam and a youth American football shoulder pad. The linear and acceleration time histories were collected from the helmeted impacts at 20 kHz using a DTS system and filtered using a CFC 180 filter. These accelerations were used as input for the finite element modelling of the youth brain to determine brain strains. A finite element model designed for 6-year-olds was used to obtain the peak maximum principal strain (MPS) for the impacts that were reported for the 5–9 age group. This model had 169,849 elements and the brain was modeled as hyperelastic [3]. The University College Dublin Brain Trauma Model (UCDBTM), scaled to 96% of original size, was used for the 9–14 age group. The UCDBTM had 32,994 elements and was modelled as viscoelastic. The resulting impact frequencies for each strain magnitude was categorized into MPS categories reflective of neurological impairment: The MPS categories were very low (<0.08), low (0.08–0.169), medium (0.17–0.259), high (0.26–0.349) and very high (>0.35)[4].

Results and Discussion

The majority of head impacts observed for both age groups studied involved very low strain magnitudes (<0.08) (Figure 1). American youth football players aged 9–14 yrs. experienced a Statistically greater number of head impacts with MPS values between 0.08 and 0.169 when compared to the 5–9 yrs. age group. This level of trauma is typically associated with asymptomatic head injuries. While there was no statistical significance in head impact frequency for the other magnitude categories or head impacts per game, the moderate and very high magnitude head impact frequencies were higher for the younger age group. Impacts at these magnitudes represented a risk for concussive injuries and were caused by a greater frequency of head-to-head impacts and greater velocities for head-to-ground impacts. These findings clearly indicate there would be merit in developing a youth-specific helmet.

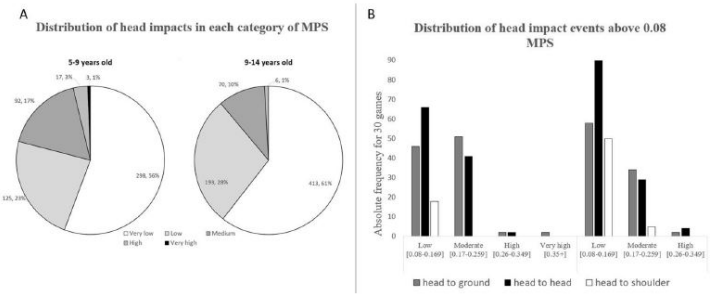

Figure 1. Frequency (A) and frequency per magnitude of strain per event type (B) for 5-9 and 9-14 datasets.

Significance

This research has described brain trauma experienced by different age groups and used this to inform the design and certification requirements for a youth-specific American tackle football helmet safety standard.

Acknowledgments

This research was funded by the National Operating Committee on Safety of Athletic Equipment (NOCSAE).

References

[1] Alosco, M. L., et al. Alzheimers Dement. (2018), 56-65.
[2] Foss, et al. Clinical j. of sport medicine (2019), 442-450.
[3] Koncan, D., et al. J. Sports Eng. Technol. (2019), 277–291.
[4] Karton, C., et al. Sci Reports. (2020), 1-14.

INFLUENCE OF PLAY TYPE ON THE MAGNITUDE AND NUMBER OF HEAD IMPACTS SUSTAINED IN YOUTH AMERICAN FOOTBALL

P. Dehghan[1*], A. Vale[1], A. Post[1,2], J. Cournoyer[1], M.D. Gilchrist[2,1]and T. B. Hoshizaki[1]
[1]Human Kinetics, University of Ottawa, Ottawa, Ontario, Canada
[2]School of Mechanical and Materials Engineering, University College Dublin, Dublin, Ireland
email: pdehg058@uottawa.ca

Introduction

American tackle football has many benefits for young athletes; however, it has also been linked to detrimental effects on brain health related to the magnitude and number of impacts to the head. To improve safety in youth American football and reduce the risk of long-term negative brain health outcomes a greater understanding of the source of repetitive impacts experienced by youth players is required.

Youth football players aged 5–14 yrs can experience more than 1000 head impacts in a single season potentially compromising their physical and mental health. Impact magnitude, which has been implicated in causing brain injuries in adult football players may also be detrimental in youth football. Play type (run vs pass) has been shown to affect head impact characteristics in the adult American football population. Determining the effect of play type on the magnitude and number of head impacts in youth players will allow for a greater understanding of causes of brain trauma in youth football. This will support improved game management strategies to reduce brain trauma at the youth level. The purpose of this research was to examine how run and pass plays affect the magnitude and number of head impacts experienced in youth American football.

Methods

Video analysis: 30 Games of youth American football in the 5-9 and 9-14 age categories were analyzed to identify the number and characteristics of the head contacts. Seven player positions from one team were followed for each play, specifically: 1 quarterback, 1 running back, 1 wide receiver, 1 offensive lineman, 1 defensive lineman, 1 linebacker, and 1 defensive back. The characteristics recorded included event type (head-to-head, head-to-shoulder, head-to-ground, head-to-hip/thigh, head-to-back/torso, head-to-knee/shin, or head-to-arm/hand), location of impact, and impact velocity (calculated using Kinovea software; version 0.8.20). The number of head impacts were then separated into play type: namely, run or passing play.

Laboratory impact procedure: The three most common event types (head-to-head, head-to-ground, and head-to-shoulder impacts) were reconstructed in the laboratory. All impact reconstructions were conducted using a NOCSAE size "small" headform that was fitted with a youth American football helmet. The headform was instrumented with accelerometers in a 3-2-2-2 array, sampling at 20 kHz, and filtered using a CFC 180 filter. The head-to-ground impacts were conducted using a monorail drop rig, where the headform was dropped onto a turf surrogate. A headform pendulum was used to conduct the head-to-head impacts. A Pendulum fitted with a compliant shoulder striker (7cm thick, VN 602) was used for the head-to-shoulder impacts. The linear and rotational acceleration time histories from these impacts were used as input for finite element modelling of the brain to determine the maximum principal strains (MPS).

Finite element model: A finite element model designed for 6-year-olds was used to obtain peak MPS values for impacts experienced in the 5–9 age group [2], with a scaled version of the University College Dublin Brain Trauma Model used for the 9–14 [3]. The number of impacts for each strain magnitude was categorized into MPS categories reflective of neurological impairment: very low (<0.08), low (0.08–0.169), moderate (0.17–0.259), high (0.26–0.349) and very high (>0.35)[4].

Statistical test: Differences in number of head impacts, and number of head impacts for each strain category normalized to number of run and pass plays for players aged 5–9 and 9–14 were determined by Mann- Whitney U test with an alpha set to 0.05.

Results and Discussion

Number of head impacts sustained was higher in run plays for both the 5–9 and 9–14 age groups ($p<0.05$). All positions across both age levels experienced higher head impact numbers during run plays ($p<0.05$) with the exception of wide receivers in both age groups, and offensive linemen and defensive backs in the 9–14 age group. The numbers of very low and low magnitude head impacts were higher in run plays for both age groups ($p<0.05$), and the number of moderate magnitude head impacts was higher in run plays in the 5–9 age category ($p<0.05$). These differences in magnitude and number of head impacts were influenced by the position played. The differences in magnitude and number of head impacts for different play types support the need for specific prevention strategies to reduce the risk of brain trauma in youth football populations.

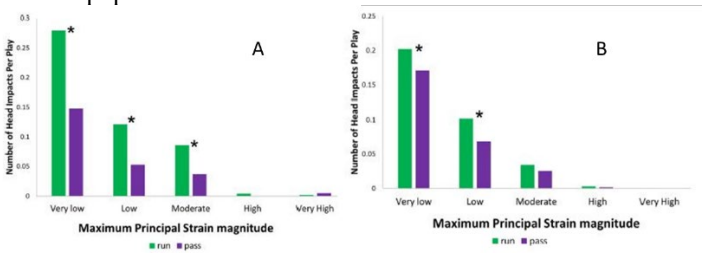

Figure 1. The number and magnitude of head impacts per run and pass play for 5-9 (A) and 9-14 (B). *Significance ($p<0.05$)

Significance

This data can be used to inform strategies to decrease head impacts and make youth football safer.

Acknowledgments

NOCSAE provided funding for this research.

References

[1] Alosco, M. L., et al. (2018), 56-65.
[2] Koncan, D., et al. J. Sports Eng. Technol. (2019), 277–291.
[3] Horgan, IJCrashworthiness. (2004), 353-366.
[4] Karton, C., et al. Sci Reports. (2020), 1-14.

HEAD IMPACT KINEMATICS DURING A BOBLSED WORLD CUP: A PILOT STUDY

April L. McPherson[1*], William M. Adams[1], Jonathan T. Finnoff[1]
[1]United States Olympic & Paralympic Committee, Colorado Springs, CO, USA
email: *april.mcpherson@usopc.org

Introduction

Despite the breadth of knowledge and awareness of sport-related concussion (SRC) and the emerging evidence suggesting associations of repetitive, sub-concussive head impacts on long term health in sports such as American Football, boxing, soccer, and ice hockey, a thorough understanding of these occurrences in sliding sports (i.e., bobsled, skeleton, and luge) is largely absent within scientific literature. While limited evidence suggests that SRC accounts for 13 – 25% of all injuries occurring during sliding sport participation,[1-4] there is no known literature that has quantified the occurrence and magnitude of head impacts during training and competition within these sports. Understanding head impact kinematics that occur in sliding sports may have important, and long-term implications for addressing the effects of both concussive and sub-concussive head impacts on health outcomes within sliding sports. Thus, this pilot study aimed to determine the frequency and magnitude of head impacts while training and competing in bobsled. It was hypothesized that there would be differences in head impact kinematics between training days and competition days.

Methods

Seven elite bobsled athletes (4 Females; 4 brakemen/push athletes, 3 pilots) competing on the International Bobsled and Skeleton Federation World Cup Tour participated in this pilot study. Athletes wore an accelerometer-enabled mouthguard (Prevent Impact Monitor, Prevent Biometrics; Edina, MN, USA) during all training sessions and competitions occurring over two consecutive weeks to quantify head impact kinematics. Number of impacts, peak linear acceleration (PLA, g), peak linear velocity (PLV, m/s), and workload (J) were calculated from raw accelerometer waveforms. A head impact was defined as an instant where PLA exceeded 8g.

Summary data, including number of days and runs captured, and number of head impacts were determined. Average values for each metric were determined for each athlete for training and competition days over a two-week period where they practiced and competed on the same track. Generalized linear mixed models via PQL were used by using a fixed effect of run number and session type (e.g. training or competition) and random effects of athlete and position (pilot or brakeman). An effect was considered to have a significant effect if $p < 0.05$.

Table 1: Group head kinematic values. Average (Standard Deviation, Minimum-Maximum)

	Training	Competition
PLA (g)	11.7 (2.9, 8.0-21.8)	11.9 (3.4, 8.0-27.8)
PLV (m/s)	0.9 (0.2, 0.3-1.6)	1.0 (0.3, 0.0-2.2)
Workload (J)	2.3 (1.0, 0.9-6.3)	2.51 (1.4, 0.1-11.2)

Results and Discussion

14 training and 13 competition days were recorded, with a mean 1 (range, 1 – 2) run per day. 290 head impacts were recorded (**Fig. 1**), with no differences in the average number of impacts per run occurring between training (4 ± 5; range, 1 – 13) or competition (6 ± 6; range, 1 – 15; $p>0.05$). There were no significant differences between training and competition days for PLA, PLV, or workload ($p>0.05$; **Table 1**).

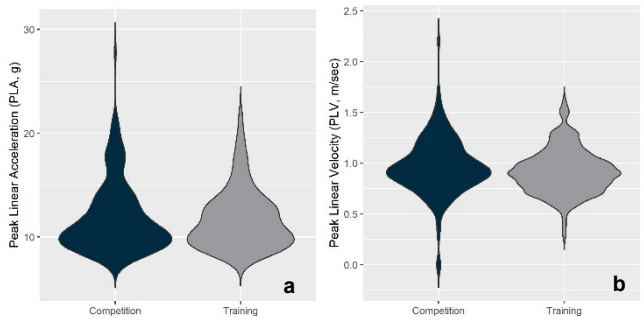

Figure 1: Distribution of (a) PLA and (b) PLV for all competition and training day head impacts (n=290).

To our knowledge, this is the first study that quantifies head impact kinematics during training and competition in elite sliding sport athletes. In sports such as American football and ice hockey, literature shows that the average number of head impacts ranges from 10.6 – 24.1 per session.[5] While our data show that the number of head impacts is 50% of the minimum occurring in other sports, we must acknowledge that the number head impacts occurring during a single bobsled run occur within approximately a two-minute timeframe, whereas the timeframes reported in other sports are much longer (i.e., 60 minutes in American football). We must also consider the differences in thresholds used to quantify a head impact. Our study used a threshold of PLA >8g, whereas other studies consider a head impact using thresholds of 10–15g; these differences may over- or underestimate the number of head impacts that occur.

Significance

This study provides a foundational understanding of head impact kinematics and forces an elite bobsled athlete experiences during training and competition. Moreover, this study serves as a baseline for future work that can determine the clinical significance of repetitive sub-concussive head impacts on health and wellness in sliding sport athletes.

Acknowledgments

We would like to thank the athletes for their participation, and Hannah Beaumont for her assistance with data collection.

References

[1] McCradden et al., 2018. *Front Neurol.* 9:772.
[2] Engebretsen et al., 2010. *Br J Sports Med.* 44:11.
[3] Soligard et al., 2015. *Br J Sports Med.* 49:7.
[4] Steffen et al., 2017. *Br J Sports Med.* 51:1.
[5] O'Connor et al., 2017. *J Ath Train.* 52:3

DYNAMICS OF HEAD-TO-SHIELDING IMPACTS IN ICE HOCKEY

Omid Vakili[1*], Olivia M.G. Aguiar[1], J. Max Donelan[1], T. Blaine Hoshizaki[2] and Stephen N. Robinovitch[1]
[1] Department of Biomedical Physiology and Kinesiology, Simon Fraser University, Burnaby, Canada
[2] School of Human Kinetics, University of Ottawa, Ottawa, Canada
email: *ovakili@sfu.ca

Introduction

Head impacts are common in ice hockey, and repeated head impacts, even at sub-concussive levels, can have serious neurological consequences[1]. One of the most common scenarios is head impact to the glass or acrylic shielding above the dasher boards[2]. Brain trauma during these events depends on the impact velocity of the head, and the stiffness of the shielding[2,3]. We sought to provide improved understanding of the magnitude of these parameters during real-life head-to-shielding impacts, based on analysis of video footage and helmet sensor data.

Methods

Head impact velocity. We collected video footage (Sony camcorder, 60 Hz; 1920x1080 px) and 3D head translational accelerations (GForceTracker helmet sensor, 3kHz) for 134 head-to-shielding impacts occurring during 44 home games of the SFU men's university hockey team. We focused on 11 cases occurring along the end boards that were captured with clear unobstructed views of the impact event by cameras oriented roughly perpendicular to the head trajectory, and involved no movement of the shielding just before impact.

These 11 cases were digitized using Kinovea (0.9.4) to track the time-varying positions of the player's head and the shielding before, during and after head impact (Fig. 1A, C, D). Position data were low-pass filtered (4th order Butterworth, 10 Hz cut-off) and head velocity was estimated by numerical integration.

Shielding stiffness. We calculated the shielding stiffness (k_s) by equating the peak head contact force (F_{peak}), given by the product of peak head acceleration times head mass ($m_h \ddot{x}_h$), to the elastic force developed in the shielding, given by the product of shielding stiffness times shielding displacement ($k_s\, x_h$) at the site of head impact: $F_{peak} = m_h \ddot{x}_h = k_s\, x_h \;\rightarrow\; k_s = \left(\frac{\ddot{x}_h}{x_h}\right) m_h$.

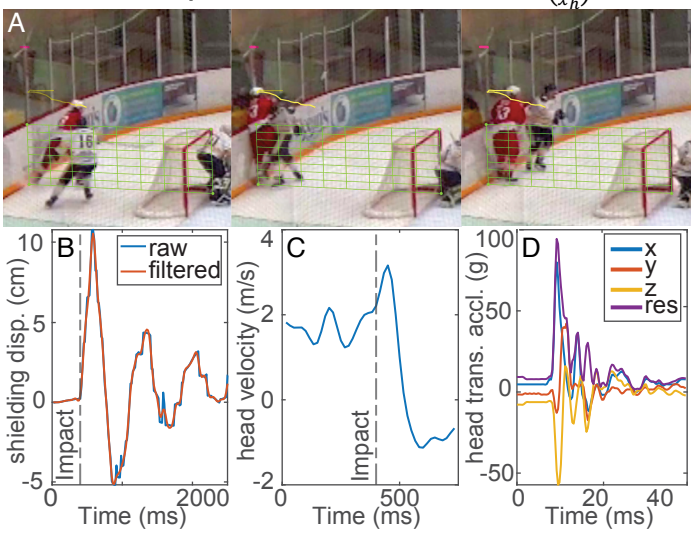

Figure 1. Example (Video ID: 4) head-to-shielding impact. (A) Kinovea analysis & video snapshot, (B) shielding displacement (marked with pink line in video), (C) head velocity (based on yellow line in video), and (D) head translational acceleration from helmet mounted sensor.

Results and Discussion

Results. The peak head acceleration averaged 43.83 g (SD= 29.51; range=13.71-94.37 g; Table 1). The head impact velocity averaged 2.51 m/s (SD=1.56; range=0.02-5.74 m/s). The shielding displacement at the impact site averaged 1.69 cm (SD=1.50; range=0.37-10.58 cm). The shielding stiffness averaged 202.34 kN/m (SD=149.47; range=24.89-480.81 kN/m).

Discussion. We used a novel approach to calculate shielding stiffness during real-life head-to-shielding impacts in hockey, based on analysis of video footage and helmet sensor data. We found that the head struck the shielding with an average impact velocity of 2.51 m/s (SD=1.56), which is consistent with the range of 1.3-3.3 m/s reported previously[3]. Shielding stiffness averaged 220 kN/m (SD=149), and varied between 25 and 481 kN/m. These values are consistent with the range of 75-400 kN/m reported from experiments with an impact pendulum[3,4].

Table 1. Parameter values for 11 head-to-shielding impacts

Video ID	$\ddot{x}_h$ (g)	$\dot{x}_h$ (m/s)	x_h (cm)	k_s (kN/m)
1	32.24	3.31	1.03	185.01
2	30.37	2.62	0.37	480.81
3	24.19	3.86	1.77	80.48
4	94.37	2.21	4.65	119.56
5	35.40	0.02	0.67	308.91
6	53.37	0.77	1.32	238.00
7	13.71	1.53	0.67	121.00
8	91.40	3.33	1.63	330.88
9	71.45	5.74	0.98	428.02
10	19.26	2.17	4.56	24.89
11	16.31	2.07	0.90	106.24
MEAN	**43.83**	**2.51**	**1.69**	**220.34**
SD	**29.51**	**1.56**	**1.50**	**149.47**

Significance

Head-to-shielding impacts are common and optimizing the stiffness of the shielding is a logical target for preserving brain health in hockey. In this study, we found that head-to-shielding impacts involved average head impact velocities of 2.5 m/s, and created peak head accelerations that averaged 43.8 g, due to a shielding stiffness that averaged 220 kN/m. Our results provide a starting point for further research on improving the design and regulation of shielding to reduce brain trauma during ice hockey.

Acknowledgments

We thank the SFU men's hockey team for their participation in this project. Supported by NSERC (RGPIN/04065-2015), the (CSA) Group and the (ASTM) International.

References

[1] Fickling et al. (2021), *Brain Comms*. 3(2)
[2] Tuominen et al. (2015), *Br J Sports Med*. 49(1):30-36
[3] Poutiainen et al. (2014), *Eur J Sport Sci.* 14(1): 11-18
[4] Schmitt et al. (2018), *Swiss Council for Accident Prevention*

EFFECT OF FILTERING ON THE AGREEMENT BETWEEN GFT HELMET MOUNTED SENSORS AND HYBRID-III MEASURES OF HEAD KINEMATICS IN BODY-TO-HEAD IMPACTS IN HOCKEY

Jeremiah Zacharias, Olivia M.G. Aguiar, Omid Vakili, Stephen N. Robinovitch
Department of Biomedical Physiology and Kinesiology, Simon Fraser University, Burnaby, Canada
email: jeremiah_zacharias@sfu.ca

Introduction

In Canada, ice hockey has the highest incidence of traumatic brain injuries among team sports [1]. Head impact accelerations and velocities associate with risk for brain injury [2]. Helmet mounted sensors (e.g., GForceTracker™ or GFT) use triaxial accelerometers and gyroscopes to detect head impacts during gameplay, and record corresponding head kinematics (linear accelerations, rotational velocities). However, GFT's accuracy in measuring head kinematics may be reduced by vibration, energy dissipation, and dislocation of the helmet during impact [3–4]. Studies have measured the accuracy of the GFT based on comparison to "gold-standard" Hybrid-III headform (HIII) measures, using mechanical testing systems more consistent with head-to-ice impacts [3–5]. In this study, we built on previous research by measuring the accuracy of GFT during real-life body-to-head impacts, and examined whether low-pass filtering of GFT data resulted in better agreement with HIII measures of peak linear acceleration and rotational velocity.

Methods

Eleven male participants (aged 21–25) were recruited from elite ice hockey teams to deliver hockey-style impacts to a dummy. The dummy was equipped with a HIII headform instrumented with accelerometers arranged in a 3-2-2-2 array sampling at 20 kHz [6]. A CCM V08 hockey helmet (with face cage) was secured to the headform and instrumented with three GFT sensors in the left back, right lateral aspect, and top of the helmet. Each GFT sensor sampled linear accelerations at 3 kHz, and rotational velocities at 0.8 kHz. Participants stood 1.4 m away and delivered either a hand, elbow, or shoulder check to the head of the dummy while wearing standard hockey padding. The frequency content of the HIII signals was analyzed via Fast Fourier Transforms (FFT). The FFTs informed the selection of a cut-off frequency range from 10–300 Hz for 4th-order Butterworth low-pass filtering of GFT data.

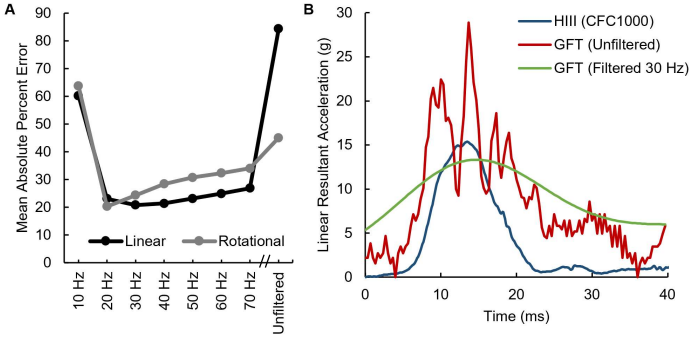

Figure 1. (A) Mean absolute percent error versus filtering cut-off frequency for the three-sensor average of the GFT data for linear acceleration and rotational velocity. (B) Improvement of an example trace (one sensor) when filtering at optimal frequency.

We then examined the effect of filter cut-off frequency on the Mean Absolute Percentage Error (MAPE), coefficient of determination (R^2), and mean difference in peak values between GFT and HIII.

Results and Discussion

For HIII, the average peak linear acceleration was 15.9±6.8 g and the average peak rotational velocity was 484.1±150.6 deg·s^{-1}. For the GFT three-sensor average, unfiltered data produced a MAPE of 84.4±70.7% and 45.1±41.0% for linear acceleration and rotational velocity, respectively (Table 1). A filter of 30 Hz for linear acceleration and 20 Hz for rotational velocity reduced the GFT MAPE to 20.8±17.9% and 20.3±18.9% (Figure 1a), respectively, and moderately improved the R^2 value between GFT and HIII (Table 1). In addition, filtering improved the mean difference between GFT and HIII, reflecting a reduction in the offset bias of the GFT.

Table 1. Measures of agreement for unfiltered GFT and optimally filtered GFT against HIII

	MAPE(SD)	R^2	Mean Difference(SD) (GFT-HIII)
$GFT_{linear,\ unfiltered}$	84.4% (70.7)	0.544	12.4 g (8.1)
$GFT_{linear,\ 30\ Hz}$	20.8% (17.9)	0.679	-1.7 g (4.3)
$GFT_{rotational,\ unfiltered}$	45.1% (41.0)	0.472	175.1 deg·s^{-1} (148.4)
$GFT_{rotational,\ 20\ Hz}$	20.3% (18.9)	0.562	7.0 deg·s^{-1} (109.3)

Our results show that, for body-to-head impacts in ice hockey, low-pass filtering of GFT data yields more accurate estimates of peak head accelerations and rotational velocities. The optimal cut-off frequency was 30 Hz for linear acceleration and 20 Hz for rotational velocity. These cutoffs are compatible with on-field head impact frequencies, which have been shown to be primarily less than 20 Hz [7]. When compared to previous results from mechanical test systems [3–5], we observed higher MAPE and lower R^2 values for checks delivered by actual hockey players. Further work is required to determine optimal filtering parameters for estimating Head Injury Criterion (HIC), acceleration duration, and for head impacts to the boards or ice.

Significance

This study demonstrates that the peak magnitude of unfiltered GFT data have poor agreement with HIII for head-to-body impacts in hockey; however, this can be substantially improved by low-pass filtering at specific cut-off frequencies. Filtering should improve the ability of helmet mounted sensors to monitor the severity of head impacts in hockey and other contact sports.

Acknowledgments

Funded by NSERC RGPIN/04065-2015.

References

[1] Cusimano et al., 2013. *PloS One*. 8(3), e58868–e58868.
[2] McCrory et al., 2017. *Br J Sports Med*. 51(11), 838–847.
[3] Allison et al., 2015. *Ann Biomed Eng*. 43(8), 1896–1906.
[4] Campbell et al., 2016. *Ann Biomed Eng*. 44(4), 1246–1256.
[5] Knowles et al., 2017. *J Appl Biomech*. 33(1), 2–11.
[6] Potvin et al., 2019. *J Biomech*. 91, 43–50.
[7] Laksari et al., 2015. *J. R. Soc. Interface*. 12(108), 20150331.

DESIGN OF A HONEYCOMB-LIKE BICYCLE HELMET FOR PREVENTION OF TRAUMATIC BRAIN INJURY

Annie King[1*], Adam Tyedmers, Sarah Gonder, Bosco Yu[1], Cheryl Quenneville[1]
[1]School of Biomedical Engineering, McMaster University, Hamilton, ON, Canada
email: *kinga12@mcmaster.ca

Introduction

Bicycle accidents are the leading cause of sports-related head injuries [1] and of these, concussions account for 42% [2]. Following a head impact, current foam helmets effectively mitigate translational kinematics (linked to skull fracture) but not rotational kinematics (associated with traumatic brain injury, TBI). A new helmet design that uses hexagonal honeycomb with pentagon-heptagon 'defects' (known as 5-7 defects) is proposed and investigated for its potential to enhance protection. Honeycomb was chosen due to its superior energy absorption potential compared to foam. As well, honeycomb can be modified to specifically achieve the anisotropy that simultaneously protects against both minor and severe injuries. The design objectives are to (1) maximize energy absorption capacity, (2) reduce the peak force on the head below the injury threshold, and (3) minimize weight. Recent efforts have been made to design foam helmets with additional rotation-damping systems, such as MIPS; however, the use of an alternate material altogether is potentially more effective.

Methods

In the development of the helmet design, the inclusion of pentagons and heptagons was inspired by graphene grain boundaries and allows the structure to fit the curvature of the head [3]. An analytical model was developed according to injury thresholds for skull fracture and concussion to define constraints on the relative density of the honeycomb. Flat hexagonal honeycomb specimens were designed in nTopology and 3D-printed using a Creality CR10 fused deposition modelling printer with Thermoplastic polyurethane. Quasi-static in-plane and out-of-plane compression tests (Figure 1a) were performed using an Instron materials testing machine to obtain stress-strain data. In-plane properties (Figure 1a) were evaluated for three design variations (Figure 1b). The effectiveness of each design was evaluated using the volumetric energy absorption efficiency given by U_v/σ_{peak} [4]. In the theoretical 'ideal' case, this ratio would be approximately equal to the densification strain (ε_d) (Figure 1c). Out-of-plane shear testing (Figure 1a) is ongoing to determine an optimal honeycomb design for multi-directional protection.

Results and Discussion

The inclusion of 5-7 defects improved the mechanical properties of the honeycomb under in-plane compression. Design 3 (honeycomb with stacked 5-7 defects) had the highest U_v/σ_{peak} ratio of 0.51 (Figure 1b), where the theoretical maximum U_v/σ_{peak} would be 0.61. Video analysis revealed that design 3 induced stable, normal collapse of the hexagons, whereas design 2 induced unstable, shear collapse corresponding to sudden drops in stress that caused a reduction in U_v/σ_{peak}.

According to the analytical model using the injury threshold of skull fracture, the optimal design would maximize energy absorption capacity while reducing out-of-plane compressive peak stress below 5.32 MPa, corresponding to an upper limit on relative density of 37%. Accordingly, flat honeycomb specimens

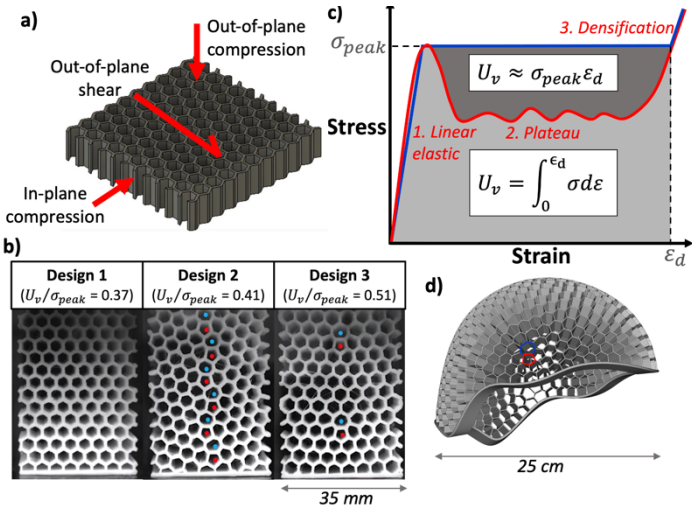

Figure 1: a) in-plane and out-of-plane loading directions; b) 3D-printed models of design 1 (regular honeycomb), design 2 (honeycomb with staggered 5-7 defects), and design 3 (honeycomb with stacked 5-7 defects), with experimental U_v/σ_{tr} ratios; c) typical stress-strain curve (red) and ideal stress-strain curve (blue); and d) full-scale helmet model

were successfully 3D-printed with relative density $\bar{\rho}$ of 21%. Stress-strain curves from preliminary out-of-plane compression tests exhibited three primary regimes: linear elastic (until peak stress was reached), stress plateau, and densification (Figure 1a). The effect of 5-7 defects on the out-of-plane compressive and shear properties will be determined to achieve the optimal honeycomb design for head protection.

The honeycomb design will be applied to a full-scale helmet (Figure 1d) that will be evaluated by measuring translational and rotational kinematics of a headform following impact.

In summary, a novel bicycle helmet design is proposed using hexagonal honeycomb with pentagon-heptagon (5-7) 'defects'. Honeycomb shows potential for head protection largely due to its anisotropy, where sufficient deformation is achievable in both the compressive and shear loading directions to offer mitigation of translational and rotational kinematics simultaneously. Results suggest that honeycomb geometry and arrangement of 5-7 defects can be modified to develop a design optimized for head protection.

Significance

A novel helmet design made of 3D-printed honeycomb with 5-7 defects can accommodate the curvature of the head while also potentially improving the mechanical properties. The bicycle helmet design demonstrates potential improvement over current foam helmets to effectively protect against both skull fracture and TBI, by mitigating the translational and rotational kinematics of the head following impact.

References

[1] National Electronic Injury Surveillance System (NEISS)
[2] E. J. Alfrey *et al.*, 2021 *J. Surg. Res.*, vol. 257
[3] C. Ophus *et al.*, 2015 *Phys. Rev. B*, vol. 92
[4] B. Yu *et al.* 2018 *Mater. Sci. Eng. A*, vol. 716

Identifying predictive variables for levels of Brain Trauma in Youth Ice Hockey

Thomas Hoshizaki*, Andrew M. Post[2,3], Clara Karton[2], Michael Robidoux[2], Blaine Hoshizaki[2] and Michael Gilchrist[3]
[1]Injury Biomechanics and Aging Laboratory, University of Waterloo, ON, Canada
[2]Neurotrauma Impact Science Laboratory, University of Ottawa, ON, Canada
[3]School of Mechanical and Materials Engineering, University College Dublin, Republic of Ireland
email: tbhoshiz@uwaterloo.ca

Introduction

Brain trauma is a concern in youth ice hockey due to its potential short and long term negative effects on brain health. Improved helmets are one method of reducing the magnitude of brain strains from impacts to the head in youth ice hockey. However current standards use adult impact parameters with linear acceleration as the performance metric; a metric with low correlations to strains in the brain tissue linked to concussion and repetitive brain trauma. As a result, current youth helmets are not tested to youth parameters of mass, velocity, and compliance, and use test metrics that are not associated with brain trauma. To improve helmets for youth ice hockey players and to reduce risk of brain trauma, methods must be developed to impact the helmet in ways that commonly occur when they play ice hockey. Also, youth specific test metrics must be developed; metrics that have a high association with strain in the brain tissues for youth players. Peak, duration, time to peak, slope to peak and integral of head impact acceleration curves as well as Gadd Severity Index (GSI) and Head Injury Criterion (HIC) represent unique dynamic response characteristics associated with brain tissue strain[1]. Understanding the relationship between impact events and these associated dynamic response characteristics for competition level and age provides a guide to improve head trauma management in youth ice hockey. The purpose of this research was to examine the relationship between these curve characteristics for youth ice hockey reconstructions to identify the kinematic variable with the highest association with maximum principal strain (MPS) in the brain tissues for three levels of play: Initiation (U6); Competitive, non-contact (U8, U10, U12); and Competitive contact (U15, U18).

Methods

Video analysis: Ice hockey game videos were analyzed for head contact events such as head-to-head, head-to-shoulder, head-to-elbow, head-to-hand/punch, head-to-ice, head-to-glass, head-to-boards, and other. The head contacts were also categorized by impact location, and velocity was determined through Kinovea analysis (Kinovea 0.8.20, 2016). Thirty games of each level were analyzed and separated into 3 groups: initiation (U6) competitive non-contact (U8, U10, U12), and competitive contact (U15, U18).

Laboratory reconstruction: All head impact events (except for "other") were reconstructed in the laboratory. Head impacts were reconstructed using an appropriately sized helmeted Hybrid III headform (6yo, 5th, or 50th) depending on age group. The headforms were equipped with accelerometers in a 3-2-2-2 array for the three-dimensional measurement of kinematics for each impact event at 20 kHz using a DTS collection module and filtered using a CFC 180 filter. The helmet used was of similar model to those used by the youth ice hockey players, which had a VN impact liner and cage. The collision events (elbow, shoulder, punch, and head-to-head) used a pendulum or linear impactor system with an appropriate surrogate striker to reflect the compliance of the event. The events where the youth player impacted an immobile object (head-to-ice, boards, glass) used a monorail drop rig with an ice, boards, or glass anvil. The impacts produced the linear and rotational acceleration time histories that were used as input for finite element (FE) modelling of the human brain to determine the MPS. A 6 year old FE model was used for the Initiation group [2], with a scaled down version of the University College Dublin Brain Trauma Model[3] used for the other groups. The MPS results were classified into the following levels of brain trauma: Very low (<0.08), Low (0.08-0.169), Medium (0.17-0.259), High (0.26-0.349), and Very High (>0.35). These categories were based upon research in injury biomechanics that identified relationships between physiological brain responses to axonal stretch and reported concussion, sub-concussion, and clinical outcomes[1].

A linear regression analysis was used to establish the relationship between the dynamic response characteristics of the head impacts with brain tissue strain within each brain trauma category.

Results and Discussion

Competitive, non-contact

Strain category	Event type (sample size)	Variable with highest R^2	R^2
Very low (0-8%)	Ice (3)	GSI	1.00
	Boards (21)	Peak resultant rotational acceleration	0.708
	Glass (8)	Peak y-axis rotation	0.501
	Elbow (41)	Velocity	0.776
	Head (18)	Peak resultant rotational acceleration	0.856
Low (8-16%)	Ice (7)	Peak resultant rotational acceleration	0.745
	Boards (11)	Peak resultant rotational acceleration	0.617
	Shoulder (18)	Peak z-axis linear acceleration	0.556
	Head (6)	Duration x-axis linear	0.988
Medium (16-26%)	Boards (4)	HIC	0.971

Competitive, contact

Strain category	Event type (sample size)	Variable with highest R^2	R^2
Low (8-16%)	Ice (6)	Peak resultant rotational acceleration	0.874
	Boards (8)	Velocity	0.564
	Glass (12)	Peak resultant rotational acceleration	0.383
	Shoulder (13)	Peak y-axis rotational acceleration	0.415
	Elbow (9)	y-axis linear acceleration duration	0.633
	Head (9)	Resulant rotational acceleration duration	0.602
Medium (16-26%)	Boards (4)	Velocity	0.986
	Elbow (4)	Peak x-axis linear acceleration	0.921

Figure 1: Linear regression results for the competitive, non-contact and competitive, contact categories.

Rotational acceleration metrics had the highest association with MPS for each category examined in this research (Figure 1). The relationship between kinematic variables varied by strain magnitude level as well as event type, suggesting that efforts to develop a test metric for the evaluation of youth ice hockey helmets need to be specific to brain trauma mechanisms. This data demonstrates that the impact data within each age category is unique, and as a result suggests that helmet technologies specific to competitive level needs to be developed.

Significance

This research indicates that metrics to evaluate the protective capacity of youth ice hockey helmets must be focused on rotational characteristics as well as age and competitive level.

Acknowledgments

This research was supported by NSERC and CCM Hockey.

References

[1] Post et al., 2012. *J Sport Eng Tech*. 226(P3-4).
[2] Koncan et al., 2019. J Sport Eng Tech. 233(2), 277-291.
[3] Horgan et al., 2004. IJCrashworthiness. 9(4), 401-418.

TWO DETERMINANTS AFFECTING THE LINK BETWEEN INJURY AND NOCICEPTION IN THE LOW BACK

Daniel Viggiani, Fasih Ahmad Rahman. Jeffery M. Barrett, Joe Quadrilatero, and Jack P. Callaghan
Department of Kinesiology and Health Sciences, University of Waterloo, Waterloo, ON, Canada
email: dviggian@uwaterloo.ca

Introduction

Low back pain is often assumed to have a mechanical origin to motivate studies on low back injuries and to guide its treatment. However, low back pain is distinct from, but often related to, the nociceptive activity in the periphery that precedes tissue damage or injury in the low back [1]. Our purpose was to apply a mechanism-based model that predicts nociceptive activity in the brainstem based on tissue loading to identify scenarios that can disrupt the presumed link between mechanical loads and low back pain. We present two cases: a simulated pressure-pain threshold exposure following a repetitive trunk flexion task and two injuries to the annulus fibrosus of the intervertebral disc.

Methods

A model of tissue loading and nociceptive neural activity was used to predict the likelihood that two sets of exposures could lead to low back pain. The first set examined pressure-pain thresholds before and after a 10-minute repetitive flexion task; the second set examined two types of annulus fibrosus tensile failure: high-stress and low-stress. The model computed tissue stresses from displacements and cross-sectional areas, which were converted into neural activity and fed into a nociceptive circuit involving the spinal cord and brainstem. This culminated in a decision that discerned what percentage of healthy individuals could find those tissues stresses painful, labelled $\Lambda_{\%}$.

Pressure-pain threshold data were collected from 37 healthy adults (19 female, 18-35 years old) before and after a 10-minute repetitive flexion task as reported in [2]. Pre-flexion peak stresses were fit to a Gumbel distribution and used to generate smoothed tent functions to permit continuously scalable simulated pressure-pain threshold stress-time curves. This same distribution also informed mechanical sensitivities used to compute $\Lambda_{\%}$.

Tissue properties and failure profiles were derived from displacement-controlled uniaxial failure tests of cadaveric posterior lumbar annulus fibrosus specimens (n=4). High-stress failures involved a 20-cycle pre-load to 5% strain followed by a single failure test, and the resulting load-displacement curves were normalized into stress-strain curves [3]. Low-stress failures involved taking the high-stress failure stress-strain approximations and increasing the cross-sectional area by a factor of 4 to reflect the failure stresses seen in chronic disc injuries [4].

Western blotting for PGP9.5 was performed on cadaveric skin (n=5) and outer annulus (n=4) from the lumbar spine to determine the relative innervation densities of both tissues. Relative protein contents informed a set of equations adapted from [5] to convert time-varying tissue stresses into electrical currents that drove a nociceptive neural activity model.

The nociceptive neural activity model consisted of ten modified Hodgkin-Huxley neurons and a brainstem decision algorithm. Eight of the ten neurons formed a simplified "base" circuit permitting temporal summation, tonic inhibition, and nociceptive gating; the other two neurons allowed for creep-related facilitation and exercise-induced hypoalgesia to reflect the post-repetitive flexion state for the pressure-pain threshold case. The membrane voltage of the end-target neuron in the brainstem was used to determine if the ensuing activity could be experienced as painful based on minimum duration (0.5 seconds) and firing rate (21 Hz) criteria [6].

In the pressure-pain threshold case, 100 pressure-pain threshold "tests" were applied to the "base" model using the pre-flexion distribution. 100 more tests sampled from this same distribution were then re-applied after activating the creep- and exercise-neurons, reflecting neurological changes post-flexion from [2]. In the annulus failure case, both the high- and low-stress failures were applied to the "base" model 100 times. Each instance used the same time-stress profile (either high or low stress) but sampled a different mechanical sensitivity. $\Lambda_{\%}$ was the percentage of simulations where the brainstem neuron was active for at least 0.5 seconds at a rate of at least 21 Hz for all four simulation sets.

Results and Discussion

Median pressure-pain thresholds before the flexion exposure were 0.84 MPa (range: 0.39 – 2.22 MPa) and were increased by 12.6% (range: 6.1% – 31.0%) post-flexion. Reapplying the pre-flexion stresses in a post-flexion state reduced $\Lambda_{\%}$ from 100% to 0% (Table 1). The increased pressure-pain thresholds following the repetitive flexion task rendered all the previously painful tissue loads not painful.

The high- and low-stress annular failure stresses were 6.9 and 1.7 MPa, respectively. PGP9.5 concentrations in the outer annulus were 7.5% (range: 1.2% – 11.7%) that of the overlying skin. Scaling inputs based on relative protein content produced nociceptive activity in 88% of the high-stress failure simulations; this was reduced to 0% for the low-stress failures (Table 1). The purpose of artificially increasing annulus cross-sectional areas was to represent a failure scenario following a chronic or repetitive exposure, as is expected following flexion-related disc herniations [4]. However, the high-stress failure having a $\Lambda_{\%} < 100\%$ demonstrates that up to 12% of people may not find catastrophic annular ruptures painful due to its poor innervation.

Table 1: Predicted Nociceptive Ratios ($\Lambda_{\%}$)

Case	Condition	$\Lambda_{\%}$
Pressure-Pain Threshold	Pre-Flexion	100%
	Post-Flexion	0%
Annular Failure	High-Stress	88%
	Low-Stress	0%

Significance

The assumed link between tissue loading and low back pain can be disrupted following repetitive flexion or in chronic injury scenarios. Other outcomes from loading-induced damage such as inflammation or central sensitization may contribute more to low back pain development than the damage itself in these scenarios.

References

[1] Raja et al, 2020. *Pain* 161: 1976-1982.
[2] Viggiani & Callaghan, 2021. *JEK* 57: 102531.
[3] Barrett & Callaghan, 2018. *J Biomech* 66: 175-179.
[4] Parkinson & Callaghan, 2009. *Clin Biomech* 24: 148-154.
[5] Gerling et al., 2018. *PLoS Comput Biol.* 14(6): 1006264.
[6] Libet et al, 1991. *Brain* 114(4): 1731-1757.

BRAIN ACTIVATION DURING DIRECT MUSCULOSKELETAL SENSORY STIMULATION OF THE TRUNK

Sheri P. Silfies[1], Jennifer M.C. Vendemia[1], Courtney M. Butowicz*[1]
[1]Applied Neuromechanics Lab, University of South Carolina
Email: butowicz@mailbox.sc.edu

Introduction

Low back pain (LBP) is a major health concern worldwide and is the most rapidly growing medical reason for disability and impaired quality of life [1]. LBP may affect up to 40% of adults annually with a lifetime prevalence of 65-80% [2]. Clinical evidence indicates sensory changes in tactile acuity exist in persons with LBP, suggesting changes in organization of the primary somatosensory cortex (S1) [3,4]. Yet, the neurophysiological effects of sensory stimuli on the cortical and subcortical regions of the brain associated with sensorimotor integration and organization are currently unknown.

Thus, the objective of this study was to validate a methodology for localizing back stimulation to the upper-, lower-thoracic and lumbar region utilizing a novel pneumatic trunk sensory localization system developed for use in functional magnetic resonance imaging (fMRI).

Methods

Eighteen right-hand dominant subjects (7 female; age: 28±8 years; mass: 71.8±16.3kg; height: 171.8±11.5cm) without LBP were recruited for this study. A pneumatic trunk sensory localization system was developed to directly stimulate bilateral thoracic and lumbar muscles. The system directs regulated airflow from an air pressure tank to one of twelve tactors on a custom-designed localization mat. Participants laid supine on a custom mat with 12 pressure stimulators, positioned bilaterally at the upper (4), lower (4) thoracic, and lumbar (4) regions.

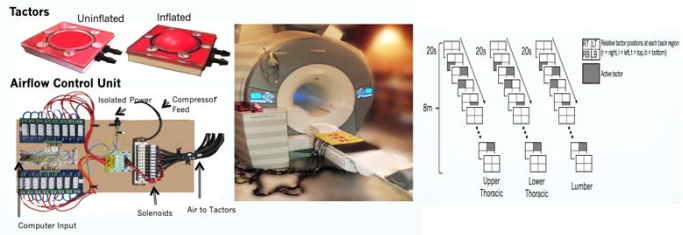

Figure 1: Left: Tactor and control system. Middle: Tactor mat in MR environment used to position tactors on each subject. Right: Illustration of 3 randomly assigned runs for each region with activated tactors represented in grayscale.

MRI scans were collected on a 3T Siemens PRISMA scanner with a 20-element head coil. During the fMRI, tactors stimulated three sensory regions across three randomly assigned runs. Each run (8min) randomly activated one of the four tactors in the respective region in 20s cycles (Fig. 1). Tactors provided a somatosensory stimulation of ~13.7-15.1N. Motion correction was done through independent components analysis-automatic removal of motion artifacts (ICA-AROMA). First-level analyses were conducted on pre-processed data using a fixed-effects model with identification of active clusters during the stimulation ($Z>2.3$; $p<.05$, cluster corrected for multiple comparisons). As few studies have investigated cortical activation related to stimulation of the back, higher-level analyses were conducted on the whole brain using a random-effects model. Follow-up analyses of significant clusters were conducted to localize significant regional activity.

Results and Discussion

Patterns of activation differentiated between anatomic regions of the back, and within these regions, clear differences between brain hemispheres existed. Tactors created a stimulus that discriminated between left and right-sided stimulation within the lumbar region. Stimulation produced activation of brain regions associated with the proprioceptive system (Fig. 2).

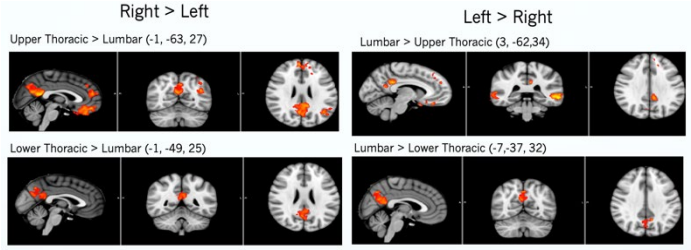

Figure 2: Comparing the effect of stimulations across participants reveals hemispheric shift in relative activity in the intraparietal parietal region associated with sensory activity within the proprioceptive system on the right vs. left sides of the body.

These data are consistent with activation of the postcentral gyrus (somatosensory cortex (S1); vibration, proprioception, and fine touch from body wall) processing region of somatic stimuli while localization of the stimuli on the body surface is associated with anterior and temporal, intra-parietal regions. If the stimulation is deep enough to influence muscle spindles in the back muscles, we would expect to see relative activation associated with proprioceptive activity on the intraparietal lobule (Fig. 2).

Significance

A novel pneumatic trunk sensory localization system produced localized cortical activation. Activation of brain regions associated with the proprioceptive system, regional S1 processing of somatic stimuli, and localization of the stimuli on the body surface suggest this system may be a valid mechanism to investigate if sensory impairments of back regions exist in persons with LBP. The system provides an MR-compatible method to record real-time brain activation associated with sensory stimuli in the posterior trunk region.

Acknowledgments

This work was funded by the National Institutes of Health under award #R01HD095959.

References

[1] Wu et al., 2020. *Ann of Translational Med*. 8(6).
[2] Deyo et al., 2006. *Spine*. 31:2724-7
[3] Luomajoki et al., 2011. *BJSM*. 45:437-40
[4] Flor et al., 1997. *Neuroscience letters*. 224:5-8.

HEAD SUPPORTED MASS, MOMENT OF INERTIA, NECK LOADS AND STABILITY: A SIMULATION STUDY

Jeff M. Barrett[1], Laura A. Healey[2], Colin D. McKinnon[3], Andrew C. Laing[1], Clark R. Dickerson[1], Steven L. Fischer[1], and Jack P. Callaghan[1]
[1]Department of Kinesiology & Health Sciences, University of Waterloo, Waterloo, Ontario, Canada
[2]Puma SE, Innovation, Somerville, Massachusetts, USA
[3]3MotionAI, Inc., Hamilton, Ontario, Canada
email: jeffery.barrett@uwaterloo.ca

Introduction

Occupations or activities where donning head supported mass (HSM) is commonplace tend to put operators at an elevated risk of chronic neck pain. Yet, there is no consensus about what features of the HSM influence the relative contributions to neck loads. Therefore, this investigation tested three potential hypotheses: (i) HSM increases the gravitational moments incurred during awkward postures; (ii) more muscle activation is required to stabilize the head with HSM; and (iii) the added moment of inertia (MOI) from HSM increases neck loads during rapid head repositioning tasks.

Methods

We performed a sensitivity analysis on C5-C6 compressive forces calculated from a 24-degree of freedom cervical spine model [1] in OpenSim for both static and dynamic movements. For static trials [2], the magnitude of HSM was varied between 0 and 8 kg in 20° of lateral bending, 30° of extension, 45° of flexion, 45° of axial rotation, and a neutral posture (Figure 1A-E, respectively). Additionally, a novel stability constraint, similar to [3], was added to the static optimization routine to quantify the additional compression required for stability. For dynamic trials [4], the mass and MOI was varied as the model moved through extension, flexion, or right-to-left axial rotation (Figure 1F-H, respectively).

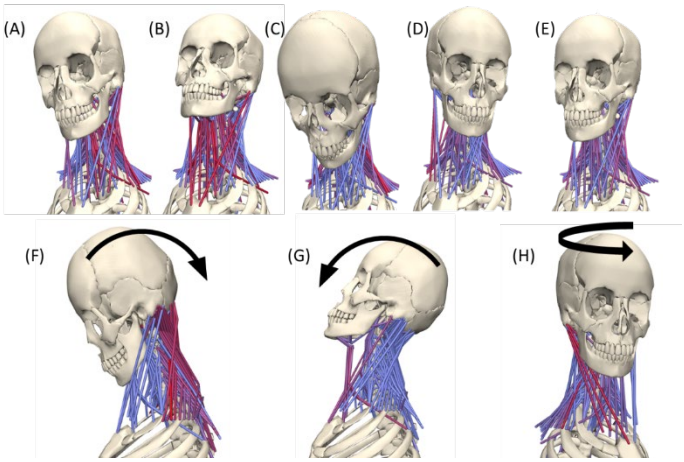

Figure 1: (A)-(E), the static postures tested in this investigation. (F) Rapid head extension from flexion; (G) Rapid head flexion from extension, and (H) rapid head twisting from right-to-left.

Results and Discussion

HSM magnitude and compression were linearly related for both static and dynamic trials, with amplification factors varying between 1.9 and 3.9 (Figures 2 and 3), which supported hypothesis (i). The relationship between peak compression and MOI in dynamic trials was generally nonlinear in twisting (Figure 3), and only weakly supported hypothesis (iii). The stability constraint generally resulted in larger magnitudes of compression with larger amplification factors as well, which supported hypothesis (ii).

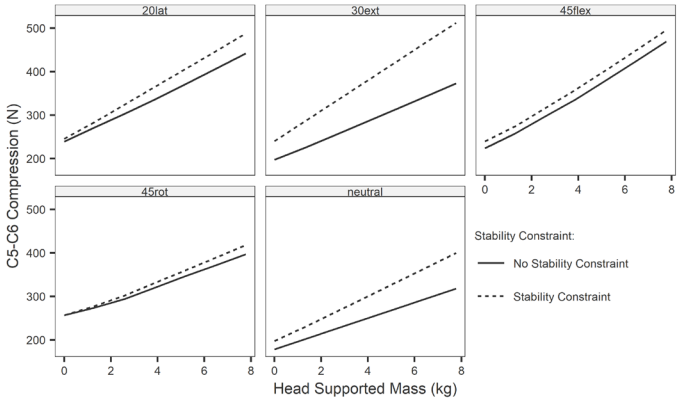

Figure 2: C5-C6 compression against head-supported mass for the five postures tested with (dashed) and without (solid) the stability constraint.

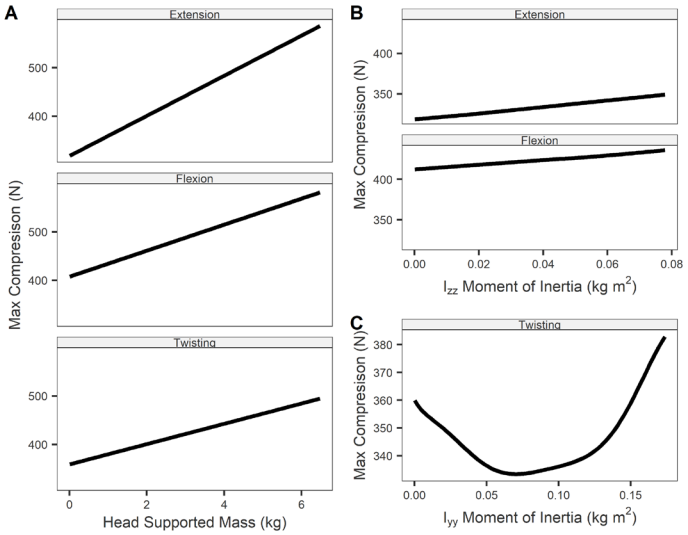

Figure 3: Maximum C5-C6 compression with respect to HSM (A), and moment of inertia (B) and (C) for dynamic extension, flexion and axial twisting movements.

Significance

This investigation supported hypotheses (i) and (ii) but found little evidence for (iii). The magnitude of HSM was the most significant contributor to increased loads in the cervical spine.

Acknowledgments

The authors acknowledge funding received from NSERC.

References

[1] Barrett et al. 2021. *J Appl. Biomech.* 37(5): 481-493.
[2] McKinnon et al. 2016. *Occup. Ergon.* 13(3):119-130
[3] Akhavanfar et al. 2019. *JBiomech.* 91: 61-68.
[4] Healey et al. 2021. *Aerosp. Med. Hum. Perform.* 92:172-181.

A COMPARISON OF FEEDFORWARD METHODS FOR CONTROL OF THE TRUNK AFTER SCI

Aidan R. W. Friederich[1*], Musa L. Audu[1], Ronald J. Triolo[1]
[1]Department of Biomedical Engineering, Case Western Reserve University, Cleveland, Ohio, USA
*email: Aidan.Friederich@case.edu

Introduction

Spinal cord injuries (SCI) at or above the thoracic level can impair seated stability due to paralysis of trunk and hip muscles. Application of a constant level of functional neuromuscular stimulation (FNS) has been shown to improve seated balance and facilitate activities of daily living [1]. However, constant stimulation is unable to respond to perturbations or enable leaning postures, which require a combination of feedforward and feedback control. Determining feedforward commands is complicated by the muscle redundancy problem, where an infinite combination of muscles can be used to accomplish a task. Some form of optimization is required, which complicates real-time implementation. Recent techniques have been shown to enable arm reaches with FNS by determining feedforward activations from subject specific models. The first method uses a nonlinear solver to minimize the activations [2]. The second method uses a quasi-Newton optimization method [3]. Lastly, Razavian *et al.* [4] first determined muscle synergies from optimal results prior to deriving feedforward commands. In this study we evaluated the feasibility of these methods for controlling the human trunk.

Methods

One participant with SCI (C5, AIS C) consented for this study. Asymmetrical charge balanced surface stimulation (100 mA, 20 hz) was applied bilaterally to their erector spinae (ES), quadratus lumborum (QL), gluteus maximus (GX), and hamstring (HS) muscles. The subject sat upright in a custom device that held their trunk and transferred applied moments to a load cell (JR3 Inc., Woodland, CA) [5]. The load cell was aligned with the S1 vertebrae allowing measurement of pitch (extension/ flexion) and roll (lateral bending) moments across the S1-L5 joint. Stimulating current was delivered three times to each electrode one at a time, and the resulting moments generated by the contracting muscles were measured. Stimulus pulse duration values were based on subject comfort or hardware limits (250 µs).

The mean moments produced by each muscle were arranged into a (2x8) matrix M where the two rows refer to the roll and pitch joint moments produced by the 8 muscle groups. From this, any desired (feedforward) joint moments (M_{des}) can be obtained by scaling the muscle moment matrix with the activations (a) as shown in equation (1).

$$[M_{des}]_{2x1} = M_{2x8} a_{8x1} \quad (1)$$

The desired feedforward command (M_{des}) was set to 10 Nm in directions behind the subject. Activations (a) were optimized with a nonlinear solver by minimizing the activation matrix norm with the constraint that Equation 1 must be true [2]. We compared that with the quasi-Newton optimization method shown in [3] and the synergy method shown in [4]. The computation time, root mean squared error (RMSE), and the sum of the activation norms were calculated and compared to the optimal solution. Computation time was obtained with Matlab's *timeit* command on a small computer (i5-4670k, RX480).

Results and Discussion

Figure 1 shows the feedforward activations determined by the optimal, quasi-Newton, and synergy approaches to produce a 10 Nm force in the target directions. A solution was unable to be found for directions greater than 150°. The quasi-Newton and synergy methods follow a similar pattern of the nonlinear optimal method, with slightly more deviations in the quasi-Newton method. The quasi-Newton method resulted in reduced RMSE of the predicted moment determined from the activations with Equation 1, than the other strategies (Table 1). However, total activation values were lowest with the nonlinear solver strategy. Reducing activations is important for reducing fatigue. The synergy method resulted in the largest error, however the execution time was two orders of magnitude lower than either method. Without further optimization or improved hardware, the nonlinear solver and quasi-Newton method would be difficult to calculate in real-time.

In this study we compared three methods of solving the muscle redundancy problem for feed-forward control of seated posture. All three methods both had comparable levels of muscle activations and error. However, the synergy method had faster computation time making it an attractive candidate for real-time feedforward control.

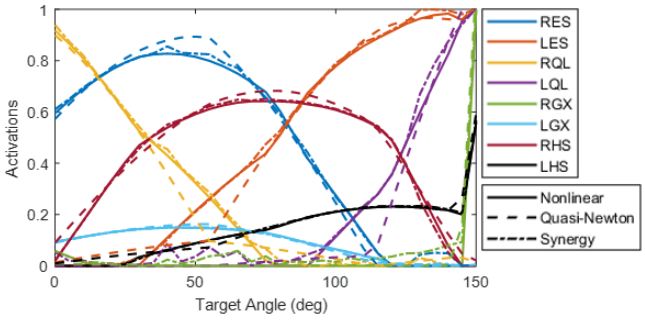

Table 1: Outcome measures from the optimal, quasi-Newton, and synergy methods.

	Total Activation	Pitch RMSE (Nm)	Roll RMSE (Nm)	Execution Time (s)
Nonlinear	40.13	0.023	0.003	0.0453
Quasi-Newton	41.23	0.001	0.001	0.0527
Synergy	41.71	0.452	0.409	0.0007

Significance

This study is an important step to implementing real-time feedforward control on the human trunk with FNS. When combined with feedback control, the system should enable individuals with SCI to lean their trunk to any position effectively expanding their workspace and increasing independence.

Acknowledgments

Funding: NIH (R01NS101043 and T32EB004314), and DOD SCIRP (W81XWH-17-1-0240). Resources: APT Center in the Louis Stokes Cleveland VA Medical Center.

References

[1] Triolo *et al.*, 2013. Arch Phys Med Rehabil 94(9) [2] Schearer *et al.*, 2013 IEEE T Neur Sys Reh. 22.3 [3] Wolf *et al.*, 2020. ICRA [4] Razavian *et al.*, 2019 J. Biomech. Eng. 141.3 [5] Friederich *et al.*, 2020 IEEE. Trans. Biomed

PORCINE VERSUS HUMAN CADAVER VERTEBRAL JOINT PROPERTIES: A COMPARISON OF ROTATIONAL AND TRANSLATIONAL NEUTRAL ZONE CHARACTERISTICS

Kayla M. Fewster[1], Jackie D. Zehr[2] and Jack P. Callaghan[2]
[1]School of Kinesiology, The University of British Columbia, Vancouver BC, Canada
[2]Department of Kinesiology and Health Sciences, University of Waterloo, Waterloo, ON, Canada
email: kayla.fewster@ubc.ca

Introduction

In vitro lumbar spine testing is necessary for the evaluation and understanding of injury mechanisms. Human cadaver specimens would typically provide the best option for biomechanical testing, however, issues such as age, bone integrity and disc degeneration pose a significant limitation in the use of cadaver specimens. Porcine cervical functional spinal units (FSUs) are frequently used as surrogates for the human lumbar spine due to their anatomical and functional similarities, coupled with the enhanced control over potential confounding factors that can impact the mechanical integrity of tissues surrounding the intervertebral joint (e.g. age, diet, physical activity).

While mechanical comparisons between the porcine cervical spine and the human lumbar spine have been heavily researched, most of such comparisons have focused on ultimate failure tolerance limits as well as failure injury mechanisms [1-2]. However, in terms sub-failure loading and understanding lumbar soft tissue injury potential and progression, the neutral zone (NZ) is typically a more sensitive measure for passive tissue injury [3]. Given that limited work has focused on porcine versus cadaver mechanical comparisons under low loading magnitudes, the purpose of this work was to compare rotational and translational NZ properties across porcine and human cadaver FSUs while under physiological compressive loading.

Methods

Sixty-four porcine FSUs (29 C3C4; 35 C5C6) and five human lumbar FSUs (age range: 85-94) underwent rotation range of motion testing (ROM) in position control (±8Nm moment applied at 0.5°/s) followed by translation ROM testing (±400N shear load applied to the caudal vertebra at 0.2mm/s) while simultaneously exposed to 300 N of compression. Moment-angle curves from flexion-extension ROM testing were created to quantify flexion-extension NZ stiffness, NZ limits and total NZ range. Force-displacement curves from anterior-posterior (AP) translational ROM testing were created. Force-displacement data were divided into two phases for separate analysis: (1) from peak posterior displacement of the inferior vertebra to peak anterior displacement of the inferior vertebra (Phase 1) and (2) peak anterior displacement to peak posterior displacement (Phase 2). For each Phase, translational NZ stiffness as well as NZ limits and NZ range were calculated. The mean differences between NZ stiffness, NZ limits and NZ range were assessed in both rotation and translation with a paired t-test at an *a-priori* level of significance (α) of 0.05.

Results and Discussion

For rotational ROM testing no significant difference in NZ stiffness was observed across porcine and human cadaver FSUs (Porcine = 0.10 Nm/degree, Cadaver = 0.36 Nm/degree). A significant difference in NZ range was observed ($p = 0.002$). Human cadaver FSUs displayed a significantly shorter NZ range in comparison to porcine (Figure 1). This was directly attributable to a significantly a greater extension NZ limit in the porcine specimens in comparison to human cadaver. No significant differences in the flexion NZ limit were observed.

For Phase 1 and 2 of translational ROM testing no significant differences were observed between porcine and human cadaver specimens for NZ stiffness, NZ Range or NZ Limits (Table 1)

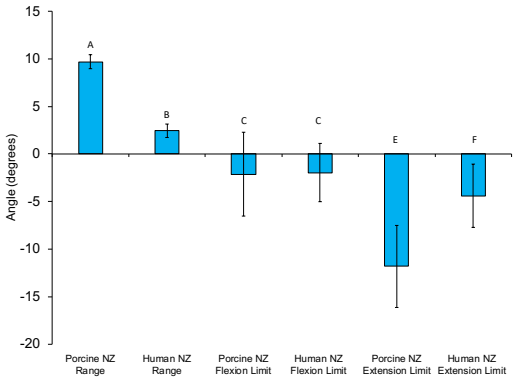

Figure 1: Rotational NZ Range and Flexion and Extension NZ limits for porcine and cadaver specimens. For NZ limits, a negative value indicates extension while a positive value indicates flexion. Standard deviation bars are displayed with a different letter donating a significant difference across measures.

Table 2: Translation NZ stiffness, NZ range and limits for porcine and human cadaver specimens. No significant differences were observed.

		NZ Boundary 1 (mm)	NZ Boundary 2 (mm)	NZ Length (mm)	NZ Stiffness (N/mm)
Phase 1	Porcine	2.28	-3.34	5.62	24.95
	SD	1.25	1.23	0.56	4.69
	Human	2.97	-3.21	6.18	22.34
	SD	2.13	1.74	1.79	7.34
Phase 2	Porcine	1.86	-3.52	5.38	22.66
	SD	1.16	1.25	0.49	4.53
	Human	3.39	-5.09	8.48	26.10
	SD	2.01	4.10	3.58	10.82

Significance

Results provide evidence that porcine and human cadaver FSUs mechanically behave similarly during translational ROM testing, justifying the use of porcine FSUs for sub-failure AP shear exposures. However, results also display that porcine FSUs have a significantly greater rotational NZ range, attributable to a greater extension NZ limit. Indicating that passive tissue resistance in the human cadaver specimens occurred at a much lower extension posture in comparison to porcine. However, given the advanced age of the human cadaver specimens, it is unknown if this difference is directly attributable to species difference or any potential age-related mechanical changes.

References

[1] Yingling et al., 1999. *J Spinal Discord Tech*. 12: 415-23
[2] Wilke et al., 2010. *Spine*. 35: E35-42
[3] Oxland & Panjabi., 1992 *J Biomech*. 25:1165-72

ESTIMATED MUSCLE GROUP FORCES ARE SENSITIVE TO MODELED MUSCLE GEOMETRIC COMPLEXITY

Jordan T. Sturdy,[1*] Pinata H. Sessoms,[2] and Anne K. Silverman[1]
[1]Department of Mechanical Engineering, Colorado School of Mines
[2]Department of Warfighter Performance, Naval Health Research Center
email: *sturdy@mines.edu

Introduction

Detailed models of the torso [e.g., 1] have been combined with lower limb models [e.g., 2] to yield full body models with the fidelity to analyze spinal loading [3,4]. While muscles in the lower limb are often represented by a single actuator, torso muscles are often represented by many actuators to represent broad physiological muscle attachments to multiple ribs or vertebral bodies. Optimization methods to find the muscle recruitment solution rely on cost functions, largely developed from walking simulations of the lower limbs, that minimize the sum of muscle activations raised to a power. Thus, the optimizer recruit fewer, stronger muscles rather than many, weaker muscles during movement. This approach may be problematic when the simplified lower limb and detailed torso musculature span the same joint. In full body models with lumbar detail, the hip joint may be spanned by many psoas actuators, which are important for lumbar joint loading, and single fiber representations of other hip flexors. Thus, the goal of this study was to compare how different levels of psoas muscle geometric complexity affected simulation results. We hypothesized that greater psoas complexity (i.e., multiple fiber representations) would result in less total psoas muscle recruitment, requiring greater force from other hip flexors such as iliacus and rectus femoris.

Methods

Three models were used for this analysis. First, a publicly available model with the psoas modeled as a single actuator [5] (1fiber) was selected as a baseline. This model was then combined with the torso from [1] with the psoas modeled as 11 actuators (11fibers). An intermediate model was developed by combining psoas actuators that attached to the same vertebral bodies, which resulted in 5 actuators (5fibers). In both the 11fibers and 5fibers models, the psoas was modified to attach to the femur identically to the 1fiber model. In addition, the optimal fiber and tendon slack lengths were modified to preserve the normalized fiber length in the default pose and fiber/tendon length ratios. The total strength of the psoas was identical for all models. Kinematic and ground reaction force data of 5 strides from a single participant (M, 38 yrs, 1.78 m, 88.0 kg) walking at 1.15 m/s was used to develop simulations with all models. For each walking trial, an inverse kinematics solution was obtained, residual reduction algorithm was performed, and a muscle solution was obtained through computed muscle control (OpenSim v3.3). Psoas muscle forces from all ipsilateral fibers were summed for model comparison. Peak muscle forces were calculated for psoas, iliacus, rectus femoris, adductor longus, gastrocnemius, and soleus for each stride.

Results and Discussion

Force output from the psoas muscle group was sensitive to the model definitions with the 5fibers and 11fibers models producing 77.4% and 86.2% less force than the 1fiber model (Figure 1). This more than 700 N discrepancy in psoas force required compensatory force production from other hip flexors (Table 1), with the greatest added contribution coming from adductor longus, which produced 47.9% and 55.7% more force in the 5fibers and 11fibers models compared to the 1fiber model. Rectus femoris produced ~8% more force in the 5fibers model and ~10% more force in the 11fibers model compared to 1fiber. Iliacus force increased with psoas complexity, but was already near full activation in the 1fiber model and was limited to <6% greater force contribution. In addition, the greater force production from biarticular hip flexors in the 5fibers and 11fibers compared to the 1fiber model resulted in greater gastrocnemius force to oppose the resulting knee extension moment, which also led to reduced soleus force (Table 1).

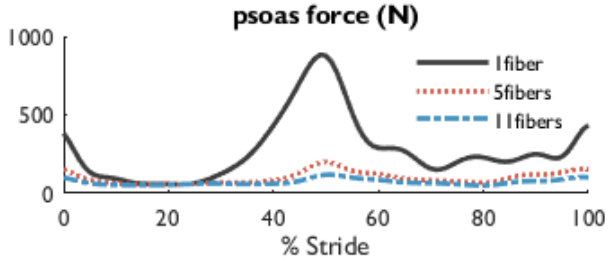

Figure 1: Net psoas force in Newtons produced for each model.

These results demonstrate that differing levels of detail within the same model can have large effects on model outcomes throughout the body. In addition, reducing the number of psoas actuators from 11 to 5 was not sufficient to restore hip muscle force contributions to a single actuator model.

Significance

Muscle and joint contact force estimates are sensitive to muscle geometric complexity when minimizing muscle activations in a movement optimization. Varying levels of muscle complexity within the same model will shift the muscle recruitment solution and cause unintended downstream effects to additional joints. Optimization cost function definition and model complexity should be considered together.

Acknowledgments

Data collection team: Paula Baluyut, Adam Bunn, Hedaya Rizeq, and Amy Silder.

References

[1] Christophy et al., 2012. *Biomech Model Mechanobiol.* 11:19-34.
[2] Hamner et al., 2010. *J Biomech.* 43:2709-2716.
[3] Actis et al., 2018. *J Biomech.* 68:107-114.
[4] Beaucage-Gauvreau et al., 2020. *J Biomech.* 100:109-584.
[5] Lai et al., 2017. *Ann Biomed Eng.* 45(12):2762-2774.

Table 1: Peak muscle force (N) produced by each muscle for the 3 different models. Mean (standard deviation) of 5 strides reported.

	psoas	iliacus	rectus femoris	adductor longus	gastrocnemius	soleus
1fiber	901.6 (111.4)	926 (33.2)	803.8 (71.6)	366.3 (39)	2982.4 (261.2)	2094 (134.1)
5fibers	203.4 (65.4)	977.1 (29.9)	873.2 (60.8)	541.6 (102)	3439.8 (156.1)	1889.7 (247.7)
11fibers	124.3 (35.4)	979.7 (30.8)	885.4 (58.6)	570.2 (113.2)	3451.8 (147.6)	1883.9 (255.1)

THE IMPACT OF HEAD-MOUNTED DISPLAY DESIGN FOR VR/AR ON CERVICAL SPINE LOADING

Amanda N. Astrologo[1*], Sarah Nano[1], Elizabeth M. Klemm[1], Sandra J. Shefelbine[1], and Jack T. Dennerlein[2]
[1]Northeastern University, Dept. of Bioengineering
[2]Northeastern University, Dept. of Physical Therapy, Movement and Rehabilitation Sciences
email: *astrologo.a@northeastern.edu

Introduction

The increasing use of head-mounted displays (HMDs) for virtual and augmented reality (VR/AR) has raised concerns about the musculoskeletal effects and potential risks of pain and discomfort in the cervical spine. Heavier HMDs (>1kg), such as night-vision goggles, are known to increase forces on the tissues of the cervical spine[1] with the potential to incite muscle fatigue[2] and induce pain[3]. Penumudi et al. (2020) examined the static, postural loading effects of a VR headset (<1kg) at different head flexion angles[4]; however, the loading effects during movement associated with headsets that have masses and inertias typical of these lighter VR/AR headsets have not been examined. Our hypothesis is that increased display mass and increased inertia through mass distribution of the HMDs increase torques due to both gravity and movement (dynamics) experienced at the occipitocervical joint (OC1) during various head movements. We also expect counterweights to decrease torques around the flexion/extension axis.

Methods

20 young adult (10f/10m) participants wore seven configurations of a custom-designed headset (mass = 235g). Four configurations consisted of different display masses at 3 cm in front of the eyes: 0g, 200g, 500g, 750g. Three configurations consisted of a 500g display mass at 7 cm in front of the eyes with varying counterweight (CW) masses placed behind the head: 0g, 333g, 500g. For each headset, participants performed four different movement types: slow and fast flexion/extension, slow and fast rotation. Inverse dynamics provided estimates of joint torques at OC1 from 3D position data of the head and torso. For each movement within each headset configuration and participant, we calculated the root mean square (RMS) value for each joint torque for the full duration of the movement (7-15 seconds). A repeated measures analysis of variance (RMANOVA), including a headset-movement type interaction, estimated least square mean values for each movement and headset configuration across the 20 participants. Tukey's post-hoc comparisons tested the hypotheses.

Results and Discussion

The results support the hypothesis that increasing display mass and increasing inertia increase torques. For flexion/extension tasks, increasing display mass significantly increased the gravitational torque component at both speeds. However, there was no effect on the dynamic component (**Fig. 1**). For rotation tasks, increasing display mass and increasing inertia through the addition of CWs significantly increased the dynamic component for fast movement but not for slow movement (**Fig. 2**). The dynamic component dominates during fast movement because it relies heavily on head acceleration. Gravity generates only a small torque because it acts in parallel to the rotational axis.

The results do not support the hypothesis that CWs decrease torques around the flexion/extension axis. Although, there was a significant decrease in the gravitational component for fast movement, there was also a significant increase in the dynamic component (**Fig. 1**). When examining the net joint torques about this axis for the same movement type, there were no significant differences among the three CW configurations.

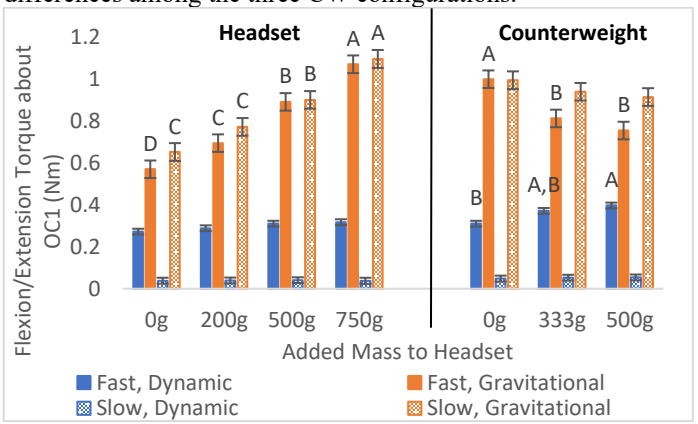

Figure 1. Flexion/extension torques at OC1. Values are least mean square from RMS values of both the gravitational and dynamic torque components about OC1 across participants. Error bars represent standard error. Within movement type and torque component, separated for the Headset and Counterweight groups, bars with the same letters and bars without letters are not significantly different from each other.

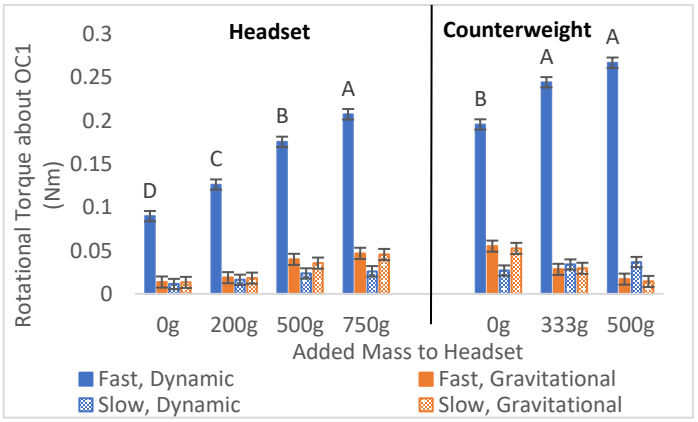

Figure 2. Rotation torques at OC1. See Figure 1 caption.

Significance

HMD design should minimize joint torques, such that cervical loading decreases, which, in theory, decreases the risk of injury. These results suggest that reducing display mass is the most effective way to reduce torques. They also suggest that adding CWs is not as effective for reducing torques.

Acknowledgments

This protocol was approved by the Northeastern University Office of Human Subject Research Protection. The study was funded in part by the Office Ergonomics Research Committee.

References

[1] Forde et al., 2011. *Int J Ind Ergonomics.* 41(2):128-135.
[2] Maithel et al., 2004. *Surg Endosc.* 19(3):406-411.
[3] Sakakibra et al., 1987. *Ergonomics.* 30(5):805-815.
[4] Penumudi et al., 2020. *Applied Ergnomics.* 84:103010.

Session 9

Thursday August 25, 2022

11:30am – 1:00pm

O9.1 – Aging

O9.2 – Sport Performance

O9.3 – Tissue Mechanics 3

O9.4 – Upper Limb 2

HOW DOES AGING IMPACT ANKLE STIFFNESS?

Kristen L. Jakubowski[1*], Daniel Ludvig[1], Sabrina S.M. Lee, and Eric J. Perreault[1]
[1] Department of Biomedical Engineering, Northwestern University
email: kristen.jakubowski@northwestern.edu

Introduction

With aging, there is a decreased ability to maintain balance when adapting to bumps, trips, or uneven terrains. Ankle stiffness plays a critical role in responding to such postural disturbances, with high stiffness being advantageous for balance as it provides greater resistance to unexpected disturbances. Ankle stiffness is strongly dependent upon the stiffness of the triceps surae and Achilles tendon. Aging has been associated with a decrease in Achilles tendon stiffness [1], and decreased muscle size and strength [1, 2], which could decrease the maximum achievable muscle stiffness. These musculotendon changes could readily affect ankle stiffness; however, their effect has not been quantified. Therefore, our objective was to investigate if there are age-related changes in muscle and tendon stiffness and determine how these influence ankle stiffness. We hypothesized that age-related changes in the muscle and tendon contribute to reduced ankle stiffness in older adults. Quantifying age-related changes in ankle stiffness, as well as the source of those changes, could lead to targeted interventions to improve balance in older adults.

Methods

Seventeen healthy young (27 ± 3 years) and 9 older (73 ± 7 years) adults were seated with their right foot rigidly secured to a rotary motor with the ankle positioned at 90°. Surface electromyograms (EMGs) were recorded from the tibialis anterior, lateral and medial gastrocnemius, and soleus. The muscle-tendon junction (MTJ) of the medial gastrocnemius muscle was imaged using B-mode ultrasound. During each trial, subjects maintained a voluntary isometric plantarflexion torque (0 - 30% of their maximum voluntary contraction (MVC) in 5% increments) with the aid of visual feedback. Visual feedback of tibialis anterior activity was also provided to prevent co-contraction.

To quantify ankle, muscle, and tendon stiffness, a rotary motor applied small, quick, stochastic perturbations to the ankle while ankle angle and torque were measured. From the measures of ankle angle, ankle torque, and MTJ displacement, we estimated ankle, muscle, and tendon stiffness [3]. Mixed-effects models were used for all statistical analyses.

Results and Discussion

Ankle, muscle, and tendon stiffness increased with plantarflexion torque (or force) for young and older adults (Fig 1). Across all levels of torque, older adults had a 10% decrease in ankle stiffness compared to young adults. However, counter to our central hypothesis, at matched levels of torque, we did not observe a significant difference in ankle stiffness between young and older adults (Fig 1A, p = 0.1). Similarly, both muscle and tendon were slightly stiffer across the range of torques in young adults (muscle: 8%; tendon: 11%), but neither of these differences reached significance (Fig 1B & C, muscle: p = 0.21, tendon: p = 0.09). This differs from previous studies that found an age-related decrease in tendon stiffness. However, these studies made comparisons at higher torque levels (up to 80% MVC) which may be less relevant to daily tasks such as standing and walking in which muscle activation typically remains below 30% MVC [4]. Our results indicate that age-related changes in tendon stiffness may differ depending on the tested level of plantarflexion torque.

While we did not observe group differences, a subset of older adults exhibited lower ankle stiffness than young adults (n = 5, Fig 1-open o's). Older adults were categorized as having lower ankle stiffness than young adults if their ankle stiffness values were lower than the 95% confidence intervals for young adults. The decrease in ankle stiffness in this subset of older adults was due to a decrease in tendon stiffness, which we were unable to explain by self-reported activity level, sex, or age.

Older adults' maximum voluntary plantarflexion torque was 37% lower than young adults (p=0.014). Since stiffness scales with torque, the decrease in strength in older adults decreased the maximum ankle, muscle, and tendon stiffness older adults could achieve. Consequently, older adults must exert more effort to achieve the same stiffness as young adults.

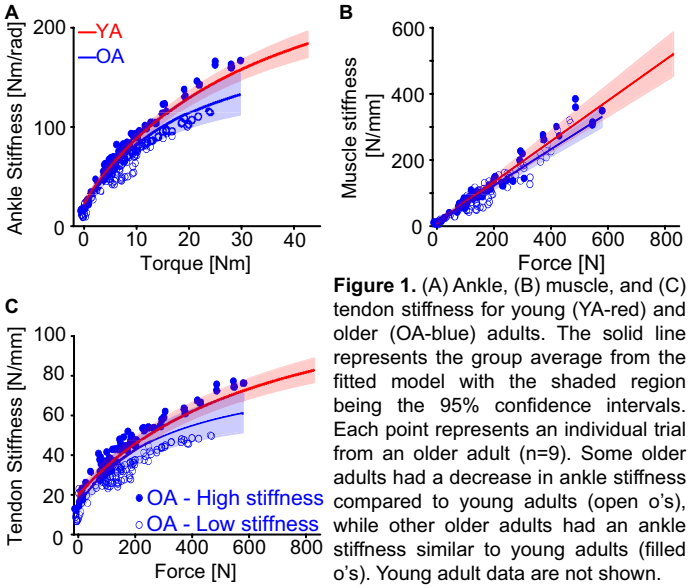

Figure 1. (A) Ankle, (B) muscle, and (C) tendon stiffness for young (YA-red) and older (OA-blue) adults. The solid line represents the group average from the fitted model with the shaded region being the 95% confidence intervals. Each point represents an individual trial from an older adult (n=9). Some older adults had a decrease in ankle stiffness compared to young adults (open o's), while other older adults had an ankle stiffness similar to young adults (filled o's). Young adult data are not shown.

Significance

Contrary to our central hypothesis, we did not observe an age-related decrease in ankle stiffness. However, our results indicate that there might be two groups of older adults: (1) those who maintain the mechanical properties of their tendon, and therefore, ankle, and (2) those that exhibit a decrease in tendon (and ankle) stiffness. Future work is warranted to determine the mechanisms leading to this heterogeneity in older adults. Determining what differentiates older adults with decreased ankle stiffness from those with similar ankle stiffness as young adults could provide insight into a mechanism contributing to impaired balance, which could ultimately aid in developing targeted interventions.

Acknowledgments

Supported by NIH F31AG069412 and ASB GIA

References

[1] Stenroth et al., 2012. *J App Phys*. 113. [2] Morse et al., 2005. *J App Phys*. 99. [3] Jakubowski et al., 2020. *Eng Med Biol Soc Ann*. [4] Nagai et al., 2011. *Arch Gerontol Geriat*. 53.

ALTERED MUSCULAR COHERENCE IS EVIDENT PRIOR TO CHANGES IN GAIT BIOMECHANICS

Francesca E. Wade[1,2*], Y. Choi[1], R. Seidler[1,3], D. Ferris[4], T. Manini[5], D. Clark[2,5], C. J. Hass[1,3] and E. Christou[1]
[1]Department of Applied Physiology & Kinesiology, University of Florida
[2]Brain Rehabilitation Research Center, Malcom Randall VA Medical Center, Gainesville, FL
email: *fwade21@ufl.edu

Introduction

Underlying neural drive to the lower limb muscles may be altered during gait due to aging, resulting in altered and more variable gait patterns. For example, older adults (OA) have lower ankle contributions to forward propulsion compared with young adults (YA) [1]. Further, OA exhibit greater step to step variability in many spatiotemporal gait parameters [2].

Electromyographic (EMG) coherence between two muscles can be interpreted as descending cortical drive to the motor neuron pool. Muscle synchrony in the Piper band (35 – 60 Hz) reflects changes to cortical input to the motor neuron pool; this is reduced in populations with impaired corticospinal pathways [3].

Here, we aim to investigate the neural control of steady state walking by understanding the common oscillatory drive to synergistic and antagonistic muscles in the lower limb in OA and YA and by investigating how neural control relates to gait variability metrics. We hypothesize that OA will have greater synergistic and antagonist coherence than YA, across the Piper frequency band, indicating greater cortical control of gait.

Methods

10 YA (age: 25 ± 1y) and 19 high-functioning (Short Physical Performance Battery Score > 10) OA (age: 75 ± 1y) walked across a 10m walkway at their "typical comfortable speed". Motion of reflective markers, placed according to Plug-in Gait model, was recorded at 100 Hz (Vicon, Oxford Metrics Inc.), while bilateral surface EMG (Trigno Avanti, Delsys Inc.) was sampled at 2000 Hz from the medial gastrocnemius (MG), tibialis anterior (TA), soleus (SO), rectus femoris (RF), vastus medialis (VM), and biceps femoris (BF). Data reported here are from the dominant limb. Spatiotemporal gait parameters were computed for all gait cycles, and stride length variability was quantified as the coefficient of variation in stride length across all gait cycles.

Cross-wavelet analysis on wavelet transforms for 4 muscle pairs (TA-SO, SO-MG, VM-RF, VM-BF) was performed. This analysis identifies the common oscillatory drive of two non-stationary signals, accounting for the relative strength of common frequencies from each signal:

$$W(s,\tau)^{XY} = W(s,\tau)^{X} W(s,\tau)^{Y*}$$

where $W(s,\tau)^{X}$ represents the Morlet wavelet transform of signal X(t), $W(s,\tau)^{Y*}$ represents the Morlet wavelet transform of signal Y(t), and $W(s,\tau)^{XY}$ represents the cross-wavelet transform of signal X(t) and Y(t).The sum of power in 35-60 Hz was calculated and normalized to total power across 0-100 Hz.

Age differences in biomechanics were assessed with independent t-tests. To test for differences in the underlying neural drive, mixed model ANOVAs were run with a between factor (age group – YA and OA), and one within factor (muscle combination: TA-SO, SO-MG, VM-RF, VM-BF). Relationships between neural drive and biomechanical function were assessed with a multiple regression model. Significance was set at $\alpha = 0.05$.

Results and Discussion

OA exhibited lower Piper band power (35-60 Hz) in all studied muscle combinations compared with YA (7.8 ± 1.03%, $p < 0001$, $\eta_p^2 = 0.570$, Figure 1). This suggests that, when compared with YA, OA have lower common oscillatory drive from the cortical input to the motor neuron pool, across both synergistic and antagonistic muscles, in contrast to our initial hypothesis.

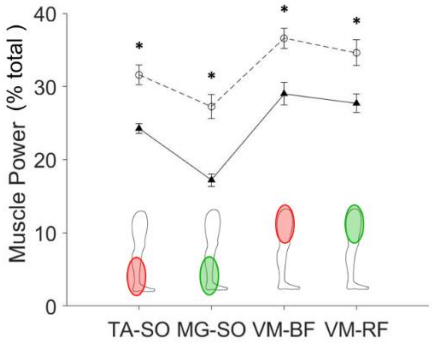

Figure 1: Mean (error bars depict SE) muscle power across 35-60 Hz antagonistic (shown via the red oval: tibialis anterior-soleus (TA-SO), vastus medialis-biceps femoris (VM-BF)) and synergistic (shown via the green oval: medial gastrocnemius-soleus (MG-SO), vastus medialis-rectus femoris (VM-RF)) muscles. *indicates significant differences between younger (○) and older adults (▲).

Much of the literature suggests OA have greater cortical control of gait. However, previous work [4] found dual-task walking resulted in lower Piper band synchrony in MG-SO, indicating that competition for cortical resources reduces that available for motor tasks. Our findings suggest that OA have less cortical resources available for motor performance than YA.

As OA were highly mobile, only stride length variability was significantly higher in OA than YA (0.72 ± 0.29%, $p = 0.018$, Cohen's d = 0.74). We found increased coherence in TA-SO in the Piper band with reduced stride length variability ($R^2 = 0.175$, $p = 0.021$). When split by age group, this relationship held for neither YA ($R^2 = 0.01$, $p = 0.78$) nor OA ($R^2 = 0.099$, $p = 0.177$). We felt confident in combining these groups functionally as we recruited high-functioning OA. Future work should include lower-functioning older adults to see if the relationship between shared neural drive to ankle antagonistic muscles and stride length variability holds.

Significance

Although our hypothesis was not supported, our findings indicate differences in the underlying control of movement patterns between younger and older adults occur prior to changes in gait behavior. and that increased shared neural drive to muscle pairs is associated with reduced stride length variability.

Acknowledgments

This project is supported by NIH U01AG0061389.

References

[1] DeVita & Hortobagyi, 2000, *J. Appl Physiol.* 88(5):1804-11.
[2] Owings & Grabiner, 2004, *Gait Posture,* 20(1):26-29
[3] Lodha et al., 2017, *J Electromyogr Kinesiol.* 37:35-40.
[4] Clark et al., 2013, *Ann Biomed Eng.* 41(8):1778-86.

SUBMAXIMAL SOLEUS FORCE LENGTH CHARACTERISTICS WITH AGING

Lindsey H. Trejo[1], Jordyn N. Schroeder[1], and Gregory S. Sawicki[1]
[1]School of Mechanical Engineering and Bio Sciences, Georgia Institute of Technology, Atlanta, GA, USA
email: ltrejo@gatech.edu

Introduction

Older adults use more energy to walk than young adults. Age-related changes in muscle-tendon units (MTU) could cause reduced muscle power and force economy. For example, reduced Achilles tendon stiffness in older adults leads to shorter, less economical muscle operating lengths [1]. But the muscle itself may also be a factor; loss of type 2 fiber percentage and muscle mass as well as increased connective tissue stiffness could all contribute to a reduced force output per muscle activation in old versus young adults and lead to increased metabolic energy expenditure. Comparative literature has shown that in healthy, young muscle there is a leftward shift of optimal muscle length with increasing activation [2] affording a potential mechanism to keep muscles operating in proximity to optimal length (l_0) despite an average shortening against series elastic tissues during more demanding tasks (e.g., faster walking). Here, we sought to examine whether this activation dependent shift in optimal length is retained in aged human soleus muscle. We hypothesized that older adults would have stiffer muscles and a smaller leftward shift in optimal length with increasing activation.

Methods

Two young (1M, 1F, 20 ± 1.4 years), and two older adults (1M, 1F, 66.5 ± 2.1 years) performed a minimum of 3 plantarflexion (PF) contractions at 5 ankle joint angles (20°PF, 10°PF, 0°, 15° dorsiflexion (DF), maxDF) and 4 activations (0, 33, 66, 100% of max voluntary contraction [MVC]). Torque at the ankle was measured using a dynamometer while prone with the knee bent 120° to isolate the soleus muscle. Muscle activity and muscle lengths of the soleus were measured using electromyography (EMG) and ultrasound respectively. MVC were performed with visual torque feedback while 33% and 66% contractions were performed with EMG feedback. Two minutes of rest were taken between every contraction. For the passive curve, torque and length were measured in increments of 5° from 10°PF to maxDF after 45 seconds of resting in this position to mitigate history-dependent effects. Soleus active muscle force (F_{sol}^{act}) was calculated as follows.

$$F_{sol}^{act} = \frac{\tau_{total} - \tau_{pedal}}{r_{ank} \cdot \cos(\theta_{penn})} - F_{sol}^{pass}$$

τ_{total} is total torque, τ_{pedal} is pedal torque, r_{ank} is ankle moment arm, θ_{penn} is pennation angle, and F_{sol}^{pass} is passive force at the length during contraction. A 2nd order polynomial was least squares curve fit to the data for the active curves, and an exponential curve for the passive data [2]. Muscle stiffness was calculated as the slope at l_0.

Results and Discussion

As expected, the normalized muscle stiffness was greater for older adults (Y: 0.118, O: 0.541). Contrary to our hypothesis, both Y and O adults exhibited a rightward shift in l_0 at the highest activations (Y:100%: 1.0, 66%: 0.896, 33%: 0.888, O: 100%: 1.0, 66%: 0.903, 33%: 0.943). The location of l_0 is highly dependent on the curve fitting method and the amount of data on the descending limb. Previous literature has reported some participants cannot reach the descending limb which could explain our observed opposite shift in l_0 compared to other studies [2]. By combining data from more participants and further refining our fitting procedure, we hope to verify our measured shifts in l_0. The absolute force-length curves for the older group had lower maximum force (Y: 6155.5 N, O: 2904.1 N) and shorter optimal length (Y: 49.5 mm, O: 40.65 mm). Lower maximum force with aging has been reported previously.

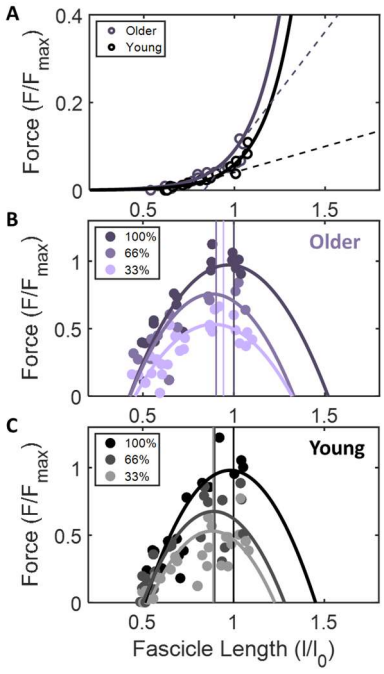

Figure 1. A. Average passive force-length curve of young (black) and older (purple) adults. The dashed lines represent respective muscle stiffness. B. Average force-length curves for 100%, 66%, and 33% activation from older adults. The vertical lines represent l_0 at respective activation. C. Average force-length curves for 100%, 66%, and 33% activation from young adults. The vertical lines represent l_0 at respective activation.

Based on these preliminary data, we conclude older adults have more stiff muscles and altered activation dependent shifts in l_0 compared to young.

Significance

Characterizing age-related shifts in muscle FL curves is a critical aspect to understanding the increase in energy cost of walking for older adults and may inform training interventions and the design of assistive devices to address the mechanical and metabolic effects of aging.

Acknowledgments

NIH NIA Grant (R0106052017), Alfred P. Sloan Foundation Graduate Scholarship, and Goizueta Foundation Fellowship

References

[1] B. Krupenevich et al., 2021 *Gerontology*
[2] N. C. Holt and E. Azizi, 2014, *Biol. Lett.*
[3] J. Rubenson et al., 2012 *J. Exp. Biol.*

The influence of age on the relationship between step width and spatial and temporal adaptation strategies during split-belt adaptation

Patrick G. Monaghan[1*], Sarah A. Brinkerhoff[1], Jaimie A. Roper[1]
[1]Auburn University, Auburn, AL

Introduction

The adaptative nature of gait is critical to maintain stability and meet the demands of our ever-changing environments. The inability to adapt gait may increase fall risk, which is even more pivotal for populations such as older adults, who are already at an elevated fall risk. To adapt gait, individuals alter both spatial and temporal parameters. Older adults and those with neurological disorders exhibit differences in spatial and temporal adaptation strategies[1,2]. Further, neurotypical older adults also demonstrate altered stability during a continuous perturbation such as split-belt treadmill walking[3,4]. Foot positioning, such as step width, is a common strategy that may influence gait adaptation strategies and stability. While shorter and wider steps have characterized older adults' gait[5], the relationship between spatial and temporal adaptation strategies during split-belt treadmill walking and step width remains unclear. Therefore, this study assesses the relationship between spatial and temporal contributions to step length asymmetry (SLA) during early adaptation and step width in healthy younger and older adults.

Methods

Nine healthy young adults (7 females, two males, 21 ± two years) and nine healthy older adults (7 females, two males, 65 ± seven years) walked on a split-belt treadmill with their non-dominant leg moving twice as fast as their dominant leg for ten minutes. Early adaptation consisted of the first ten strides of the adaptation period. Spatial contributions to SLA refer to contributions of step position to SLA, while temporal contributions to SLA refer to the product of step timing asymmetry and foot velocity asymmetry[2]. Step width was defined as the distance between the ankle markers at foot strike and measured during three minutes of baseline tied-belt walking. A moderation analysis was conducted to examine if the relationship between baseline step width and spatial or temporal gait adaptation strategy was moderated by age. Bivariate correlations were also conducted to assess the relationship between step width and spatial and temporal gait adaptation strategies during early gait adaptation in healthy older and younger adults.

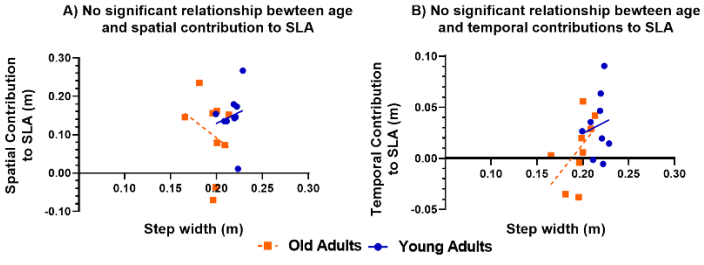

Figure 1: Relationship between baseline step width and A) spatial contributions to step length asymmetry and B) temporal contributions to step length asymmetry in younger and older adults. SLA = step length asymmetry

Results and Discussion

Our analysis revealed no significant effect of age (p= .52) or baseline step width (p = .39) on spatial contribution to SLA during early adaptation. Similarly, there was no significant effect of age (p =.63) or baseline step width (p = .36) on temporal contribution to SLA during early adaptation. Further, there was no significant moderating effect of age on the relationship between step width and spatial and temporal contribution to SLA during early adaptation (p = .47 & p = .64). Results of the correlation analysis indicated that there were no significant relationships between baseline step width and spatial contributions to SLA during early adaptation for both older, $r(7)$ = -.27, p = .48) and younger, $r(7)$ = .16, p = .68) healthy adults. Similarly, no significant relationships between baseline step width and temporal contributions to SLA during early adaptation for both older, $r(7)$ = .52, p = .16) and younger, $r(7)$ = .13, p = .74) healthy adults. While individuals adjust walking strategies during split-belt treadmill walking[6], our early findings indicate that step width during tied walking does not relate to spatial or temporal adaptation strategies during early gait adaptation. Although increased step width is a hallmark of older adults' gait, we reveal no age-related differences between step width and gait adaptation strategy. However, it is essential to highlight these initial findings from a limited sample size. As our sample size and statistical power increase, monitoring these relationships is critical to understanding age-related differences that may impact gait adaptation. It is also important to note that participants walked with one foot on each belt and held on to handrails for all trials.

Significance

Understanding how stability parameters relate to temporal and spatial gait adaptation strategies and how this may be impacted by age is essential to understanding gait abnormality in older adults. For example, if markers of decreased stability (such as increased step width) were found to use more spatial contributions to modify and adapt SLA, more specific and patient-centered therapeutic approaches may be employed. Continued research into the causative relationship between spatiotemporal aspects of gait and gait adaptation strategies in older adults can enhance rehabilitation approaches and ultimately increase the ability of older adults to interact optimally with their environment.

Acknowledgments

An Auburn University seed grant supported this project.

References

[1] Roper et al., 2019. *J Neurophysiol,*
[2] Finley et al., 2015. *J Neurorehab & Neur Repair.*
[3] Fettrow et al., 2021. *Sci Reports*
[4] Vervoot et al., 2020. *Medicine&Sci in Sports and Exercise*
[5] Winter et al., 1990. *Phys Ther*
[6] Buurke et al., 2018. *J Exp Biology*

.

Assessment of aging related changes in postural control using time to contact

Ross J. Brancati[1*], Jane A. Kent[1], Kate L. Hayes[1], Fany Alvarado[1], Katherine A. Boyer[1],
[1]Department of Kinesiology, University of Massachusetts Amherst, Amherst, MA
email: *rbrancati@umass.edu

Introduction

Performance fatigability, a decline in performance in response to a standardized activity[1] is an early predictor of mobility decline in older adults. Muscle fatigue (decrease in maximal power with activity) in older adults could contribute to greater performance fatigability and has been shown to impact postural control.[2] The advanced version of the Short Physical Performance Battery (SPPB-A) may be used to quantify performance fatigability as it includes tasks that evaluate an individual's postural control in challenging positions. However, only stance time is used to evaluate performance.[3] An individual may hold a position for the full task time, 30 seconds, but information about their center of pressure (COP) vector is not captured.

Time-to-contact (TTC) is a measure that accounts for both the spatial and temporal aspects of postural control because it quantifies how much time it would take the center of pressure to contact a stability boundary.[4,5] Functionally, TTC represents the time until a person would need to make a postural correction, such as taking a step, in order to prevent a fall.[6,7] TTC has been shown to be lower in older adults in basic postural stances,[4] but it has not yet been quantified in progressively challenging stances or in response to a standardized activity to quantify performance fatigability. The purpose of this study was to compare TTC in younger and older adults in the four stances of the SPPB-A before and after a prolonged walk that has been shown to result in knee extensor muscle fatigue and postural disturbances.

Methods

Five young adults (35.6±3.0 yr, BMI: 23.3±3.9 kg·m^{-2}, 1 male) and five older adults (72.0±1.9 yr, BMI: 24.5±3.4 kg·m^{-2}, 3 male), all healthy and sedentary, stood on a force plate (AMTI., MA, USA) in standardized lab footwear in four positions: side-by-side (SBS), semi-tandem (ST), full-tandem (FT), and single leg (SL) stances, attempting to hold each stance for the full 30s. A motion capture system (Qualysis, Sweden) collected marker positions on both feet during each trial. Force data were sampled at 100Hz and filtered with a 2nd order low-pass Butterworth filter with a cut-off frequency of 10Hz. Participants then completed a 30-min treadmill walk (30MTW)[2] at their self-selected speed, determined by a 400m overground walk test, and then repeated the four balance positions. Minimum TTC (s) was calculated for each trial by solving for the time variable, τ, in the equation:[4] $P_i(\tau) = r(t_i) + P(t_i) \cdot \tau + a(t_i) \cdot \tau^2/2$. At least 50% of the trial had to be completed to accurately quantify TTC. For each stance, a 2 x 2 ANOVA was conducted using age and time (pre or post 30MTW) as factors. Muscle fatigue was quantified the change in peak knee extensor torque (at 240 dps) following the 30MTW.

Results and Discussion

All young participants held each stance for 30s. All older participants held the SBS and ST, but not the FT and SL, stances for 30s. For FT, older group stance times were 27.3±6s before and 24.3±11s after the 30MTW. For SL, older group stance times were 18.9±11s before and 10.5±7.8s after the 30MTW. The older group did no hold the SL stance for sufficient time and thus it was excluded from the TTC analysis. There was a main effect of age for minimum TTC ($p<0.05$) for the SBS, which agrees with previous data.[4] ST and FT stances also showed an age effect ($p<0.01$). There was no effect of time for any stance, which is supported by a lack of muscle fatigue in response to the 30MTW (data not shown). Reduced TTC in the older adults reveals diminished postural control in the spatio-temporal domain in all 3 stances, suggesting an increased risk of falls due to perturbations compared with younger adults.

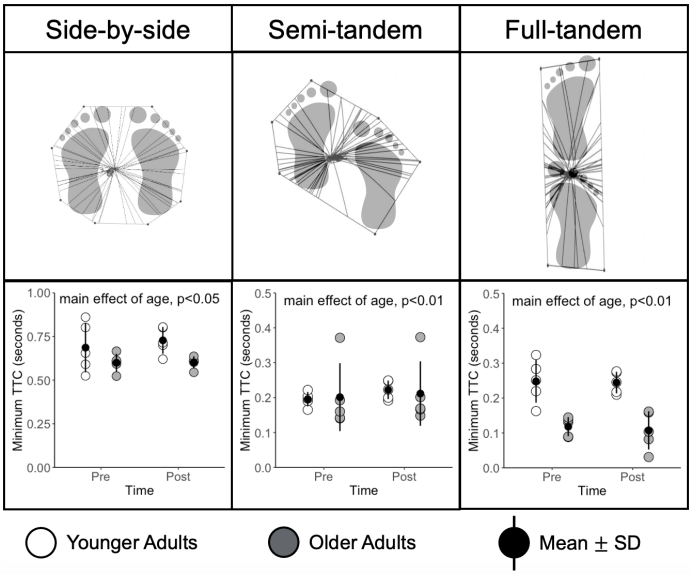

Figure 1: Trajectory plots of TTC (top) for the three stances included in the analysis. Minimum TTC (in seconds) for pre and post 30MTW (bottom). There was a main effect of age for the SBS ($p<0.05$), ST ($p<0.01$) and FT ($p<0.01$) stances.

Significance

TTC detected lower in postural control at baseline in the healthy older compared with younger adults. Notably, this was the case whether or not they failed to complete the full 30 s of the balance tasks. Thus, this metric may be effective at capturing reduced postural performance despite task completion.

Acknowledgments

Funding: NIH AG058607. Aidan Gross, for data processing.

References

[1] Shrack et al., 2020. *J of Gerontology*. 9: e63-e66.
[2] Foulis et al., 2017. *Plos One*. 12: e0183483.
[3] Simonsick et al., 2001. *J of Gerontol. Ser. A*. 56: M644-M649.
[4] Slobounov et al., 1998. *J of Gerontol. Ser. A*. 53A: B71-B80.
[5] van Emmerik et al., 2010. *Gait & Posture*. 32: 608-614.
[6] Richmond et al., 2020. *J of Sport Sciences*. 38: 21-28.
[7] Hasson et al., 2008. *J of Biomechanics*. 41: 2121-2129.

THE CIRCUMSTANCES AND CONSEQUENCES OF FALLS IN LONG-TERM CARE RESIDENTS

Mayank Kalra[1,2*], Jaimie Killingbeck[2], Andrew C. Laing[1]
[1]Dept. of Kinesiology, University of Waterloo, Waterloo, ON; [2]Schlegel Villages, Waterloo, ON; email: *mayank.kalra@uwaterloo.ca

Introduction

It is well established that falls and fall-injuries are a hardship that affect approximately 1/4 to 1/3 of community dwelling older adults [1]. The falls and fractures incidence rates are 2-3 times higher in institutions such as nursing homes or long-term care (LTC) facilities [2,3]. There are different underlying circumstances that contribute to higher fall incidence rates in LTC, some of which have been previously reported [4-6]. This study aims to add to this limited body of work by contextualizing fall circumstances and consequences such as fall location, activity, injury site, and injury severity within a sizeable Canadian LTC sample population.

Methods

A database comprised of LTC residents from 13 care facilities in Ontario, Canada that experienced a fall between October 1, 2012 to December 31, 2015 was analysed. The location of the fall within the LTC site, the action resulting in the fall, the resulting injury site, and injury severity were extracted. Descriptive statistics were conducted to quantify the number of falls, and absolute values and relative percentages were obtained for the different fall circumstances.

Results and Discussion

19 869 falls occurred amongst 2557 LTC residents, resulting in a mean of approximately 2.4 annual falls/resident (that experienced a fall), with 78% (n=1987) of residents experiencing multiple falls, and 24% (n=623) of residents experiencing at least 10 falls.

The bedroom was the most common fall location (Figure 1), which is concurrent with prior studies [4,5]; although, this study had relatively fewer falls in the bedroom (53% vs. 62% [4]). Walking and transfers were respectively the most and second most common identifiable actions leading to a fall (Table 1), which have also been reported in prior literature, though not necessarily in the same relative order [4-6].

14 010 total injuries were reported equating to a mean of 1.7 annual injuries/resident. Among the classified injuries 'aches/pain' (n=2730) were the most frequent injury type followed closely by 'bruises/bumps' (n=2480) and 'skin tear' (n=2478). 39% of injuries (n=5462) were further categorized by anatomical location (Table 2) with head injuries as the most frequent injury type.

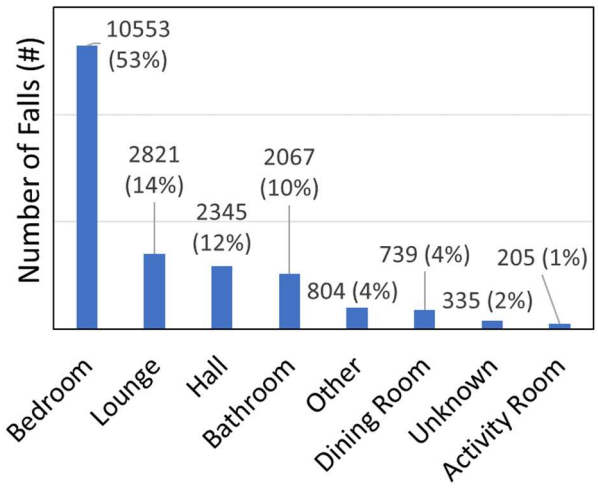

Figure 1: Number of falls categorized by Location.

Significance

The present study reaffirmed previous findings related to fall location and actions leading to a fall, while providing novel insights on injury incidences by relating anatomical location with injury severity. Further identifying the circumstances and consequences of falls are crucial in the clinical prevention and management of falls and fall injuries.

Acknowledgements

Funding support was provided by Mitacs and Schlegel Villages.

References

[1] Stinchcombe et al., Chronic Diseases Injuries Can. 2014 34(2-3):171-174.
[2] Rubenstein et al., Ann Intern Med 1994;121:442-51.
[3] Luukinen et al., J Clin Epidemiol 1994;47:843-50.
[4] Büchele et al., JAMDA 2014;15(8):559-63.
[5] McArthur et al., Cdn J. Aging 2016;35(4):491-8.
[6] Jensen et al., Scandinavian J. Public Health. 2002;30(1):54-61.

Table 1: Number of falls categorized by Activity leading up to the fall.

Unknown	Walking	Transfer	Sitting	Standing	Lying	Other	Reaching	Turning
7259 (37%)	3203 (16%)	2565 (13%)	2257 (11%)	1284 (7%)	1233 (6%)	1066 (5%)	738 (4%)	264 (1%)

Table 2: Number of fall related injuries categorized by Anatomical Location and Injury Severity.

	Uncategorized (n=8548)	**Head** (n=3052)	**Arm** (n=1159)	**Leg** (n=576)	**Hip** (n=424)	**Torso** (n=251)
Bruises/bumps	120	1397	413	254	167	129
Skin tears	241	1362	574	205	48	48
Soft tissue	58	160	77	61	39	28
Fractures	-	80	68	42	147	26
Aches/pain	2593	53	27	14	23	20
Unclassified	5536	-	-	-	-	-

KINEMATIC SEQUENCE IN BASEBALL PITCHING: A THREE-DIMENSIONAL APPROACH

Jun M Liu[1], Christopher Knowlton, Matthew Gauthier, Zach Tropp, Antonia Zaferiou[1]
[1] Musculoskeletal Control and Dynamics Lab, Dept. Biomedical Engineering, Stevens Institute of Technology, Hoboken, NJ, USA
Email: jliu130@stevens.edu

Introduction

Baseball pitching has been described as a whole-body activity that requires kinetic energy transfer from the lower extremities to the torso and then the throwing hand [1]. The sequence with which the body segments change velocity describes the kinematic sequence [1]. Delayed pelvis rotation relative to trunk rotation was associated with increased upper limb joint loads [2]. Instead, a proximal-to-distal kinematic sequence (PDS) is believed to be more efficient and may reduce likelihood of injury [3], though only one study directly investigated PDS in fastball pitching using a five-segment (pelvis-to-hand) model [4]. In that study, no pitches by any pitcher demonstrated a full PDS from pelvis to hand. However, only segment angular velocity *magnitude* relative to the global axes was investigated.

This study investigated whether PDS was used by professional pitchers when analysed about each global axis. We hypothesized that a full PDS from pelvis to hand will be used as the primary sequence about at least one global axis.

Methods

Professional pitchers (n=4) volunteered for the study in accordance with the IRB. They pitched five to eleven fastballs on an instrumented mound while 3D positional data were collected (Optitrack; 250 fps for pitchers 1&2 and 360 fps for pitchers 3&4 due to change in software capabilities). The global axes were defined with the forward axis in the direction of the pitcher's throw (mound to home plate), the global vertical axis, and the left axis which was a cross product of the vertical and forward axes. A fourth-order, zero-lag Butterworth low-pass filter with a cut-off frequency of 10 Hz was used to processed marker data [5]. The pelvis, trunk, upper arm, lower arm, and hand segment axes were defined according to McConville's anthropometric data [6].

Segment angular velocity were calculated relative to the global axes. For each body segment, the time at which the component of angular velocity vector about each global axis reached a peak (positive/negative) is referred to as "peak time" for that segment. The progression of peak times of the five segments is the kinematic sequence [4]. A *full* PDS follows the progression from pelvis to trunk, upper arm, forearm, and ends with the hand. If there was a PDS between adjacent segments, the sign test (α=0.05) was used to further compare peak times between adjacent segments within pitcher.

Results and Discussion

We found that pitchers demonstrated full PDS about the global left axis in 67-100% of their trials, depending on the pitcher. For two pitchers, there were significant differences between peak times of each set of adjacent segments from pelvis to hand ($p<0.05$) (**Fig. 1A**). No pitcher demonstrated full PDS about the global vertical axis. For three pitchers, there were significant differences between peak times of each set of adjacent segments from pelvis to upper arm ($p<0.05$) (**Fig. 1B**). There was no discernable sequence about the global forward axis (and segment angular velocity about the forward axis accounted for 16-30% of the angular velocity magnitude). No pitcher demonstrated full PDS when angular velocity magnitude was used. In one pitcher, there were significant differences between peak times of each set of adjacent segments from pelvis to upper arm ($p<0.05$) (**Fig. 1C**). The sequence observed varied across the global axes, which could explain why no PDS was found when angular velocity magnitude was used previously [4]. In this study, we observed that peak segmental angular velocity about the global left axis were always positive for all segments. In contrast, peak angular velocities about the global vertical and forward axes for some segments (even the pelvis and trunk) exhibited negative or positive peaks, depending on the pitcher.

Significance

This study revealed full PDS when examining the peak times of segmental angular velocity about the global left axis but did not reveal PDS when using angular velocity *magnitude* only. Therefore, analysing 3D segment angular velocity may be more suitable than magnitude alone to better understand pitching.

Acknowledgments

This study was funded by Major League Baseball.

References

[1] Putnam, C.A., 1993. *J Biomech.* 26
[2] Elliot, B. et al, 1988, *Int. J Biomech.* 4
[3] Calabrese, G., 1995, *Int. J Sports Phys. Therapy.* 8
[4] Scarborough, D. et al, 2020, *Sports Biomech.* 19
[5] Crenna, F. et al, 2021, *Sensors,* 21: Iss.13
[6] McConville, J. et al, 1980, *AFMRL Tech. Report*

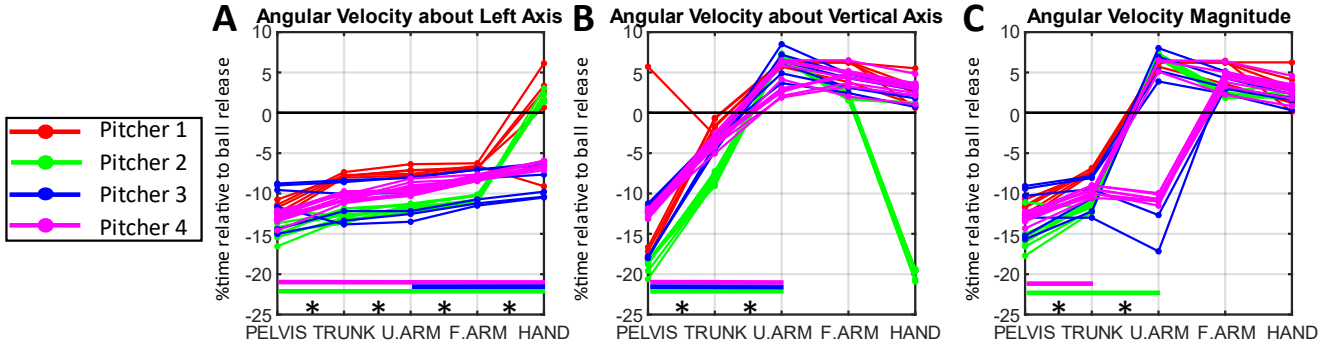

Figure 1: Peak times for pelvis, trunk, upper arm (U.ARM), forearm (F.ARM), and hand for all trials and pitchers about global (A) left and (B) vertical axes. (C) Peak times for segmental angular velocity *magnitudes*. Ball release is at 0% time relative to ball release, with positive % time being after ball release. Colored bars at the bottom show significance for specific pitchers with PDS between adjacent segments (*p<0.05).

THE ANALYSIS OF FORWARD ACCELERATION ASYMMETRIES DURING ON-WATER SPRINT KAYAKING

Joshua A. Goreham[1*] and Michel Ladouceur[1]
[1]Kinesiology, School of Health and Human Performance, Dalhousie University, Halifax, NS, Canada
email: *josh.goreham@dal.ca

Introduction

To increase kayak velocity, athletes must propel themselves forward by applying large amounts of force to the water via a double-bladed paddle. As the energy exerted transfers from the water to the athlete and kayak, it causes the kayak to accelerate towards the finish line. Throughout the stroke the forward acceleration fluctuates from positive (i.e., entry and pull phases of the stroke) to negative (i.e., exit and aerial phase of the stroke).[1] Information regarding how the kayak accelerates in the water may uncover technical inefficiencies (e.g., stroke asymmetry), which could be hindering performance.

The study's aim was to investigate the effect of stroke rate (SR) on the critical features of forward acceleration asymmetries (i.e., range, maximum, and minimum) in sprint kayaking. As SR (and velocity) increases, we would expect power output to increase as well. Previous research[2] showed that power asymmetries in ergometer kayaking was not modulated by SR. Our hypothesis is that on-water forward acceleration asymmetries will not change as SR increases.

Methods

Fifteen national-to-world class level sprint kayak athletes consented to participate in accordance with Dalhousie University's Research Ethics Board. The experimental protocol consisted of an individual-led warm-up followed by four 30-second paddling trials (SRs in random order: 60 strokes per minute (spm), 80 spm, 100 spm, and maximum spm) with a three-minute rest period between trials. Kayak velocity and forward acceleration data were collected using a 50 Hz tri-axial inertial measurement unit (±2 *g*, STMicroelectronics©, Indiana, USA) with a 5 Hz GPS/GNSS module.

The kayak's forward acceleration was analyzed by extracting 10 stroke waveforms (five left and five right strokes) from each SR trial when athletes were paddling at a constant velocity. After signal filtering, critical features were extracted from the forward acceleration waveforms, and then averaged for each SR trial. Asymmetries for each critical feature between the left and right strokes were calculated for each SR condition using an asymmetry index (ASI), where an ASI of 0% indicated the strokes were symmetric.[3] A one-way, repeated measures ANOVA with a Tukey's *post-hoc* analysis and a linear trend test was used to analyze ASI data ($\alpha = 0.05$).

$$ASI(\%) = \frac{|(Left\ stroke - Right\ stroke)|}{½\,|(Left\ stroke + Right\ stroke)|} \bullet 100\%$$

Results and Discussion

Average kayak velocities increased as SR conditions increased (Table 1). There was a significant effect of the SR condition on the maximum forward acceleration ASI ($F(2.6, 36.7)=4.1$, $P=0.016$, $\eta^2=0.23$). There was no significant effect of the SR condition on the minimum or range of forward acceleration ASI's. However, linear trend analyses were statistically significant for all three critical features (Table 1).

This finding is important for two reasons. First, it informs the sport biomechanist and coach to analyze the left and right strokes independently. Prior to this research, no data had been published on how the left and right strokes produce kayak acceleration during on-water paddling. Second, if athletes are shown to have a large forward acceleration asymmetry between sides of the stroke cycle, it can be expected to increase as their SR increases. Although a small asymmetry may not affect technical efficiency at lower SR's (i.e., during training), it can be expected that inefficiencies will increase as the athlete reaches higher SR's (i.e., during racing). Due to the potential effect on boat steering, future research should investigate how asymmetries affect other planes of boat movement (i.e., vertical and side-to-side accelerations, and pitch, yaw, and roll).[4]

Significance

This is the first study to investigate forward acceleration asymmetries during on-water sprint kayaking providing coaches with normative asymmetry values in elite sprint kayakers. These normative values could provide appropriate benchmarks when assessing technical efficiency.

Acknowledgments

The authors would like to thank the study participants, and Mitacs and Own the Podium for their financial support.

References

[1] Gomes et al., 2020. *Sport Biomech*. 1-9.
[2] Bjerkefors et al., 2017. *Sport Biomech.* 17(3), 414-427.
[3] Robinson et al., 1987. *J Manipulative Physiol Ther.* 10(4), 172-176
[4] Michael et al., 2009. *Sport Biomech*. 8(2). 167-179

Table 1: Average ASI and velocity for each SR condition, as well as linear trend results.

	60 spm	80 spm	100 spm	Maximum spm	Linear Trend?
Velocity ($m \bullet s^{-1}$)	3.53±0.24	4.01±0.18	4.51±0.28	4.99±0.53	-
ASI Range (%)	8.01±11.70	10.13±14.07	10.66±13.18	13.55±10.84	P=0.007, b=1.71
ASI Maximum (%)	10.34±13.59	10.72±16.31	15.29±19.41	16.43±15.95	P=0.002, b=2.28
ASI Minimum (%)	9.62±10.10	13.35±16.97	16.03±13.88	19.28±12.40	P=0.022, b=3.17

Data presented as mean ± standard deviation. *P, p*-value; *b*, slope.

SPRINT KAYAKER'S KINETIC ASYMMETRIES AT INCREASING STROKE RATES

Kayla B. Miller[1*], Joshua A. Gorehamt[1], Ryan J. Frayne[1] and Michel Ladouceur[1]
[1] Kinesiology Division, School of Health and Human Performance, Dalhousie University, Halifax, NS, Canada
email: michel.ladouceur@dal.ca

Introduction

In kayaking, ergometers are used for research, training, and performance testing. To date, the kayak paddle force profile has been studied, where the forces at the seat and footboard are not well understood. In sprint kayaking, the upper body is the main contributor to force production [1,2]; however, mean kayak speed decreases by 16 % and mean paddle force decreases by 21 % when lower body movement is constrained [3]. Therefore, the lower body forces should also be considered when assessing measures of performance.

In a performance analysis context, it is important to understand an athlete's level of asymmetry to make corrections to their training program. Kayakers' lower body force and moment asymmetries have not yet been studied in any plane. Therefore, the purpose of this study is to determine if stroke rate influences the level of asymmetry on a kayak ergometer. It is hypothesized that as kayaking stroke rate increases on an ergometer, the ASI between left and right footboard, and seat forces will decrease.

Methods

A Dansprint® paddling ergometer (Dansprint, ApS, Denmark) was instrumented with three AMTI AD2-5D load cells (AMTI Force and Motion, Watertown, MA): one for the left and right footboards, separately, and one for the seat. The footboard and seat load cells were adjusted to participant's preferences. All data were collected at 1000 Hz. Ten participants (4 females, 20 ± 6 years, 72 ± 9 kg, 12 ± 5 years spent kayaking) of provincial to national team level were recruited. Participants were asked to perform a 10-minute warm-up prior to completing four randomized 30-second trials at 60 strokes per minute (spm), 80 spm, 100 spm, and maximum (max) spm with a three-minutes rest between trials. Recorded forces were translated into a global coordinate system. Ten stroke cycles were analyzed for each individual trial. Mean force, impulse, and impulse*SR discrete measures were identified for the individual components (anteroposterior, lateral, and vertical) of the resultant forces within each stroke cycle. Impulse*stroke rate were calculated to approximate impulse per minute. A Shapiro-Wilk's test was used to determine if the data was normally distributed. A one-way repeated measures analysis of variance (ANOVA) was used when data was normally distributed, whereas a Friedman's ANOVA was used when data was not normally distributed. Tukey's post hoc analysis was used when statically significant differences were found using a RM ANOVA, where a Dunn's multiple comparison post hoc was used when a Friedman's ANOVA was performed. Data was tested at $p<0.05$ for all tests.

An asymmetry index (ASIi) was calculated for all discrete measures of force and moments.

$$ASI(\%) = \frac{\left|\left(|X_{left}| - |X_{right}|\right)\right|}{\left(|X_{left}| + |X_{right}|\right) * 0.5} * 100$$

where Xleft is the measure of the left side, Xright is the measure of the right side, and ASI is the calculated ASI. An ASI equal to zero, corresponds to complete symmetry. The ASI was calculated to have no direction to the value.

Results and Discussion

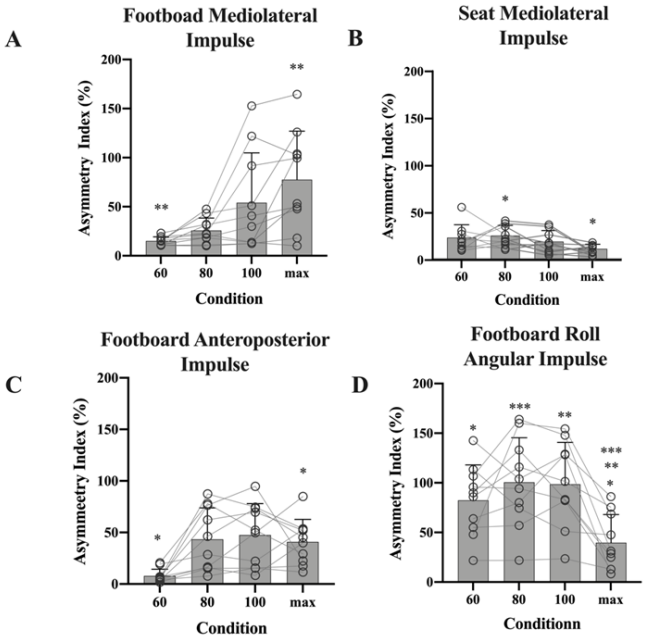

Figure 1: Stroke cycle had a significant effect on total stroke cycle impulse (TSI) and total stroke cycle angular impulse (TSAI). This graph represents individual participant TSI and TSAI asymmetry indexes (ASI) (circles) compared to the group means and standard deviations (bars). (A) Stroke rate had a significant effect on mediolateral TSI ASI in the footboard, where ASI increased with stroke rate, (B) stroke rate had a significant effect on mediolateral TSI ASI in the seat, where 80 spm demonstrated the highest ASI of the four conditions, and the ASI decreased from 80 – maximum spm, (C) stroke rate had a significant effect on anteroposterior TSI ASI in the footboard, where ASI increased until 100 strokes per minute (spm) and then slightly decreased at maximum spm, (D) stroke rate had a significant effect on roll TSAI ASI in the footboard, where ASI was lowest at max spm. * $p < 0.05$, ** $p < 0.005$, *** $p < 0.0005$

Significance

The result from this study shows that athletes use difference in the magnitude of footboard and seat forces and moments to counteract each other to maintain themselves on their seat while on the ergometer.

Acknowledgments

The authors would like to thank the study participants, and Mitacs and Own the Podium for their financial support.

References

[1] Michael JS, Smith R, Rooney KB. Determinants of kayak paddling performance. Sport Biomech. 2009;8(2):167–79.
[2] Shephard RJ. Science and Medicine of Canoeing and Kayaking. Sport Med An Int J Appl Med Sci Sport Exerc. 1987;4(1):19–33.
[3] Nilsson JE, Rosdahl HG. Contribution of leg-muscle forces to paddle force and kayak speed during maximal-effort flat-water paddling. Int J Sports Physiol Perform. 2016;11(1):22–7.

COMPARISON OF MARKER-LESS AND MARKER-BASED MOTION CAPTURE FOR BASEBALL PITCHING

Glenn S. Fleisig[1,2*], Jonathan S. Slowik[1], Derek Wassom[2], Yuki Yanagita[1], Jasper Bishop[1], Alek Z. Diffendaffer[1]
[1]American Sports Medicine Institute, Birmingham, AL, USA
[2]Dari Motion, Overland Park, KS, USA
email: *glennf@asmi.org

Introduction

Commercially available marker-less motion capture has recently emerged in biomechanics and professional sports. A survey by the American Baseball Biomechanics Society found that 70% of Major League Baseball organizations used 3D marker-less motion capture technology in 2021. Understanding the accuracy of marker-less motion capture is essential to justify its use in on-field research and performance enhancement. The purpose of this study was to compare baseball pitching kinematics measured with a marker-less system against data measured with a marker-based system.

Methods

275 fastball pitches were captured at 240 Hz simultaneously with a 9-camera marker-less system (DARI Motion, Overland Park, KS) and a 12-camera marker system (Motion Analysis Corporation, Rohnert Park, CA). The pitches were thrown by a diverse group of 30 baseball pitchers (age 17.1 ± 3.1 yrs), ranging from youth to professional level. Data for each trial were time-synchronized between the two systems using the instant of ball release. Five kinematic time series (lead knee flexion, trunk rotation, throwing shoulder abduction, throwing shoulder external rotation, throwing elbow flexion) and 12 discrete kinematic measurements were calculated from the joint center data of each system using computations previously described.[3,5,6]

Coefficients of Multiple Correlations (CMC) were computed to assess the similarity of waveforms between the two systems.[2,4] Discrete measurements at foot contact, during arm cocking, and at ball release were compared between the systems using Bland-Altman plots and descriptive statistics.[1]

Results and Discussion

CMC values for the five time series ranged from 0.88 to 0.97, indicating consistency in movement patterns between systems. As shown in Table 1, mean differences for discrete measurements ranged from 0 to 16 degrees. Standard deviations in the difference between systems ranged from 0 to 12 degrees across subjects, and from 0 to 5 degrees within subject.

Thus, the marker-based and marker-less motion capture systems produced similar patterns for baseball pitching kinematics. However, based on the variations between the systems, it is recommended that a database of normative ranges should be established for each system.

Significance

Biomechanics is changing as marker-less technologies enter the field. This study provides fundamental information for baseball and all applications of motion capture, detailing the variations between two systems for measuring complex and dynamic movement in athletes.

Acknowledgments

The authors would like to acknowledge the support of the 2020 International Society of Biomechanics in Sports Internship Grant.

References

1. Bland JM, Altman DG. *Lancet* 1986;1(8476):307-310, 1986.
2. Drazan JF, et al. *J Biomech* 2021;125:110547, 2021.
3. Escamilla RF, et al. *J Appl Biomech* 34(5):377-385, 2018.
4. Ferrari A, et al. *Gait Posture* 31(4):540-542, 2010.
5. Fleisig GS. (Doctoral dissertation). *UAB*, 1994.
6. Zheng N, et al. In: Hung GK, Pallis JM, eds. *Biomedical Engineering Principles in Sports*. Plenum Publishers, 2004.

Table 1. Differences, based upon mean marker-less system value minus mean marker system value for each subject.

Parameter	Lower Limit of Agreement	Mean	Upper Limit of Agreement	Standard deviation across subjects	Standard deviation within subject
At the instant of foot contact					
Stride length (% height)	0.2	1.8	3.3	0.8	0.3
Lead foot position (cm)	-4.8	-1.2	2.7	1.9	0.4
Lead foot angle (°)	-8.3	1.5	11.4	5.0	1.8
Lead knee flexion (°)	4.4	11.5	18.7	3.7	1.4
Trunk axial rotation (°)	-28.1	-10.8	6.5	8.8	2.4
Shoulder external rotation (°)	-23.9	-1.5	20.8	11.4	5.2
Arm cocking					
Maximum shoulder external rotation (°)	-24.7	-8.5	7.7	8.3	2.2
Maximum elbow flexion (°)	-37.5	-13.9	9.6	12.0	2.7
At the instant of ball release					
Lead knee flexion (°)	7.9	15.8	23.7	4.0	1.3
Trunk forward tilt (°)	-6.0	-0.1	5.7	3.0	0.8
Trunk side tilt (°)	-9.8	-5.5	-1.1	2.2	0.7
Shoulder abduction (°)	-11.0	-0.9	9.01	5.1	1.4

SHOULDER-TRUNK COORDINATION AND SEQUENCING DURING SLAP SHOTS IN ICE HOCKEY PLAYERS

Shawn Robbins[1*], Philippe J[2]. Renaud, Neil MacInnis[2], and David J. Pearsall[2]
[1]School of Physical and Occupational Therapy, McGill University
[2]Department of Kinesiology and Physical Education, McGill University
email: *shawn.robbins@mcgill.ca

Introduction

In ice hockey, slap shots produce the fastest puck speeds of all shot types. Research evaluating slap shot performance has focused on stick properties or player characteristics.[1] There has been limited research examining optimal body kinematics during shooting on real ice, and comparing these variables between skill levels. The objective was to compare shoulder-trunk inter-joint coordination and joint sequencing between high and low calibre ice hockey players when completing a slap shot on the ice surface. We hypothesized that high calibre players would demonstrate more out-of-phase shoulder-trunk inter-joint coordination and earlier onset of peak trunk angular velocity compared to low calibre players.

Methods

High (n=10; mean age 26 years) and low (n=9; mean age 26 years) calibre male ice hockey players were recruited. High calibre players played at least at the major junior level and/or Canadian university level, while low calibre players played at lower levels. Reflective markers were placed on the players, stick, and puck. A 14-camera Vicon motion capture system sampled at 240 Hz captured marker data. Participants completed ten skating slap shot trials on real ice where they shot 9.25 m from the net. They aimed for a target in the middle of the net. Players used the same stick type (Nexus 1N, 87 flex, Bauer Ltd).

The slap shot was divided into backswing and downswing based on the position of the stick blade. Peak puck speed was calculated. Trunk and shoulder angles were calculated using Euler YXZ and ZYZ sequences, respectively. Both lead and trail shoulders were considered (e.g., right shoulder is the trail side and left shoulder is the lead side for right-handed shooters). Inter-joint coordination between the shoulder-trunk was determined using continuous relative phase (CRP), and both magnitude and inter-trial variability measures were calculated. To determine sequencing, the norm of the joint angular velocity was calculated for the trunk and shoulders. Then, peak velocity in relation to puck release was determined. Mann-Whitney U tests examined differences in puck speed, inter-joint coordination magnitude and variability, and sequencing between high and low calibre players.

Results and Discussion

High calibre players produced faster puck speeds (mean difference=2.94 m/s), although this was not statistically significant (p=0.105). For shoulder-elevation plane/trunk rotation (p=0.050) and shoulder-elevation/trunk rotation (p=0.028) inter-joint coordination on the trail shoulder, high calibre players had greater CRP magnitude values than low calibre players. Thus, high calibre players were more out-of-phase, specifically during the backswing phase (Figure 1). There were no differences in lead shoulder/trunk CRP magnitude and CRP inter-trial variability. For sequencing, peak trunk angular velocity occurred earlier in relation to peak shoulder (trail side) angular velocity (p=0.038) for high calibre players. There were no group differences for sequencing of the trunk/lead side shoulder (p=0.574).

Consistent with our hypothesis, high calibre players were more out-phase for shoulder-trunk inter-joint coordination during the backswing on the trail shoulder, potentially allowing them to adapt more easily to varying shot environments. However, there were no differences in inter-joint coordination during downswing or between the lead shoulder and trunk. Also consistent with our hypothesis, high calibre players had earlier onset of peak angular velocity of the trunk relative to the trail shoulder. This proximal to distal sequence might help them produce faster puck speeds, similar to a golf swing. Again, there was no significant findings with sequencing of the lead shoulder.

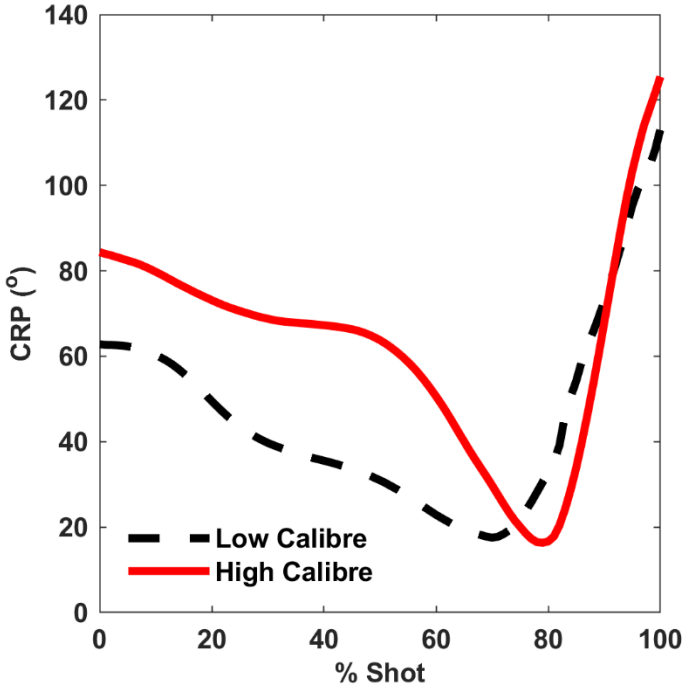

Figure 1: Group mean continuous relative phase (CRP) waveforms during a slap shot in high and low calibre players. Higher values represent more out-of-phase coordination.

Significance

When coaching players on how to take a slap shot, more attention should be paid to the backswing phase including the proper mechanics of the shoulder and trunk. In addition, earlier onset of trunk rotation towards the net should be encouraged in order to ensure a proximal to distal sequence in the trunk and shoulder.

Acknowledgments

Funding was provided by a Collaborative Research and Development Gant from the Natural Sciences and Engineering Research Council of Canada and Bauer Ltd.

References

[1] Wu TC et al., 2003. *Sports Eng.* 6: 31-39.

NEUROMUSCULAR CONTROL OF LOWER LIMB MUSCLES DURING HIGH CADENCE CYCLING

Brett Still[1,2], Alexander Willmott[1], Steven Lindley[2], David Mullineaux[1], Franky Mulloy[1]
[1]School of Sport and Exercise Science, University of Lincoln, UK [2]Delsys Europe, Manchester, UK
Email: bstill@lincoln.ac.uk

Introduction

Athletes employ a range of fast-paced whole-limb movements during competitive skill acquisition but our understanding of neuromuscular control during these tasks remains limited. Surface electromyography (EMG) decomposition has provided useful insight into neuromuscular control of a small number of muscles during slow paced single muscle activities [1, 2]. However, increases in limb segment acceleration and coordination of multiple muscle groups across multiple joints during fast-paced whole-limb tasks may limit the extent to which current findings can be applied to sporting activities. Recent evidence suggests that as the speed of movement increases motor unit firings become synonymous with an initial firing rate distinct from the moving time window average firing rate normally reported during slower movements [3]. This initial firing rate may be lower and facilitate quicker adjustments in force output, improving control of limb segment accelerations and better coordination of muscle activity [4]. What impact this motor unit firing behavior has on motor unit recruitment and subsequent effect on neuromuscular control during fast-paced movement is currently unclear. To investigate the effect of speed of movement on neuromuscular control, surface EMG decomposition was applied to measure the motor unit firings of six lower limb muscles during high cadence cycling.

Methods

Eight recreationally active males (mean ± SD; age 25 ± 8 years; height 177 ± 6 cm; mass 72 ± 11 kg) completed 75 s of sub-maximal cycling at cadences of 60, 75, 90 and 105 RPM on a cycle ergometer at 40% of maximal power (determined by a 10 s sprint test at each cadence). Surface EMG data were recorded and decomposed for six muscles (rectus femoris (RF), vastus lateralis (VL), gastrocnemius medialis (GA), tibialis anterior (TA), biceps femoris (BF) and semimembranosus (SM)). A novel approach was used to time normalise motor unit firings to 100% of the pedal cycle (determined via marker data collected with a motion capture system). Data was analysed for 15 consecutive pedal cycles. Adaptations in neuromuscular control were determined by identifying differences in the slope and y-intercept of linear regression of motor unit firings per pedal cycle (ppc) and motor unit recruitment thresholds (%Cycle) for each muscle at each cadence using a repeat measures ANOVA and post hoc analysis.

Figure 1. Experimental setup with a cycle ergometer placed in front of a monitor displaying power output and cycling parameters.

Results and Discussion

At 60 RPM both RF and VL had a regression slope significantly steeper than that for the other three cadences (RF, F = 7.38; VL, F = 9.48). At 105 RPM motor unit firing instances per pedal cycle for four muscles (RF, VL, GA and SM) averaged across the motor unit pool were smaller when compared with the other three cadences. The most significant differences occurring between 90 RPM and 105 RPM (RF, F = 7.86; VL, F = 6.21; GA, F = 4.73; SM, F = 4.44).

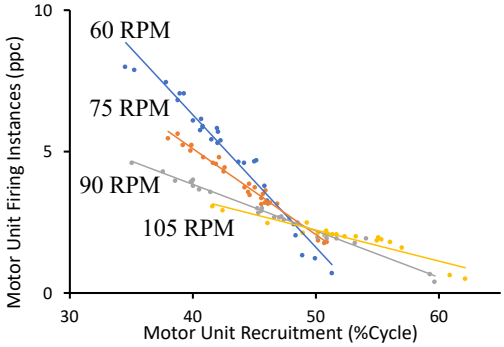

Figure 2. Regression analysis for the rectus femoris recorded for an individual participant at four pedal speeds. Each data point represents an individual motor unit. All data is the average of 15 consecutive pedal cycles. ppc = pulses per cycle. Pedal cycle defined using bottom dead centre.

Change in the motor unit recruitment activity of the RF and VL at 60 RPM is supported by previous research [5]. A decrease in motor unit firing instances per pedal cycle of four of the six muscles at 105 RPM is a novel finding and supports the hypothesis of a decrease in motor unit firing activity at faster pedal speeds relative to a defined movement cycle. This may be related to an increased requirement for quicker force adjustments improving control of limb segment accelerations and better coordination of muscle activity as the speed of movement increases [4, 6].

Significance

Reporting motor unit firing instances per pedal cycle has allowed greater understanding of the interactive effect of motor unit firing behavior and movement control. When developing exercise and training programs it may be important to consider the speed at which an exercise is performed for specific adaptations in neuromuscular control.

References

[1] De Luca et al., 2015. *J. Neurophysiol*., 113(6). 1941-1951
[2] Oliveira et al., 2021. *J. Appl. Physiol*., 130(6). 1798-1813
[3] Kirk et al., 2020. *The FASEB Journal*., 34(s1). pp. 1-1
[4] Celichowski et al., 2019 *Muscle. Exerc. Physiol.* pp. 51-91
[5] Blake et al., 2015. *J. Neurophysiol*., 114(6). 3283-3295
[6] Pratt et al., 2021. *Med. Sci. Sport Exerc*., 53(11). 2436-2444

SERVE KNEE FLEXION CONTRIBUTES TO SERVE SPEED OF JUNIOR TENNIS PLAYERS

Joana F. Hornestam[1,2*], Thales R. Souza[1], Fabrício A. Magalhães[1], Mickäel Begon[3] and Sérgio T. Fonseca[1]
[1]Graduate Program in Rehabilitation Sciences, Federal University of Minas Gerais, Belo Horizonte, MG, Brazil
[2]School of Rehabilitation Sciences, University of Ottawa, ON, Canada
[3]School of Kinesiology and Exercise Sciences, Université de Montréal, Montreal, QC, Canada
email: *fhjoana@gmail.com

Introduction

The serve is one of the most important strokes to win a tennis match. Speed is the main key to a successful and strategic serve[1]. It is well known that the shoulder internal rotation is one of the major contributors to serve speed[1,2]. However, the lower limbs are believed to be at the base of the serve's kinetic chain and so in charge of starting energy generation and transfer to superior body segments and, finally, to the tennis racket during serve[2]. However, the effects of knee flexion on the biomechanics of superior body joints and racket have not been clearly established in junior tennis players.

This study aimed to examine the effects of knee flexion during tennis serve preparation phase on serve speed and on the biomechanics of superior joints that could contribute to serve speed.

Methods

Twenty-six right-handed junior competitive tennis players were equally divided into two groups based on their peak knee flexion (PKF) during the preparation phase of the tennis serve[3]: Smaller (SKF; n=13, male n = 9, 13.85 ± 1.14 yrs; 1.66 ± 0.07 cm; 53.72 ± 4.56 kg) and Greater (GKF; n=13, male = 10, 14.38 ± 1.26 yrs; 1.67 ± 0.06 cm; 56.15 ± 6.32 kg) Knee Flexion.

Wireless inertial sensors (Xsens Technologies B.V., Enschede, The Netherlands) were used to record full body and racket motion tennis serve while the participants performed 5 flat, first, and valid serves on the tennis court. The means were used for analysis.

The maximum angular velocities of knee, hip, trunk, and shoulder and pelvic vertical velocity during serve, and the racket resultant velocity just before racket-ball impact were compared between groups. Additionally, the groups were compared for PKF, for characterization, and for variables that could potentially impact serve speed, such as age, body height, body mass, weekly training volume, and years of practice. These analyses were conducted using the independent samples t-test.

Results and Discussion

There were no differences in age (p=0.265), body height (p=0.591), body mass (p=0.271), weekly training volume (p=0.068), and years of practice (p=0.690) between groups. PKF was 20° greater in the GKF compared to the SKF.

The maximum racket velocity (p=0.006) was higher in the GKF, indicating a better serve performance of this tennis players that flex more their knees during the serve preparation. The maximum knee (p=0.004) and hip (p<0.001) extension, pelvic upward (p=0.008), and trunk anterior flexion (p=0.033) velocities were higher in the GKF than the SKF (Figure 1). These findings show that greater knee flexion contributes increases in joint velocities that may explain serve speed.

No difference was found for the maximum trunk lateral flexion (p=0.095) and rotation (i.e., rotation on the transverse plane) (p=0.119) and shoulder internal rotation velocities (p=0.116). Curiously, the shoulder is typically overload and one of the most injured joints in tennis[4]. These results show that larger serve knee flexion relates to higher serve speed, without greater contribution of the shoulder.

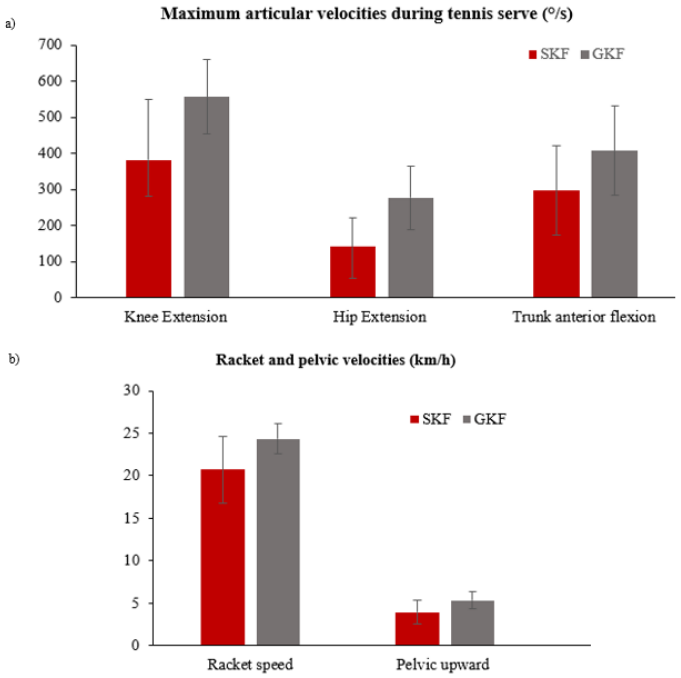

Figure 1. Joint, segments and racket velocity

Significance

Knee flexion should be seen as a contributor to serve speed of junior competitive tennis players. It is associated with greater lower limb, pelvic and trunk velocities, but not with shoulder velocity. Coaches should consider evaluating knee flexion during tennis serve and preparing training strategies to increase it, when planning training to improve serve performance. Also, rehabilitation and injury prevention team members examining junior tennis players should consider assessing and preparing them to increase knee flexion during serve, as these can potentially gain in serve performance without increasing shoulder load.

Acknowledgments

We thank the Brazilian funding agencies: CAPES (finance code 001 and process number 88887.364812/2019- 00) and CNPQ for the financial support. We also thank the SESI/FIEMG – Minas Gerais Industrial Federation - for the availability of the inertial measuring system.

References

1. Martin, 2014. *J Med Sci Tennis.*
2. Kibler, 1995. *Clin. Sports Med.*
3. Kovacs et al., 2011. *Sports Health.*
4. Lynall et al., 2016. *Br J Sports Med.*

An Automatic Knee Joint Geometry Construction From MRI

Reza Kakavand[1*], Mehrdad Palizi[2], Olivia L. Bruce[1], Samer Adeeb[2], W. Brent Edwards[1] and Amin Komeili[1*]
[1]Schulich School of Engineering, Department of Biomedical Engineering, University of Calgary
[2]Faculty of Engineering, Civil and Environmental Engineering Dept, University of Alberta
email: * reza.kakavand@ucalgary.ca

Introduction

Specific sports and occupations involving intense physical activity or prolonged loading of the knee are highly associated with OA[1,2]. The precise prediction of OA is therefore useful for developing preventative treatments. One efficient method for such prediction is the Finite Element Method (FE). FE is used to estimate the internal pressure at contact surfaces and deformation of cartilage due to external forces. Constructing accurate bone geometry is a major initial step for developing patient-specific FE models of the knee joint. MRI images are frequently used to manually segment knee geometry. However, manual segmentation is time-consuming. An automatic segmentation approach, that is as accurate as the manual one, would significantly facilitate knee joint biomechanics analysis. Therefore, we proposed an automatic method, where a 2D U-Net convolutional neural network (CNN) and a statistical shape model (SSM) were combined to extract the distal femur and proximal tibia from MRI images of the Osteoarthritis Initiative (OAI) database (https://nda.nih.gov/oai/). The validity of the predictions was verified by evaluating the maximum principal stress between the manual and automatic segmentations.

Methods

First, the femur and tibia were segmented using a 2D U-Net CNN. The outcome was fed into a SSM to improve the accuracy of segmentation[3]. The CNN included 4 layers. In the downstream path, each layer had 2 convolutions (5×5, ReLU) and 0.1 dropout, followed by a maxpooling of 2×2 between layers. 32 filters were used for the first layer, duplicated for the next layers. Zero-padding was employed to preserve the image size. The upstream path was similar to the downstream. The maxpooling was replaced with an up-convolution of 2×2, concatenated by the corresponding convoluted layer in the downstream. At the end of this path, there was a 1×1 convolution to generate a probability map with the same size of the input image. The SSM was fitted to the femoral condyles and tibial plateaus predicted from the CNN. A limited-memory Broyden-Fletcher-Goldfarb-Shanno (L-BFGS) algorithm was used for the fitting process[4]. In this process, the vector of weights for principal components and translation were the unknowns.

256 MRI images (61.87±9.33 years; 29.27±4.52 BMI [kg/m^2]; 0.36×0.36×0.7 image resolution [mm]) from the OAI database whose masks are publicly available[3] were used for training. Another 20 MRI images from the same resources were used for testing. For 3 test patients, we compared the mechanical stress between FE models developed using manual and automatic segmentations. Articular cartilage was added to the bones. Forces associated with gait were applied to the femur while the tibia was held fixed. The maximum principal stress in the cartilage was compared.

Results and Discussion

The difference between the maximum principal stress of the two FE models, one developed by manual segmentation and the other with the automatic segmentation, was not statistically significant. The results showed that the automatic segmentation is reliable in terms of the induced stress in FE. The Jaccard similarity index[3] of 80 ±1.5 % was obtained.

The combination of CNN and SSM is a novel method for automatic segmentation and geometry development of patient-specific FE models of the knee joint. This method relies on both intensity (CNN) and coordinate (SSM) data of the region of interest. Studies that used only CNN or SSM were susceptible to noise and resulted in local anomalies on the geometry[3]. When the intensity of a test image differs considerably from the intensity of training data sets, the CNN-based method predicted a poor segmentation[3]. Moreover, an SSM-based method requires anatomical landmarks for the prediction. The manual selection of landmarks is a tedious task and also human errors might occur in detecting their exact location (Figure 1). This manual task was performed by the CNN in our study. The choice of condyles and tibia plateaus in SSM ensures a precise geometry in contact areas.

Significance

The automatic segmentation is one crucial step further towards developing patient-specific FE models of the knee joint. In this study, the CNN and SSM were used for automatic geometry reconstruction from knee MRI scans. The long-term objective of this study is to develop a user-friendly software package for geometry reconstruction and knee joint external loads prediction using machine learning approaches. Such tools would make the application of patient specific FE modelling more accessible for clinicians and researchers.

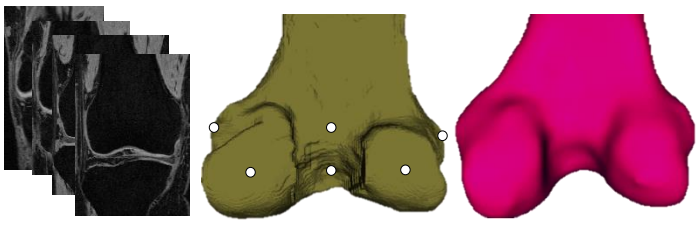

Figure 1. Manual segmentation (middle) and automatic segmentation using the SSM and CNN (right) from MRI (left). White circles are anatomical landmarks.

Acknowledgments

The project was supported by the Natural Sciences and Engineering Research Council Canada (NSERC) Discovery grant.

References

1 Driban, J. B. *et al. J. Athl. Train.* 52, 497–506 (2017)
2 Andersen, S. *et al. Occup. Environ. Med.* 69, 325–330 (2012)
3 Ambellan, F. *et al. Med. Image Anal.* 52, 109–118 (2019)
4 Bruce, O. L. *et al. Comput. Methods Biomech. Biomed. Engin.* 1–12 (2021)

DEVELOPMENT OF MULTI-BUNDLE VIRTUAL LIGAMENTS TO SIMULATE KNEE MECHANICS AFTER TOTAL KNEE ARTHROPLASTY

Samira Vakili[1*], Brent Lanting[2], Alan Getgood[2,3], and Ryan Willing[1]
[1]Western University, [2]London Health Sciences Centre University Hospital, [3]Fowler Kennedy, London, Ontario, Canada
email: *svakili4@uwo.ca

Introduction

Total knee arthroplasty (TKA) aims to improve joint kinematics and hence restore joint stability. Preclinical testing of TKA implants is essential to understanding their mechanical performance and for developing strategies to improve joint stability [1]. Ideally, such preclinical tests should reproduce the physiological behaviour of the knee joint, which is guided by the articular geometries of the implants in conjunction with the capsule and ligaments. The purpose of our study was to design subject-specific virtual ligaments based on native ligaments and to determine if subject-specific virtual ligaments accurately reproduce the same mechanical behaviour as real ligaments surrounding TKA implants on a joint motion simulator.

Methods

Five cadaveric knee specimens with TKA implants were mounted onto the 6 degrees of freedom AMTI VIVO joint motion simulator (Advanced Mechanical Technology, Inc, Watertown, MA). Each knee was subjected to loads that simulated neutral flexion-extension (FE) and knee laxity tests. FE kinematics were determined by flexing and extending the knee between 0° and 90° while applying a 200N constant compression force. Knee laxity tests also were simulated by applying constant anterior-posterior (AP) forces, varus-valgus (VV), or internal-external (IE) torques to the tibia while maintaining 200 N of compression, across the full range of flexion and extension. Tibiofemoral kinematics were recorded during each motion. The forces transmitted through major ligaments (medial, lateral, and the posterior cruciate ligament) were measured using a sequential resection and superposition technique whereby each ligament was individually dissected, the kinematics were repeated, and the changes in joint reaction force were measured. Ligament lengths were calculated based on the point-to-point distances between the femoral and tibial insertions. Ligament properties (stiffness, slack length, ligament insertion points, and the number of bundles) were calibrated by tuning the measured ligament force to an established nonlinear force-length relationship. Based on this, virtual ligaments were developed for each specimen and were used to simulate the soft tissue envelop around isolated TKA implants mounted on the motion simulator. The same motions were then repeated allowing the comparison of joint kinematics resulting from native versus virtual ligaments.

Results and Discussion

The mean difference between virtual and native ligament knee kinematics during FE was less than 3 mm in terms of AP displacement, 2° for IE rotation, and 2° for VV. The average RMSE between virtual and native ligament knee laxities was less than 3.6 mm for AP, 7.6° for IE, and 1.7° for VV. There were similar errors recorded in the present study as in previous studies, such as an average RMSE of less than 2 deg during VV rotations, less than 6 deg during IE rotations, and less than 3 mm of translation during AP displacements [2].

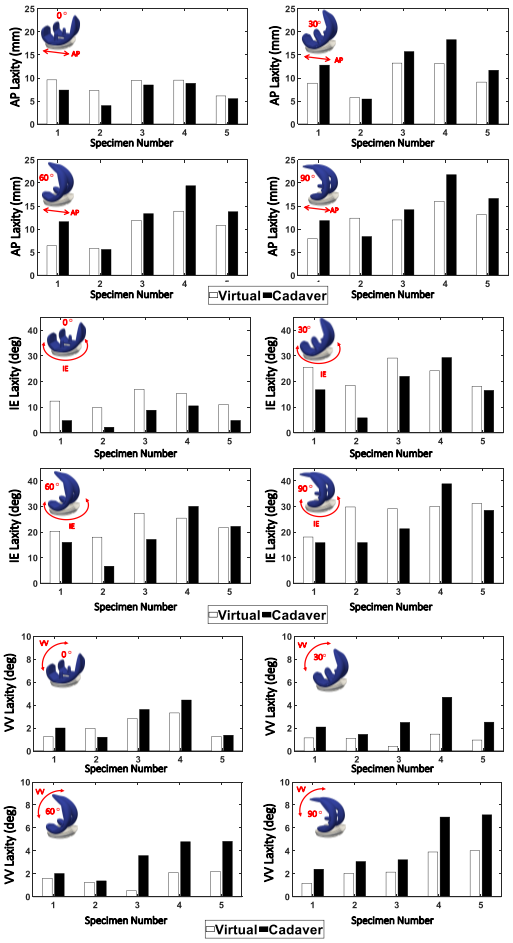

Figure 1: AP, IE, and VV laxity in TKA joint with native ligaments (cadaver) and with virtual ligaments (virtual) tests in 0, 30, 60 and 90 degrees of flexion

Significance

In this study, virtual ligament properties were calibrated to best match native ligament behaviours. When used to stabilize isolated implants, the resulting behaviours were comparable to those of the real ligaments. These results suggest that databases of subject-specific knee ligaments could be developed and employed on joint motion simulators to simulate prosthesis behaviours in a large population of knees.

References

[1] H. Haider and P. S. Walker., 2005. *J Biomech.* 38.
[2] Harris et al., 2016. *J Biomech Eng.* 138.

AGE-RELATED REDUCTIONS IN ACHILLES TENDON STIFFNESS PERSIST AT MATCHED TRICEPS SURAE ACTIVATIONS

Rebecca L. Krupenevich[1*], Gregory S. Sawicki[2], and Jason R. Franz[1]
[1]Joint Department of Biomedical Engineering, UNC Chapel Hill and NC State University, Chapel Hill, NC
[2]George W. Woodruff School of Mechanical Engineering, Georgia Tech, Atlanta, GA

email: *rlkrup@email.unc.edu

Introduction

Ankle muscle-tendon unit (MTU) stiffness is thought to arise from a combination of activation-independent (*i.e.*, Achilles tendon) and activation-dependent components (*i.e.*, muscle). Indeed, we have shown that MTU stiffness is regulated via activation-dependent changes in triceps surae length-tension behavior [1]. This neuromechanical behavior is critical to help explain clinically-relevant declines in ankle power output during walking – for example those due to aging. Historically, most human subject comparisons have shown *in vivo* evidence of reduced Achilles tendon stiffness (k_{AT}) with age [2]. However, these previous studies may have inadvertently compared k_{AT} between young and older adults at different regions on their respective tendon length-tension curves. Indeed, tendon length-tension relations are nonlinear at lower tissue strains and the effective stiffness "seen" by muscle can vary as a function of activation – something overlooked in our previous theoretical considerations of muscle-tendon interaction dynamics. Thus, it is unknown how aging effects on the effective stiffness of the Achilles tendon varies as a function of triceps surae activation. The purpose of this study was to quantify age-related differences in apparent K_{AT} across a broad range of matched muscle activations prescribed using electromyographic biofeedback. We hypothesized that (1) young and older adults would exhibit greater k_{AT} at higher triceps surae activations – consistent with a shift from the nonlinear to the linear region of their tendon length-tension curves, and (2) older adults would exhibit lesser k_{AT} compared to young adults at matched activations.

Methods

Thus far, 15 young adults (8F/7M, 23±4 yrs, 1.7±0.09 m, 72.9±14.2 kg) and 13 older adults (7F/6M, 71±5 yrs, 1.7±0.07 m, 71.3±12.0 kg) performed passive ankle rotation and a series of isokinetic plantarflexion contractions while using biofeedback to match targets representing 25 and 75% of their maximum voluntary isometric contraction (MVIC) triceps surae activation. Specifically, participants performed isokinetic eccentric contractions at 20°/s from 30° plantarflexion to maximum dorsiflexion. Ultrasound imaging captured displacement of the gastrocnemius muscle-tendon junction (MTJ) and surface electromyography measured muscle activation. Achilles tendon force was estimated by dividing ankle torque by subject-specific Achilles tendon moment arm. Achilles tendon stiffness was then calculated as the slope of the relation between tendon force and tendon elongation, from 20-80% of each subjects' dorsiflexion range of motion (i.e. starting from a neutral ankle angle). A mixed ANOVA compared Achilles tendon stiffness across activation levels, and between young and older adults (p<0.05).

Results and Discussion

We found a significant interaction between activation level and age (p=0.045), a significant main effect of activation level (p<0.001), and a significant main effect of age (p=0.028) on k_{AT}. First, consistent with our first hypothesis, Achilles tendon stiffness increased with muscle activation in both young and older adults. We interpret these data to suggest that the non-linear region of the tendon length-tension relation is functionally meaningful not only at negligible levels of muscle activation, but across a broad range relevant to daily activities such as walking. In addition, and consistent with our second hypothesis, older adults displayed lesser Achilles tendon stiffness than young adults. Pairwise comparisons revealed that this effect was activation-dependent and specific to passive rotation (-56%, p=0.045) and 75% MVIC activation (-63%, p=0.005). These results confirm prior reports that older adults exhibit lesser k_{AT} stiffness compared to young but add that this difference: (i) exists during passive rotation and (ii) persists despite matched activations at those representative of walking.

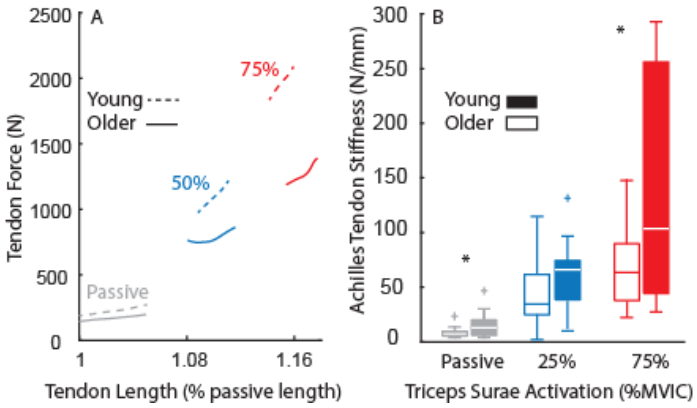

Figure 1. (A) Tendon force-length relations and (B) Achilles tendon stiffness across 0, 25, and 75% MVIC triceps surae activation in young (dashed line/filled box) and older adults (sold line/open box). Asterisks (*) indicate significant age effects.

Significance

Our results suggest that the effective tendon stiffness "seen" by the triceps surae muscles varies across a functionally-relevant range of activations and that age-related reductions in Achilles tendon stiffness persist even at matched muscle activations. These findings have functional implications for the origins of neuromechanical deficits in ankle push-off power observed in older adults. Indeed, in support of our recently published hypothesis [3], reduced Achilles tendon stiffness may precipitate an unfavorable cascade of muscle dysfunction.

Acknowledgments

This work was supported by an NIH grant (R01AG058615).

References

[1] Krupenevich et al. (2020). *JAB.* 36(4) 209.
[2] Delabastita et al. (2021). *Scand J Med Sci Sports.* 31(5) 1036
[3] Krupenevich et al. (2021). *Gerontology.*

ESTIMATION OF PATELLAR TENDON LOAD DURING BILATERAL AND UNILATERAL MOVEMENTS IN YOUNG ADULTS

Matthew Beerse[1*], Breven Perry[1], Allison Kinney[1], and Joaquin Barrios[1]
[1]University of Dayton
email: *mbeerse1@udayton.edu

Introduction

Patellar tendinopathies might arise, in part, from repetitive loading of the patellar tendon [1]. Prior studies have estimated patellar tendon forces during different jumps [2], and jump-stops [3]. However, a range across movements with likely low loads, e.g. walking, to high loads, e.g. drop vertical jumps, is unknown but necessary to make recommendations away from high load movements. Moreover, evaluation of unilateral variations is imperative, as many sport-specific skills require jumping and landing on one leg. Therefore, the purpose of this study was to estimate patellar tendon force, impulse, and loading rate across a range of movements and compare unilateral variations.

Methods

Thirty young adults (20F, 20.8 (1.25) years) participated. We collected kinematic data using a Vicon motion capture system (Oxford, UK). Kinetic data was captured using a Bertec force plate (OH, USA). Subjects completed five successful trials of overground walking, overground running, two-legged hopping in-place (HOP), countermovement jump (CMJ), drop landing (DL), and drop vertical jump (DVJ). Subjects completed unilateral variations of the HOP, CMJ, DL, and DVJ movements. Knee joint moment was estimated using an inverse dynamics approach. Patellar tendon moment arm was approximated from a polynomial regression curve based on knee joint angle [4]. Patellar tendon force was then calculated as the quotient of knee moment and patellar tendon moment arm. Contact time and time to peak were identified to evaluate impulse and loading rate, respectively. A one-way repeated measures ANOVA was used to compare bilateral tasks. A two-way repeated measures ANOVA was used to compare bilateral and unilateral variations of tasks.

Results and Discussion

Across bilateral movements (Fig.1), the DVJ demonstrated significantly greater peak patellar tendon force than all others, greater patellar tendon impulse except compared to running and CMJ, and greater loading rate except compared to DL. This finding is likely a result of a large extension moment about the knee joint and greater peak knee flexion where the moment arm of the patellar tendon becomes smaller [4].

Unilateral variations were performed with less peak knee flexion, except for HOP (Fig. 2). Interestingly, unilateral variations did not result in significantly different peak patellar tendon force though the entire bodyweight was supported on one leg. Instead, for the DVJ, the bilateral variation was significantly greater than the unilateral. A strategy adopted for these unilateral movements might be to limit maximum knee flexion to maintain a larger patellar tendon moment arm, reducing the required force. There were no statistically significant differences of impulse. Similarly, there were no significant differences of loading rate between unilateral and bilateral variations, but similar task differences across both variations.

Our findings suggest landing and jumping movements, particularly performed together, i.e. DVJ, result in the greatest load and loading rate of the patellar tendon. Unilateral variations of these movements pose similar loading risks, but individual variations of technique might influence patellar tendon loads.

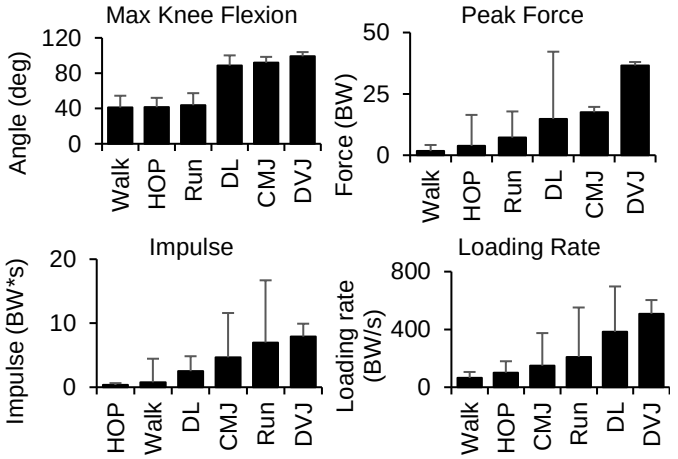

Figure 1: Mean (SD) of bilateral movements. Ordered lowest to highest.

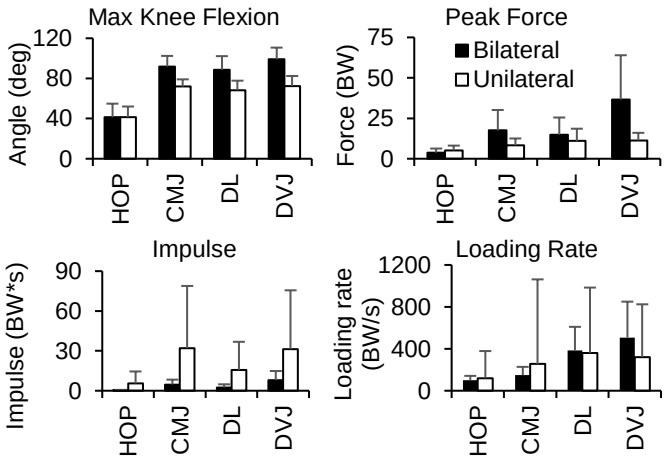

Figure 2: Mean (SD) of bilateral and unilateral variations.

Significance

Our results provide insight to patellar tendon specific loads during common movements and their unilateral variations. These results can inform clinicians and practitioners which movements should be minimized or avoided when working with individuals at risk or presenting with patellar tendinopathies, such as Osgood-Schlatter's disease.

References

[1] Cook et al. 2000 *Scan J Med Sci Sports*. 10: 216-220.
[2] Finni et al. 2000. *Euro J Appl Physiol*. 83: 416-426.
[3] Edwards et al., 2012. *Scan J Med Sci Sports*. 22: 2-11.
[4] Herzog & Read, 1993. *J Anatomy*. 213-230.

SQUAT EXERCISE VARIATIONS REQUIRE UNIQUE THREE-DIMENSIONAL HIP MUSCLE STRATEGIES

Zachary A. Fielding[1*], and Loren Z.F. Chiu[1]
[1]Faculty of Kinesiology, Sport, and Recreation, University of Alberta
*email: zfieldin@ualberta.ca

Introduction

The mechanical loading of lower extremity muscles in resistance training exercises has primarily emphasized quantifying the sagittal plane net joint moments (NJM). Less is known regarding frontal and transverse plane NJMs during resistance training exercises. Three-dimensional hip NJMs are particularly relevant as muscles crossing this joint have moment arms in two or three axes [1]. Consequently, a multi-planar investigation could elucidate differences in muscle strategy between seemingly similar exercises. This study sets out to explore the multi-planar NJMs exerted during four loaded squat exercise variations.

Methods

Females (n = 18) who could perform a bilateral back squat (BS) with ≥80% of their body mass for 5 repetitions were included. Participants performed bilateral back squat, forward split squat (FSS), lateral split squat (LSS), and single limb squat (SLS). The five repetition maximum (5 RM) was determined for each exercise during the first two visits. On the third visit, participants performed three repetitions of each exercise at their 5 RM standing on force platforms (f_s = 1000 Hz) with retroreflective markers recorded using eight optoelectronic cameras (f_s = 100 Hz). Hip NJMs were computed in Visual 3D Software (C-Motion Inc., Germantown, Maryland, USA) and expressed in the local coordinate system of the thigh. Negative values represent hip extensor (X-axis), abduction (Y-axis), and external rotation (Z-axis) moments. Hip flexion was expressed using the pelvis as the reference segment with an X-Y-Z Cardan rotation sequence. NJM were averaged across 9.9° intervals of hip flexion (i.e., >10° to 20°, >20° to 30°, etc.), for descent and ascent phases. NJM from the greatest hip flexion interval during ascent was used for analysis. Non-parametric Friedman's Test and pairwise Sign Tests assessed for statistical differences due to non-normality and low sample size. A Bonferonni correction factor was applied to pairwise tests (adjusted significance: $p < 0.0083$). Data is presented as median, 25th-, and 75th-quartiles.

Results and Discussion

Friedman's Test revealed a significant group difference for sagittal ($X^2(3) = 34.67$, $p < 0.01$), frontal ($X^2(3) = 25.2$, $p < 0.01$), and transverse ($X^2(3) = 25.0$, $p < 0.01$) plane hip NJMs. Pairwise comparisons revealed some differences between exercise, demonstrating collectively, that three different multi-planar hip muscle strategies were exhibited (Table 1). The SLS exercise utilized a hip *extensor-abductor-internal rotator* muscle strategy. The FSS and LSS employed the same strategy, requiring hip extensors and internal rotators, with minimal frontal plane muscle loading. The BS exercise utilized a hip extensor-adductor strategy, with minimal transverse plane NJM. The BS demonstrates a hip extensor strategy that may primarily require the adductor magnus posterior head [1]. The variance in the transverse plane NJM may indicate additional contribution from the gluteus maximus for individuals with external rotator NJM, versus adductor longus and adductor magnus anterior head for individuals with internal rotator NJM [1]. The SLS, FSS, and LSS would require more complex muscle synergies as no single hip extensor – or combination of hip extensor - muscles could explain the multi-planar NJMs [1]. Further investigation is necessary to explore the specific hip muscle contributions to these exercises, which is pertinent to understand the practical meaningfulness of these exercises for eliciting muscle strength adaptations.

Significance

There are divergent frontal and transverse plane NJM strategies during loaded squat exercise variations. As muscles may act in one, two, or all three planes, the multi-planar hip NJMs indicate that different muscle synergies are required for the BS versus the FSS, LSS, and the SLS, and the SLS versus the LSS. As all exercises demonstrated hip extensor NJMs with varying frontal and transverse plane demands, squat exercises may require distinct hip extensor muscles. Identifying these muscle strategies may allow appropriate exercises to be used to target specific muscles. As hip muscle strategies during weight-bearing tasks may be multi-planar, the collective analysis of NJM in all three planes is required, as opposed to traditional uniplanar analyses.

References

[1] Dostal, W., et al. Actions of Hip Muscles. *Physical Therapy*. 66:351-359. doi.org/10.1093/ptj/66.3.351

Acknowledgments

Bethany Jantz and Caitlin Coulombe assisted with this study.

Table 1. Hip Net Joint Moments at Peak Hip Flexion during Squat Exercise Variations

Plane	Back Squat	Forward Split Squat	Lateral Split Squat	Single Limb Squat
Sagittal (Nm/kg)	-2.50 [-2.60, -2.26]	-3.47 [-4.00, -3.19]†	-3.28 [-3.36, -2.69]†‡	-2.92 [-3.10, -2.54]‡
Frontal (Nm/kg)	0.31 [-0.05, 0.53]*	-0.02 [-0.22, 0.28]*	0.05[-0.07, 0.36]*	-0.45[-0.57, -0.34]
Transverse (Nm/kg)	-0.02 [-0.15, 0.32]*	0.29 [0.22, 0.42]*	0.27 [0.14, 0.36]*	0.48 [0.39, 0.59]

Data are median [25th-, 75th-quartiles]; †different than back squat ($p < 0.0083$); ‡different than forward split squat ($p < 0.0083$); *different than single limb squat ($p < 0.0083$).

VALIDATION OF [^{18}F]NaF PET AS A MEASURE OF BONE REMODELING USING FINITE ELEMENT ANALYSIS

Anthony A. Gatti[1], Bryan Haddock, Ryan S. Alcantara, Sarah R. St. Pierre, Mathias Peirlinck, Scott D. Uhlrich, Ellen Kuhl, Charlotte Suetta, Garry Evan Gold[1], Akshay Chaudhari[1], Jennifer L. Hicks, Scott L. Delp, Feliks Kogan[1*]
[1]*Dept. of Radiology, Stanford University, Stanford, CA, USA.* email: * fkogan@stanford.edu

Introduction

Quantifying the acute effect of mechanical loading on bone remodeling is crucial to understanding the etiology of bone stress injuries. Fluoride is attracted to hydroxyapatite and thus has a high affinity for bone. Positron emission tomography (PET) studies can use [^{18}F]NaF as a tracer to measure and map the location of increased activity associated with bone formation [1]. Increased uptake of [^{18}F]NaF has not been validated as a measure of load-induced bone remodeling in humans, or at physiologic loads. Bone remodeling is driven by mechanoreceptors which are sensitive to tissue strain that can be estimated using finite element analysis (FEA). The aim of this study was to explore whether increased [^{18}F]NaF uptake in response to exercise-induced loading is related to FEA based tibial strains following a high impact drop landing exercise.

Methods

Twelve healthy subjects underwent an imaging protocol where a [^{18}F]NaF PET scan (GE Signa PET/MRI) of the lower leg was performed before and after a bout of high-impact exercise. Between scans, subjects performed 100 right-leg step ups and left-leg drop landings from a 25cm box at 0.25 Hz. We calculated the mean percent increase in [^{18}F]NaF uptake in the left tibia from pre to post-exercise across participants (**Figure 1**).

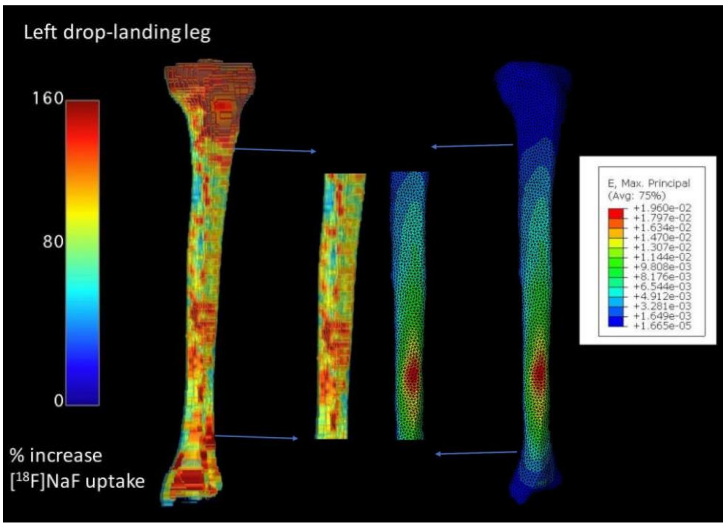

Figure 1. Mean percent increase in [^{18}F]NaF uptake and maximum principal tensile strains on the left landing leg.

To estimate the distribution of tibial strains during a drop landing, we measured kinematics and ground reaction forces for a representative subject during the drop landing exercise. We calculated muscle forces and knee joint reaction forces acting on the tibia using static optimization in OpenSim [2]. We computed muscle and knee reaction force vectors and locations of application at the time of the peak knee joint reaction force. A personalized finite element model with 331,680 tetrahedral mesh elements was created from an MRI of the subject's lower leg. The tibial bone was modelled as a homogeneous linear elastic material with a Young's Modulus of 18GPa [3]. Using the OpenSim muscle and knee reaction forces as inputs, we used the Abaqus/Standard FEA software suite (Dassault Systemes Simulia Corp., Johnston (RI), USA) to compute the maximum principal strains of the tibia during drop landing (**Figure 1**).

To spatially compare strains and percent increase in [^{18}F]NaF, the surface of the representative subject's tetrahedral mesh was non rigidly registered to a surface mesh of the mean percent increase in [^{18}F]NaF of all subjects. We extracted maximal principal strain and percent increase in [^{18}F]NaF uptake from each node in the tibial diaphysis and fit a linear model to the data.

Results and Discussion

The drop landings induced a higher mean increase in [^{18}F]NaF uptake in the tibial diaphysis of the left drop landing leg (+53%), compared to the right step-up leg (+4%). Tensile strain modelled from FEA and the measured increase in [^{18}F]NaF uptake both showed high values in the distal medial tibial diaphysis (**Figure 1**) suggesting convergent validity. The point-by-point analysis showed that tibial strain explained 16% of the variance in the increase in [^{18}F]NaF uptake (**Figure 2**). The line of best fit had diminishing returns, suggesting that [^{18}F]NaF uptake, and theoretically bone remodeling, saturated at higher tensile strains.

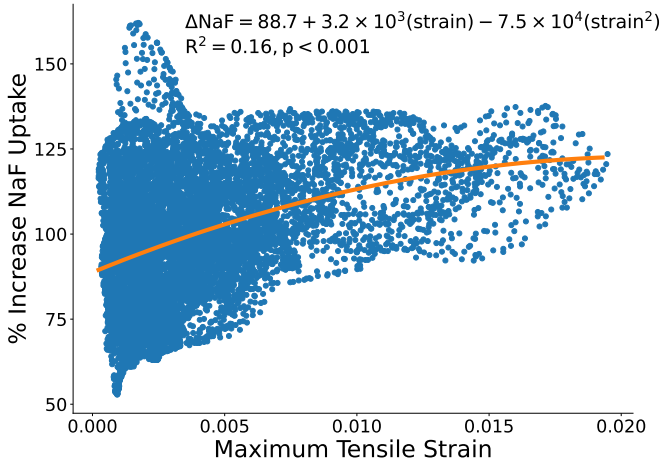

Figure 2. Node-wise relationship between tensile strain and percent increase in [^{18}F]NaF uptake from the drop landing.

Significance

We found a relationship between non-invasive estimates of bone strain and *in vivo* estimates of increased bone remodeling, which suggests that [^{18}F]NaF PET may be used to study acute changes in bone remodeling in response to loading. Combining FEA with change in [^{18}F]NaF PET could enable novel understanding of the pathophysiology as well as the design of better treatments for bone conditions such as bone stress fractures and osteoporosis.

Acknowledgments

This research was supported by the Wu Tsai Human Performance Alliance, GE Healthcare, and NIH grants R21EB030180, R00EB022634, and R01AR074492.

References

[1] Haddock et al., 2019. *Eur. J. Nucl. Med. Mol. Imaging*. 46
[2] Seth et al., 2018. *PLOS Computational Biology*. 14(7)
[3] Gray et al., 2008. *J. Biomech. Eng.* 131(3)

A NOVEL ULTRASOUND PROTOCOL FOR MEASURING SOFT TISSUE THICKNESS OVER THE FEMUR

Alyssa Tondat[1], Becky Knarr[1], Sukirat Kaur Bhullar[1] and Andrew Laing[1*]
[1]Department of Kinesiology and Health Sciences, University of Waterloo, Waterloo, ON, Canada
email: actlaing@uwaterloo.ca

Introduction

Fall-related hip fractures are a common injury in older adults, with hip fracture risk highest for lateral falls[1] and sideways landing configurations.[2] Trochanteric soft tissue thickness has been shown to influence hip fracture risk.[3] However, previous research on the relationship between soft tissues and lateral falls has only considered the total thickness of the tissues lying directly over the greater trochanter (GT). While the soft tissues overlying the GT are impacted during a lateral fall, the soft tissues overlying a larger area of the femur are impacted as well. Accounting for these tissues and the differing contributions of muscle and adipose tissue may serve to improve hip fracture risk predictions. Accordingly, the goal of this study is twofold: 1. To assess the reliability of a novel ultrasound protocol for measuring soft tissue thickness over a larger area of the femur. 2. To test the hypothesis that there are differences in total soft tissue thickness (TST), muscle thickness (MT), and adipose tissue thickness (AT) over a larger area of the femur based on measurement location and sex.

Methods

To simulate a lateral fall, participants were asked to lie on their right side on a specially designed table with a cut-out to allow for imaging of the side of the femur that would impact the ground (Figure 1a). B-mode ultrasound images were taken from participants' right hip and femur at 6 cm intervals throughout a 3 x 4 grid centred over the GT (Figure 1b) using a GE LOGIQ E10 commercial ultrasound machine and a L2-9VN-D linear array ultrasound probe (GE Healthcare Canada, ON, Canada). Three images were taken at each location in the grid. Using built-in software on the ultrasound machine, TST, MT, and AT were measured. Average, standard deviation (SD), and coefficient of variability (CV) were calculated at each measurement location for TST, MT, and AT.

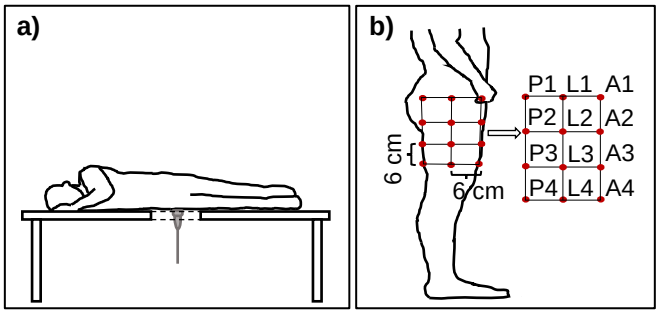

Figure 1: a) Shows the side-lying position all ultrasound images are taken in. b) Circles indicate the 12 locations where ultrasound images are taken. These locations cover the posterolateral (P), lateral (L), and anterolateral (A) aspects of the femur. Point L2 is over the GT and points L3 and L4 are aligned along the femur diaphysis.

Results and Discussion

Based on pilot data (n=1 female), TST was largest over P1 and L1 with averages ± SD of 82.95 mm ± 2.48 mm and 79.2 ± 2.58 mm respectively and lowest over L3, L4 and L2 (45.94 mm ± 2.42 mm, 48.71 ± 1.11 mm, and 48.55 ± 10.28 mm respectively; Figure 2). MT made up a larger proportion of TST over the anterolateral femur (59.2 – 82.7%) compared to the posterolateral (41.2 – 59.6%) and lateral femur (29.4 – 55.8%). AT made up a larger proportion of TST over the lateral femur (41.2 – 66.7%) compared to the posterolateral (36.9 – 55.3%) and anterolateral (13.8 – 37.3%) femur. These results highlight that TST, and the proportions of MT and AT differ across different regions of the femur. More data is needed to determine if these differences are seen in a larger sample and if they are significant.

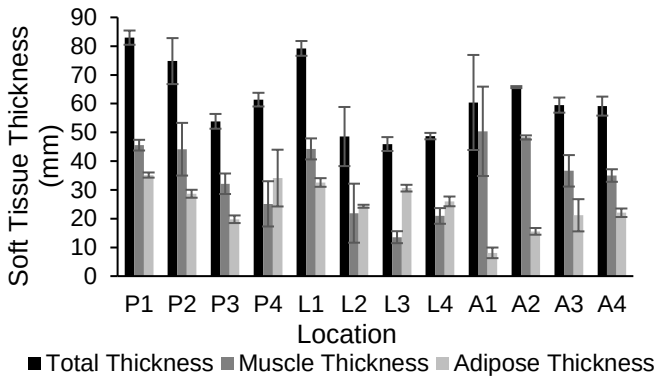

Figure 2: Average TST, MT, and AT at each of the 12 measurement locations. Error bars represent standard deviation.

CV ranged from 0.52% for TST at A2 to 46.9% for MT at L2. CV was < 10% for all thickness measurements (TST, AT, MT) at P1, L1, A2, and A4. CV was also < 10% for AT at the following locations: P2, P3, L2, L3, and L4. There were no additional locations where CV for MT was < 10%. CV was > 10% for all thickness measurements (TST, AT, MT) taken at A1. CV was also > 10% for MT at the following locations: P2, P3, P4, L2, L3, L4, and A3. CV was also > 10% for AT at the following locations: P4 and A3. These results highlight that there is variability among ultrasound measures of soft tissue thickness across the femur, with the least variability in all measurements taken at P1, L1, A2, and A4; and in general, there is greater variability among measures of MT compared to TST and AT. More data is needed to determine if these differences in variability are seen in a larger sample.

Significance

These results highlight the variability in ultrasound measurements of soft tissue thickness over different locations on the femur and the need for a standardized approach to measuring femoral soft tissue thickness. Additionally, it is important to consider the contribution of MT and AT to TST when developing models of hip fracture.

Acknowledgments

This research is funded in part by the Natural Sciences and Engineering Research Council of Canada.

References

[1] Nankaku et al., 2005. *Osteoporosis Int*. 16(11):1315-1320.
[2] Yang et al., 2020. *J Bone Miner Res*.
[3] Bouxsein et al., 2007. *J Bone Miner Res*. 2007. 22(6):825-831.

CARPAL TUNNEL VOLUME DISTRIBUTION AND MORPHOLOGY CHANGES WITH FLEXION-EXTENSION AND RADIAL-ULNAR DEVIATION

Drew A. Anderson[1*], Michele L. Oliver [1], Karen D. Gordon[1]
[1] School of Engineering, University of Guelph, Canada
*email: dander04@uoguelph.ca

Introduction

Non-neutral wrist postures are a risk factor for carpal tunnel syndrome (CTS). Deviation from neutral posture is thought to cause a decrease in carpal tunnel volume (CTV) leading to impingement of the median nerve. In recent work, we found that CTV did not significantly change over ± 20º of flexion-extension (FE) while a significant CTV decrease was observed between –5º and 15º of radial-ulnar deviation (RUD) [1]. This finding suggests that CTV may be too coarse a measurement to capture the effects of slight FE postures. It is possible that changes in carpal tunnel morphology with posture cause a redistribution of volume rather than a change in overall CTV. Further, morphology change could produce localized compression of the nerve despite no change in CTV. The objective of this study was to assess volume distribution and morphology changes with FE and RUD postures.

Methods

Analysis was conducted in MATLAB on a dataset of segmented computed tomography scans collected on ten cadaveric specimens (5 male; age = 80.7 ± 10.9), over a range of ± 20º of FE and –5º to 15º of RUD [1]. The range of postures was based on the maximum range of motion that could be achieved by all specimens. Proximal and distal boundary planes for each carpal tunnel were defined with anatomical landmarks [2]. To quantify volume distribution, each tunnel was divided into quartiles defined by planes at 25%, 50%, and 75% of the distance between the proximal and distal planes (Q1 proximal, Q2, Q3, and Q4 distal). Several morphology metrics were calculated on cross-sections defined at 0.5 mm increments along the tunnel and quartile averages were determined for each metric. Like previous studies of carpal tunnel morphology, cross-sectional area (CSA) was calculated in addition to width and depth which were found using a minimum bounding box. Morphology was further quantified with novel metrics demonstrated in a companion abstract. Centroid-to-boundary distance shape signatures were generated for each quartile, along with a template function for each specimen defined as the ensemble average of its shape signatures. From the shape signatures, Euclidean distance from the template, and phase shift relative to the template were calculated. In addition, the angle between the main principal component of each cross-section and the medial-lateral axis of the radius was calculated. Multiple linear regression ($p < 0.05$) was performed for each metric (quartile volume, CSA, width, depth, distance from the template, phase shift, principal component angle) to assess the effects of quartile, FE angle, RUD angle, and all two-way interactions.

Results and Discussion

Significant effects were observed for all metrics by quartile, as well as quartile*posture interactions. Moving from extension to flexion, the volume of Q1 and Q2 increased, whereas Q3 did not change, and Q4 decreased (**Figure 1a**). While overall CTV did not change with flexion, the volume decrease in the distal quartile with flexion could cause impingement of the median nerve. Moving from radial to ulnar deviation, the volume in all quartiles decreased with the greatest decrease occurring in the proximal quartile Q1 (**Figure 1b**). This result supports the previous finding of CTV decreasing with ulnar deviation, and further clarifies that the greatest effect occurs in the proximal region of the tunnel [1].

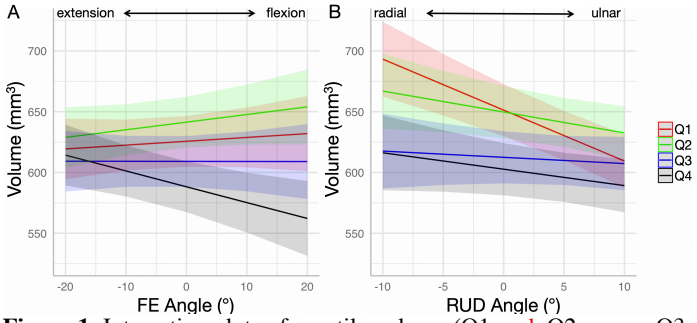

Figure 1: Interaction plots of quartile volume (Q1: red, Q2: green, Q3: blue, Q4: black) with FE angle (A) and RUD angle (B) demonstrate redistribution of volume in the carpal tunnel with varying wrist posture.

Morphology metrics provide insight into the cause of quartile volume changes. CSA changes with posture followed similar trends to quartile volume, with Q4 having the lowest mean CSA. With flexion as well as ulnar deviation Q4 width increased, while depth decreased, indicating volar-dorsal compression of the distal aspect of the tunnel with these postures. Distal compression and decreased CSA align with previously reported flattening of the median nerve in the distal region of the tunnel in individuals with CTS [3]. The cross-section principal component angle, and the phase shift metrics both exhibited twist between the proximal and distal aspects of the tunnel which became more exaggerated with flexion as well as ulnar deviation. Shape signature distance from the template was greatest in Q1 and Q4, both of which increased with flexion and radial deviation. This result indicates the greatest shape change is occurring at the proximal and distal ends of the tunnel. Agreement between distance from the template and other metrics in this study demonstrate utility in quantifying morphology with shape signatures.

Significance

This study is the first to demonstrate redistribution of CTV with wrist posture and to quantify the associated morphological changes using novel metrics. The findings provide new insight into CTS aetiology and risk factors which could be applied clinically for applications such as carpal tunnel release surgery.

Acknowledgments

This research was supported by NSERC and DJO Global.

References

[1] Anderson et al., 2022. *Clin. Biomech.*, 92: 105575.
[2] Anderson et al., 2021, *Comput. Methods Biomech. Biomed. Eng. Imaging Vis.*, 1–6.
[3] Uchiyama, et al., 2005, *J. Neurol. Neurosurg. Psychiatry*, 76(8): 1103–1108.

Different aspects of hand grip performance may be explained by connectivity of distinct sensorimotor networks in chronic stroke

Christian Schranz, PhD[1*], Shraddha Srivastava, PhD, Bryant A. Seamon, PhD, Barbara Marebwa, PhD, Leonardo Bonilha, PhD, Viswanathan Ramakrishnan, PhD, Janina Wilmskoetter, PhD, Richard R. Neptune, PhD, Steve Kautz, PhD, Na Jin Seo, PhD[1]
[1]Department of Health Sciences and Research, Medical University of South Carolina
email: *schranz@musc.edu

Introduction

More than two thirds of stroke survivors suffer from upper extremity impairment, which impacts the ability of an individual to perform activities of daily living [1]. Substantial heterogeneity exists in upper extremity impairment presentation and response to rehabilitation therapy among individual following a stroke [2]. This heterogeneity poses a significant hurdle to clinical decision making for rehabilitation treatments. Therefore, it is of paramount importance to improve our understanding of the origin of heterogeneous presentation of upper limb impairment, so that rehabilitation therapies can be personalized for maximal effectiveness.

Previous research has shown that while standard clinical assessments for upper extremity motor impairment such as the Fugl-Meyer Assessment were not able to distinguish different aspects of hand function such as strength versus Control. However, lesion characteristics may be able to distinguish between them [3]. A similar relationship has not been investigated for brain networks which also provides information on white matter integrity. Therefore, the aim of this study was to determine if distinct brain networks explain different aspects of hand function. We hypothesized that distinct brain networks are responsible for different aspects of hand grip performance.

Methods

Twenty-two chronic stroke survivors (>6 months post stroke) were assessed for biomechanical grip performances. Specifically, reaction time, relaxation time, force directional control, force magnitude estimation and maximum force performance were obtained. These 5 grip performances represent the individual's ability to contract/relax muscles timely [4], ability to apply grip force with an adequate direction [5] and magnitude [6] for a given task, and strength [4], respectively.

In addition, each participant's brain connectome was reconstructed from structural diffusion weighted MRI obtained using a 3T scanner. Tractography was estimated using FSL diffusion toolbox probabilistic method [7]. We performed two-step factor analysis with 10 regions of interests within connectome that are involved in sensorimotor control to reduce dimensionality and identify prominent sensorimotor networks.

Correlations between connectivity of these sensorimotor networks and the 5 grip performances were examined. If each of the 5 grip performances correlates best with a distinct network (vs. a single network), it would support our hypothesis.

Results and Discussion

Factor analysis identified 7 sensorimotor networks. Of these, 5 distinct networks' connectivity correlated best with each of the 5 grip performances (Figure 1). These results suggest that different networks may be responsible for different biomechanical grip performances that lead to different clinical presentations of upper extremity impairment following stroke.

Significance

Understanding distinct brain networks associated with different grip performances may facilitate the development of personalized rehabilitation interventions to directly target the responsible brain network for individual patients. For example, brain stimulation may target the brain network responsible for the individual patient's most impaired grip performance.

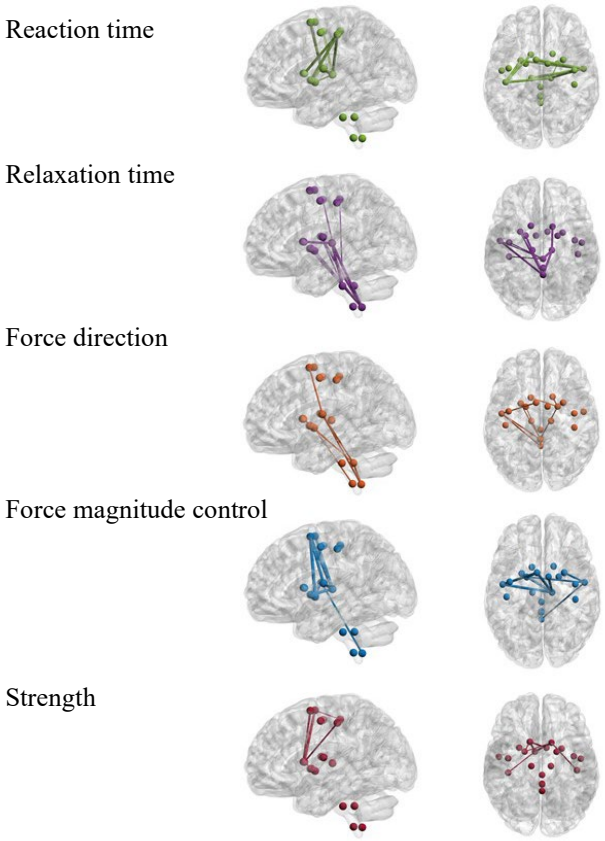

Figure 1: Lateral and top view of the five distinct brain networks that correlated best with each of the five grip performances. The lesioned hemisphere is shown on the left and the non-lesioned hemisphere on the right for the top view (right column).

Acknowledgements: VA Office of Research and Development Rehabilitation R&D Service 1I01RX001935, Senior Research Career Scientist Award 1IK6RX003075, NIH/NIGMS P20GM109040, and NIH/NICHD R01HD094731.

References

[1] Lawrence et al. Stroke, 32 (2001) 1279–1284
[2] Legg et al. Br Med J, 335 (2007) 922–925.
[3] Xu et al. J Neurophysiol, 118 (2017) 1151–1163
[4] Molenaar et al., J Appl Physiol, 124 (2018) 1597–1604
[5] Seo et al, J Biomech, 48 (2015) 383-387
[6] Takamuku et al. Sci Reports, 91 (2019) 1–12
[7] Behrens et al. Neuroimage, 34 (2007) 144–155

THE EFFECT OF FOREARM CRUTCH LENGTH ON UPPER LIMB KINEMATICS

Amanda L. Chen[1], Gregor Kuntze, PhD[2], Janet L. Ronsky, PhD[1], and Ranita H.K. Manocha, MD, MSc[3]
[1]Department of Mechanical and Manufacturing Engineering, University of Calgary, Calgary, Alberta, Canada
[2]Faculty of Kinesiology, University of Calgary, Calgary, Alberta, Canada
[3]Division of Physical Medicine & Rehabilitation, University of Calgary, Calgary, Alberta, Canada
email: amanda.chen1@ucalgary.ca

Introduction

Forearm crutches (FC) are commonly prescribed as an ambulatory aid to individuals with impairment of one or both legs [1]. FCs result in weight-bearing primarily through the hands, wrists, and forearms. FC use has been associated with forearm nerve injuries and stress fractures, and improper crutch length may increase the risk of such injuries [2].

The aim of this investigation was to explore the effects of forearm crutch length on upper limb kinematics to better understand upper limb injury risk. It was hypothesized that upper limb kinematics would be affected by crutch length being longer or shorter than standard-fit crutches.

Methods

Seven healthy male participants (mean±SD age 24.4±5.4, BMI 24.3±1.7 kgm^{-2}) with no prior crutch experience were fitted with FCs for 3 length conditions: standard fit [3]; 5cm longer than standard fit; and 5cm shorter than standard fit. Crutches were instrumented with uniaxial accelerometers. Participants were instructed on single-limb swing-through gait (STG) and then walked across an 8 x 2 m raised walkway. Whole body and crutch kinematics were recorded using a 10-camera motion capture system (Motion Analysis, USA; 120Hz) for ten trials per crutch length condition. The order of crutch length tested was randomized [4].

Joint angles were computed in Visual 3D (C-Motion, USA) and then normalized to the STG gait cycle using the accelerometer data. Statistical analysis was conducted in SPSS (IBM, USA). The effects of crutch length on joint angles at initial crutch contact (IC) and joint range of motion (ROM) were analyzed using the multivariate Wilcoxon Signed Ranks Test. Differences between conditions were reported using medians and interquartile ranges (Q1, Q3).

Results and Discussion

Significant effects of crutch length on joint angles at IC were found for the long-standard and the short-standard length comparisons. Joint ROM was not influenced by crutch length. At crutch initial contact, the long crutch condition produced greater upwards rotation of the scapula [-5.4 (-5.9, -4.3)˚, p=0.02], abduction [-5.0 (-5.7, -3.7)˚, p=0.03] and extension of the shoulder [-1.4 (-5.8, -0.6)˚, p=0.02], and flexion of the elbow [2.5 (1.9, 7.0)˚, p=0.02] in comparison to the standard crutch condition. The short crutch condition produced greater downwards rotation of the scapula [3.2 (2.2, 4.3)˚, p=0.02] and flexion of the shoulder [2.9 (0.2, 4.1)˚, p=0.03] compared to the standard crutch length.

Altering FC length affected upper limb kinematics during crutch-assisted gait, particularly with respect to downward/upward scapular rotation and shoulder flexion/extension. Further research on how altered upper limb kinematics correlate with long-term injury risk is necessary. These findings may speak to the importance of ensuring appropriate crutch fitting in long-term crutch users.

Significance

Altered forearm crutch length affected scapular, glenohumeral, and elbow kinematics during swing-through gait in this healthy male population. Prior research suggests that altered crutch length correlates with increased upper limb injury risk with crutch use. These findings provide a biomechanical basis for the risks of improper crutch length on upper limb injury in novice crutch users. Further research on the impacts of altered crutch length in long-term users such as those with cerebral palsy or spinal cord injury is needed.

Acknowledgments

Support was received by the University of Calgary Cumming School of Medicine and Alberta Health Services Clinical Research Fund (CRF18-1202), the NSERC Undergraduate Student Research Award, and the Alberta Innovates iCORE Strategic Research Chair.

References

[1] Rasouli & Reed, 2020. *J Biomech.* 98: 109489.
[2] Manocha et al., 2021. *PM&R.* 13: 1176-1192.
[3] Potter & Wallace, 1990. *BMJ.* 301: 1037-1039.
[4] Urbaniak & Plous. Research randomizer (version 4.0). 2013.

Table 1: Differences between forearm crutch length conditions. *Abbreviations: D/U (downward/upward), Add/Abd (adduction/abduction), F/E (flexion/extension), R/U (radial/ulnar), IC (initial contact), ROM (range of motion).*

Joint	Measure	Standard - Long Condition				Standard - Short Condition			
		Median	Q1	Q3	P-value	Median	Q1	Q3	P-value
Scapula D/U Rotation	IC	-5.42	-5.86	-4.31	**0.02**	3.16	2.18	4.30	**0.02**
	ROM	-0.49	-2.34	1.58	0.69	1.14	-0.33	2.02	0.11
Shoulder Add/Abd	IC	-4.99	-5.66	-3.73	**0.03**	2.76	0.69	3.78	0.08
	ROM	-0.92	-1.46	0.52	0.30	0.36	-0.85	2.43	0.38
Shoulder F/E	IC	-1.40	-5.80	-0.62	**0.02**	2.93	0.22	4.10	**0.03**
	ROM	-0.41	-5.04	2.39	0.81	1.92	-0.99	5.31	0.16
Elbow F/E	IC	2.47	1.94	6.96	**0.02**	-2.94	-4.52	0.19	0.38
	ROM	-3.05	-4.74	1.02	0.16	3.01	1.02	5.84	0.16
Wrist R/U Deviation	IC	-0.54	-0.71	-0.32	0.16	0.21	-0.42	1.71	0.47
	ROM	0.09	-0.11	0.43	0.58	-0.19	-0.31	1.62	0.94

QUANTIFICATION OF ELBOW SPASTICITY (PRELIMINARY RESULTS)

Yinan Pei[1*], Yiyue Feng[2], Seung Yun (Leo) Song[1], Liu Tao[2], Christopher M. Zallek[3] and Elizabeth T. Hsiao-Wecksler[1]
[1]U Illinois Urbana-Champaign, USA [2]Zhejiang Univ, China [3] OSF Healthcare/U Illinois Col Med, USA email: *pei2@illinois.edu

Introduction

Accurate clinical assessments of spasticity and rigidity are needed for effective patient management and treatment. These abnormal muscle behaviors arise from upper motor neuron or basal ganglia lesions observed with some neurological conditions. Assessment involves a clinician passively stretching the patient's muscles and assessing the resistance to movement. Clinical scales, e.g., Modified Ashworth Scale (MAS) [1], are used to rate a patient's severity level based on behaviors observed or felt by the clinician. The qualitative nature of these scales can result in poor consistency and low reliability. Quantitative measurements could improve assessment.

We are conducting a cross-sectional study targeting 110 test participants to build a quantitative database on measured elbow kinematic and kinetic behaviors in patients with spasticity, lead-pipe rigidity, and cogwheel rigidity across severities and healthy controls during passive stretch tests. This abstract presents preliminary results from a first cohort with spasticity. Data collection has been delayed due to the COVID-19 pandemic.

Methods

In this preliminary report, eight spasticity subjects were assessed by two experienced clinicians from Zhejiang Hospital and Pudixin Rehabilitation Hospital in Hangzhou, China. IRB approval obtained from University of Illinois Urbana-Champaign and Zhejiang Hospital.

Table 1: Subject demography. MAS level assessed before testing.

Subject ID	Age	Gender	Affected side	Biceps MAS	Triceps MAS	Cause*	Post Injury	Clinician
1	49	M	R	0	1	HS	2 months	1
2	36	M	L	2	2	HS	3 months	1
3	79	F	L	1	1	IS	3 months	1
4	61	M	L	2	2	HS	6 yrs	1
5	60	M	R	2	2	IS	2 yrs	1
6	68	M	L	2	0	IS	1 month	2
7	57	F	L	2	3	IS	7 yrs	2
8	72	F	L	1	3	IS	9 yrs	2

*HS: hemorrhagic stroke, IS: ischemic stroke

A multi-sensor wearable instrumented setup was established (Figure 1, left). A custom device, the Position, Velocity, and Resistance Meter (PVRM) [2], consisted of moving (wrist) and main (forearm) modules, each containing an IMU (MPU 6050, InvenSense, USA). The PVRM recorded elbow joint angular position and velocity, and clinician's applied load via a 6-axis F/T sensor (M3703C, Sunrise Instruments, China). Biceps and triceps muscle activity were monitored by a wireless surface electromyography (sEMG) system (Kine, Kiso Inc., Iceland).

The compact design of the moving module allowed clinicians to use their regular manual assessment technique (Figure 1, right). Each subject's elbow was first passively moved in slow speed (i.e., peak speed < 30 °/s) for five extension-flexion cycles and then stretched in the clinician's preferred fast speed for three trials per muscle group (i.e., biceps and triceps).

Elbow joint angular position and velocity were obtained by sensor fusion and subtraction of gyroscopic data from the two IMUs, respectively, at 100 Hz. Applied forces and moments were sampled at 400 Hz and used to calculate resultant elbow moment (M_{elbow}). Muscle resistive moment (M_{spas}) was calculated by removing inertial and gravitational moments ($M_{inertia}$ and M_{elbow}). All data were filtered by a 4th order Butterworth filter with cut-off frequency of 2 Hz for angular position and velocity and 20 Hz for force and moment signals.

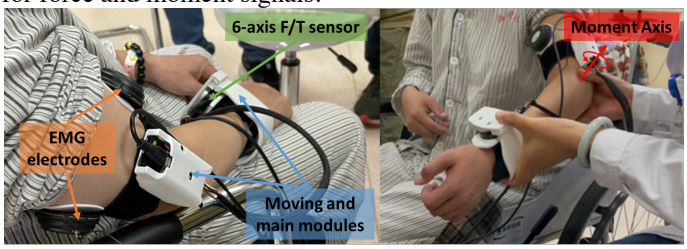

Figure 1: (Left) Sensor placements of the PVRM. (Right) Clinician's assessment technique with the instrumented setup.

Results and Discussion

The proposed protocol and PVRM setup were able to quantify the speed dependent tone (muscle resistance of ~2.4 Nm at slow speed vs. 4.2 Nm for biceps and 5.3 Nm for triceps at fast speed), and the well-known catch-release behavior of spastic muscle of each subject (Figure 2). The protocol and PVRM system were designed to align with the regular clinical assessment procedure and technique used, so that the quantified responses documented in this study also reflect the type of exam observations that clinicians normally encounter in their daily routines.

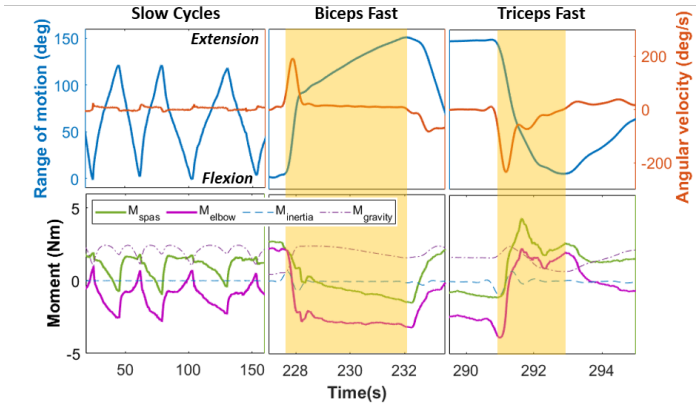

Figure 2: Sample angle, angular velocity, and moment data from Subject 2 during slow and fast passive stretch trials.

Significance

The establishment of a quantitative database containing kinematic, kinetic, and muscle activation patterns of abnormal muscle tone during clinical assessments can be useful for 1) clinicians to objectively track the severity of their patient's impairment with a PVRM-like device, 2) scientists to understand the underlying neuromuscular mechanics of abnormal muscle tones, and 3) engineers to develop medical education robotic task trainers to supplement practice patients in neurology training.

Acknowledgments

We thank Dr. Lin Li and Dr. Xuemeng Sun for their assessments, and Prof. Tao Liu's students for help on the sEMG system.

Reference

[1] Bohannon et al., 1987, *Phys Ther*, 67(2): 206–207
[2] Song et al., 2017, *Front Biomed Dev*, 40672: V001T11A02

IMU-DERIVED METRICS OF REPETITIVE ARM MOTION IN THE COMMUNITY ENVIRONMENT FOR MANUAL WHEELCHAIR USERS

Omid Jahanian [1], Meegan G. Van Straaten [1], Jasmine B. Nakum[1], Sydney M. Lundell[1], Kathylee Pinnock Branford[2], Stephen M. Cain[2], and Melissa M. B. Morrow[1]
[1]Mayo Clinic, Rochester, MN, USA; [2]West Virginia University, Morgantown, WV, USA
email: jahanian.omid@mayo.edu morrow.melissa@mayo.edu

Introduction

Manual wheelchair (MWC) users with spinal cord injury (SCI) are extensively exposed to physical risk factors including upper arm elevation, repetitive motions, and shoulder loading that accelerate shoulder pathology and pain progression beyond that of natural aging. To better understand and assess these risk factors, free-living data collection is necessary. In this study, we propose and investigate the feasibility and accuracy of a novel approach based on inertial measurement unit (IMU) data to interpret repetitive arm motion in the community environment in MWC users with SCI.

Methods

Humeral angles were calculated from body segment orientations using linear acceleration and angular velocity from IMUs (Opal, APDM Inc., USA) worn on the upper arms [1]. One movement cycle was defined as an arm elevation greater than a movement threshold (e.g., 10°; Elevation) followed by arm lowering of greater than the movement threshold (Lowering). The movements with smaller ranges of motion than the movement threshold that occurred between successive Elevation and Lowering events were called Idle and were treated as a part of the movement cycle. The intervals (time) between the consecutive cycles were calculated and a bout of activity was defined as the consecutive cycles with intervals less than 7 seconds [2]. The intervals greater than 7 seconds were considered as sedentary bouts. Finally, the number of cycles per activity bout and the kinematic and temporal features of each cycle and each bout of activity were calculated.

Video and IMU data were collected from 4 MWC users with SCI (4 males, 32 ± 3 years old, 5 ± 2 years since injury, T5-L1 injury levels). Participants completed MWC-based activities including level and inclined propulsion, car transfer, cross body lifting, and reaching in a community environment. Video data were coded as sedentary, propulsion activity (defined as hand moving the MWC hand-rim including small maneuvers), or non-propulsion activity and used as gold standard data to evaluate the accuracy of the estimated active and sedentary times. To evaluate the applicability of this approach for characterization of arm use during active bouts, the number of MWC propulsion stroke cycles, as an exemplar of repetitive arm activities, was estimated using the developed model and compared with the actual number of stroke cycles from video data.

Results and Discussion

The rated video data indicated that the total time of data collection for all participants was 3123 seconds. They were active for 1592 seconds including 43 active bouts (median active time per bout: 25 sec, IQR: 26 sec) and they were sedentary for 1531 seconds including 22 sedentary bouts (median sedentary time per bout: 50 sec, IQR: 51 sec). Comparisons of model estimates of active time and sedentary time using different movement thresholds (5°, 10°, 15°, 20°) to gold standard data demonstrated that the model with both 5° and 10° had the highest accuracies (Table 1). Therefore, using smaller movement thresholds in the proposed approach has the potential to accurately estimate the active and sedentary time during the day for the MWC users. This is an essential step toward objective interpretation of free-living environment data for this population. Model estimates of the number of MWC propulsion stroke cycles when implementing a 10° movement threshold had the lowest error (< 2% underestimation error; Figure 2). Movement thresholds smaller than 10° led to overestimation and greater than 10° led to underestimation of the number of push counts.

Table 1. Accuracy measures of the model in estimating the active time and sedentary time. Accuracy is the ratio of true active and true sedentary to the total time, sensitivity is the ratio of true active to the total active time, and specificity is the true sedentary to the total sedentary time.

Measures	5 Deg	10 Deg	15 Deg	20 Deg
Accuracy	0.995	0.984	0.939	0.761
Sensitivity	0.995	0.969	0.880	0.527
Specificity	0.996	0.999	0.999	0.999

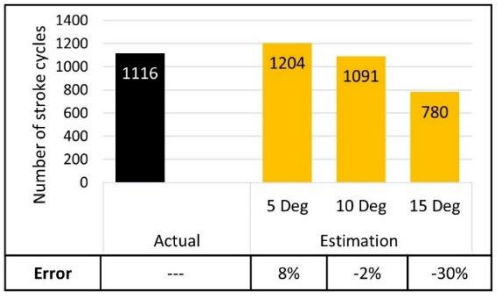

Figure 1: Estimated number of stroke cycles when using different movement thresholds (5-15 degrees). Negative errors indicate underestimation and positive errors indicate overestimation.

Significance

Accurate interpretation of free-living IMU data collected from upper arms could help to better assess potential risk factors for shoulder pathology progression. Additionally, the proposed approach has the potential to be utilized for the classification of daily activities and characterization of arm use in MWC users. Data collections and analyses with larger sample sizes of MWC users are warranted to confirm the findings of this study and refine the interval and movement thresholds to achieve accurate estimation of active and sedentary bouts, classification of wheelchair-based activities during active bouts, and characterization of arm use during these activities.

Acknowledgments

This research was supported by the NIH (2R01 HD84423).

References

[1] Goodwin et al. (2021). PLoS One, 16(4), e0248978.
[2] Tolerico et al. (2007), JRRD, 44(4), 561.

CHARACTERIZING SHOULDER-RELATED QUALITY OF LIFE IN BREAST CANCER SURVIVORS: A CLUSTER ANALYSIS

Jacquelyn M. Maciukiewicz and Clark R. Dickerson
University of Waterloo, Faculty of Health
email: cdickers@uwaterloo.ca

Introduction

Breast cancer is prevalent among Canadian women, but treatment may cause functional impairments and reduced shoulder related quality of life. Over 22,000 new survivors join the population each year in Canada [1]. Current research spans a wide range of individual and treatment variables [2,3], making general conclusions difficult. Additionally, much work focuses on limb differences [4,5] or compares survivors to control groups [2,6,7]. To address this diffuse literature, it is important to investigate which factors differentiate survivor functional outcomes.

Multivariate analyses, such as cluster analysis, allow identification of distinct clinical subgroups without assuming relationships between variables. A cluster analysis determined cohorts of breast cancer survivors and distinguish factors that differed between them. These clusters were hypothesized to be formed based on physical activity, time since treatment ended, perceived disability, force production and range of motion and that one group would have lower measures of shoulder-related quality of life (SR-QOL), force production and range of motion.

Methods

Thirty-five female breast cancer survivors (Stage I – IIIa) who were within 3 months – 2 years post treatment participated in the study. Participants completed a general health questionnaire and four self-reported questionnaires [8-11], followed by a DXA scan. Maximal isometric strength and range of motion (ROM) trials measurements of the affected side. Peak force was extracted from strength trials (flexion, extension, abduction, adduction, internal rotation, and external rotation). Humerothoracic joint angles were defined via ISB standards [12]. Maximal elevation angle was extracted from flexion, extension, abduction and scapular abduction, and range was extracted for internal and external rotation. In total, 47 collected variables were analyzed.

Prior to the cluster analysis, the dependent variables were reduced. A low variance filter yielded 24 variables. These were input in a backward feature elimination to find the 5 dependent variables that were most predictive of group membership (internal rotation force, extension range of motion, and 3 RAND-36 variables (energy/fatigue, social function and pain).

These 5 variables were used for a k-means clustering method. 2-9 clusters were investigated, and average silhouette dictated 2 clusters was the most appropriate (deemed high score cluster (HSC) and low score cluster (LSC)). Two tailed t-tests were used to determine the differences of each cluster based on strength measures, range of motion, time since treatment, body composition, age, physical activity and SR-QOL ($p<0.05$).

Results and Discussion

No significant differences existed between the two clusters for age, height, BMI weight or months since treatment ($p<0.05$). The HSC had 11.5% higher lean muscle mass of the affected limb ($p<0.05$). The HSC had 19.5-102.2% greater shoulder related quality of life measures, and 111% less perceived disability, and participated in 34% more physical activity than the LSC.

Functional differences were exhibited between the clusters in both strength and range of motion tasks. The HSC participants produced 47.8-82.6N more force across all isometric force production measurements. Only flexion differed in ROM, with the HSC having 18° larger ROM compared to the LSC.

Of the 5 variables to distinguish the clusters, 2 were physical function measures, and three were SR-QOL. This does not infer other variables are un-important, but that there are overlapping facets of survivorship expressed by multiple variables. The pectroalis major assists with internal rotation and extension, and therefore the two physical function measures were expected due to damage from surgery and adjuvant therapies [13]. The three SR-QOL measures showed the importance of social support, but also that both fatigue and pain are persistent in a subset of survivors. As strength was different across all motions, it is suggested that force production is an important factor in regaining SR-QOL after treatment.

Significance

This study determined there are 5 variables that can distinguish between breast cancer survivors. These variables formed two groups, that differed in 33/47 factors of survivorship (spanning body composition, SR-QOL, range of motion and strength). These differences have vast implications for survivors in their activities of daily living and return to work. Therefore, these should be considered in treatment programs, and may assist clinicians and physiotherapists to identify and aid individuals who may be more likely to experience more functional deficits. Specifically, that increasing force production across the shoulder motions will assist in increasing SR-QOL.

Acknowledgments

This project was partially funded through an NSERC Discovery Grant (311895-2016). Equipment was funded through the Canada Foundation for Innovation and the Ontario Research Fund. A Canada Research Chair (NSERC) in Shoulder Mechanics also supports Dickerson. This project also was funded by the Canadian Breast Cancer Foundation (#316317).

References

[1] Canadian Cancer Society (2020). *Canadian Cancer Statistics*
[2] Kaur et al (2018). *Breast.* 41:120-126.
[3] De Vrieze et al (2020). Lymphat Res Biol. 439-449
[4] Merchant et al. (2008). Disabil. Rehabil. 30:1098-1105
[5] Hagstrom et al (2019). J. Strength Cond. 33:225-233
[6] Brookham & Dickerson (2016). J Electromyogr Kinesiol. 26:100-106
[7] Galiano-Castillo et al. (2011). Am J Phys Med Rehabil 90:349-355.
[8]Brady et al. (1997). Am. J. Clin. Oncol. 15:974-986
[9] Hays et al. (1992). Health Econ.. 2:217-227
[10] Hudak et al. (1996) Am. J. Ind. Med. 29:602-608
[11]Godin & Shephard (1985). Can. J. Appl. Sci. 141-146
[12] Wu et al. (2005). J. Biomech. 38:981-992
[13]Lipps et al. (2017). Radiat. Oncol.. 122:431-436

CHANGES IN PECTORALIS MAJOR STIFFNESS AND THICKNESS OVER THE FIRST 12 MONTHS AFTER RADIOTHERAPY FOR BREAST CANCER

Susann Wolfram[1*], James A. Hayman[2], Lori J. Pierce[2], Reshma Jagsi[2], David B. Lipps[1]
[1]School of Kinesiology, University of Michigan; [2]Department of Radiation Oncology, University of Michigan
email: *swolfram@umich.edu

Introduction

Breast cancer is the most common cancer diagnosis and the leading cause of death in women worldwide (1). Radiation therapy (RT) following breast cancer surgery reduces loco-regional recurrence (2) but has been associated with pectoralis major (PM) fibrosis and muscle atrophy (3). Muscle stiffness of the PM was shown to be increased approximately 2.5 years after initiation of RT (4). However, adaptations in muscle stiffness during the first year of completing RT are unknown. The current study investigated longitudinal changes in PM muscle stiffness and thickness in breast cancer survivors up to one year after RT using ultrasound shear wave elastography (SWE) and B-mode imaging.

Methods

We examined seven breast cancer patients (age 53.9 ± 6.0 years, height 166 ± 6.2 cm, body mass 77 ± 6.8 kg) who had undergone breast conserving surgery with sentinel lymph node biopsy followed by RT to the breast only. Participants visited the laboratory for data collection before RT initiation (Visit 1) with follow-ups four weeks (Visit 2), six months (Visit 3) and twelve months (Visit 4) after RT completion. At each visit, participants' affected arm was examined with the elbow at 90° flexion and shoulder at 90° abduction.

SWE maps and B-mode images of the clavicular (CL) and sternocostal (SC) regions of the PM were obtained as participants were relaxed (Supersonic Imagine Aixplorer). Mean shear wave velocities (SWV) were obtained from each SWE map, serving as a measure of muscle stiffness. Muscle thickness from the CL and SC regions was measured in B-mode images. Changes in muscle stiffness of CL and SC between visits were determined with a linear mixed model with SWV as outcome variable, muscle region (CL and SC) as fixed factor and participant and visit as random factors. A similar approach was used to determine changes in muscle thickness of CL and SC between visits.

Results and Discussion

SWV and muscle thickness were similar between CL and SC at Visit 1, but the two muscle regions showed different changes following RT (Fig. 1). SWV measured for CL did not change after RT ($p = 1.0$), indicating that stiffness of this muscle region remains unchanged within twelve months of RT. SC showed an initial, but non-significant ($p = 0.311$), reduction in SWV at Visit 2, followed by a significant increase ($p = 0.003$) at Visit 3, which persisted at Visit 4. SC receives greater radiation doses than CL when two tangent fields targeting only the breast are used (5). Therefore, the reduction in SC stiffness observed at Visit 2 may indicate immediate responses to RT, such as seroma formation.

Muscle thickness of CL did not differ between visits ($p = 1.0$). There was a trend towards the thickness of SC decreasing after RT ($p = 0.054$). However, SC thickness was significantly lower than CL thickness at all time points following the completion of RT (all $p < 0.05$). This decrease in SC thickness is indicative of muscle atrophy in the muscle region where radiation dose is greatest. This atrophy may be a direct result of RT or caused by disuse of the affected arm after RT.

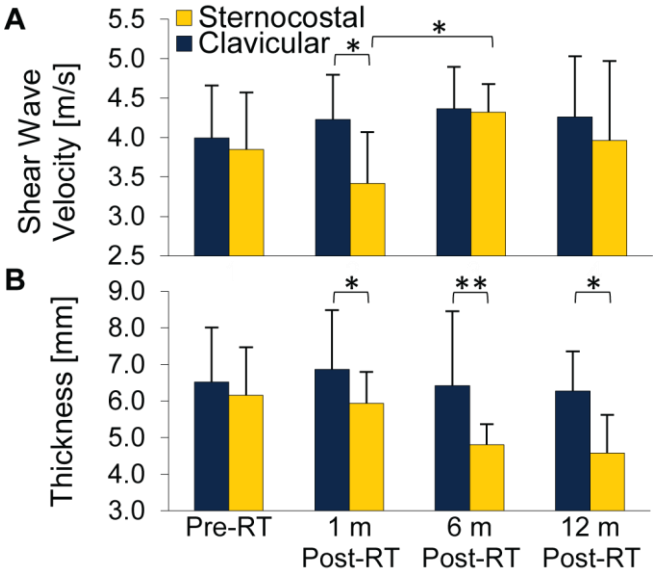

Figure 1: Mean SWV (A) and mean muscle thickness (B) of the clavicular and sternocostal regions before RT (Visit 1), and four weeks (Visit 2), six months (Visit 3) and twelve months (Visit 4) after completion of RT. Error bars are standard deviations.
* $p < 0.05$; ** $p < 0.001$

Overall, the SC region was more affected after RT than the CL region, especially with respect to muscle thickness. We detected atrophy one month after RT completion. Atrophy of the PM muscle was previously detected after two months and continued for up to four years after completion of RT (6). Future work is needed to expand the sample size and investigate the effect of regional nodal irradiation, which could further increase muscle stiffness and atrophy.

Significance

The present study shows that RT to the breast affects the SC region of the PM more than the CL region during the first twelve months following RT. Rehabilitation programs to restore shoulder function in breast cancer survivors managed with RT should place particular focus on the SC region.

Acknowledgments

This study was funded by a Susan B. Komen Postdoctoral Fellowship (PDF15329262) grant to David B. Lipps.

References

(1) Sung et al., 2021. *CA: A Cancer Journal for Clinicians*, 71.
(2) Early Breast Cancer Trialists' Collaborative Group, 2011. *Lancet*, 378.
(3) Shamley et al., 2007. *Breast Cancer Research and Treatment*, 106.
(4) Lipps et al., 2019. *Science Reports*, 9:17737.
(5) Lipps et al. 2017. *Radiotherapy and Oncology*, 122.
(6) Seo et al., 2019. *Scientific Reports*, 9:7038

Session 10

Thursday August 25, 2022

2:15pm – 3:45pm

O10.1 – Locomotion

O10.2 – Lower Limb

O10.3 – Upper Limb 3

O10.4 – Wearable Sensors 2

Thematic Poster Session 4 – Low Back/Ergonomics

From dwarfs to giants: using predictive musculoskeletal simulations to explore the limits of human locomotor speed with increasing body size

Taylor J.M. Dick[1*], Friedl De Groote[2], Christofer J. Clemente[1,3]
[1] School of Biomedical Sciences, University of Queensland, St Lucia, Queensland, Australia
[2] Department of Movement Sciences, KU Leuven, Leuven, Belgium
[3] Faculty of Science, Technology and Engineering, University of the Sunshine Coast, Sippy Downs, Australia
email: t.dick@uq.edu.au

Introduction

Throughout the evolution of hominins body size has varied remarkably. We know from studies in quadrupedal mammals that body size is tightly linked to maximum speed, such that the fastest animals are not the largest nor the smallest, but rather an intermediate size [1]. It is unclear if this similar pattern exists in hominins, since a large enough extant size range does not currently exist. Furthermore, the biological phenomena that underpin this relationship amongst all mammals remains unresolved.

Predictive musculoskeletal simulations are the only tool available to explore the limits of locomotor speed with body size because they enable us to predict *de novo* movements based on first principles of the neuro-musculoskeletal system, without relying on experimental data [2]. The overarching goal of this study is to use predictive musculoskeletal simulations to determine the maximum human locomotor speed as body size increases from 0.1 kg to 2000 kg. We hypothesized that the speed-mass relationship would display a hyperbolic pattern whereby speed is maximized at an intermediate body mass. To unveil the biomechanical factors that limit speed at both small and larger body masses, we investigated how stride parameters, forces, kinematics, and muscle activation patterns varied across the body size and speed landscape.

Methods

We used an OpenSim musculoskeletal model with 29 dof, 92 muscles actuating the lower limbs and trunk, 8 ideal torque actuators at the arms, and 6 contact spheres per foot [2]. We scaled a generic model to create 33 models across a body size range of 0.1 kg to 2000 kg. Musculoskeletal properties were scaled according to geometric similarity such that muscle forces scaled $\alpha\ m^{0.67}$ and linear dimensions (skeletal dimensions, muscle fibre and tendon lengths) scaled $\alpha\ m^{0.33}$. We used a previously established predictive muscle-driven simulation framework [2] to generate simulations at different gait speeds (from 0.1 ms^{-1} to 6.3 ms^{-1} in increments of 0.1 ms^{-1}). We established the maximum gait speed at each body size were as the maximal speed for which (i) a locally optimal solution was found within 10,000 iterations, and (ii) the simulated ground reaction force was characterized by a ground contact and an aerial phase. Our simulation outcomes were compared, where possible, to patterns available in the literature.

Results and Discussion

Based on 553 simulations, 414 were able to successfully compile over 1,190,787 total iterations. The three largest models (>1000 kg) failed to find a feasible solution given all imposed constraints. As expected, the speed-mass relationship displayed a hyperbolic pattern whereby a 60 kg model moved at the maximum speed of 6.3 m s^{-1} (Figure 1). We explored the rise and fall of speed with mass in more detail. Including only models with body masses below this maximum speed model, the increase in speed scaled with $m^{0.68}$ and above, speed decreased more steeply, scaling as $m^{-1.06}$. Stride length and stride frequency displayed opposing trends. Stride length increased, reaching a maximum at 84 kg (CIs: 34-139 kg), before declining at larger body sizes. Stride frequency decreased to a minimum at 18 kg (CIs: 9-34 kg), before increasing at larger body sizes. Smaller models took longer and less frequent steps whereas larger models took shorter but more frequent steps.

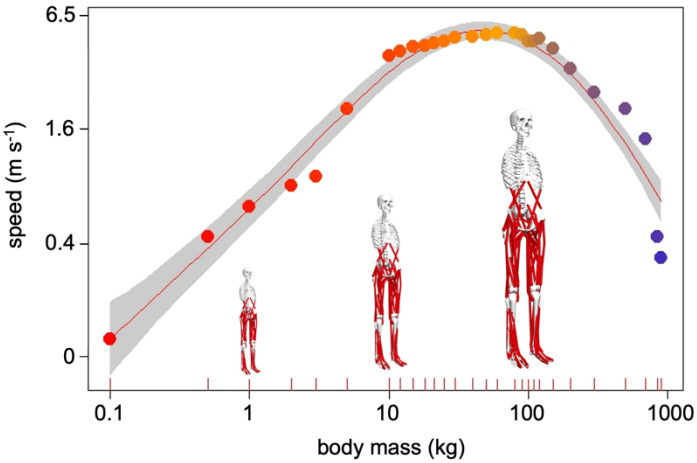

Figure 1: Speed-mass relationship displays the maximum predicted gait speed from whole-body predictive musculoskeletal simulations across a size range of 0.1 kg to 900 kg. All models >1000 kg failed to converge.

The trends in joint angles follow those observed in quadrupedal animals, becoming more upright at larger body sizes [3]. This was evidenced by more extended ankle, knee, and hip angles.

Consistent with human musculoskeletal modelling studies, the ankle extensors and hip flexors play an important role in maximum speed locomotion [4, 5]. Here, we find that muscle activation in the ankle extensors and hip flexors increased rapidly with increasing body mass and remained high for maximum speed gait across all models >10 kg.

Significance

With rapid advances in computational tools to simulate novel movement patterns, we can for the first time, explore the theoretical limits to movement at different body shapes and sizes. These results provide important insights into where the limits of locomotor performance lie, independent of the evolutionary selective pressures which have guided the phenotypes of both extant and extinct animals.

References

[1] Garland, 1983. *J Zoology,* 199(2)
[2] Falisse et al., 2019. *Interface,* 16(157)
[3] Biewener, 1989. *Science,* 245(4913)
[4] Lai et al., 2016. *Interface,* 13(121)
[5] Schache et al., 2014. *JOSPT,* 44(10

TEST-RETEST RELIABILITY OF TRANSIENT BALANCE FEATURES ACROSS SENSORY, COGNITIVE, AND STANCE PERTURBATIONS

Kshithij M. Nandishwara,[1] Nicholas Benson,[1] Gregory M. Freisinger,[2] Janet E. Simon,[3] Kimberly E. Bigelow,[4] and Scott M. Monfort[1]
[1]Montana State University; [2]United Stated Military Academy; [3]Ohio University; [4]University of Dayton
email: scott.monfort@montana.edu

Introduction

Transient periods (5-15 seconds) of increased postural sway following sensory transitions (e.g., closing eyes) or starting/stopping a cognitive task have been reported during standing balance, which spurs their potential to probe aspects of how sensory reweighting and attention reallocation influence balance control [1,2]. These transient features appear largely unrelated to balance parameters that are calculated over entire trials and have shown the ability to distinguish between older and younger adults [1]. However, a critical gap in understanding the potential clinical utility of transient balance features is their unknown consistency over time. The purpose of this study was to determine the test-retest reliability of transient balance features in response to sensory, cognitive, and stance perturbations. We hypothesized that the reliability of transient balance measures would be supported by: 1) significant correlations of transient metrics between testing sessions, and 2) no significant differences in transient metric means between testing sessions.

Methods

Eighteen healthy, younger adults (25.5 ± 4.5 years, 67.4 ± 11.6 kg, 1.71 ± 0.10 m, 7 males/11 females) performed a series of postural control tasks at two testing sessions that were scheduled two weeks apart. The balance conditions were selected to introduce sensory, cognitive, and/or stance perturbations to evaluate reliability characteristics across a broad set of scenarios. Balance conditions consisted of 1) eyes open, single task (**EOST**), 2) eyes closed, single task (**ECST**), 3) eyes open, dual task (**EODT**), 4) eyes closed, dual task (**ECDT**), 5) an anticipated shift from bipedal stance to single limb stance (**ASFT**), and 6) a reactive bipedal to single limb stance transition where participants reacted as quickly as possible to stand on the limb indicated by a visual directional cue (**RSFT**). The dual-task for EODT and ECDT conditions was an auditory Stroop task. Condition order was randomized between participants, and five 60-second trials were collected for each condition.

Both whole-trial and transient balance metrics were calculated in an attempt to benchmark test-retest characteristics of the transient metric. 95% confidence ellipse area (EA) was calculated for the entire 60-second trial (whole-trial) and separately for 12 five-second epochs throughout the trial [1]. The difference in EA from the first epoch to the last epoch was used to characterize transient features (**ΔEA**). The natural logarithm of EA estimates (whole-trial and epoch-based) was taken to obtain normally distributed data within conditions. Averages of the five trials were used in statistical analyses.

Test-retest reliability was assessed by 1) performing paired t-tests to determine whether the means differed between visits, and 2) performing Pearson correlations to identify the extent that balance metrics were related across visits.

Results and Discussion

There were no differences in transient metric means between visits for any condition (**Figure 1**). ECST demonstrated a difference between visits for whole-trial EA ($P = 0.003$).

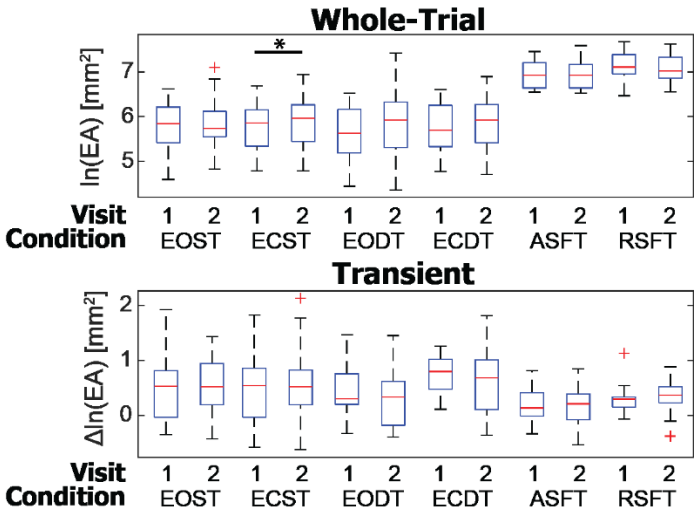

Figure 1: Distributions of whole-trial (top) and transient (bottom) metrics for all conditions and over both visits. + are outliers. * indicates statistically significant differences between visits.

Moderate to strong correlations between visits were observed for the transient metric for all balance conditions except for RSFT (**Table 1**). The test-retest consistency for the transient metric was highest in a challenging bipedal condition, which may indicate that tasks that introduce challenging perturbations (but not too challenging - e.g., RSFT) may enhance the reliability for this outcome. Test-retest correlations were consistently stronger for the whole-trial metric for all conditions (**Table 1**).

Table 1. Pearson correlations between visits.

Condition	Whole-Trial	Transient
EOST	0.867 (<0.001)*	0.487 (0.040)*
ECST	0.951 (<0.001)*	0.572 (0.013)*
EODT	0.851 (<0.001)*	0.544 (0.020)*
ECDT	0.776 (<0.001)*	0.708 (0.001)*
ASFT	0.861 (<0.001)*	0.548 (0.019)*
RSFT	0.840 (<0.001)*	0.110 (0.664)

Note: Values are: r (*P*-value); * indicates $P<0.05$

Significance

Test-retest reliability of transient balance features was demonstrated over a period of two weeks in healthy adults; however, the consistency over time was typically less than that of traditional whole-trial estimates. The premise of longitudinal stability of transient measures was largely supported, although further opportunities to refine the transient metrics to obtain clinically-acceptable levels of reliability are highlighted.

Acknowledgements

Research was sponsored by the United States Military Academy (USMA) (Awards W911NF-20-2-0240; W911NF-22-2-0060).

References

[1] Reed et al., *PLOS ONE,* 2020. 15(8):e0237246.
[2] Reed et al., *Hum Mov Sci*, 2022. 83:102950

NAVIGATING NEGATIVE CONSEQUENCES DURING OBSTACLE CROSSING

Isabella Champenois[1], Ashlyn M. Jendro[1*], Jessica Passarelli[1], Tiphanie E. Raffegeau[2] and Abigail C. Schmitt[1]
[1]University of Arkansas [2]Ohio University
email: acs063@uark.edu

Introduction

The ability to successfully cross obstacles while walking is essential to carrying out everyday activities. Unsuccessful obstacle crossings result from inadequate foot clearance over an obstacle, most often with the trailing foot[1,2]. When individuals are focusing on not contacting an obstacle, they tend to increase their foot clearance measures and adopt a more cautious strategy during crossing[3]. It is well known that unsuccessful obstacle crossings can have serious physical consequences (i.e., injuries)[4], but little is known about how motivation and perceived consequences affect the ways in which we cross obstacles. It is likely that young adults feel less threatened by physical consequences[5] and, thus, prioritize reduced effort during obstacle crossing as opposed to safety. The use of external motivation may provide insights into how young adults cross obstacles when consequences beyond potential physical threats exist. Thus, the purpose of this study was to measure how the threat of negative, non-physical, motivational consequences alter the strategy used by individuals during obstacle crossing.

Methods

Twenty-six healthy, young adults (10 control, 16 consequence, age: 22 ± 2yrs, mass: 70.3 ± 13.2kg, height: 1.71 ± 11m, 14 women, 12 men, 25 right leg dominant) completed a series of walking tasks on an 8m walkway, including 10 trials of obstacle crossing. 3D motion capture (Vicon Motion Systems) was used to measure participant kinematics during crossing and the position of the 150mm dowel rod obstacle. All participants were asked to "*cross the obstacle in your path and continue walking at your typical, comfortable speed*." Participants self-selected their lead limb during crossing. The control group was given no additional instruction. The consequence group was told there were negative consequences for contacting the obstacle in any way, including losing payment for participation and an additional study visit to redo any unsuccessful trials. Following data collection, participants were unblinded to the deception and told that they would receive the full payment ($15) and would not need to return for any follow-up visits.

A custom MATLAB program calculated the measures of foot clearance, which were used to assess obstacle crossing strategy. Foot clearance for both the leading and trailing limbs was defined as the vertical distance between the respective marker and the obstacle when the toe and the heel crossed over the dowel rod. The horizontal distance between the toe marker of the trail limb and the obstacle on approach and the heel marker of the lead limb after crossing were also calculated. T-tests were used to evaluate differences in the variables of interest between the control and consequence groups (α=.05). Cohen's d was used for effect size, with 0.2, 0.5, and 0.8 denoting small, medium, and large effect sizes, respectively.

Results and Discussion

Participants chose to use their dominant foot as the lead foot during 56% of obstacle crossing trials (control: 43.7% consequence: 63.2%). There were no unsuccessful trials in either group. Generally, participants in the consequence group crossed the dowel rod with a larger margin of safety than the control group, evidenced by the greater foot clearance values (Table 1). Specifically, the consequence group exhibited greater lead foot clearance for both the toe (p= *.019*, Cohen's d= 1.01) and the heel (p= *.028*, Cohen's d= 0.94), as well as greater trailing foot clearance for both the toe (p= *.002*, Cohen's d= 1.38) and the heel (p= *.005*, Cohen's d= 1.26), all with large effect.

The horizontal distances on approach and landing did not significantly differ between groups (p= .14, Cohen's d= 0.62 and p= .964, Cohen's d= 0.02, respectively) and small/medium effect sizes suggest these measures are not meaningfully different, either.

Table 1: Mean ± SD of foot clearance measures (in mm), with respect to leading limb (LL) and trailing limb (TL).

	Control	Consequence
Toe Clearance (LL)	145 ± 35	191 ± 51
Heel Clearance (LL)	136 ± 38	182 ± 54
Toe Clearance (TL)	157 ± 31	243 ± 75
Heel Clearance (TL)	320 ± 43	407 ± 80
Approach Distance (TL)	252 ± 64	296 ± 76
Landing Distance (LL)	246 ± 63	247 ± 47

These results suggest that motivational consequences do affect the strategies used to cross obstacles. Foot clearance measures for both the lead and trail feet were greater in the group that was presented with consequences. This suggests the presence of motivational consequences likely led to participants choosing a more conservative, safer strategy during obstacle crossing. Additionally, previous literature suggests that most obstacle contacts occur from the trailing foot[4,5], where we observed the greatest difference in toe clearance between the groups further highlighting the shift toward a safer crossing strategy in the consequence group.

Significance

These data suggest that individuals alter their obstacle crossing strategies based on the presence of motivational consequences. This data may lead to more meaningful and realistic assessments of obstacle crossing and may provide insights into how different groups of people choose to navigate obstacles.

Acknowledgments

Funding for this project was provided by a University of Arkansas Honors College Research Grant.

References

1. LoJacono et al., 2018. J Mot Learn Dev. 6(2):234-249.
2. Heijnen et al., 2012. Exp Brain Res. 223(2), 219–231.
3. Chen et al., 1991. J Gerontol. 46(6):M196-203.
4. Pocinki, 1990. Feb PT Bulletin,: Am Phys Ther Assoc, p 13.
5. Muir et al., 2020. Gait & Posture, 77, 100–104.

Wearable sensors reveal propulsion-based locomotor phenotypes among endurant individuals after stroke

Dheepak Arumukhom Revi[1,2], Johanna Spangler[1], Stefano M.M De. Rossi[1], William L. Swift[1], Lillian Ribeirinha-Brage[1], Terry D. Ellis[1], Conor J. Walsh[3] and Louis N Awad[1,2]
[1]College of Health & Rehabilitation Science, Boston University, USA [2]Department of Mechanical Engineering, Boston University, USA, [3]John A. Paulson School of Engineering and Applied Sciences, Harvard University, USA
email: *louawad@bu.edu

Introduction

The 6-minute walk test (6MWT) is a clinical measure of functional walking capacity where the total distance walked[1] and distance-induced change in speed[2] are strong indicators of post-stroke community walking activity. In prior work, we showed that non-endurant individuals—i.e., those who decrease their walking speed over the minutes of the test—walk 62% less in the community compared to endurant individuals who do not decrease walking speed[2]. In recent work, we demonstrated the feasibility of instrumenting the 6MWT with a minimal set of wearable sensors to produce stride-by-stride estimates of walking speed[3] and its spatial-temporal[3] and propulsion[4] determinants. The aim of this study was to use this sensor-based estimation approach to identify performance-based locomotor phenotypes among endurant individuals with the potential to inform the diagnosis and treatment of post-stroke walking impairments.

Methods

Twenty-six endurant[2] individuals with chronic post-stroke hemiparesis and eight healthy controls completed a 6MWT over a 26.6m walking track instrumented with forceplates (Bertec) and an optical motion capture system (Qualisys) while wearing five IMUs (Xsens) securely attached to the pelvis, thighs, and shanks. Forceplate and motion capture data collected during the 6MWT were used to calibrate subject-specific estimation models driven by IMU measurements to yield robust estimates of spatiotemporal[3] and propulsion determinants[4] for each stride. For each variable, the median was computed for every 30-second interval. The difference between first and last intervals was used to identify the distance-induced change for each variable. In addition, the Borg rating of perceived exertion (RPE) scale was administered before and after the 6MWT. Individuals post-stroke were dichotomized into two subgroups based on median propulsion impulse asymmetry (Pp) using a cutoff of 36%, which is indicative of moderate hemiparetic severity after stroke[5]. Individuals with Pp>36% were defined to have severe hemiparesis (N=13), whereas individuals with Pp<36% were defined to have mild hemiparesis (N=13). Group-level comparisons were conducted using Wilcoxon Signed Rank tests, with alpha set to 0.05.

Results and Discussion

Both the mild- and severe-hemiparesis subgroups differed from healthy controls in total 6MWT distance, as well as walking speed, cadence, stride length, and propulsion asymmetry measured during the first 30-sec interval of the 6MWT. Neither healthy controls nor the mild-hemiparesis subgroup showed distance-induced changes in any variable. In contrast, compared to the mild-hemiparesis subgroup, 11 out of 13 individuals in the severe-hemiparesis subgroup reduced their cadence, with the overall group reducing cadence by a median 5.2% ($p = 0.004$). Similarly, 11 out of 13 increased their stride length, with the overall group increasing stride length by a median 5.3% ($p = 0.06$). These spatiotemporal differences were observed without a concurrent change in speed (Δ: 0.3%, $p = 0.84$), and were associated with a higher post-test RPE for 8 out of 13 individuals in the severe-hemiparesis subgroup.

Significance

We show that wearable sensors can potentially identify propulsion-based locomotor phenotypes associated with spatiotemporal modulation during the 6MWT. Specifically, though individuals with severe post-stroke hemiparesis walk similar 6MWT distances as individuals with mild hemiparesis, those with severe hemiparesis maintain speed by increasing stride length and reducing cadence. This spatiotemporal strategy is treading towards a higher RPE after the test, which might help explain why individuals with severe hemiparesis are less active in the community[6], despite similar baseline walking speeds and 6MWT distance. Instrumenting the 6MWT with wearable sensors may provide treatment-shaping diagnostic and prognostic information not currently available from conventional measures of walking capacity.

Acknowledgments

We thank our participants for their participation in our study.

References

[1] Fulk2017, doi: 10.1161/STROKEAHA.116.015309
[2] Awad2019, doi:10.1097/NPT.0000000000000293
[3] ArumukhomRevi2021, doi: 10.3390/s21216976
[4] ArumukhomRevi2020, doi: 10.1186/s12984-020-00700-7
[5] Bowden2006, doi: 10.1161/01.STR.0000204063.75779.8d
[6] Awad2020, doi: 10.1186/s12984-020-00747-6

Table 1: Summary of sub-group level differences in baseline measurements and change over six-minute walk test

	Baseline			Change over the 6MWT (last 30 sec – first 30 sec)			
	median speed (m/s)	median Pp (%)	6MWT (m)	ΔSpeed (m/s)	ΔStride length (m)	ΔCadence (step/min)	ΔRPE (score)
Healthy Control	1.84 (0.31)	48.2 (1.4)	677 (126)	0.01 (0.04)	0.03 (0.07)	0.3 (3)	-
Mild Hemiparesis	0.86 (0.43)	42.6 (7.9)	303 (170)	-0.00 (0.02)	0.01 (0.05)	-2.0 (4)	2 (2)
Severe Hemiparesis	0.84 (0.45)	24.0 (19.9)	289 (159)	-0.01 (0.03)	0.04 (0.06)	-6.5 (5)	3 (3)
Mild - Severe	0.02 m/s	18.6%*	15m	0.01 (0.3%)	-0.04 (-5.3%†)	4.5 (5.2%*)	-1†

*$p < 0.05$; †$p < 0.10$; Pp = propulsion asymmetry (50% = perfect symmetry); 6MWT = six-minute walk test distance

SOFT ROBOTIC EXOSUIT ASSISTANCE FACILITATES HIGH INTENSITY GAIT TRAINING AFTER STROKE

Anna Roto Cataldo[1], Johanna Spangler[1], Lillian Braga-Ribeirinha[1], Karen Hutchinson[1], and Louis N Awad[1*]
[1]College of of Health and Rehabilitation Sciences, Boston University, Boston, Massachusetts, USA
email: *louawad@bu.edu

Introduction

Stroke-induced gait deficits often limit gait training intensity and repetition—training parameters known to drive experience-dependent neuroplasticity. We posit that soft robotic exosuits[1] that provide paretic plantarflexor and dorsiflexor force assistance during the appropriate phases of the gait cycle have the potential to facilitate gait training at higher intensities and for longer durations than may be achieved without exosuit assistance. Our prior work shows that exosuit assistance leads to greater energetic efficiency, improved propulsion symmetry and ground clearance[1], and reduced gait compensations[2] during steady-state treadmill walking. People post-stroke also self-select faster overground walking speeds and walk farther distances with exosuit assistance[3]. Taken together, these orthotic benefits have potential to be applied during gait training to enhance therapeutic outcomes. However, gait training often does not occur at comfortable, self-selected walking speeds. Fast training speeds are often prescribed not only to address speed deficits after stroke, but to also increase training intensity and, in turn, enhance experience-dependent neuroplasticity. We hypothesize that exosuit assistance will provide the propulsive support required to achieve faster walking speeds and the ground clearance support needed to reduce or delay gait instabilities at faster speeds, thus facilitating faster walking for longer durations, and consequently, a higher training intensity and dose, as measured by exercise test time and VO_2 peak achieved before physiological deterioration, gait instability, or fatigue require that testing be terminated.

Methods

We evaluated the effects of exosuit assistance using two speed-based maximal effort graded exercise tests[4] that spanned participants' self-selected speed range, up to the maximum walking speed they could safely tolerate. Participants completed one with and one without exosuit assistance (no-exosuit). Tests started at 80% of comfortable overground walking speed for 2 minutes followed by an increase in treadmill speed by 10% of the starting speed every 2 minutes until test termination. Stopping criteria included reaching peak volitional fatigue or meeting any physiological or physical (e.g., gait instability judged to be unsafe by a licensed physical therapist) criteria[4,5]. Indirect calorimetry and electrocardiogram data were collected continuously during the tests. The final 30 seconds of steady-state walking—identified based on standard deviation[6] and visual inspection of indirect calorimetry data—were averaged and normalized to body mass to compute VO_2 peak (ml O_2/kg/min). Test duration is presented in minutes. Maximum walking speed refers to the final treadmill speed (m/s) achieved.

This study is ongoing. Available data for test duration, fastest walking speed, and VO_2 peak achieved for all completed subjects are presented in this preliminary report. Descriptive statistics and individual data are reported as median ± semi-interquartile range.

Results and Discussion

Data from 8 individuals >6 months post-stroke (58±13 yrs. old, 2 females, 2 right paretic) are presented. Participants walked a median two stages longer (range: -2 to +5 stages) with exosuit assistance compared to no-exosuit, resulting in a longer test duration (+17%; 14±2.8 vs. 10±1.5 minutes) (Fig. 1A), faster maximum speed (+7%; 1.01±0.12 vs. 0.95±0.13 m/s) (Fig. 1B), and higher VO_2 peak (+9.5%; 16.6±2.5 vs. 14.7±1.3 ml O2/kg/min) (Fig. 1C). At the individual level, six out of eight participants increased both test duration and fastest walking speed achieved, one reduced both measures (Fig. 1A & 1B, red), and one had no change in either measure (Fig. 1A & 1B, black). In addition, five participants achieved a higher VO_2 peak (range: +1.8% to +24%), and three achieved a lower VO_2 peak (range: -3.1% to -21%) (Fig. 1C, red). During no-exosuit testing, three participants were stopped due to gait instability, three due to physiological deterioration, and two because of volitional fatigue. For two participants, the reason for stopping the test was altered by exosuit assistance: one continued to a later stage without physiological deterioration and was later stopped due to gait instability, and one stopped at an earlier stage due to gait instability. A third participant presented with physiological deterioration during the same stage as the no-exosuit condition. For all other participants, tests were stopped for the same reasons across conditions, with exosuit assistance delaying the onset of stopping criteria.

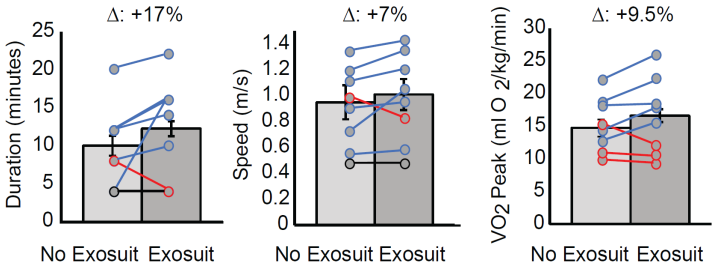

Figure 1: Median test duration (A), maximum speed (B), and VO_2peak (C) between conditions.

Significance

These preliminary results suggest that soft robotic exosuits may enable individuals with post-stroke hemiparesis to walk for longer durations and at faster training speeds, and thus facilitate clinical gait training at the intensities and durations necessary to drive experience-dependent neuroplasticity and maximize locomotor recovery.

Acknowledgments

We thank our participants for their generous donation of time.

References

1. Awad, L. *et al.* 2017 *Sci. Transl. Med.* DOI: 10.1126/scitranslmed.aai9084
2. Awad, L. *et al.* 2017 *Am. J. Phys. Med. Rehabil.* DOI: 10.1097/PHM.0000000000000800
3. Awad, L. *et al.* 2020 *IEEE Open J. Eng. Med. Biol.* DOI: 10.1109/ojemb.2020.2984429
4. Fletcher, G. F. *et al.* 2013 *Circulation*. DOI: 10.1161/CIR.0b013e31829b5b44
5. Macko, R. F. *et al.* 1997 *Stroke*. DOI: 10.1161/01.str.28.5.988
6. Taylor, H. L. *et al.* 1955 *J. Appl. Physiol.* DOI: 10.1152/jappl.1955.8.1.73

THE EFFECT OF DIFFERENT TYPES OF ANKLE FOOT ORTHOSES ON STATIC AND DYNAMIC BALANCE

Martin P. Kilbane[1], Adam J. Jones[1], Sophia G. Chirumbole[2] and Kimberly E. Bigelow[1*]
[1]University of Dayton, Dayton, Ohio, USA; [2]Ohio State University, Columbus, Ohio, USA
email: [*]kbigelow1@udayton.edu

Introduction

Previous work suggests that wearing AFOs may negatively affect aspects of dynamic balance, while having little impact, or even positive, impact on static balance.[1,2] These effects may be related to the style, materials, and characteristics of the AFO. The cost of carbon composite AFOs (cAFOs) is relatively high compared to the cost of traditional polypropylene AFOs (pAFOs), yet there is limited research comparing the effectiveness of the two. This study aimed to determine the effect of using carbon (Allard Toe-Off®) and polypropylene (OPTEC USA) AFOs on static and dynamic balance in a group of healthy young adults. We hypothesized that postural sway would be reduced when wearing the cAFO (which have an anterior shell) compared to the pAFO.

Methods

Twenty healthy college-aged students participated in this study. The individuals tested included 9 men and 11 women, mean age: 20.55±1.50 years; mean height: 169.70±10.25 cm; and mean weight: 75.57±13.21 kg. 79% of the study population was white, non-Hispanic; the remaining 21% of test participants came from other racial-ethnic groups.

Participants first completed a sequence of 30 second quiet-standing trials of the Modified Test of Sensory Interaction on Balance (mCTSIB) while standing on a Bertec force-measuring platform. The tasks were: (1) Eyes Open on the Flat Platform, (2) Eyes Closed on the Flat Platform, (3) Eyes Open on the Memory Foam Pad, (4) Eyes Closed on the Memory Foam Pad. Participants completed this entire sequence twice for three AFO conditions: noAFO, cAFO, and pAFO, in a randomized order. For all trials, study participants stood with arms crossed across their chest, and looking straight ahead, trying not to talk or move for the trial duration. Participants then completed a sequence of 30 second Sit-to-Stand trials, completing the sequence three times for each AFO condition. For all trials, study participants began sitting in a chair, placed their feet on the flat plate and rose to a standing position, and then returned to sitting. AFOs were sized from XS-XL and laboratory shoes were provided.

Anterior-posterior and medial-lateral center of pressure (COP) data were collected from the force plate at 1000 Hz. These data were filtered with a fourth-order low-pass Butterworth filter with a 20 Hz. Cutoff. To account for the transient balance movements that often exist early in a balance trial[3], only the final 25 seconds of data was analyzed. A number of traditional postural sway measures were calculated. Root-mean square displacement (RMS) results are presented here. Paired-Samples T-Tests were conducted between the three AFO conditions using IBM's SPSS Statistics software ($p<0.05$).

Results and Discussion

Our results (Table 1) suggest that there are some statistically significant differences in RMS results obtained based on the presence of an AFO, with these differences observed mostly in the sit-to-stand task. For most quiet-standing conditions, it was found that there were no statistical differences between cAFO and pAFO on balance. This suggests that the choice of AFO prescribed may be able to be driven by patient comfort and preference rather than its positive, or negative, impact on balance. In the eyes open on the foam pad, it was found that the AFOs, while not significantly different from each other, did result in increased sway over the no AFO condition. This might indicate that individuals who wear AFOs may wish to be cautious when encountering challenging terrains (sand, hiking paths, thick carpets, etc.). There were no differences in dynamic balance between cAFO and pAFO, but it was found that both the cAFO and pAFO elicited significantly larger RMS COP displacements in Sit-to-Stand trials than without an AFO being worn. This suggests that AFO users may have difficulty performing this routine task, likely due to the way in which the AFO restricts ankle function. Future work should examine how a hinged AFO may assist in performing this task more naturally; and investigate other routine dynamic tasks.

Significance

Our findings suggest that an AFO appears to make it more challenging to perform a sit-to-stand task, though does not generally affect standing balance. When prescribing an AFO or training a new AFO user, clinicians should consider using assessment tools that measure various aspects of both static and dynamic balance to evaluate individual response to AFOs.

Acknowledgments

We would like to thank Jaxie Brokamp, Drew Geise, Ryan Gigiano, Vivian Mota, Katherine Perille, Annie Robinson, Jordan Wilson, and Celena Wirth for assisting this study.

References

[1] Ramstrand N, et. al. *JPO*. **22(8)**, 4-23, 2010.
[2] Jackson K, et al. *JPO*. **33(3)**, 227-233, 2021.
[3] Reed A, et. Al. *PLoS ONE*. **15(8)**, 2020.

Table 1: Mean ± Standard Deviation RMS (in mm) per trial, per AFO condition. Significance compared to the No AFO condition: * $p < 0.001$, ** $p < 0.01$, *** $p < 0.05$. Significance compared to the Carbon AFO condition: + $p < 0.001$, ++ $p < 0.01$, +++ $p < 0.05$.

	No AFO	Allard Toe-Off® Carbon AFO	OPTEC USA Plastic AFO
Eyes Open Flat Plate	4.23 ± 1.4	3.98 ± 1.3	4.33 ± 2.1
Eyes Closed Flat Plate	5.14 ± 2.3	4.42 ± 1.4	4.54 ± 1.7
Eyes Open Foam Pad	7.33 ± 3.3	8.79 ± 3.5***	9.05 ± 4.0
Eyes Closed Foam Pad	13.91 ± 4.5	15.27 ± 5.9	15.51 ± 4.4
Sit-to-Stand	23.53 ± 9.2	29.33 ± 9.2**	31.60 ± 11.3**

FEEDBACK OF WHOLE-BODY MOTION CONTRIBUTES TO PERCEPTION OF LOCOMOTOR DISTURBANCES

Daniel J. Liss[1], Jessica L. Allen[1]
[1]West Virginia University, Morgantown, WV
Email: djl0024@mix.wvu.edu

Introduction

We previously found that young adults could perceive small slip-like locomotor disturbances [1]. Prior studies have identified that the muscular response used to maintain balance in response to similar perturbations during both standing and walking can be explained based on the feedback of whole-body motion [2]. Therefore, we hypothesize that estimates of whole-body motion play a role in perceiving small locomotor disturbances. To test this hypothesis, we investigated differences in whole-body angular momentum (WBAM) between perceived and not perceived slip-like locomotor disturbances in young adults.

Methods

Eleven young adults (7M, 22±2.3 yrs) walked on a split-belt instrumented treadmill (Bertec, Inc.) at self-selected walking speed while experiencing balance disturbances every 8-12 strides. Disturbances were imposed through short duration decreases in treadmill belt velocity (dV) triggered at heel-strike, where dV was 0, 0.02, 0.05, 0.1, 0.15, 0.2, 0.3, 0.4 m/s. Disturbances were randomized and repeated 5 times on the dominant leg with nondominant leg disturbances interspersed to reduce learning effects. After each disturbance, subjects were asked if they perceived a balance disturbance and responded "yes" or "no". The conscious perception threshold was determined by fitting a psychometric curve to the percentage of perceived responses for each dV.

We then analyzed disturbance-induced deviations in WBAM derived from whole-body kinematics [3] in response to the two perturbation levels nearest each subject's perception threshold. For each of the three planes of motion, the deviation between WBAM in the perturbed gait cycle and the five preceding gait cycles was calculated as $(x_i - \bar{x}_i)/SD_i$ and then averaged across the gait cycle, where i is gait cycle %, x is the perturbed gait cycle, and $\bar{x}$ and SD are the average and standard deviation of the five pre-perturbation gait cycles.

A rank-sum test was used to determine in which planes of motion WBAM differed between perceived and non-perceived perturbations, with Bonferroni corrections to account for the multiple comparisons (α=0.05/3). We then used logistical mixed-effects models to examine the extent to which each perturbation-induced deviation could explain whether a perturbation was perceived. Separate models were used for each direction of WBAM, with each plane of motion treated as a fixed effect and subject as a random effect.

Results and Discussion

Young adults perceived small locomotor disturbances of 0.08±0.03 m/s. Ten perturbations were analyzed per subject, with the median number of perceived perturbations across subjects equal to 5 (range: 3-7). Disturbance-induced deviation in sagittal plane WBAM was the only variable that significantly differed between perceived and non-perceived perturbations (p=0.001, Fig. 1A). Sagittal WBAM was also the only variable whose 95% confidence interval on the odds ratio did not cross one, with an estimated odds ratio of 1.65 (Fig. 1B). This means that for every 1 SD increase in sagittal-plane WBAM from unperturbed walking, a subject was over 1.5 times as likely to perceive that a walking disturbance occurred.

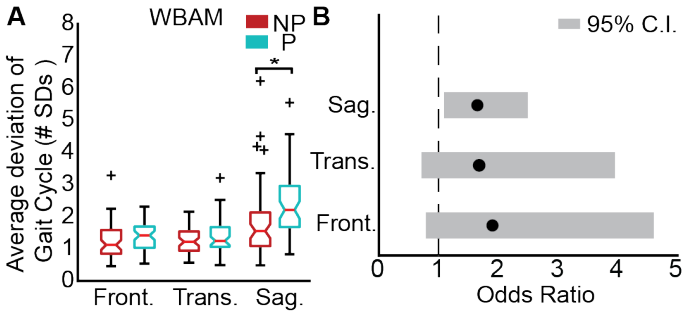

Figure 1: A) Rank-sums test compared perceived (P) to not perceived disturbances. B) Odds ratio on the ability of each WBAM plane to predict whether a disturbance was perceived.

These results suggest that whole-body feedback may play a role for young adults in their perception of small locomotor disturbances, which is consistent with prior studies demonstrating that whole-body motion drives corrective muscle responses to perturbations [2]. Whole-body motion is sensed by integrating feedback across multiple sensory modalities (e.g., visual, vestibular, proprioceptive, and somatosensory). We previously found deviations in ankle motion (but no other joint) contributed to the perception of locomotor disturbances [4]. Taken together, these results suggest that young adults may use ankle proprioception as the dominant contributor to estimate whole-body motion during subtle slip-like disturbances. Reduced proprioceptive feedback at the ankle that occurs with aging may cause an increased reliance on other sensory modalities, e.g., a shift from ankle to hip feedback. Whether this shift in reliance towards other joints or sensory modalities makes the aging population less sensitive to disturbances remains unknown.

Significance

These results suggest whole-body motion may play a crucial role in perceiving locomotor disturbances. Clinical measurement of the ability to estimate whole-body motion may therefore be important for assessing fall risk.

Acknowledgments

This research was supported by NIH NIGMS under Award Numbers 5U54GM104942-04 and T32GM133369.

References

[1] Liss et al., 2021. *Gait Posture.*
[2] Afschrift et al. 2021, PLoS *Comput. Biol.*
[3] Herr & Popovic, *J. Exp. Biol., 2008.*
[4] Liss et al. *45th Annual ASB Meeting,* 2021.

INVESTIGATING THE EFFECT OF SUBCUTANEOUS FAT THICKNESS ON SURFACE AND INTRAMUSCULAR-BASED ELECTROMYOGRAPHY SIGNALS IN THE LOWER LIMB

Matthew S. Russell[1], Samuel Vasilounis[1], Daniel Desroches[1], Talia Alenabi[2], Janessa D.M. Drake[1], Jaclyn N. Chopp-Hurley[1]
[1]School of Kinesiology and Health Science, York University, Canada
[2]Department of Kinesiology, University of Waterloo, Canada
email: jnhurley@yorku.ca

Introduction

Compared to intramuscular electromyography (iEMG), surface electromyography (sEMG) is a relatively quick, non-invasive method to capture muscle activity in biomechanics research. However, sEMG can be affected by intrinsic and extrinsic properties including crosstalk, musculoskeletal anatomy and physiology.[1] Subcutaneous fat thickness (SCFT) in particular may be an important factor affecting the agreement between surface and intramuscular-based signals and may be differentially impacted by contraction level.

This research investigated whether the difference between surface-based (sEMG) and intramuscular-based (iEMG) measured electromyography signals of the rectus femoris (RF) and vastus lateralis (VL) muscles was related to the magnitude of SCFT, measured using ultrasound. Further, the effect of submaximal exertion level (30%, 50% maximum knee extensor force) on this relationship was evaluated. Findings from this research will provide insight into whether a particular range of SCFT magnitudes yields larger discrepancies between sEMG and iEMG signals. This may have implications for the usability of surface-based approaches for measuring quadriceps muscle activity.

Methods

7 (5M, 2W) healthy adults (23-35y; BMI 24.9 ± 3.1 kg/m^2) have initially participated in this research. Resting ultrasound images (Logiq e, GE Healthcare) of the RF and VL were captured in a longitudinal view with the knee positioned at 90° using published methods to guide transducer placement.[2] SCFT superficial to each of the RF and VL was measured in FIJI[3] at the midpoint and medial and lateral-most image borders of the ultrasound image from which a mean value was calculated. Following resting ultrasound images, participants were instrumented with iEMG and sEMG (Delsys Trigno, Natick MA) electrodes to capture RF and VL muscle activity.[4] In a seated position, participants performed five-second maximal static knee extension exertions with the knee flexed to 90°. Force during maximal exertions was recorded by an ergoFET® force gauge (Hoggan Scientific, LLC) with exertions resisted by a rigid steel frame. Following maximal exertions, participants completed two repetitions of five-second static submaximal exertions at 30% and 50% of their force recorded during maximal exertions. sEMG and iEMG signals were linear enveloped and normalized to their muscle-specific maximal voluntary exertion magnitudes and the average between repeated trials used for analysis.

Differences between iEMG and sEMG were computed (ΔiEMG-sEMG) and correlation coefficients calculated between signal differences and SCFT for each muscle (RF, VL) and each exertion level (30%, 50%).

Preliminary findings from this research are reported. We expect to collect an anticipated sample size of n=20-30. Further, data from both men and women will be captured to permit sex-based analysis.

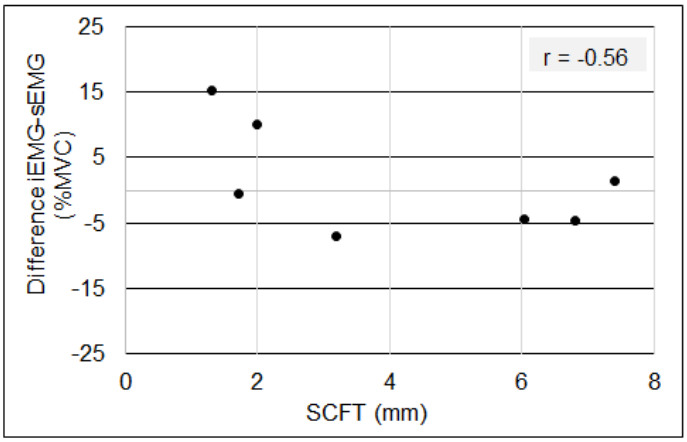

Figure 1: Difference between iEMG and sEMG (ΔiEMG-sEMG) (%MVC) by SCFT (mm) for the 30% exertion level for vastus lateralis.

Results and Discussion

Preliminary results show variable differences between iEMG and sEMG between participants, with iEMG both underestimating and overestimating sEMG signals at magnitudes that ranged from -21.5% MVC (underestimate) to 15.2% MVC (overestimate) across studied muscles and exertion levels. SCFT ranged from 1.5 mm to 15.6 mm for RF and 1.3 mm to 7.4 mm for VL. Correlation coefficients calculated between ΔiEMG-sEMG and SCFT were r=-0.1 (RF) and r=-0.56 (VL) for the 30% exertion level (Figure 1) and r=-0.33 (RF) and r=-0.14 (VL) for the 50% exertion level. Contrary to our expectations, the negative relationship suggests that a smaller difference between iEMG and sEMG was related to a greater magnitude of subcutaneous fat. However, the marked inconsistency in the direction of amplitude differences (overestimation versus underestimation) may partially explain these initial findings, in addition to a number of potential confounding factors, including crosstalk and intramuscular fat.

Significance

Initial results of this research provide little evidence to suggest that the magnitude of SCFT has a systematic effect on the agreement between surface-based and intramuscular-based methods to capture muscle activity. However, a larger sample size is required before conclusively discounting its effect.

Acknowledgments

The authors would like to acknowledge Alexandra Mahna for her assistance with data collection.

References

[1] De Luca, 1997. J Appl Biomech 13, 135-163.
[2] Moreau et al, 2009. Dev. Med. Child Neurol. 51, 800–806.
[3] Schindelin et al., 2012 Nat Method, 9(7), 676-82.
[4] Perotto, 2011. Anatomical Guide for the Electromyographer: The Limbs and Trunk (5th ed.). Springfeild, Il: Charels C. Thomas.

USE OF A POWERED PROSTHESIS INCREASES PEAK ANKLE POWER BUT NOT EFFECTIVE FOOT ARC LENGTH COMPARED TO A PASSIVE PROSTHESIS DURING WALKING ON SLOPES

Janet H. Zhang-Lea[1,*], Jana R. Montgomery[2], Alena M. Grabowski[1,3]
[1]University of Colorado, Boulder, CO, USA; [2]Evidation Health, San Mateo, CA, USA; [3]VA Eastern Colorado Healthcare System, Denver, CO, USA
email: *Hanwen.Zhang@colorado.edu

Introduction

People with transtibial amputation (TTA) using a passive-elastic prosthesis walk with a shorter effective ankle-foot "rocker" arm length compared to non-amputees, and thus have a shorter moment arm about the ankle joint compared to non-amputees. Effective foot length ratio (EFLR) has been used to assess ankle-foot effective arch length and adjust design and alignment of passive-elastic prostheses for people with TTA [1].

Use of a stance-phase powered ankle-foot prosthesis (BiOM) that provides prosthetic ankle plantarflexion power during the second half of the stance phase during walking increases peak prosthetic ankle power [2]. To match peak prosthetic ankle joint power and moment with values from a biological ankle joint, several tuning parameters of the powered prosthesis such as the duration of power output and push-off timing can be adjusted [3]. However, it is not clear if use of a biomimetic powered prosthesis results in a longer EFLR compared to use of a passive-elastic prosthesis by people with TTA.

We hypothesized that use of the BiOM prosthesis would increase peak ankle power and EFLR in the affected leg (AL) compared to use of a passive-elastic prosthesis during walking on level-ground and uphill slopes.

Methods

Nine healthy adults with TTA walked on a force-measuring treadmill (Bertec, OH) at 1.25 m/s on level ground and uphill slopes of 3°, 6°, and 9° using their own passive-elastic prosthesis, and a powered ankle-foot prosthesis (BiOM T2, Bedford, MA). We objectively and iteratively tuned the BiOM prosthesis until prosthetic ankle range of motion, peak moment, peak power, and net work of each subject were within 2 SDs of average non-amputee values [4].

We measured 3D ground reaction forces, center of pressure and lower limb joint kinematics. We used a 20 N vertical ground reaction force threshold to determine the stance phase. We used Visual 3D to calculate ankle power and determined peak ankle power during the stance phase.

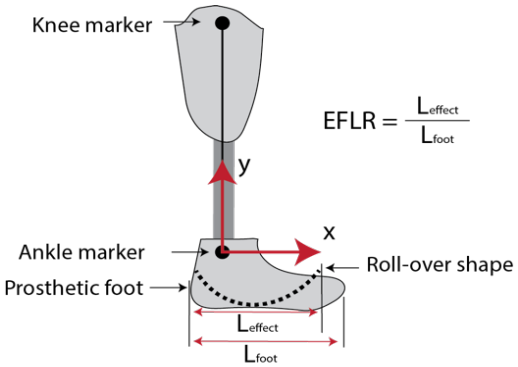

Figure 1. We determined roll-over shape by transforming the center of pressure into an ankle-foot coordinate system. EFLR indicates effective foot length ratio, which is the quotient of the roll-over shape distance (L_{effect}) and the foot length (L_{foot})

We calculated EFLR to quantify ankle-foot arch length. We first transformed center of pressure data from the single leg support phase for each foot into an ankle-foot coordinate system to obtain roll-over shape (Fig. 1), where EFLR is the distance between the heel of the foot to the anterior end of the ROS [1], normalized by foot length. We used repeated measures ANOVAs to assess the effect of prosthesis type and slope on peak ankle power and EFLR and significance was set at $p<0.05$.

Results and Discussion

Use of the BiOM compared to a passive-elastic prosthesis significantly increased AL peak prosthetic ankle power by up to 53.6% (Fig 2A, $p=0.045$), in agreement with previous findings [1]. However, this increase in peak prosthetic ankle power did not lead to an increased EFLR in the AL. We controlled for slope and interaction effects and found that use of the BiOM prosthesis *reduced* AL EFLR by 0.086−0.12 ($p=0.014$) compared to use of a passive-elastic prosthesis (Fig. 2B). Our results suggest that although use of the BiOM powered prosthesis increased peak prosthetic ankle power compared to a passive-elastic prosthesis in people with TTA, it did not result in a longer effective foot arch length.

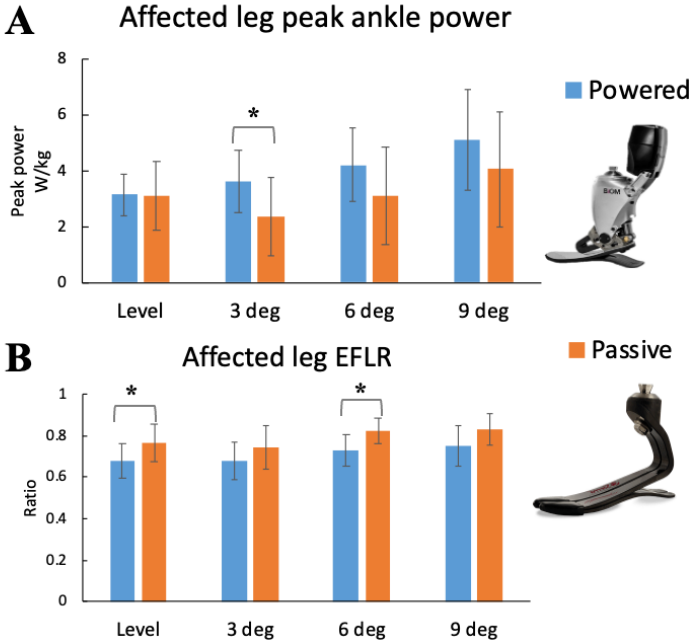

Figure 2. Affected leg peak prosthetic ankle power (A) and EFLR (B) when subjects used a passive-elastic and powered prosthesis during walking. * $p<0.05$

Significance

The tuning strategy used for the BiOM powered prothesis did not yield a longer EFLR compared to a passive-elastic prothesis during walking on level-ground and uphill slopes for people with unilateral TTA. Future studies are needed to understand if and how tuning parameters of a powered prosthesis affect effective arch length of the ankle-foot "rocker".

Acknowledgments

Funding from the VA RR&D Service RX002943-01A2.

References

[1] Hansen and Childress 2010 *Disability and Rehablitation*
[2] Herr and Grabowski, 2012 *Proc. R. Soc. B*
[3] Malcolm et al., 2015 *J. Neuroeng. Rehabilitation*
[4] Jeffers and Grabowski, 2017 *Front. Robot. AI*

IMU-BASED ESTIMATION OF ANKLE AND HIP JOINT CENTERS USING AN ERROR-STATE KALMAN FILTER

Michael V. Potter[1], Stephen M. Cain, Lauro V. Ojeda, Reed D. Gurchiek, Ryan S. McGinnis, and Noel C. Perkins
[1]Department of Physics and Engineering, Francis Marion University
email: michael.potter@fmarion.edu

Introduction

Body-worn inertial measurement units (IMUs) are an increasingly popular tool for biomechanical studies outside of traditional laboratory environments. In some applications, IMUs are placed on individual body segments and the raw IMU signals are used in combination with advanced methods to estimate traditional human kinematic measures (e.g., joint angles). Importantly, such methods rely on accurately knowing the relationships (i.e., the relative positions and orientations) between the IMU sense axes and the anatomical axes of the associated body segment. These relationships are commonly known as the sensor-to-segment alignment parameters. Accurate estimates of these parameters from IMU data only remains a difficult, but important challenge [1].

We present a novel method for estimating two critical sensor-to-segment alignment parameters, namely the locations of the ankle and hip joint centers in the IMU sense frames. Specifically, these parameters are the XYZ coordinates of the joint centers in their associated segments' IMU frames (e.g., the location of the ankle center in the foot IMU frame and in the shank IMU frame).

Methods

The error-state Kalman filter (ErKF) method in [2] is expanded to a full seven-body model of the human lower limbs composed of the feet, shanks, thighs, and pelvis. This method estimates the positions, velocities, and orientations of each of the seven associated body segments. In contrast to [2], we further expand the estimated state to include (i.e., estimate) the joint center locations in the associated segments' IMU sense frames. Thus, the new method simultaneously estimates the lower-limb kinematics and the joint center alignment parameters.

One healthy adult subject wore reflective markers whose trajectories were recorded via optical motion capture as the subject performed various activities. Motion from two activities (approx. 1 minute each) were selected for this study, namely: 1) a treadmill walk at a self-selected speed and 2) a dynamic calibration procedure designed to exercise all major lower-limb joint degrees of freedom. OpenSim software was used to create a scaled model of the subject and compute the lower-limb kinematics for each activity using the marker trajectories. Using these data, an approach similar to that in [2] was used to calculate noise-free IMU data for "virtual IMUs" on the feet, shanks, thighs, and pelvis for each activity.

The effectiveness of the proposed method in accurately estimating joint center locations was evaluated by performing 100 simulations per activity. In each simulation, random noise was added to the calculated (i.e., virtual) IMU data to simulate the effects of real sensor noise. Additionally, random noise was added to the initial state estimate of the joint center locations ($\sigma = 5\ cm$ in each axis) to simulate the effects of reasonable errors in the initial guesses of these alignment parameters. Finally, the positional errors in the joint center estimates at the end of each simulation were investigated.

Results and Discussion

Table 1 presents the mean and standard deviation of the magnitudes of the positional errors in joint center location estimates from the walking trial and dynamic calibration trial. Note that each joint center is estimated from two IMUs (e.g., the ankle joint center must be determined in both the foot and shank IMU frames).

Table 1: Mean ± SD positional errors (in mm) in hip and ankle joint center estimates from ErKF method.

Joint	IMU	Walk	Dynamic Calibration
Ankle	Foot	4.8±1.3	1.7±1.5
	Shank	15.5±8.8	4.1±2.9
Hip	Thigh	26.1±19.1	4.7±2.9
	Pelvis	25.2±9.5	32.0±20.4

These data demonstrate errors in the ankle joint center location estimates less than 5 millimeters using the dynamic calibration procedure. Note that for most of the four joint center estimates (rows in Table 1), the dynamic calibration yields superior errors to the walking trial. The only exception is for the estimated hip center from the pelvis IMU. Further note that the dynamic calibration movement is designed to provide significant motion of the thighs, shanks, and feet; however, the pelvis remains nearly static. In contrast, all segments move during the walking trial; but, the three leg segments generally move with lower accelerations and ranges of motion than in the dynamic calibration. In combination, these results suggest that the proposed method accurately estimates joint center locations provided sufficient accelerations and ranges of motion in the individual segments and joints.

Significance

For IMU-based kinematic estimation methods to achieve full utility in broad biomechanical study designs, they must be capable of accurately estimating kinematics from the IMU data alone (e.g., without using optical motion capture to initialize the estimates). This research represents an important step towards achieving this goal by presenting a method that can successfully estimate important sensor-to-segment alignment parameters from IMU data only. This work also provides evidence of important considerations for future IMU-only sensor-to-segment alignment methods; specifically, that the accuracy of such methods may rely critically on having subjects initially perform movements that have sufficient accelerations and ranges of motion for each body segment.

References

[1] Vitali and Perkins, 2020. *J. Biomech*. 106: 109832.
[2] Potter et al., 2019. *PLOS ONE.* 16(4): e0249577.

Stoko K1: Supportive apparel to reinterpret lower extremity bracing

Calvin T.F. Tse[1*], Ryan Bakker[2], Joseph Ardell[2]
[1] Graduate Programs in Rehabilitation Sciences, University of British Columbia, Vancouver, BC
[2] Stoko Design Inc., Vancouver, BC
email:* calvin.tse@ubc.ca

Introduction

Knee bracing is commonly used to support weightbearing activities in individuals with knee injuries or instability [1]. Conventional knee braces use a rigid hinged frame for structural support, and Velcro straps for attachment onto the thigh and lower leg. After long periods of wear, these braces can become uncomfortable or migrate down the leg from their intended positions. The K1 (Stoko Design Inc., Vancouver, BC) is a novel knee bracing device that integrates an adjustable network of inelastic cables (spans across the knee joint, anchors around pelvis) into the fabric of a compressive athletic tight designed to support the knee (Fig. 1). During tests using a simulated triaxial knee loading apparatus, a white paper released by Stoko Design Inc. reported the K1 reduced external frontal plane knee moments similar to an industry-accepted 'gold standard' brace [2]. Considering its departure from traditional bracing design, a biomechanical assessment of the K1 is warranted to understand its effects during in vivo weightbearing activities.

Methods

Lower body biomechanics of ACL-deficient adults (n = 20, 8M/12F, mean age = 34.5 [8.8]) were assessed during overground walking, treadmill running, and single-leg drop landing (SL-Drop). In a randomized order, all activities were performed in the K1 and a control athletic tight. 3D motion capture of the lower body and ground reaction force (GRF) data were measured synchronously. Relative angles and external joint moments were calculated for the hip and knee with Visual 3D.

Figure 1. *Marker placements while donning Stoko K1*

Self-perceived knee stability in each apparel condition and activity was rated on a 0 – 10 scale (0 = completely unstable, 10 = perfectly stable). A SL-Drop time to stabilization (TTS) was calculated as the time elapsed from initial contact to maintenance of vertical GRF between 95-105% bodyweight for one unbroken second. Differences in outcomes between the K1 and control tights were explored with T-Tests (α<0.05).

Results and Discussion

Table 1 summarizes selected outcomes comparing the K1 with the control tight. At the knee, the peak valgus angle was reduced with the K1 during running and SL-Drop. At the hip, the frontal plane angle was more abducted with the K1 during all activities. This combined effect at the knee and hip suggests the K1 may serve to position the lower extremity further from the body's midline in the frontal plane. Considering the dynamic valgus knee injury mechanism involves both knee valgus angle and hip adduction, the observed changes in knee and hip frontal plane mechanics, as well as perceived stability with K1, could have implications for improving confidence in movement, and potentially injury risk.

A negative correlation between the SL-Drop TTS (control) and the change in TTS with K1 was observed (Fig. 2). This suggests that individuals who are less stable (long TTS-control) may also experience greater improvements in TTS when supported with K1 (larger reduction in TTS).

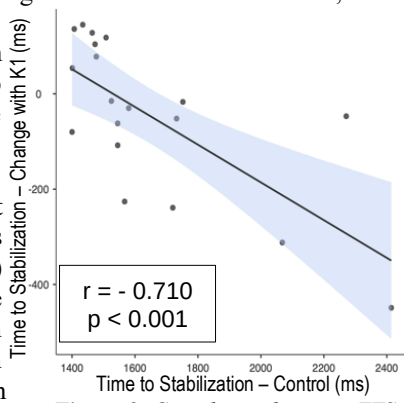

Figure 2. *Correlation between TTS-Control and TTS-Change with K1*

Significance

The Stoko K1 is a novel knee brace that addresses many pitfalls of conventional rigid hinged frames while providing similar levels of support. Early investigation of the K1 indicates this brace may shift knee and hip joint angles away from joint positions frequently identified as injury mechanisms. Improved perceived stability could also benefit K1 users prophylactically and functionally support individuals recovering from injury.

Acknowledgments

Research funding was provided by the Mitacs Accelerate program, in collaboration with Stoko Design Inc.

References

[1] Chew et al., 2007. *Am J Phys Med Rehabil.* 86(8): 678 – 686
[2] Ardell & Bakker, 2020. Stoko K1 Support Verification

Table 1. Knee and hip biomechanical and perceived stability outcomes during activities with control tight and the change with Stoko K1.

Activity:	Walking		Running		Single-Leg Drop Landing	
Observed Outcome	Control	Mean Change	Control	Mean Change	Control	Mean Change
Knee Valgus Angle Peak (°) *	1.3 [3.1]	- 0.6 [1.4]	- 2.1 [2.8]	**- 1.1 [2.0]**	- 0.7 [3.7]	**- 0.8 [1.7]**
Knee Adduction Moment Peak (Nm/kg)	0.53 [0.14]	- 0.02 [0.07]	–	–	0.85 [0.32]	+ 0.05 [0.11]
Hip Adduction Angle Peak (°) *	5.6 [2.8]	**- 5.5 [2.5]**	7.8 [3.2]	**- 6.3 [2.4]**	0.6 [4.2]	**- 5.0 [2.0]**
Hip Adduction Moment Peak (Nm/kg)	0.79 [0.13]	**- 0.07 [0.11]**	–	–	1.27 [0.26]	- 0.06 [0.17]
Perceived Stability (0 – 10)	8.6 [1.0]	**+ 0.7 [0.7]**	7.5 [1.4]	**+ 1.5 [1.5]**	6.4 [1.7]	**+ 2.1 [1.4]**

Values reported as mean [standard deviation]. Bolded values indicate a significant difference between control tights and K1 ($p < 0.05$).
* Positive/negative angles indicate valgus/varus for the knee, and adduction/abduction for the hip, respectively.

MEASURING SAGITTAL KNEE ANGLE AND MOMENT USING SENSORS EMBEDDED IN A PROSTHESIS

Sabina Manz[1,2,*], Thomas Schmalz[1], Veit Schopper[1,3], Strahinja Dosen[2], Jose Gonzalez-Vargas[1]
[1]Ottobock SE & Co. KGaA, Duderstadt, Germany
[2]Department of Health Science and Technology, Aalborg University, Aalborg, Denmark
[3]Institute of Biomechanics and Orthopaedics, German Sport University Cologne, Cologne, Germany
email: *sabina.manz@ottobock.de

Introduction

Optoelectronic motion capture systems and force plates are typically used to assess kinematics and kinetics in clinical gait analyses. However, these systems are bound to laboratory environments only [1]. For this reason, the performance of a patient in the laboratory often does not represent entirely real-life gait due to various limitations such as confined spaces and constrained but perfectly even pathways [1].

Inertial measurement units (IMUs) are wearable sensors that overcome some of the limitations of optoelectronic systems. These sensors can be used for the clinical gait analyses outside of a laboratory environment with good precision with respect to optoelectronic systems (e.g., less than 1° error in the knee angle [2]). However, IMUs are not without limitations, as for instance, the errors introduced when positioning the units to the limbs can translate into errors in the derived movements [3]. Importantly, some mechatronic lower limb prostheses are already equipped with embedded sensors (for control purposes), which are an attractive and easy solution for clinical gait analyses as they do not require external positioning. These sensors can measure orientation, acceleration, angular velocity, joint angles and loads when using a prosthetic device [4]. However, the validity and accuracy of these sensor data with respect to clinical gait analyses originating from laboratory measurements are still unknown. Therefore, there is a need to investigate how movement kinematics and kinetics obtained from the embedded sensors compares to that measured using laboratory-based clinical gait analyses.

Methods

Kinematic and kinetic data were collected from two patients with unilateral transfemoral amputation (mean ± standard deviation, age: 53.5 ± 3.5 years, height: 173.5 ± 6.4 cm, weight: 82.3 ± 3.9 kg, time since amputation: 42.5 ± 2.1 years, knee joint: GeniumX3) using an optical motion capture system and ground embedded force plates, as well as the sensors integrated in the microprocessor-controlled knee joint (GeniumX3, Ottobock, Germany). The embedded sensors provided hydraulic loading of the knee, knee joint angle, and orientation of the prosthesis in the sagittal plane (shank angle). The data were collected during level walking at three self-selected speeds (normal, slow, and fast), ramp ambulation (at 10° and 15° incline/decline), and stair ambulation. Five trials were collected for each task.

The variables of interest in this study were the sagittal knee angle (measured directly) and moment (estimated external moment). The outcome measures for the comparison between the optical motion capture system (gold standard, GS) and the device sensors (DS) were Pearson correlation coefficients, root mean square errors (RMSE), and maximum relative errors. The relative error was computed as the error over time divided by the range of GS values of the same trial.

Results and Discussion

The knee angle and moment measured in both subjects during level walking at normal speed is shown in Figure 1 (average, n=5 trials). In general, both were strongly correlated (ρ>0.9). Therefore, the overall trend and shape of the knee angle and moment obtained by GS is very well replicated by DS.

The knee angle RMSE and relative error were between 2.1-3.1° and 2.2-3.2%, respectively, and hence the deviations between DS and GS signals were rather small. Larger deviations were seen in the moments (6.4-7.0 Nm and 10.8-14.1%). Figure 1 further shows that both DS and GS could capture interindividual differences in the gait patterns.

Overall, these results demonstrate that the kinematics and kinetics measured using DS are close to that obtained using GS in shape as well as in amplitude. Further analysis including more participants, other tasks and measures are needed in order to generalize these results and establish that the embedded sensors are indeed a useful tool for clinical gait analyses.

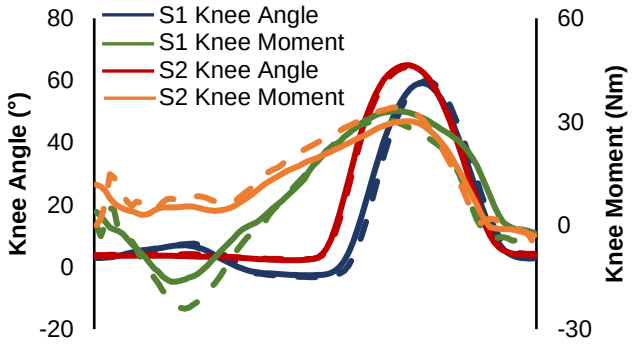

Figure 1: Knee angle and moment of subject one (S1) and two (S2), for gold standard (GS, dashed lines) and device sensor (DS, solid lines) data, respectively. The lines each represent the average of five trials. The data is normalized to one gait cycle (angle) and one stance phase (moment), respectively.

Significance

These results are relevant for the field of lower limb prosthetics in order to facilitate the development of more appropriate gait assessment tools which can be used for the assessment in real world and outside of a gait laboratory. The preliminary analysis indicated that the embedded sensors can be used to determine the knee angle and moment of the prosthetic leg during walking, while future work will evaluate if this also holds true for other measures and more participants.

Acknowledgments

This work is supported by the Marie Skłodowska-Curie Actions (MSCA) Innovative Training Networks (ITN) H2020-MSCA-ITN-2019 - 860850 – SimBionics.

References

[1] Cutti et al., 2015. *G Ital Med Lav Ergon* **37**: 45-8.
[2] Seel et al., 2014. *Sensors* **14**: 6891–909.
[3] Bolink et al., 2016. *Med Eng Physics* **38**:225–31.
[4] Bellmann et al., 2019. *Biomed Eng* **64**:407–20.

KNEE FLEXION ANGLE AND VERTICAL GROUND REACTION FORCE PREDICTS KNEE EXTENSION MOMENTS DURING GAIT AFTER ANTERIOR CRUCIATE LIGAMENT RECONSTRUCTION: A LONGITUDINAL ANALYSIS

Alexa K. Johnson[1*], Riann M. Palmieri-Smith[1,2], Chandramouli Krishnan[1,3,4,5]
[1]School of Kinesiology, University of Michigan, Ann Arbor, MI USA
email: *akjohns@umich.edu

Introduction

Altered knee biomechanics during gait is commonplace after anterior cruciate ligament reconstruction (ACLR). In particular, smaller knee flexion angles and knee extension moments are seen early following surgery and persist for years after. [1] These abnormal knee mechanics observed after ACLR have been linked to cartilage degradation and therefore are believed to contribute to the pathogenesis of post-traumatic knee osteoarthritis. Researchers have determined that reduced vertical ground reaction forces (vGRF) contribute to decreases in knee extensor moments during gait, [2] and increasing vGRF can improve knee moments and restore normal gait patterns after ACLR. [3] While previous research has established the cross-sectional association between vGRF and knee extension moment, [2,3] the longitudinal nature of this relationship is currently unknown - i.e., the change in vGRF with time is associated with the change in knee moment with time. Therefore, the purpose of this study was to examine the relationship between knee joint angles, vGRF, and knee moments during walking in individuals who had recently undergone ACLR. We hypothesized that the change in knee flexion angle and vGRF would be positively associated with the change in peak knee moments during the stance phase of walking.

Methods

Twenty-six individuals who had recently undergone ACLR (17 females; Age: 20.7±5.5yrs; Height:1.72±0.09m, Mass: 69.9±11.9kgs) completed a gait analysis at three time-points following surgery, time1 = 2.2 months after surgery, time2 = 4.6 months after surgery and time3 = 6.6 months after surgery. Three-dimensional motion capture and two in-ground force platforms were used to analyze kinematic and kinetic data during overground walking at an average self-selected speed. Data were time normalized, and knee flexion angle at initial contact, peak knee flexion angle, peak vGRF, and peak knee extension moment were calculated for each limb during the loading phase of the gait for all three time points. Change from baseline, utilizing time1 as baseline were calculated as Change1 = time2 – time1, and Change2 = time3 – time1.

Multiple linear regressions utilizing classical and Bayesian Interference methods were used to determine the contribution of the change in knee flexion angle and vGRF to the change in peak knee extension moment during gait in both the ACLR limb and the non-ACLR limb. A significance level of $\alpha = 0.05$ was used for classical regression analyses and Bayesian analyses were performed to estimate the Bayes Factor in favor of the alternative hypothesis (BF_{10}).

Results and Discussion

Regression analyses on the ACLR limb indicated that changes in peak knee flexion angle and peak vGRF significantly predicted the changes in peak knee extension moment during the loading phase of the gait at both Change1 ($P < 0.001$, $R^2 = 0.775$, fig 1A) and Change2 ($P < 0.001$, $R^2 = 0.731$, fig 1C). Bayesian regression evaluating the likelihood of these prediction models showed that there was decisive evidence favoring the regression model that included changes in peak knee angle and peak vGRF as opposed to the null model (ACLR BF_{10} at Change1 = 329729, and ACLR BF_{10} at Change2 = 27481). The non-ACLR limb analyses indicated changes in knee angle at initial contact, peak knee angle, and peak vGRF significantly predicted the changes in peak knee moment during the loading phase of the gait in Change1 ($P < 0.001$, $R^2 = 0.844$, fig 1B) and Change2 ($P < 0.001$, $R^2 = 0.883$, fig 1D). Bayesian regression of these prediction models showed decisive evidence favoring the regression model that included changes in knee angle at initial contact, peak knee angle, and peak vGRF as opposed to the null model (non-ACLR BF_{10} at Change1 = 2.526e +6 and non-ACLR BF_{10} at Change2 = 1.779e +7). Standardized beta coefficients indicated that changes in knee flexion angle had a greater impact (>2x) on knee extension moments than vGRF at both time points in both limbs.

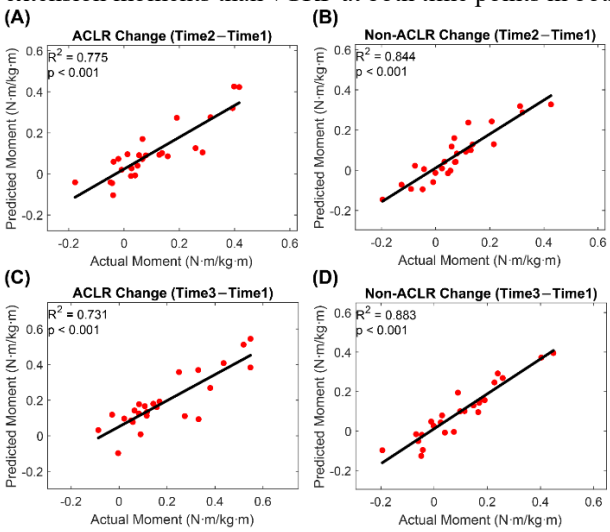

Figure 1: Scatterplots of actual vs. predicted changes in knee moment of the ACLR and non-ACLR limbs using regression models that used changes in knee angle and peak vGRF during the loading phase of the gait of the respective limbs across timepoints.

Significance

Real-time biofeedback of vGRF has been used to improve knee loading after ACLR; however, the results of this study indicate that targeting knee flexion angles may have a bigger impact on improving knee joint loading than vGRF. Knee flexion angles are also easier to target in a clinic due to the increasing availability of low-cost camera systems that can provide real-time feedback of knee joint angles. Further research is warranted to determine if targeting knee flexion angle during gait can improve knee joint loading and cartilage health following ACLR.

Acknowledgments

This research was supported by the NIH R21-HD092614 grant.

References

[1] Hart et al., 2016. *Br J Sports Med.* 50; 597-612.
[2] Lin & Sigward., 2018. *Gait & Posture,* 66; 83-87.
[3] Luc-Harkey et al. 2018. *J Biomech,* 76; 94-102.

ACUTE EFFECTS OF KNEELING EXPOSURE ON PASSIVE FRONTAL PLANE KNEE LAXITY

Kimberly H. Peckett[1], Daniel K. Mines[1], Michelle Loo[1], Stacey M. Acker[1]
[1]Department of Kinesiology and Health Sciences, University of Waterloo, Waterloo, ON
email: stacey.acker@uwaterloo.ca

Introduction

Previous work has found that prolonged kneeling exposure changes knee joint mechanics [1] and has links to knee osteoarthritis [2,3]. Individuals with knee osteoarthritis have been shown to have an increase in knee laxity compared to healthy individuals [4,5] leading to speculation that there may be an increase in knee joint laxity following prolonged kneeling in full flexion that leads to the later development of osteoarthritis in habitual kneelers. The purpose of this study was to compare frontal plane knee laxity before and after 30 minutes of kneeling exposure. It was hypothesized that prolonged kneeling will increase frontal plane knee joint laxity when varus and valgus forces are applied.

Methods

A laxity measurement system was used to evaluate passive frontal plane knee laxity (EMG amplitude <5% of MVC) in 15 right leg dominant healthy participants (8 males and 7 females) from a university population before and after a kneeling exposure protocol (10 minutes full flexion kneeling + 5 minutes seated rest, x 3 cycles). The system consisted of a seat where the thigh was strapped and clamped down, a sled to which the tibia was strapped, a table with ball bearings over which the sled could slide freely, a 2.28kg medially or laterally directed load applied 0.45m distal to the femoral condyles to create a 10Nm adduction or abduction moment, and infrared markers affixed to the thigh and shank, tracked using an optical motion capture system (Optotrak Certus, NDI, Waterloo, Canada). In pilot work, the laxity device was determined to have a minimal detectable change (MDC) of 1.8°. Joint angles were calculated using a Z-X-Y (flexion/extension – adduction/abduction – axial rotation) Cardan Sequence in Visual3D software (v6, C-Motion, Germantown, MD). Total passive knee joint laxity was defined as the range between the loaded maximum adduction and maximum abduction joint angles. The participants' means and standard deviations from the three pre-kneeling and post-kneeling trials were calculated. Statistical analysis of the data was performed using a one-tailed paired sample t-test with an alpha value of 0.05.

Results

There was no overall significant difference in passive knee laxity in the frontal plane before (8.8° ± 3.5°) and after kneeling (8.5° ± 3.2°) (p=0.17). Examined individually, only 3 participants had laxity changes greater than the MDC. The average within-participant change (post-pre) was -0.3° ± 1.2°, ranging from -2.9° to 1.8°.

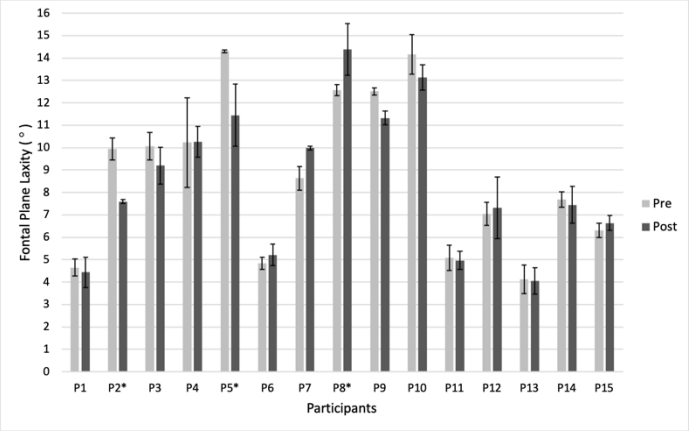

Figure 1: Mean frontal plane knee laxities (sum of maximum adduction and maximum abduction) pre- and post-kneeling. Error bars represent standard deviations. Asterisks (*) next to the participant's code on the x-axis indicate a change in laxity greater than the MDC of 1.8°.

Discussion

The hypothesis that 30 minutes of kneeling exposure would cause a significant increase in passive knee laxity in the frontal plane was rejected. It should be noted that this study only examined acute exposure and used only one kneeling position, whereas many high knee flexion occupations adopt several kneeling positions throughout the course of a workday. However, the outcomes from this acute exposure do not support the possibility that laxity increases after exposure. Future work should investigate laxity in participants who are habitually exposed to kneeling.

Significance

It is understood that individuals with knee osteoarthritis have an increase in frontal plane knee laxity when compared with healthy controls. However, after a prolonged kneeling protocol, the non-habitual kneelers in our study did not exhibit a significant change in frontal plane knee laxity. This finding refutes the possibility that acute changes in passive knee laxity after kneeling could contribute the development of kneeling related knee osteoarthritis.

Acknowledgments

The authors gratefully acknowledge the Biomechanics of Human Mobility Lab members assistance with data processing as well as our funding sources including the Canadian Foundation for Innovation and NSERC Canada.

References

[1] Kajaks et al., 2015. *Applied Ergonomics, 46*, 224-230.
[2] Cooper et al., 1994. *Annals of the Rheumatic Diseases, 53*(2), 90-93.
[3] Coggon et al., 2000. *Arthritis and Rheumatism, 43*(7), 1443-1449.
[4] Sharma et al., 1999. *Arthritis & Rheumatism, 42*(5), 861-870.
[5] van der Esch et al., 2005. *Scandinavian Journal Of Rheumatology, 34*(4), 298-30

RAPID UPPER LIMB ASSESSMENT OF BURKINABE WEAVERS USING TRADITIONAL HANDLOOMS

Samuel Brost[1*], Amidou Sawadogo[2], Timothy J. Bryant[1], Genevieve A. Dumas[1] and Qingguo Li[1]
[1]Department of Mechanical and Materials Engineering, Queen's University, Canada
[2]Institute of Sport Sciences and Human Development, Joseph Ki-Zerbo University, Burkina Faso
email: *16sb97@queensu.ca

Introduction

Burkinabe artisans who produce woven cotton goods are a vital part of the large informal work sector present in Burkina Faso. In low-income countries these informal workers are responsible for over 50% of the gross domestic product [1]. The large population of weavers in Burkina Faso are primarily women, despite the work having been traditionally reserved for men in the past [2].

Weavers typically work for 6-9 hours per day and 5-7 days per week [3]. While working, weavers are performing repetitive motions and experiencing high loads from the tension placed on the woven strings. Many weavers report pain and injury because of the occupation. In a recent survey done in Ouagadougou, 98% of the 213 weavers surveyed reported experiencing musculoskeletal disorders (MSDs) in the past year [3]. The two most prevalent regions reported were the low back (76.5%) and the shoulders (70.4%) [3]. This work aims to explore the biomechanical factors in the weaving cycle that may be contributing to the MSDs being reported by Burkinabe weavers using the Rapid Upper Limb Assessment (RULA) [4].

Methods

Video data of the weaving process performed by 10 weavers (height of 163.05 ± 7.0 cm, mass 65.45 ± 14.8 kg, 48.70 ± 15.2 years of age, and 19.80 ± 13.7 years of experience weaving [3]) recruited from weaving centres in Ouagadougou, Burkina Faso was analyzed [3]. Videos were collected in the sagittal and coronal planes using two video cameras (DCR-SR80, Sony, USA).

The weaving process used in Burkina Faso is highly complex and cyclical in nature. To properly evaluate the postures and loading experienced, the weaving cycle was subdivided into two phases which were then subdivided. The two primary phases are: interlacing which accounts for approximately 80% of the 1.9-minute weaving cycle and requires repetitive low load motion; and the shorter winding phase that requires weavers to exert a large force to wind the tensioned string.

Four key extreme postures in the weaving cycle were analyzed using the RULA. These postures included the highly repetitive weft passage from interlacing, the high loading lift and push actions found in winding, and adjustment which represents the greatest trunk flexion observed in the weaving cycle and occurs at the end of winding. To perform the RULA, the postures of the weavers recorded were independently analyzed by three researchers using Kinovea (version 0.8.15). Loading at the pedals during interlacing and the loading at the hand-operated lever required for beam rotation were measured on one loom using a mechanical force gauge (MFD-06, Nidec-Shimpo, USA).

Results and Discussion

The results of the RULA analysis, summarized in Table 1, indicate that none of the weaving actions were acceptable and all require additional investigation and potential changes. A non-parametric Kruskal-Wallis H-Test indicated several significant differences between the actions analyzed.

Table 1: Summary of RULA scores for the four weaving actions

	Weft Passage	Lift	Push	Adjustment
Posture A	3.1 ± 0.1†	3.3 ± 0.2†	3.5 ± 0.1*	3.7 ± 0.1*
Wrist and Arm	4.1 ± 0.1	6.3 ± 0.2*†	6.5 ± 0.1*†	3.7 ± 0.1
Posture B	2.8 ± 0.1	4.0 ± 0.2*	4.9 ± 0.2*†	3.5 ± 0.2
Neck, Trunk and Legs	6.7 ± 0.1†	4.0 ± 0.2*	4.9 ± 0.2*†	3.5 ± 0.2*
Grand Score	6.0 ± 0.1†	5.7 ± 0.2†	6.3 ± 0.2†	3.7 ± 0.2*

* Significantly different from Weft Passage
† Significantly different from Adjustment

A post-hoc Dunn's test investigated the differences between postural scores with and without loading and the grand score for each of the actions. This analysis shows that weft passage has a significantly lower mean postural score for the neck, trunk, and legs (posture B) than lift and push but a significantly higher score when considering loading (neck, trunk and legs). This result indicates that the external load of the pedals that exceeds 10 kg is a key factor in the high grand score.

The lift and push actions both had high postural scores, however results indicated that the most important factor was the loading experienced at the lever. Lift had a poor posture score for the wrist and arm as well as the neck, trunk, and legs, however the no-load wrist and arm score was not significantly higher than weft passage whereas the scores including the 10 kg loading at the lever (wrist and arm and neck, trunk, and legs) were significantly higher than weft passage. This result indicates that an intervention or loom redesign to decrease the loading experienced during the weaving cycle is required.

RULA analysis demonstrated that the poor postures combined with high loading could be the most significant factor in the prevalence of MSDs being reported by the weavers.

Significance

This study identified factors relating to weavers in Burkina Faso that may cause MSDs and are unique to the regional weaving process. Furthermore, the methodology and analysis are not resource intensive and can be applied to study more of the nearly two billion informal workers in developing countries [5].

Acknowledgments

This study is partially supported by a NSERC Discovery Grant.

References

[1] Sawadogo et al., 2019. Int J Med Pharm Sci. 9(6):83–94.
[2] Igué J., 2003. Le secteur informel en Afrique de l'Ouest
[3] Sawadogo A., 2019. Universite D'Abomey–Calavi.
[4] McAtamney, Corlett, 1993. Appl Ergon. 24(2):91–9.
[5] International Labour Office. Women and men in the informal economy: a statistical picture. 3rd ed. 2018.

MEDIAN NERVE DEFORMATION AND VELOCITY CHANGE IN CONCERT DURING A POWER GRIP IN THE TRANSVERSE PLANE OF THE CARPAL TUNNEL

Michelle B. Campbell[1], Kaylyn E. Turcotte[1], Gabrielle Racine[1], Michael W.R. Holmes[2] and Aaron M. Kociolek[1*]
[1]Biomechanics and Ergonomics Lab, School of Physical and Health Education, Nipissing University, North Bay ON, Canada
[2]Neuromechanics and Ergonomics Lab, Department of Kinesiology, Brock University, St. Catharines ON, Canada
Email: *aaronk@nipissingu.ca

Introduction

Carpal tunnel syndrome (CTS) is characterized by compression and entrapment of the median nerve (MN); however, the underlying pathomechanisms are complex and multi-factorial [1]. Patients with CTS present with increased MN cross-sectional area proximal to the carpal tunnel inlet, which is consistent with edema-based enlargement due to increased hydrostatic pressure inside the carpal tunnel [2]. Our study using ultrasound within the carpal tunnel found greater migration and reduced cross-sectional area of the MN during a sustained chuck grip in nonneutral wrist postures [3]. These results are consistent with a compression-based pseudoneuroma work-related injury mechanism. However, active tendon tension during gripping may also influence MN migration and deformation patterns, either due to increased contact stress with neighbouring anatomical structures such as the transverse carpal ligament, or alternatively via increased subsynovial connective tissue strain in the carpal tunnel.

There remains a need to understand to what extent MN deformation is related to tendon dynamics within the carpal tunnel. Therefore, the purpose of this study was to quantify MN deformation and motion relative to the finger flexor tendons. Ultrasound analysis was conducted throughout the time series of a forceful grip task (loading and unloading) to better understand tissue interactions within the carpal tunnel.

Methods

Twelve participants completed a power grip while ramping force up from 0% to 50% of their maximal voluntary force (MVF), before ramping force down from 50% to 0% MVF. Feedback of the force matching task was provided using a custom program (LabVIEW, National Instruments), which was also used to collect grip forces produced on a digital dynamometer (MIE Medical) at 1000 Hz. The transverse carpal tunnel was imaged at the distal wrist crease using B-mode ultrasound (Vivid Q, General Electric). Scanning depth was set to 3 cm while cineloops were captured at an acquisition frequency of 13 MHz and sampling rate of 30 Hz. A custom-built triggering device was used to synchronize grip force data and ultrasound cineloops, allowing the extraction of ultrasound images at specific force levels for analyses. Carpal tunnel images were extracted using MATLAB (MathWorks) in 5% increments of 0-50% MVF during both the ramp up and ramp down phases of the grip task. Additional images were extracted immediately before and after the ramp up and down phases to represent rest (0% MVF) and sustained gripping (50% MVF). Images were analyzed in ImageJ (National Institutes of Health) to determine MN cross-sectional area, circularity [$4\pi(Area/Perimeter^2)$], width (radioulnar axis), and height (palmar-dorsal axis) as well as the relative displacement and velocity between the MN and flexor digitorum superficialis tendon of the long finger (FDS-L). Two-way repeated measures ANOVAs tested the effects of grip force level (0%-50% in 5% increments of MVF) and ramp direction (loading vs unloading) on all outcome variables ($\alpha = 0.05$).

Results and Discussion

We found a force level by ramp direction interaction on MN circularity ($F_{12,120}$=2.599, p=0.004). While ramping force up (loading), the MN became more circular from 0%-10% MVF, with little change from 10%-50% MVF. While ramping force down (unloading), there were no further changes in MN shape, retaining deformation from the previous loading phase. There was also a significant force level by ramp direction interaction on MN displacement ($F_{12,120}$=4.397, p<0.001) and velocity ($F_{8,80}$=3.228, p=0.003) relative to the FDS-L in the radioulnar axis. Interestingly, MN velocity data coincided with changes to MN deformation, with significantly greater velocity while ramping force up from 0-10% MVF (Figure 1), followed by very little movement for the rest of the grip task (velocities approaching 0 mm/s).

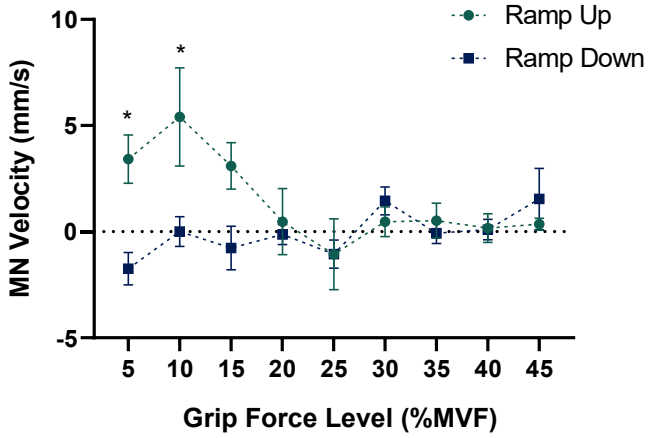

Figure 1: Mean (± 95% CI) MN velocity in the radioulnar axis while ramping up and down grip force. Significance indicated by asterisks (*).

Significance

We found coinciding changes in MN circularity and velocity throughout the time series (loading and unloading) of gripping, which matched previous findings documenting time-dependent strain of the subsynovial connective tissue [4]. Together, these results suggest that MN deformation is, in part, caused by viscoelastic strain within the carpal tunnel. This data supports the etiology of fibrosis and thickening of the subsynovial connective tissue, thereby causing pressure-induced pseudoneuroma.

Acknowledgments

Natural Science and Engineering Research Council of Canada Discovery Grant # 2017-0409.

References

[1] Vignais et al., 2016. *Crit Rev Biomed Eng.* 44(5): 397-410.
[2] Fu et al., 2015. *PLoS One.* 10(1): e0116777.
[3] Turcotte & Kociolek, 2021. *Peer J.* 9: e11038.
[4] Tat et al., 2016. *J Biomech*. 49(15), 3682-3687.

PERCEPTIONS OF AFFORDANCE AND KINEMATICS FOR A LATERAL MANUAL MATERIALS HANDLING TASK ARE MODIFIED BY PHYSICAL LITERACY TRAINING

Jon B. Doan[1*], Kayla D. Walker[1], Conor Tosh[1], Dean Stewart[1], and Claudia Gonzalez[2]
[1]Engineering and Human Performance Lab, University of Lethbridge, Lethbridge AB Canada
[2]Brain in Action Lab, University of Lethbridge, Lethbridge AB Canada

*Email: jon.doan@uleth.ca

Introduction

Employee training as a control method for limiting work-related musculoskeletal diseases and discomforts (WR-MSDs) continues to deliver highly equivocal results [1]. A recent position paper highlights the potential of high physical literacy as an important component of effective, theory-based interventions for WR-MSDs, building on the raised physical and psychological capacities that form of training can generate [2]. The purpose of the current research was to examine how specific training and subsequent high physical literacy influences perceptions and behaviours for safe manual materials handling. We predicted that high physical literacy would lead to perceptions of increased work capacity but more controlled MMH kinematics, in line with limiting the risk of WR-MSDs.

Methods

25 healthy young adults (21.8 +/- 1.3 years, 171.5 +/- 12.8 cm, 16 F) participated in the study. 12 of these participants (8 F) were regular and proficient rock climbers, and this expertise was used as the model of training-developed high physical literacy. All participants were tasked with standing in front of a mock conveyor belt and centred on a fixed MMH load in a rigid container, with the centre of that load raised to 51% of participant height (Figure 1). Participants were asked to determine their maximum affordance [3], that is largest distance they could safely and repeatedly reach up the conveyor (to their right) to grasp and handle a load. Participants then completed a series of trials at this affordant distance (AT), plus at relative distance (RT) of 20% their height and fixed distance (FT) of 20 cm right of their centre line. All MMH trials were captured and processed (Vicon MOTUS) then averaged within subject then within group.

Figure 1. Visualization of MMH experiment. Participant standing in defined experimental workspace and handling load along conveyor. Visual cue wall behind task is stimulus for a different experiment, and presentation of the cue was balanced amongst the climber and non-climber participants.

Results and Discussion

Climbers had larger perceived affordances for handling than non-climbers (Figure 2A) and they had increased self-reported risk behaviour (Figure 2B). Conversely, climbers-highly physically literate used smaller relative axial rotation (X-factor between shoulders and hips) to handle loads at fixed absolute or height-relative distances from the centre line (Figure 3).

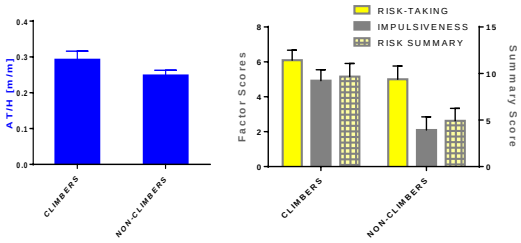

Figure 2A (left) . Perceived safe affordance thresholds for lateral MMH. Perception for safe lateral handling affordance (height-normalised; AT/H) was increased for climbers.

Figure 2B (right) . Risk-taking behaviour amongst MMH participants. Climbers had a higher summary value for self-reported risk taking behaviour, plus higher factor scores for Risk-Taking and Implusiveness [4].

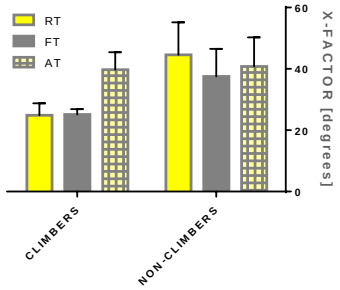

Figure 3. MMH kinematics for industrial targets at 3 distances. Climbers used significantly decreased relative axial rotation of the trunk to MMH targets at set relative (RT) and absolute (FT) lateral distances.

Significance

Non-occupational physical literacy training may transfer to positively modified perceptions of affordance and behavioural kinematics for MMH, particularly when the training activity includes whole body mobility and upper body strength [5]. Psychological gains found during the development of high physical literacy may also transfer to MMH behaviours. In this study, high physical literacy of a specific type was associated with higher risk taking behaviour, but succeeding despite those risks may generate both motivation and confidence [6] plus awareness [7] that could be useful for consistently perceiving and performing safe manual materials handling behaviours at work [2]. More study of high physical literacy training embedded in an MMH training program is warranted.

Acknowledgments

Welcome support from NSERC-DG (JBD), UL-Chinook (DS), and undergrad research assistants Jaclyn Knol and Josh Austin.

References

[1] Denis et al. 2020. *Appl Erg*, *89*;103186
[2] Beach & Dutta, CRE-MSD Position Paper 4204-2
[3] Gibson. 1977. *Perc, Acting, Knowing.*
[4] Eysenck & Eysenck. 1978. *Psych Reports, 43*: 1247-1255.
[5] Giles et al. 2021. *J Sports Sci, 39(1)*; 48-56.
[6] Langseth & Salvesen. 2018. *Front in Psych, 9*:001793.
[7] Coelho et al. 2019. *EBR, 237*: 137-146.

Brain Connectivity Patterns Associated with Different Aspects of Motor Performance

Adam Baker[1*], Christian Schranz, PhD[1], and Na Jin Seo, PhD[1,2]
[1]Department of Rehabilitation Sciences, College of Health Professions, Medical University of South Carolina, Charleston, SC
[2]Ralph H. Johnson VA Medical Center, Charleston, SC
email: *bakerdon@musc.edu

Introduction

In the United States, over 800,000 people suffer from a stroke annually.[1] Stroke often impairs motor function, specifically in the upper extremities. Because the ability to use the arms and hands is critical for performing activities of daily living, these impairments greatly reduce quality of life. It has previously been established that functional brain networks are altered after stroke, and that these changes may be associated with post-stroke motor impairments.[2] However, post-stroke functional neural networks have mostly been studied in relation to clinical motor function assessments. These clinical assessments only indicate gross motor function and do not quantify specific motor control processes. Elucidating the relationship between specific motor control processes and functional brain networks could inform the design of personalized rehabilitation treatments that target the brain networks responsible for the specific motor control impairment for individual patients. To elucidate this knowledge gap, we hypothesized different aspects of motor control will be associated with different patterns of brain network connectivity.

Methods

This is a retrospective analysis of baseline data from a triple-blind randomized controlled trial with 12 chronic stroke survivors (>6 months post stroke). Participants performed a hand grip-and-relax task using the thumb and index finger of the affected hand against 6-axis load cells (Mini40, ATI, Apex, NC) with 100 repetitions while electroencephalography (EEG) was recorded using 96 channel actiCAP and BrainAmp MR plus (BrainVision, Morrisville, NC). From the hand grip task, the following motor control measures were obtained: reaction time, relaxation time, force magnitude control (i.e., difference from instructed force magnitude), and force direction control (i.e., angular deviation of digit force from the normal direction).[3]

For brain network connectivity, EEG data was pre-processed.[4] A structural T1 weighted brain MRI was used for lesion-specific source modelling. Cortical surface was reconstructed/segmented in FreeSurfer. A boundary element head model was created and EEG sources were computed using the minimum norm estimate.[5] Functional connectivity within the bilateral sensorimotor cortices (primary motor, primary sensory, premotor cortices) was computed as coherence between EEG signals in the brain regions.[6] Connectivity was computed separately in the α (8-12 Hz) and β (13-30 Hz) frequency bands during the grip preparation and execution phases. Correlations were drawn between the connectivity and motor control measures.

Results and Discussion

Reaction time correlated best with α connectivity in the non-lesioned hemisphere during grip preparation (r = -0.61; **Figure 1**), which may represent attention/readiness.[7] Relaxation time correlated best with β connectivity in the lesioned hemisphere during grip execution (r = 0.75), which may represent motor control based on sensory feedback.[8] Force magnitude control was found to best correlate with α connectivity in the lesioned hemisphere during grip preparation (r = 0.66) and with inter-hemispheric connectivity during grip execution (r = 0.56), which may represent motor control based on short-term memory.[9] Force direction control best correlated with α connectivity between the non-lesioned premotor and sensory cortices during grip execution (r = -0.57). The non-lesioned hemisphere may be involved in either compensating for or disinhibiting the lesioned hemisphere for the paretic hand grip.[10]

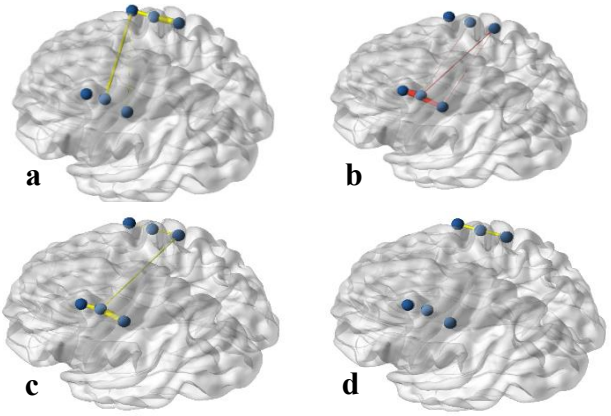

Figure 1: Brain networks correlating best with each motor control measure. Thicker lines indicate stronger correlation magnitude. Yellow indicates α band. Red indicates β band. Lesioned hemisphere pictured at bottom left. **a)** Reaction time best correlated with α connectivity in the non-lesioned hemisphere during grip preparation. **b)** Relaxation time best correlated with β connectivity in the lesioned hemisphere during grip execution. **c)** Force magnitude control best correlated with α connectivity in the lesioned hemisphere during grip preparation. **d)** Force direction control best correlated with α connectivity between the non-lesioned premotor and sensory cortices during grip execution.

Significance

This research paves the way to elucidate how functional brain network connectivity patterns associate with different aspects of motor control. This work encourages development of a personalized rehabilitation paradigm in which individual motor control aspects are assessed to determine and treat the functional brain network responsible for clinical motor impairment to improve recovery outcomes of individual patients.

Acknowledgments

NIH/NIGMS P20GM109040, NIH/NICHD R01HD094731-01A1, and VA RR&D I01 RX003066.

References

1. Virani SS, et al., *Circulation*. 2020;141:e139-e596
2. Carrera E, et al., *Brain*. 2014;137:2408-2422
3. Seo NJ., et al., *J Biomech*. 2015;48:383-387
4. Seo NJ., et al., *Physiol Rep*. 2015;3
5. Gramfort A., et al., *Biomed Eng Online*. 2010;9:45
6. Nolte G., et al., *Clin Neurophysiol*. 2004;115
7. Cooper N., et al., *Int J Psychophysiol*. 2003;47:65-74
8. Struber L., *Neuroimage*. 2021;245:118645
9. Jensen O., et al., *Cereb Cortex*. 2002;12:877-882
10. Kobayashi M., et al., *NeuroImage*. 2003;20:2259-2270

MARKERLESS MOTION CAPTURE OF THE HAND AND FINGERS

Nigel Majoni, Daanish M. Mulla, & Peter J. Keir*
Department of Kinesiology, McMaster University, Hamilton, ON, Canada, L8S 4K1
email: pjkeir@mcmaster.ca

Introduction

Hand and finger movements are poorly captured in most workplace assessments but play important roles in the development of hand-related musculoskeletal disorders [1]. All manual tasks require the use of the hands and loading of the upper extremity typically occurs through the hands. However, the hands are often poorly represented in most biomechanical and ergonomic research studies. Marker-based systems have been used to evaluate the kinematics of the hand but are typically limited to laboratory settings [2]. Marker-based motion capture systems may provide the desired accuracy but are not practical or feasible in the workplace. Computer vision is a field of artificial intelligence that allows computers to extract information from images and videos. Recent developments in computer vision have influenced the production of programs with the ability to track motion by recording a simple video of the desired motion, without the use of markers. This work aims to use an open source markerless motion capture program and train a network to evaluate and track hand and finger movements and postures, allowing easier collection in the workplace.

Methods

DeepLabCut is an open-source Python package used for 2D and 3D markerless animal pose estimation [3, 4]. Currently, a 2D model was developed to track hand motion using DeepLabCut. Preparing to train the network began with collecting a sample video at 60 Hz and 1080p. The video contained 420 frames that were manually digitized to allow the program to identify joint locations. Twenty-one anatomical landmarks were identified and tracked throughout the two trials of forearm supination and pronation. Specifically, this markerless motion capture program identified the wrist, the carpometacarpal joint of the thumb, the metacarpal joints of digits 1-5, the proximal interphalangeal joints of digits 2-5, the distal interphalangeal joints of digits 1-5, and the endpoints of digits 1-5 The network was trained with 1,000,000 iterations using a training dataset to enable 2D motion capture. Evaluation of the trained network determined the performance of the trained neural network. Figure 1 shows the results of the trained network in identifying joint locations of the hand.

Results and Discussion

The current model is limited to analyzing movements in two dimensions using a single camera. Following successful model development in 2D, a second camera will be included to move to three-dimensional tracking of hand motion. The multicamera system will be developed with mobility in mind such that non-laboratory settings may be used for video capture. Training will also include the industrial use of gloves and tools to ensure capability. This will allow us to develop a model that is capable of markerless capture of hand and finger movements in the workplace that has the capability of being integrated with other force-sensing equipment. These kinematic and external force data may then be used as input to our hand simulations in OpenSim. Ultimately, this data will be used to improve the representation of the hand in biomechanical and ergonomics assessments to improve our assessment of the risk of developing musculoskeletal disorders in the workplace

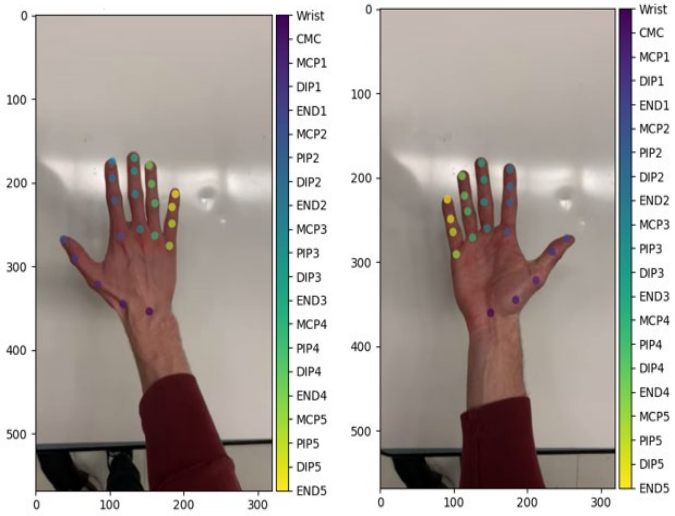

Figure 1: (a) Joint locations of the hand modelled in pronation within DeepLabCut. (b) Joint locations of the hand modelled in supination within DeepLabCut. Marker colours represent each joint or anatomical location based on the scale at the right of each image.

Significance

The hand and fingers are currently poorly represented, or even neglected, in most evaluations of external loads acting on the body. An accurate markerless system to capture the kinematics of the hand and fingers in the workplace would immensely improve our ability to assess the injury risk in the upper extremity. Concurrent to the 2D model, we are also working on using multiple cameras to track 3D bilateral hand movements with the open-source Python toolkit Anipose [5]. Ultimately, this will be incorporated with real-time force inputs for the rapid output of assessments.

Acknowledgments

Funding was provided by NSERC (RGPIN-2016-06460).

References

[1] Amell et al., 2001. *J Occupational rehabilitation.* 11:255-265
[2] Cocchiarella et al., 2016. *Comput Method Biomech Biomed Engin*. 19:639-647
[3] Mathis et al., 2018. *Nat Neurosci.* 21:1281-1289.
[4] Nath et al., 2019. *Nat Protoc.* 14:2152-2176.
[5] Karashcuk et al. 2021. *Cell Rep*. 36:109730.

The effect of rotator cuff tear severity and external load on aspects of muscle force compensation: A modeling study

Zoe M. Moore[1], Joshua Pataky[1], Sujata Khandare[1], Meghan E. Vidt[1,2]
[1]Biomedical Engineering, Pennsylvania State University, University Park, PA, USA
[2]Physcial Medicine and Rehabilitation, Penn State College of Medicine, Hershey, PA, USA
email: zmm5238@psu.edu

Introduction

Rotator cuff tears (RCT) negatively impact shoulder function and are common in adults[1]. RCT are characterized by partial or full thickness tearing of the supraspinatus tendon, which is often accompanied by tearing of the infraspinatus and subscapularis tendons. RCT can diminish an individual's ability to complete everyday tasks, such as reaching or lifting an object. However, it is currently unknown how RCT severity influences one's ability to perform daily tasks with varying loads. Specifically, it is unclear how unaffected muscles compensate to enable loaded movement. Therefore, the objective of this study is to examine the impact of RCT severity on performance of a loaded forward reach task using a computational modeling approach.

Methods

A unilateral upper extremity musculoskeletal model[2] was developed in OpenSim software (v.3.3)[3]. The nominal model representing the muscle force-generating properties of young adult males was used, then modified using our prior methods of reducing peak isometric muscle force of muscle actuators in the model[4,5] to represent 3 RCT severities: a partial-thickness supraspinatus tear, a full thickness supraspinatus tear with infraspinatus involvement, and a massive, 3-tendon tear involving supraspinatus, infraspinatus, and subscapularis. Representative forward reach kinematics from a prior study[6] were used to perform a computed muscle control[7] simulation followed by joint force and point kinematics analyses. For all simulations, external loads representing 0N, 4.5N (1lb), 13.3N (3lb), 22.2N (5lb), 44.5N (10lb) were applied to the hand in the model in the negative vertical direction (Fig. 1). All permutations of tear severity and external load were performed for a total of 20 simulations. Outcomes included: average percent muscle activation, peak resultant joint contact force, and root mean squared error for hand kinematic deviation. Predicted outcomes were compared across rotator cuff tear severity and increasing external load.

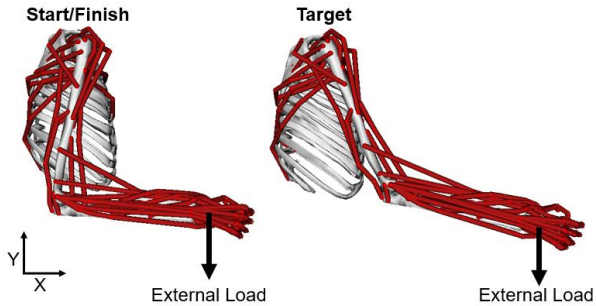

Figure 1: Simulations of a forward reach task were performed with an upper extremity model. The task start/finish was with the arm at the side and the target location was a distance 80% of forearm length. External loads (0N, 4.5N, 13.3N, 22.2N, 44.5N) in the global negative vertical direction were applied to the origin of the hand.

Results and Discussion

Results revealed that the magnitude of peak joint contact force decreases with increased tear severity, which is consistent with our prior work[5], but here we observed small (6.4 ± 3.2%) decreases in joint contact forces with increasing external load. Average root mean square error of hand kinematic deviation was 37.3 ± 13.5mm in the global x-direction, 42.2 ± 21.8mm in the global y-direction, 14.3 ± 21.8mm in the global z-direction, and 13.9 ± 1.9 mm for the magnitude of the resultant vector across all models and loads, suggesting that movement kinematics are preserved with increased injury and increased load. Results of muscle force contributions were different across models and loads, indicating that muscles are compensating to enable successful task performance. We observed a force increase in the middle deltoid (41.7 ± 5.5%), anterior deltoid (21.9 ± 5.1%), infraspinatus (13.1 ± 5.7%), teres minor (0.68 ± 15.2%), and clavicular compartment of pectoralis major (12.5 ± 14.9%) muscles with increased tear severity and increased load (Fig. 2).

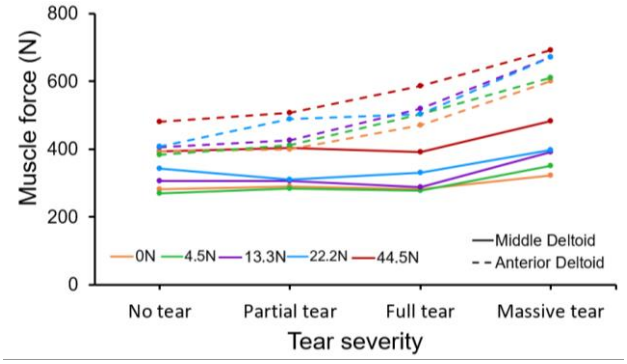

Figure 2: Muscle force contributions for the middle deltoid and anterior deltoid muscles for all tear severity models and external loads.

Significance

This model-based study revealed that movement kinematics during a loaded forward reaching task were not altered by load or rotator cuff tear severity. Remaining intact muscles, particularly the deltoid and teres minor, help compensate for the reduced force-generating capacity of muscles affected by the RCT. Deltoid is a large compensating muscle that has reserve activation capacity, rendering it a target for development of rehabilitation interventions to increase arm function in individuals with RCT. Ongoing work continues to examine the influence of external load in other functional tasks and also in the context of aging.

Acknowledgments

Penn State start-up funds (Vidt).

References

1. Oh JH. et al. Clin Orthop Surg. 2018;10:119-134
2. Holzbaur KR. et al. Ann Biomed Engr. 2005;33(6):829-840
3. Delp SL. et al. IEEE Trans Biomed. Eng. 2007;54(11):1940-50.
4. Khandare S. et al. J Electromyogr Kinesiol. 2022;62:102335.
5. Pataky J. et al. Clin Biomech. 2021;90:105494.
6. Vidt ME. et al. J Biomech. 2016;49(4):611-617.
7. Thelen DG. et al. J Biomech. 2003;36(3):321-328.

Impact of post-mastectomy breast reconstruction on pectoralis major stiffness, shoulder strength and self-report function

Mary Jane Bouman[1], Adeyiza O. Momoh[2], and David B. Lipps[1]
[1]School of Kinesiology, Department of Surgery[2], University of Michigan, Ann Arbor, MI USA
email: mjbouman@umich.edu

Introduction

Post-mastectomy breast reconstruction patients commonly report shoulder pain and restricted mobility post-operatively [1]. Post-operative stiffening of the pectoralis major, resulting from the dissection or full disinsertion of the muscle during breast reconstructive surgery, may contribute to post-operative pain and restricted mobility. Pectoralis major passive stiffness was found to increase up to two years post-reconstruction [2]. This increased stiffness was associated with increased patient-reported Shoulder Pain and Disability Index (SPADI) scores [2]. However, prospective assessments of pectoralis major stiffness in women undergoing mastectomy and breast reconstruction have yet to be performed. We performed the first longitudinal study of peri-operative changes in pectoralis major stiffness and their association with self-reported functional deficits. We hypothesized post-mastectomy breast reconstruction would increase pectoralis major passive stiffness over the first 12 months post-surgery and these changes would be associated with decreased shoulder strength and function.

Methods

Seven women that underwent a mastectomy to treat or prevent breast cancer, followed by breast reconstruction, participated in the study. Patients underwent one of three types of breast reconstruction surgery: two deep inferior epigastric perforator flaps, three sub-pectoral implants, and two latissimus dorsi flaps. Patients were evaluated before surgery and an average of 13 months after surgery.

The affected arm of patients was evaluated at both time points with the same procedures. Ultrasound shear wave elastography images were collected from the clavicular and sternocostal regions of the pectoralis major muscle while the participant was relaxed (Supersonic Imagine Aixplorer). The mean shear wave velocity (SWV) of the elastography map was measured, which is indicative of muscle stiffness [3]. Patients completed the Shoulder Pain and Disability Index (SPADI) surveys and had their maximum shoulder strength measured in 3-degrees of freedom. Strength and SWV were collected while the participant's arm was in a plastic cast positioned at 90° of elbow flexion and 90° of shoulder abduction.

Wilcoxon signed-rank test compared pre-to-post surgery changes in SPADI scores, strength, and SWVs. Spearman's correlations were performed to identify post-surgery associations between these outcome measures. Significance was set at $p<0.05$.

Results and Discussion

Post-mastectomy breast reconstruction patients had a significant pre-to-post surgery increase in SPADI scores ($p = 0.027$), indicative of greater shoulder morbidity. They also exhibited a significant decrease in vertical adduction strength ($p = 0.018$). The pectoralis major is disinserted to varying degrees during the three breast reconstruction surgeries evaluated, which likely contributes to this adduction weakness. There was also a trend towards decreasing vertical abduction strength ($p = 0.063$). However, there were no pre-to-post surgery differences in SWV for the clavicular ($p = 0.128$) or sternocostal ($p = 0.866$) regions of the pectoralis major.

Increasing post-surgery SPADI scores were significantly associated with increasing post-surgery SWV of the clavicular ($\rho = 0.812$, $p = 0.05$) or sternocostal ($\rho = 0.841$, $p = 0.036$) regions of the pectoralis major, and reduced post-surgery adduction strength ($\rho = -0.812$, $p = 0.05$). These results confirm SWV of the pectoralis major is associated with greater shoulder morbidity in breast reconstruction patients at 12 months post-surgery, supporting prior results reported at 24 months post-surgery [2].

Increasing post-surgery SWV of the sternocostal fiber region was further associated with reductions in shoulder strength, including abduction ($\rho = -0.821$, $p = 0.023$), extension ($\rho = -0.821$, $p = 0.023$) and flexion ($\rho = -0.786$, $p = 0.036$). Increasing clavicular SWV was also associated with reductions in extension strength ($\rho = -0.786$, $p = 0.036$). Together these findings indicate that increasing post-surgery stiffness of the pectoralis major is related to shoulder strength and function. Future work will expand the sample size to control for surgical variations and evaluate associations between the pre-to-post surgery changes in self-reported function and biomechanical measures.

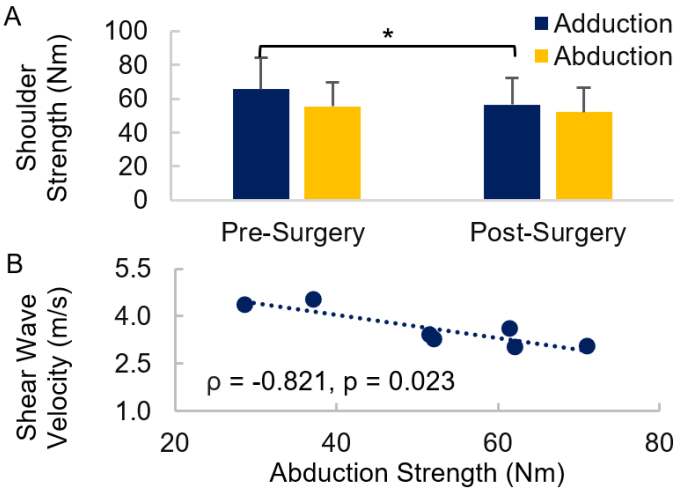

Significance

Women who undergo post-mastectomy breast reconstruction have decreased shoulder strength and function an average of 13-months post-surgery that are associated with pectoralis major stiffness. These are the first reported insights into the peri-operative progression of pectoralis major stiffness and its association with patient strength and function.

Acknowledgments

This project was funded by NIH/NICHD R03HD097704.

References

[1] Tarantino et al. 2006. Plast Reconstr Surg. 117:5, 1387-94.
[2] Leonardis et al. 2019. J Orthop Res. 37(7): 1610-1619.
[3] Bernabei et al. 2020. J Appl Physiol. 128: 8-16

EFFICACY OF IN-SOLE SENSORS TO DETECT LIMB LOADING CHANGES USING BIOFEEDBACK

Ricky Pimentel[1], Cortney Armitano-Lago[2], Brian G. Pietrosimone[2], Jason R. Franz[1]
[1]Joint Dept. of BME, UNC Chapel Hill and NC State University, USA [2]Exercise and Sports Science, UNC Chapel Hill, USA
email: rickypim@live.unc.edu

Introduction

Clinicians lack precise, accessible, and evidence-based technology to detect and treat subtle, yet potentially harmful changes in walking biomechanics. For example, accurate, user-friendly, and reliable devices capable of measuring the most relevant outcomes of knee joint loading during walking could improve clinical outcomes by detecting aberrant biomechanics and integrating with biofeedback to optimize loading. Altered peak vertical ground reaction force (vGRF) during the impact phase of gait associates with biochemical markers indicative of joint tissue breakdown.[1,2] Furthermore, modifying peak vGRF via biofeedback elicits favorable changes in knee joint biomechanics, showing practicality for gait retraining in populations at risk for chronic knee dysfunction.[3,4] However, detecting vGRF changes during walking and implementing biofeedback typically requires using laboratory-grade force-sensing treadmills. Commercially-available devices do not yet exist to provide these services to clinicians and patients seeking to mitigate risk of chronic pain and dysfunction. In-sole wearable sensors may provide an accessible option for: (*i*) estimating vGRF profiles during walking and (*ii*) driving real-time biofeedback to modify gait biomechanics and tissue biology.

Our purpose was to determine if in-sole sensors (SS) can serve as a sufficient alternative to force-sensing treadmills (FT) to estimate changes in vGRF signals prescribed using real-time biofeedback. We hypothesized that SS would provide a comparable vGRF estimate to that derived via FT, and that SS would be as sensitive as FT to biofeedback-induced changes.

Methods

We recruited a convenience sample of 17 participants (10 female, age: 26.0±3.6 years, height: 1.74±0.08 m, mass: 69.1±8.5 kg, preferred walking speed 1.35±0.14 m/s [*mean ± standard deviation*]) to walk at their preferred speed for 5 minutes (*Control*) on a FT. We recorded their typical loading peak vertical ground reaction force from the FT for each leg during the last minute of the control trial. The participants then performed two 5-minute targeted biofeedback trials at +/- 5% (*Over/Under*) of their typical loading peak vGRF measured from the FT (Fig. 1A). During biofeedback trials, participants saw their average loading peak vGRF for each side (left & right) from their previous 2 steps.

During each trial, we recorded force platform kinetics (Qualisys Track Manager, Qualisys AB, Göteborg, Sweden) and bilateral in-shoe sole forces (LoadSol, Novel, Saint Paul, Minnesota, USA). After resampling the signals to a common 100 Hz, we synchronized the FT and SS signals using a cross-correlation function and extracted the peak loading force across both systems using a peak finding algorithm. We used a repeated measures ANOVA (with Tukey post-hoc) to test for differences between FT and SS and across biofeedback conditions ($\alpha = 0.05$). We also present (partial) eta square ($\eta_{(p)}^2$) effect sizes.

Results and Discussion

We found a significant main effect for biofeedback condition ($p<0.001$, $\eta_p^2=0.713$, Fig. 1B). However, we found no main effect of measurement modality (FT vs. SS) nor an interaction between measurement modality and biofeedback condition ($p\geq0.312$, $\eta_p^2\leq0.057$). Loading peak vGRFs estimated via SS were similar to those from FT ($p\geq0.516$, $\eta^2\leq0.013$, Fig. 1B-C). However, only FT could distinguish between loading biofeedback conditions (SS under & over vs. control: $p\geq0.076$, $\eta^2\leq0.128$; FT under & over vs. control: $p\leq0.017$, $\eta^2\geq0.193$, Fig. 1B). On average, compared to FT, SS estimated loading peaks within ~5% (Fig. 1C) and displayed 7% RMS error overall (Fig. 1D).

Significance

In-shoe wearable sensor systems show promise to estimate limb loading profiles during walking. However, their precision must be improved to better detect altered vGRF magnitudes for use in biofeedback paradigms. Future investigations could seek to incorporate other measurement capabilities, such as IMUs, to refine accuracy for portable vGRF biofeedback systems.

Acknowledgements

The Eshelman Institute for Innovation funded this study.

References

1. Pietrosimone, B. *et al. Am. J. Sports Med.* 44, 425–432 (2016).
2. Pietrosimone, B. *et al. J. Orthop. Res.* 35, 2288–2297 (2017).
3. Evans-Pickett, A. *et al. Clin. Biomech.* 76, 105014 (2020).
4. Luc-Harkey, B. A. *et al. J. Biomech.* 76, 94–102 (2018).

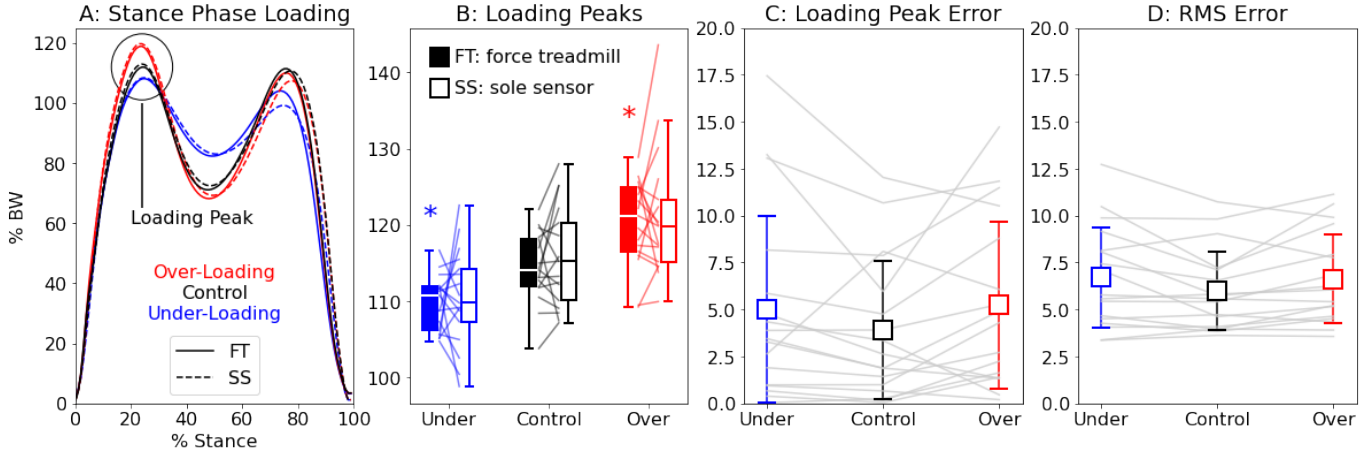

Figure 1: Compared to FT, SS displayed 7% RMS error and estimated loading peaks within ~5% on average. SS similarly matched FT loading peaks, however SS did not significantly distinguish between biofeedback conditions. Asterisks (*) indicate significant Tukey's post-hoc difference vs. control.

COMPARISON OF 3-D TORSO ANGLES USING LOW-COST VS. HIGH-COST IMU

Seung Yun (Leo) Song*, Yinan Pei, Elizabeth T. Hsiao-Wecksler
Department of Mechanical Science and Engineering, University of Illinois at Urbana-Champaign, Urbana, IL USA
*email: ssong47@illinois.edu

Introduction

Inertial measurement units (IMUs) have become a common tool in biomechanics. Many studies have used expensive 9-axis IMUs with well-developed software packages. 6-axis IMUs, which do not include magnetometers, may be preferable in indoor/lab environments since magnetometers are susceptible to electro-magnetic noises. Various computational methods have been proposed for computing absolute and relative angles within and between IMUs. In our previous work, we used a custom test apparatus to collect data from two low-cost 6-axis IMUs across multiple rotation axes, movement speeds, and extended collection times. IMU data were used to compare up to 7 common computational methods to calculate relative joint angle between IMUs (e.g., [1]). Open-source code and documentation were developed to help biomechanics researchers develop similar low-cost IMU systems for their applications [2].

In this study, we compare the accuracy of relatively simple computation methods using a 6-axis IMU to an expensive research grade IMU (with magnetometer), as well as a gold standard motion capture system. The data were collected on a human subject to calculate the absolute angle of the torso.

Methods

The test setup consisted of a low-cost 6-axis IMU without magnetometer (US$2-$5, MPU-6050; TDK-InvenSense, San Jose, CA), a high-cost research grade 9-axis IMU with magnetometer (US$800-$1,000, VN-100; VectorNav, Dallas, TX), and a 6-camera research-grade motion capture (MoCap) system (Oqus; Qualisys, Sweden) (Fig. 1). Three motion markers were placed on the subject's manubrium to measure 3-D torso angles, which served as the ground truth. The two IMUs were also placed on the manubrium to estimate the same 3-D torso angles as the MoCap. The two IMUs and the motion markers were placed on a single rigid 3-D printed module to ensure that the IMUs and MoCap measure the kinematics of the same moving body (Fig. 1). MoCap and IMU data were collected at 100 Hz.

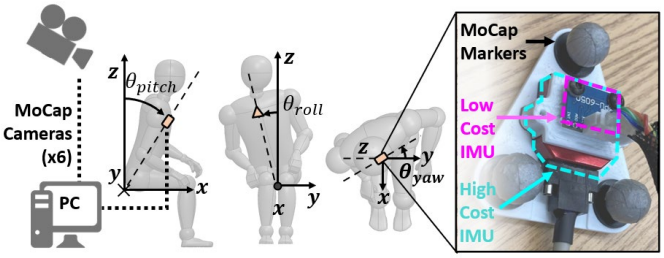

Figure 1: Test setup definition of 3-D torso angles (yaw, pitch, roll). A module containing the low-cost IMU, high-cost IMU, and markers was placed on the subject's manubrium.

For the low-cost IMU, the roll and pitch angles were estimated using projections of gravity on low-pass filtered accelerometer readings, and the yaw angle was estimated using and a sensor fusion method (i.e., Complementary Filter) [2]. For the research grade IMU, the 3-D angles were estimated using the proprietary algorithm provided by VectorNav.

The subject, wearing the IMUs and three markers, sat on a stable platform and performed a series of torso movements involving leaning in the sagittal and frontal planes, and twisting in the transverse plane.

Results and Discussion

Compared to the gold-standard MoCap values, the low-cost IMU demonstrated high accuracy for estimating pitch and roll torso angles ($RMSE_{pitch,roll} < 5°$), which were similar to the high-cost IMU (Fig. 2). Even at sudden directional changes where high acceleration and decelerations were involved, the accuracy of the low-cost IMU still remained high.

For yaw angle, larger error ($RMSE_{yaw} \cong 12°$) was observed due to an initial offset difference between the low-cost IMU and MoCap. As expected, the high-cost IMU was able to estimate yaw angle accurately. This offset may be caused by the inability of finding the reference axis for the yaw angle due to the lack of magnetometers. Thus, the IMU's yaw angle always started from zero position; the IMU estimated the changes in yaw angle and not the absolute yaw angle. Overtime, however, the low-cost IMU was able to track yaw with similar accuracy.

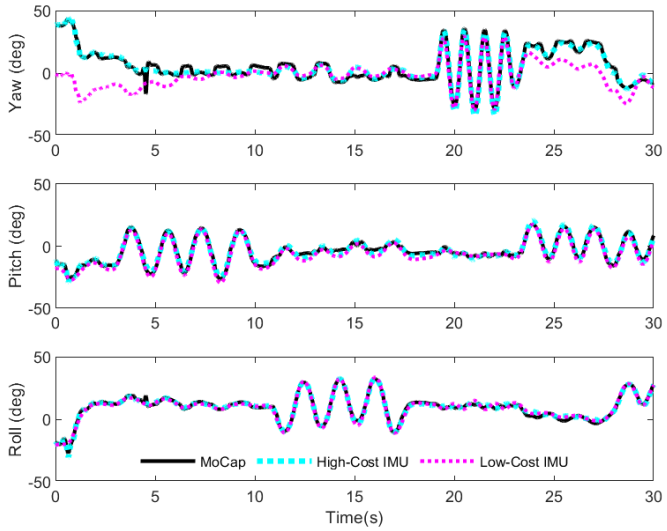

Figure 2: Preliminary results comparing the 3-D torso angle readings from low-cost IMU, high-cost IMU, and MoCap system.

Significance

These preliminary results suggest that low-cost IMUs without magnetometers can produce absolute body segment angles comparable to more expensive IMU systems or motion capture systems. This information can be helpful to researchers who wish to develop their own low-cost IMU systems.

Acknowledgments

Funded provided by the Jump ARCHES partnership between OSF HealthCare and the University of Illinois, and NSF NRI 2024905.

References

[1] Song, S.Y., Pei, Y., Hsiao-Wecksler, E.T., ASB. 2020
[2] https://github.com/ssong47/compute_relative_angle_between_two_IMU

ARE 4D MOTION SENSORS VALID AND RELIABLE FOR STUDYING BASEBALL PITCHING?

Stacy R. Loushin, Christopher L. Camp, Kenton R. Kaufman
Department of Orthopedic Surgery, Mayo Clinic, Rochester, MN, USA
email: kaufman.kenton@mayo.edu

Introduction

Inertial measurement units (IMUs) are emerging as an attractive alternative for motion capture in the sports world, allowing for the evaluation of kinematics and kinetics outside of the traditional lab setting. Recently, IMU technology has been used for the evaluation of baseball throwing [1]. While this technology is cost effective and easy to use, investigations into the reliability, consistency, and validity of each IMU system need to be conducted. The motusBASEBALL sensor was found to be inaccurate compared to motion capture for 3 out of 4 commonly used metrics [2].

A six sensor IMU system from 4D Motion has recently become commercially available and provides the user with kinematic analyses of multiple segments. A systematic analysis of this system has not been completed. Therefore, the goals of this study were to evaluate the validity of the 4D Motion IMU system compared to motion capture and evaluate the internal reliability and consistency of the device.

Methods

Ten high school pitchers participated in this study (10/10 Male, Age = 16.6±1.3 years, BMI = 24.1±3.9 kg/m^2). Subjects wore IMU sensors (Gen3, 4D Motion, Allendale, NJ) on the throwing upper arm and forearm, trunk, pelvis, and bilateral thighs. Each IMU was placed and calibrated according to the company's instructions. Thirty-seven retroreflective markers were simultaneously placed on anatomic landmarks of the throwing arm, trunk, pelvis, and thighs to create corresponding segments.

Subjects threw fastballs off a mound at maximum effort until 5 strikes were recorded. IMU data was captured at 100 Hz. 3D trajectories of the reflective markers were collected at 500 Hz with a 14-camera motion capture system (Raptor 12HS, Motion Analysis, Rohnert Park, CA).

A comparison was made between the IMUs and corresponding motion capture values for shoulder rotation, elbow flexion, chest extension, pelvis and chest rotation velocity and rotation acceleration. Due to the differing data collection rates, the max value for each metric were used. The Wilcoxon signed-rank test was used to compare the motion capture and IMU data. Percent error was calculated, using the motion capture value as the expected value, preserving the sign convention. To assess the IMU reliability, the root mean square error (RMSE) and percent difference were calculated for each metric. The range, median (med) and interquartile range (IQR) were reported. Based on previous studies, acceptable limits for RMSE were <5° for all angles and <240°/s for chest rotation velocity and 100°/s for pelvis rotation velocity [3]. For all other metrics, a percentage difference of <5% was considered acceptable.

Results and Discussion

Significant differences were found for 5 of 7 metrics analyzed. The IMU over reported most metrics, except for elbow flexion and pelvis rotation acceleration, where both positive and negative error was observed (Figure 1). The RMSE and percent errors indicate smaller discrepancies for chest extension, and pelvis and chest rotation velocity, with elbow flexion having the largest variance (Table 1). While shoulder rotation displayed a median RMSE value within acceptable limits (<5°), the wide RMSE range (1°-44°) could lead to misleading interpretation.

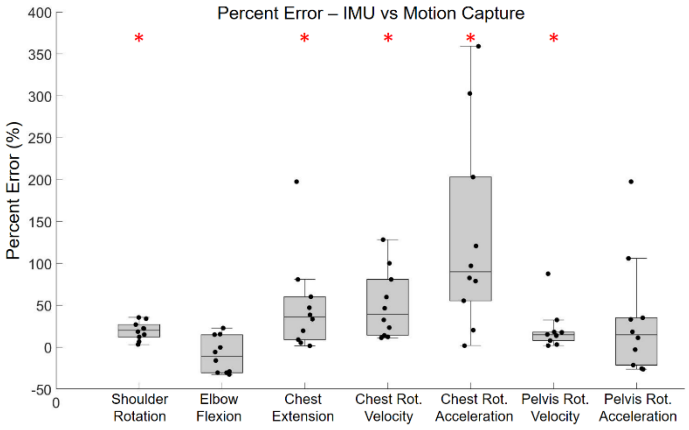

Figure 1: Percentage error of the IMU data compared to motion capture. A negative value indicates underreporting, while a positive value indicates overreporting. * Indicates significant difference from motion capture, with $p<0.05$.

Table 1: Reliability and consistency of the 4D Motion system metrics

Metric	RMSE		Percent Difference	
	Range	Med±IQR	Range	Med±IQR
Shoulder Rotation (°)	1-44	4±12	1-28	2±5
Elbow Flexion (°)	7-37	37±9	7-22	18±7
Chest Extension (°)	1-11	5±4	1-14	5±4
Chest Rot. Velocity (°/s)	38-166	96±38	2-10	5±3
Chest Rot. Acceleration (°/s^2)	1618-8715	4161±5027	6-17	11±5
Pelvis Rot. Velocity (°/s)	10-61	38±14	1-7	4±3
Pelvis Rot. Acceleration (°/s^2)	529-4094	1599±1327	5-20	11±9

The 4D Motion IMU system did not demonstrate acceptable validity for 5 of 7 metrics tested. It also lacked internal consistency and reliability, with angular velocities being the most consistent. Caution should be used when using the metrics provided by an IMU based system for individualized monitoring.

Significance

If found valid and reliable, IMUs could be used for longitudinal workload monitoring, individualized throwing and rehabilitation programs, and ultimately injury prevention. The study demonstrates the data obtained from a 4D Motion system using Gen 3 sensors are not equivalent to the data obtained from a marker-based motion capture system.

References

[1] Fleisig, GS. 2018. *Arthroscopy*. 34:823-824.
[2] Camp et al., 2021. *Am J Sports Med.* 49:3094-3101.
[3] Kageyama et al., 2014. *J Sports Sci Med.* 13:742-750.

SMARTWATCH-BASED ESTIMATION OF STRIDE-TO-STRIDE GAIT VARIABILITY AND STABILITY

Christopher A. Bailey[1*], Alexandre Mir-Orefice[1], Thomas K. Uchida[2], Julie Nantel[1] and Ryan B. Graham[1]
[1] School of Human Kinetics, University of Ottawa, Canada
[2] Department of Mechanical Engineering, University of Ottawa, Canada
email: * cbailey2@uottawa.ca

Introduction

Compromised dynamic control of gait, including adjustments in the variability of stride timing and the stability of the trunk and centre of mass, is well-linked to fall risk [1,2]. Monitoring these features of gait during daily living is therefore of interest to researchers and clinicians. However, current methods of quantifying these features typically require optoelectronic technologies with restrictive fields of view or trunk-worn inertial measurement units (IMUs) that are not widely available.

A potential alternative sensor solution is to leverage the availability of smartwatches and the link between arm swing and gait stability. For example, accentuation of arm swing (i.e. increased arm swing amplitude) increases trunk local dynamic stability (i.e. decreases local divergence exponent, λ_{max}) [3] but decreases centre-of-mass smoothness (i.e. decreases harmonic ratio, HR) in young adults [4]. In the same arm swing condition, adults simultaneously increased the magnitude of variability and decreased the local dynamic stability of lower-limb kinematics [5], suggesting that stride-to-stride motor variability of limb movement is directly related to gait stability. Currently, these arm swing patterns remain unexplored. We investigated whether stride-to-stride gait variability and stability could be estimated by arm swing motor variability, measured with a smartwatch-based IMU. We hypothesized that higher variability and lower stability of smartwatch kinematics would be related to higher variability in stride timing and lower trunk stability, respectively.

Methods

Ten young adults (five females) completed seven-minute trials of constant-speed treadmill gait at 100%, 70%, and 130% of preferred speed. Inverse kinematics during 200 consecutive right-leg strides were computed in OpenSim v4.2 [6] using a full-body model [7,8], driven by marker trajectories measured by an 11-camera optoelectronic system (60 Hz; Vantage, Vicon). Arm swing accelerations and angular velocities were measured by a smartwatch-based IMU worn on the left wrist (60 Hz; Apple Watch Series 5, Apple Inc.) using the HemiPhysioData application available for watchOS/iOS. Gait variability was quantified by the stride-to-stride coefficient of variation (CV) of stride time; gait stability was quantified by trunk λ_{max}, calculated from a state space of linear and angular velocities, and HRs of centre-of-mass linear acceleration. Arm swing motor variability was quantified by mean standard deviation (meanSD), λ_{max}, and sample entropy (SaEn) of the Euclidean norm linear acceleration and Euclidean norm angular velocity of the smartwatch. Pearson correlation coefficients were computed to evaluate relationships between stride-to-stride gait and smartwatch parameters.

Results and Discussion

Higher stride time CV was correlated with lower meanSD of smartwatch linear acceleration (Figure 1; r = -0.48, p = 0.008). Higher trunk λ_{max} was not correlated with the selected smartwatch parameters. Lower centre-of-mass HR was not correlated with the selected smartwatch parameters in the anterior–posterior or mediolateral directions, but was correlated with higher λ_{max} of smartwatch linear acceleration in the vertical direction (Figure 1; r = -0.46, p = 0.011).

These results provide the first known evidence for a link between motor variability of gait and that of arm swing. As hypothesized, lower vertical trunk stability was related to lower local stability of smartwatch acceleration. In contrast, higher variability in stride timing was related to lower variability of smartwatch linear acceleration. We suggest that this contrast may be due to a potential motor variability trade-off in gait of young adults, where less-variable stride timing may be achieved by having a more variable arm swing, and vice versa.

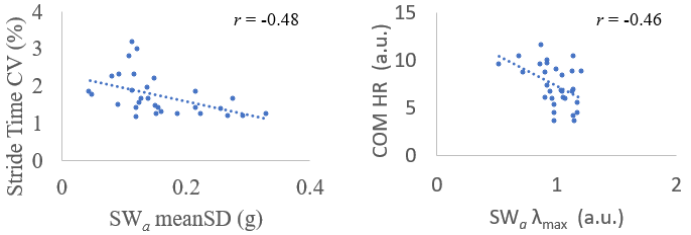

Figure 1. Relationships between smartwatch acceleration (SW_a) mean standard deviation (meanSD) and stride time variability (CV), and between SW_a local divergence exponent (λ_{max}) and centre-of-mass vertical harmonic ratio (COM HR). Pearson coefficients (r) are shown.

Significance

Our findings support the feasibility of monitoring stride-to-stride gait variability and stability using a smartwatch-based inertial measurement unit. Increased sample size from further data acquisition will enable development of a machine learning algorithm and smartwatch application to accurately predict these gait parameters. This work is an important step towards providing a wearable monitoring solution that is (1) available to users and (2) able to estimate gait stability and walking-related fall risk in real time. However, evaluation in older populations and in different overground gait environments is still needed to investigate how these groups and conditions affect relationships between stride-to-stride gait and arm swing parameters.

Acknowledgments

This project is supported by a uOttawa-CHEO Research Fellowship, NSERC, and the Ontario Early Researcher Award Program. Apple Inc. provided Apple Watches through its Investigator Initiated Research program. Supporters have no role in the design, data acquisition, data interpretation, or decision to disseminate findings from this project.

References

[1] Hausdorff, 2005. *J NeuroEng Rehabil*. 2: 19.
[2] Toebes et al., 2012. *Gait Posture*. 36: 527-31.
[3] Hill et al., 2019. *PLOS ONE*. 14: e0218644.
[4] Siragy et al., 2020. *J Biomech.* 99: 109529.
[5] Bailey et al., 2022. *J Biomech*. 130: 110855.
[6] Seth et al., 2018. *PLOS Comput Biol.* 14: e1006223.
[7] Rajagopal et al., 2016. *IEEE Trans Biomed.* 63: 2068-79.
[8] Bailey et al., 2021. *Sensors.* 21: 7690.

THE NUMBER OF STEPS NEEDED TO OBTAIN STABLE VARIABLES FROM REAL-WORLD WALKING

Jesse M. Charlton[1*], Calvin Kuo[2] and Michael A. Hunt[1]
[1]Department of Physical Therapy, University of British Columbia, Canada
[2]School of Biomedical Engineering, University of British
email: jesse.charlton@ubc.ca

Introduction

Inertial sensor systems are becoming an increasingly popular method to record gait mechanics in real-world settings and over extended time periods [1]. Compared to laboratory studies, this allows gait analysis to occur in environments that are representative of daily life. Moreover, we can collect many thousands of steps over days or weeks, incorporating more variability, environmental factors, and changes over time.

To maximize efficiency when conducting real-world gait analysis with inertial sensors, we must identify when enough data is collected. One strategy is to establish when a walking pattern has stabilized, indicating the dataset is representative of the natural walking pattern and environmental factors typical for that person. In the context of healthy runners [2], 4-5 running sessions (15-20 mins in length) were needed to observe a stabilization of variables derived from healthy runners using a waist-mounted sensor. A similar analysis for walking data does not yet exist.

Sensor-driven gait analysis in both healthy [1] and clinical populations, like knee osteoarthritis [3], are becoming more prevalent; so too is the transition of gait analysis into real-world contexts. Establishing a guideline for observing stable walking data is needed to inform time and resource allocation. The goal of this study was to identify when real-world walking foot biomechanics stabilize in a healthy and clinical population.

Methods

This study involved seven days of unsupervised community walking and included two groups: 15 healthy adults (HA) and 15 adults with mild-severe, symptomatic medial compartment knee osteoarthritis (KOA). The participants wore a shoe-embedded 3-D magneto-inertial sensor [4] on their dominant (HA) or most severe limb (KOA) to record at least 20 mins/day of walking in their usual environments (sidewalks, trails etc.). From each recorded step, we extracted the peak magnitudes from the accelerometer (AC) and gyroscope (G) Euclidean norms at heel strike (HS) and toe off (TO), gait cycle time (GC), foot strike angle (FSA), and foot progression angle (FPA).

We performed a stability analysis adapted from previous work [2]. We first compiled a participant's data into testing sets (unique sets of n=5 steps). We then compiled training sets of j=5 steps in the same manner. The 95% confidence intervals of every training set were identified, and for every unique combination of testing-training set pairs we calculated the percent of testing set steps that were within those bounds. The analysis was then repeated with the number of steps in the training set increasing by five for each repetition (j=10, 15…), until every step was within the training set. The average percent of testing steps within the training set bounds was calculated across all unique comparisons per repetition. Stability was defined when the average percent was >95% and the increase in percent from the previous repetition was <1%. The number of steps in the training set when the criteria were met was considered the stability point.

The stability points (steps) were compared across the *variables* and *groups* using generalized linear mixed effects with a negative binomial distribution and log-link function (α=0.05).

Results and Discussion

From the seven days of data collection, participants contributed an average (min, max) of 10,919 (4698, 23904) steps to the analysis. In support of our first hypothesis, we observed a significant effect for *variable* ($p<0.001$). Compared to FPA (the variable requiring the fewest steps to reach stability), all other variables (Table 1) needed significantly more steps ($p<0.001$), except for FSA ($p=0.439$). The healthy adult and knee osteoarthritis groups were not significantly different ($p=0.708$).

Unsupervised, real-world walking biomechanics will stabilize, though the number of steps required for this differs by variable. For example, our data suggest at least 665 steps should be collected to examine the FPA, which equates to approximately 12 minutes of walking (assuming 55 ipsilateral steps/min). Meanwhile, outcomes like ACTO may require upwards of 2 hours of walking. The feasibility of these collection requirements should be weighed prior to starting real-world walking studies. Not all participants and variables reached stability based on our criteria (42/210). In these instances, the variables stabilized but at a lower percent (e.g., 80% or 90%). This indicates that some individuals walk with more inherent variability; whether that arose from external or internal factors is not yet clear. These results may be due to including all walking data, regardless of environment, while the previous running study only used data during level-ground running [2].

Table 1: The median (25th, 75th percentile) steps to stabilize.

Variable	HA (n=15)	KOA (n=15)	All (n=30)
ACHS	4410 (2480, 9965)	5185 (3736, 6679)	4645 (3009, 6796)
ACTO	5360 (2815, 10125)	6090 (4048, 7314)	6090 (3628, 8015)
GHS	5788 (3620, 9980)	5635 (4256, 7660)	5635 (3858, 8202)
GTO	3685 (871, 4851)	2550 (878, 5646)	2990 (950, 5250)
GC	5230 (3600, 7605)	5475 (3520, 7555)	5390 (3600, 7605)
FSA	745 (161, 3461)	540 (280, 2635)	695 (232, 2721)
FPA	595 (352, 885)	665 (485, 846)	612 (470, 875)

Significance

Our study provides the first investigation of how many steps are needed to reach stable foot biomechanics variables while walking in unsupervised, real-world conditions. This builds on previous work that used 15-20 min running bouts, by using a more precise 5 step interval for comparing test-training sets. Ultimately, our results support the feasibility of real-world walking studies.

Acknowledgements

Thanks go to the Canadian Institutes of Health Research for funding support, and Drs Pete Shull and Haisheng Xia for their guidance.

References

[1] Shull et al., (2014) Gait Posture, 40:11-9. [2] Benson LC et al., 2019 J Biomech, 85:187-92. [3] Kobsar et al., (2020), Sensors, 20. [4] Xia et al., (2017), J Biomech, 61:193-8.

DETERMINING WHOLE-FOOT GROUND CLEARANCE KINEMATICS BY AUGMENTING IMU TRAJECTORY WITH PERSONALIZED 3D SCANS

Katherine Heidi Fehr[1*], Jennifer Nicole Bartloff[1], Yisen Wang[1], Katherine Konieczka[1], Julia Mastej[1], and Peter G. Adamczyk[1]
[1]University of Wisconsin–Madison, Madison WI, USA
email: kfehr@wisc.edu

Introduction

Estimation of minimum foot clearance using wearable IMU's typically assumes that the toe or a point on the midfoot is the lowest vertical point relative to the walking surface during swing phase [1]. This assumption could lead to inaccurate foot clearance estimates in individuals with gait impairments who demonstrate atypical swing phase kinematics such as excessive inversion or lack of controlled dorsiflexion [2]. Further, this assumption does not hold during stair negotiation for healthy individuals [3]. Our pilot study aims to accurately characterize whole-foot minimum clearance during gait through observing the true lowest point on the shoe via use of 3d scanning to reconstruct and analyze entire shoe movement along a trajectory described by a shoe-mounted IMU.

Methods

Experimental Protocol

Two adult, female, unimpaired participants consented to participate in this pilot study. We securely placed one Opal (APDM) IMU sensor in a small pouch on each participant's running shoes. We scanned participants' feet/shoes with a Structure Sensor (Occipital Inc.) connected to an iPad (Apple) using the companion Occipital "Scanner" app. To properly locate the position and orientation of the IMU we placed a 3D printed fixture inside the pouch during the scan. Participants walked in a straight line down a hallway at a self-selected speed. Eight strides per participant were analyzed.

Processing of the 3D Scans

We used CAD software (Autodesk) to place points describing the IMU's center and axes, the toe, the heel, and a grid of points that covered the bottom surface of the participant's shoe. These salient points were located based on the fixture's rectangular "ears" that were visible to establish datum planes and edges.

Trajectory Reconstruction

The trajectory was reconstructed using a Kalman Smoother from the foot IMU's acceleration and gyroscope data. To reduce drift due to sensor bias, we applied Zero Velocity Update (ZUPT) at every footfall and Zero Attitude Rate Update (ZARU) for long stationary periods. This procedure yielded the IMU's position and orientation relative to global reference frame at each instant.

Minimum Clearance Calculation

Having the global pose of the IMU from the reconstruction and the pose of the salient points on the shoe with respect to the IMU in the 3D scan's reference frame, we calculated the location of the foot's points in the global frame throughout of the trials. "Lowest" clearance was defined as the lowest height of the lowest point on the shoe during the forward swing, defined between the maxima of heel and toe height during swing phase. For comparison, we calculated virtual IMU clearance as the minimum height above a line connecting successive footfalls during forward swing, here defined between the two maxima [4].

Results and Discussion

Clearance values are shown in Table 1. In addition to providing a more sensitive metric of whole foot clearance during forward swing, this method provides information on the magnitude and at-risk location of minimum foot clearance. Further, our analysis revealed strikingly different patterns between participants in the anatomical location of the lowest points during forward swing, shown in Figure 1.

Table 1: Vertical clearance in millimeters (Mean±St.Dev.)

Participant	Lowest	Toe	Heel	Virtual IMU
A	18.2±4.9	32.4*±6.7	36.3*±6.2	14.26±4.2
B	4.1±4.5	13.4*±3.0	20.8*±3.0	10.2*±3.3
Average	11.1±8.6	22.9*±11.2	28.6*±9.27	12.2±4.2

*denotes significantly greater average clearance than Lowest, p<0.0167

Significance

This novel approach results in a more comprehensive understanding of minimum foot clearance than current methods and enables precise identification of anatomical locations most likely to lead to scuffing, tripping, and falls during gait. Such information collected from real-world mobility via IMU's, could offer a new objective comparison of prosthetic & orthotic effectiveness and can better inform selection and design of such devices based on individual foot clearance patterns.

Acknowledgments

Funding provided by DOD W81XWH-19-2-0024.

References

[1] Delft et al., 2021. *Int. J of Env. Research and Public Health*., **[2]** Lee & Hogan, 2015. *IEEE Transactions on Neural Sys. And Rehab. Eng*. **[3]** Telonio et al., 2013. *J Biomech*. **[4]** Wang & Adamczyk, 2019. *Sensors*.

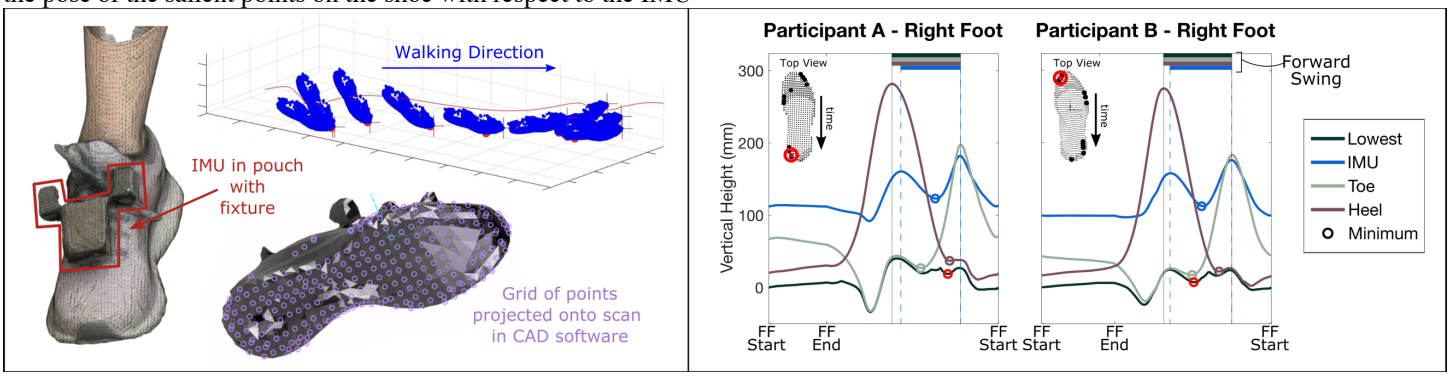

Figure 1: Left—images of the scan of a participant's foot and an example reconstruction of a single stride. Right— representative trajectories for each participant between consecutive foot falls (FF).

SYNTHESIZING BIOMECHANICAL MEASUREMENTS USING A SEQUENTIAL TRANSFORMER MODEL

Paul Quinlan[1*], Qingguo Li[1] and Xiaodan Zhu[2]
[1]Queen's University, Department of Mechanical and Materials Engineering
[2]Queen's University, Department of Electrical and Computer Engineering
Email: *15pwq@queensu.ca

Introduction

Biomechanics research relies heavily on sensor measurements, where the number of sensors constrains the amount of information that a study can acquire. Instead of collecting data with many sensors, synthesizing sensor data based on available measurements from a smaller set of sensors could be a viable alternative. We hypothesize that the use of modern deep learning technologies could help reducing the number of sensors required without losing key biomechanical information

In this study, we demonstrated that synthetic sensor data can be generated using a transformer-based model using a small amount of training data from sensor measurements. The sensor glove records positions at 21 different points within the hand. After removing 13 sensors from the wrist, middle, ring, and pinkie fingers, we used the remaining 8 sensors, located on the thumb and index finger, to generate synthetic sensor data.

Methods

The Xsens Glove (Manus) was used to collect hand gesture data. The glove records 4 positions on each finger and one at the wrist. 15 hand gestures were recorded continuously at 60Hz with a total of 750 training samples. The gestures chosen were yes, no, name, help and number 0 through 10 in American Sign Language. Each gesture has a length up to a maximum of 300 data points. These gestures were chosen to help ensure variations between hand positions within the dataset of recorded gestures.

We chose to keep the sensors related to thumb and index finger motion. Each sensor contains relative position information in the X, Y and Z axis. Our model will take 24 channels of position information from the 8 input sensors. At each timestep the model can output X, Y and Z positions for up to 4 sensors simultaneously.

We trained an attention-based encoder model as presented by Vaswani et al [1]. First, we project the input data from each timestep into an embedding vector of size 64 using a series of 1x1 convolutions as shown by Shavit and Klein [2]. We then add a learned positional encoding at each timestep. Since each sequence is of different lengths, we added a mask over the padded time series data to ensure that our model is not using them to make predictions for our synthetic sensor data. The embeddings are passed to 4 stacked encoders with 8 self-attention heads. Finally, the encoder output is fed to the classification head. This consists of a feed-forward neural network to predict a value for the synthetic sensor data at each timestep and for each axis. We employ layer normalization within the classification head and within the encoder model.

Of the 750 samples recorded, 600 were used to train the model and 150 were used for model validation. To train our model we used an initial learning rate of 0.01 which is decreased by an order of magnitude when the loss plateaus during training. The Stochastic gradient descent algorithm and mean absolute error were used for optimization. The glove and corresponding location renderings are shown in figure 1.

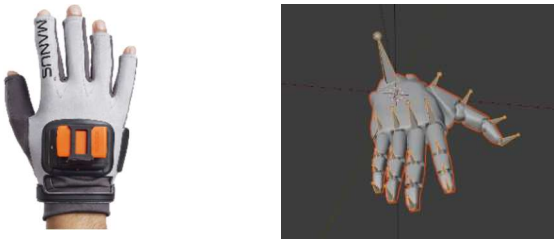

Figure 1:Xsens Glove by Manus (left) and corresponding measured positions(right) as shown in Blender.

Results and Discussion

Using our model, we can obtain a mean absolute error (MAE) of 0.008m and a product-moment correlation (PMC) coefficient of 0.97 between the synthetic and real sensor data on the validation dataset for predicting values from the primary sensor. When we adjust the model to output all 4 sensors on the middle finger simultaneously, we can achieve an MAE of 0.012m and a PMC coefficient of 0.96. A sample timeseries is shown in figure 2 for the sensor on the knuckle of the middle finger.

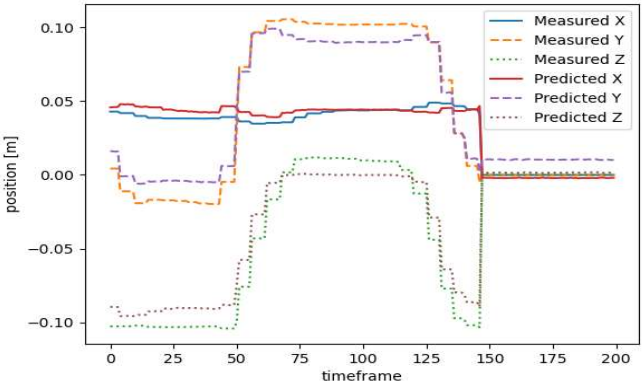

Figure 2: Measured vs synthetic sensor position data.

These results demonstrate that the movement of a constrained biomechanical system such as the hand has redundancy. Deep learning algorithms can discover the inherent correlation between measurements of sensors at different locations. Consequently, a small set of sensors could be sufficient to capture the overall movement of the biological system.

Significance

This research could have very broad impacts within the field of biomechanics involving sensor measurements. This approach alleviates the constraints of placing sensors at each location of interest and instead can generate the information from a relatively small amount of training data.

Acknowledgments

We would like to acknowledge the support of the Ingenuity Labs Research Opportunity Seed Funds, Queen's University.

References

[1] A. Vaswani *et al.*, "Attention Is All You Need".
[2] Y. Shavit and I. Klein, "Boosting Inertial-Based Human Activity Recognition with Transformers"

THE INFLUENCE OF A SOFT ACTIVE EXOSUIT ON VERTEBRAL LOADS DURING LIFTING

Jacob J. Banks[1,2*], D. Adam Quirk[3], Jinwon Chung[3], Conor J. Walsh[3], Dennis E. Anderson[1,2]
[1]Center for Advanced Orthopaedic Studies, Beth Israel Deaconess Medical Center, Boston, MA, United States
[2]Department of Orthopaedic Surgery, Harvard Medical School, Boston, MA, United States
[3]John A. Paulson School of Engineering and Applied Sciences, Harvard University, Boston, MA, United States
email: *jbanks3@bidmc.harvard.edu

Introduction

Back related workers-compensation claims are prevalent and costly industrial injuries[1]. Ergonomists, engineers, and clinicians strive to reduce back injury via a variety of interventions aimed at reducing back demands during manual materials handling tasks[2]. A promising and exciting intervention are back support exoskeletons/suits[3]. Support exosuits are designed to provide comfortable assistive force(s) to back muscles during lifting tasks, but their influence on thoracolumbar spine loads is mostly unknown.

The purpose of this study is to estimate *in vivo* back demands during different lifting tasks with and without a soft active back support exosuit (Exo)[4]. We hypothesize the Exo will reduce demands, but effects will vary by vertebral level. By examining the impact at multiple levels, the results from this study will improve our understanding of this and other exosuits as a potential intervention.

Methods

Fourteen healthy participants (♂=10; 31±4 years) consented to a multi-institute review board approved protocol. All participants' donned form fitting clothing to facilitate full-body motion capture (Qualisys AB) while squat lifting a 6 kg box at a prescribed 5 lift/min pace from the floor with and without an Exo suit. The Exo studied here was designed to provide kinematically compliant trunk and hip extension assistance via a nylon cord linking a backpack-mounted electromechanical actuator to each thigh[4]. Assistance forces of up to 250 N were applied based on measured real-time kinematics.

An OpenSim[5] full-body thoracolumbar musculoskeletal model[6] was used to estimate back demands. Models were scaled to participant specific measures of marker distances, IMU recorded angles, and predictive regressions[7]. Trial specific kinematics, musculotendon recruitment, and joint reactions were estimated with custom MATLAB to OpenSim API scripts. Additionally, the Exo condition was modelled by adding rigid-bodies of appropriate inertial properties (2.7 kg in total) attached dorsally to the trunk at the T6 vertebrae and each thigh, connected via actuators replicating a measured assistive force.

Back demands for both conditions were quantified at the L5, L3, T12, and T10 vertebrae as the average compression force during the ascending portion of three lift repetitions. A repeated-measures ANOVA, and when applicable post hoc Tukey HSD pairwise comparisons, tested ($\alpha < .05$) the main effects and interaction of the two suit conditions and four vertebral levels (independent variables) on average compression force (dependent variable).

Results and Discussion

The average compression forces during the lift were different for both main effects and their interaction (p-values < .01 for each; Fig. 1). Post hoc groupings showed that during the Exo suit condition forces were reduced relative to the No Exo suit condition, supporting our primary hypothesis. Vertebral level forces were all unique from one other, with larger magnitudes at more inferior vertebral levels. A significant interaction effect and corresponding pairwise comparison complemented both main effects and our secondary hypothesis, and highlighted how the relative benefits of the Exo suit are more prominent at more superior vertebral levels (e.g., 11.4% reduction in compression force during the Exo condition at T10 versus 1.8% at L5).

The observed main effect of the Exo (e.g., reducing vertebral compression forces) support the benefits of having an external assistive force working at a more advantageous distance in relation to the trunk extensors muscles. However, such benefits seemingly lessen at inferior vertebral levels. Further analyses indicate this reduced efficacy could be a consequence of exosuit assistive forces becoming less beneficial in relation to larger inherent kinetic demands, a smaller exosuit moment arm length, and a deleterious effect of the thoracically located Exo mass.

The interpretation of these results is limited to our experimental analysis and modeling approaches. Future work should examine whether these observed effects are consistent across other lifts, participants, and modeling assumptions.

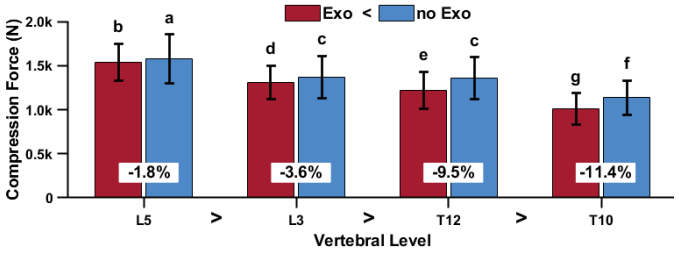

Figure 1: L5, L3, T12, and T10 vertebral compression forces for Exo (red) and no Exo (blue) suit conditions. Percentages represent differences between Exo and No Exo suit conditions for each vertebrae. Greater/less than signs and letters denote significant ($\alpha < .05$) main and interaction effect pairwise groupings, respectively.

Significance

This study demonstrates that a soft active back support exosuit can reduce musculoskeletal model estimated spinal loading during a lifting task. However, the impact of the suit seems to vary by vertebral level. Thus exosuit design processes should more broadly consider their variable effect on spinal loading to ensure they meet expectations.

Acknowledgements

Funded via a collaborative DOD CDMRP: W81XWH-20-1-0608

References

1. Liberty Mutual Insurance (2021) *Workplace Safety Index*
2. Marras & Karwowski (2006) *Occup. Ergo. Handbook*
3. Ali et al. (2021) *Frontiers Bioeng. Biotech.* 9
4. https://wyss.harvard.edu/technology/soft-exosuits-for-back-support-during-strenuous-tasks/
5. Delp et al. (2007) *IEEE* 54(11)
6. Burkhart et al. (2020) *J Biomech.* 112
7. Anderson et al. (2012) *J Biomech*. 45

KINEMATIC ADAPTATIONS TO LIMITING LUMBAR SPINE FLEXION ACROSS LIFTING TASKS

Danielle R. Carnegie*, Steven M. Hirsch[1], Samuel J. Howarth[2], and Tyson A.C. Beach[3]
[1]Faculty of Kinesiology and Physical Education, University of Toronto, Toronto, ON
[2]Division of Research and Innovation, Canadian Memorial Chiropractic College, Toronto, ON
[3]Department of Kinesiology and Health Sciences, University of Waterloo, Waterloo, ON
email: danielle.carnegie@mail.utoronto.ca

Introduction

Approximately 80-100% of maximum available lumbar flexion range-of-motion is used when lifting [1]. Our unpublished data suggests compensatory adaptations in trunk and lower extremity joint range-of-motion are observed when lumbar flexion motion is experimentally limited during lifting [2]. However, these specific observations were made using a single lift origin height and object mass. It is likely that the nature and magnitude of adaptations vary based on lifting task parameters. The current study sought to describe kinematic changes that result from limiting lumbar flexion motion when executing lifts with different origin heights and object masses. It was expected that effects of limiting lumbar flexion on lifting kinematics would be largest when loads were greatest and lift origin heights were lowest.

Methods

20 participants (10 male and 10 female) performed a series of 8 lifting tasks in block randomised order which varied in combinations of the following task factors: 1) lift origin height (high = knee height, low = mid shank height); 2) mass of object lifted (light = 20kg women and 34kg men; heavy = 34kg women and 58kg men); and 3) presence or absence of lumbar flexion motion limiting harness. This custom-built harness was designed to limit lumbar spine flexion exclusively, while allowing all other joints to move freely. Five contiguous repetitions for each possible combinations of lifting task parameters were performed. Optoelectronic motion capture (Vicon, Oxford, UK) recorded segment kinematics during lifting tasks, and participant-specific linked-segment models were used to calculate sagittal trunk, spine, hip, knee, and ankle angles. Peak angles for each segment or joint were determined for each lifting repetition, averaged across all 5 repetitions for a single task, then compared using repeated measures ANOVAs.

Results and Discussion

A significant interaction effect between use of harness and lift origin height was observed for lumbar flexion ($F=8.822$, $df = (1,133)$, $p<0.01$). This indicated that the magnitude of change in lumbar flexion that resulted from different lift origin heights depended on the presence or absence of harness. However, use of the harness reduced the magnitude of lumbar flexion motion in all conditions compared to not wearing the harness, confirming the harness functioned as intended. A statistically significant interaction effect was also observed for hip flexion ($F=6.615$, $df = (1,133)$, $p<0.05$) (Figure 1). Hip flexion was greater in lower lifts compared to higher lifts, however there was an 18^0 difference in hip flexion between high and low origin heights when lumbar flexion motion was limited, compared to a 10^0 difference between high and low origin heights when spine motion was unlimited. A main effect of harness was also observed for knee flexion ($F=5.779$, $df = (1,133)$, $p<0.05$) and ankle dorsiflexion ($F=3.996$, $df = (1,133)$, $p<0.05$). When the harness was in place, lifters exhibited greater knee flexion and ankle dorsiflexion compared to when lumbar flexion motion was not limited. Further, a main effect of lift origin height was observed for trunk inclination ($F=177.101$, $df = (1,133)$, $p<0.001$), ankle dorsiflexion ($F=54.359$, $df = (1,133)$, $p<0.001$), and knee flexion ($F=114.974$, $df = (1,133)$, $p<0.001$). Specifically, lifters increased trunk inclination, knee flexion and ankle dorsiflexion when lifting lower-lying objects compared to higher lift origin heights. Contrary to previous findings [2], in comparison to not wearing the harness, trunk angle was not significantly reduced by wearing it. Unexpectedly, no significant main effect was found for object mass for any dependent variable and no three-way interactions were observed.

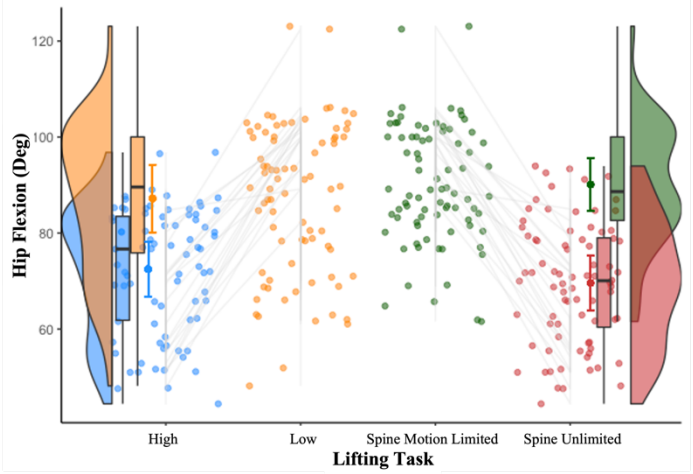

Figure 1: Raincloud plot for hip flexion angle. Scatter points displays intraparticipant change in hip flexion (y axis) between conditions (x axis). Boxplots display central tendency. Line plot display mean hip flexion angle for condition with confidence interval (0.95). Violin plots display distribution of participants. Blue plots display hip flexion angle during high lift origin heights and orange plots indicate low lift origin heights. Green plots denote hip flexion angle during lumbar flexion motion limited tasks and red plots show motion unlimited lifts.

Significance

Because limiting lumbar spine flexion during lifting reallocates necessary joint range-of-motion demands to the lower extremity, individuals without sufficient lower extremity joint range-of-motion capacity may not be able to limit lumbar spine flexion when lifting. Further, the nature and magnitude of kinematic adaptations required to limit lumbar flexion motion during lifting depend on lift origin height but do not appear to be affected by mass lifted.

Acknowledgments

This research was jointly supported by the University of Toronto's Faculty of Kinesiology and Physical Education and the Canadian Memorial Chiropractic College.

References

[1] Dolan et al., 1994. *J Biomech*. 27; 1237.
[2] Carnegie et al., 2022. *In Progress*.

THE RELATIONSHIP BETWEEN PAIN CATASTROPHIZING, PAIN SENSITIVITY, AND INTER-JOINT COORDINATION DURING A LIFTING TASK IN PEOPLE WITH CHRONIC LOW BACK PAIN

Patrick Ippersiel[1*], Richard Preuss[1], Timothy H. Wideman[1], and Shawn M. Robbins[1]
[1] McGill University, School of Physical and Occupational Therapy, Montreal, Quebec, Canada
*Email: Patrick.ippersiel@mail.mcgill.ca

Introduction

Pain may serve as a protective mechanism, prompting guarding of a region that is perceived to be injured or threatened [1]. This may manifest as tighter inter-joint coordination and reduced movement variability in people with low back pain (LBP). Persistence of these "protective" behaviors, however, may cause uneven tissue loading and complicate recovery, and may be a factor in chronic LBP. Despite calls for conceptualizing movement within a biopsychosocial framework, key risk factors for disability such as heightened pain catastrophizing and pain sensitivity are often considered independent from biomechanical metrics – leaving our understanding of movement somewhat limited.

Therefore, we aimed to determine if pain catastrophizing and pain sensitivity were related guarded movement (via joint coordination and variability) during a lifting task in people with chronic LBP.

Methods

Fifty-four adults with chronic non-specific LBP (>3 months) were recruited (36F, mean age=44.4, SD=10.5). Baseline demographics, pain (Brief Pain Inventory), and pain catastrophizing (pain catastrophizing scale) were measured. Pain sensitivity was quantified via temporal summation of pain and pressure pain thresholds at the lumbar spine.

Participants performed a crate lifting task (partitioned into lifting and replacing phases). An electromagnetic TrakSTAR motion capture system (Ascension Technology, Milton, VT, USA) collected spinal kinematics (sampled at 200Hz) using sensors on the right thigh, and S1, L3, T12, and T9 spinous processes. Hip and lower lumbar joint angles (L3-S1) were extracted by calculating the relative orientation of adjacent segments (e.g., thigh relative to S1 defines the hip angle).

Continuous relative phase (CRP) analysis determined inter-joint coordination of the Hip-Lower lumbar joint pair. Phase angles were determined using the Hilbert transform method [2]. The absolute difference between the two joints quantified coordination, where a value of 0 corresponds to perfect in-phase synchronization, while 180 refers to out-of-phase behavior. The mean absolute relative phase (MARP) quantified coordination amplitude. The deviation phase (DP) quantified variability of coordination patterns [3].

Linear regression analyses tested the hypotheses that (i) pain catastrophizing and (ii) pain sensitivity were associated with more in-phase Hip-Lower lumbar coordination amplitude (MARP) and less variable coordinative variability (DP), after accounting for other factors.

Results and Discussion

For Hip-Lower lumbar coordination amplitude, the base model (age, sex, BMI, pain severity) was statistically significant for crate lifting (Table 1) and replacing (R^2=0.219, p=0.023) phases. Adding pain catastrophizing improved our model for lifting (Table 1) and replacing (R^2=0.331, p=0.003; b=-1.43, p=0.010, ΔR^2=0.112) phases, showing that greater pain catastrophizing was related to more in-phase guarded movement. Adding temporal summation of pain and pressure pain thresholds in a separate step did not improve our models. For Hip-Lower lumbar variability, no models were statistically significant.

Table 1. Regression analyses with coordination amplitude (MARP) as dependent variable during crate lifting.

Step	Variable	β	95% CI	Δr^2 (p-value)
1	BMI	0.287	0.07 to 3.50	0.192
	Age	0.211	-0.27 to 2.04	(0.044)
	Sex	-0.066	-30.6 to 18.9	
	Pain Severity	-0.231	-13.9 to 1.22	
2	PCS	-0.437	-2.45 to -0.45	0.130 (0.006)

PCS: pain catastrophizing scale

Pain catastrophizing was related to more in-phase Hip-Lower lumbar coordination (i.e., guarding) during a lifting task, while measures of pain sensitivity were not. Hip-Lower lumbar variability was largely unrelated to pain catastrophizing and pain sensitivity. This suggests that psychological factors and certain movement behaviors are intertwined – to some degree – and that different metrics of movement may show distinct relationships with biopsychosocial variables.

Significance

This work provides evidence that psychological factors and movement biomechanics are not entirely distinct. Clinically, rehabilitation strategies might consider integrated treatment approaches (e.g., psych-informed physiotherapy) as opposed to more traditional 'siloed' approaches. Researchers should consider the possibility that psychological factors could influence biomechanics and should account for this in future studies.

Acknowledgments

Patrick Ippersiel is supported by an IRSST doctoral fellowship and an OPPQ-REPAR project grant clinical research.

References

[1] Hodges P and Tucker K. (2011). *Pain* Vol **152**;

[2] Lamb P and Stockl M. (2014). *Clin Biomech.* Vol **29(5)**

[3] Stergiou N and Decker L. (2011). *Hum Mov Sci.* Vol **30(3)**;

AUTOMATED CONTROL OF QUASI-PASSIVE BACK EXOSUITS USING RECURRENT NEURAL NETWORKS

Laura J. Elstub[1*], Cameron A. Nurse[1], Paul R. Slaughter[1], Peter Volgyesi[2], Chad C. Ice[1] and Karl E. Zelik[1]
[1]Center for Rehabilitation Engineering and Assistive Technology, Vanderbilt University
[2] Institute for Software Integrated Systems, Vanderbilt University, Nashville, Tennessee, United States
*email: laura.judson@vanderbilt.edu

Introduction

Low back disorders due to overexertion are a common cause of missed work, pain and disability. When traditional ergonomic controls are unable to remove or mitigate risks then emerging wearable assist devices called exos (exoskeletons and exosuits) provide a promising alternative. Back exos reduce muscular demands, effort, and fatigue [1] and are useful in occupational settings where repetitive lifting takes place and low back injuries are prevalent [2]. Passive and powered back exos have each been developed and shown to be feasible, but they have different strengths, weaknesses, and use cases. Quasi-passive (also known as semi-active) exos have also been developed and contain some of the benefits and drawbacks of both passive and powered devices. In some instances, quasi-passive exos use small actuators to engage a spring to provide elastic assistance when it is needed, then disengage the spring to remain transparent (unobstructive) when assistance is not needed. In theory, this engagement/disengagement can be automated using wearable sensors and a control algorithm, but user intent recognition and coordinating the exo's actions with the user remain a grand challenge in the field. This human-device coordination is difficult in part due to potential safety issues that can occur if a device were to perform the wrong action or be in the wrong mode at the wrong time, and in part due to users of wearable assist devices having relatively low tolerance for device control and coordination errors, which may perturb their balance or comfort.

One prior control algorithm for a quasi-passive exo achieved an overall accuracy of 87% in support activation using Gaussian Mixed Models [3]. However, we expect this level of accuracy is insufficient for real-world applications, as users become frustrated when wearable devices behave inconsistently, and this negatively affects user adoption [4]. Errors in exosuit control can be particularly problematic, as failing to correctly engage would mean assistance is not provided when required or expected by the user and failing to disengage could interfere with other tasks such as sitting. The aim of this work is to develop a quasi-passive exo control algorithm with very high mode-switching accuracy. We initially targeted an accuracy of >95%, while focusing on control methods that we believe have the potential (with sufficient refinement) to be > 99% accurate.

Methods

Using video footage and insight from industry, we developed user stories focused on material handlers (e.g., movers) whose job involves repetitive lifting, walking, carrying, and other movement tasks. We defined what we term 'critical' transitions: exo mode switches (from engaged to disengaged, or vice versa) that would be difficult to perform manually, for instance, if both hands are already occupied or required to complete the occupational task. As such, we labeled long-distance walking (specifically while carrying an object with two hands) as the start of a critical transition to exo spring disengagement, and then stopping to lower the carried object afterwards as the start of a critical transition to spring engagement. Other examples where a change in mode may be required or desired, such as sitting down or climbing stairs, were thought of as non-critical since both hands are generally not in use and therefore a manual mode switch (e.g., button press) would be simple and practical.

We focused on developing an automated control algorithm based on a heuristic that disengages the exo spring after a set number of sequential steps (e.g., 3), then engages the spring as the user comes to a stop regardless of whether they subsequently perform a lift or not.

Training data were collected from one participant during a range of lifting and walking tasks with an inertial measurement unit (IMU) placed on the sternum, pelvis and the left and right thigh to record accelerations alongside orientation and Euler angles in the x,y,z directions. In total, 11 trials of 5 to 20 minutes were recorded, resulting in 25,747,400 data points provided for initial algorithm development. The machine learning algorithm used was a recurrent neural network (RNN) with stacked LSTM (long short-term memory) nodes that use the previous sample(s) to predict the engage/disengage command of the next sample.

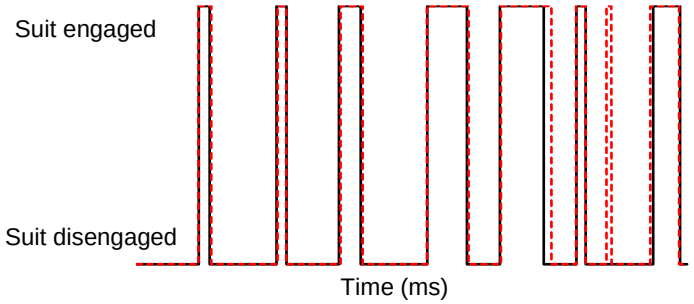

Figure 1: A representative trial where the red dashed line shows RNN predictions, and the solid black line shows the target control signal based on the critical transition control heuristics we defined.

Results and Discussion

By combining accelerometer and gyroscope signals from four IMUs with a RNN algorithm, we achieved a preliminary accuracy of 93.5%. We intend to further development with a state-machine-based supervisor and implementing online learning with real-time user feedback. Through these additional steps, we expect to achieve overall control accuracy >95%.

Significance

Successful development of the proposed control algorithm has the potential to improve quasi-passive exo capabilities and use cases, which may help reduce low back injury prevalence in the workplace and throughout society.

References

[1] Lamers et al., 2020. *Scientific Reports.* 10.1038/s41598-020
[2] US Department of Labor, 2016
[3] Jamŝek et al., 2020. *Sensors*. 10.3390/s20092705
[4] Orlando et al., 2021. *Medicina.* 10.3390/medicina5

SHOULD WE ESTIMATE INJURY RISK BASED ON KINEMATICS FROM A SINGLE MOVEMENT STRATEGY?

Daniel P. Armstrong[1*] and Steven L. Fischer[1]
[1]Department of Kinesiology and Health Sciences, University of Waterloo
email: dparmstr@uwaterloo.ca

Introduction

Movement and posture prediction tools such as digital human models (DHMs) can be used to proactively assess injury risk, but their predictive validity is reliant on their ability to accurately predict postures [1]. Movement strategy, in concert with body segment parameters (BSP), influence resultant biomechanical exposures on the body [2] and therefore are important considerations in proactive risk assessment. Currently, movement prediction models tend to predict a single movement trajectory for a given task (i.e., deterministic) but based on motor control literature we know that human movement is inherently variable [3] (i.e., probabilistic). Therefore, reliance on deterministic models to predict kinematics used to inform risk assessment may not be sufficient. However, using principal component analysis (PCA) to quantify modes of variance in kinematic data and then calculating the biomechanical exposures as a function of variability in the feature-reduced kinematic data may be a solution to consider movement variability in proactive risk assessment.

The purpose of this sensitivity analysis was to understand the range of peak low back loads observed across variability in feature-reduced kinematic data collected during a lifting task across a range of BSP assumptions. Second, to confirm that variability in peak low back loads is a primarily a product of kinematic variability opposed to BSP assumptions, the standard deviation of predicted low back load ranges (calculated using feature-reduced kinematics) across BSP conditions was investigated. It was hypothesized that peak low back loads would differ across the variability in lifting kinematics, and that these differences would be consistent across differing BSP conditions.

Methods

A sample of 28 participants completed 30 floor-to-waist height lifts while whole-body kinematics were collected at 100 Hz. Time-series *x, y,* and *z* coordinates of 29 anatomical landmarks were used to define segment orientations (consistent with ISB standards [4,5]), and were normalized to 101 points. PCA was applied to these data to identify modes of variance, referred to as principal components (PCs), in the whole-body kinematic data [6]. Ten PCs were retained for analysis.

For the 5th, 50th and 95th percentile score for each retained PC, kinematic data were reconstructed using single component reconstruction (10 PCs x 3 percentiles = 30 unique kinematic patterns). A load mass of 34 kg was applied to the distal end-point of the forearms for each reconstructed kinematic pattern. Using a top-down rigid link model with a single muscle equivalent peak low back compression and anteroposterior (AP) shear forces were calculated. This process was completed in 6 body mass conditions representing each of a 5th, 50th and 95th percentile male and female, which were used to scale BSPs (30 kinematics patterns x 6 BSP settings = 180 low back load estimates). The range of peak low back loads in each PC were calculated and expressed as a percentage of peak loads in the 50th percentile PC score reconstruction. The average and standard deviation of normalized range of peak low back loads within each PC across the 6 body mass conditions are reported as dependent measures.

Results and Discussion

Across the 10 retained PCs the range of peak low back compression and AP shear forces differed by as little as 4.4%, and by as much as 57.3% from the 50th percentile reconstruction (PC 4 - Table 1). While the peak low back compression and AP shear forces did appreciably vary in some PCs, these relative ranges were consistent across BSP conditions with a maximum standard deviation of normalized low back load range of 6.6%.

Table 1: Average range of normalized peak compression and AP shear forces between the 5th and 95th percentile PC reconstructions across all body mass conditions.

PC	Compression (%)	AP Shear (%)
1	9.9 (2.5)	8.6 (1.9)
2	4.3 (1.0)	9.0 (1.6)
3	12.1 (0.3)	20.8 (0.3)
4	50.6 (6.5)	57.3 (5.9)
5	9.8 (0.2)	18.9 (0.6)
6	11.5 (2.2)	38.3 (1.9)
7	4.6 (0.5)	14.0 (0.3)
8	24.5 (1.1)	31.5 (1.3)
9	1.9 (3.1)	17.4 (2.2)
10	11.3 (1.0)	19.2 (0.6)

Our hypothesis that peak low back loads would appreciably differ as a function of kinematic variability, and be consistent across BSP conditions, was supported. This is demonstrated by large ranges of low back loads across variability in some PCs (table 1 averages) and low variability in low back load ranges as a function of BSP conditions (table 1 standard deviations).

While this study uses a 'worst case' example by considering kinematic variability across the data set, it is a proof-of-principle demonstrating the potential impact of movement variability on peak low back loads in movement prediction.

Significance

This study supports that modelling variability in human movement prediction is important to inform risk assessment. Normalized peak low back compression and shear forces ranging by as much as 50% from the peak loads estimated from a mean movement (i.e., reconstruction from a 50th percentile PC score) demonstrate that the naturally occurring variability in lifting strategy can drastically influence peak low back loads. As such, use of deterministic modelling approaches that fail to consider movement variability may lack sufficient external validity when aiming to proactively assess risk. These reported methods could be used in the development of future probabilistic movement prediction models that would have potentially higher predictive validity than existing deterministic solutions such as DHMs.

References

[1] Chaffin, 2005. *Ergonomics.* 48:5, 478-491.
[2] Kingma et al., 2004. *Ergonomics.* 47:13, 1365-1385.
[3] Latash, 2012. *Experimental Brain Research.* 217:1, 1-5.
[4] Wu et al., 2002. *J. Biomech.* 35:4, 543-548.
[5] Wu et al., 2005. *J. Biomech.* 38:5, 981-992.
[6] Armstrong et al., 2021. *J. Occ. Rehab.* 31:1, 50-62.